EGG-TMI-6853 pt 2
Part 2--Appendixes
DRAFT

DRAFT REPORT: TMI-2 CORE DEBRIS GRAB SAMPLES--EXAMINATION AND ANALYSIS

Douglas W. Akers
Eric R. Carlson
Beverly A. Cook
Scott A. Ploger
Johan O. Carlson

Idaho National Engineering Laboratory
Operated by the U.S. Department of Energy

Informal Report

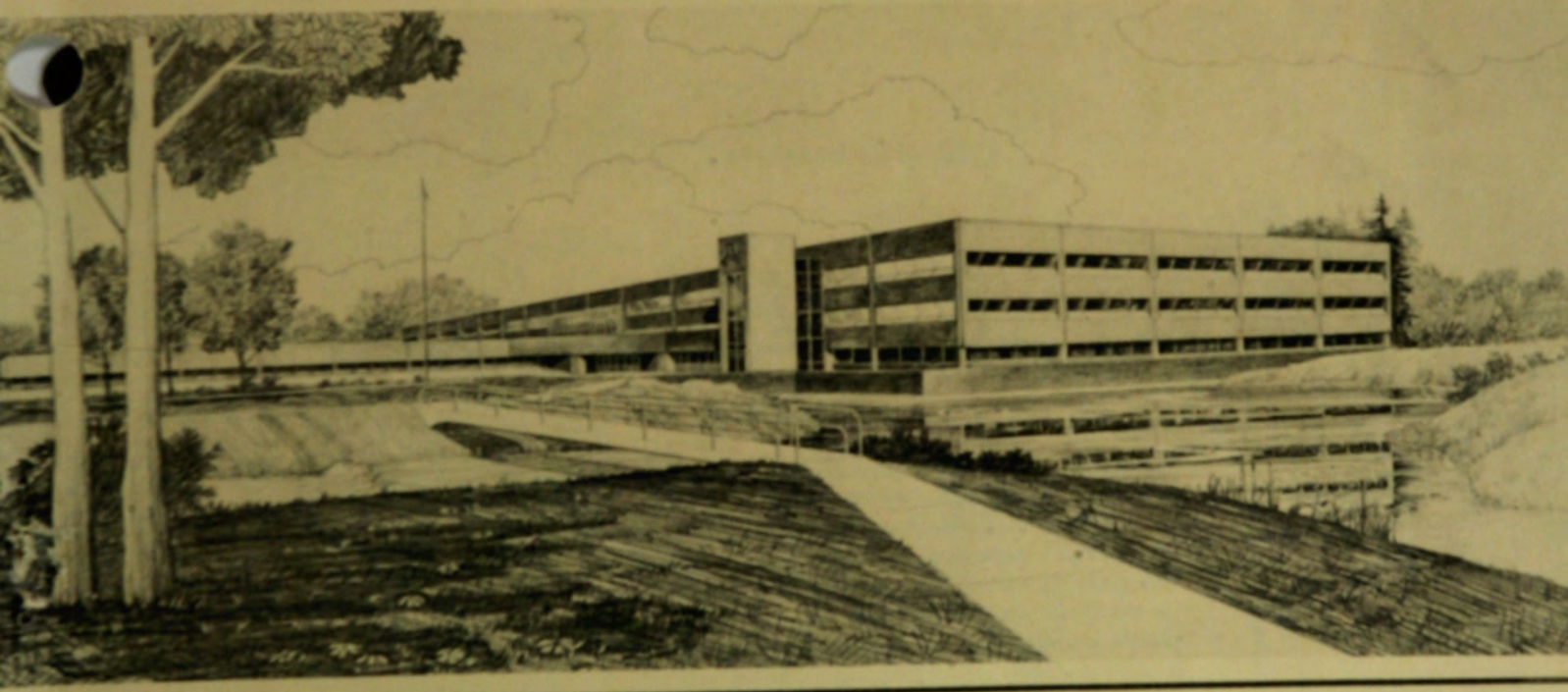

Prepared for the
U.S. DEPARTMENT OF ENERGY
Under DOE Contract No. DE-AC07-76ID01570

EG&G Idaho

EGG-TMI-6853
DRAFT

DRAFT REPORT: TMI-2 CORE DEBRIS GRAB SAMPLES--EXAMINATION AND ANALYSIS

PART 2

Douglas W. Akers
Eric R. Carlson
Beverly A. Cook
Scott A. Ploger
Johan O. Carlson

Published July 1985

EG&G Idaho, Inc.
Idaho Falls, ID 83415

Prepared for the
U.S. Department of Energy
Idaho Operations Office
Under DOE Contract No. DE-AC07-76ID01570

CONTENTS

DRAFT REPORT: TMI-2 CORE DEBRIS GRAB SAMPLES--EXAMINATION AND ANALYSIS

PART 2

Due to its large volume, this report has been divided into two parts. Part 1 contains the main body of the report, and Part 2 contains the appendixes.

APPENDIX A
EXAMINATION TECHNIQUES

APPENDIX A
EXAMINATION TECHNIQUES

This appendix contains a brief overview of techniques used during examination of the TMI-2 core debris grab samples, including physical, metallurgical, chemical, and radiochemical examinations.

Physical Examinations

Visual Examination and Photography

The visual and photographic examinations of the bulk core debris grab samples were performed through a glove box window for Samples 1 through 6, and through a hot cell periscope for Samples 7 through 11. Individual particles were removed and examined in the glove box.

Weight

The samples were weighed in the hot cell using an electronic balance (Sartorius Model 1205 MP).

Bulk Tap Density Measurement

The volume of each sample was determined by placing the bulk sample in a graduated beaker, tapping the beaker to compact the material, and measuring the sample volume. The weight (g) was divided by the volume (cm^3) to obtain the bulk tap density. The uncertainty associated with this analysis is large ($\leq$25%) because the irregular top surface of the sample in the beaker prevented precise measurement of the volume.

Particle Size Distribution

The core debris grab samples were subjected to a particle size distribution analysis by sieving each bulk sample into progressively smaller (4000 μm to <20 μm) particle size fractions (9 to 10 groups

in most cases). Sieve sizes were predetermined during visual examination of the samples, and new sieves (manufactured by Tyler, Inc.) were used for each sample to prevent cross contamination. Each bulk sample was placed in the top of the sieve column, and the larger (>1000 μm) particle size fractions were separated using dry, mechanical or hand-agitated sieving. Smaller (<1000 μm) particle size fractions were separated by wet sieving to prevent loss of particles by aerosol transport or adherence to sieve surfaces. Freon was used as the wash solution because it is not chemically reactive. Each sieve fraction was visually examined, photographed, and weighed.

Sample 4 was not sieved because it consisted of large particles. Sample 5 consisted of mostly large particles and was sieved into only four particle size fractions. Sample 7 was sieved after being agitated for 5 min and then again after 1 h to determine whether or not the sieving technique had an effect on results of the particle size distribution.

Ferromagnetic Material Content

The quantity of ferromagnetic material present in each sieve fraction was determined for Sample 6 (E9, 56 cm). This analysis was performed by placing a small (2-lb pull) magnet in a small beaker and then placing the beaker in contact with each sieve fraction. After stirring the beaker in the sample material, the magnet, beaker, and attached magnetic material were removed and placed in a container. The magnet then was removed from the beaker, allowing the magnetic material to drop into the container. No material adhered to the beaker after removing the magnet; therefore, it was assumed that all material in the container had a ferromagnetic component.

Pyrophoricity

Pyrophoricity (pilot ignition) tests were performed on portions of the core debris grab samples to evaluate potential safety hazards during core recovery operations. The test procedure was verified by igniting zirconium hydride powder, using a small Tesla coil (Fisher Scientific Model BD 10) rated at 50,000 volts. Ignition of the powder was recorded both by video

tape and still photography before beginning the actual core debris pyrophoricity tests. An additional method used to produce higher temperatures (a propane torch) also was tested on the zirconium hydride powder before beginning the actual test on the core debris material. The sample material was tested dry; then a drop of water was added and the material was tested wet.

A differential thermal analysis was performed by Rockwell Hanford Operations on small pieces of material which had been removed from some of the larger sized particles. Appendix H contains the report describing the examination and analytical technique.

Metallurgical Examinations

Optical Metallography

This technique involved viewing highly polished particles using a light microscope at magnifications up to about 500X. In addition, the particles often were treated with etchants to highlight grain boundaries and second phases.

The following grinding and polishing sequence was used for the TMI-2 core debris particles:

1. Course ground with water-lubricated silicon carbide 120 grit paper in a Whirlamat

2. Medium ground with 400 grit paper

3. Final ground with 600 grit paper

4. Initial polish with kerosene-type, fluid-lubricated 6-μm diamond grit on a hard paper in a Whirlamat

5. Final polish with 1-μm diamond grit on a short nap nylon

6. Metallic (non-zircaloy) particles were polished further with 0.3-μm Al_2O_3 grit in a vibratory polisher.

In general, either an immersion or swab etching technique was used, depending on whether a heavy or light etch was appropriate. The following etchants were used on the various materials:

- Fuel - 85% H_2O_2, 15% H_2SO_4
- Zircaloy - 55% lactic acid, 19% HNO, 19% H_2O, 7% HF
- Non-zircaloy metallic - 9.5% HNO_3, 90.5% methanol.

Scanning Electron Microscopy (SEM)

For this technique, a finely focused electron beam is swept in a raster across the surface of a sample. The types of signals which are produced when the focused electron beam impinges on a sample surface include secondary electrons, backscattered electrons, and characteristic x-rays. In SEM, the primary signal of interest is the variation in secondary electron emission that occurs. The variation is due to differences in surface topography. The secondary electrons are collected by a scintillator-photomultiplier system, and the resultant signal is displayed on a cathode ray tube (CRT). The scanning electron beam is synchronized with the scanning of the CRT such that images can be presented on a storage oscilloscope or a monitor oscilloscope for photographing. This procedure also is used for backscattered electron images. These electrons have a higher energy than secondary electrons, resulting in greater escape depths. The primary advantage of backscattered electron images is that they show different brightness values of phases of different composition.

Energy-Dispersive X-ray Spectroscopy (EDS)

EDS analysis is performed by measuring characteristic detectable x-rays from elements above atomic number 10 on the periodic table, which are excited by a scanning electron beam. The beam is typically 1 μm in diameter, but scattering produces x-rays over a region up to ten times wider. A SEM/EDS system is very convenient for speedy area surveys of elemental content and spectral uniformity, and produces good images and photographic records. Other advantages are the low beam energy and relatively low vacuum required, both of which limit absorption of deposited molecules. The usefulness of this instrument is reduced by susceptibility to background radiation, inability to detect oxygen and carbon, and absence of binding energy information.

Scanning Auger Spectroscopy (SAS)

This instrument rasters an electron beam over a sample region, ionizing surface atoms and generating characteristic x-rays and secondary electrons in the process. Rather than the x-rays, Auger spectroscopy collects and energy-analyzes the emitted Auger electrons from elements above atomic number 2. The double-focusing electron optics and tight energy resolution essentially eliminate interferences from background radiation. Moreover, the detected secondary electrons are only able to escape the outermost atomic or molecular layers, so depth resolution is extremely fine. Most SAS systems incorporate inert gas ion sputter-etching for both specimen cleaning and depth profiling; the positive ion flux counter balances charging by incident electrons. The elemental detection threshold is typically 0.1 at. %, which is comparable to EDS. SAS spatial resolution is equal to the beam diameter, which varies between models from 0.1 to 20 μm.

Chemical Examinations

Inductively Coupled Plasma Spectrometry (ICP)

Liquid-based samples are nebulized and pulse-injected into an inductively (radio frequency) heated plasma, causing all elements present

to emit characteristic light wavelengths. The light is separated on a diffraction-grating monochromator, and the wavelength intensities are sequentially measured by photomultiplier tube. [As such, ICP is a refinement of atomic emission spectroscopy.] This technique generally is free of elemental interferences, is highly accurate, and has a detection threshold of approximately 0.001 at. % (10 ppm). This analysis is performed on liquids (dissolved sample material). The equipment used was an ISA 2000 Scanning Spectrometer.

X-Ray Diffraction

Every crystalline substance scatters x-rays in its own unique diffraction pattern, producing a "fingerprint" of its atomic and molecular structure. The intensity of each reflection provides limited semiquantitative information on the molecular structures present. One unique feature of x-ray diffraction is that components are identified as specific compounds. Small (<10 mg) portions of the samples were placed in a powder camera, exposed to the x-ray beam, and characteristic x-ray diffraction patterns produced. The equipment used was a Phillips X-ray Diffractometer.

X-ray diffraction analysis was performed on several samples. However, the following problems were encountered in analyzing the samples and data:

- Because of high radiation levels associated with the samples, only small (1 to 2 mg) portions could be analyzed. Therefore, several (up to 10) portions would have had to be analyzed and averaged to characterize a large (20 to 30 mg) sample.

- The heterogeneity (many different phases structures) of the TMI-2 core debris grab samples made it difficult to characterize a sample, because the lattice structure observed contained all phases present.

- Crystalline structures of most importance are the mixed oxides of U and Zr. There are few or no materials standards for the variety of lattice structure observed.

- where U or Zr is a minor component, it is difficult to resolve the minor oxide species with available equipment. This makes identifying minor but important structures in the samples difficult.

Radiochemical Examinations

Gamma Spectroscopy

The initial radiochemical analysis performed was gamma spectroscopy. This technique is based on gamma-ray emissions which produce a spectrum specific to individual radionuclide species. The spectra were analyzed by a computerized gamma spectroscopy system using DEC PDP-15 or PDP-11/44 computers with a GAUSS VI analysis program.[a] This program identifies the radionuclides associated with the gamma-ray energy peaks and determines their emission rates corrected for detector efficiency, random pulse summing, and decay during the count. The values were converted to disintegration rates by dividing them by the gamma-ray emission probability. The equipment used was fabricated at EG&G Idaho and calibrated using standards of the National Bureau of Standards.

Dissolved portions of samples were diluted and analyzed in 60-mL bottles at calibrated distances with the computerized Ge(Li) gamma spectroscopy system. They were analyzed as point source geometries at distances ranging up to 195 cm from the detector. The mass of each portion analyzed was less than or equal to 100 mg to keep the gross radioactivity low and minimize the effects of mass attenuation. The effects of mass attenuation were evaluated and corrections applied, using different gamma-ray emission lines from one radionuclide. The uncertainty of the gamma spectroscopy analysis method is less than 10%, with the exception of those radionuclides whose concentrations were measured using low energy gamma rays (^{152}Eu and ^{125}Sb). The uncertainty associated with these radionuclides is approximately 30%.

---

a. J. E. Klein, M. H. Putnam, R. H. Helmer, GAUSS VI, A Computer Program for the Automatic Analysis of Gamma Rays from Germanium Spectrometers, ANRC-113, June 1973.

Neutron Activation/Delayed Neutron Analysis

The fissile/fertile material content was measured by neutron activation/delayed neutron analysis at the Coupled Fast Reactivity Measurement Facility (CFRMF) at the Idaho National Engineering Laboratory.[a] The total fissile/fertile material content was measured by remotely exposing individual 1 x 5-cm cylinders containing sample material to a fast spectrum neutron flux in the central region of the CFRMF core. The cylinder was removed after a 1-min exposure, and the delayed neutrons were measured after about 40 s, using a ^{3}He detector in a hydrogen moderator.

The fissile material content was measured by exposing the cylinder to a thermal spectrum neutron flux, causing only the ^{235}U and ^{239}Pu within the material to fission and emit delayed neutrons. It was assumed that the quantity of ^{239}Pu was insignificant (<2 wt% based on theoretical predictions). However, a 5 to 8% bias may have resulted. The fertile material contents were determined by subtracting the measured fissile material content (^{235}U and ^{239}Pu) from the total fissile/fertile material content using appropriate calibrations. Calibration measurements were made for both mass differences and enrichment. Standards were depleted U, natural U, 4.3%-enriched U, and 93%-enriched U.

^{129}I, ^{90}Sr, and Tellurium Analyses

Analyses for ^{129}I, ^{90}Sr, and Te were performed on the dissolved sample material. After organic separation, the volatile sample fraction was analyzed for ^{129}I via neutron activation with a subsequent gamma spectroscopy analysis. The ^{129}I present in the dissolved material was activated to ^{130}I, a gamma-ray emitting radionuclide. The sample material then was analyzed via gamma spectrometry, and the ^{129}I concentration calculated from the measured ^{130}I.

---

a. Y. D. Harker, Feasibility of Measuring the Fissile Content of Irradiated Fuel Samples, REA-83-022, February 16, 1983.

The ^{90}Sr analysis was performed on the nonvolatile sample fractions by precipitating the Sr carrier and ^{90}Sr from the other radionuclides, followed by beta analysis performed in a liquid scintillation counter (Packard Tricarb 3385).

The elemental Te analysis was performed on the nonvolatile sample fractions by ICP. Tellurium is slightly volatile under the dissolution conditions. Therefore, experiments were performed using a ^{125}Te tracer that indicated a relatively consistent retention of approximately 80% in the nonvolatile portion of the sample. No tracer was used for the sample analysis.

There is a total uncertainty associated with the ^{129}I, ^{90}Sr, and Te analyses of 10 to 15%. Uncertainties resulted from the sample dissolution and individual analytical techniques. The uncertainty associated with the dissolution is due to potential material losses on glassware surfaces and the occasional presence of small (<10%) amounts of insoluble material after the dissolution. However, for some samples, the uncertainties are 30 to 50%, due to uncertainties in the sample weight for small (<10 mg) portions and losses during dissolution, as determined by comparing the fissile/fertile and chemical analysis results.

Cesium Release and Settling Tests

Cesium release and settling (turbidity and airborne fission product release) tests were conducted on material from recombined bulk Sample 6. Tests were performed on both as-received and crushed materials. Crushing was intended to simulate the breakup of TMI-2 core material during reactor defueling.

For the leaching tests, the core debris material was mixed with simulated reactor coolant (adjusted to the correct chemistry and pH).

For the cesium release test, the quantity of fission products leached into the coolant was measured as a function of time (0 min, 5 min, 20 min, 1 h, 24 h, up to 3 days). Cesium was the main fission product of interest, although other radionuclides were measurable.

A two-part settling test also was performed which measured (a) turbidity of the sample material/coolant mixture as a function of time and (b) airborne fission product release as a function of time, with a continuous air flow (0.5 linear m/s) over the liquid. Aliquots were removed at the aforementioned times, and the turbidity was measured using a turbidimeter (H. F. Instruments Co., Model DRT-100D). The airborne fission product release test was performed on the liquid portion of the mixture after 40 h of leaching. Radionuclide concentrations present in the airstream were measured using a particulate air sampling system developed by Science Applications, Inc.

APPENDIX B
PHOTOGRAPHS OF SAMPLES AND PARTICLES

APPENDIX B

PHOTOGRAPHS OF SAMPLES AND PARTICLES

As part of the initial unloading and weighing activities, visual examination was undertaken and photographs made of the bulk samples after their removal. Several larger sized ($\geq$1000 μm) particles from each sample were then selected for follow up examination and analysis. This appendix contains photographs of the bulk samples and individual particles taken from all samples. The exceptions are Sample 2 (which was sent to B&W) and Sample 3, in which the large individual particles were not photographed. Photographs of individual particles smaller than 1000 μm are not included in this report due to the lack of acuity in the photos.

TABLE B-1. SAMPLE CROSS REFERENCE INDEX

Sample No.	Description	Figure(s)
1	Bulk material/eleven particles	B-1 thru B-7
3	Bulk material	B-8 thru B-7
4	Bulk material/five particles	B-10 thru B-14
5	Bulk material/eleven particles	B-15 thru B-21
6	Bulk material/eleven particles	B-22 thru B-29
7	Bulk material/one particle size fraction/eleven particles	B-30 thru B-41
8	Bulk material/two particle size fractions/eleven particles	B-42 thru B-54
9	Bulk material/two particle size fractions/eleven particles	B-55 thru B-67
10	Bulk material/one particle size fraction/eleven particles	B-68 thru B-78
11	Bulk material/two particle size fractions/eleven particles	B-79 thru B-93

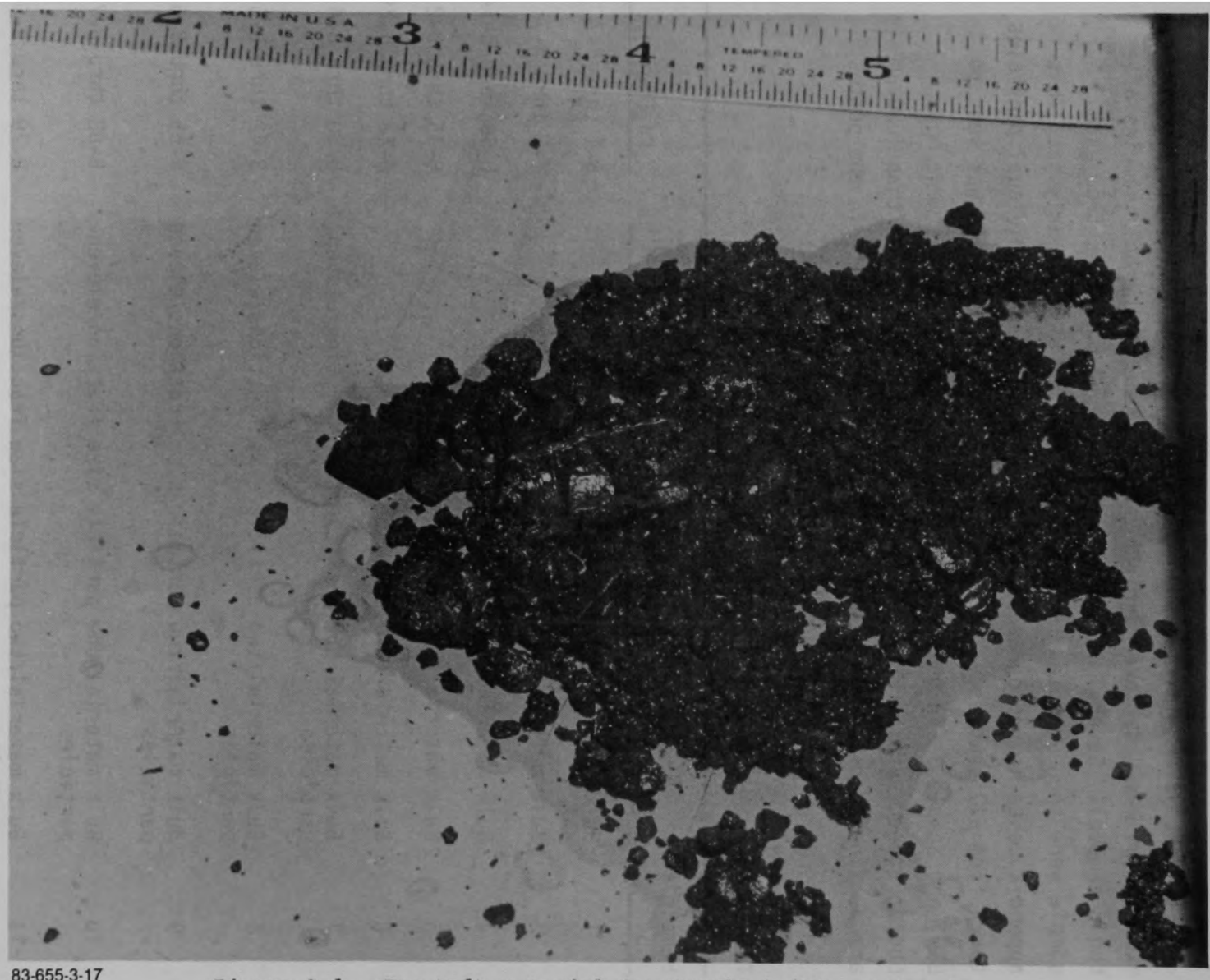

83-655-3-17

Figure B-1. The bulk material for Sample 1 (H8, surface).

84-216-2-22

a) Front view of particle

84-216-2-30

b) Back view of particle

Figure B-2. Particle 1A from Sample 1 (H8, surface), size range: >4000 μm.

84-216-3-4

a) Particle 1B (size range: >4000 μm)

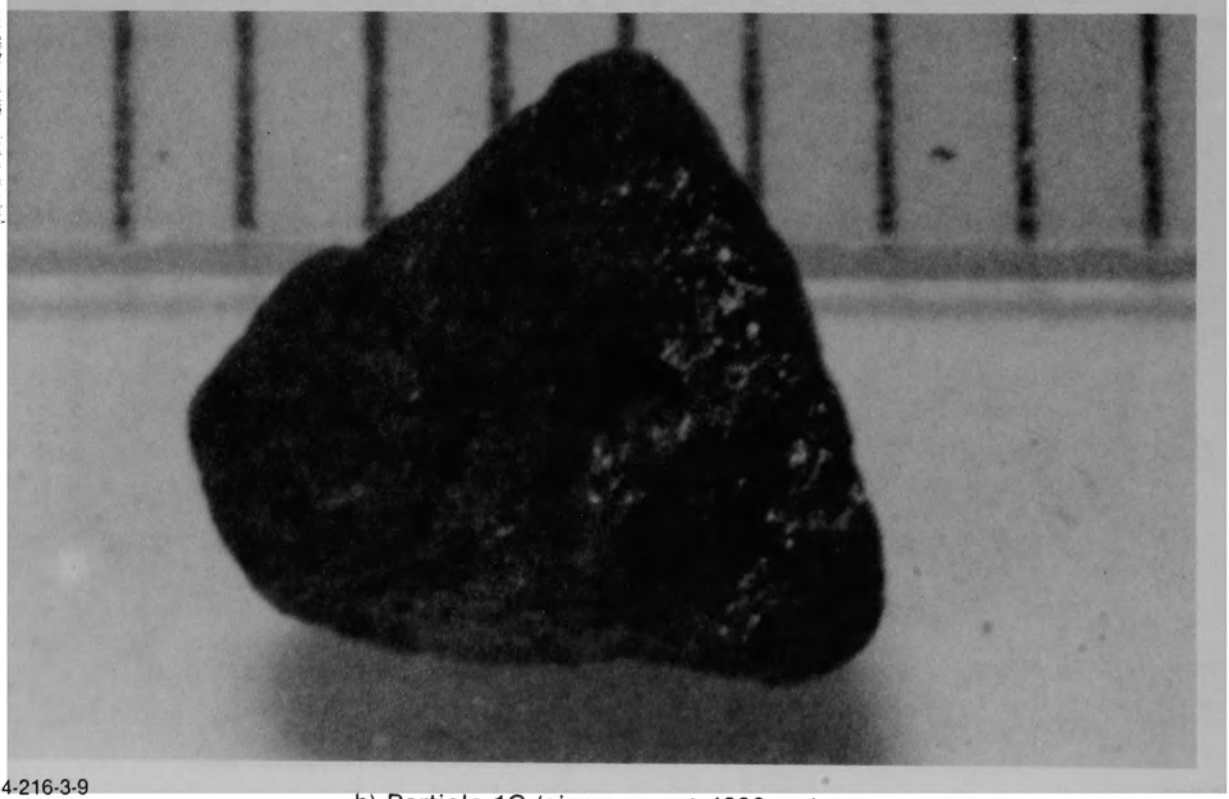

84-216-3-9

b) Particle 1C (size range: >4000 μm)

Figure B-3. Particles from Sample 1 (H8, surface).

83-216-3-12

a) Particle 1D (size range: >4000 μm)

84-216-3-17

b) Particle 1E (size range: >4000 μm)

Figure B-4. Particles from Sample 1 (H8, surface)

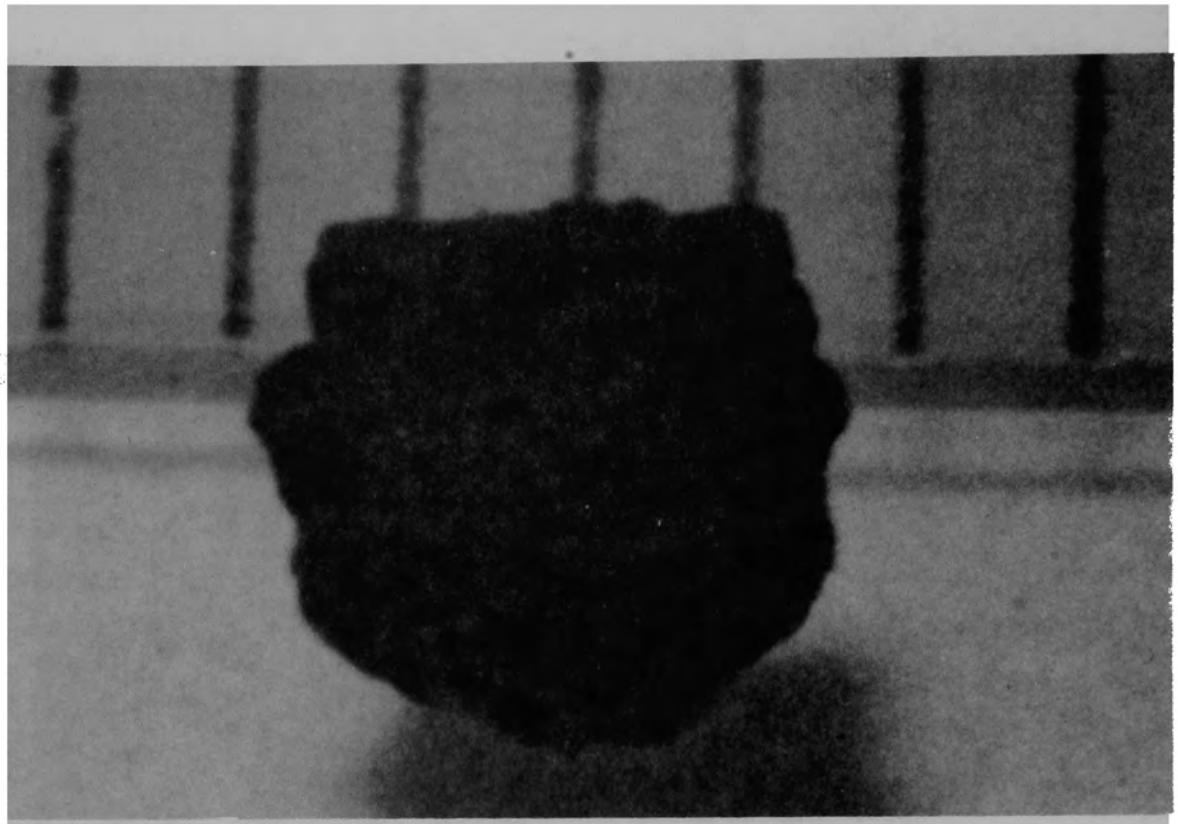

84-216-3-18

a) Particle 1F (size range: 1680-4000 μm)

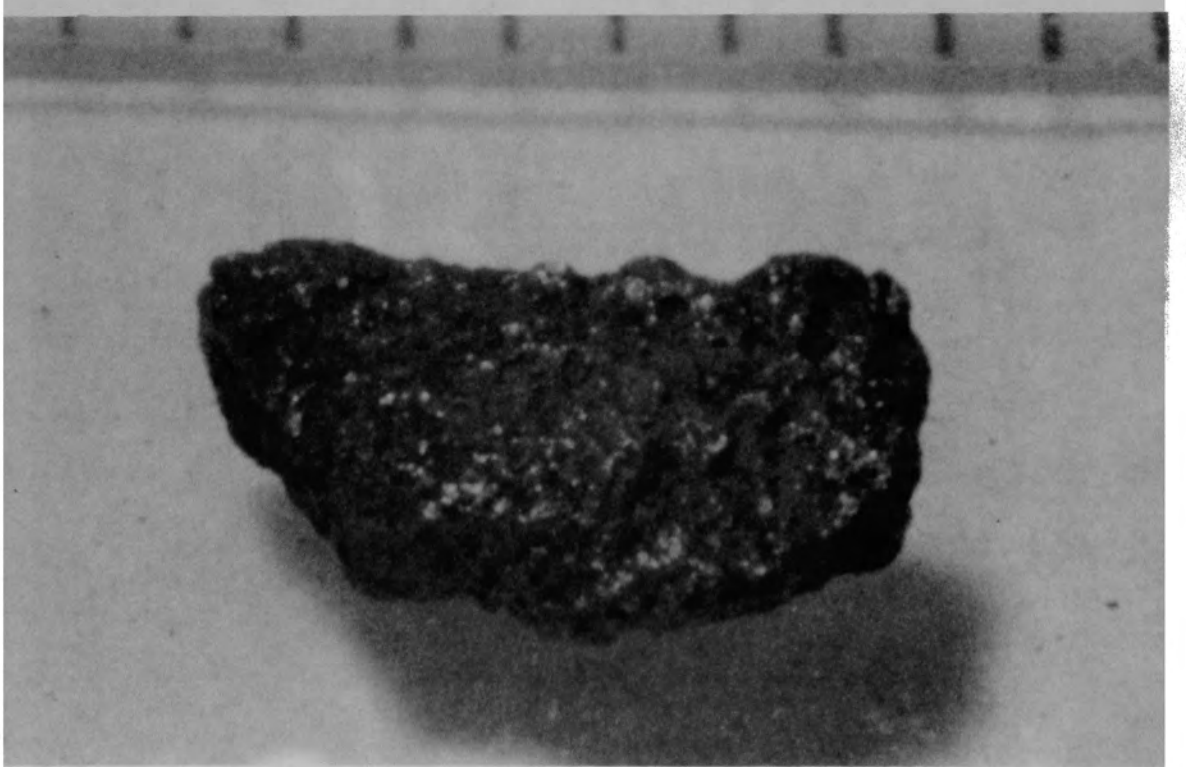

84-216-3-21

b) Particle 1G (size range: 1680-4000 μm)

Figure B-5. Particles from Sample 1 (H8, surface).

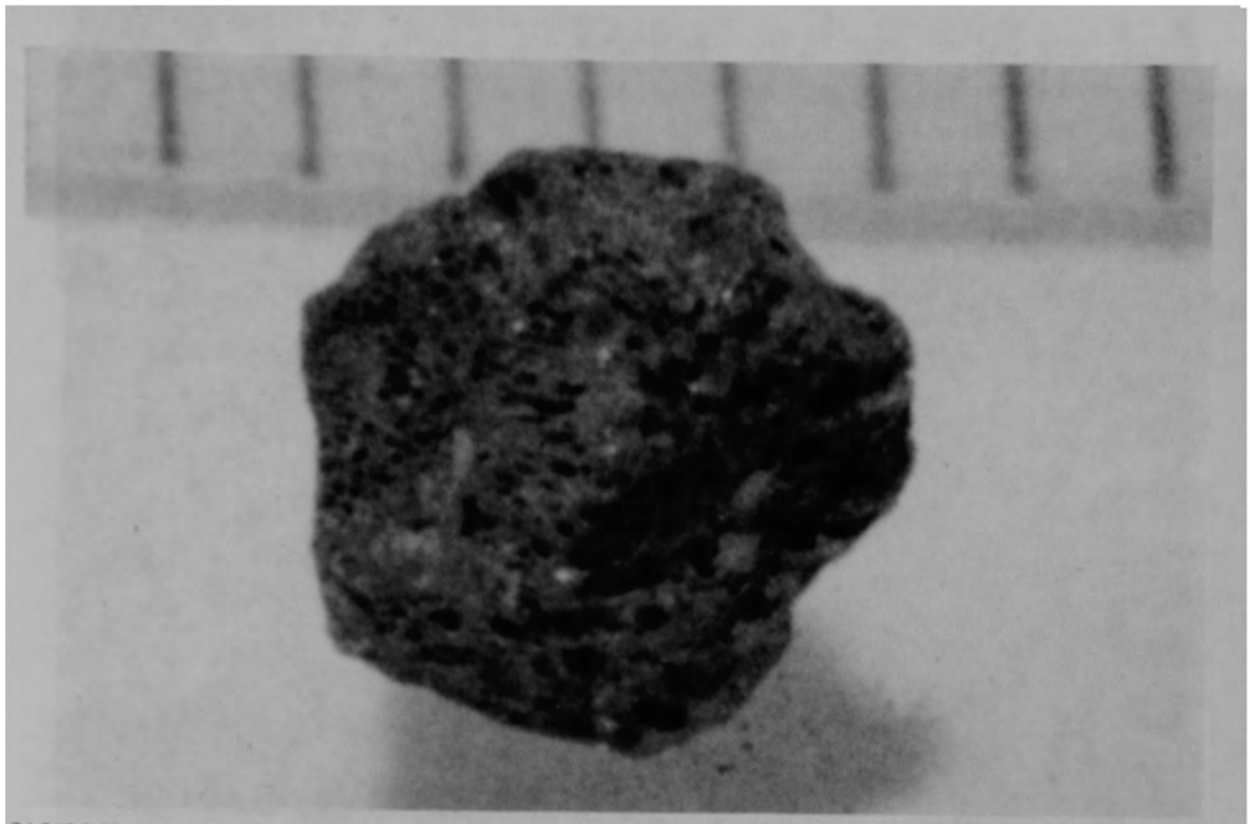

84-216-3-23

a) Particle 1H (size range: 1680-4000 μm)

84-216-3-24

b) Particle 1I (size range: 1000-1680 μm)

Figure B-6. Particles from Sample 1 (H8, surface).

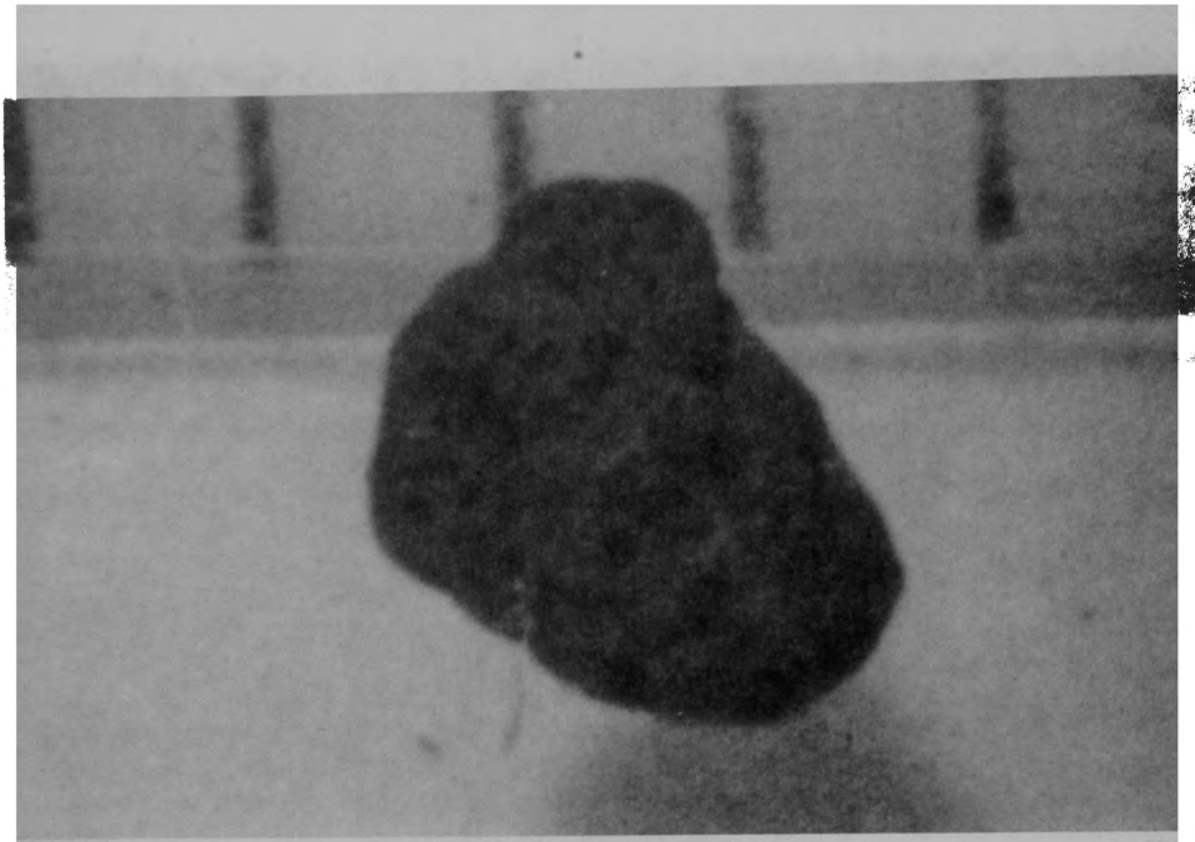

84-216-3-27

a) Particle 1J (size range: 1000-1680 μm)

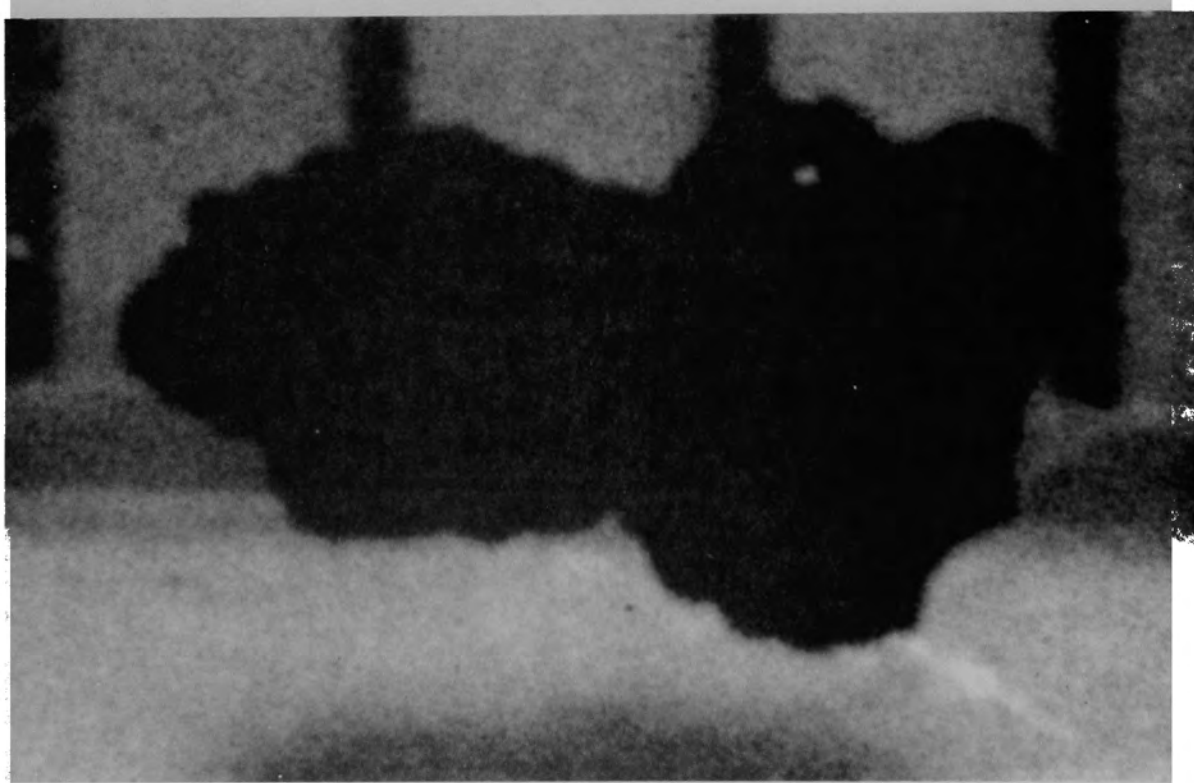

84-216-3-28

b) Particle 1K (size range: 1000-1680 μm)

Figure B-7. Particles from Sample 1 (H8, surface).

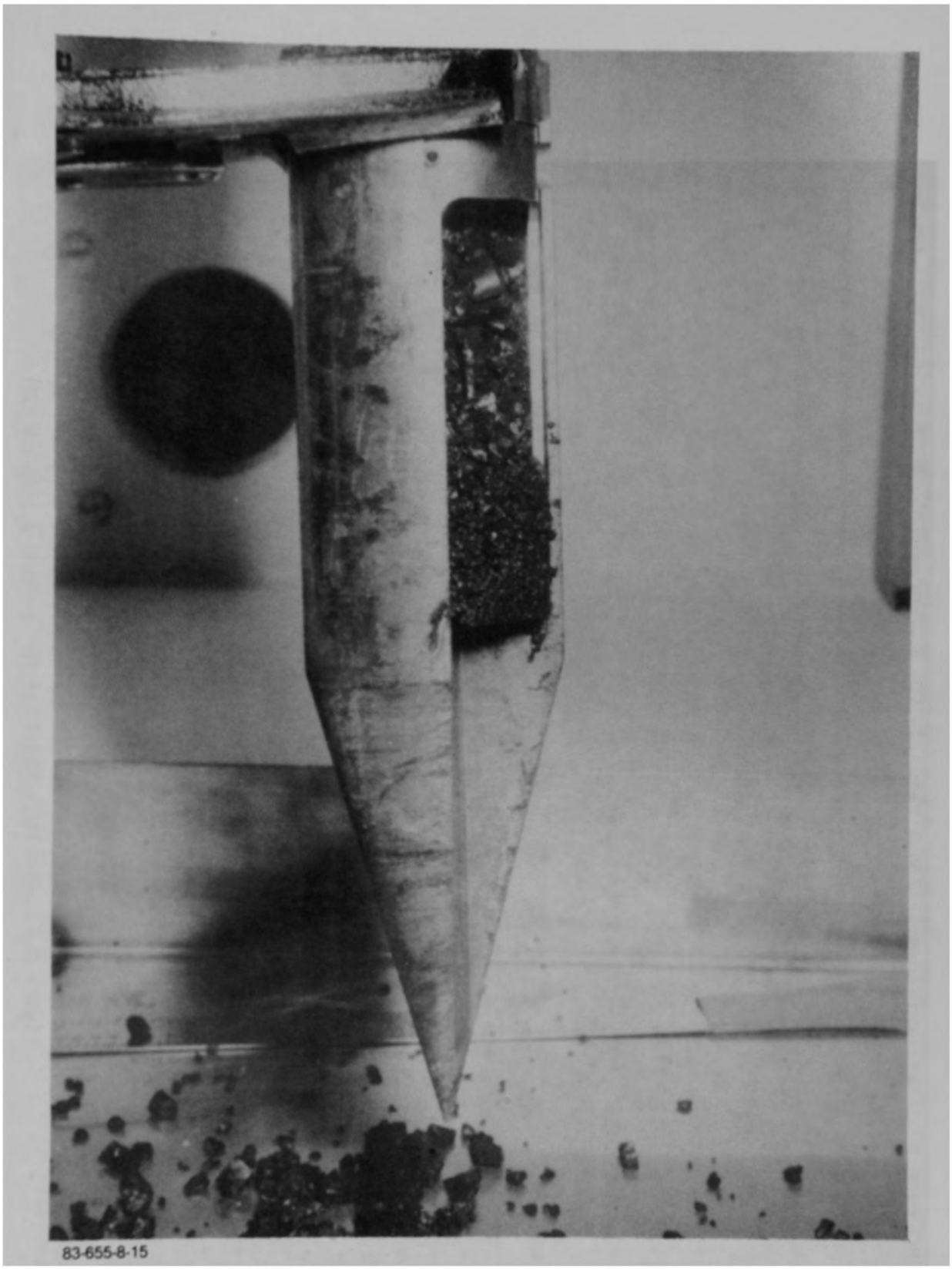

Figure B-8. Stratified material in sampling tool for Sample 3 (H8, 56 cm).

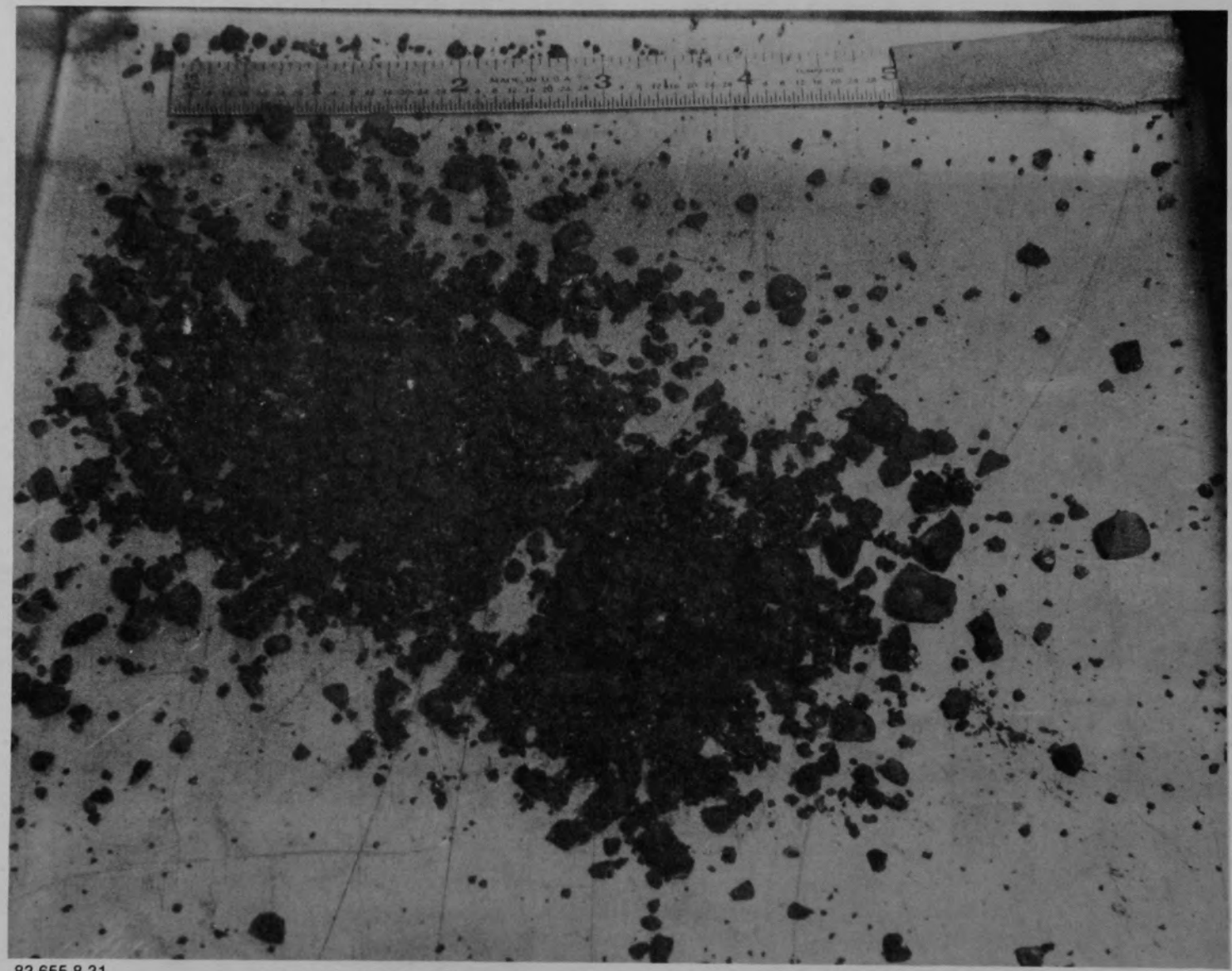

83-655-8-31

Figure B-9. The bulk material for Sample 3 (H8, 56 cm).

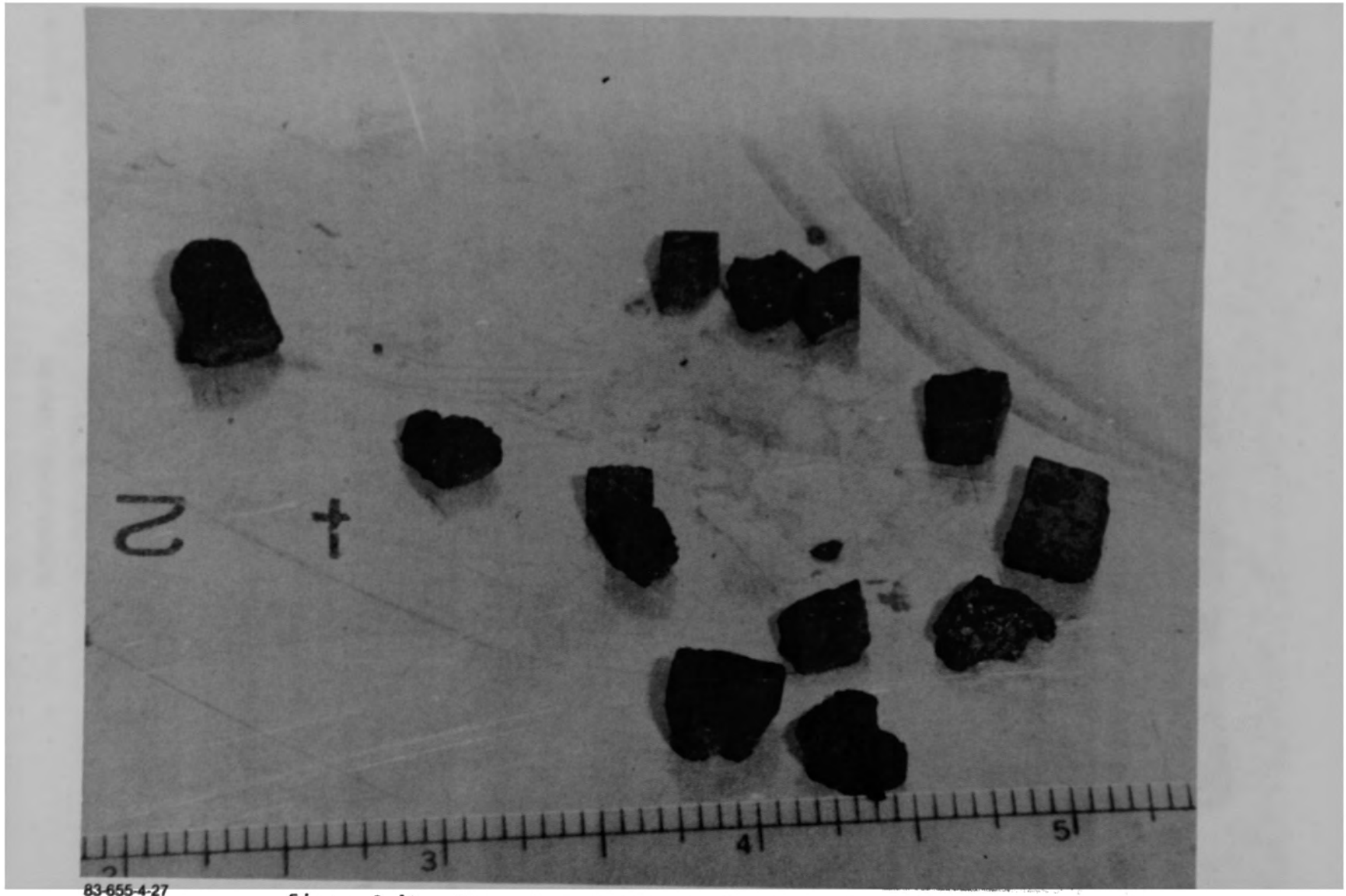

83-655-4-27

Figure B-10. The bulk material for Sample 4 (E9, surface).

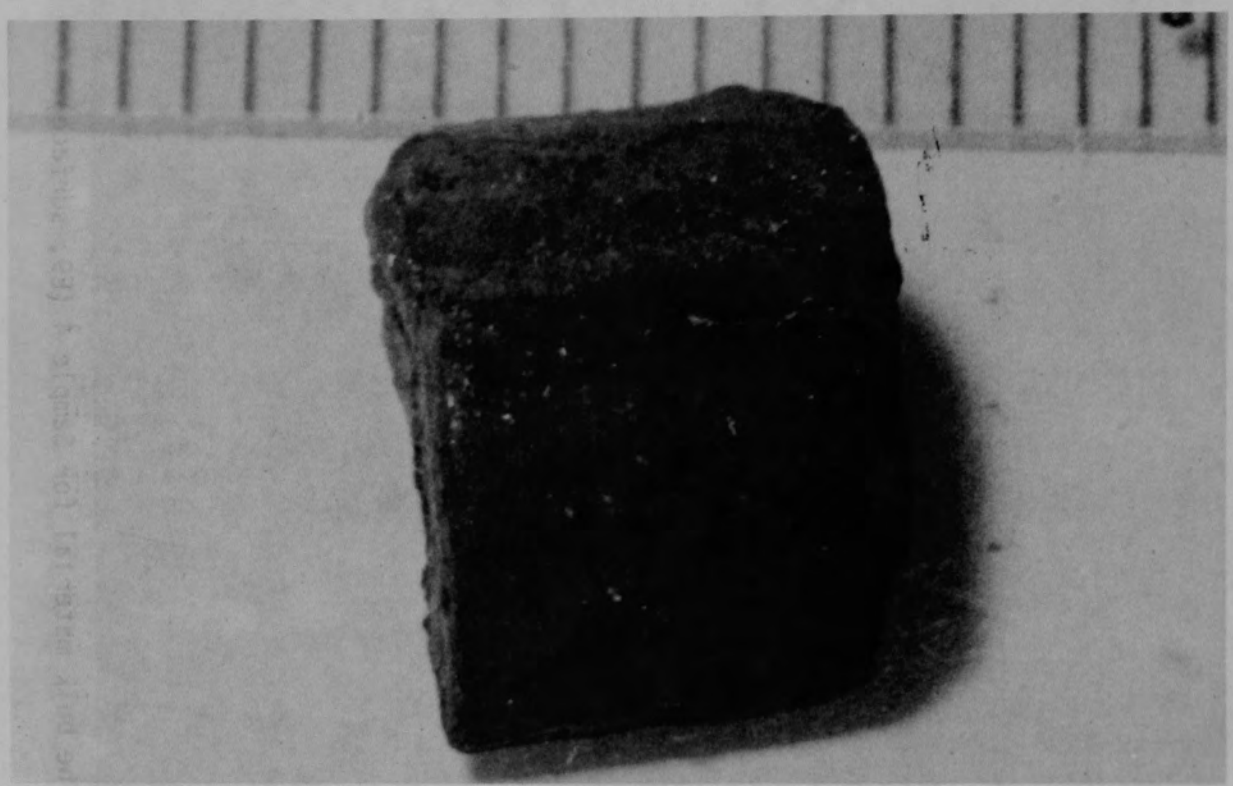

84-157-2-28

Figure B-11. Particle 4A from Sample 4 (E9, surface), size range: >4000 μm.

84-157-2-11

a) Front view of particle

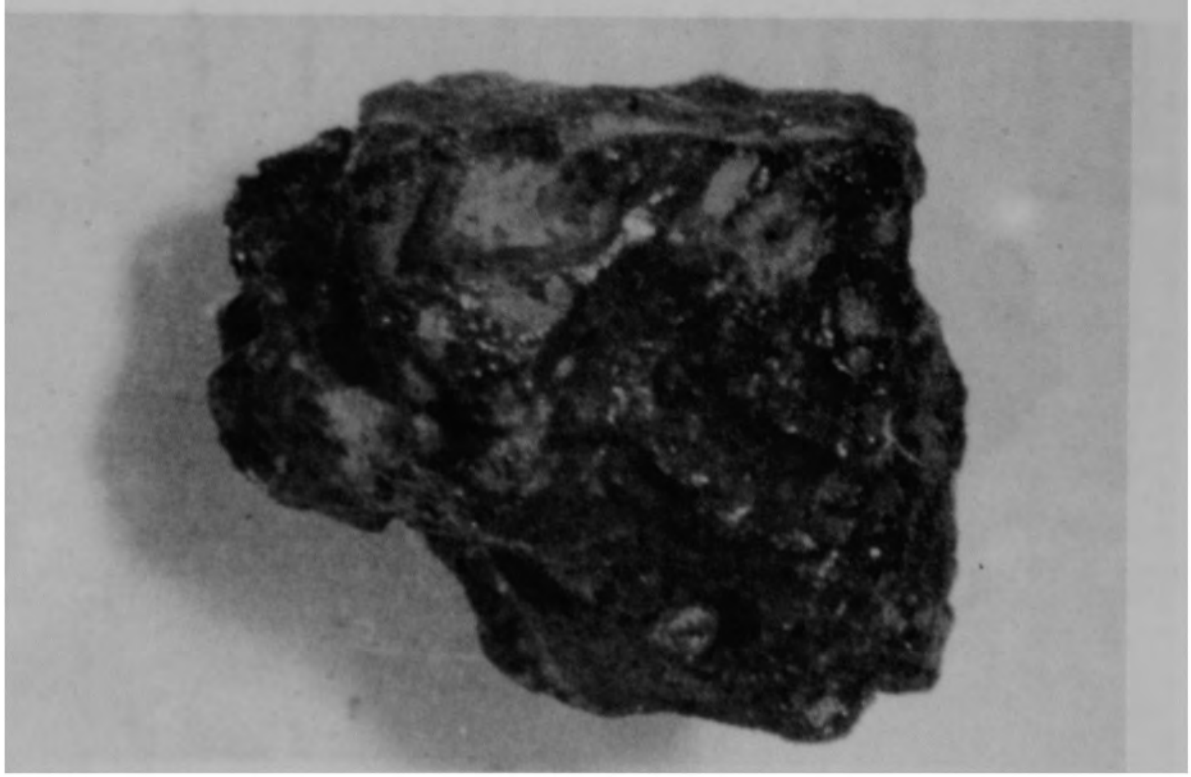

84-157-2-16

b) Back view of particle

Figure B-12. Particle 4B from Sample 4 (E9, surface), size range: >4000 µm.

84-157-2-22

a) Particle 4C (size range: >4000 μm)

84-157-2-32

b) Particle 4D (size range: >4000 μm)

Figure B-13. Particles from Sample 4 (E9, surface).

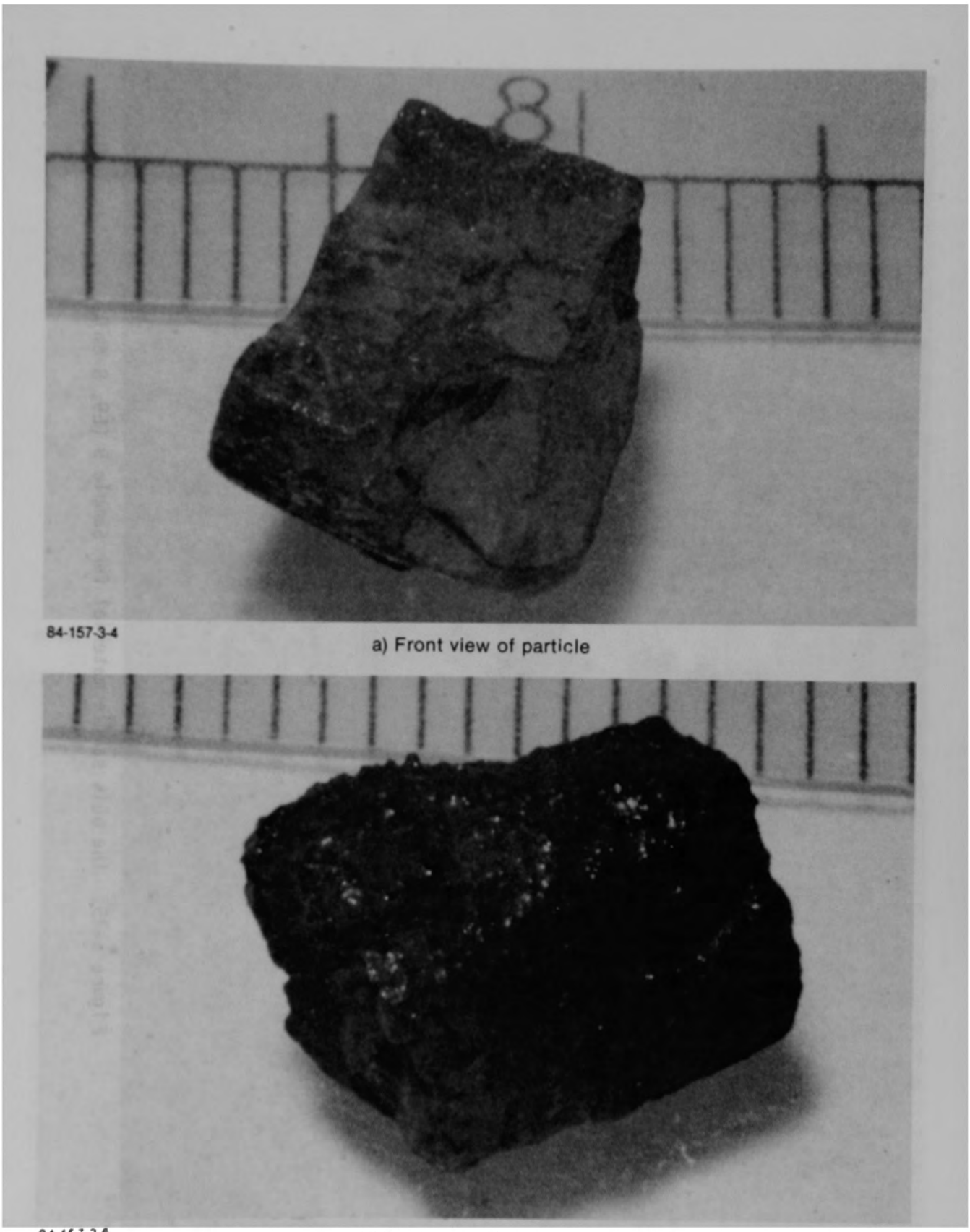

84-157-3-4

a) Front view of particle

84-157-3-6

b) Back view of particle

Figure B-14. Particle 4E from Sample 4 (E9, surface), size range: >4000 μm.

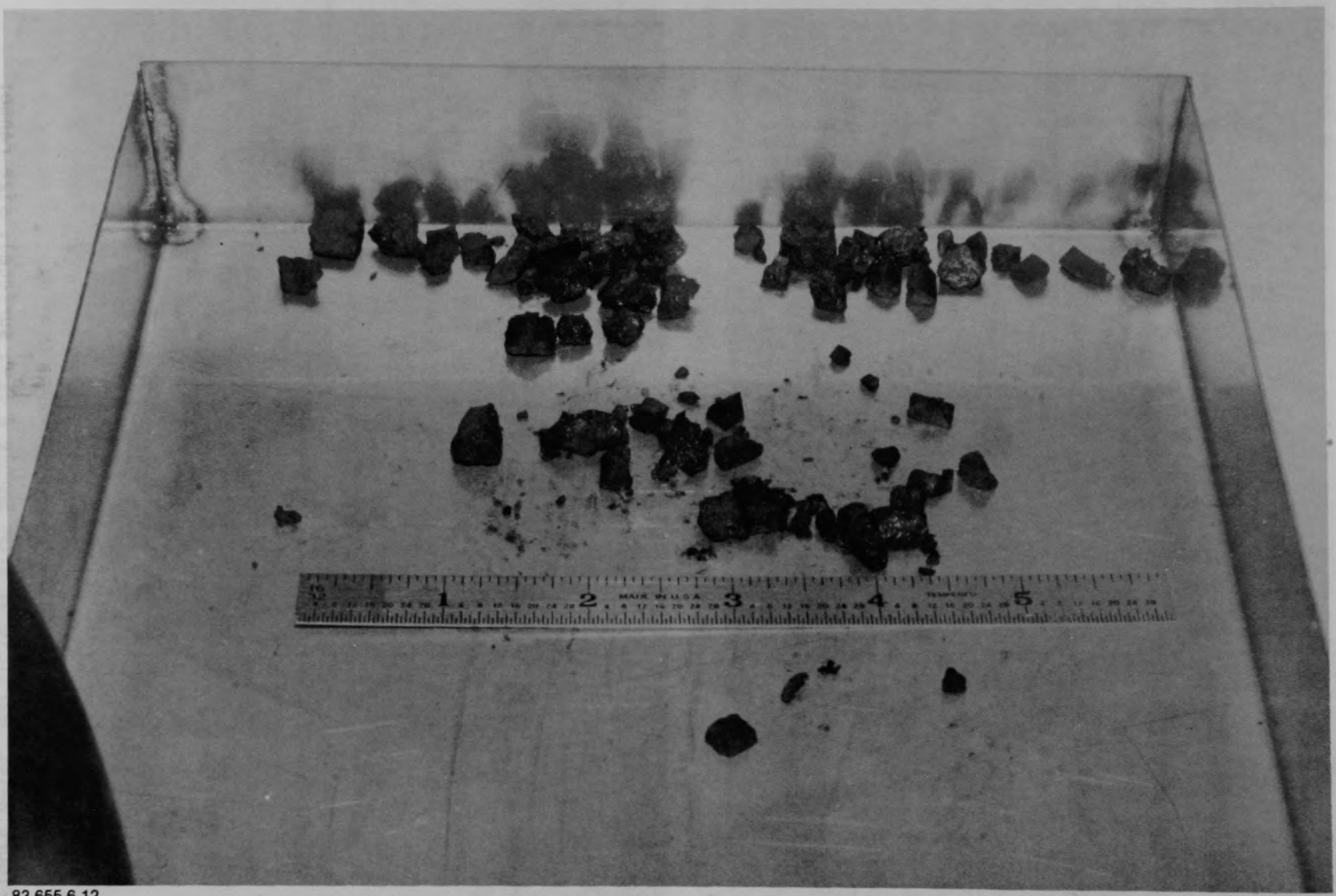

83-655-6-12

Figure B-15. The bulk sample material for Sample 5 (E9, 8 cm).

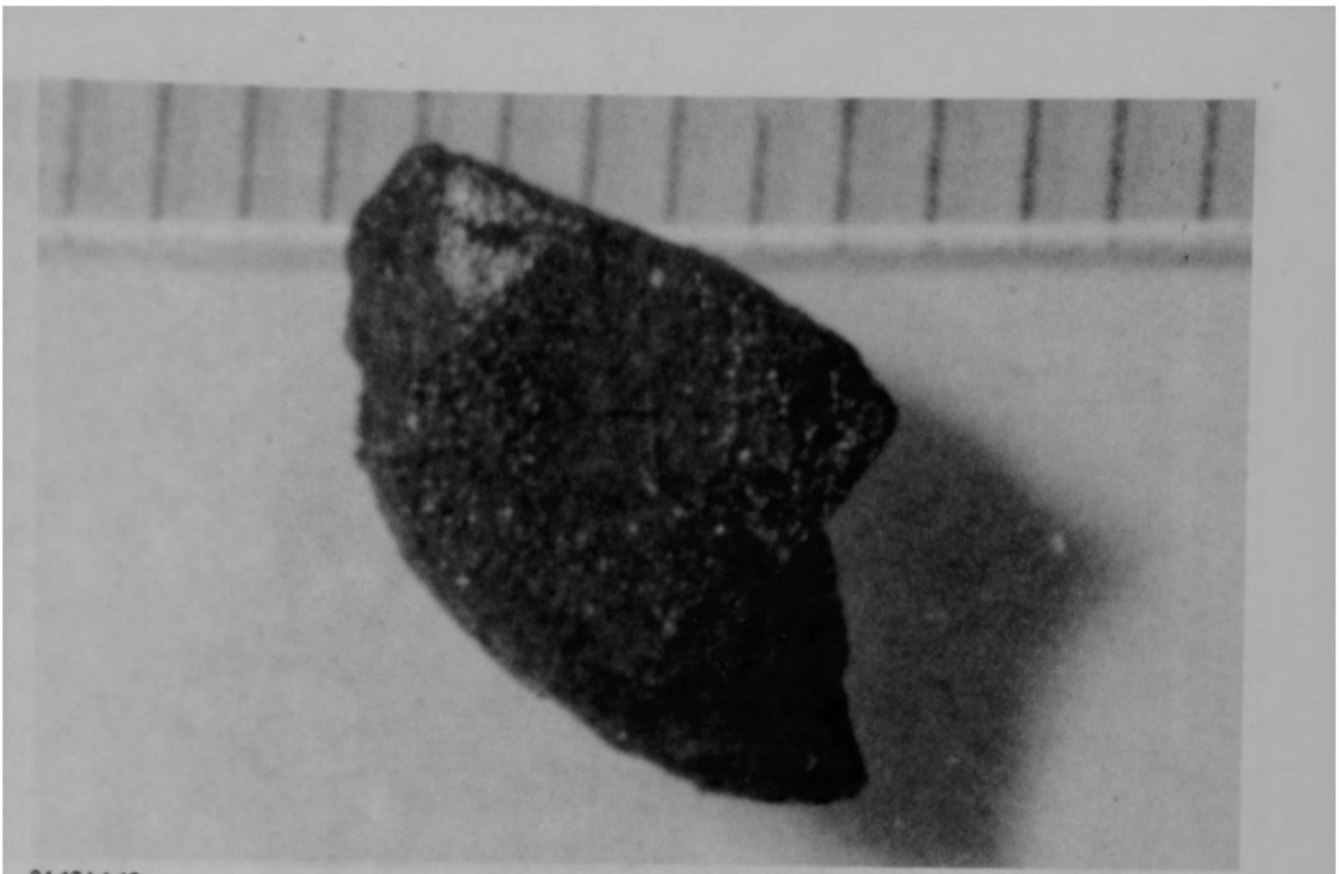

84-194-1-19

a) Front view of particle

84-194-1-27

b) Back view of particle

Figure B-16. Particle 5A from Sample 5 (E9, 8 cm), size range: >4000 μm.

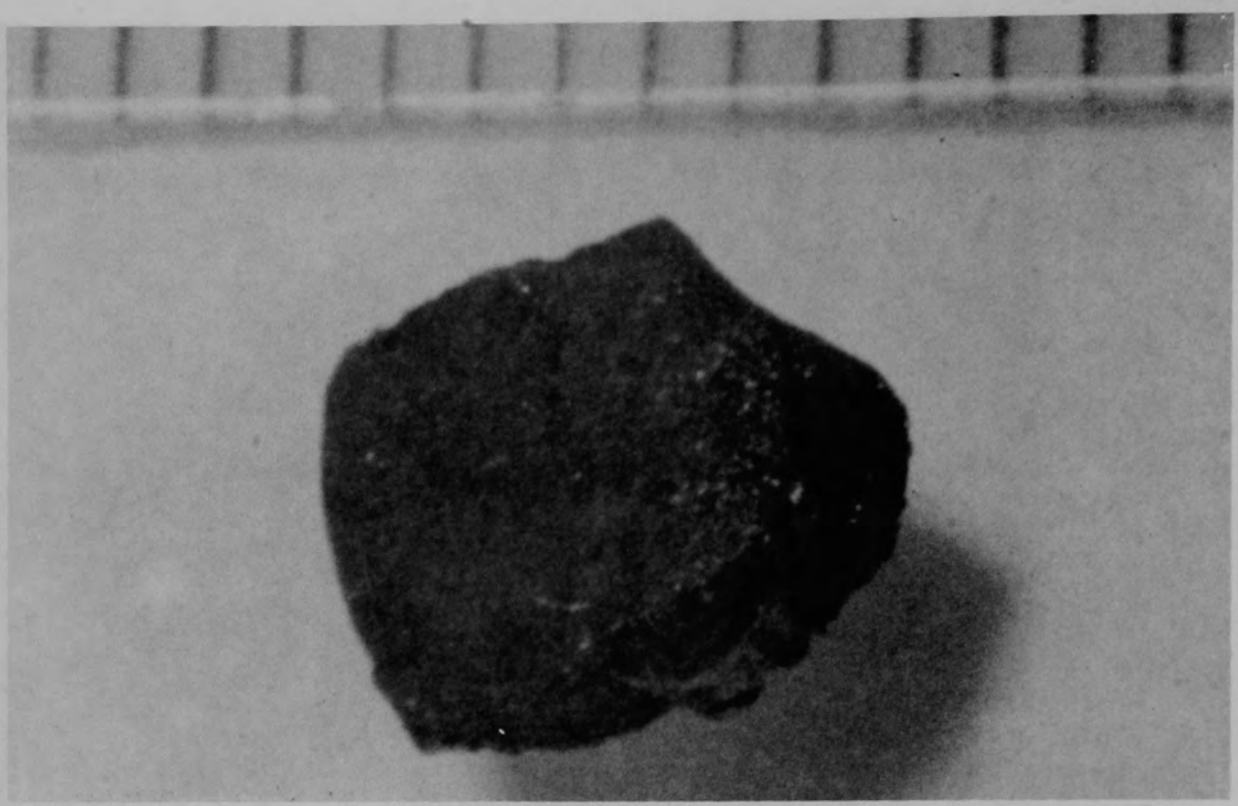

84-194-1-30

a) Particle 5B (size range: >4000 μm)

84-194-2-8

b) Particle 5C (size range: >4000 μm)

Figure B-17. Particles from Sample 5 (E9, 8 cm).

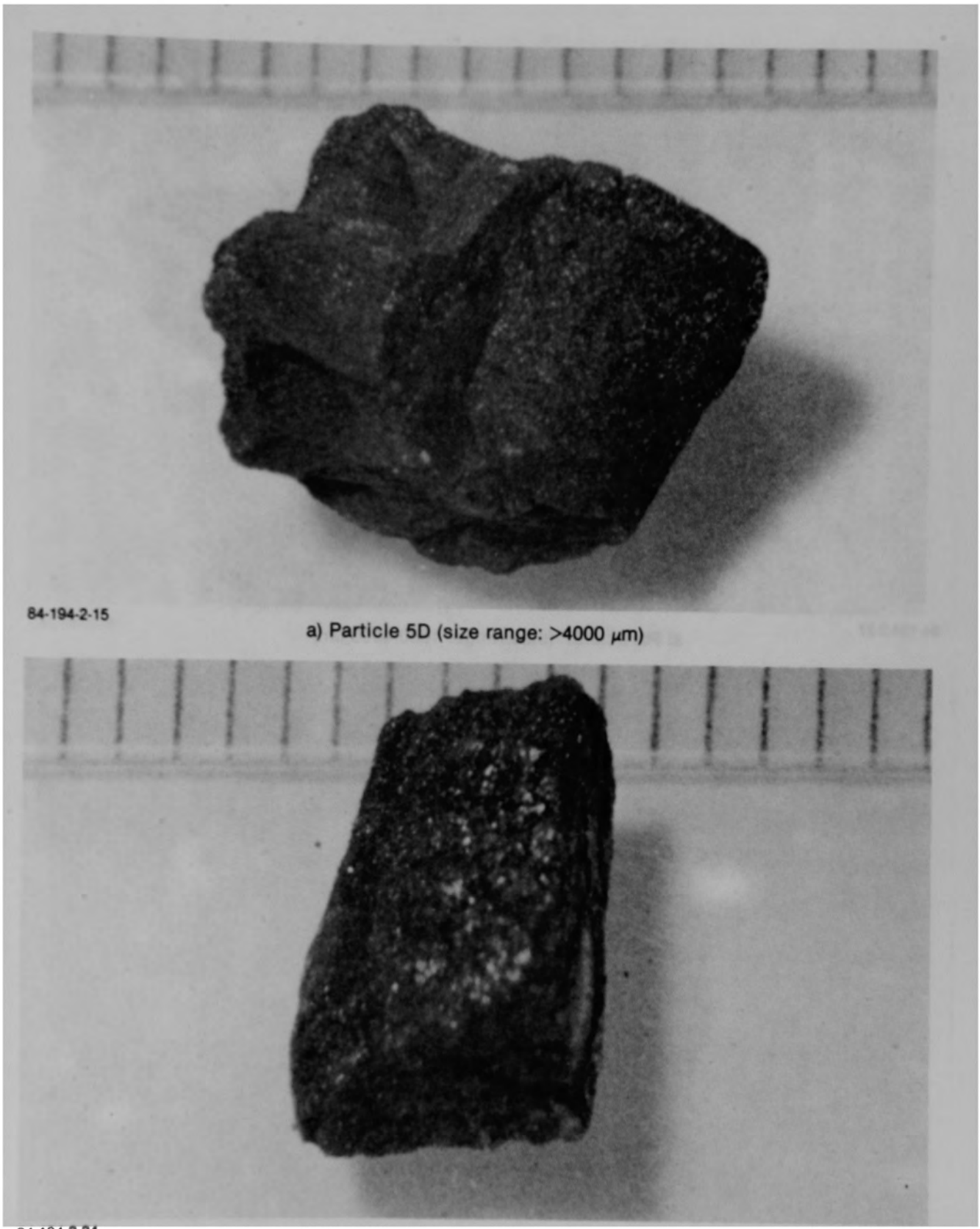

84-194-2-15

a) Particle 5D (size range: >4000 μm)

84-194-2-24

b) Particle 5E (size range: >4000 μm)

Figure B-18. Particles from Sample 5 (E9, 8 cm).

84-194-2-27

a) Particle 5F (size range: 1680-4000 μm)

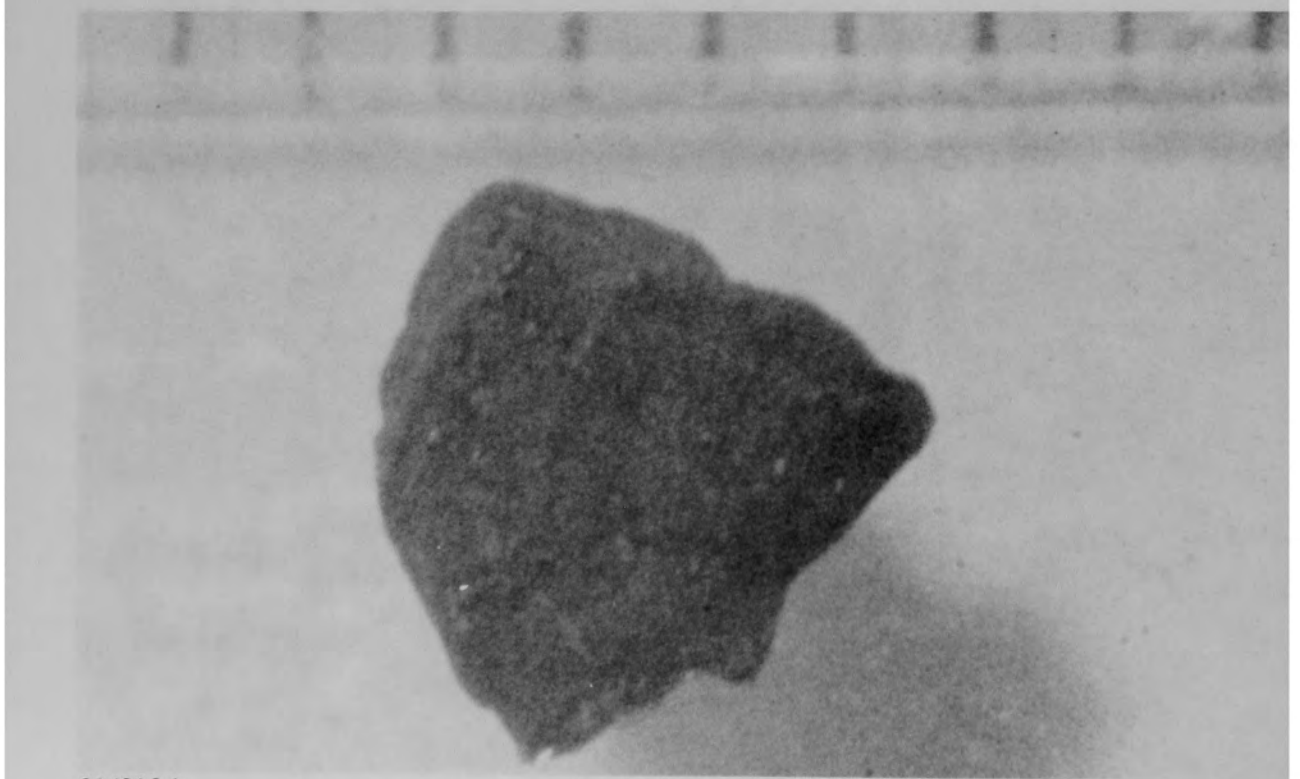

84-194-3-4

b) Particle 5G (size range: 1680-4000 μm)

Figure B-19. Particles from Sample 5 (E9, 8 cm).

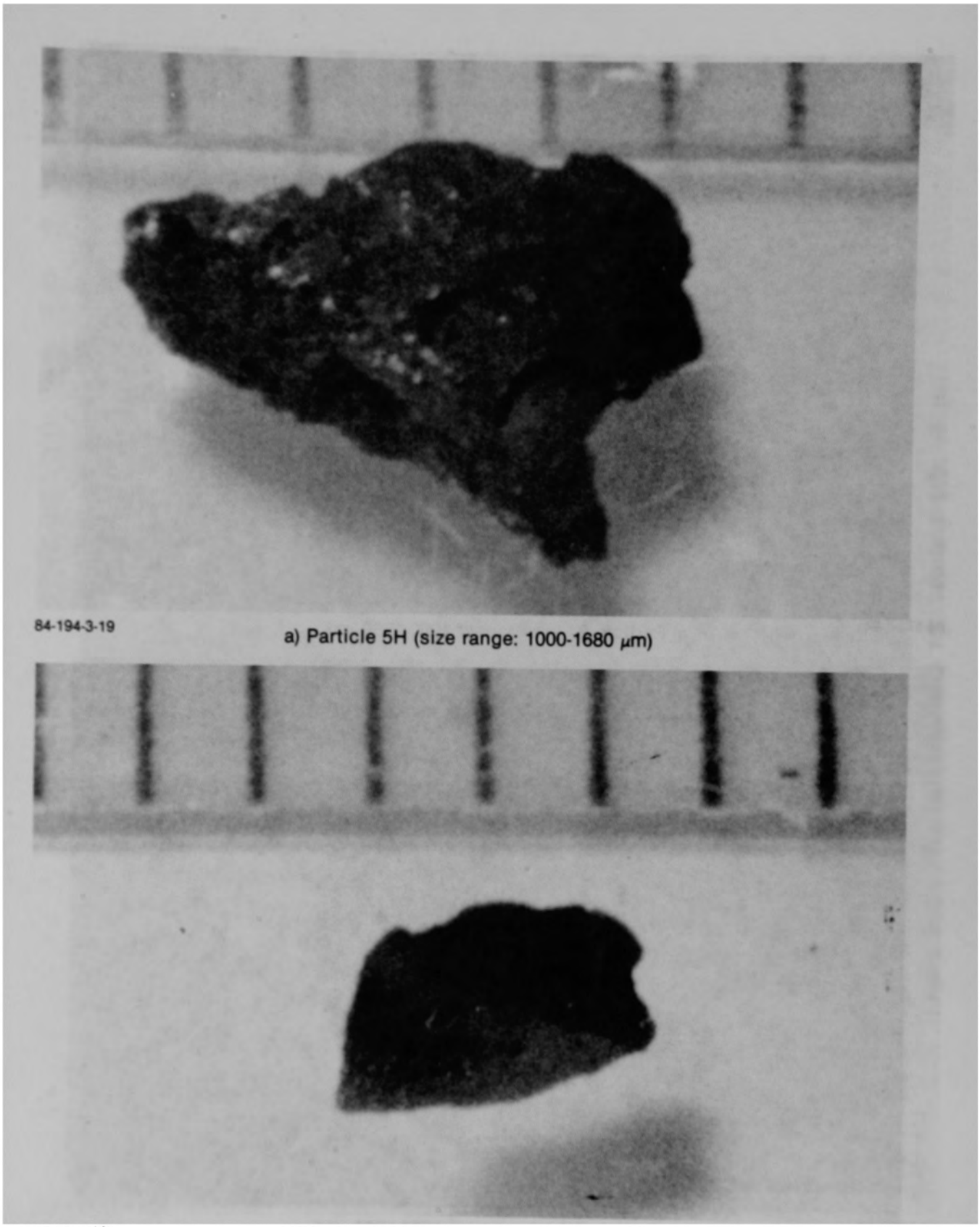

84-194-3-19

a) Particle 5H (size range: 1000-1680 μm)

84-172-1-22

b) Particle 5I (size range: 1000-1680 μm)

Figure B-20. Particles from Sample 5 (E9, 8 cm).

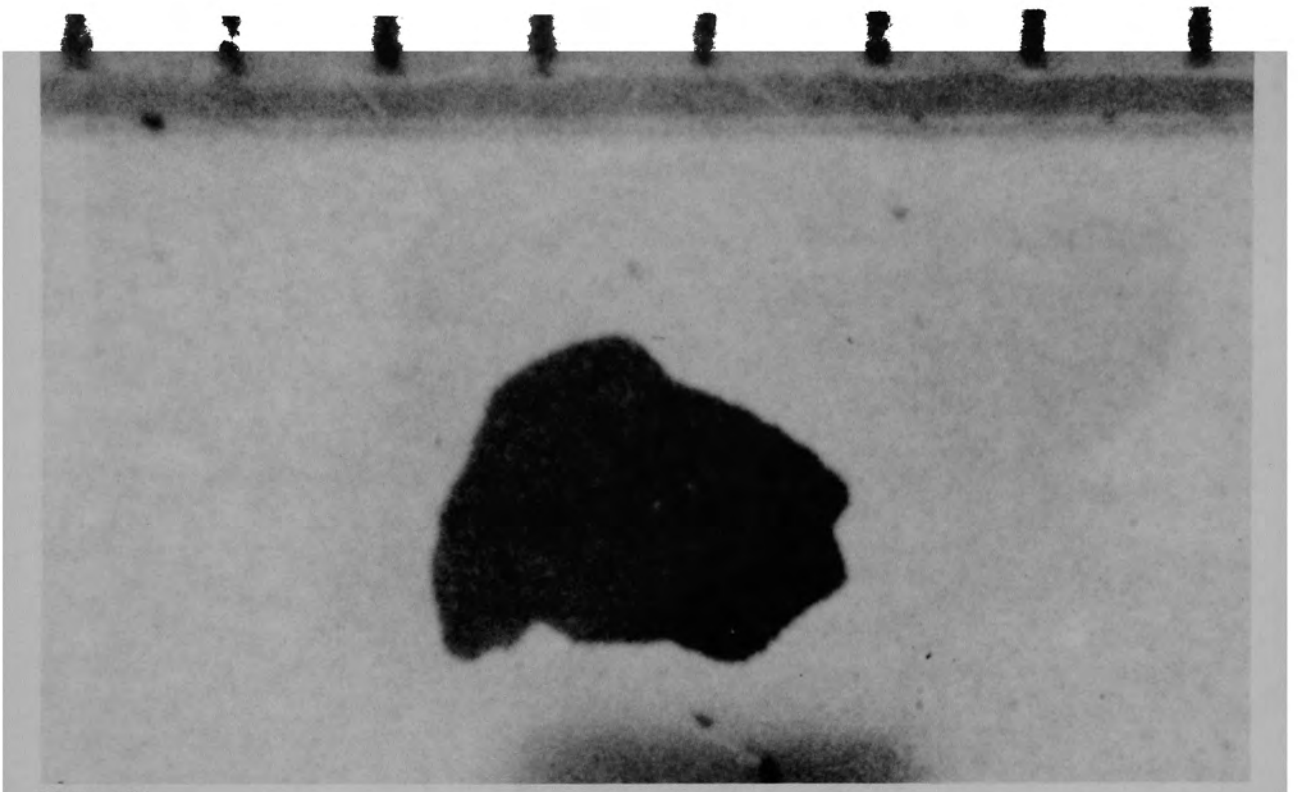

84-172-1-24

a) Particle 5J (size range: 1000-1680 μm)

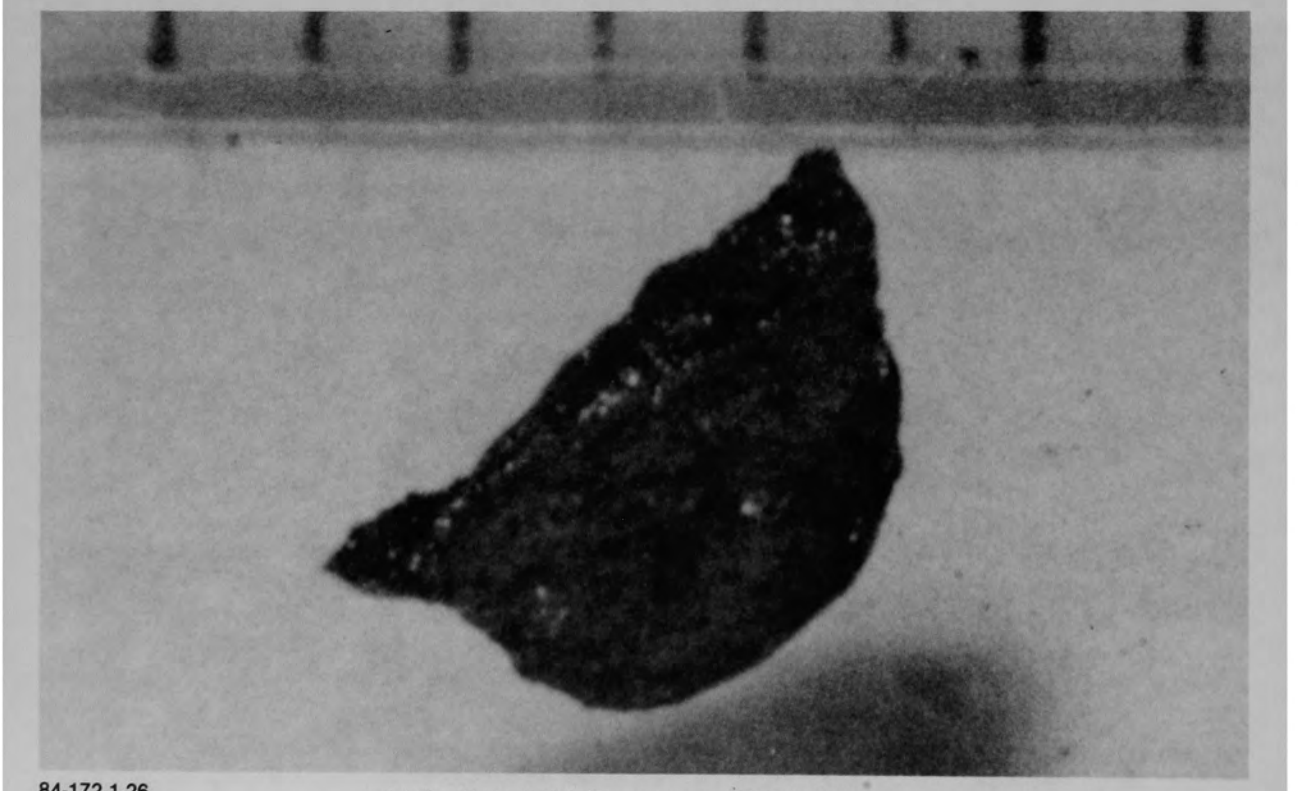

84-172-1-26

b) Particle 5K (size range: 1000-1680 μm)

Figure B-21. Particles from Sample 5 (E9, 8 cm).

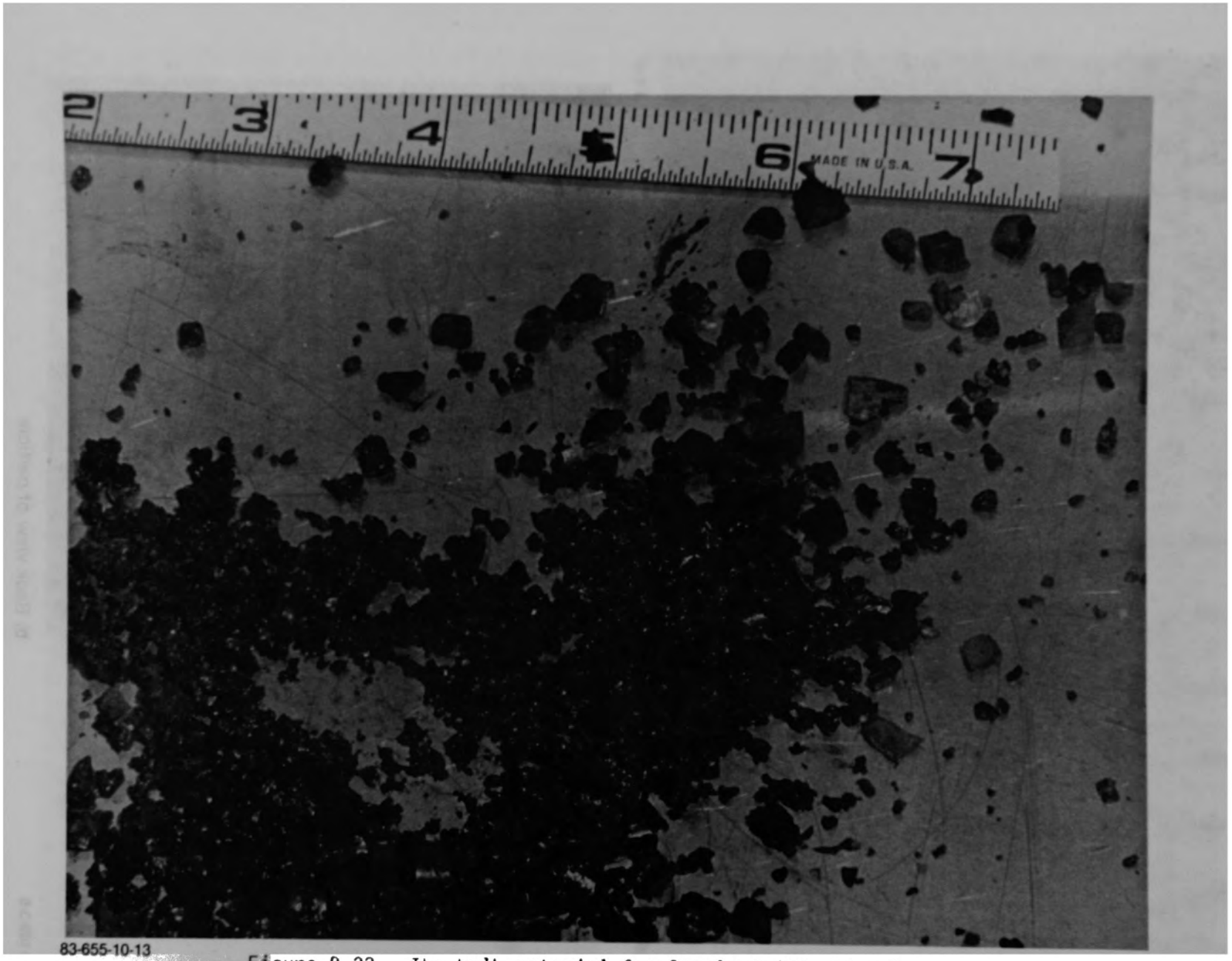

83-655-10-13

Figure B-22. The bulk material for Sample 6 (E9, 56 cm).

84-199-3-4

a) Front view of particle

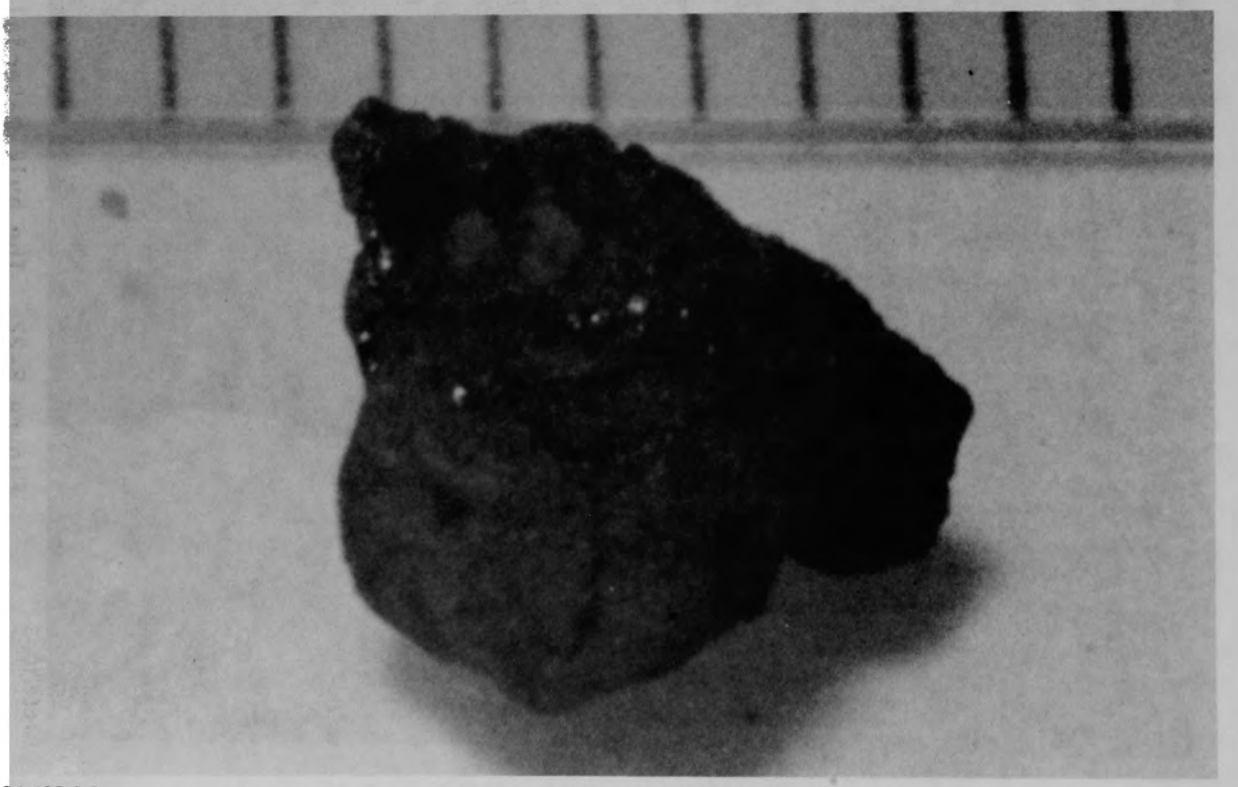

84-199-3-6

b) Back view of particle

Figure B-23. Particle 6A from Sample 6 (E9, 56 cm), size range: >4000 μm.

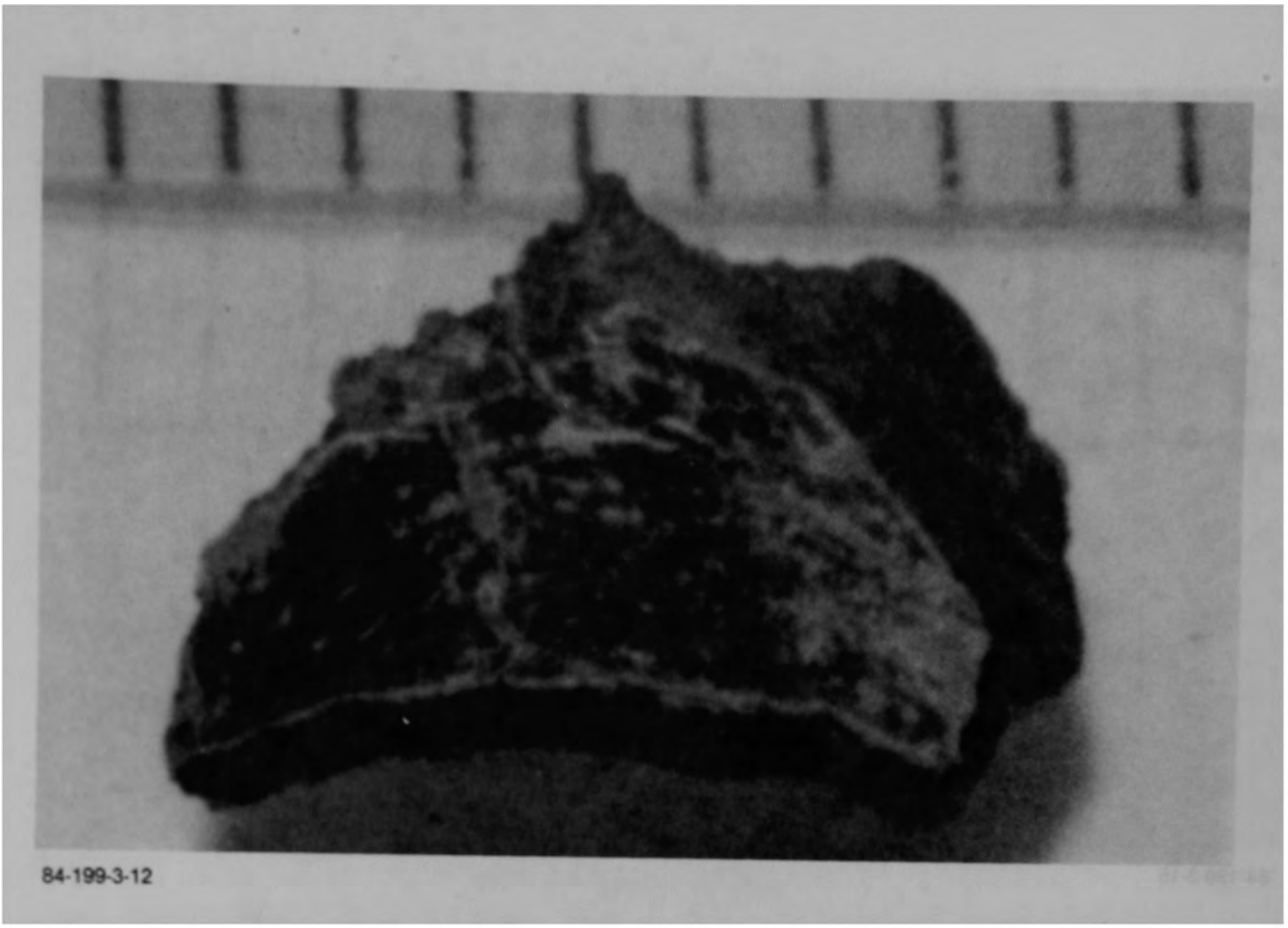

Figure B-24. Particle 6B from Sample 6 (E9, 56 cm), size range: >4000 μm.

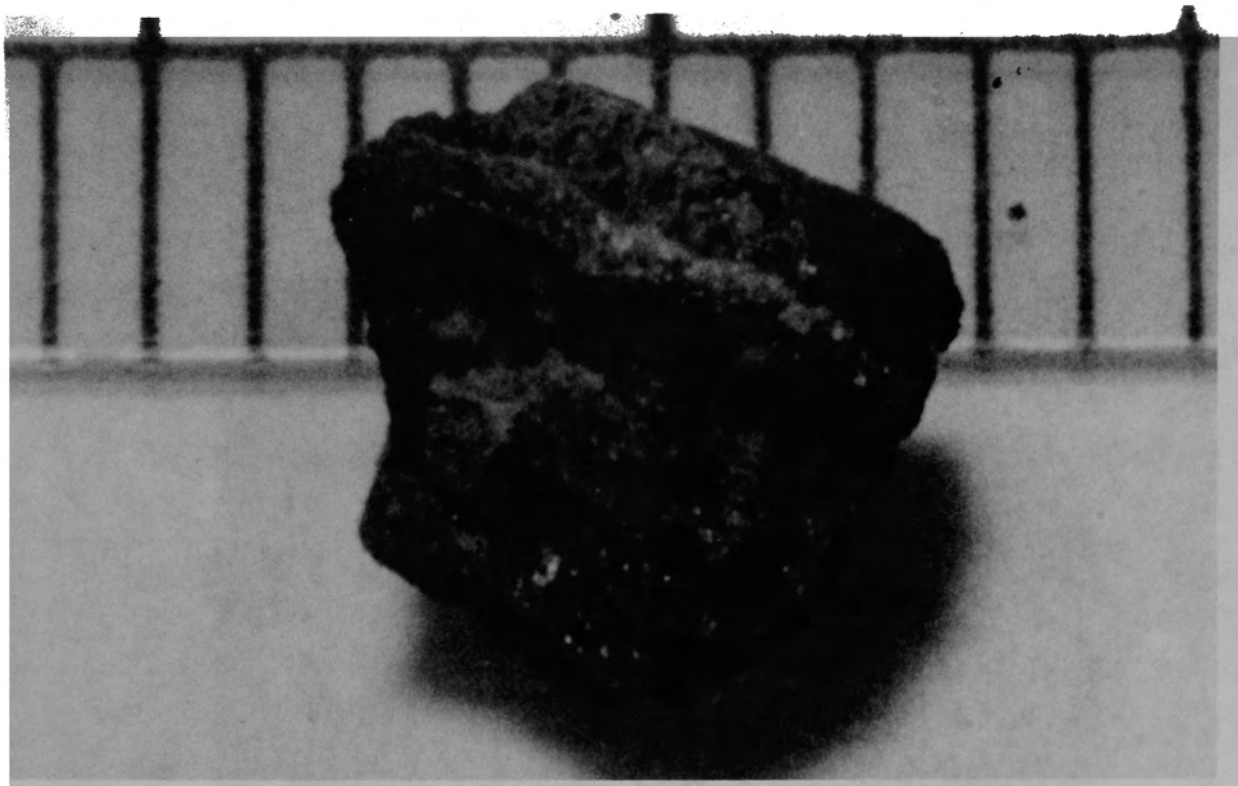

84-199-3-15

Figure B-25. Particle 6C from Sample 6 (E9, 56 cm), size range: >4000μm.

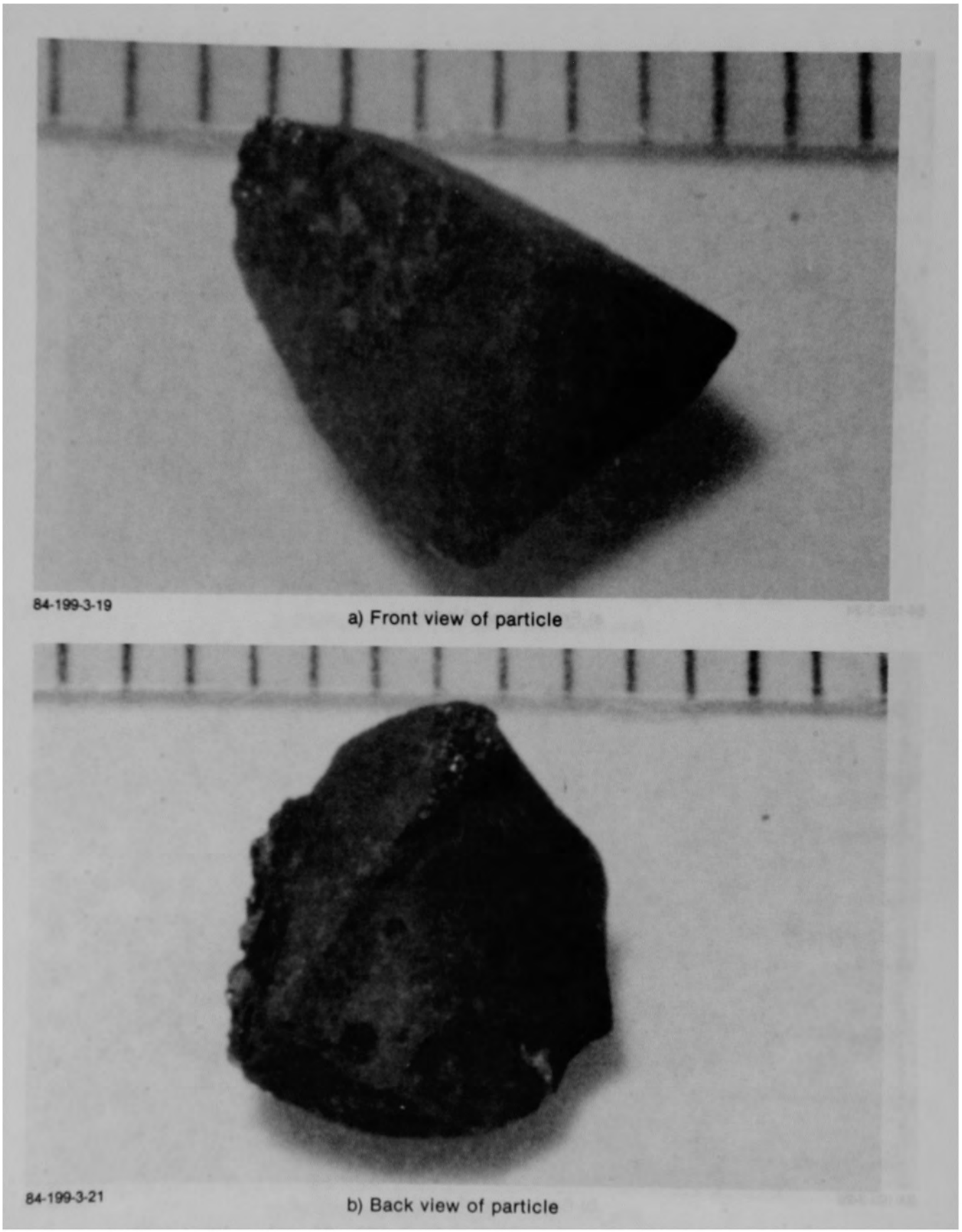

Figure B-26. Particle 6D from Sample 6 (E9, 56 cm), size range: >4000 μm.

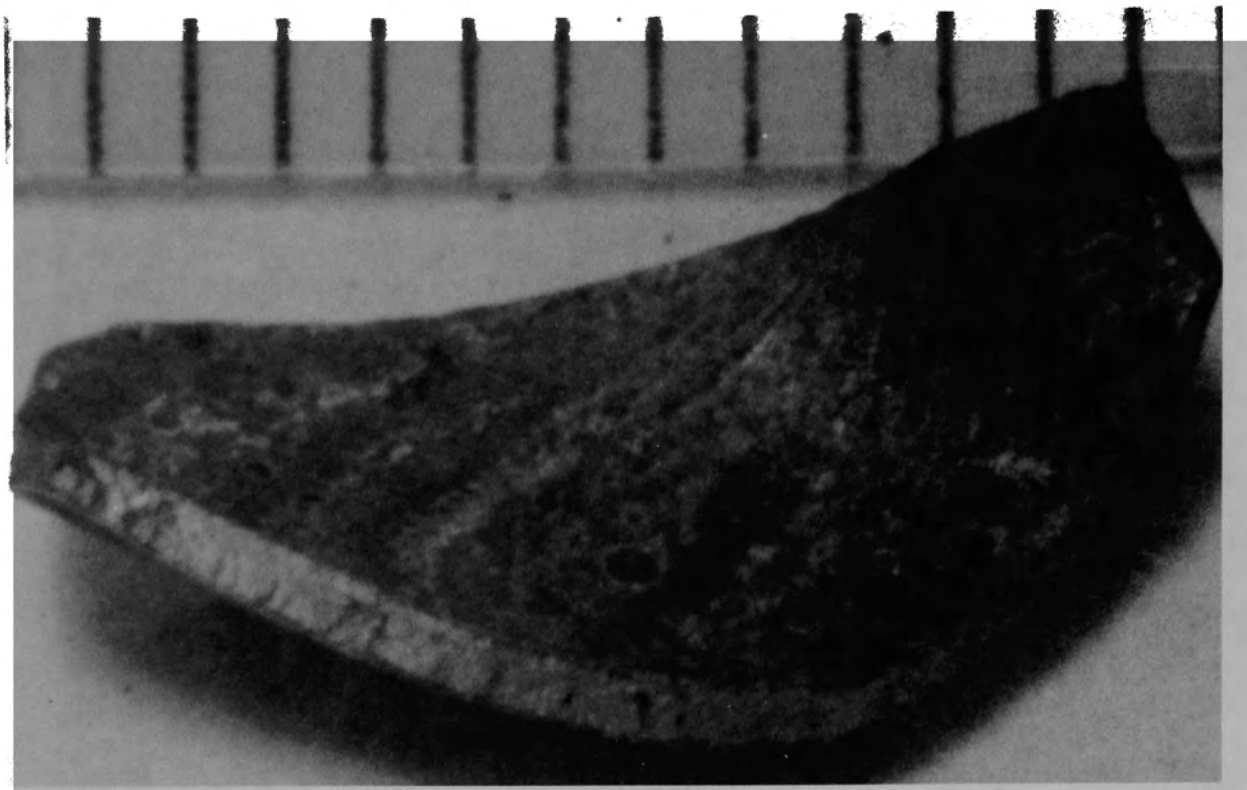

84-199-3-24

a) Front view of particle

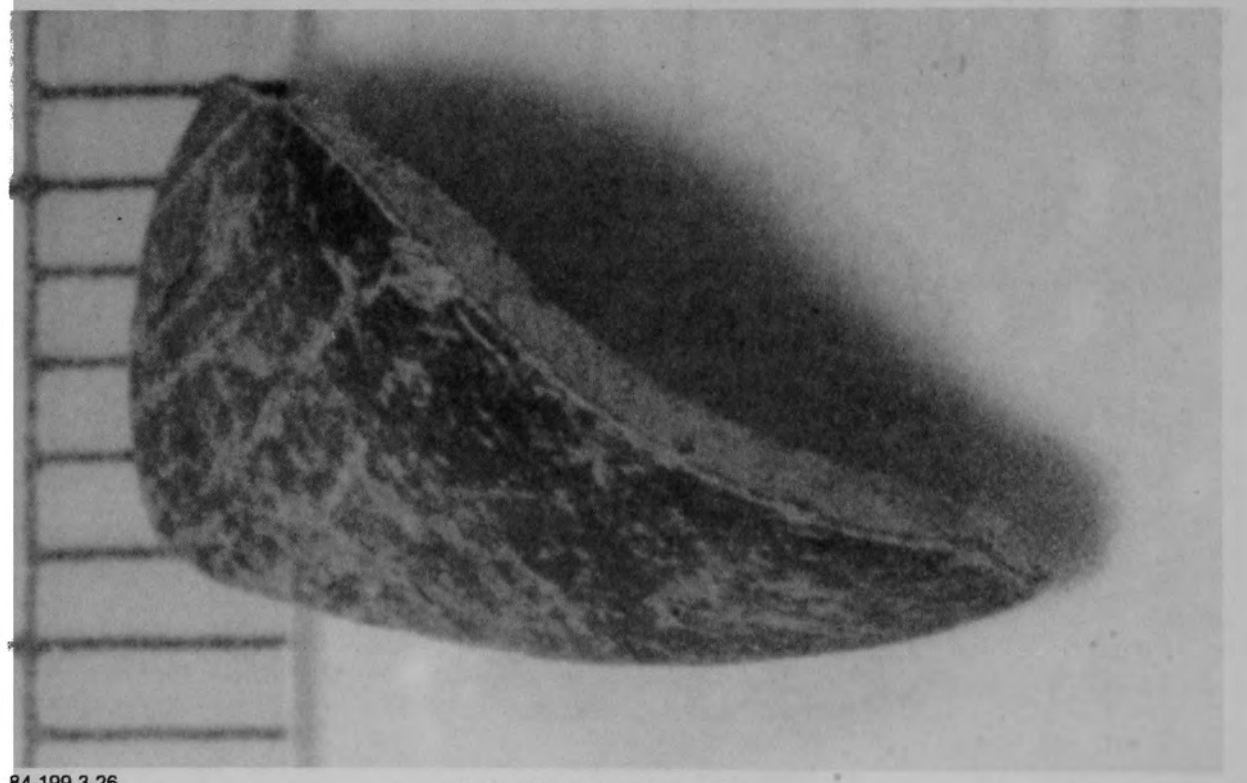

84-199-3-26

b) Back view of particle

Figure B-27. Particle 6E from Sample 6 (E9, 56 cm), size range: >4000 μm).

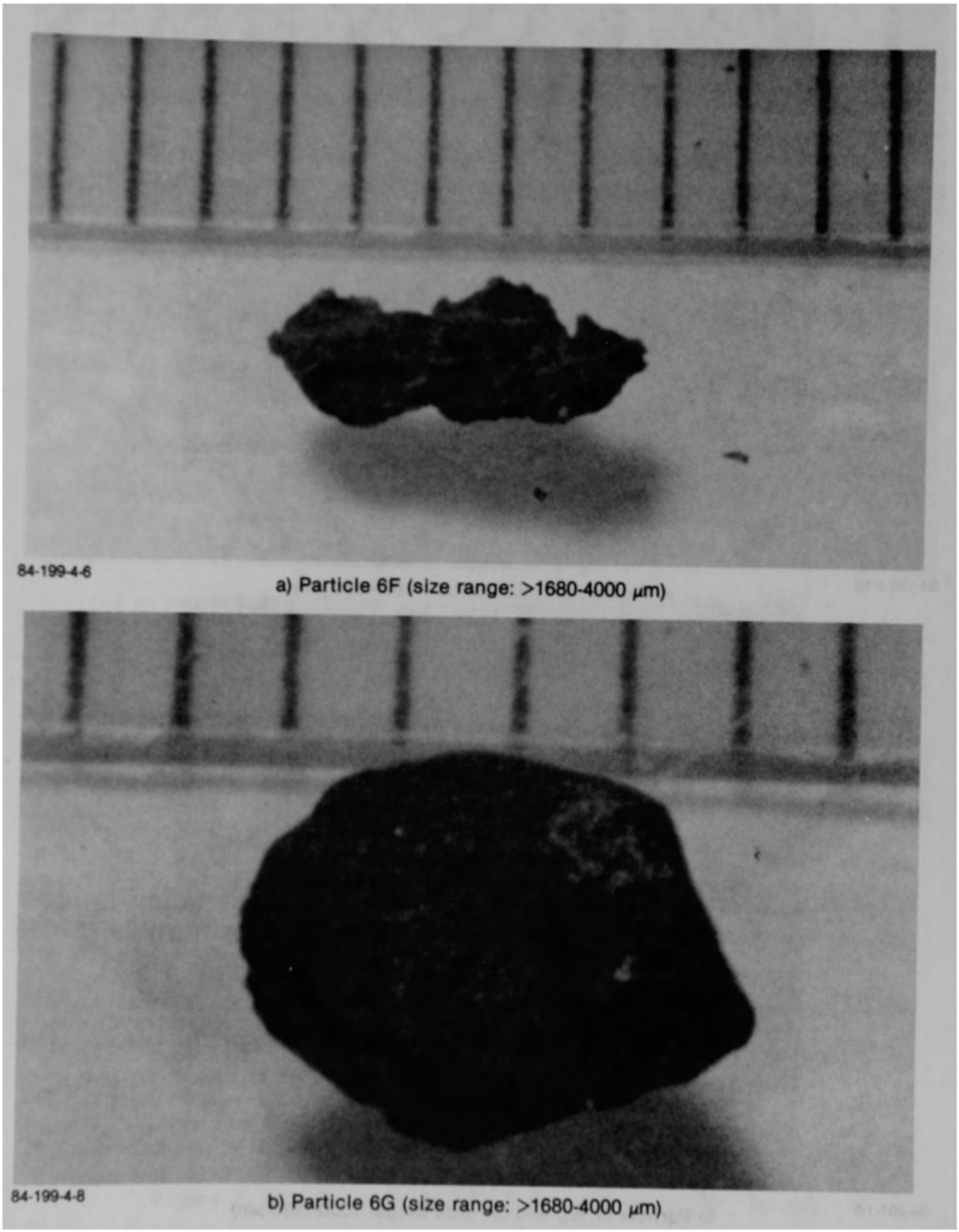

Figure B-28. Particles from Sample 6 (E9, 56 cm).

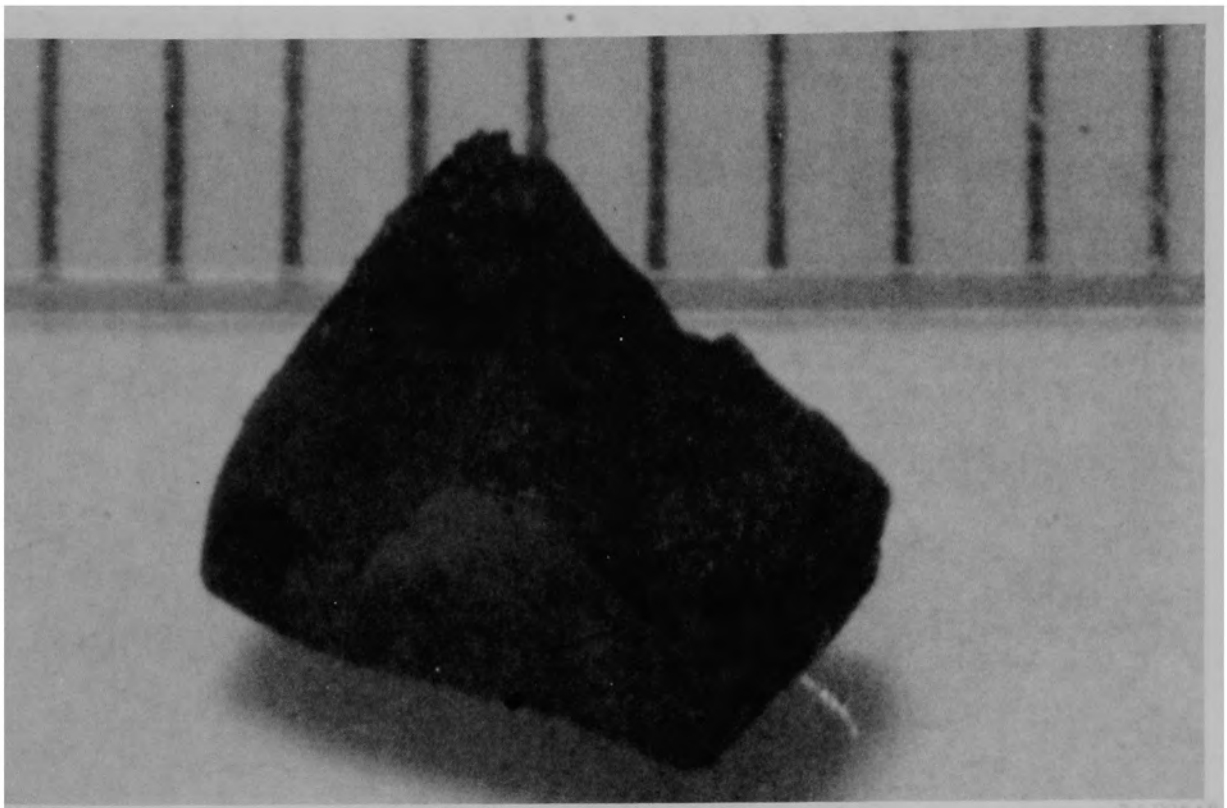

84-199-4-10

a) Particle 6H (size range: 1680-4000 μm)

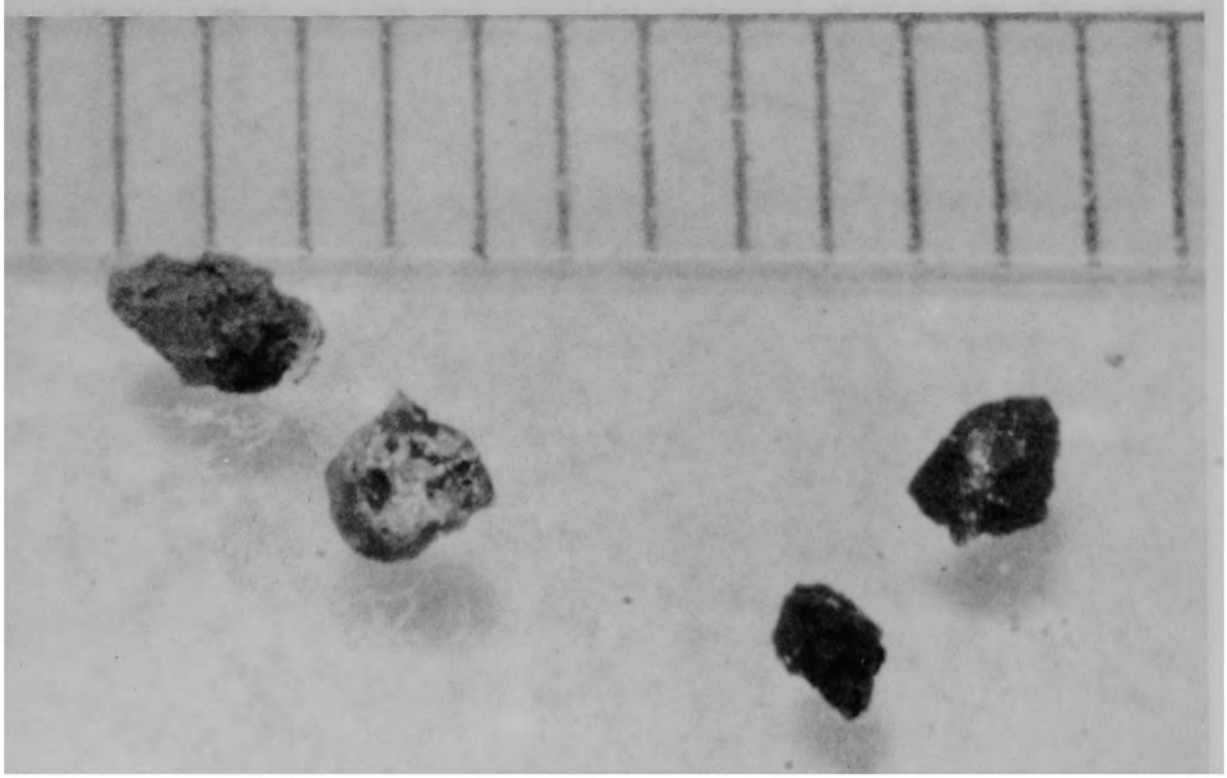

84-201-1-5

b) Particle 6I, 6J, and 6K (size range: 1000-1680 μm)

Figure B-29. Particles from Sample 6 (E9, 56 cm).

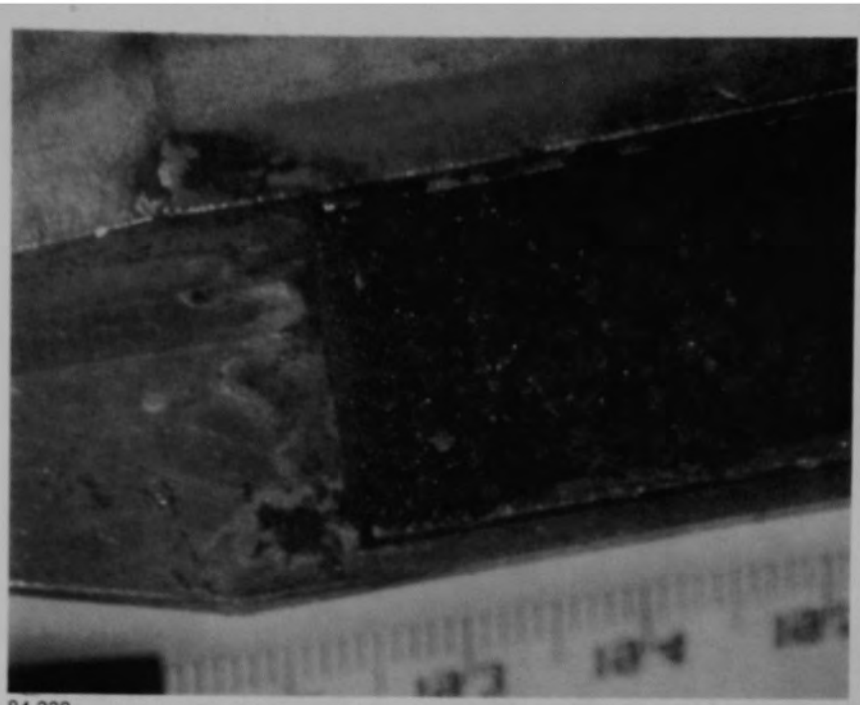

84-238

a) Material in sampling tool (shows stratification)

84-240

b) After removing material from sampling tool

Figure B-30. The bulk material for Sample 7, (H8, 36 cm).

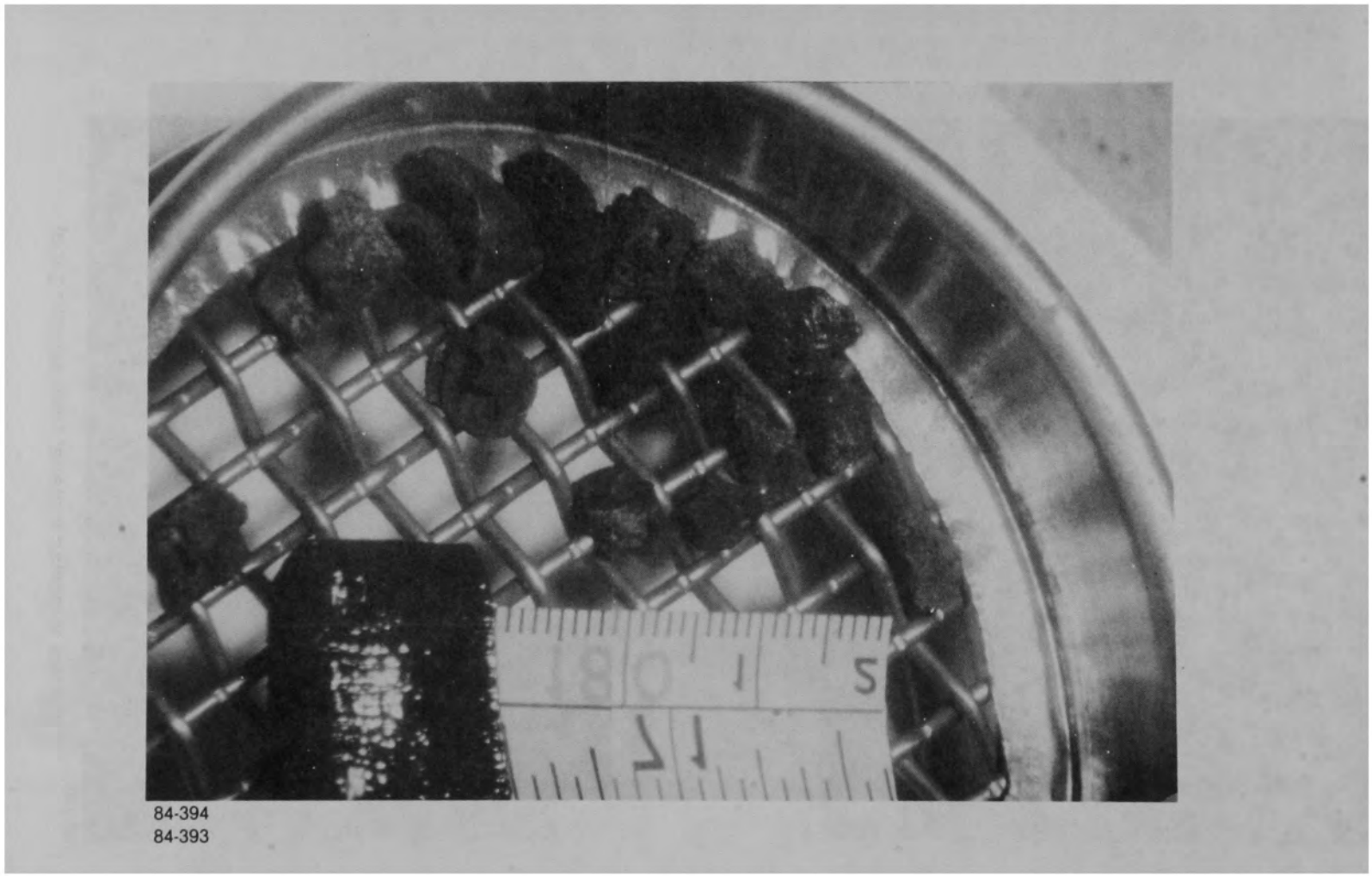

Figure B-31. Particles >4000 μm from Sample 7 (H8, 36 cm).

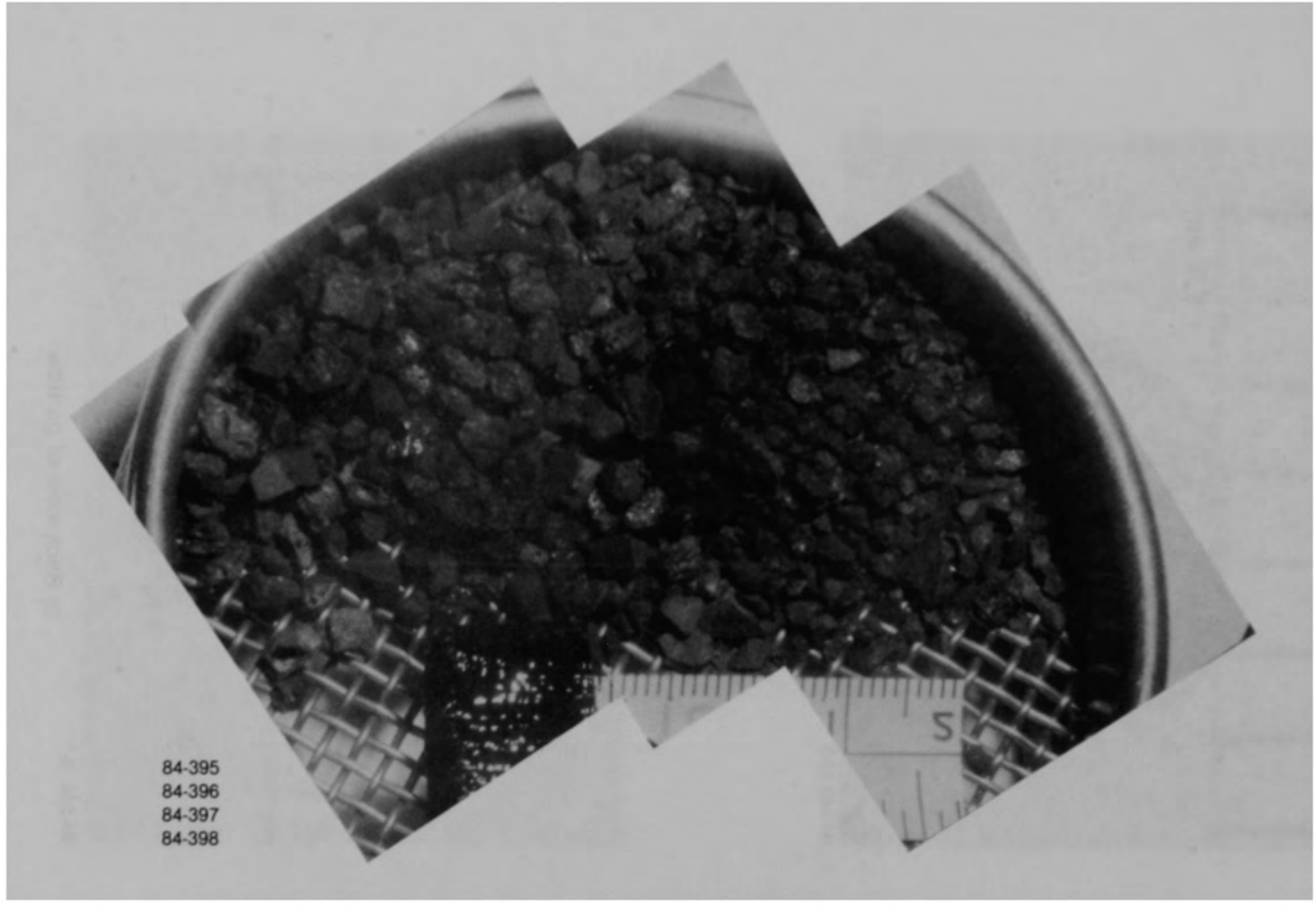

Figure B-32. Particle size fraction (size range 1680-4000 µm) from Sample 7, (H8, 36 cm).

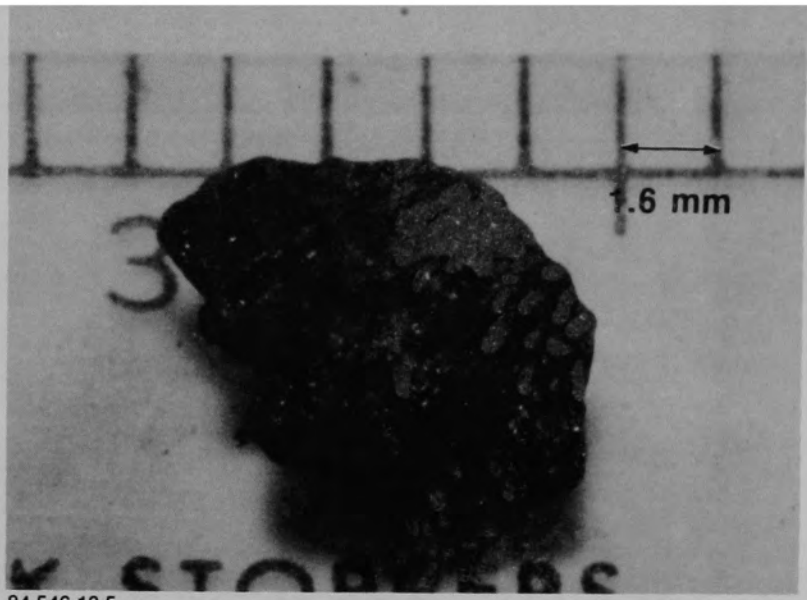

84-546-13-5

a) Front view of particle

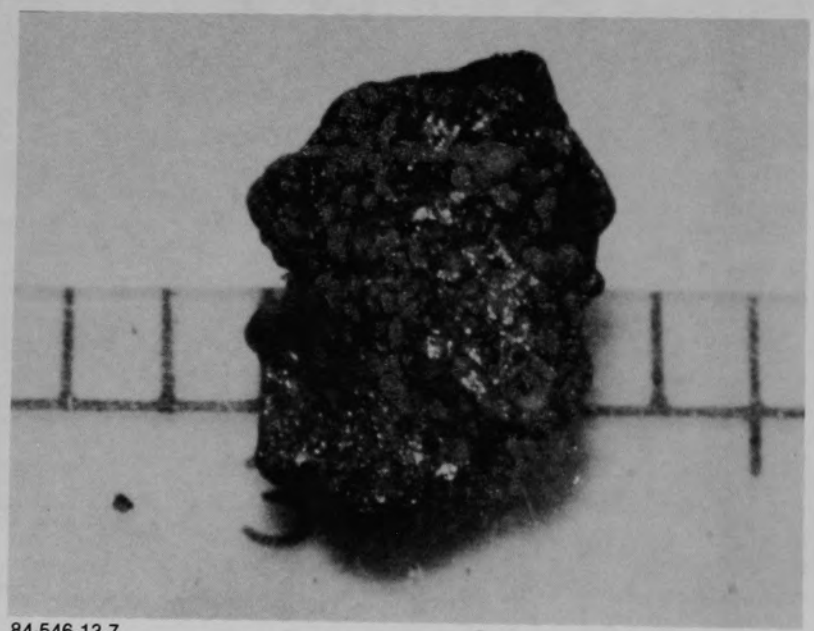

84-546-13-7

b) Back view of particle

Figure B-33. Particle 7A from Sample 7 (H8, 36 cm), size range: >4000 μm.

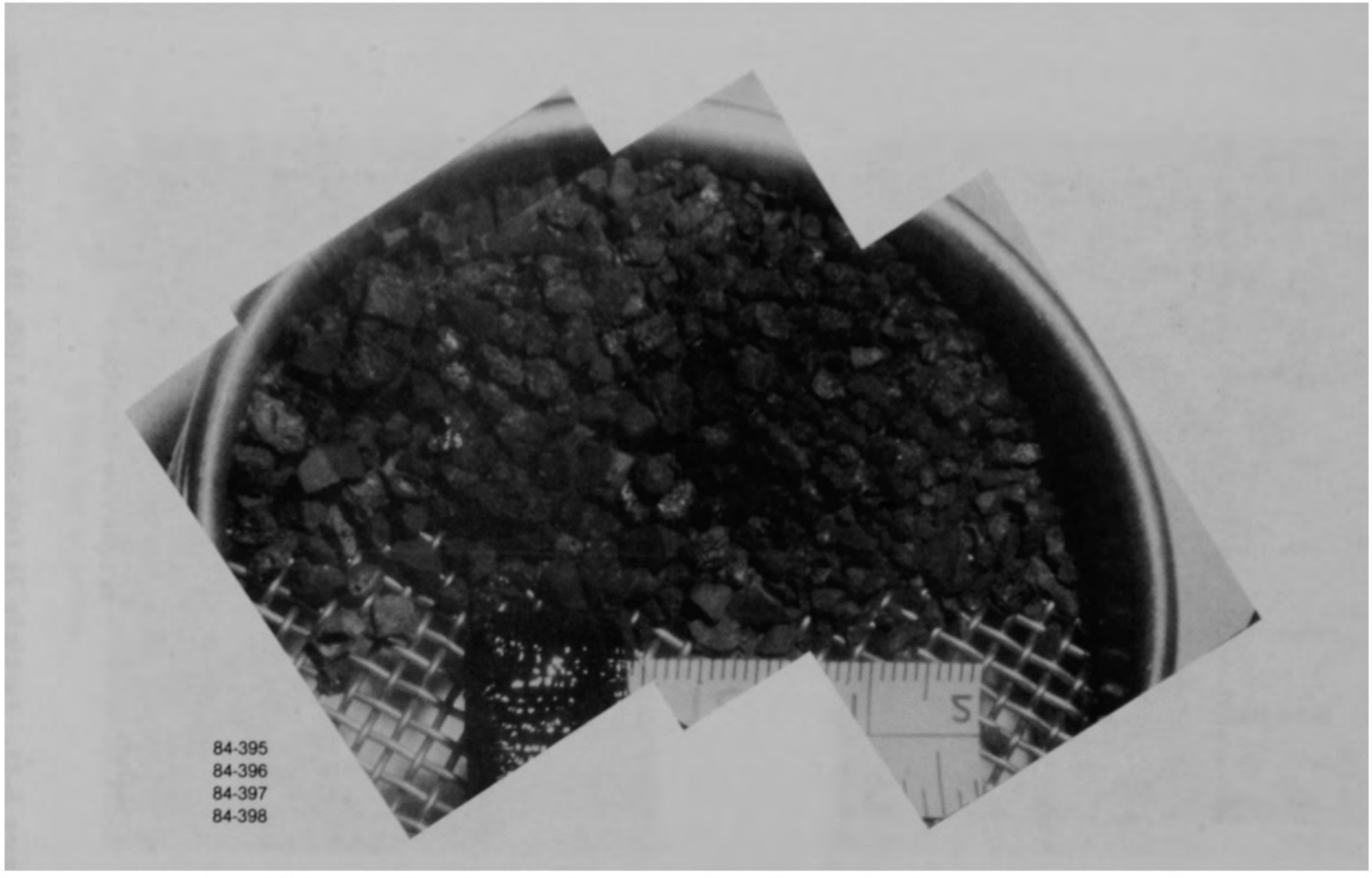

Figure B-32. Particle size fraction (size range 1680-4000 μm) from Sample 7, (H8, 36 cm).

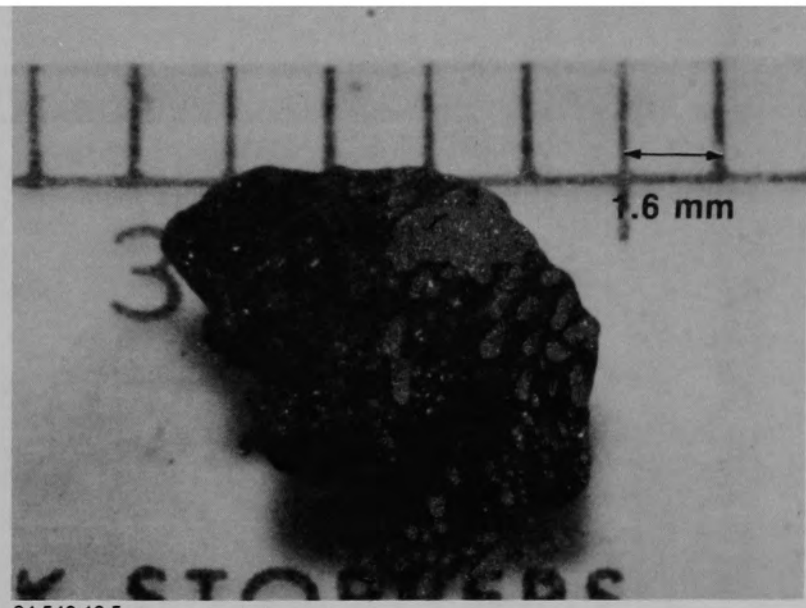

84-546-13-5

a) Front view of particle

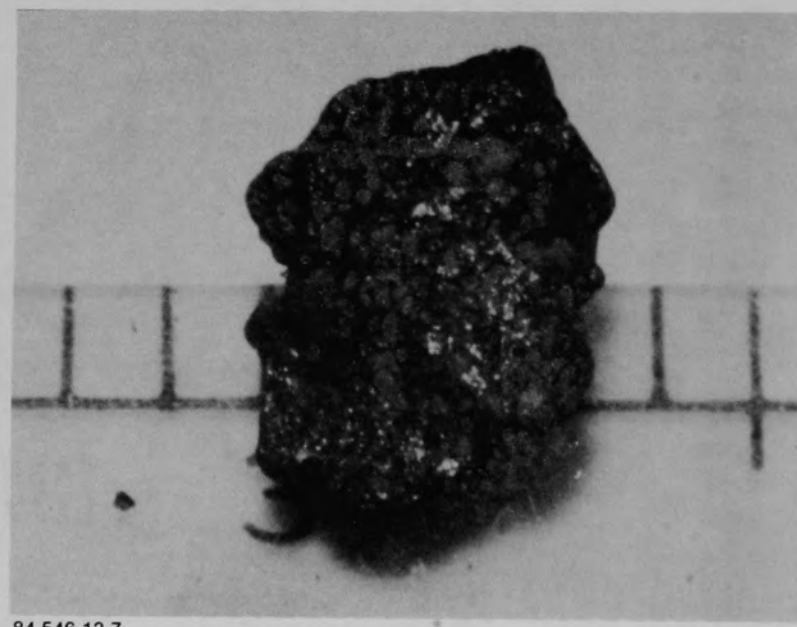

84-546-13-7

b) Back view of particle

Figure B-33. Particle 7A from Sample 7 (H8, 36 cm), size range: >4000 μm.

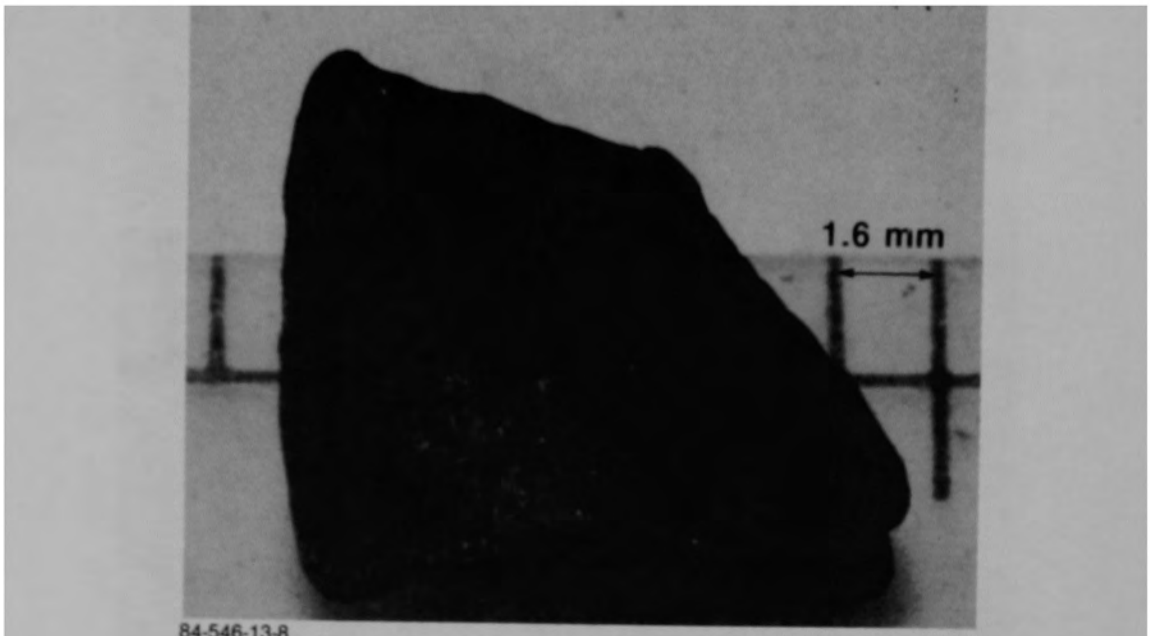

84-546-13-8

a) Front view of particle

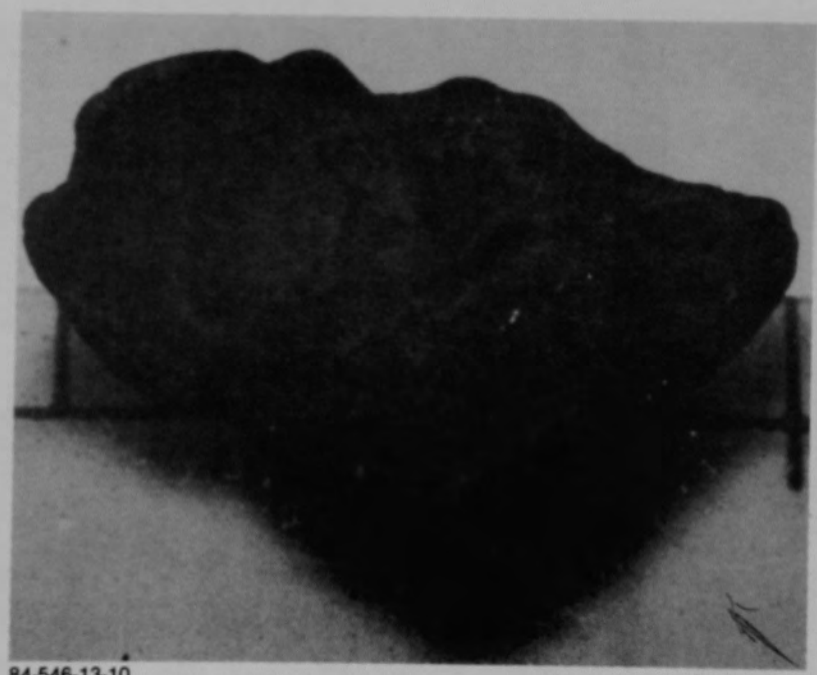

84-546-13-10

b) Back view of particle

Figure B-34. Particle 7B from Sample 7 (H8, 36 cm), size range: >4000 μm.

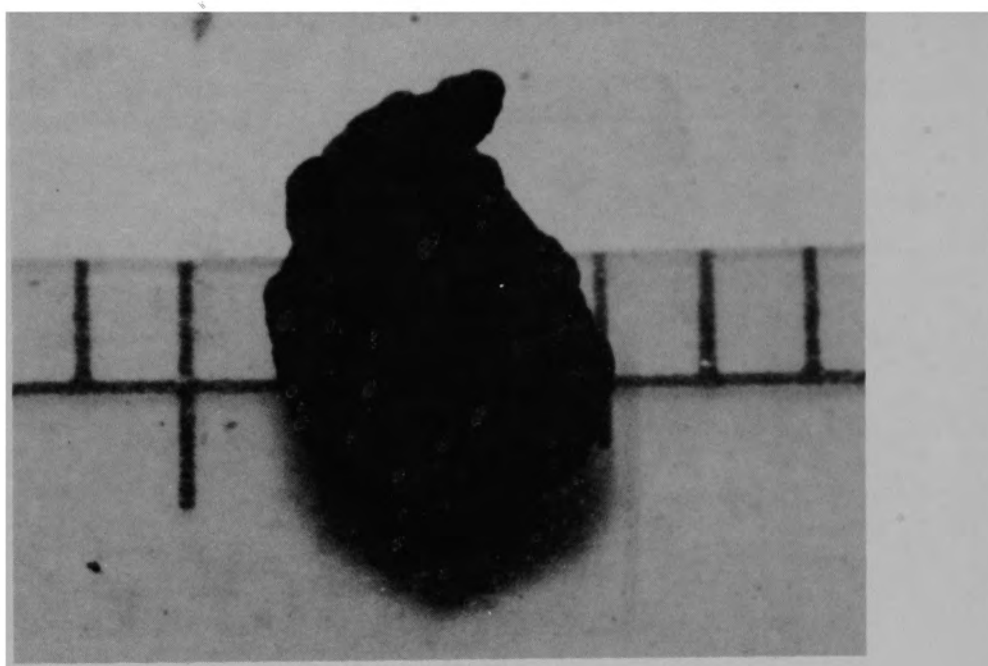

84-546-13-12

a) Front view of particle

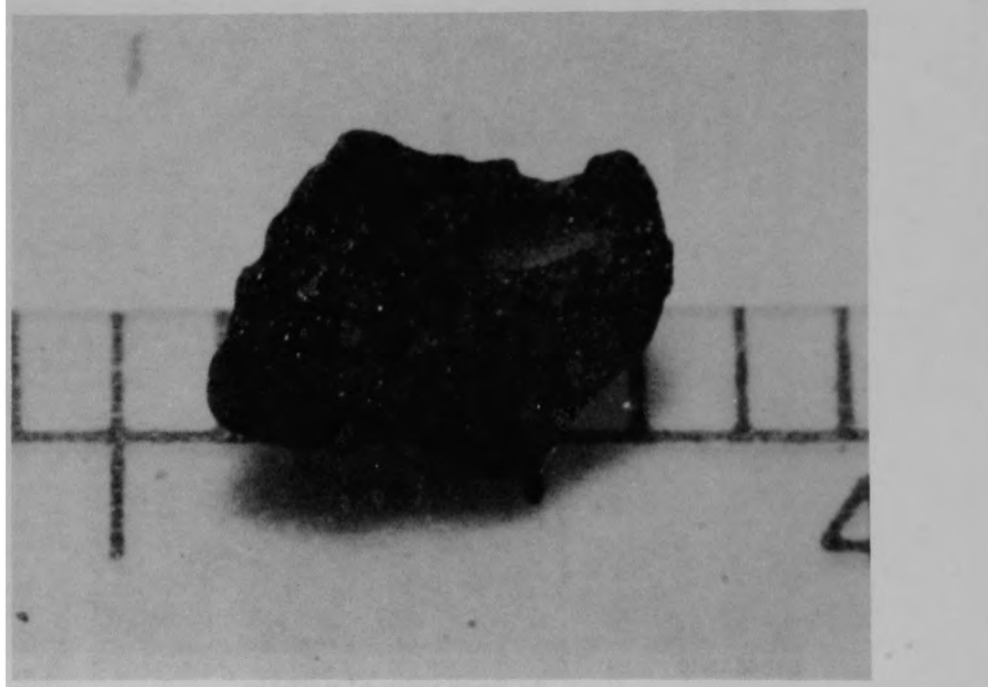

84-546-13-14

b) Back view of particle

Figure B-35. Particle 7C from Sample 7 (H8, 36 cm), size range: >4000 μm.

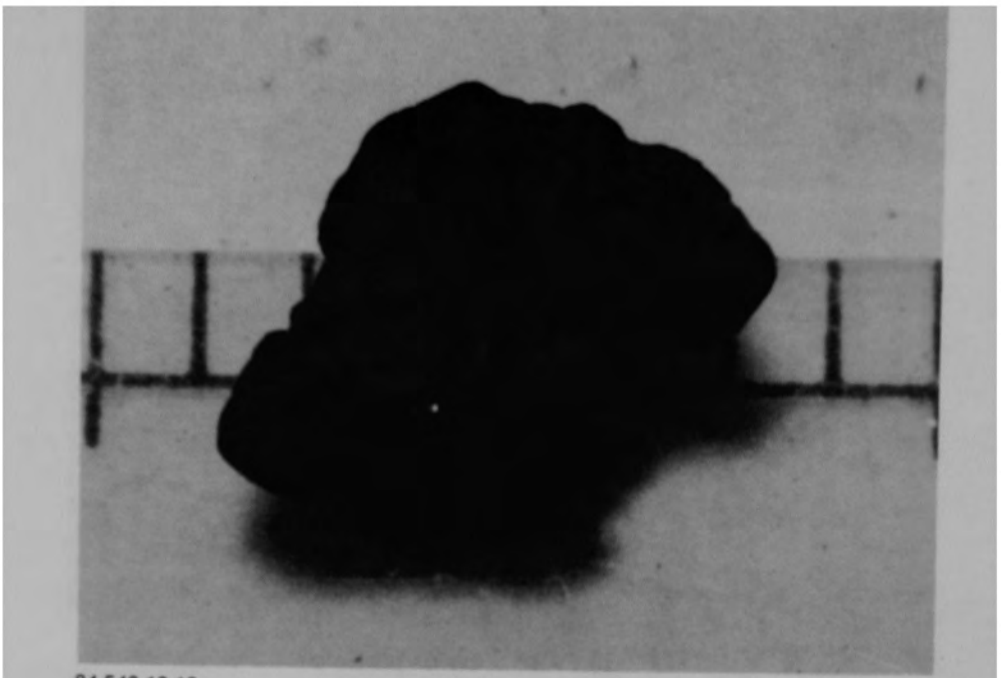

84-546-13-16

a) Front view of particle

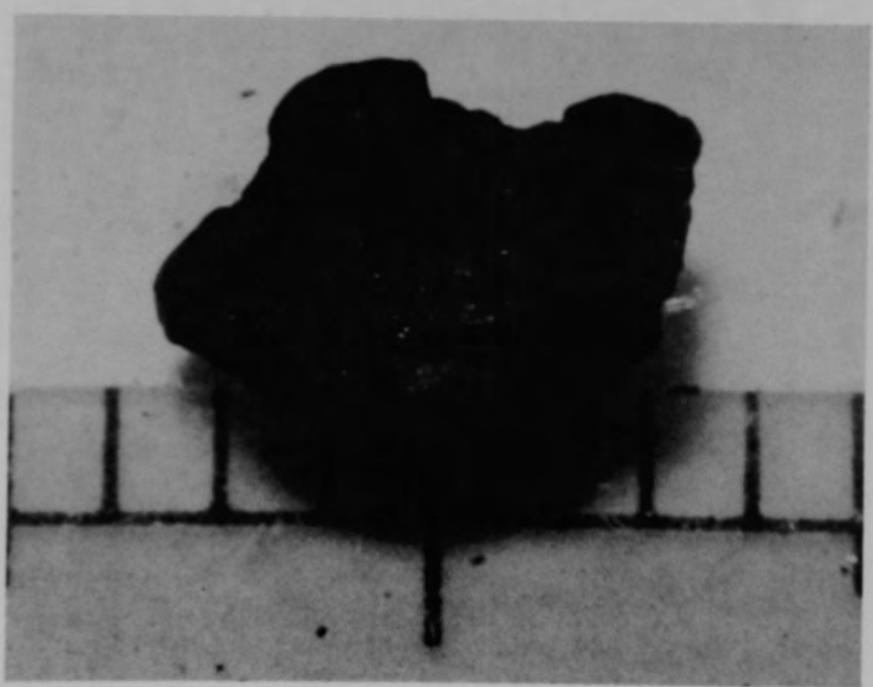

84-546-13-18

b) Back view of particle

Figure B-36. Particle 7D from Sample 7 (H8, 36 cm), size range: >4000 μm.

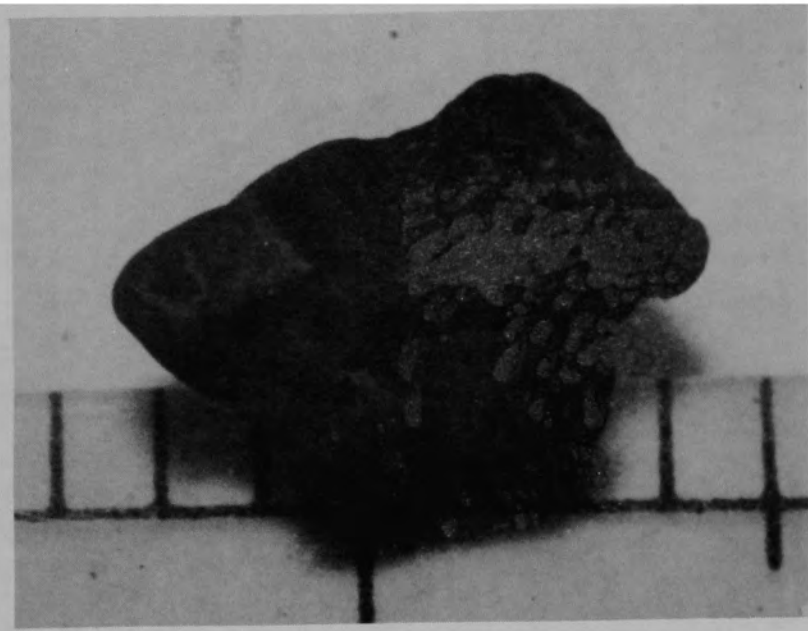

84-546-13-20

a) Front view of particle

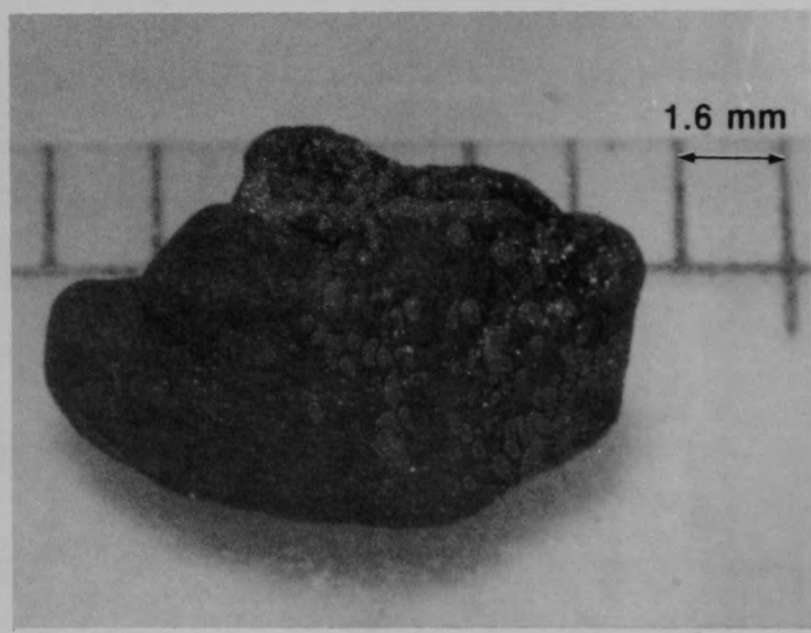

84-546-13-22

b) Back view of particle

Figure B-37. Particle 7E from Sample 7 (H8, 36 cm), size range: >4000 µm.

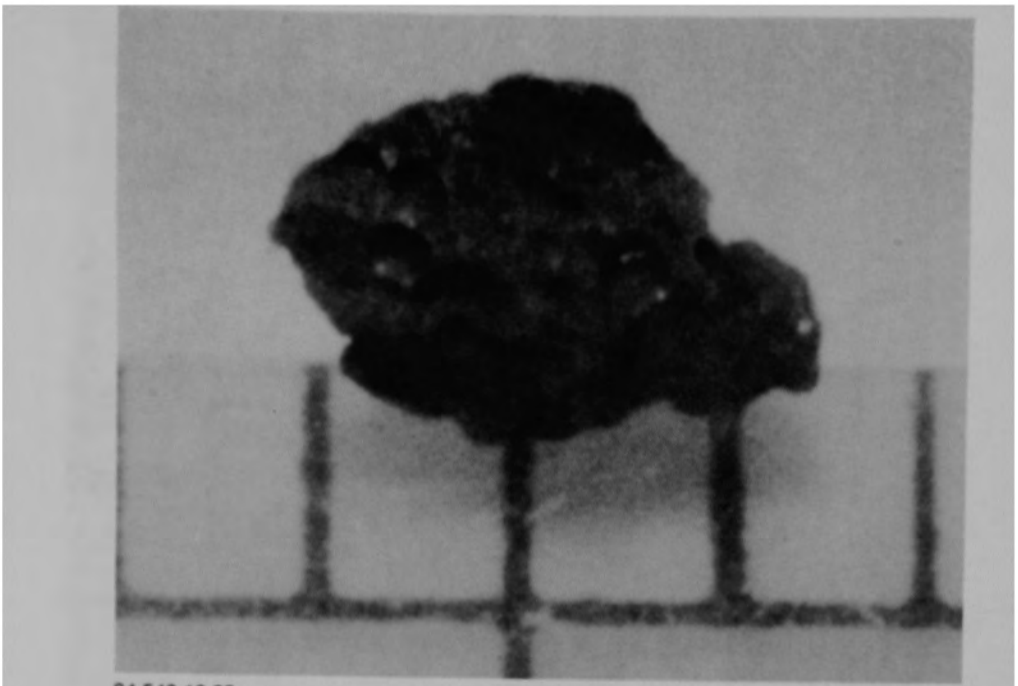

84-546-13-25

a) Front view of particle

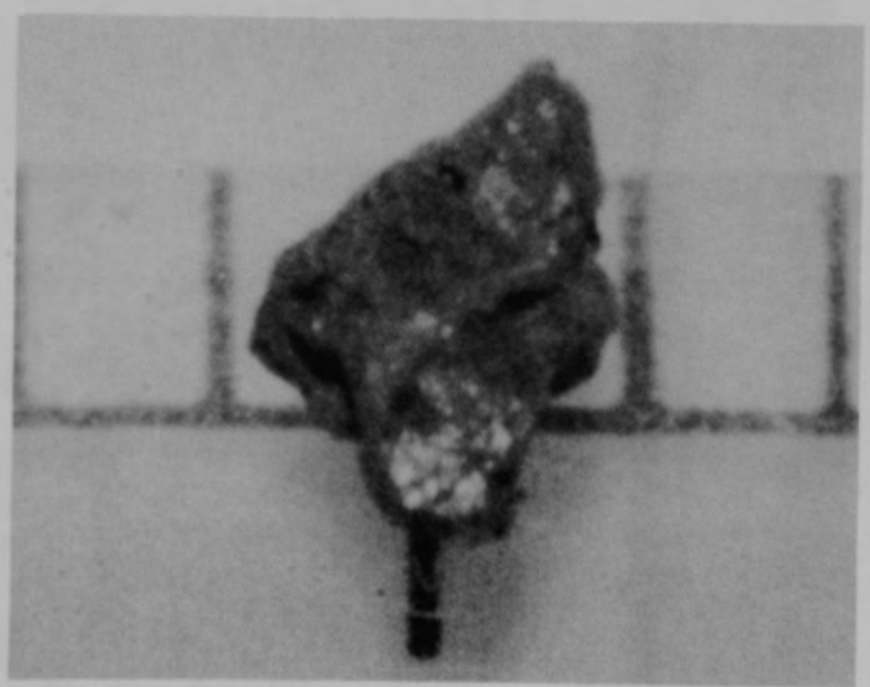

84-546-13-26

b) Back view of particle

Figure B-38. Particle 7F from Sample 7 (H8, 36 cm), size range: 1680-4000 µm.

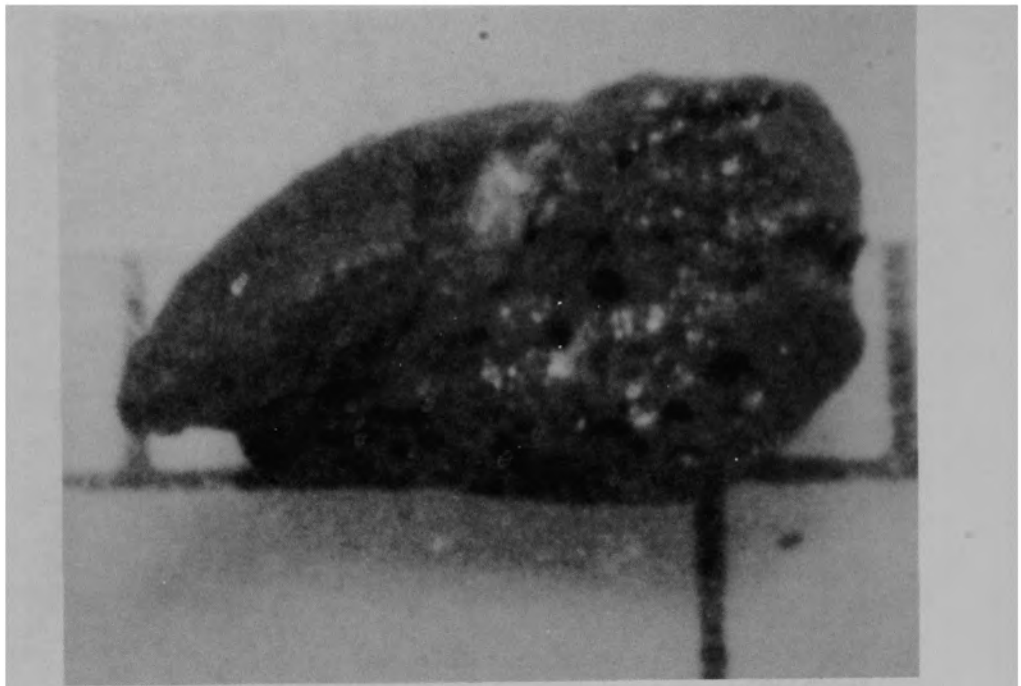

884-546-13-29

a) Front view of particle

84-546-13-30

b) Back view of particle

Figure B-39. Particle 7G from Sample 7 (H8, 36 cm), size range: 1680-4000 μm.

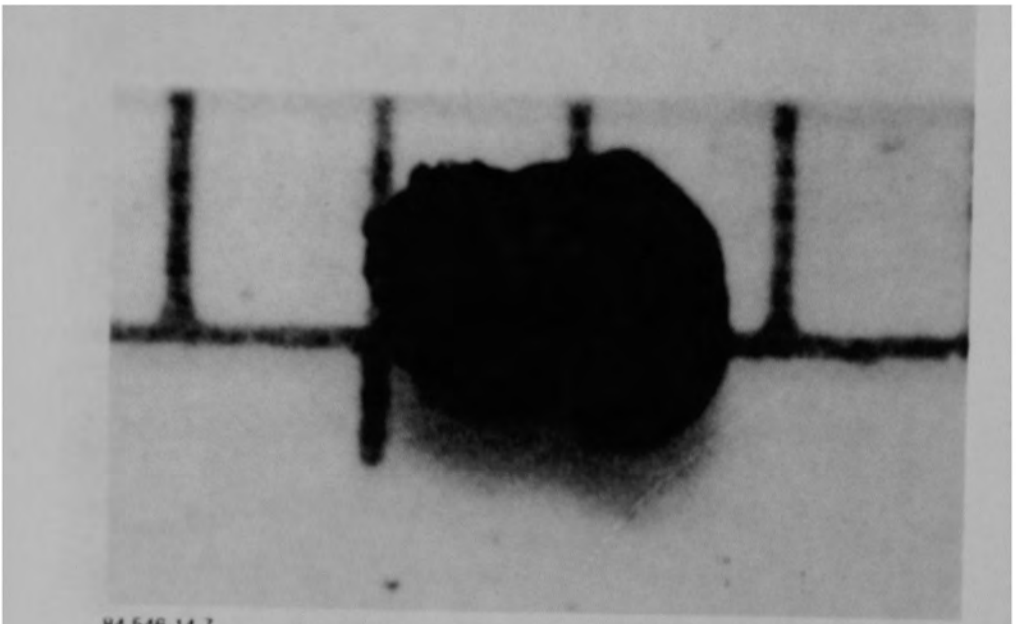

84-546-14-7

a) Particle 7H (size range: 1680-4000 μm)

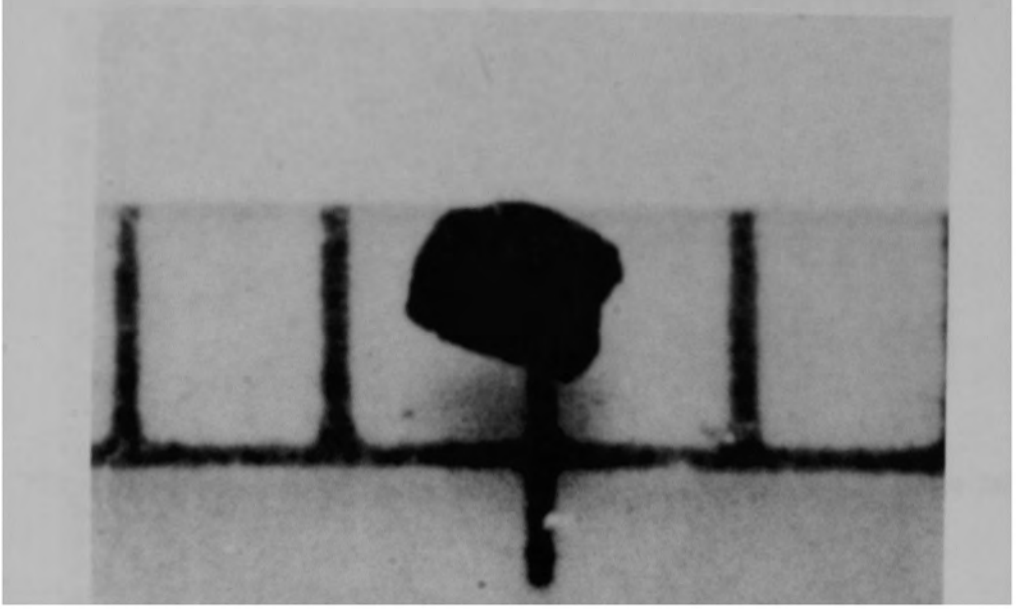

84-546-14-9

b) Particle 7I (size range 1000-1680 μm)

Figure B-40. Particles from Sample 7 (118, 36 cm).

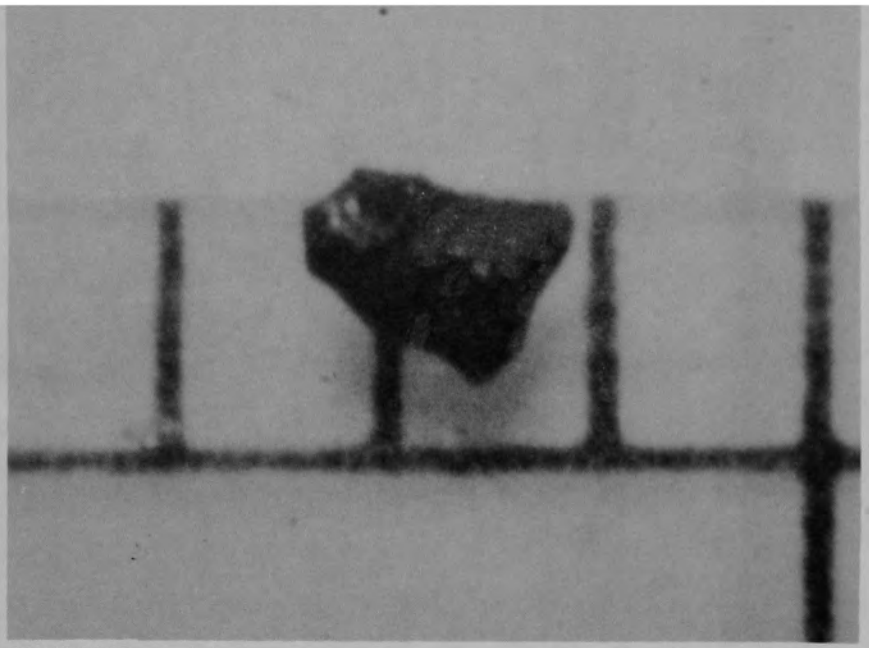

84-546-14-12

a) Particle 7J (size range: 1000-1680 μm)

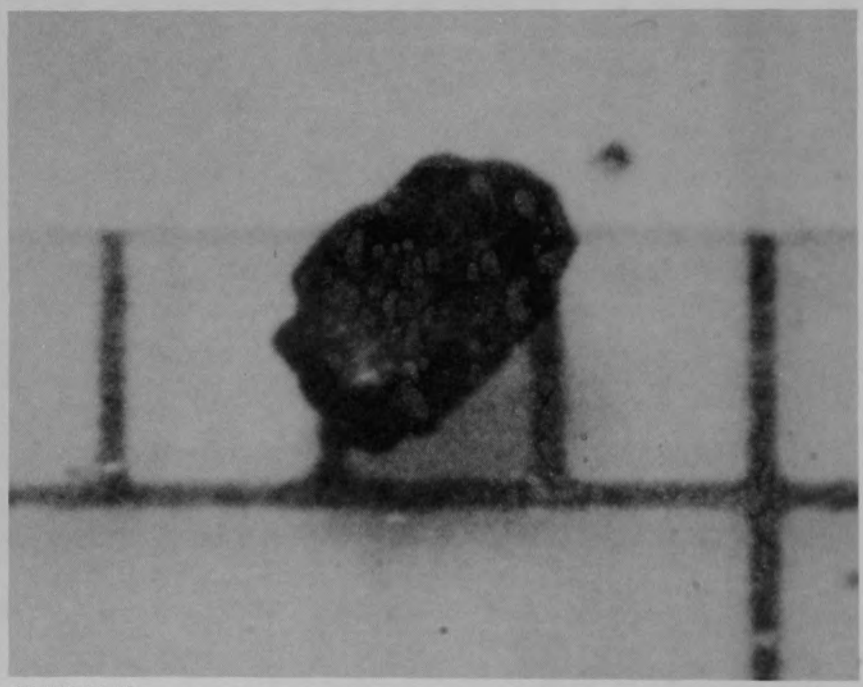

84-546-14-13

b) Particle 7K (size range: 1000-1680 μm)

Figure B-41. Particles from Sample 7 (H8, 36 cm).

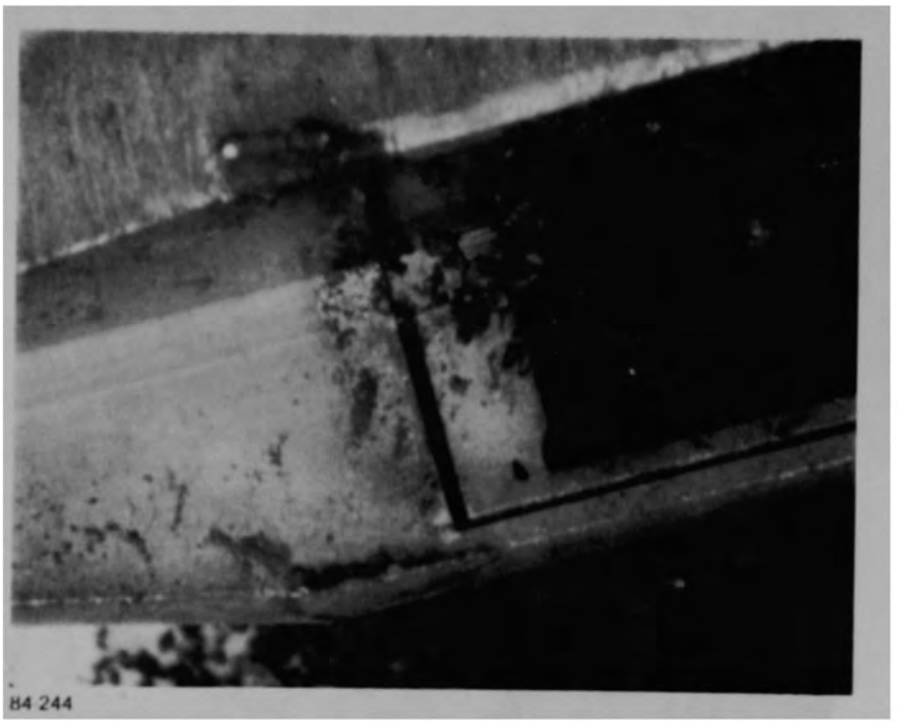

Figure B-42. Sample 8 (H8, 70 cm) being removed from sampling tool.

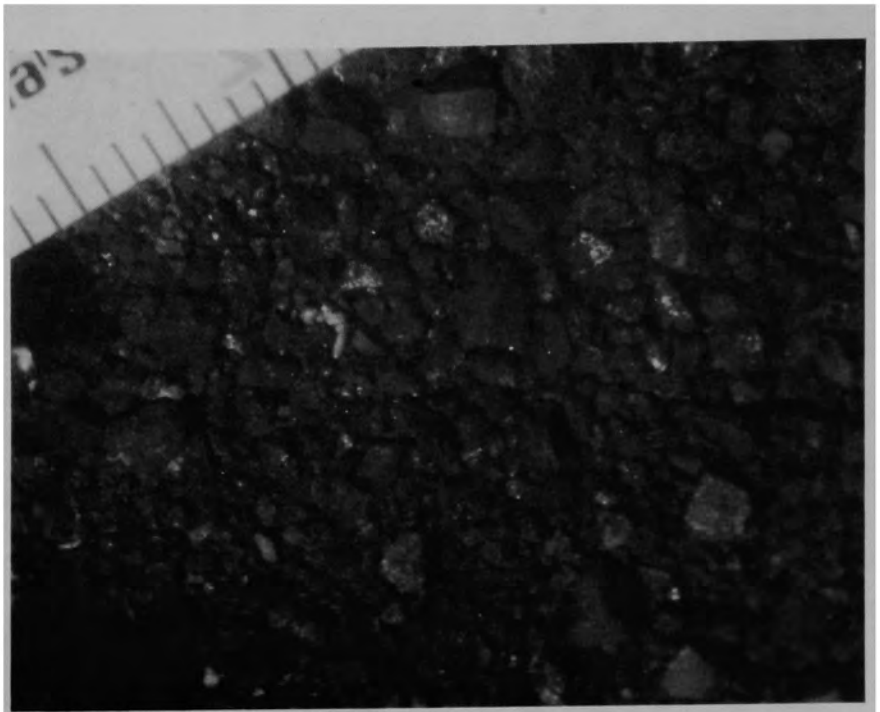

84-247

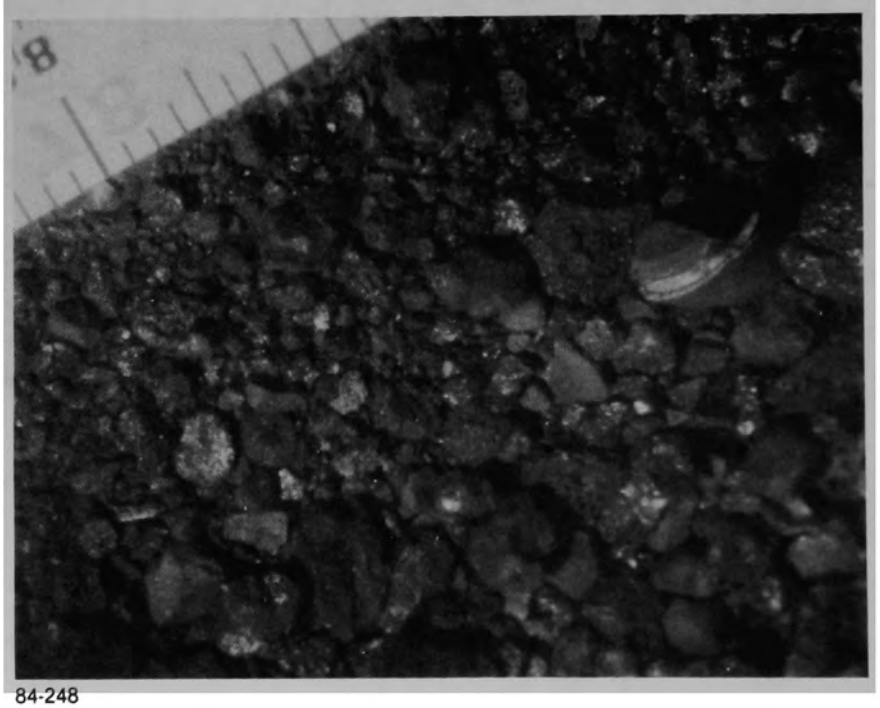

84-248

Figure B-43. Views of the bulk material for Sample 8 (H8, 70 cm) after removal from the sampling tool.

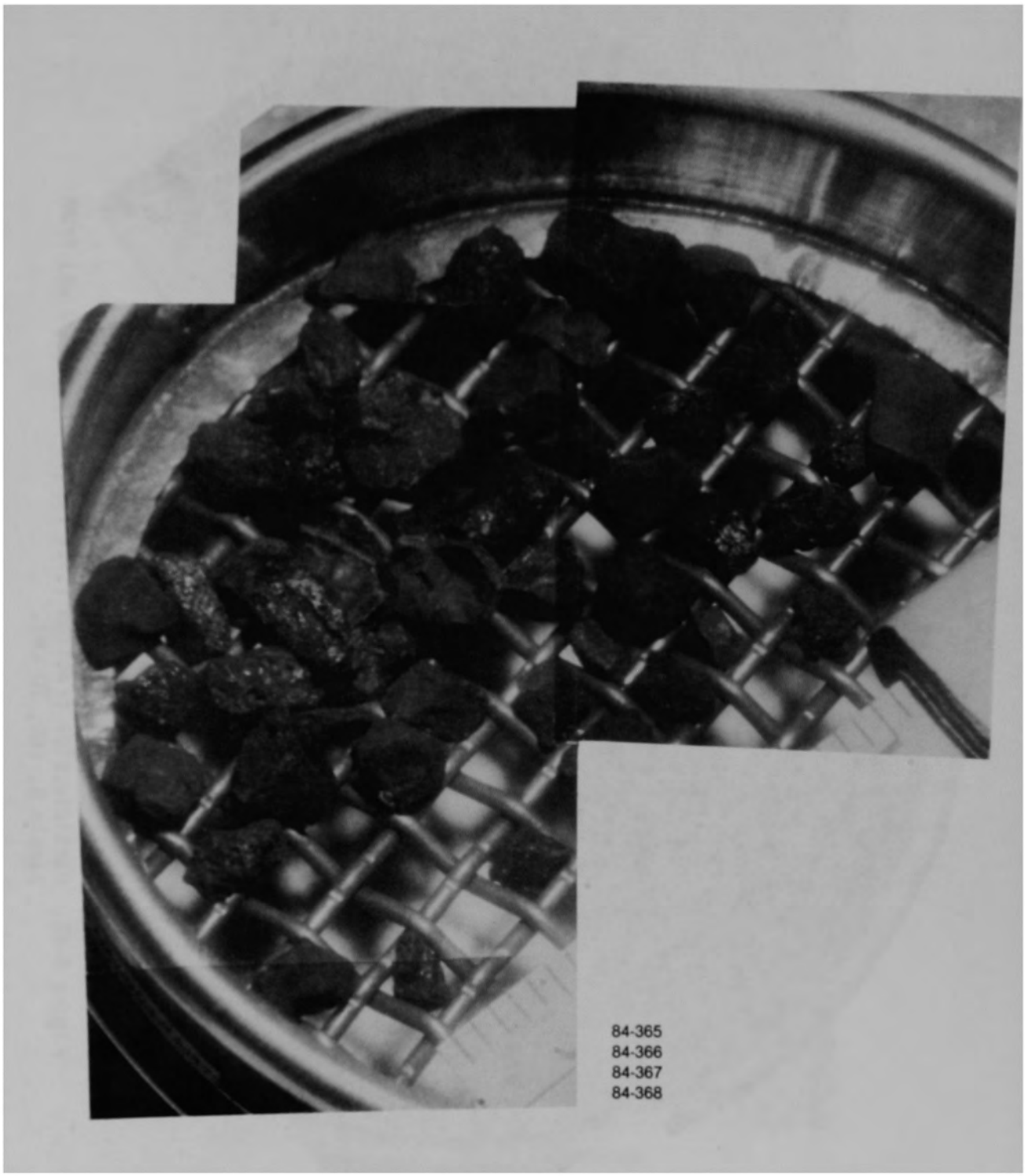

Figure B-44. Particles >4000 μm from Sample 8 (H8, 70 cm).

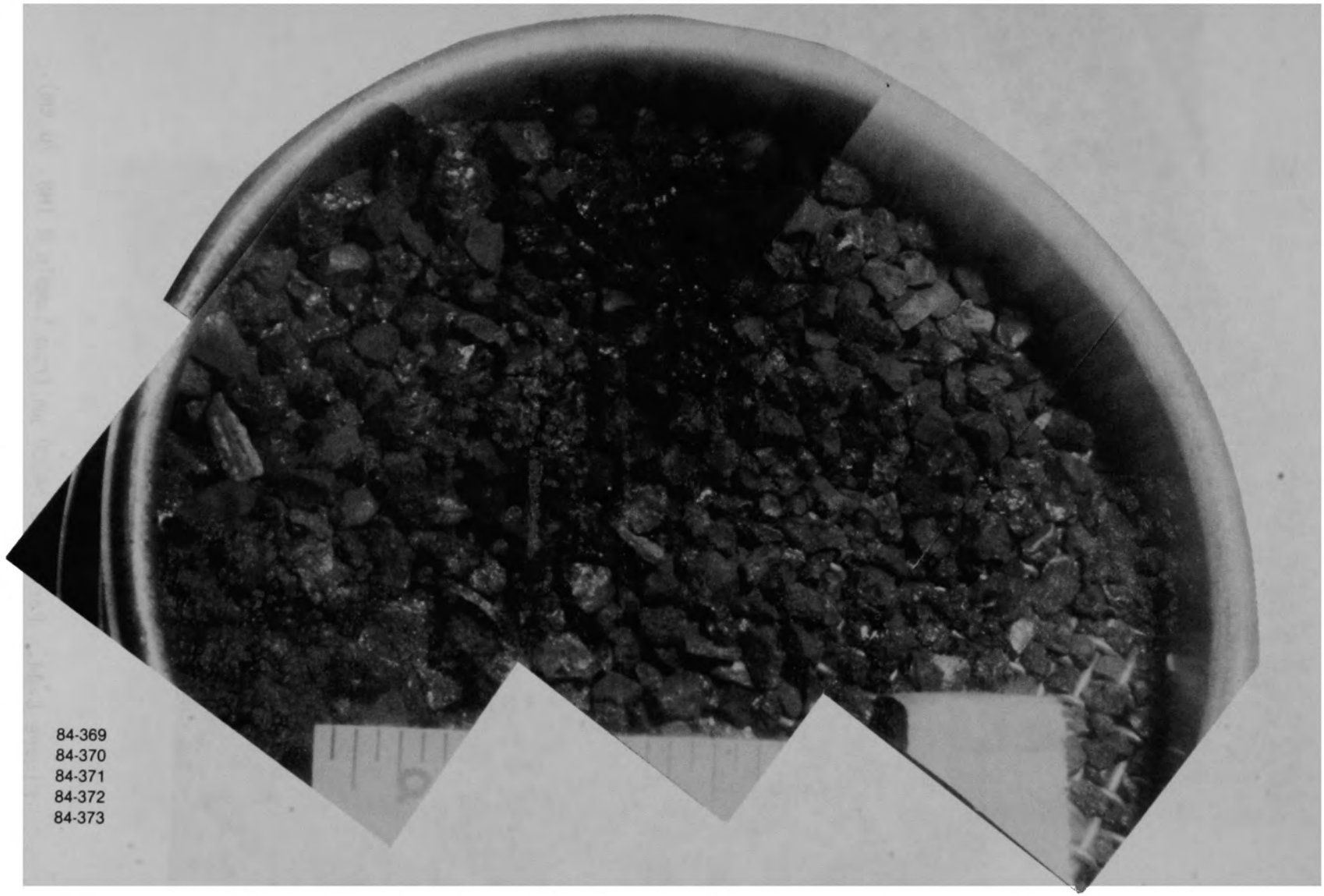

Figure B-45. Particle size fraction (size range: 1680-4000 μm) from Sample 8, (H8, 70 cm).

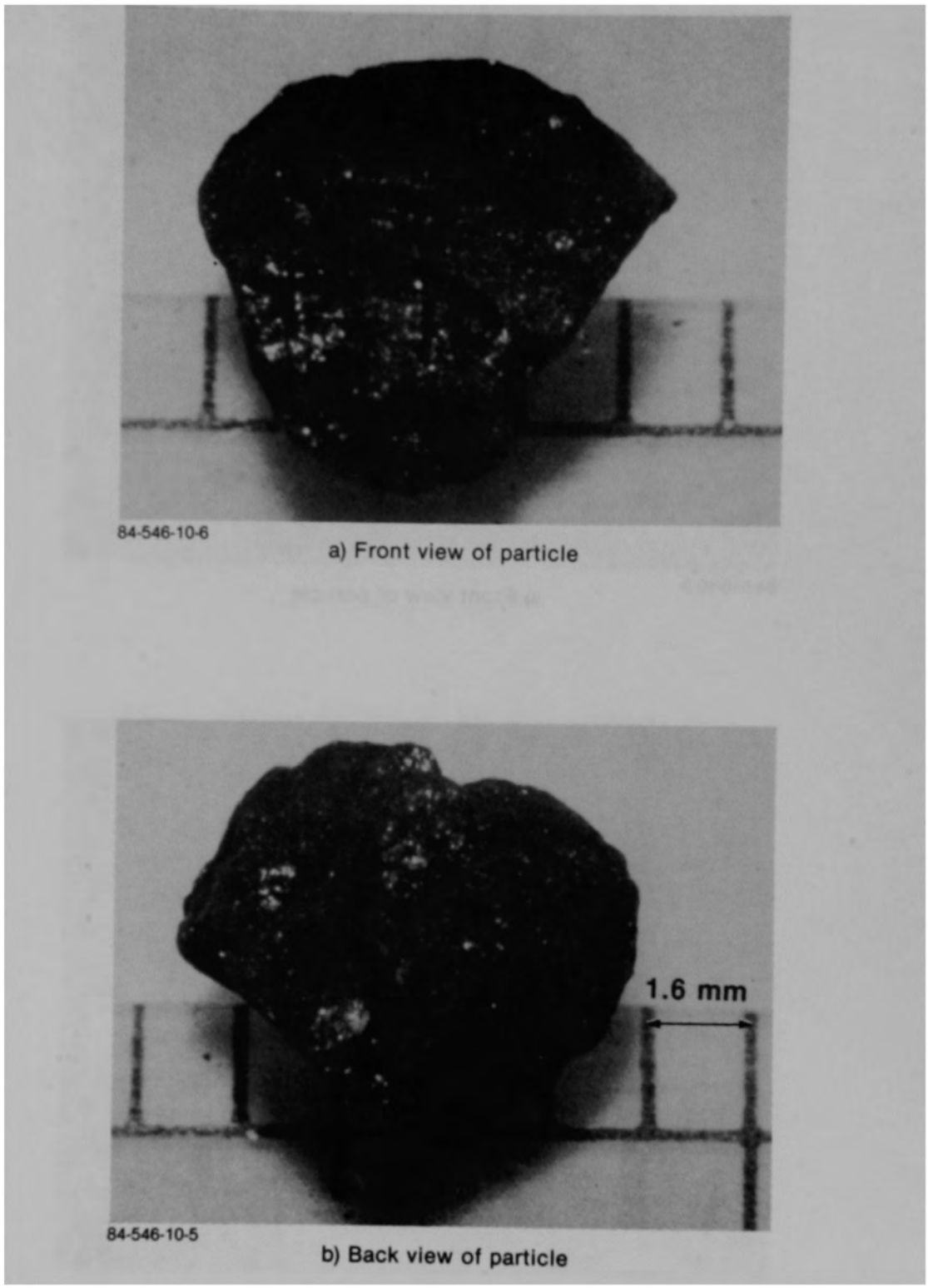

Figure B-46. Particle 8A from Sample 8 (H8, 70 cm), size range: >4000 µm.

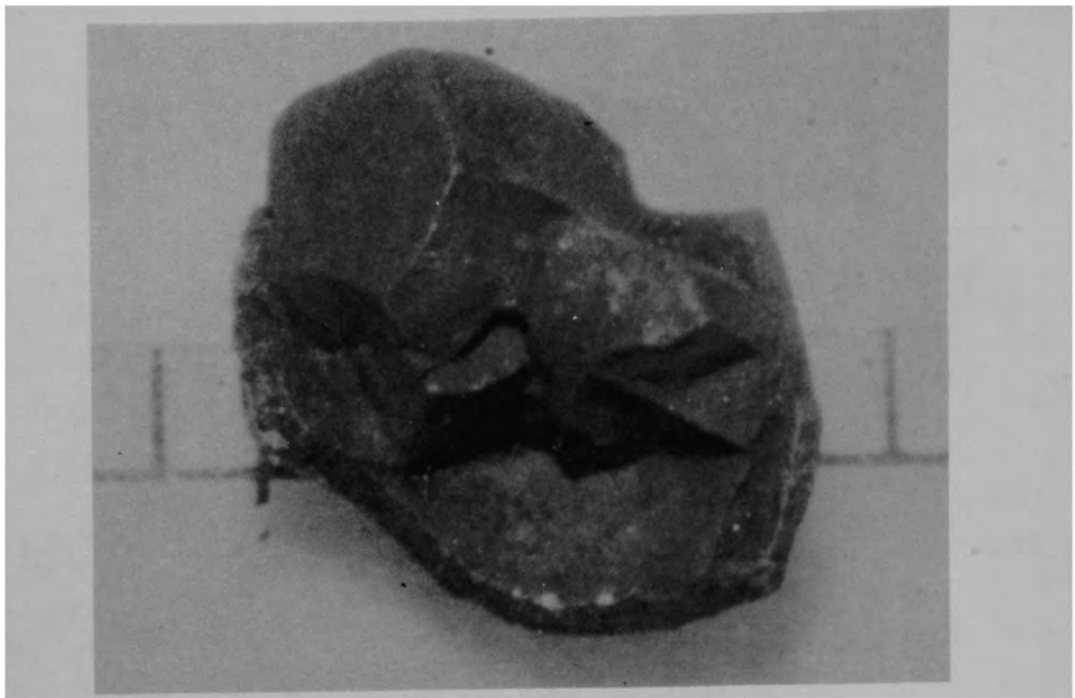

84-546-10-9

a) Front view of particle

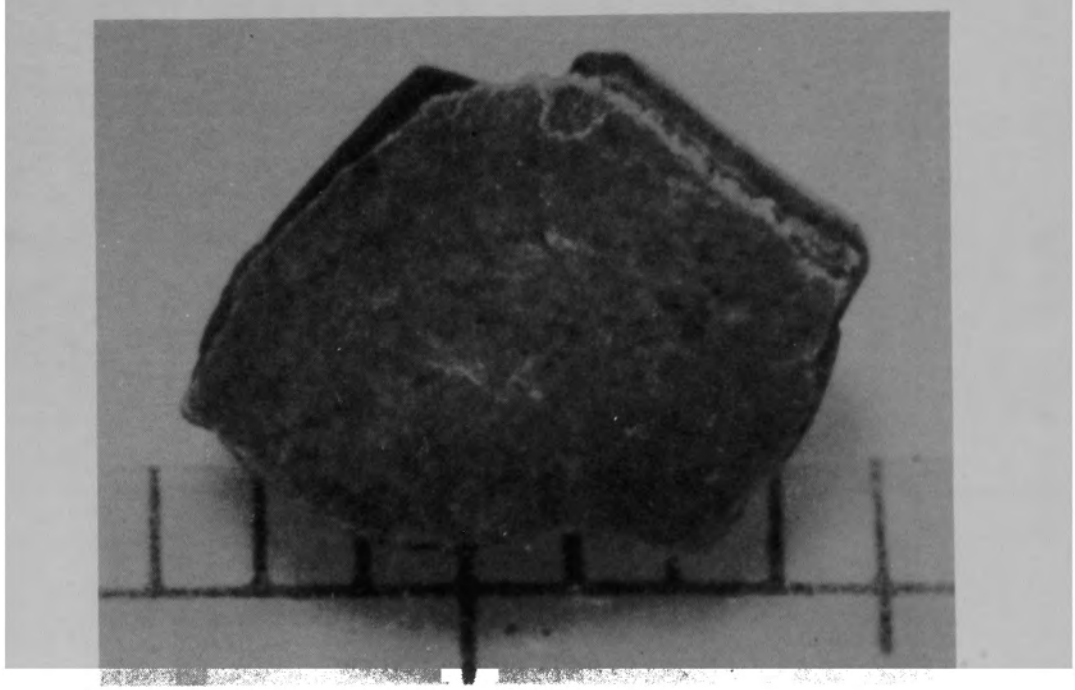

84-546-10-11

b) Back view of particle

Figure B-47. Particle 8B from Sample 8 (H8, 70 cm), size range: >4000 µm.

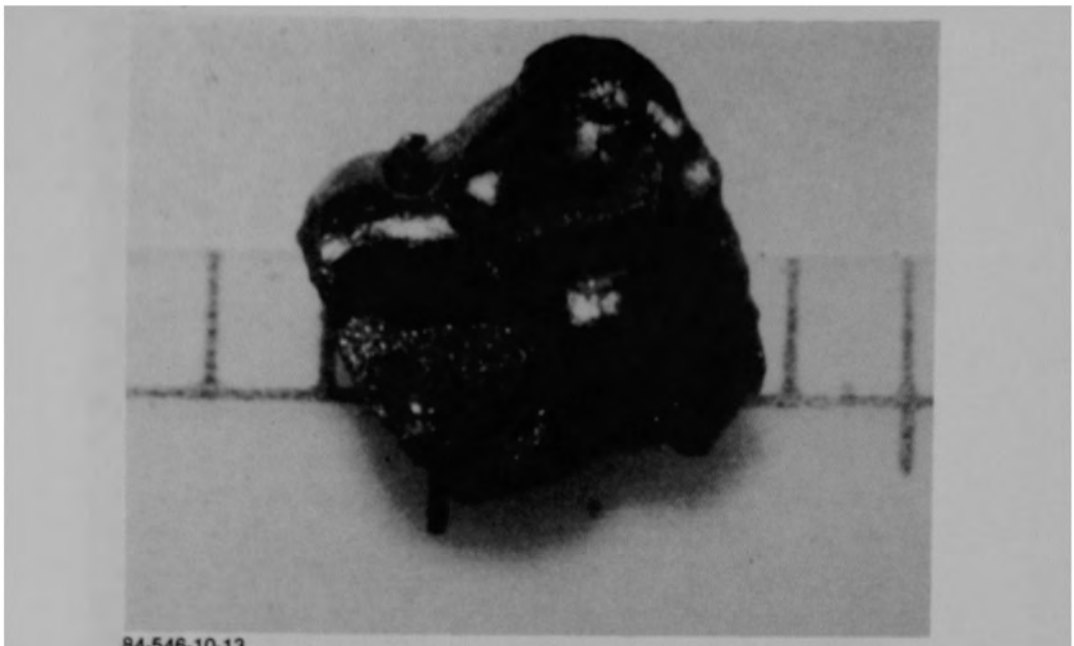

84-546-10-13

a) Front view of particle

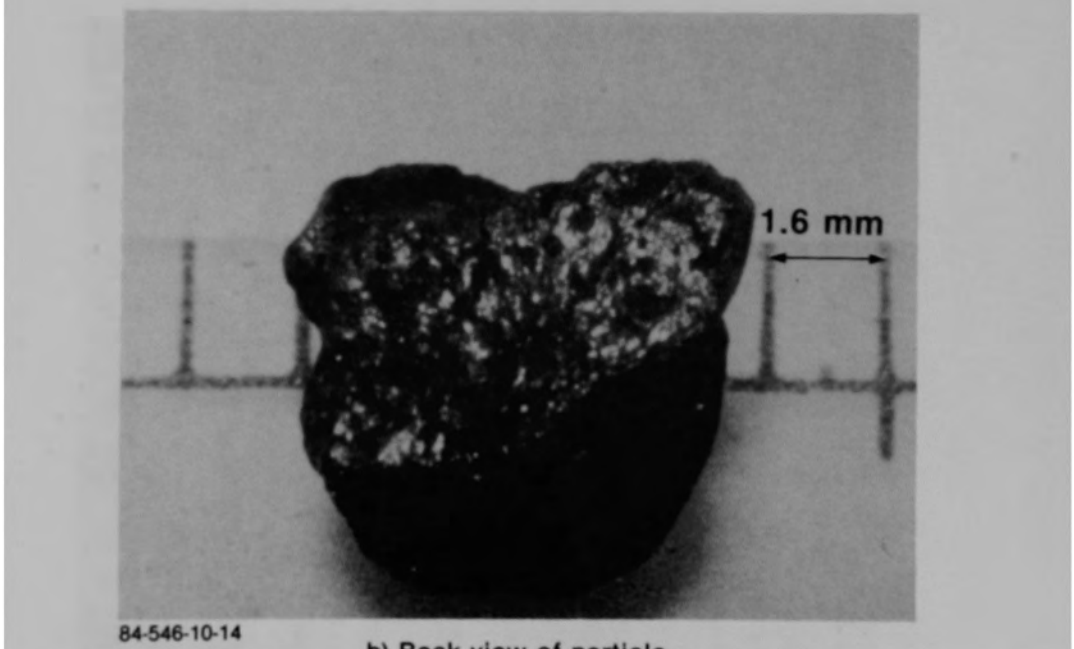

84-546-10-14

b) Back view of particle

Figure B-48. Particle 8C from Sample 8 (H8, 70 cm), size range: >4000 μm.

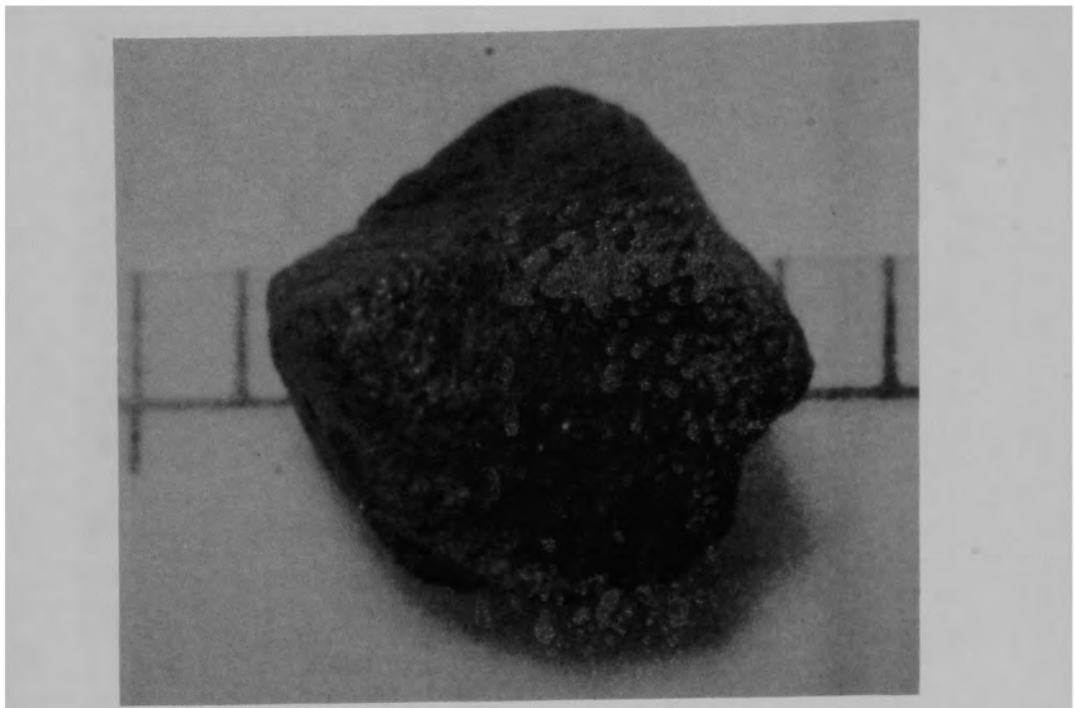

84-546-10-17

a) Front view of particle

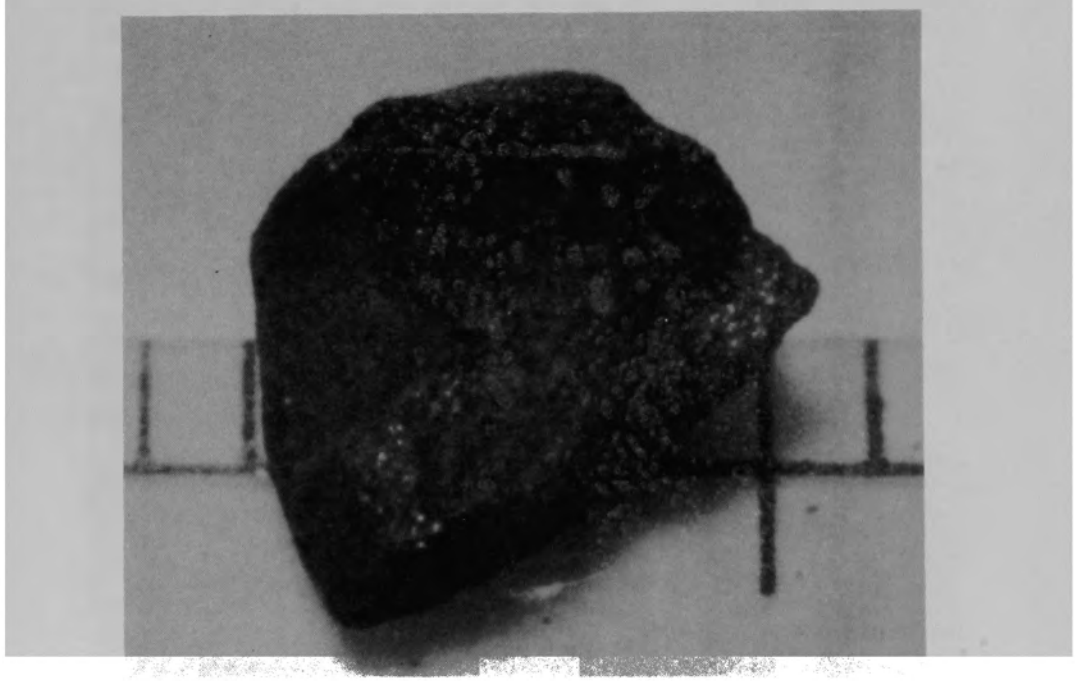

84-546-10-18

b) Back view of particle

Figure B-49. Particle 8D from Sample 8 (H8, 70 cm), size range: >4000 μm.

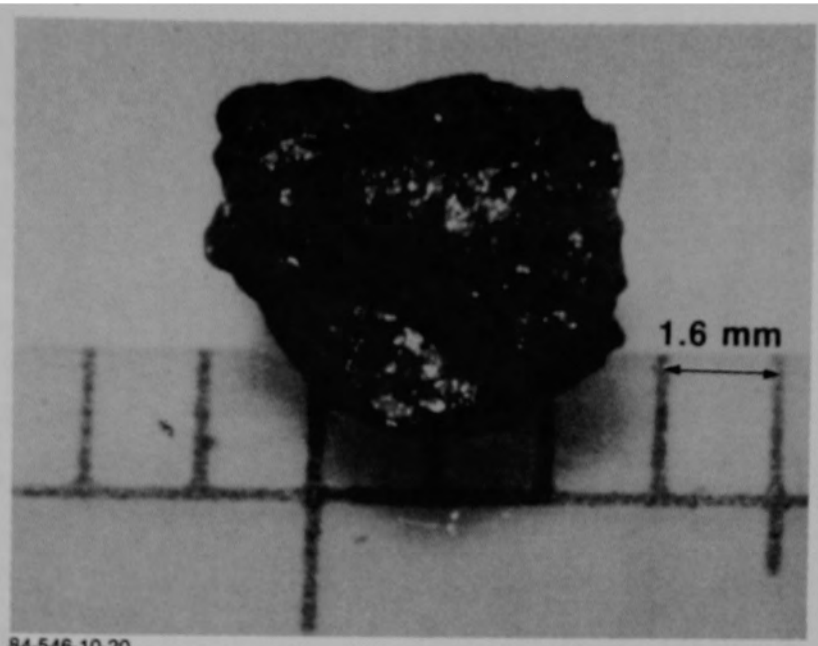

84-546-10-20

a) Front view of particle

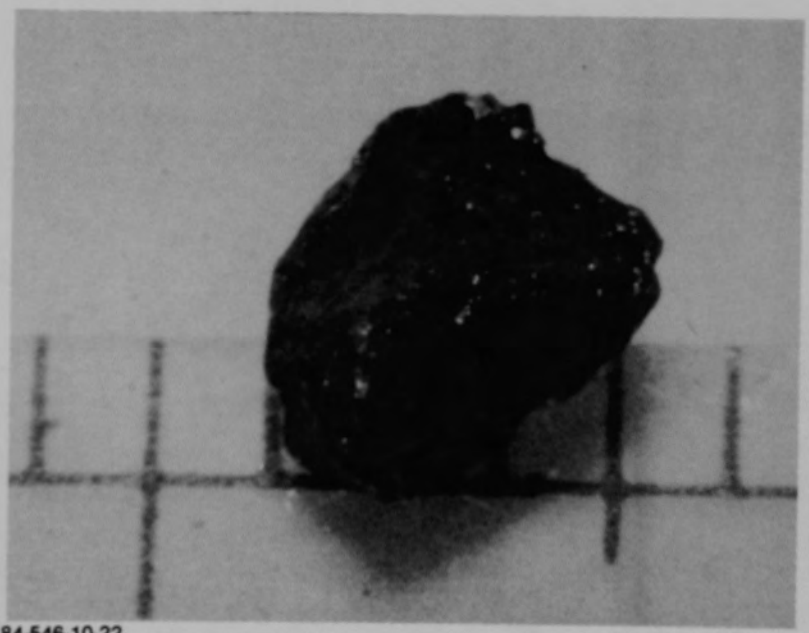

84-546-10-22

b) Back view of particle

Figure B-50. Particle 8E from Sample 8 (H8, 70 cm), size range: >4000 μm.

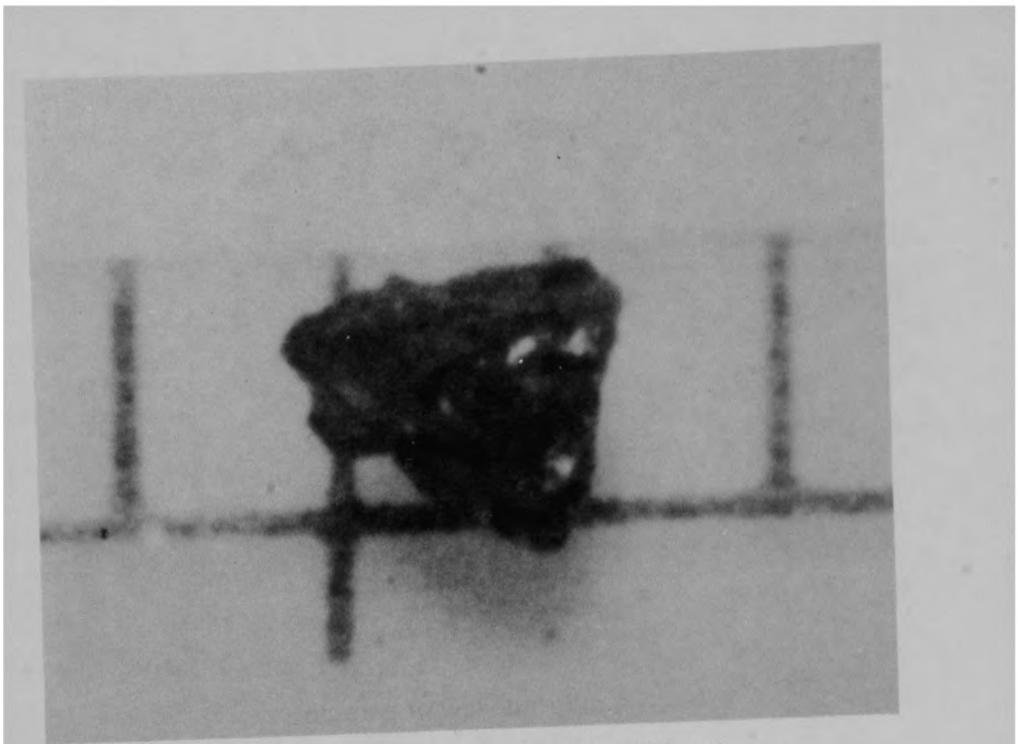

84-546-10-25 a) Particle 8F (size range: 1680-4000 μm)

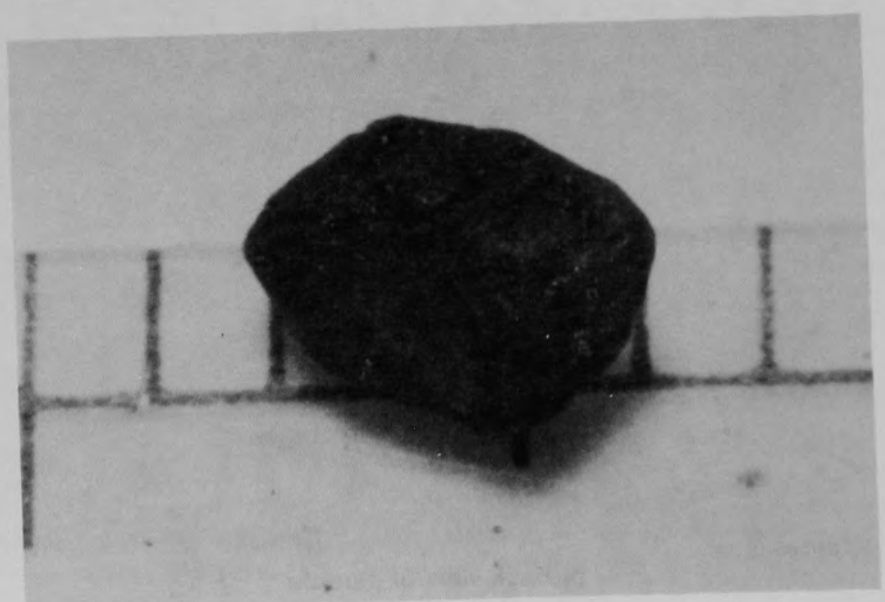

84-546-10-26 b) Particle 8G (size range: 1680-4000 μm)

Figure B-51. Particles fom Sample 8 (H8, 70 cm).

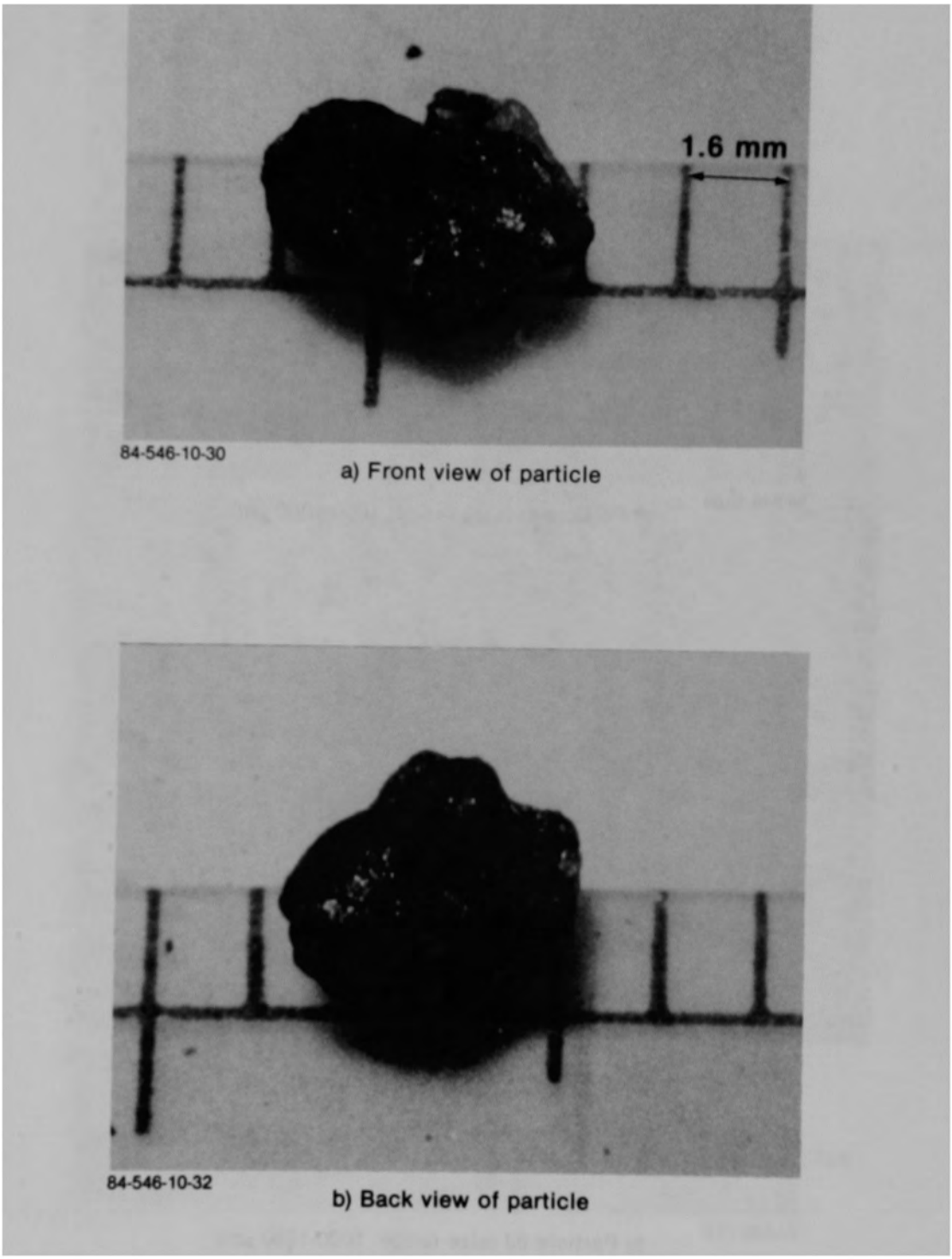

Figure B-52. Particle 8H from Sample 8 (H8, 70 cm), size range: >4000 μm.

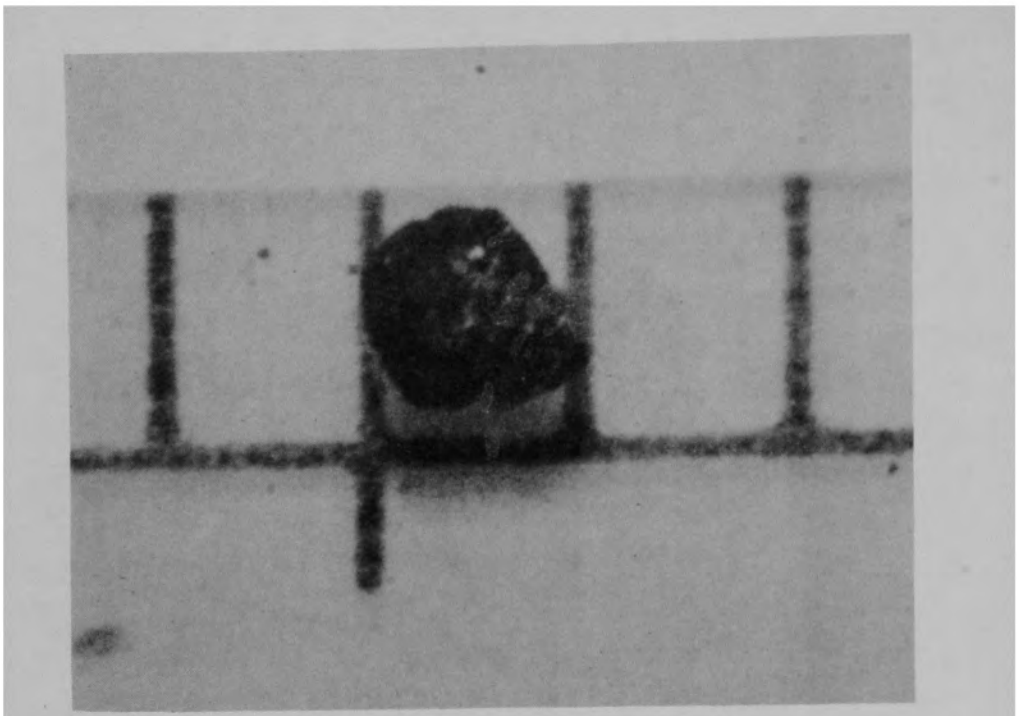

84-546-10-34

a) Particle 8I (size range: 1000-1680 μm)

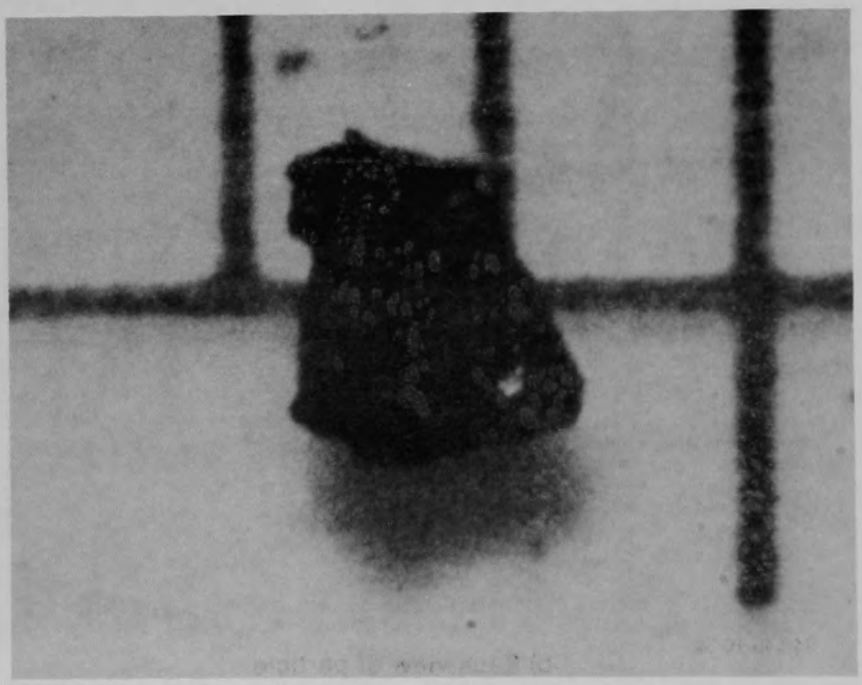

84-546-11-6

b) Particle 8J (size range: 1000-1680 μm)

Figure B-53. Particles from Sample 8 (H8, 70 cm).

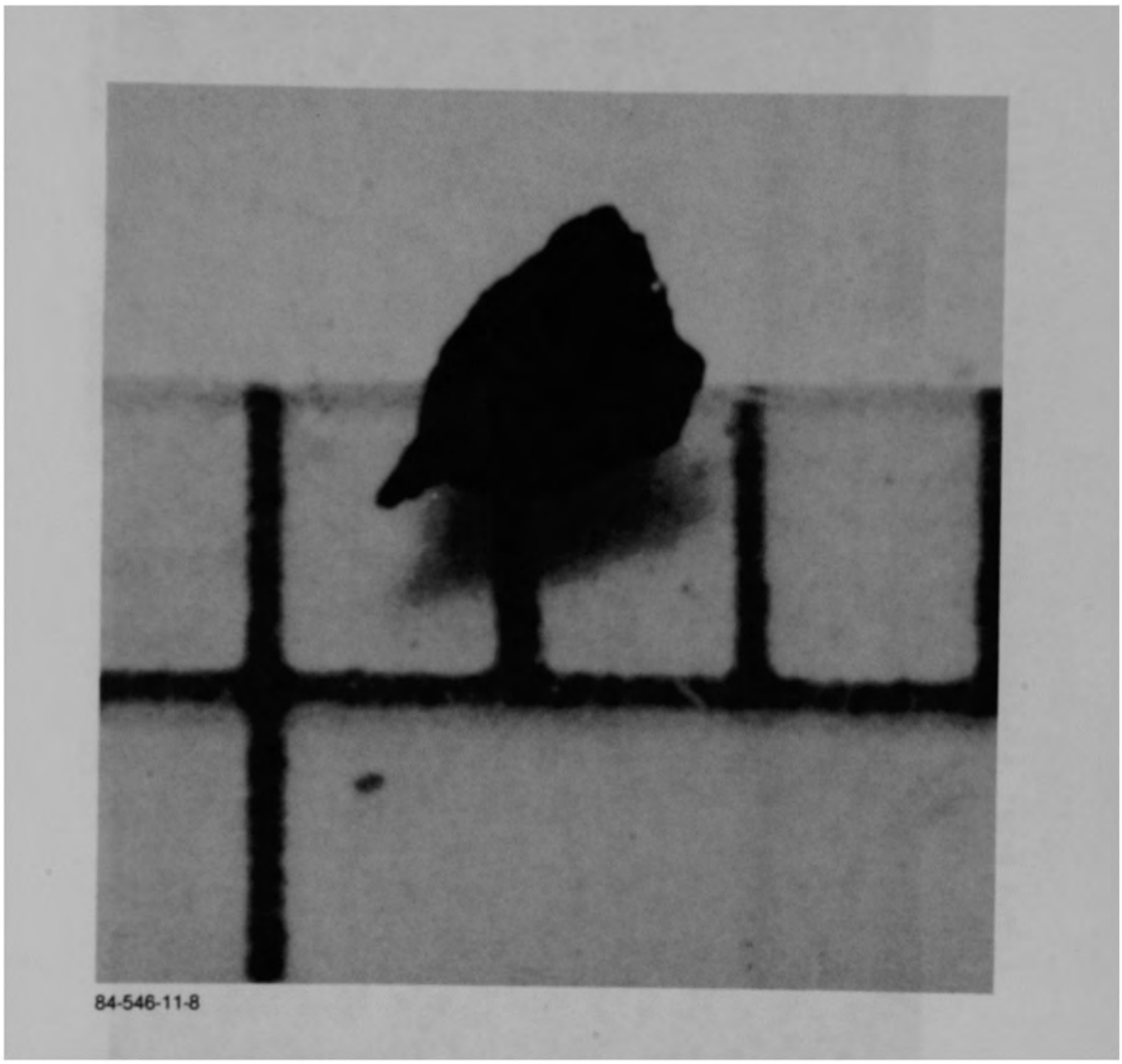

Figure B-54. Particle 8K from Sample 8 (H8, 70 cm), size range: 1000-1680 μm.

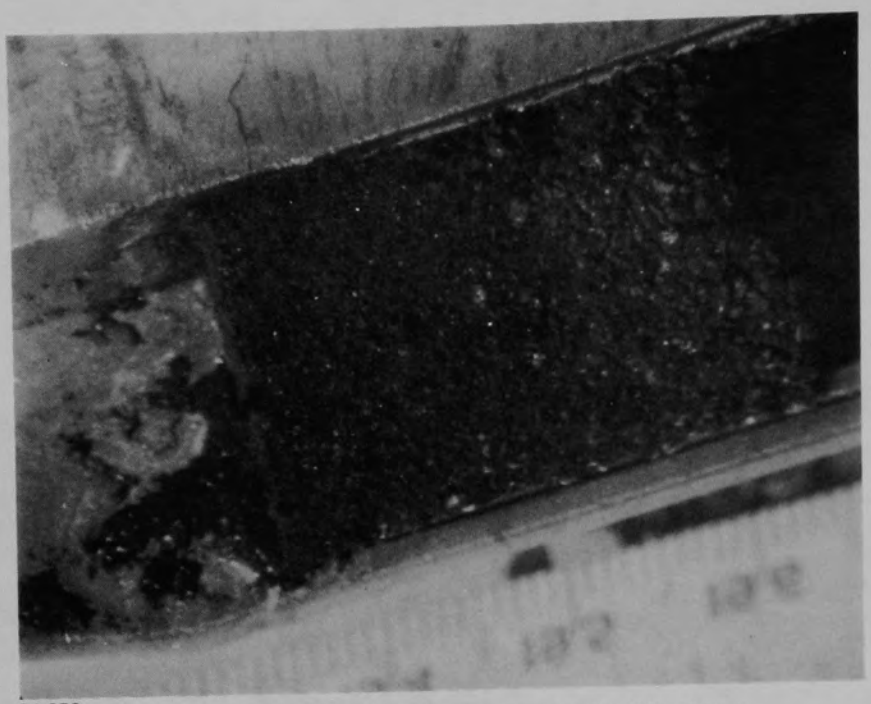

84-250 a) Material in sampling tool (shows stratification)

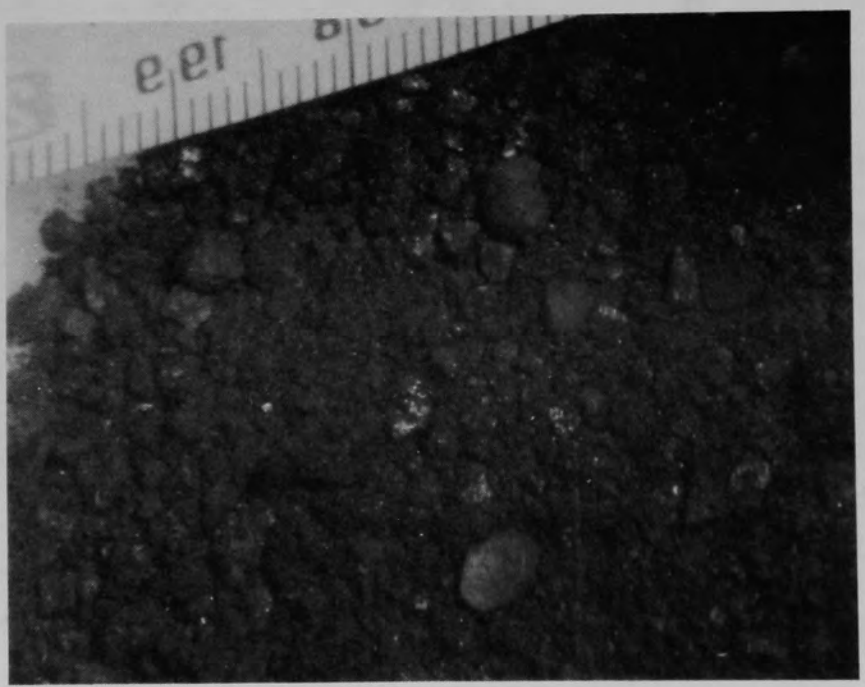

84-253 b) After removing material from sampling tool

Figure B-55. The bulk material for Sample 9 (H8, 77 cm).

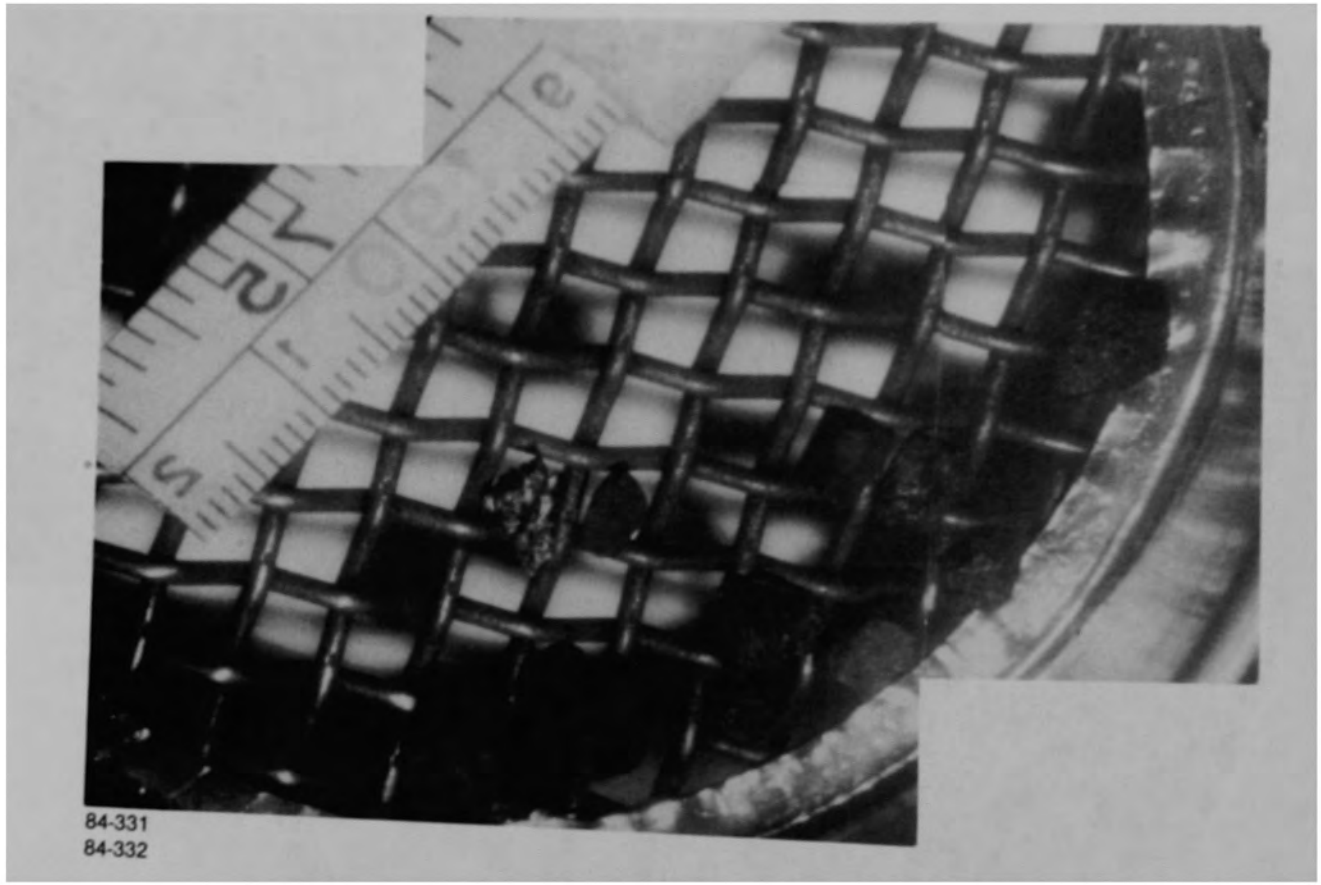

Figure B-56. Particles >4000 µm from Sample 9 (H8, 77 cm).

Figure B-57. Particle size fraction (size range: 1680-4000 μm) from Sample 9, (H8, 77 cm).

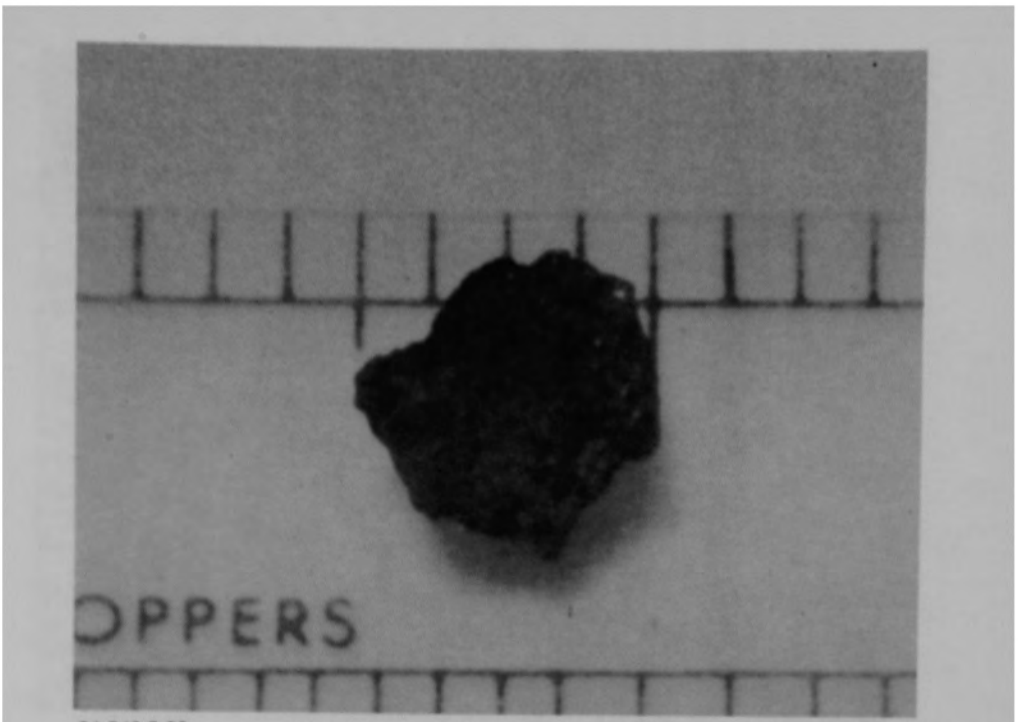

84-546-5-20

a) Front view of particle

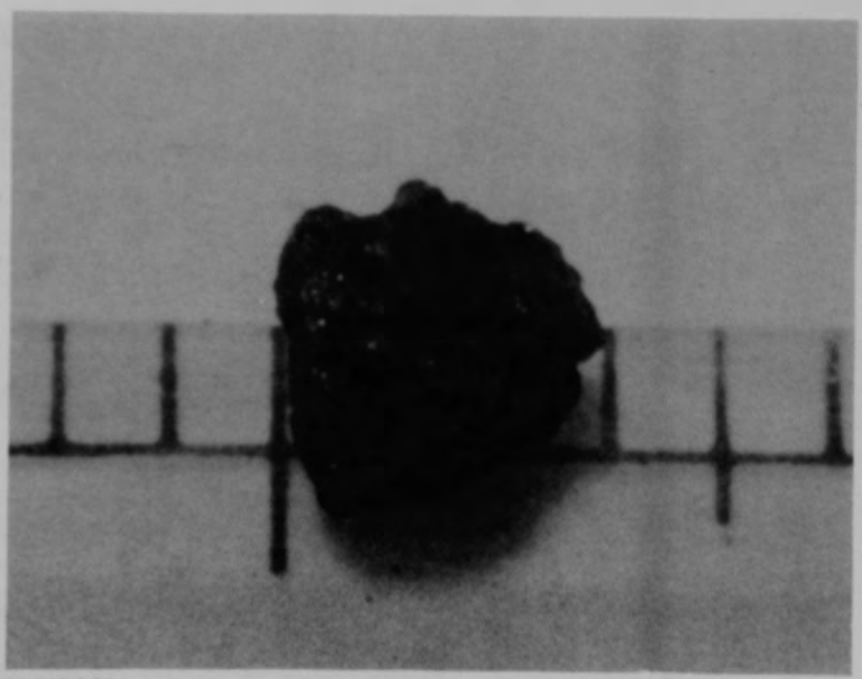

84-546-5-22

b) Back view of particle

Figure B-58. Particle 9A from Sample 9 (H8, 77 cm), size range: >4000 μm.

84-546-5-24

a) Front view of particle

84-546-5-26

b) Back view of particle

Figure B-59. Particle 9B from Sample 9 (H8, 77 cm), size range: >4000 µm.

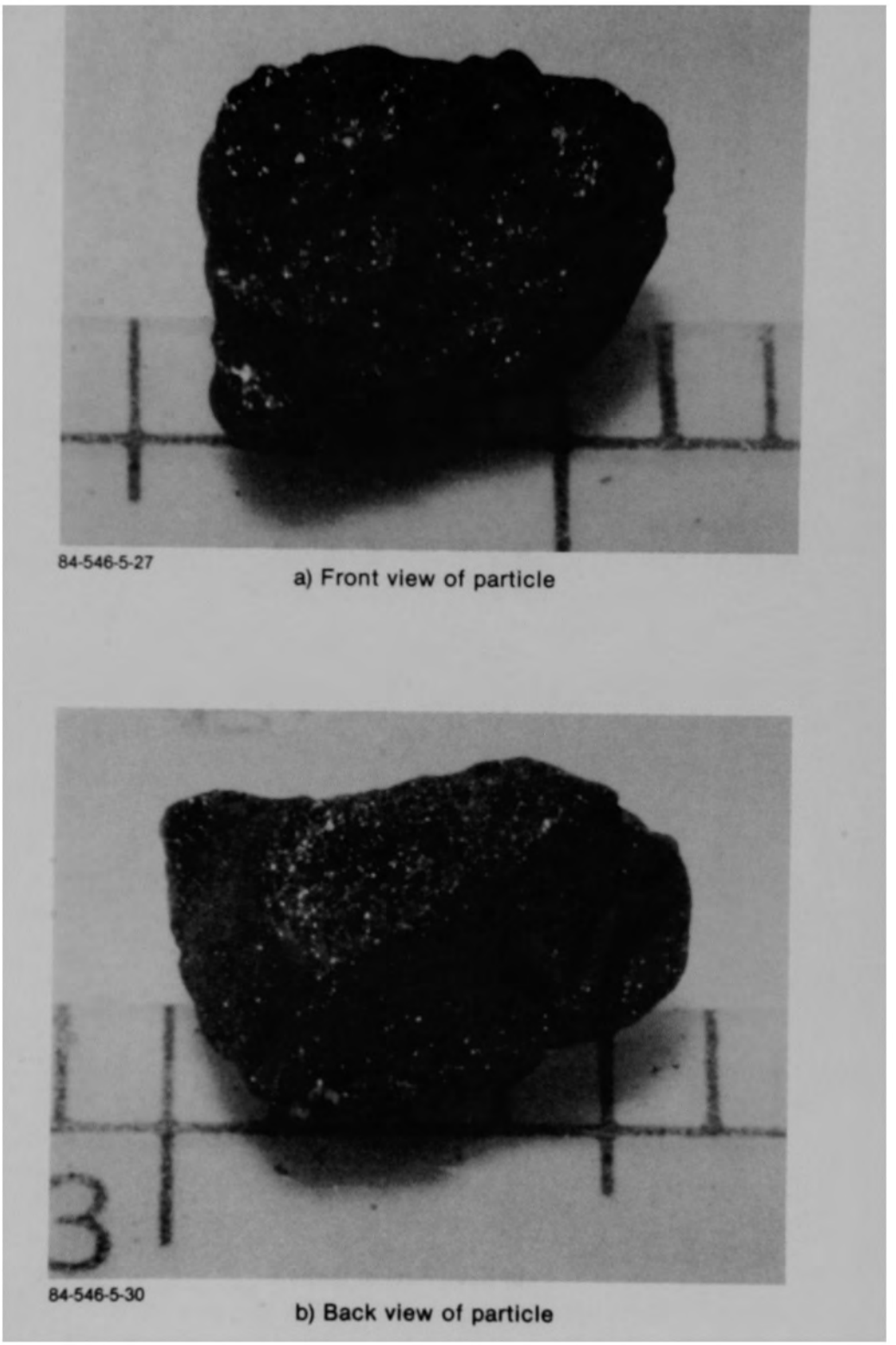

Figure B-60. Particle 9C from Sample 9 (H8, 77 cm), size range: >4000 µm.

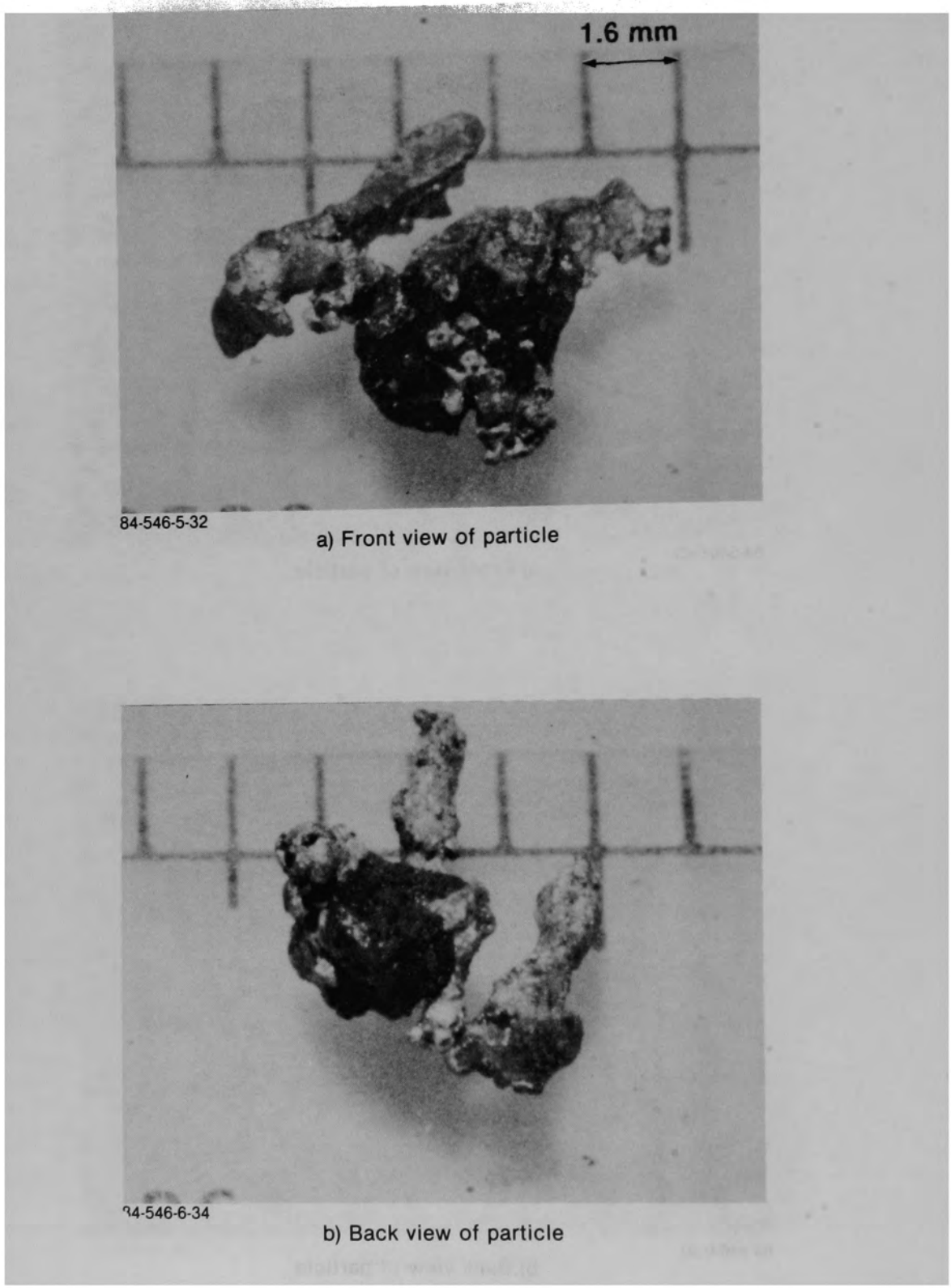

Figure B-61. Particle 9D from Sample 9 (H8, 77 cm), size range: >4000 μm.

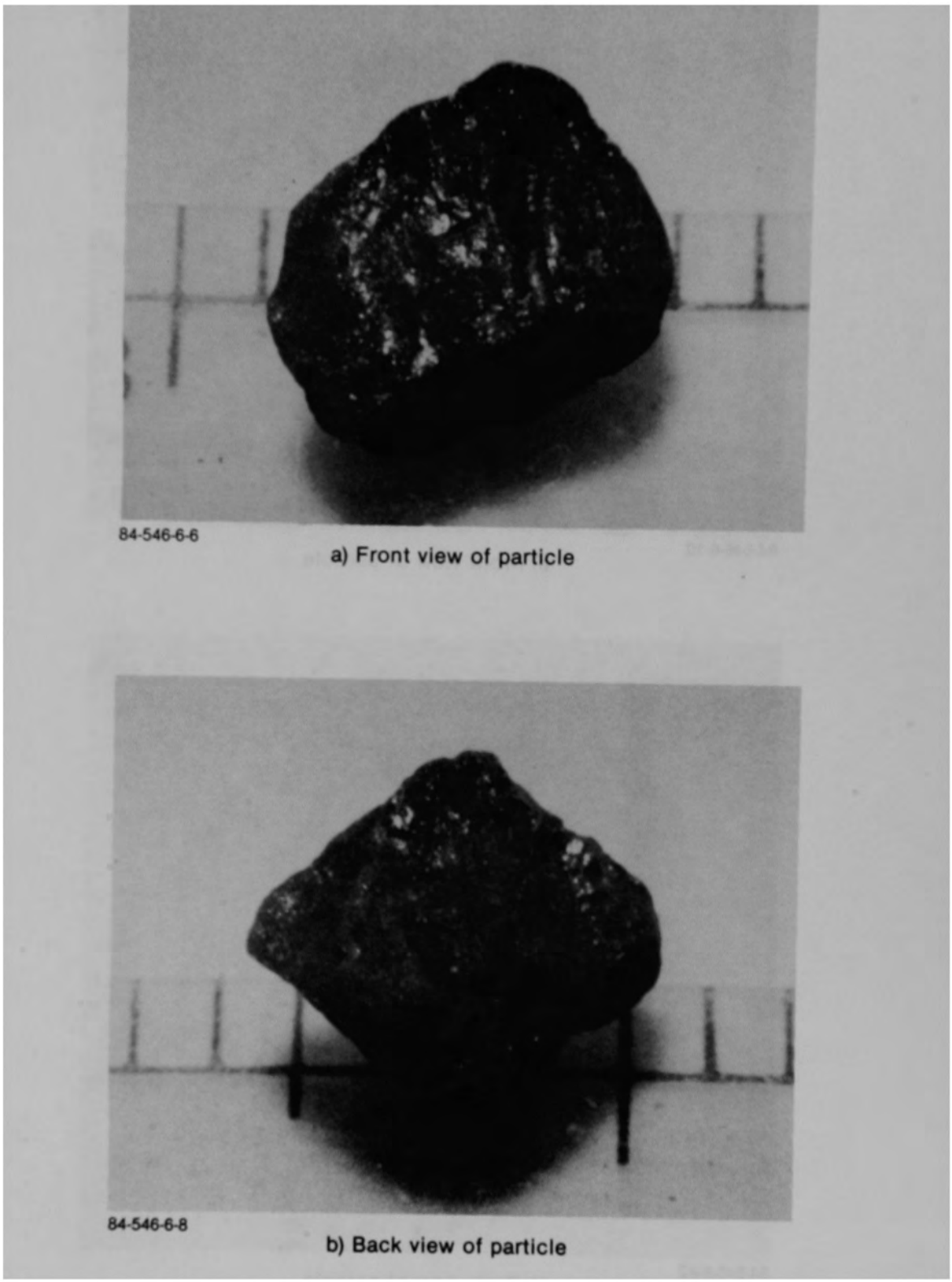

Figure B-62. Particle 9E from Sample 9 (H8, 77 cm), size range: >4000 μm.

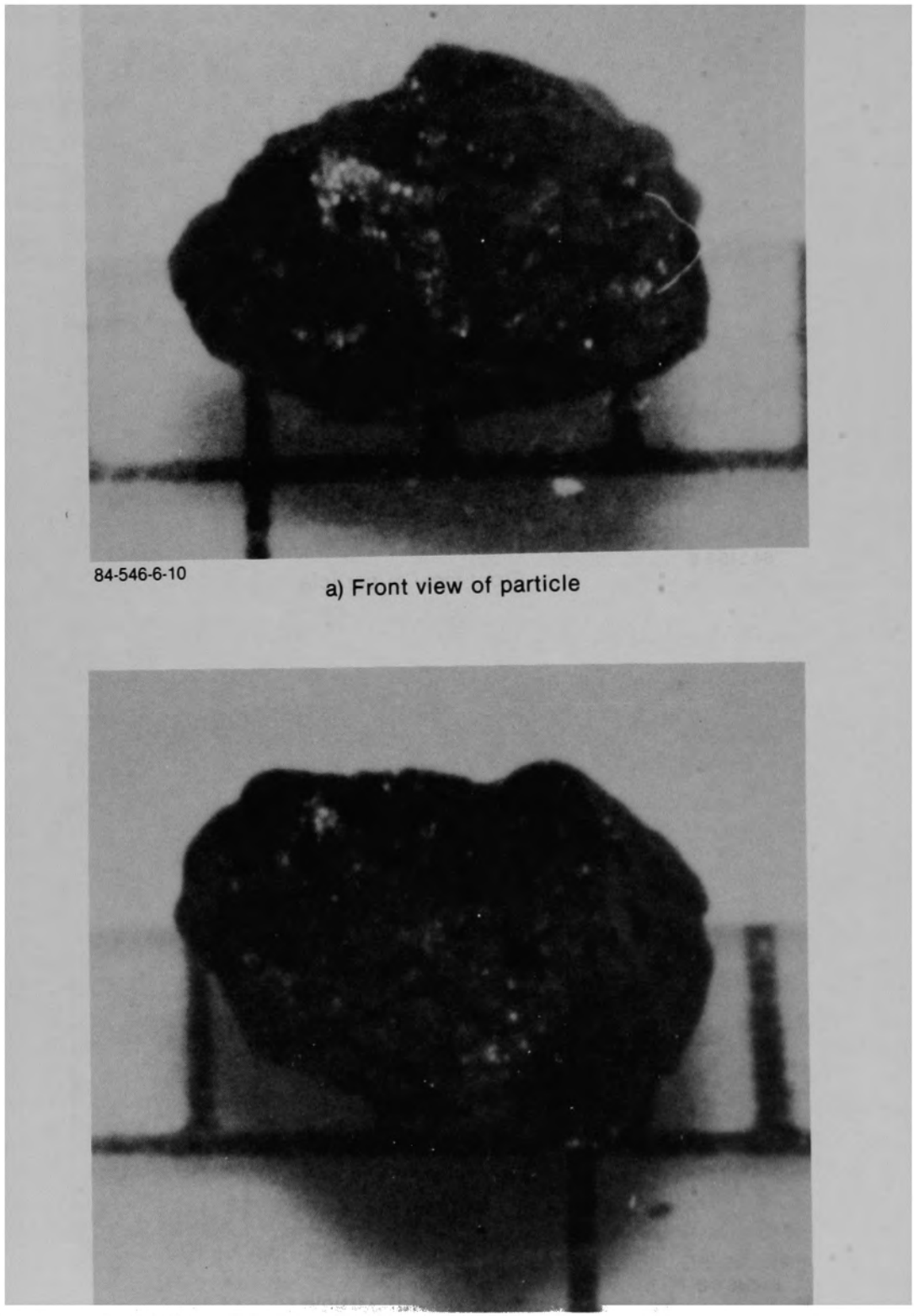

84-546-6-10

a) Front view of particle

84-546-6-12

b) Back view of particle

Figure B-63. Particle 9F from Sample 9 (H8, 77 cm), size range: 1680-4000 μm.

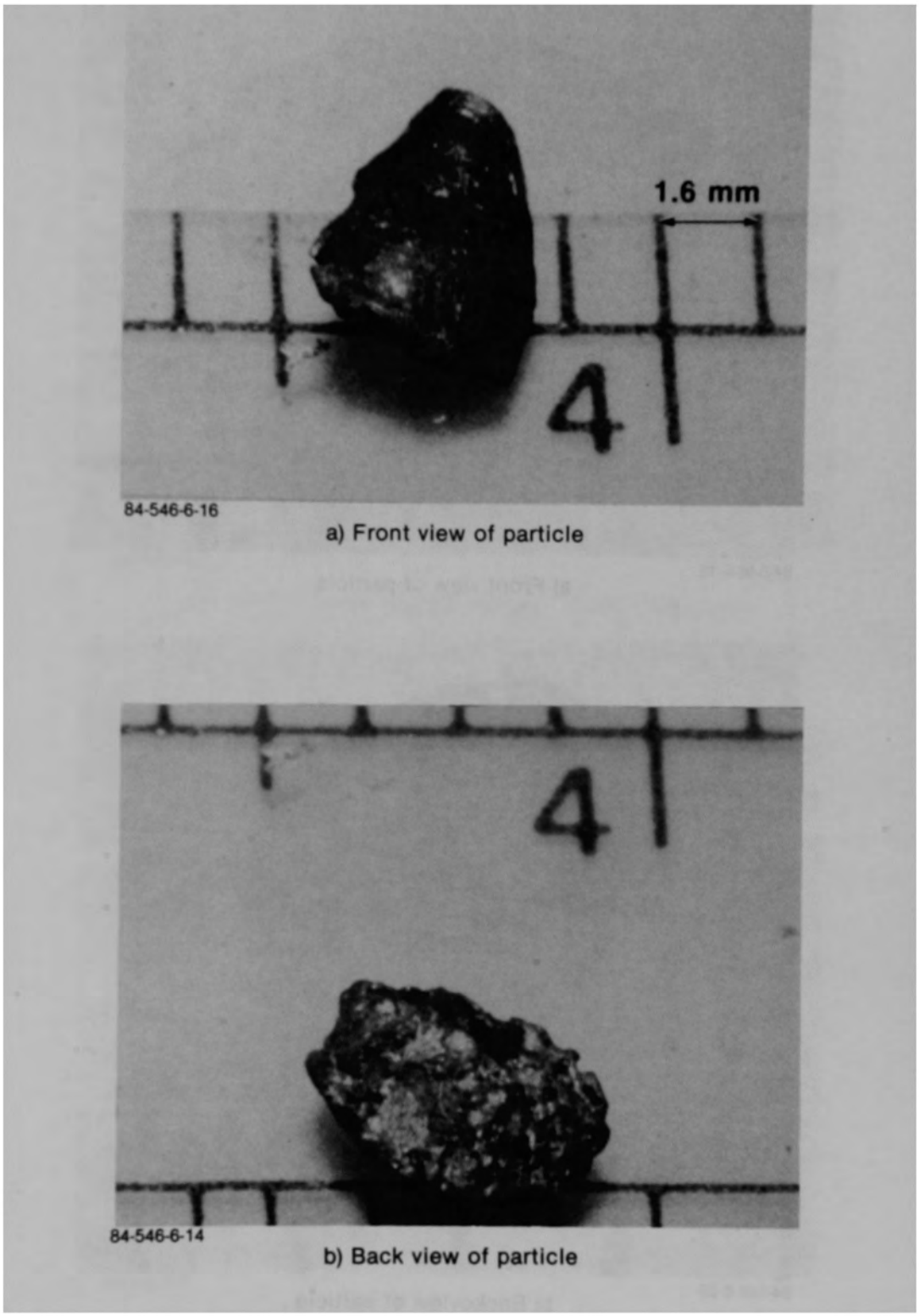

Figure B-64. Particle 96 from Sample 9 (H8, 77 cm), size range: 1680-4000 μm.

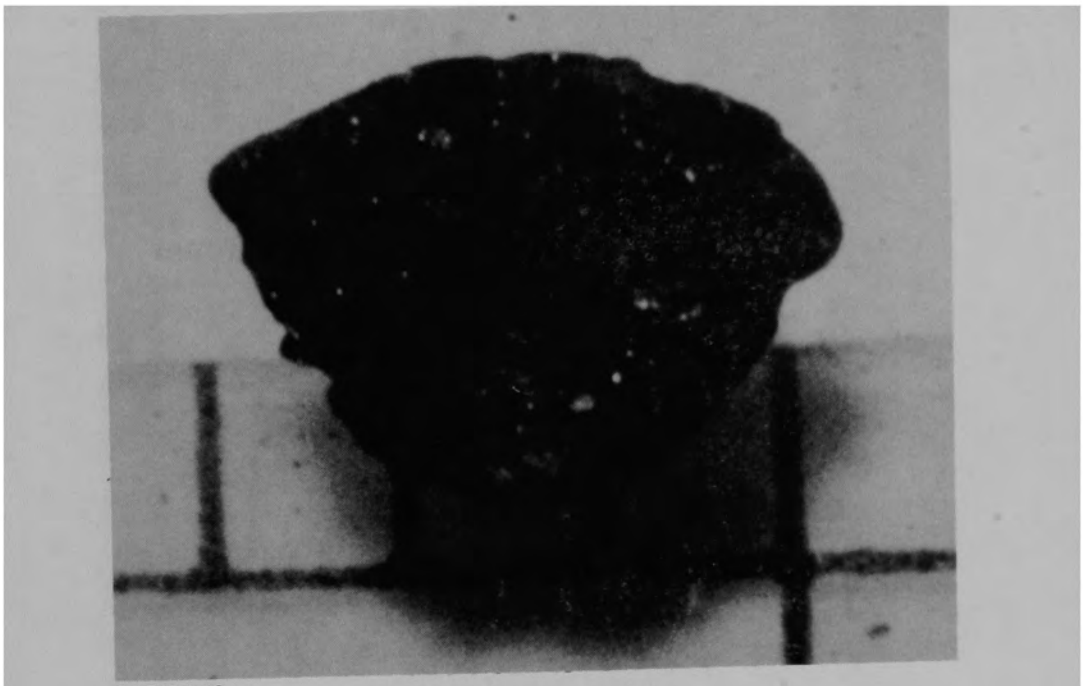

84-546-6-18

a) Front view of particle

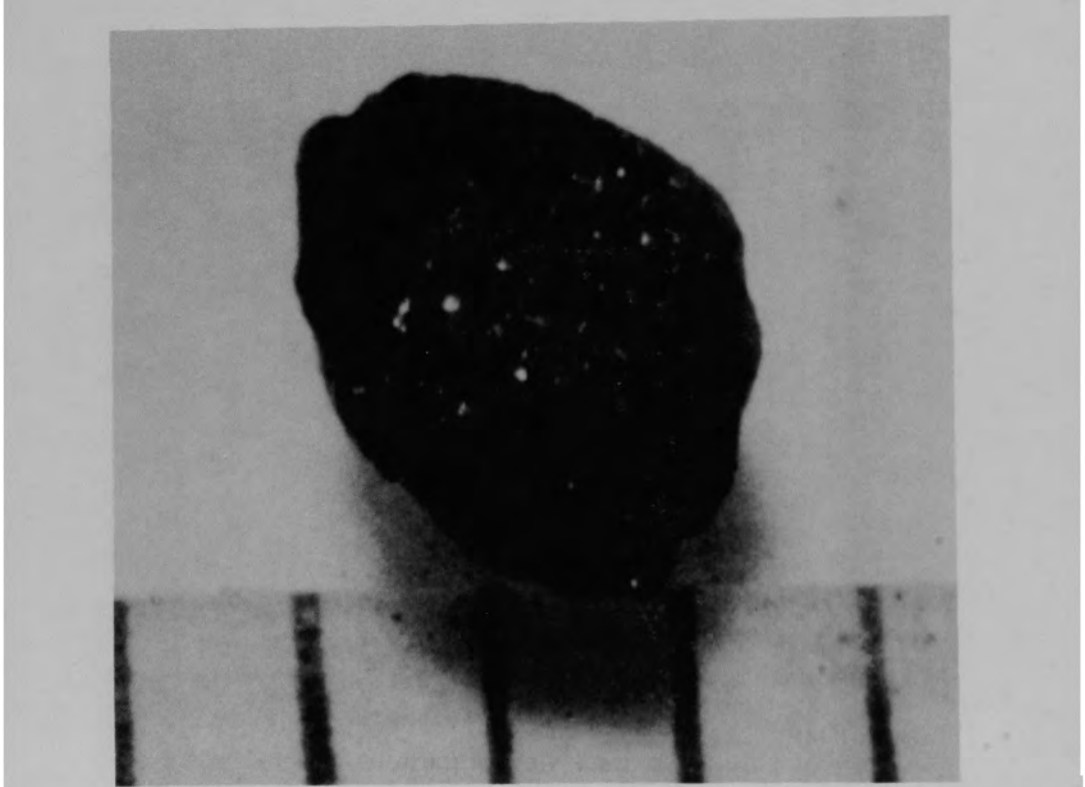

84-546-6-20

b) Backoview of particle

Figure B-65. Particle 9H from Sample 9 (H8, 77 cm), size range: 1680-4000 μm.

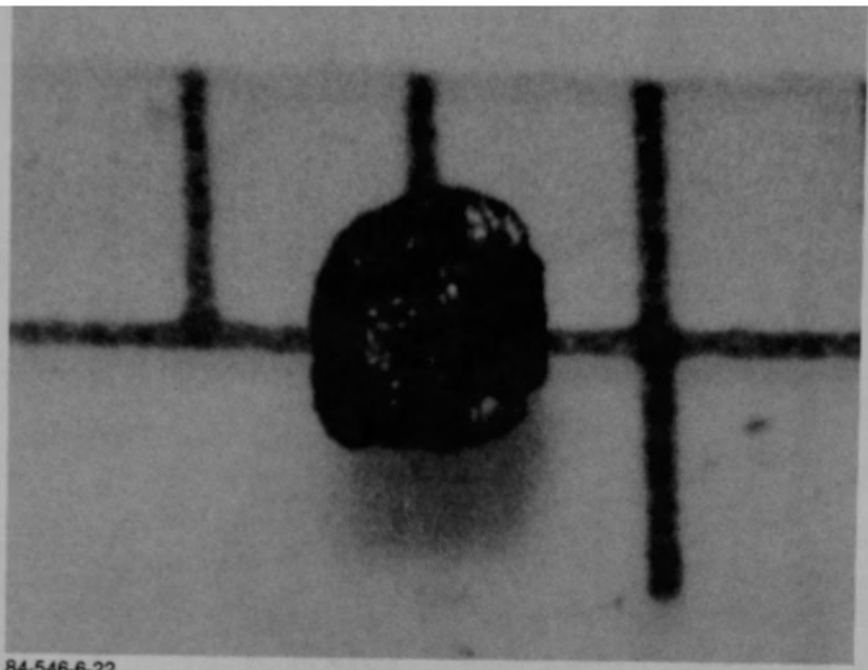

84-546-6-22

a) Particle 9I (size range: 1000-1680 μm)

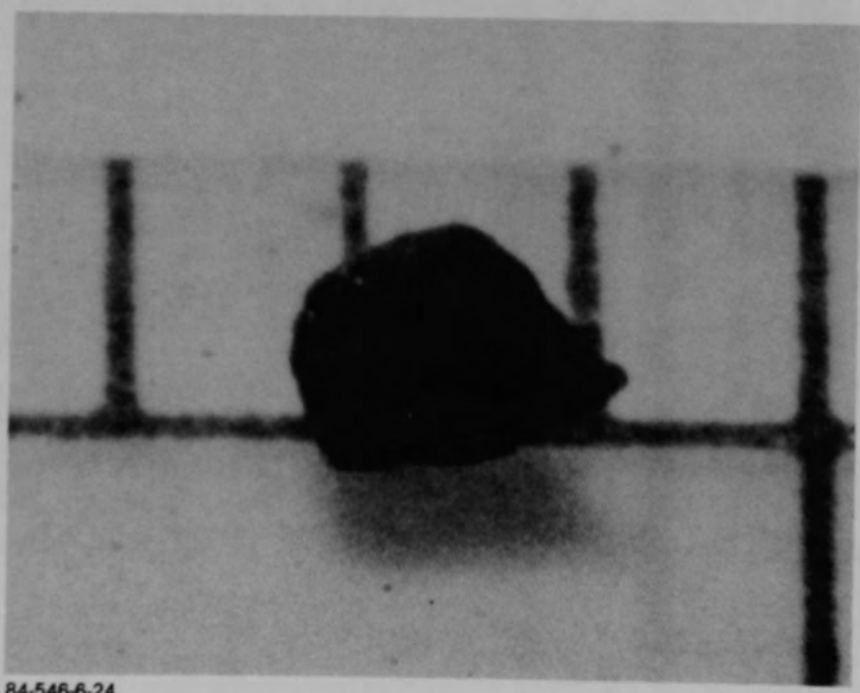

84-546-6-24

b) Particle 9J (size range: 1000-1680 μm)

Figure B-66. Particles from Sample 9 (H8, 77 cm).

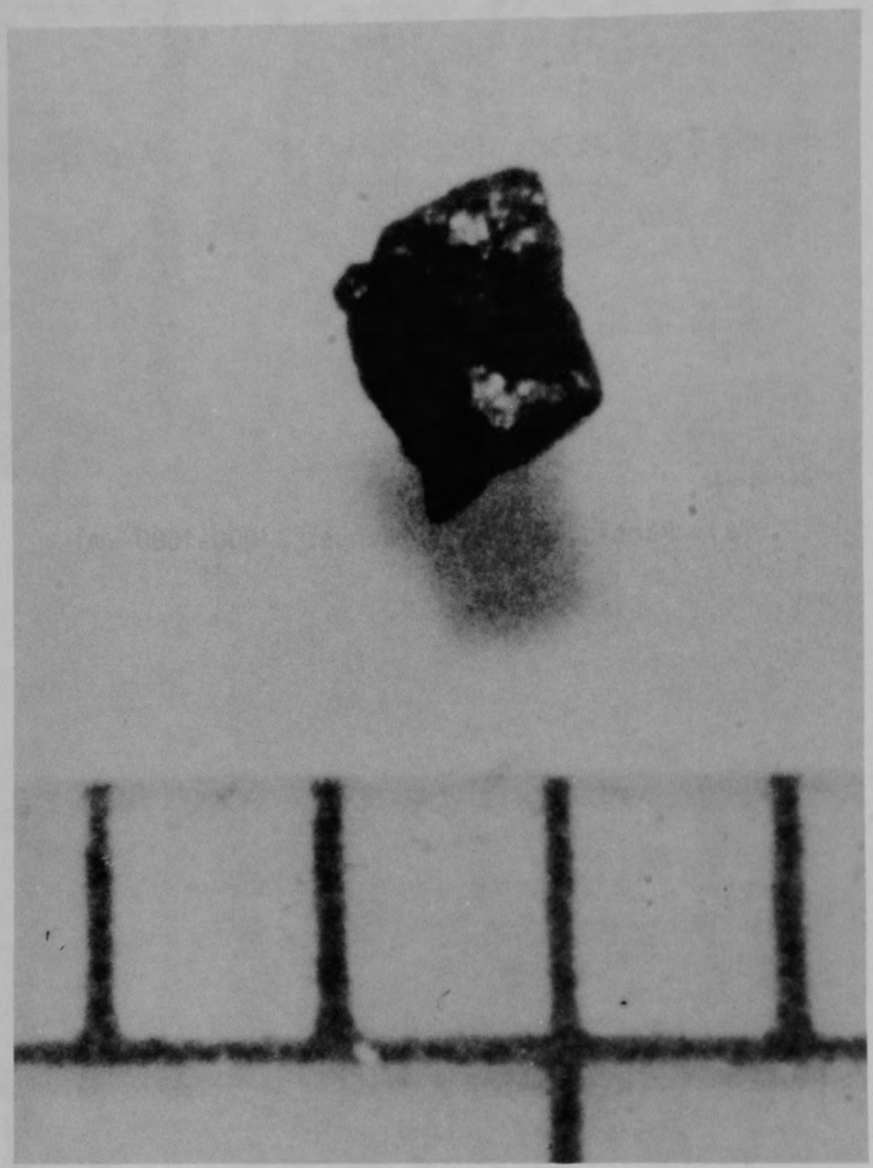

84-546-6-26

Figure B-67. Particle 9K from Sample 9 (H8, 77 cm), size range: 1000-1680 µm.

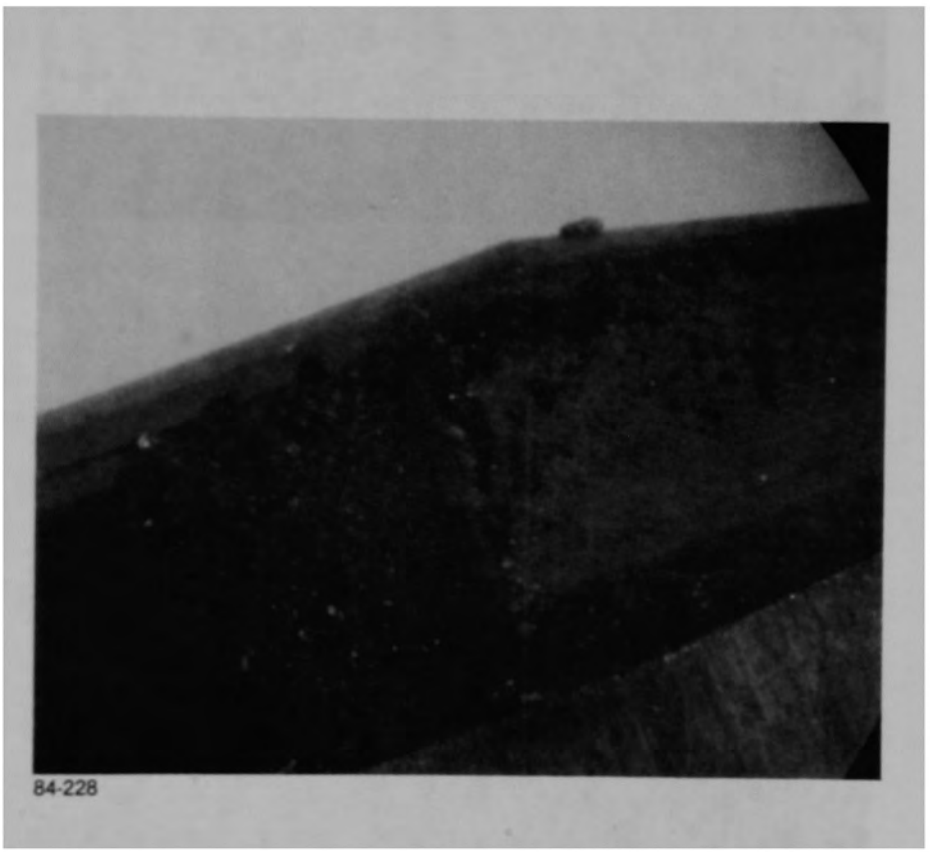

Figure B-68. Sample 10 (E9, 74 cm) being removed from sampling tool.

84-230

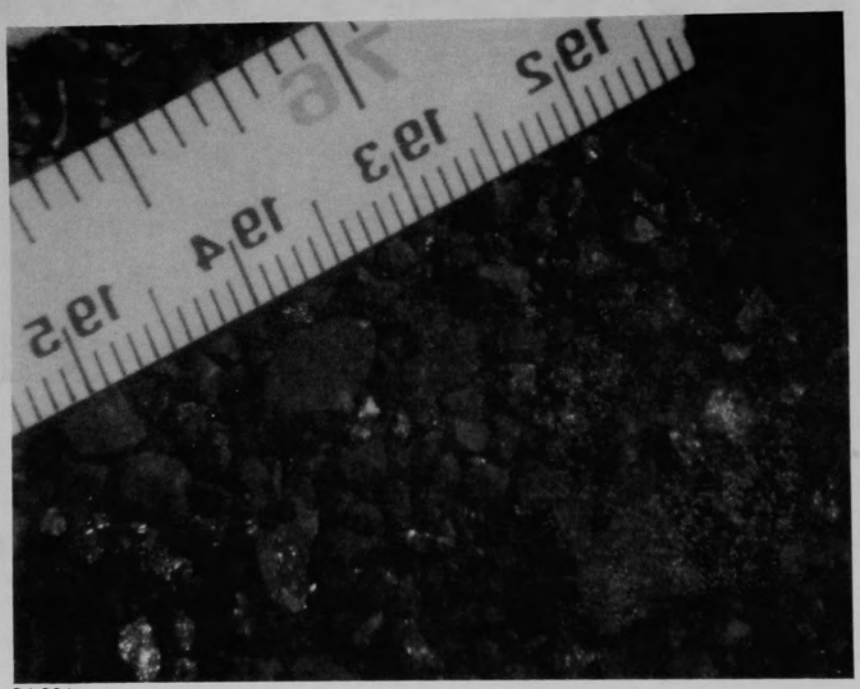

84-231

Figure B-69. Views of the bulk material for Sample 10 (E9, 74 cm) after removal from sampling tool.

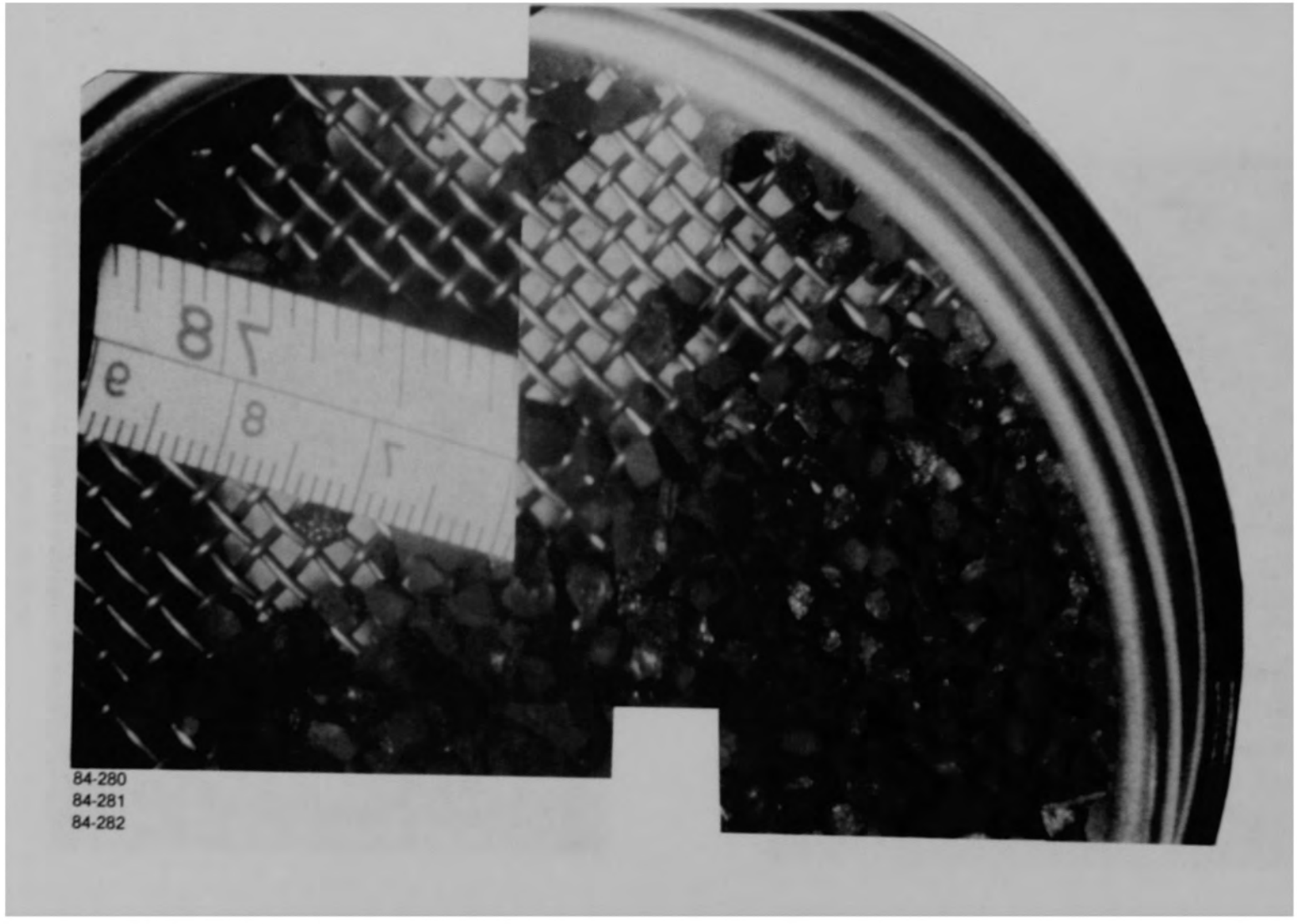

Figure B-70. Particle size fraction (size range: 1680-4000 μm) from Sample 10 (E9, 74 cm).

84-546-4-4

a) Front view of particle

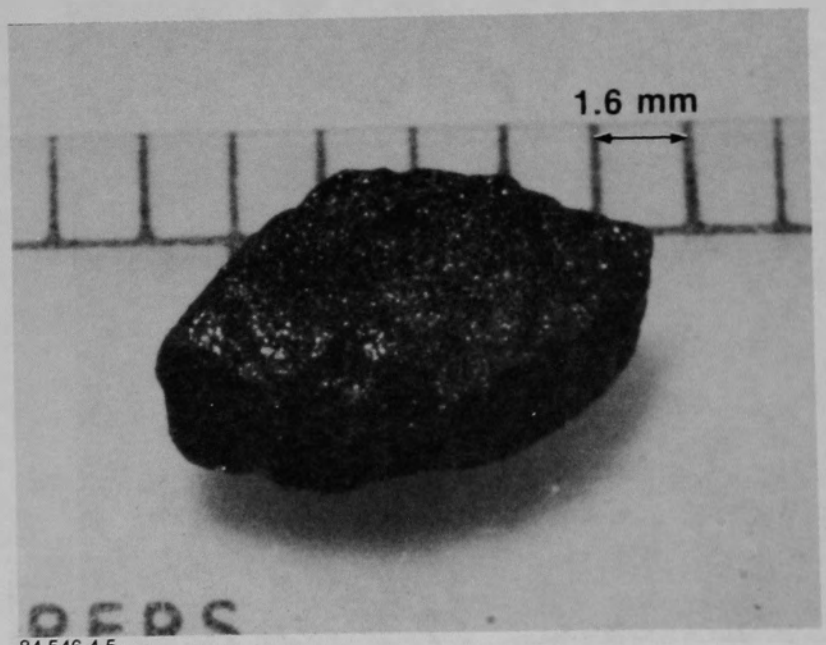

84-546-4-5

b) Back view of particle

Figure B-71. Particle 10A from Sample 10 (E9, 74 cm), size range: >4000 µm.

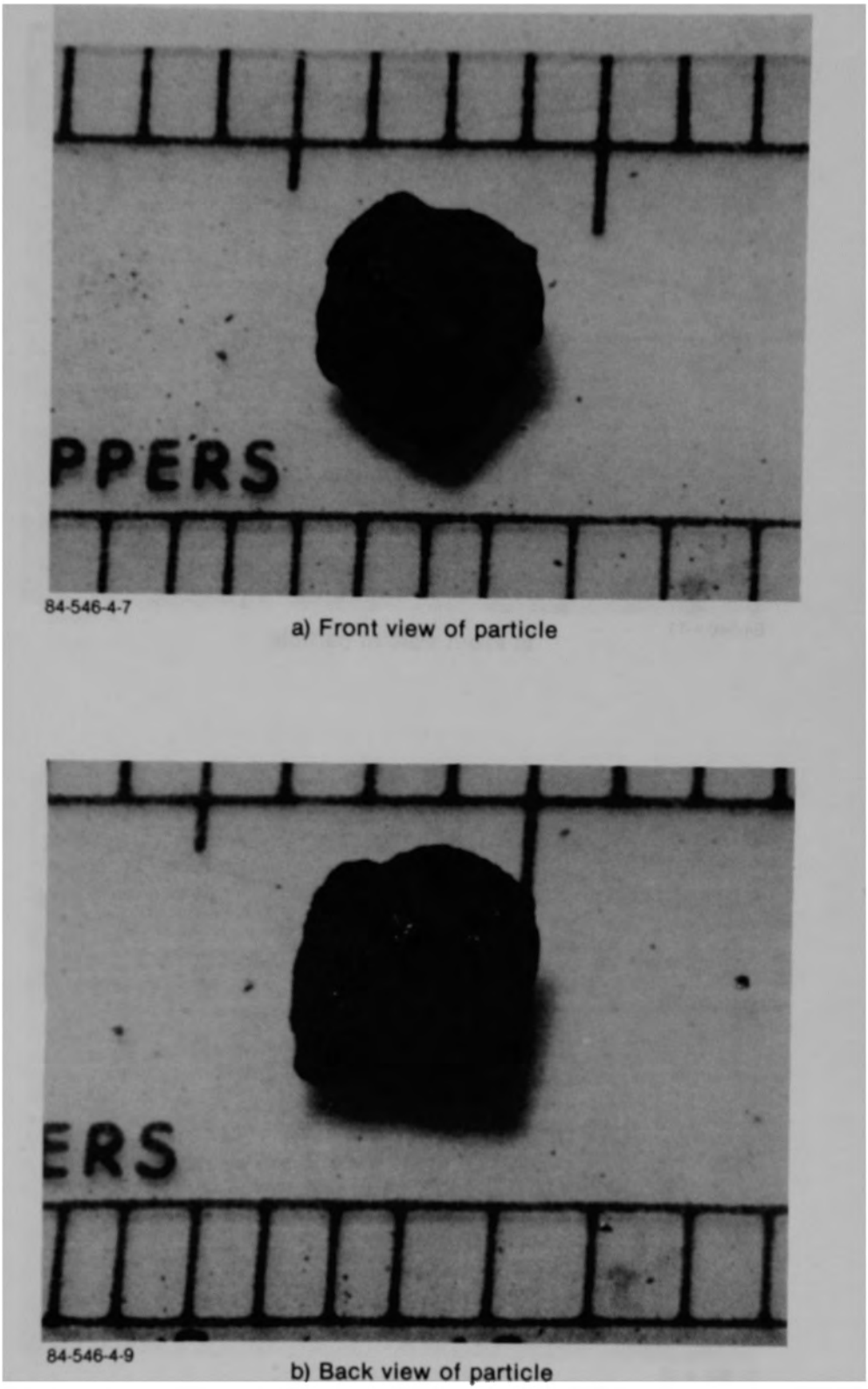

Figure B-72. Particle 10B from Sample 10 (E9, 74 cm), size range: >4000 μm.

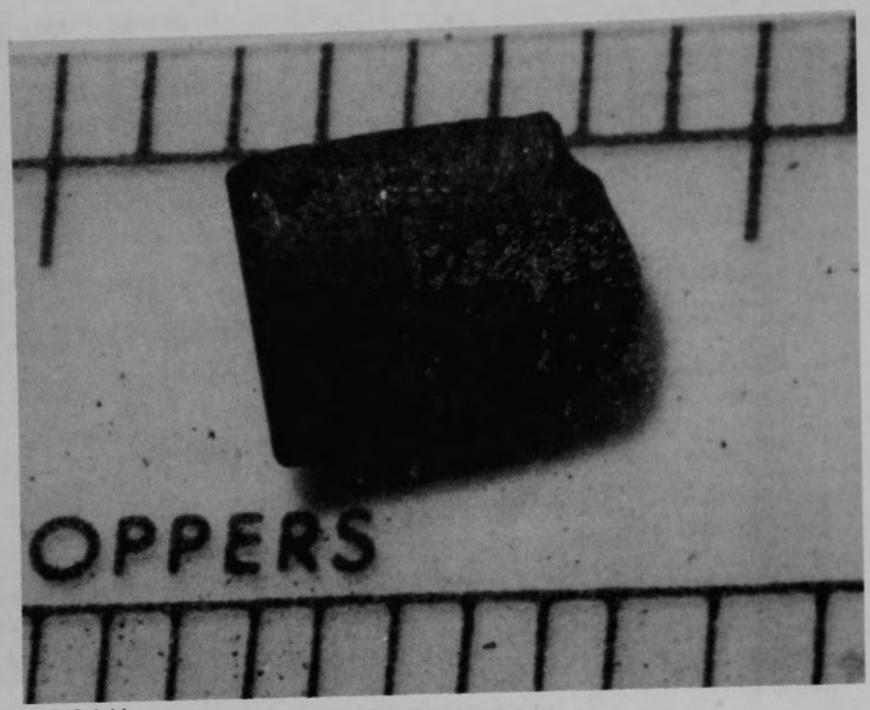

84-546-4-11

a) Front view of particle

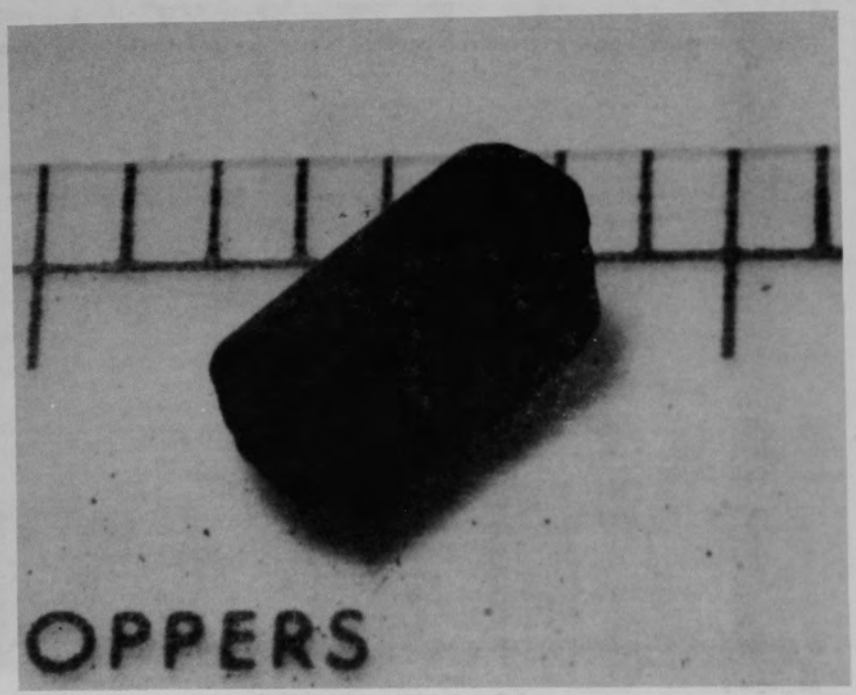

84-546-4-13

b) Back view of particle

Figure B-73. Particle 10C from Sample 10 (E9, 74 cm), size range: >4000 µm.

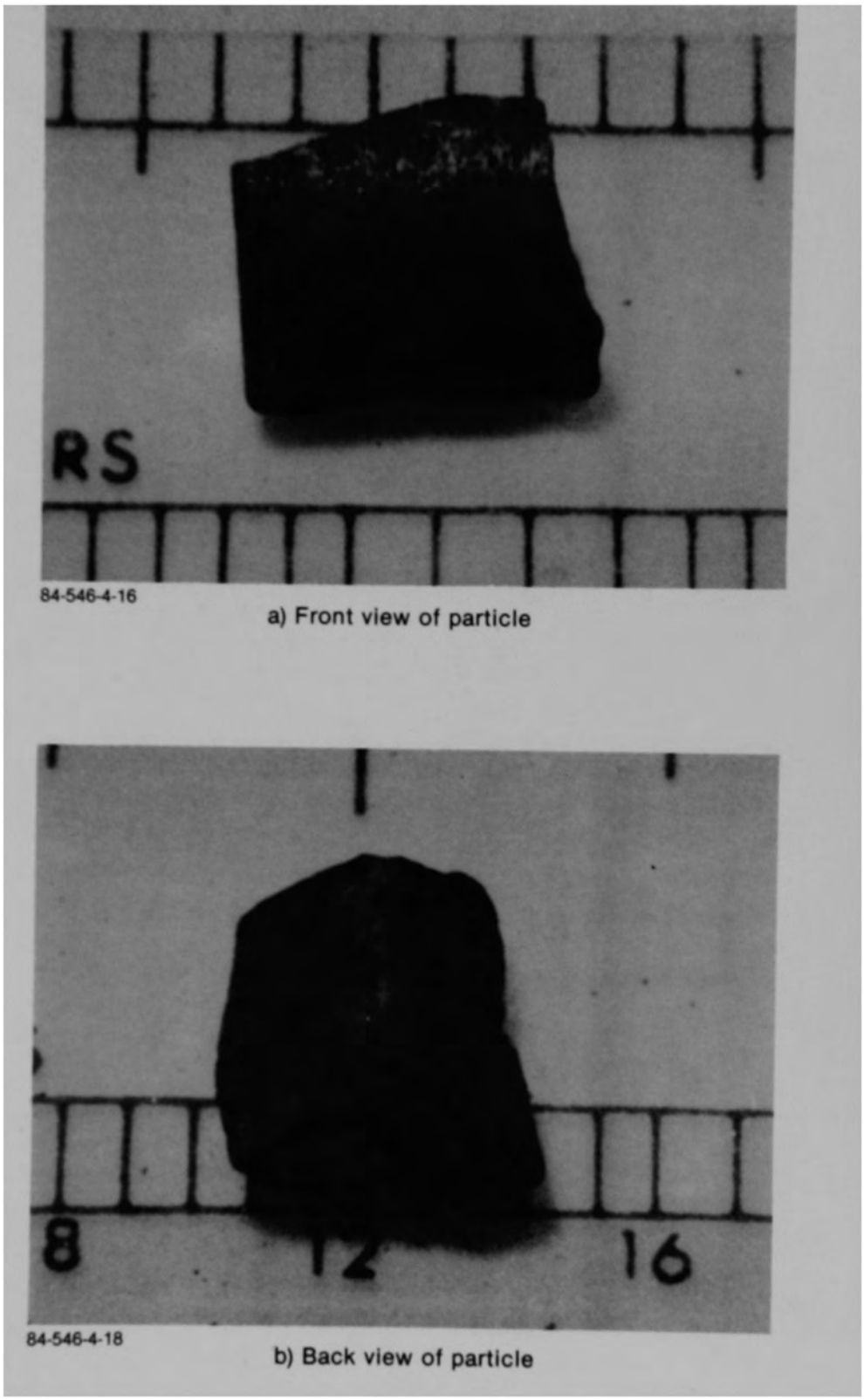

Figure B-74. Particle 10D from Sample 10 (E9, 74 cm), size range: >4000 μm.

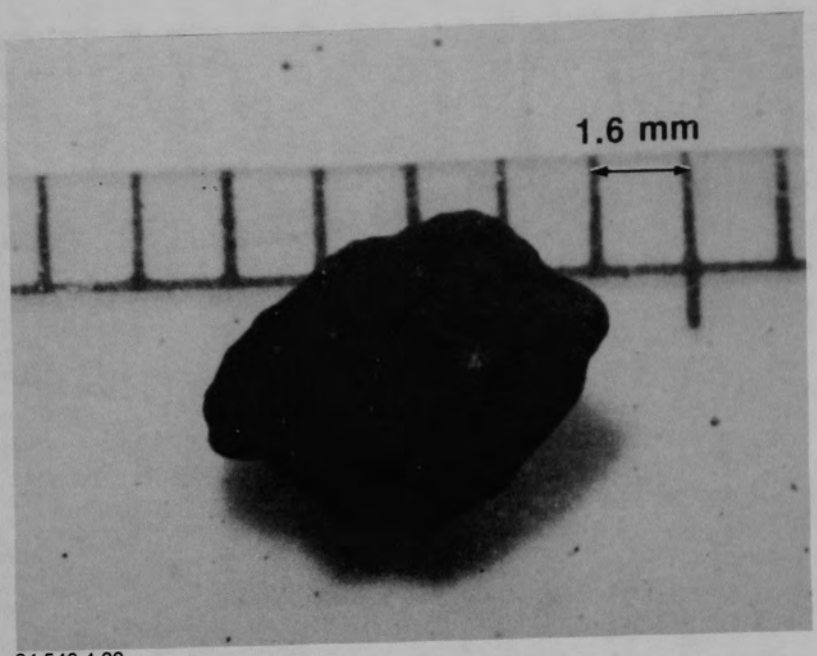

84-546-4-20

a) Front view of particle

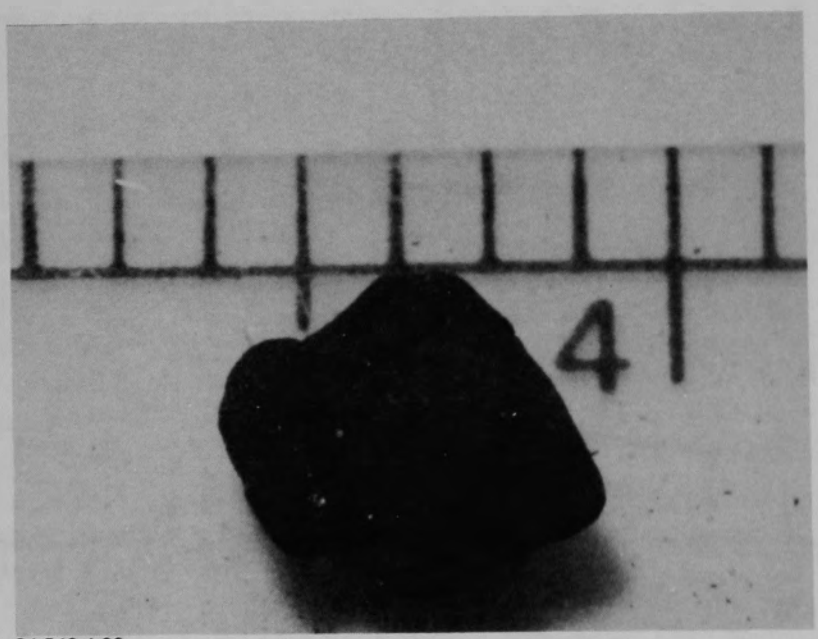

84-546-4-22

b) Back view of particle

Figure B-75. Particle 10E from Sample 10 (E9, 74 cm), size range: >4000 µm.

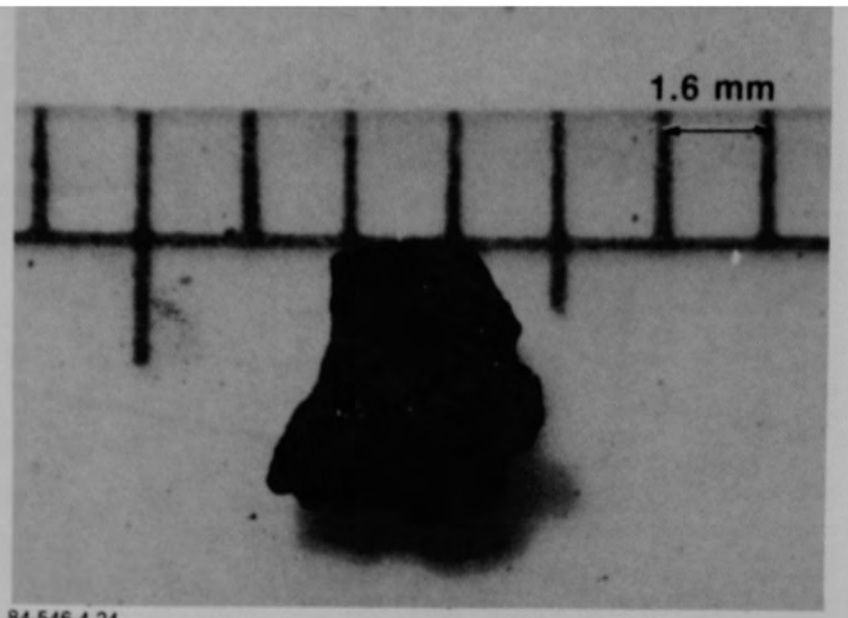

84-546-4-24

a) Particle 10F (size range: 1680-4000 μm)

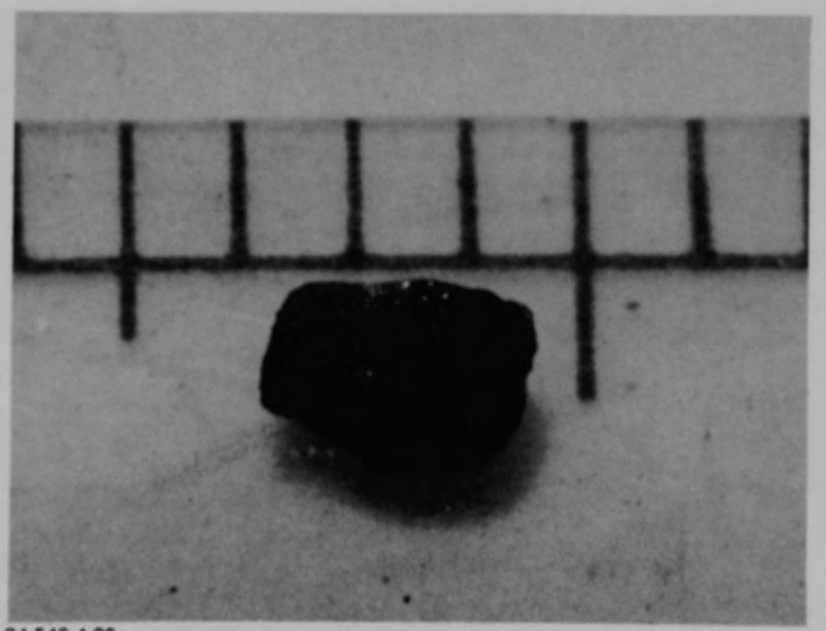

84-546-4-26

b) Particle 10G (size range: 1680-4000 μm)

Figure B-76. Particles from Sample 10 (E9, 74 cm).

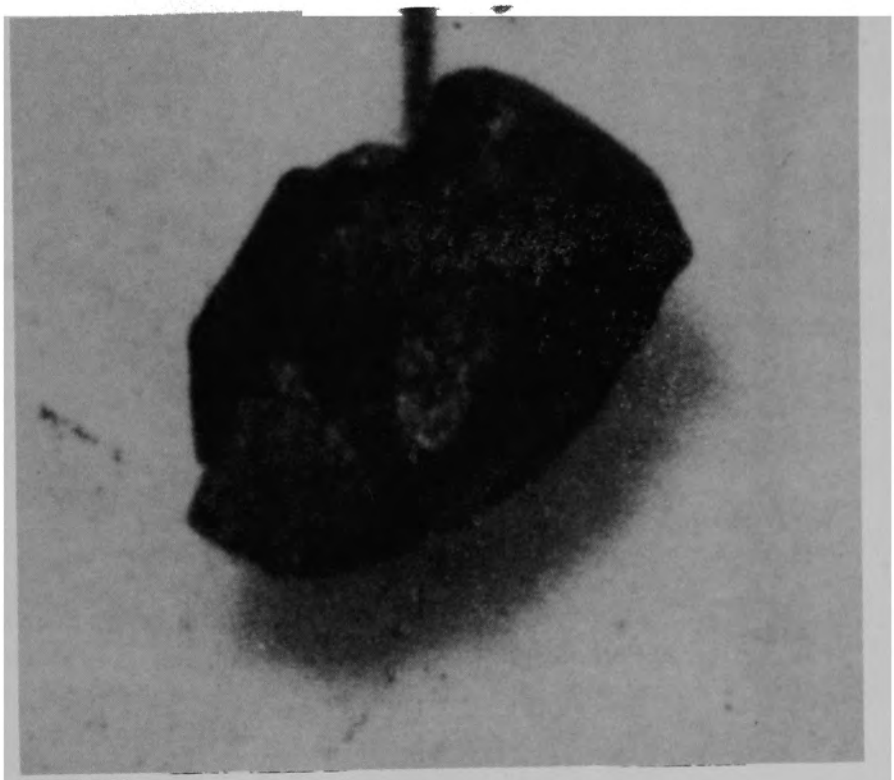

84-546-4-28

a) Particle 10H (size range: 1680-4000 μm)

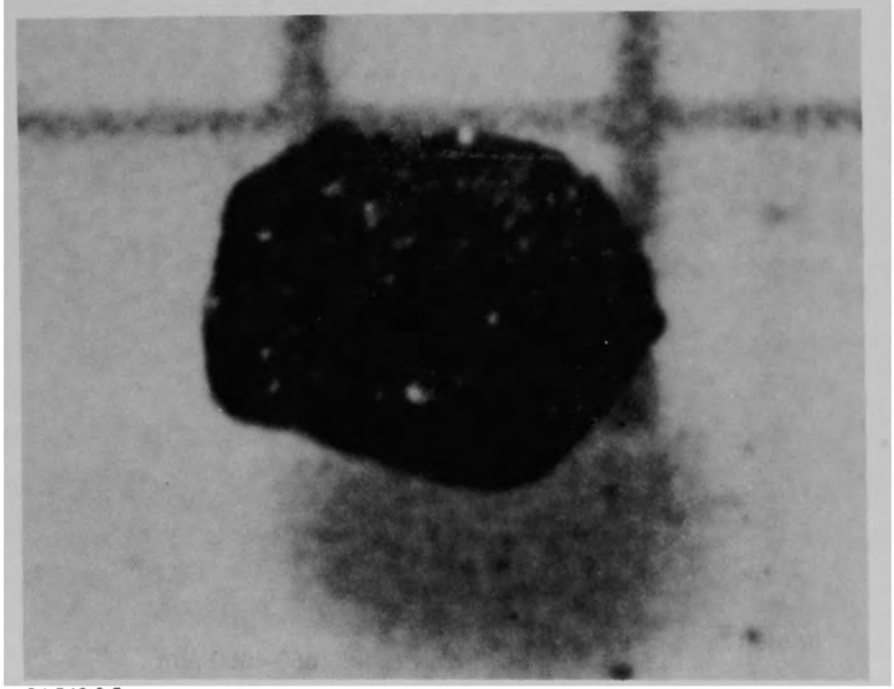

84-546-3-5

b) Particle 10I (size range: 1000-1680 μm)

Figure B-77. Particles from Sample 10 (E9, 74 cm).

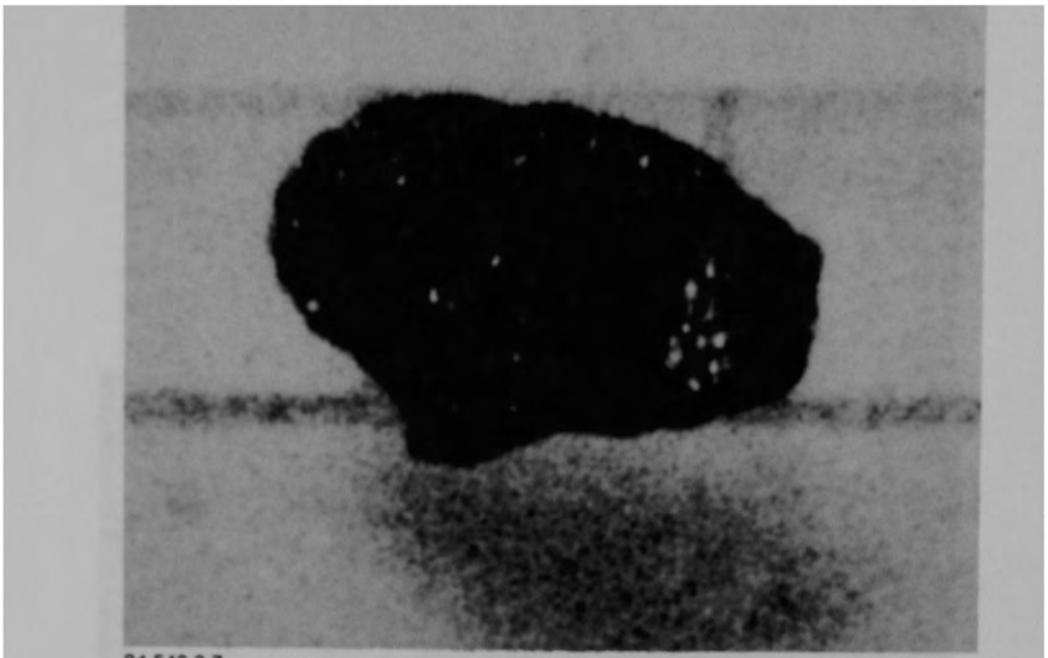

84-546-3-7

a) Particle 10J (size range: 1000-1680 μm)

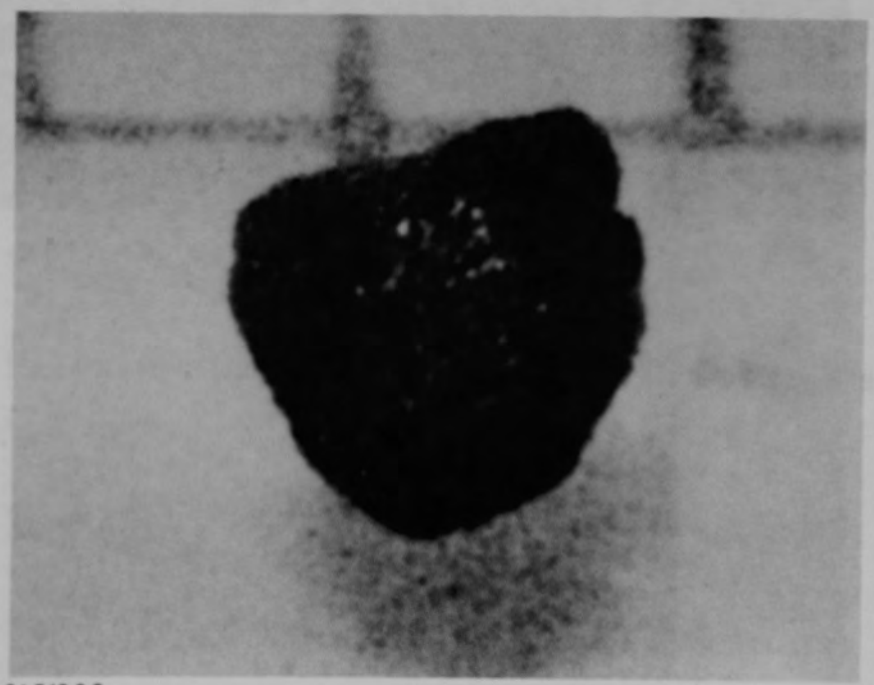

84-546-3-9

b) Particle 10K (size range: 1000-1680 μm)

Figure B-78. Particles from Sample 10 (E9, 74 cm).

84-233

Figure B-79. Sample 11 (E9, 94 cm) being removed from sampling tool.

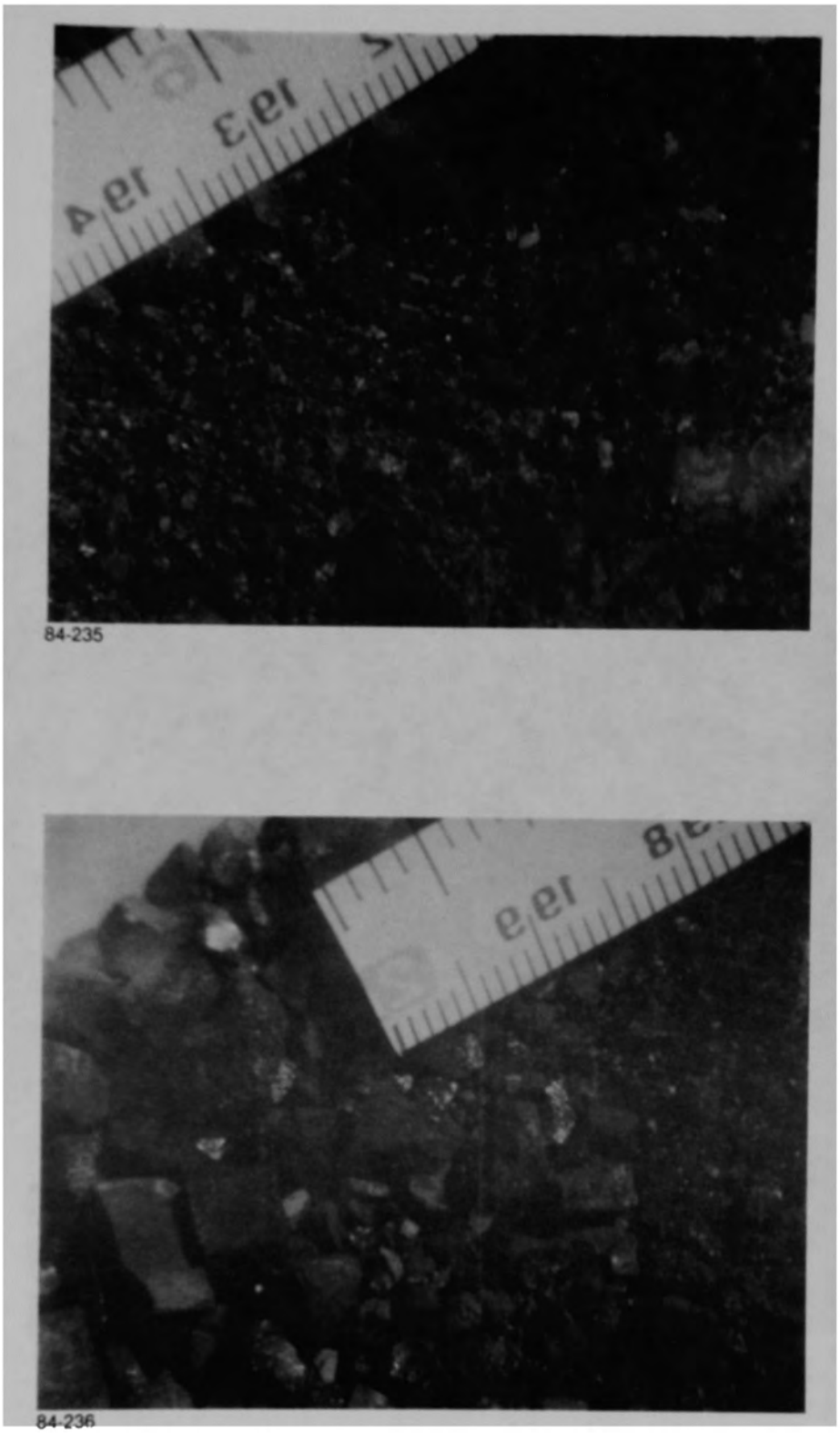

Figure B-80. Views of the bulk material for Sample 11 (E9, 94 cm) after removal from the sampling tool.

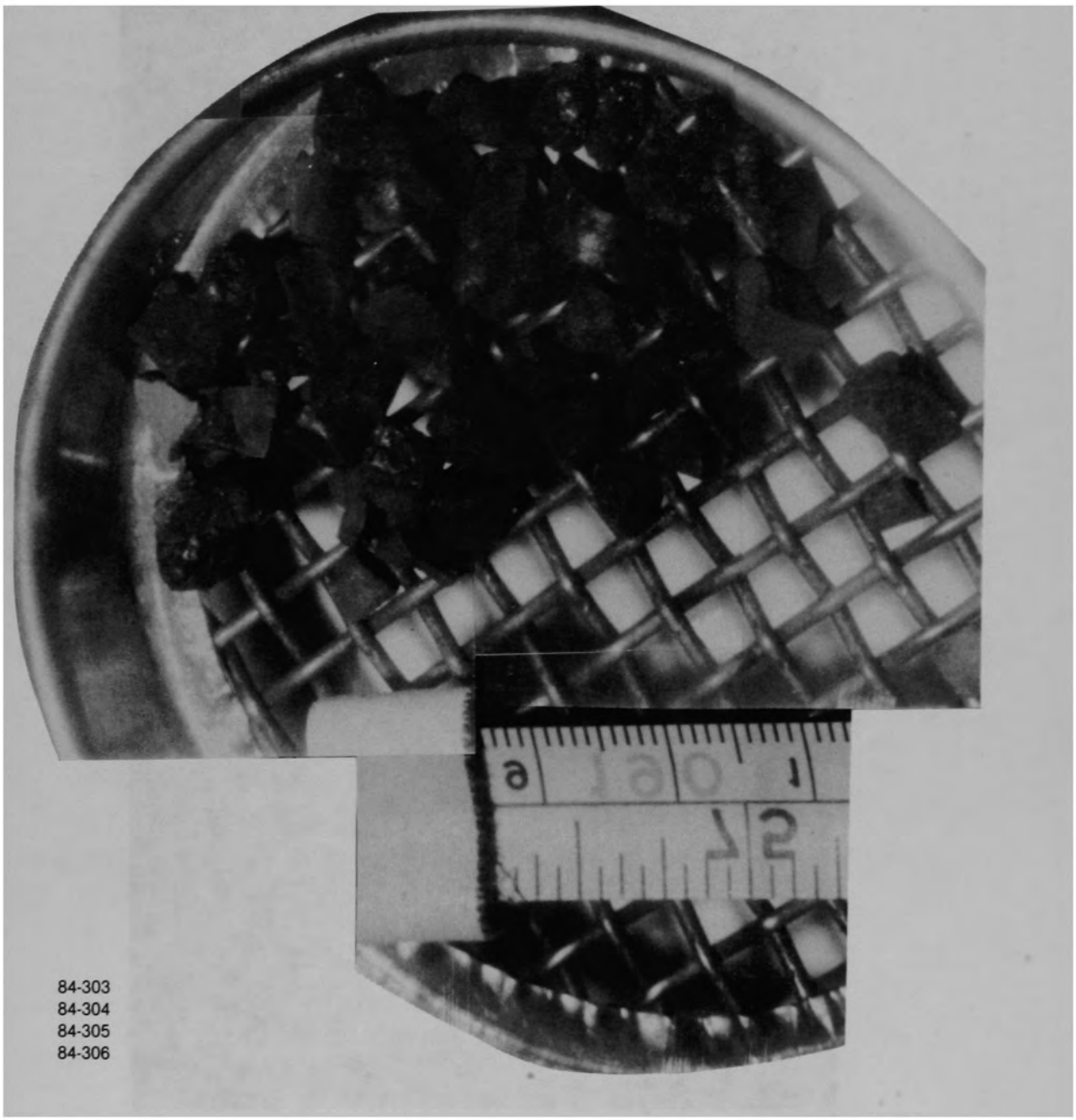

Figure B-81. Particles >4000 μm for Sample 11 (E9, 94 cm).

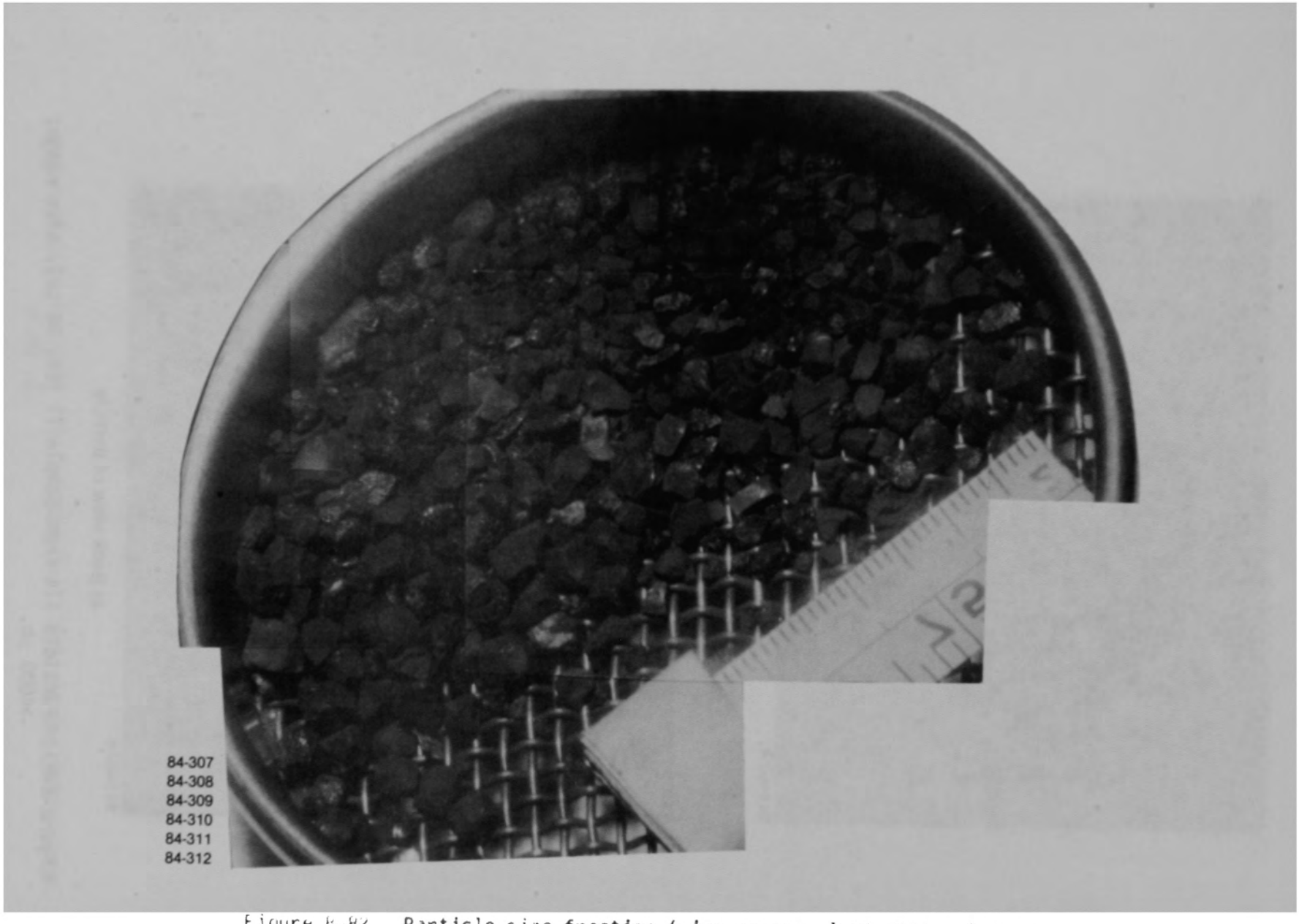

Figure 8-82. Particle size fraction (size range: 1680-4000 µm) from Sample 11 (E9, 94 cm).

84-546-7-4

a) Front view of particle

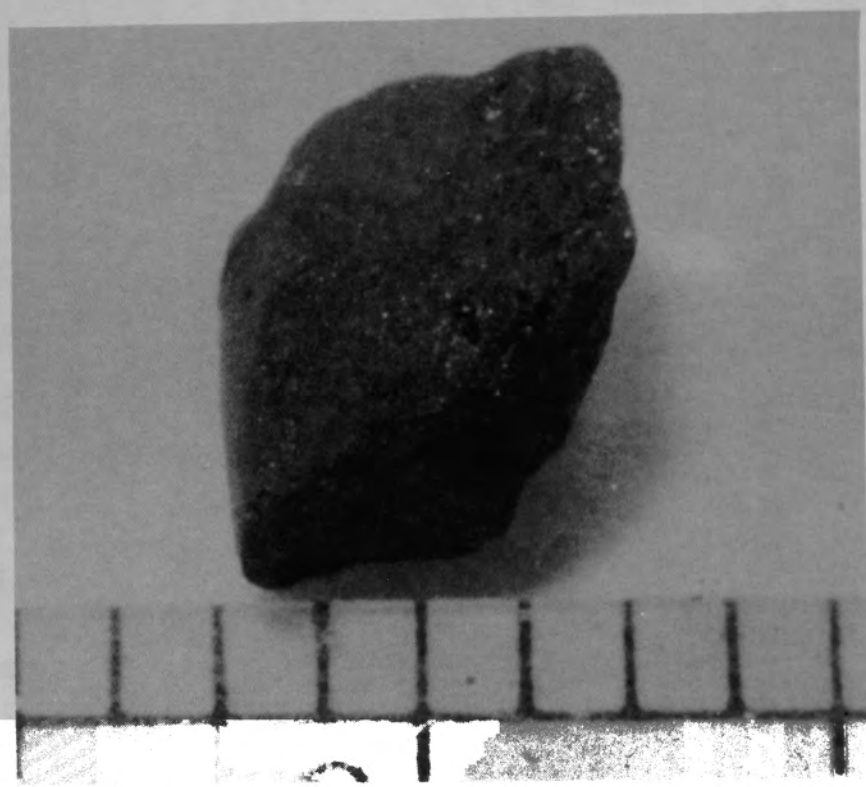

84-546-7-6

b) Back view of particle

Figure B-83. Particle 11A from Sample 11 (E9, 94 cm), size range: >4000 μm.

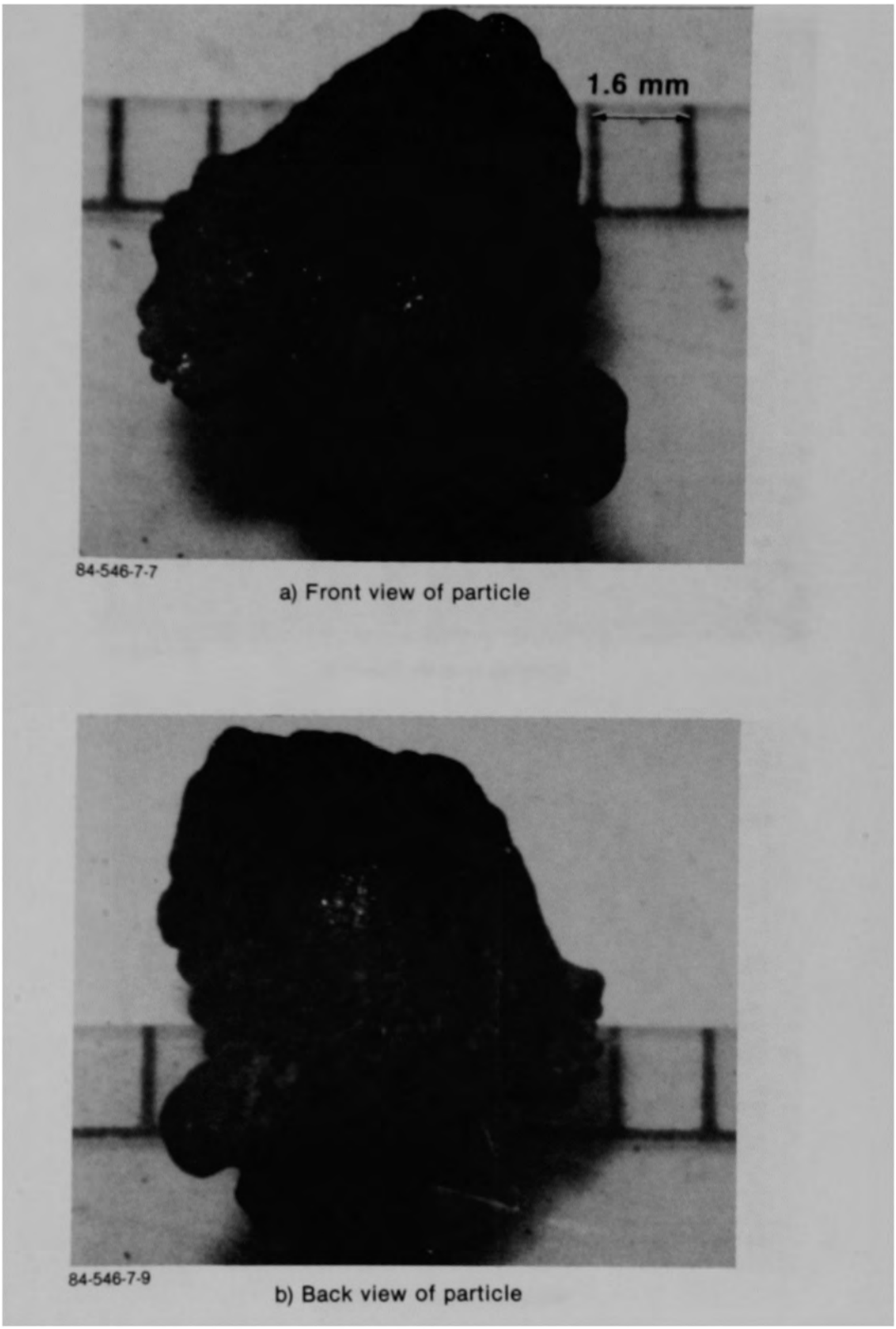

Figure B-84. Particle 11B from Sample 11 (E9, 94 cm), size range: >4000 µm.

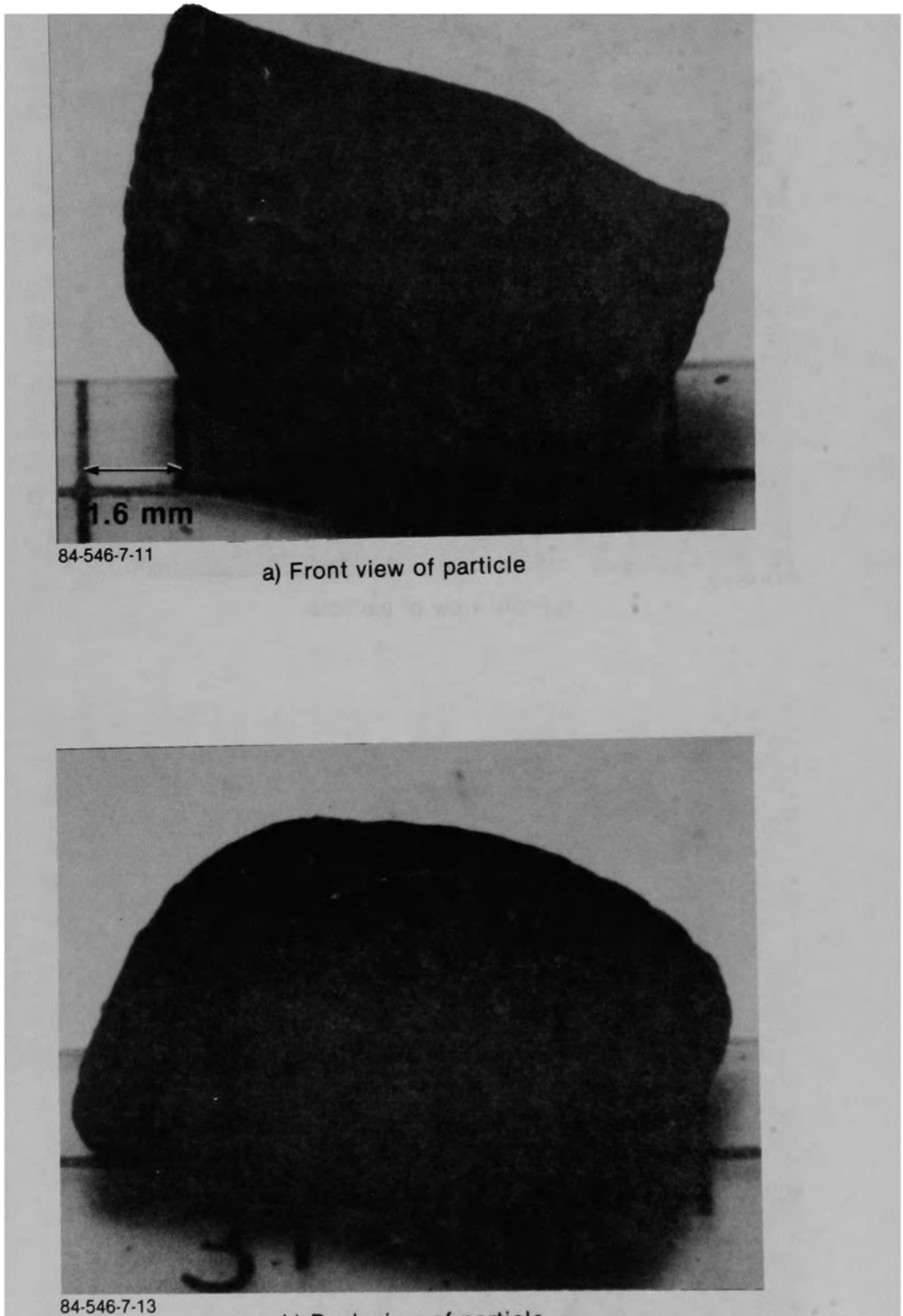

Figure B-85. Particle 11C from Sample 11 (E9, 94 cm), size range: >4000 μm.

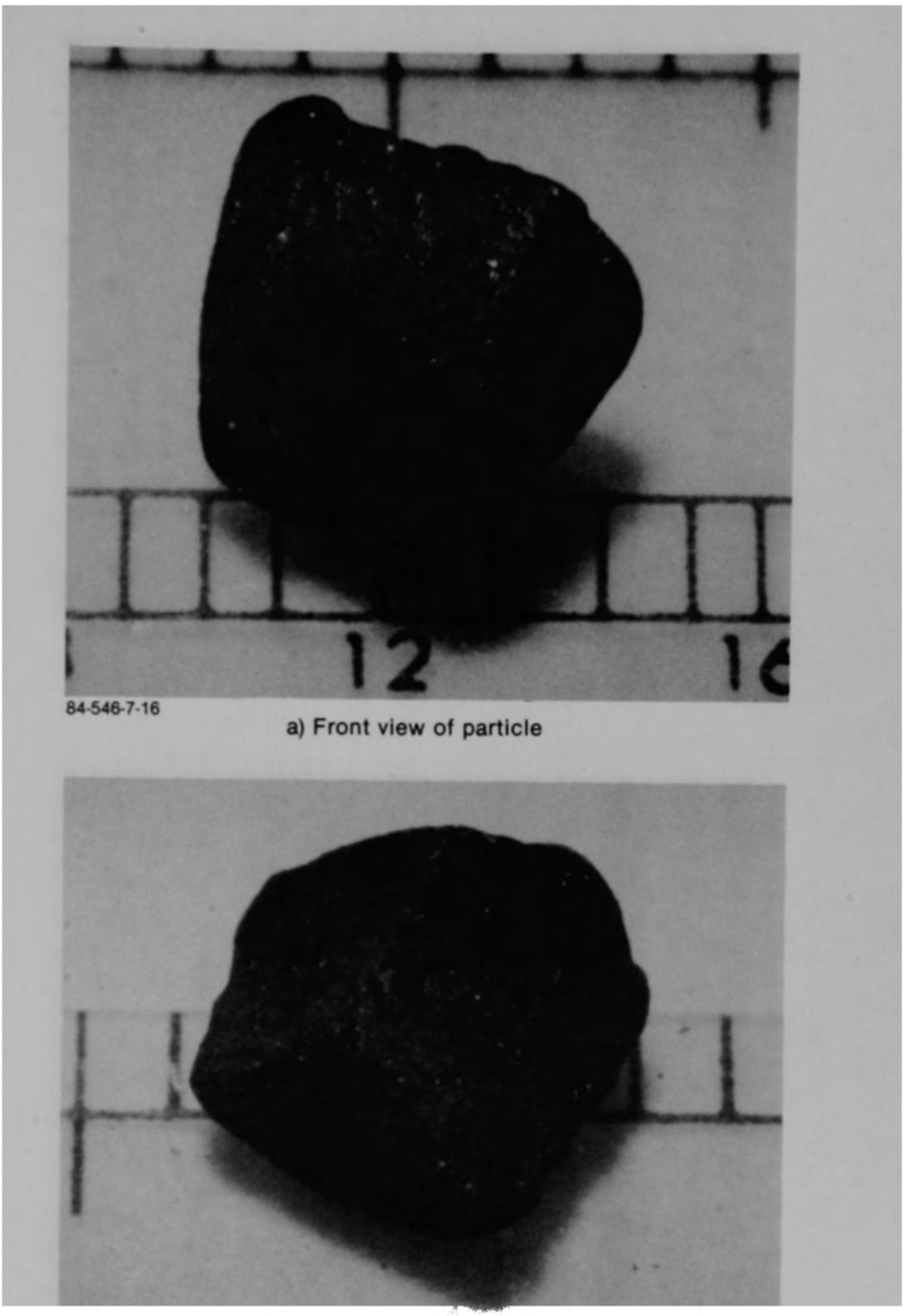

Figure B-86. Particle 110 from Sample 11 (E9, 94 cm), size range: >4000 µm.

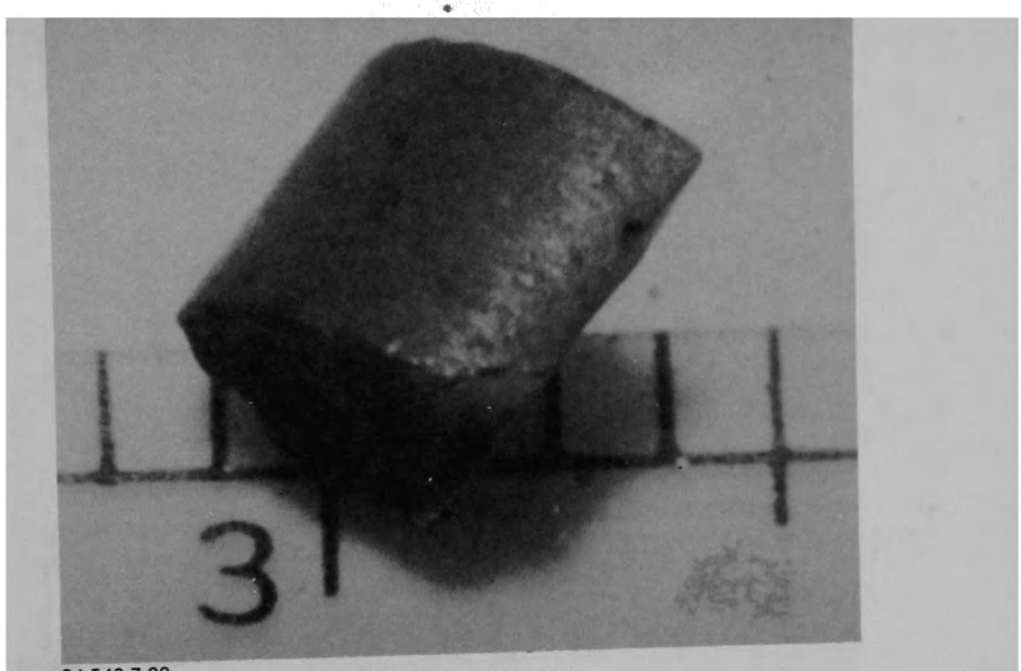

84-546-7-20

a) Front view of particle

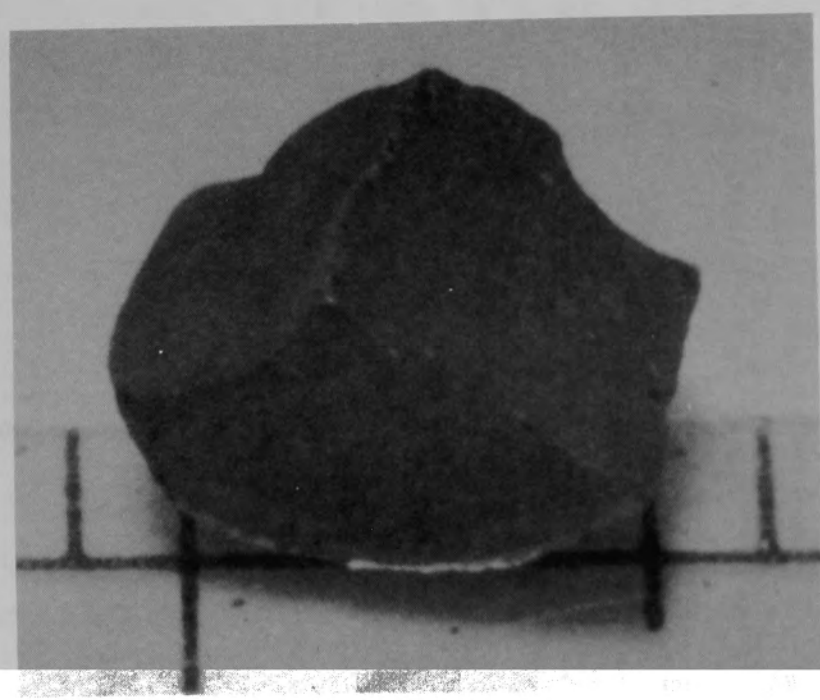

84-546-7-22

b) Back view of particle

Figure B-87. Particle 11E from Sample 11 (E9, 94 cm), size range: >4000 μm.

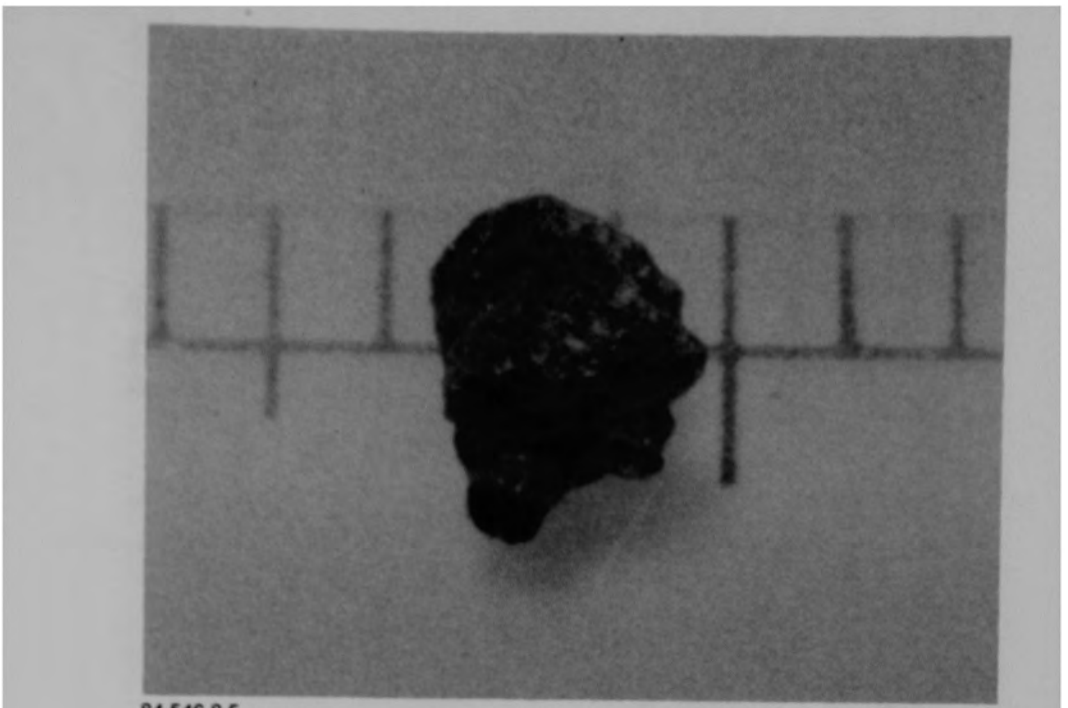

84-546-8-5

a) Front view of particle

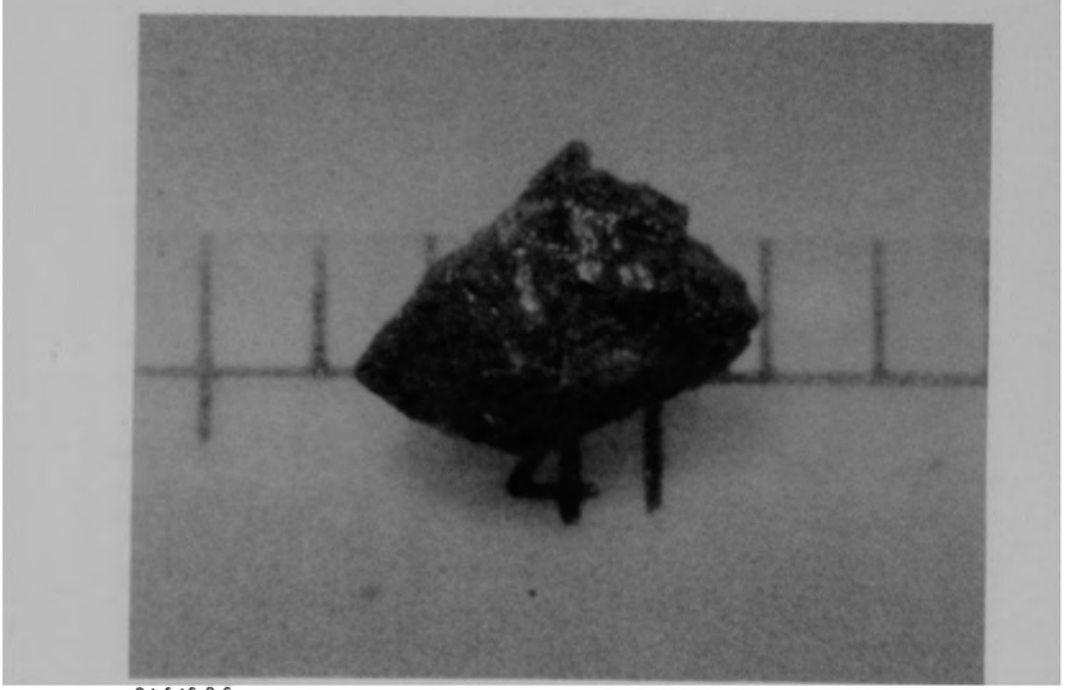

84 546-8-6

b) Back view of particle

Figure B-88. Particle 11F from Sample 11 (E9, 94 cm), size range: 1680-4000 μm.

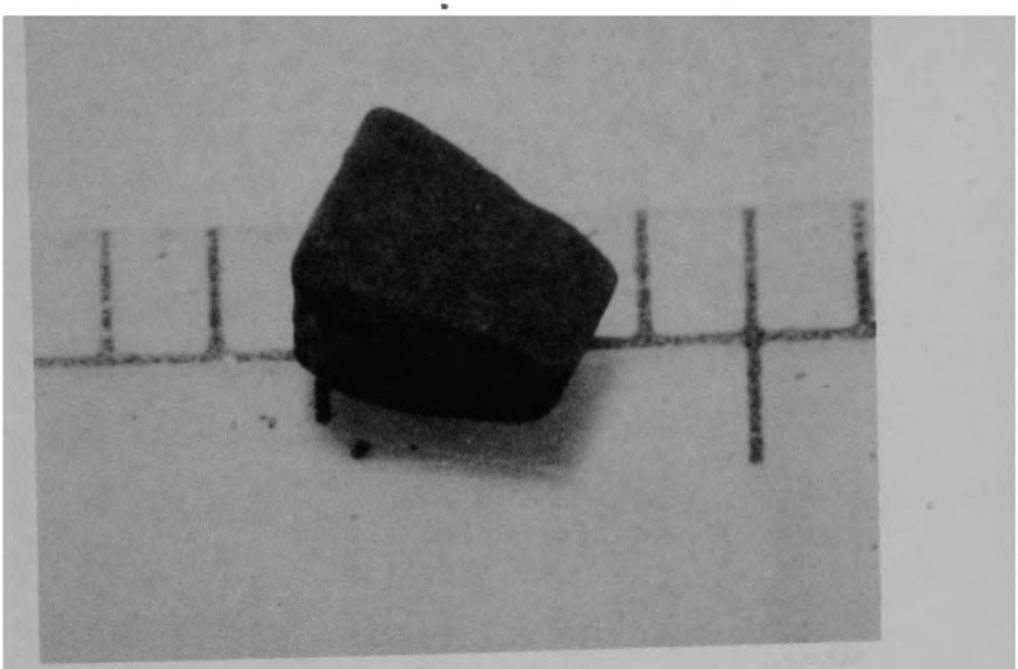

84-546-8-9

a) Front view of particle

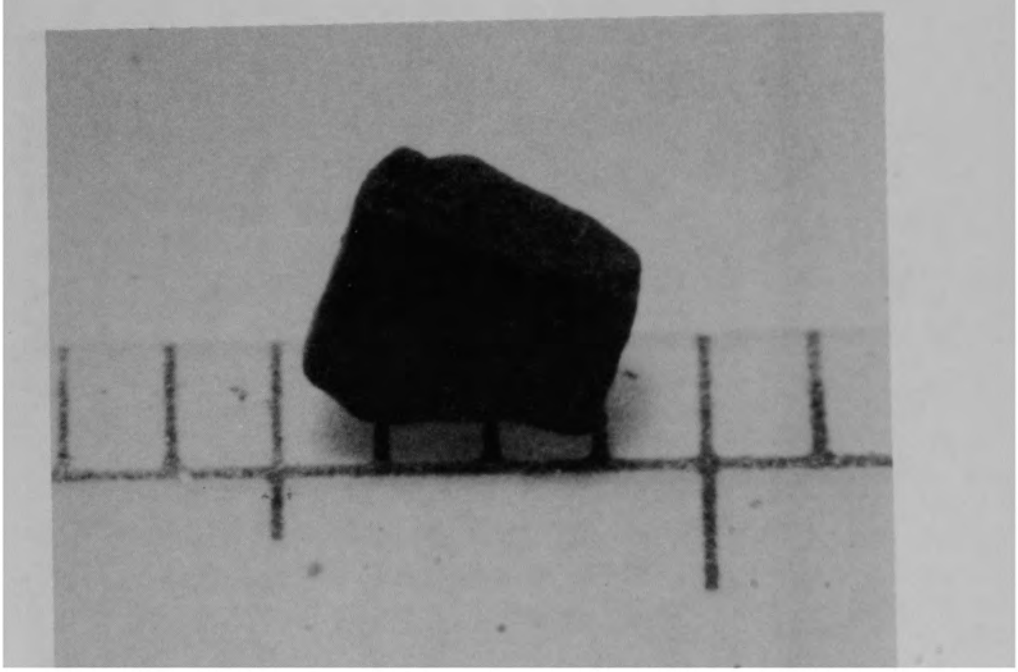

84-546-8-10

b) Back view of particle

Figure B-89. Particle 11G from Sample 11 (E9, 94 cm), size range: 1680-4000 µm.

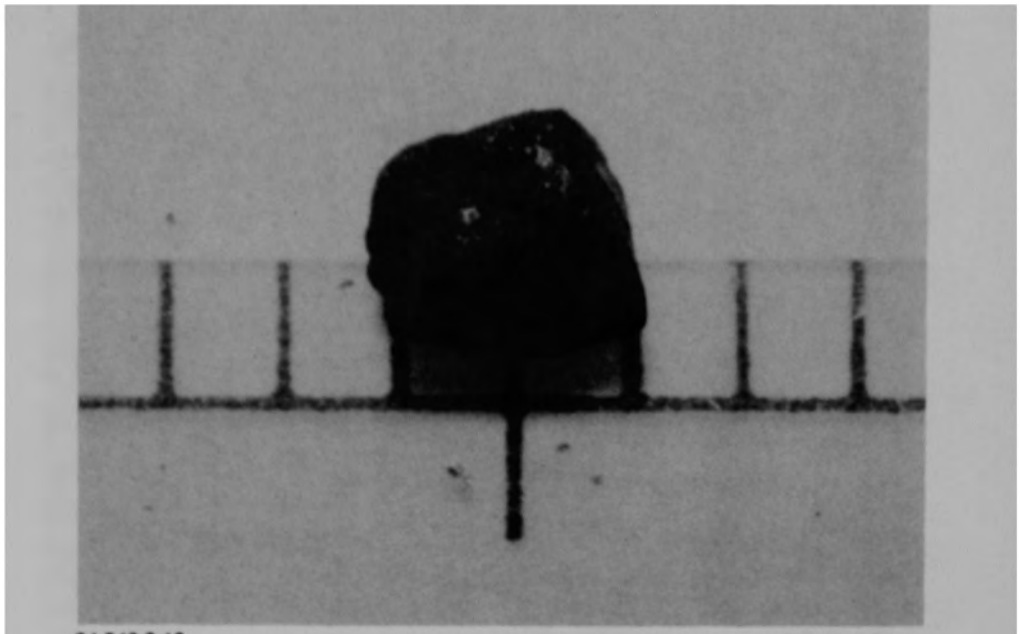

84-546-8-13

a) Front view of particle

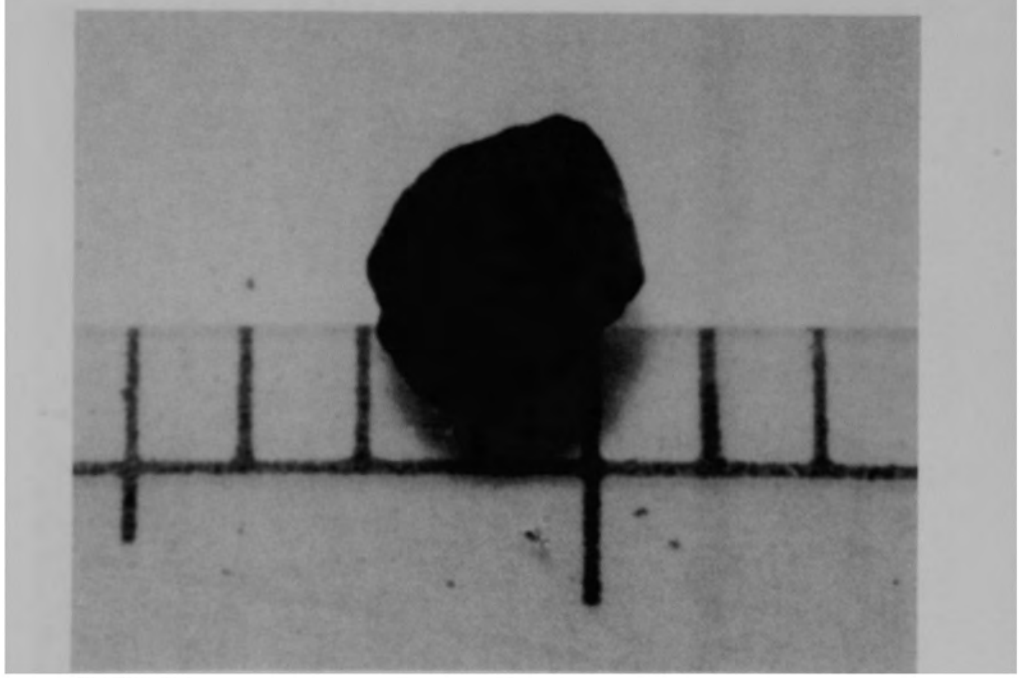

84-546-8-14

b) Back view of particle

Figure B-90. Particle 11H from Sample 11 (E9, 94 cm), size range: 1680-4000 μm.

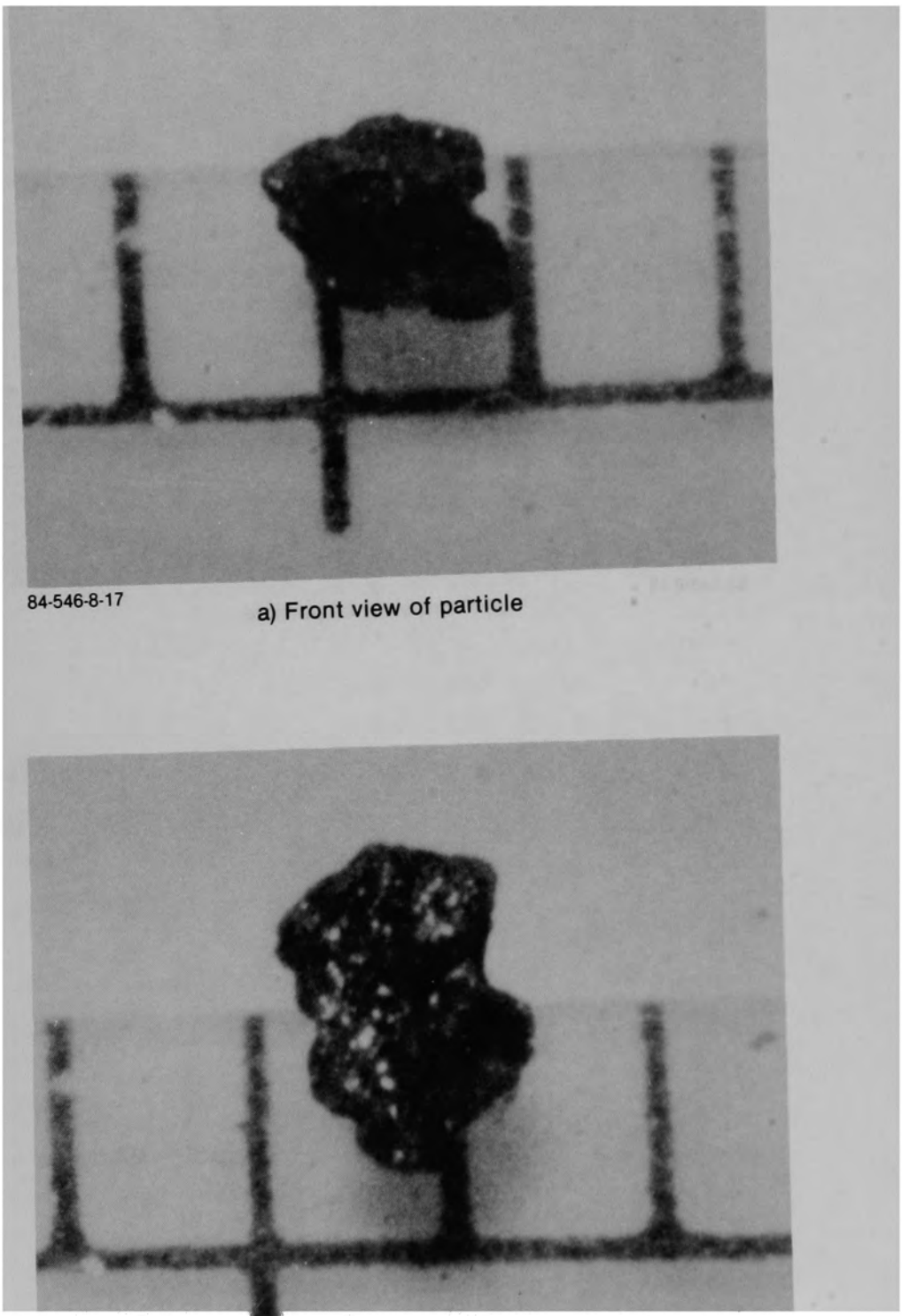

84-546-8-17

a) Front view of particle

84-546-8-19

b) Back view of particle

Figure B-91. Particle 111 from Sample 11 (E9, 94 cm), size range: 1000-1680 μm.

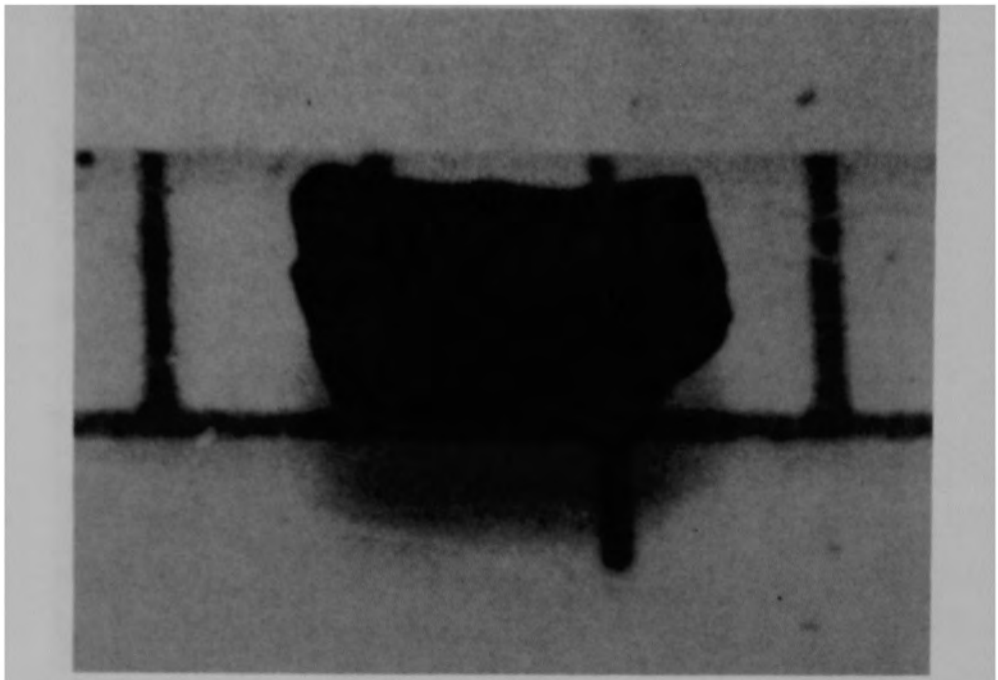

84-546-8-21

a) Front view of particle

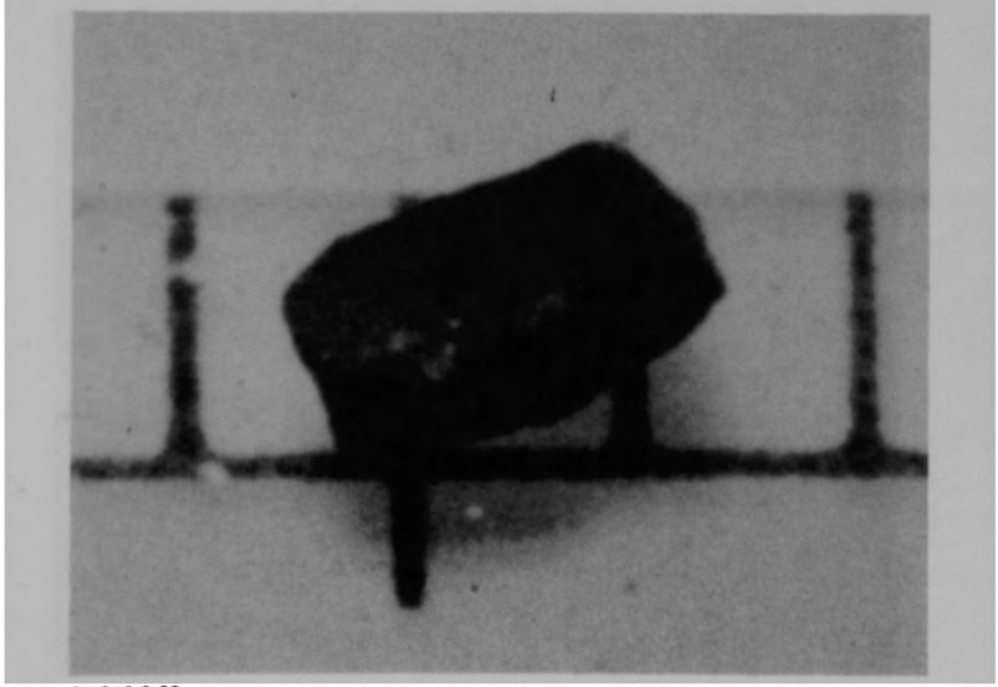

84-546-8-23

b) Back view of particle

Figure B-92. Particle 11J from Sample 11 (E9, 94 cm), size range: 1000-1680 μm.

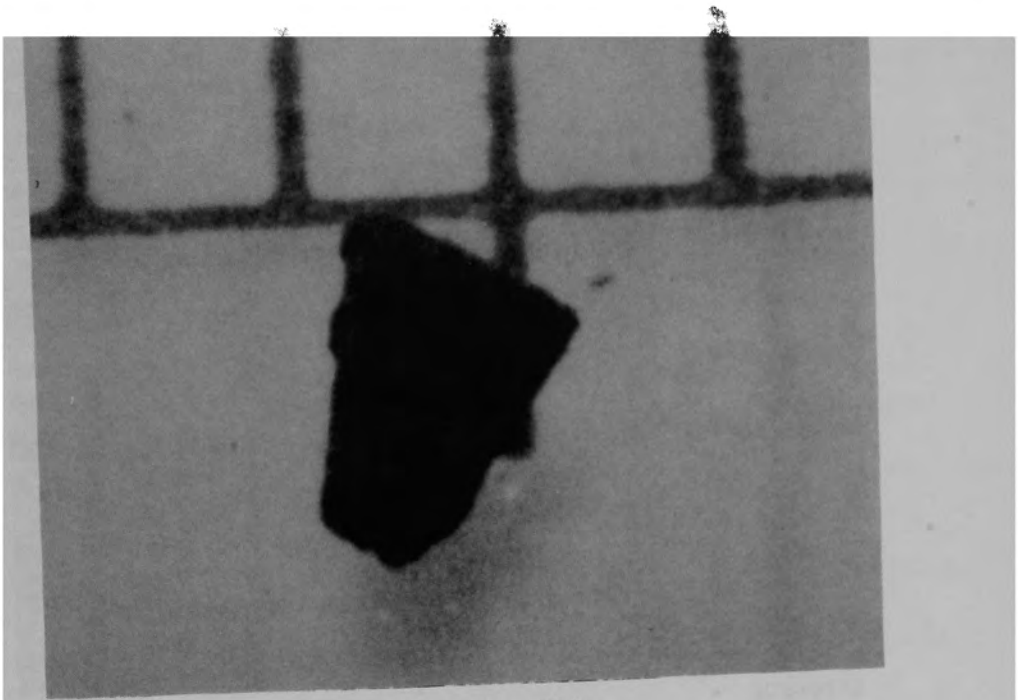

84-546-8-25

a) Front view of particle

84-546-8-27

b) Back view of particle

Figure B-93. Particle 11K from Sample 11 (E9, 94 cm), size range: 1000-1680 μm.

APPENDIX C

METALLURGICAL DATA

CROSS REFERENCE INDEX FOR THE PARTICLES AND ASSOCIATED FIGURES AND TABLES

Particle	Figure(s)	Tables
1A[a]	C-1 through C-8	--
1B[b]	C-9 through C-20	C-1
1E[a]	C-21 through C-26	--
1H[a]	C-27 through C-30	--
3L[b]	C-31 through C-38	C-2
3M[b]	C-40 through C-49	C-3
4A[b]	C-50 through C-58	C-4
4B[b]	C-59 through C-69	C-5
4D[b]	C-70 through C-85	C-6
5E[b]	C-86 through C-95	C-7
6B[a]	C-96	--
6C[b]	C-97 through C-109	C-8
6D[a]	C-110 through C-114	--
6E[a]	C-115 through C-116	--
6F[a]	C-117 through C-119	--
7A[b]	C-120 through C-130	C-9
7B[b]	C-131 through C-141	C-10
7E[b]	C-142 through C-152	C-11
8A[b]	C-153 through C-165	C-12
8C[b]	C-166 through C-176	C-13
8E[b]	C-177 through C-189	C-14
8H[b]	C-190 through C-204	C-15
9D[b]	C-205 through C-219	C-16
9G[b]	C-220 through C-232	C-17
10A[b]	C-233 through C-247	C-18
10E[b]	C-248 through C-260	C-19
10F[b]	C-261 through C-270	C-20
11B[b]	C-271 through C-281	C-21
11C[b]	C-282 through C-294	C-22

a. Examination performed by EG&G Idaho and Westinghouse Idaho Nuclear Co. personnel.

b. Examination performed by Argonne National Laboratory personnel.

APPENDIX C

METALLURGICAL DATA

The optical metallographic, scanning electron microscope (SEM) and scanning Auger spectroscopy (SAS) analysis of the twenty-nine particles examined from the TMI-2 core debris samples are presented in this appendix. Twenty-two particles were studied jointly by EG&G Idaho and Argonne National Laboratories (East and West), while the remaining seven were characterized by EG&G Idaho and Westinghouse Idaho Nuclear Co. Representative photographs of each sample are presented, along with tables of chemical composition for locations analyzed by electron dispersive x-ray analysis (EDS), (in conjunction with the SEM examinations), and SAS analysis.[a] The first one or two figures in each section are photomacrographs of the particle with the locations of the subsequent photographs identified usually by letters. The three digit number identifications refer to chemical analysis locations reported in the tables.

The SEM/EDS data presented here are interpretations of the x-ray spectrums at representative locations. The location of peaks within the spectrum identified elements; the relative peak areas were used to classify the elements as major, minor or trace constituents. In instances where there was difficulty in distinguishing between overlapping peaks or background, the element was classified as questionable. Oxygen concentrations are not included in this data because oxygen can not be measured by this technique.

Quantitative concentrations were determined from the raw SAS data through the use of separate normalization factors (S_x) for each element. These factors relate the peak height of a standard material to the peak height of silver which is the normalizing element. The peak height for normalization factors can be obtained from "handbook" data or, for best

---

a. Note that not all particles were analyzed by SAS.

accuracy, measured from standard materials which contain the element of interest in the form expected in the unknown material. Using the S_x values, peak heights of different elements are put on a common basis so that relative ratios of measured peak heights become relative compositions.

The Zr and O_2 S_x values used on the initial two particles (6C and 4B) were measured from a piece of ZrO_2 which had been quantitatively analyzed by EDX. The S_x values for the remaining particles were measured from a piece of ZrO_2 which had been quantitatively analyzed by wet chemical techniques. The S_x value for U on the initial two particles was measured using UO_2 test fuel, assuming an S_x value for O_2 from the ZrO_2 standard. This value was updated for the majority of the remaining particles using the corrected S_x value for O_2. Finally, a direct measurement of the S_x value for U and O_2 from depleted UO_2 (which had not been used in a high temperature test) was used on the final three particles (10E, 10A, and 7E). The S_x values for the remaining elements were obtained from NBS standards (Cr, Fe, and Ni), theoretical interpolations (Tc, Ru, Rh, Pd, and Sn), or "handbook" data (C and Al).

A measure of the accuracy of the SAS system was obtained from 14 readings of the Ag peak. These were taken on pure silver foil, under conditions similar to those of the analysis. From these measurements, a standard deviation of 0.87 and a mean of 63.9 was determined which results in a scatter band of about ±2%. This represents the best precision possible. However, most measurements are not this good. The scatter of the data is lowest when the surface being measured is smooth and well polished. Region G of Sample 5E, and to a lesser extent, Region 2 of Sample 10A are examples of rough surfaces with corresponding high scatter.

Particles 1A, 1E, 1H, 6D, and 6F were separately characterized on WINCO instruments in a somewhat different format. Semi-quantitative SEM/EDS data were acquired from all five particles, while quantitative SAS was performed only on Particles 1E and 6D. This was done primarily to verify metallographic inferences on oxygen concentrations and to confirm

related interpretations on peak temperatures. Detailed SEM/metallogrphic images, comprehensive data listings, and thorough discussions on these five particles are presented in this appendix.

EDS derived composition information is termed "semi-quantitative" for two reasons: (a) oxygen concentrations cannot be measured, which induced significant upward biases in weight percentages for those elements that were detected; and (b) area fractions for x-ray peaks were converted into elemental weight percentages without calibration to standards. The theoretical corrections applied compensate for mass attenuation, self-fluorescence, and atomic number effects. They are more appropriate to metals than oxides. Deficiences in these correction factors can cause uncertainties of ±5wt%. In addition, bias errors result from the inability to detect oxygen. Consequently, the EDS values reported for Particles 1A, 1E, 1H, 6D, and 6F should be interpreted as relative indications of elemental amounts, rather than absolute determinations.

By comparison, the SAS measurements on Particles 1E and 6D of Zr, U, and O contents were performed with rigorous calibrations and are accurate to within ±2 at.%. A UO_2/Zr interaction standard was graciously donated by the Kernforschungszentrum Karlsruhe (Federal Repbulic of Germany) where UO_2, α-Zr(O), and (U,Zr) alloy were assessed by both Auger spectroscopy and electron microprobe, each of which had been previously calibrated to numerous standard materials. An extruded ZrO_2 rod (Corning Glass Co.) was also supplied by Babcock & Wilcox Co. to provide a known Zr-O ratio for Auger spectroscopy calibration where the rod composition was precisely determined by inductively coupled plasma spectrometry at INEL. While the 15-μm electron beam diameter prevented analysis of small discrete phases, the relatively large beam also reduced sensitivity to local sample topography, with a beneficial effort on data scatter.

Particle 1A

Particle 1A (Figure B-2) is composed of an outer shell of partially oxidized cladding, an intermediate region of prior-molten U-Zr-O mixture, and an interior piece of UO_2 fuel. Thickness variations in the prior β-Zr wall, and in the melt layer, indicate that the cladding ballooned asymmetrically (presumably as a consequence of unbalanced heat transfer), with a radial increase of approximately 1 mm at the orientation shown in Figure C-1. Zircaloy in direct contact with fuel pellets above the ballooned region reacted to create a homogeneous (U,Zr,O) melt that relocated downward to fill the balloon space. The large voids with oxidized surfaces represent two portions of the melt that slumped further downward to be replaced by steam. The extent of oxidation on Figure C-2 suggests that steam flow occurred through these voids between two axially separated cladding breaches. Figure C-2 also demonstrates that the heat of oxidation permitted some segregation of melt constituents along the void surfaces, since the random arrangement of α-Zr(O) grains and (U,Zr) alloy precipitates in the melt interior has been restructured into parallel bands of dark-gray ZrO_2 and light-gray $(U,Zr)O_2$ in the oxidized regions.[a]

SEM/EDS results from Particle 1A are summarized on Figure C-3 and presented in detail on Figures C-4 through C-8. One noteworthy finding on Figure C-3 is Point 1, a Fe-rich deposit on the exterior surface that indicates post-accident rust accumulation. This explains the reddish-yellow external coloration of many grab sample particles. The melt composition (neglecting oxygen) was measured for area 6 as approximately 87-wt% Zr, 11-wt% U, and 2-wt% Ni, plus traces of Fe and Cr. The Fe and Cr content could be attributed to Zircaloy-4 alloying ingredients, but the Ni originated from another component source.[b] As shown in Figure C-4, the

---

a. Oxidized areas appear darker on backscattered scanning electron micrographs, due to dilution of the heavy metal scattering centers by large concentrations of oxygen atoms.

b. An Inconel spacer grid, control rod guide tube, fuel assembly end fitting, etc.

melt segregated into three phases upon cooldown: grains of α-Zr(O), irregular patches of (U,Zr) alloy, and a transition metal phase (Ni, Fe, Cr, plus substantial Zr) squeezed between the other two phases. Figure C-4 also demonstrates that very little chemical and diffusional interaction occurred across the cladding-melt boundary, despite the melt's tendency to wet both cladding and fuel. This was evident from the oval shape of both voids in Figure C-1. Therefore, melt solidification probably happened shortly after arrival at this fuel rod elevation.

Figure C-5 illustrates the phase make-up of the interior melt region (Area 7), which is very similar to that near the cladding. However, a Sn x-ray peak was partially resolved at this position, so the area distribution of this element was indirectly mapped. As indicated, Sn was found within both the (U,Zr) alloy and the transition metal phase, but not inside the α-Zr(O) grains to any noticeable extent. Figures C-6 and C-7 display phase structures for Areas 8 and 9, respectively, that are nearly identical to Areas 6 and 7.

Figure C-10 presents the fuel morphology and elemental distributions adjacent to the melt. As shown, some inward diffusion of Zr and Fe has occurred, but no clear signs of fuel liquefaction were found. This suggests prompt melt solidification after contact. Note also that the UO_2 grains in Figure C-10 are typically in the 10-μm range, approximately the as-fabricated size. The lack of equiaxed grain growth, plus the thin ZrO_2 layer thickness on the cladding exterior, confirm that the fuel rod region from which Particle 1A originated stayed relatively cool--within a few hundred degrees of the 1245 K β-zircaloy transition temperature.

Particle 1B

Particle 1B (Figure B-3) appears to be a quarter section of a fuel pellet with a thin layer of prior-molten U-Zr-O as shown in Figure C-9. Initial preparation of this particle was difficult due to severe pullout of

individual fuel grains so the particle was backfilled with epoxy to hold the grains in place. Figures C-10 through C-13 are optical photos which show the etched grain structure from pellet center to outside surface. The grain size is consistently about 12 μm across the particle. Figures C-14 and C-15 are optical photos which show the thin U-Zr-O layer at two locations on the surface. Figures C-16 and C-17 are SEM secondary electron images of the fuel (note the interlinked porosity in C-16) and Figures C-18, C-19, and C-20 are SEM Back Scatter Electron (BSE) images which correspond to Figures C-14, C-15, and C-12, respectively. Note the layers shown in Figure C-18. Table C-1 displays the SEM/EDS elemental analysis indicating the outer surface of this film is pure Zr with U content increasing with position toward the fuel, and with little penetration of Zr into the fuel.

Particle 1E

Particle 1E (Figure B-4) is a partially oxidized cladding section with UO_2 fuel bonded to the interior surface and ZrO_2 on the outer surface. The two parallel, circumferentially oriented cladding bands in Figure C-21 (that are rich in uranium content) provide evidence of high temperature zircaloy-UO_2 interactions. Radially oriented patches of ZrO_2 within the cladding matrix and large metallic stringers along the interior of the ZrO_2 layer indicate that cladding melting occurred. In addition, a small amount of prior-molten $(U,Zr)O_2$ ($T > 2810$ K) has solidfied on the exterior of the ZrO_2 layer.

Because of prolonged oxidation, the cladding structure at one point during the TMI-2 transient consisted of the following layers (from the outside inward): ZrO_2, α-Zr(O), large β-Zr grains at the cladding center, $\alpha\text{-Zr(O)}_b$, (U,Zr) alloy, $\alpha\text{-Zr(O)}_a$, and the UO_2. Then this cladding structure melted, which accelerated oxygen uptake from both the UO_2 and external ZrO_2. For a brief time, UO_2 dissolution by molten cladding must have proceeded rapidly. Upon cooldown, the oxygen-depleted, hypostoichiometric portion of the ZrO_2 decomposed into ZrO_2 and metallic stringers of α-Zr(O). Meanwhile, the heterogeneous (U,Zr,O)

melt near the fuel interface transformed into α-Zr(O), (U,Zr) alloy, and $(U,Zr)O_2$. The timing of the molten, single-phase $(U,Zr)O_2$ attachment to the exterior ZrO_2 surface cannot be directly inferred from this scenario.

Figures C-22 and C-23 (high magnification) detail the semiquantitative elemental analyses that were performed near the fuel-cladding interface. Only relative weight percentages for U and Zr were measured, because oxygen cannot be detected by EDS. Therefore, the approximate degree of oxidation must be inferred from the gray-level contrast on the backscattered scanning electron images, where brighter regions correspond to higher average atomic numbers. For example, the bands of $(U,Zr)O_2$ are considerably darker than the small patches of (U,Zr) alloy, due both to lower U concentrations and substantial dilution by oxidation. Point 7 of Figure C-23 demonstrates that microsegregation of a Fe- and Cr-rich phase occurred at isolated portions of this interface. UO_2 grains on the left side of this micrograph are typically 30 μm in diameter, so some grain growth has taken place at this position. This observation is consistent with the determination that the cladding exceeded the α-Zr(O) melting point of 2245 K.

Figure C-24 illustrates how the ZrO_2 layer was reduced by the metallic cladding, creating patches of ZrO_2 in the α-Zr(O) cladding matrix and leaving radially oriented stringers of α-Zr(O) within the ZrO_2 region. However, the sizable separation between these two phases in both instances means that this area was not quenched abruptly from its maximum temperature. As shown by the EDS results from Point 1 and the Al x-ray image, a thin layer of Al-rich material collected at the interface, which suggests an earlier cladding reaction with Al_2O_3, the dominant Al source within the TMI core. Figure C-25 shows a different view across the ZrO_2 layer, where substantial amounts of a Fe/Cr/Al-rich phase are conspicuous at mid-thickness. Here, the metallic stringers were found to contain significant U concentrations. These (presumably) originated across the cladding in the fuel. Note also that the adherent $(U,Zr)O_2$ at the top of Figure C-25 has not reduced the adjacent ZrO_2, which confirms the

metallographic interpretation that the $(U,Zr)O_2$ arrived as a molten ceramic (T > 2810 K) as opposed to a metallic melt oxidized in place at a lower temperature.

Although the $(U,Zr)O_2$ adhered as a single-phase ceramic melt, the attachment did not necessarily occur at a single time. As shown by the EDS results on the left side of Figure C-26, significant differences were detected in concentrations of transition metals between melt adjacent to and away from the ZrO_2 layer. Some variation in U and Zr composition was also found across the melt during quantitative SAS measurements, according to the right side of Figure C-26. Therefore, the molten ceramic probably arrived at this fuel rod elevation in separate rivulets, solidifying in succession much like candle wax. Nevertheless, the temperature estimation of at least 2810 K is unaffected, because SAS oxygen values are uniformly close to 67 atom%. The exception is Point 9 from the ZrO_2 portion that was reduced by the molten cladding.

Particle 1H

Particle 1H, (Figure B-6), as shown in multiple views on Figure C-27, has a very porous (foamy) appearance and is a quench-frozen agglomerate of two distinctly different types of material. Single-phase, large-grained, pore-free fragments have been surrounded by a fine-grained, porous, multi-phase melt. After metallography, it was initially thought that this particle was probably composed of fuel pellet pieces coated by a quenched melt, which would have accounted for the apparent chemical dissolution of the single-phase ceramic blocks. However, very little gray-level contrast is evident between the porous and pore-free regions on the backscattered scanning electron micrograph. This means there is overall similarity in average elemental composition and extent of oxidation.

Metallographic and SEM images are presented on Figure C-28 of area A, one of the regions of Particle 1H where porous melt attack of a solid fragment is especially apparent. The upper photomicrograph shows the grain facets of the pore-free material quite clearly, but grain surfaces along

the melt interface are irregular and pitted from dissolution. Melt penetration along grain boundaries is evident from the wide thickness variations of the intergranular material. This eliminates precipitation of a second phase during cooldown of the pore-free solid as a cause for the presence of this grain boundary substance. As shown in the lower micrograph on Figure C-28, melt-solid interaction was evidently related to pore production, because small pores nucleate near the interface and combine to form larger voids with increasing distance.

Two smaller portions of area A were analyzed by EDS, and are shown at high magnification on Figure C-29. Negelecting oxygen, which cannot be detected by EDS, the melt has an average composition of 68-wt% U, 28-wt% Zr, and 4-wt% Fe, plus traces of Ni, Cr, and Al.[a] The Fe content is much higher than the nominal 0.225-wt% in Zircaloy-4 and Ni should not normally be detected, so the melt almost certainly interacted with Inconel or stainless steel early in its evolution. Three phases are apparent in the melt: bright, relatively distinct grains, dark stringers, and mottled patches, with the grains containing the largest U concentrations and the stringers being high in transition metals. However, phase segregation seems incomplete as a consequence of quenching, so the mottled patches may in fact be a multi-phase mixture; the phase compositions might have been different had equilibrium been attained. Note also, that the composition and appearance of the mottled patches are very close to the material between grains of the pore-free solid. This suggests that this phase preferentially wetted the large-grained fragments.

The single-phase, pore-free fragments are almost definitely $(U,Zr)O_2$ solid solutions, although this identification is a metallographic deduction and has not been precisely confirmed by SAS. The $(U,Zr)O_2$ "islands" could represent a ceramic melt ($T > 2810$ K) or a metallic melt oxidized in the liquid state to saturation and solidification ($2175\ K < 2675\ K$). No shrinkage pores, nor other features clearly associated with a prior molten state, were observed, unlike the ceramic melt on Particle 1E. However,

---

a. The approximate atomic Zr:U:Fe ratio is 13:12:3.

mixed ceramic melts that have been superheated and quenched can appear pore-free. But, because the $(U,Zr)O_2$ regions were found to vary from 67-wt% U and 33-wt% Zr to 59-wt% U and 41-wt% Zr[a] with no detectable Al, Ni, Fe, and Cr, the pore-free solids did not originate within a single molten region.

Figure C-30 presents micrographs from areas B (upper) and C (lower) of Particle 1H. Area B is quite similar in appearance and average composition to the upper portion of area A, showing the same three-phase melt microstructure. Like area A, area C illustrates how porosity from melt-solid interfaces has coalesced into larger void features. Tiny deposits of Fe, Cr, Al, Ni, and Sn were occasionally detected within the smallest pores during EDS surveys at this position, so the porosity may be nucleated at temperature by miniscule bubbles of metal vapor.[b] Nevertheless, area C demonstrates that melt shrinkage during cooldown was equally important in void formation. Note the parallel, elongated melt strands pulled between two $(U,Zr)O_2$ fragments in response to the strong melt tendency to wet the $(U,Zr)O_2$. In addition, area C supplies additional proof that mixed oxide dissolution occurred along all exposed $(U,Zr)O_2$ surfaces and not just within grain boundaries; two regions are indicated where $(U,Zr)O_2$ grains are almost completely dissolved. The rounded, bulbous shape of one of these grain remnants suggests incipient melting, in which case the melt temperature was greater than 2810 K. Note that the melting point of the $(U,Zr)O_2$ would be the same whether the $(U,Zr)O_2$ formed by ceramic melting or by liquid-state oxidation of a metallic melt.

The melt behavior at temperature is difficult to precisely deduce from the phase make-up after quenching. Because the dissolution of the $(U,Zr)O_2$ blocks had progressed quite far, some of the melt represents previously dissolved mixed oxide. Thus, it is not certain whether the melt

---

a. See Figure C-30.

b. Such deposits might be more common on unetched samples.

was initially homogenous or heterogeneous. The melt surrounding the $(U,Zr)O_2$ blocks and along block grain boundaries was nearly indentical to the average mottled patch composition. Therefore the patch phase was likely responsible for attacking the mixed oxide fragments. Because Fe forms a complex eutectic system with U, Zr, and O, the dissolution mechanism was probably eutectic decomposition. However, the melt temperature may also have been higher than 2810 K, as suggested by the bulb shape in area C. In that case $(U,Zr)O_2$ melting would have accelerated the dissolution process. In any event, the melt penetration along grain boundaries confirms that the $(U,Zr)O_2$ had definitely solidified before melt contact concurred.

Particle 3L

From the photomacrograph of Particle 3L in the as-polished condition, shown in Figure C-31, this particle appears to be formed from several different pieces of ceramic material. There are regions of large elongated pores, large round pores, and small pores. Figure C-32 shows closer views of the central section as polished and Figures C-33 and C-34 show typical areas (no visible microstructure) after a very heavy etch with the fuel etchant.

Figure C-35 is a BSE overall image, with Figure C-36 showing a very fine grain structure from Region A. This type of structure is found throughout the band of the particle identified by large elongated pores. Figure C-37 is from the bottom of Figure C-35. Figures C-38 and C-39 are SEM images of two regions containing large round pores with an Al-Cr-Fe-Ni phase within.

Table C-2 displays the SEM/EDS and SAS analysis. This particle is predominantly $(U,Zr)O_2$ with slight variations in Zr/U ratios between regions ranging from about 2.4 in the top edge, to about 2.2 in the bulk of the sample, to about 1 in a small region seen in Figure C-38. The only occurrence of other elements is in and around a few large pores (see Figures C-37 and C-38).

Particle 3M

Particle 3M appears to be a piece of (UO_2) fuel which has interacted with zircaloy and structural material along one side and in cracks. Figure C-40 shows the two region types that make up Particle 3M. Region Type 1 is UO_2 fuel which has experienced very little grain growth (current grain size ~11μm) but has a large void fraction. Region Type 2 is mostly uranium with varying amounts of Zr and a trace of Fe. A Cr, Fe, Ni material fills grain boundaries and occurs in voids in Region 2. Figure C-41 through C-49 are typical optical and SEM images of the particle (see Figure C-40 for locations). Table C-3 displays the SEM/EDS elemental analysis. A gradient in Zr was detected by the SEM/EDS at the interfaces between Regions 1 and 2.

Particle 4A

Figure C-50 shows Particle 4A (Figure B-11) as-polished and after a 5 min. fuel etch. The base material in the over etched region is UO_2 with a trace of Fe in some places. The base material in the region that did not over etch is U with some Zr and Fe; the amount of Zr increases with distance away from the over etched region. There is an Al-Cr-Fe-Ni second phase found throughout the particle but more often in the Zr bearings regions. See Table C-4 for a summary of the chemical composition from the SEM/EDS analysis.

There is a gradient in the pore and grain size across this particle where the minimum grain size (which is on the right side of the particle) is about 18 μm. Figure C-51 shows three as-polished optical photos of the same magnification from opposite sides of the particle and Figure C-52 shows equivalent SEM images. The grain boundary phase seen in the SEM images in Figure C-53 can be seen in the etched optical images in Figures C-54 and C-55. Figure C-56 SEM images showing the Al-Cr-Fe-Ni bearing grain boundary phase in the over etched region are seen in Figure C-56. Figures C-57 and C-58 are representative SEM and optical images of the particles.

Particle 4B

Figure C-59 shows all of Particle 4B (Figure B-12) as-polished and the middle section after being etched for fuel. The center portion of this particle is UO_2 fuel which has experienced some grain growth (to about 18 μm) and void formation. Pullout of individual grains of UO_2 occurred in this region when etched (see Figure C-60). All around the edge of this particle is $(U,Zr)O_2$ with a small amount of an Al-Cr-Fe-Ni second phase material and a few Ni-Sn inclusions. The amount of Zr in the rim decreases with position from the edge toward the center fuel region. See Table C-5 for composition data and Figures C-61 through C-69 for typical optical and SEM images.

Particle 4D

From the optical as-polished photographs (see Figures C-70 through C-73) Particle 4D appears to be a relatively homogeneous and dense particle. Figure C-74 shows the effect of a two minute immersion fuel etch which tended to preferentially dissolve material around clusters of small pores. Figures C-75 through C-77 show the effect of a one minute swab fuel etch which also did not reveal any grain structure. Figures C-78 through C-85 are typical SEM-BSE images of Particle 4D. The different shades of gray indicate that the particle is not homogeneous. In general there was no grain structure or second phase material detected, but there were inclusions of a Cr-Fe-Ni-Al material.[a]

Particle 5E

Particle 5E (Figure B-18) can be divided into six regions based on Zr content. Figures C-86 shows the as-polished and etched view of the particles. A map of the regions is shown in Figure C-87; Table C-7 shows the composition in the different regions. Region 5 in the bottom tip of

---

a. See Table C-6 for a summary of chemical compositions.

the particle has less than 1 atom% Zr and Region 6 within Region 5 has only a trace of Zr and appears to be U_4O_9 from the SAS data. The four regions in the upper areas of the particle vary from 2 to 9 atom% Zr. There is a small amount of Ni-Fe-Cr in some of the grain boundaries and a few Ru-Ni inclusions. Figures C-88 through C-96 are typical optical and SEM images of Particle 5E.

Particle 6B

Particle 6B appears to be a piece of zircaloy; SEM or SAS measurements were not performed on this particle. Figure C-96 is the photomacrograph and Figure B-24 in the particle macro-photograph.

Particle 6C

Particle 6C (Figure B-25) appears to be two pieces of oxidized cladding stuck together with prior molten material as shown in Figure C-97. Assuming the cladding pieces became stuck together while part of an intact fuel bundle, the radius of curvature and relative positions of the cladding pieces indicate about 30% ballooning strains. See Figures C-98 through C-109 for typical optical and SEM magnified images. Table C-8 shows representative compositions. In general, the cladding pieces are ZrO_2 with small amounts of carbon and the prior molten base material is $(Zr,U)O_2$ with a high Zr to U ratio. There is a large amount of second phase materials and inclusions in the prior molten material made up of Al-Ni-Sn-Fe-Cr. There is an inordinate amount of Al and C in this particle indicating a possible interaction with a Al_2O_3-B_4C poison rod.

Particle 6D

Particle 6D (Figure B-26) is a large fuel pellet fragment with a tiny portion of (U,Zr,O) melt attached at one end. As shown in Figure C-110, the fracture surfaces appear atypically irregular for UO_2, while the fuel matrix has a distinctly unusual speckled cast. The external surface of the particle appears "glazed."

The photomicrograph at the upper-left of Figure C-111 shows that the fuel experienced elevated temperatures, since considerable porosity has accumulated at grain boundaries. This phenomenon is also observed in fuel operated at standard reactor conditions, but only after burnups of approximately 15 to 20 GWd/t. The extent of equiaxed grain growth is small, indicating that the peak fuel temperature did not greatly exceed 1900 K over a significant time duration. Figure C-111 also shows the fuel appearance after etching to expose grain boundaries, whereupon a second fuel phase emerged. The existence of a second ceramic fuel phase suggests fuel oxidation, but the U-O phase diagram (see Figure 31 of the main text) shows several possibilities for two-phase mixtures, depending on the average oxygen content. Accordingly, SAS was performed on two representative, widely separated fuel regions, the results of which are listed on the right side of Figure C-111. The average concentration of approximately 71 atom% (± 2 atom% at worst) converts to $UO_{2.44}$, which means that the fuel was oxidized beyond the UO_2 crystal structure into a two-phase mixture of U_4O_9 and $UO_{2.6}$.[a] Despite efforts to center the 15-μm SAS beam on grains of each phase, the oxygen concentrations of the major and minor phases could not be separately identified within the resolution and accuracy limitations of the instrument.

The most probable mechanism for fuel oxidation is inward diffusion of oxygen gas, which necessarily presupposes a hyperstoichiometric excess of oxygen in the steam at some phase of the TMI-2 transient. As shown in the U-O phase diagram, this could only have occurred at fuel temperatures above 1900 K, where the two phases segregated during subsequent cooldown. However, temperatures much above 1900 K would presumably have induced more equiaxed grain growth than was observed. Consequently, an approximate temperature of 2000 K is tentatively concluded for the fuel oxidation process. Diffusion calculations are recommended to bracket the time duration involved and to help determine the source of the surplus oxygen, which is not readily apparent at present.

---

a. The crystal structure of $UO_{2.6}$ is in dispute, with opinions divided between U_5O_{13} and U_8O_{21}.

Behavior and origin of the adherent melt on Particle 6D were similarly of major interest. EDS derived melt data are summarized on Figure C-112. As shown, the melt composition was uniformly measured as approximately 66-wt% U and 34-wt% Zr, excepting near the melt-fuel interface where the U/Zr ratio increased abruptly. No traces of Fe, Cr, Ni, Sn, nor other alloying impurities were detected. Figure C-112 further demonstrates that melt interactions were not confined to the metallurgical examination plane, because a second Zr-rich area is evident about 100 μm below the conspicuous interface. Therefore, the fuel region near the interface was almost surrounded by melt.

Metallographic examinations of the fuel-melt interaction zone were also quite revealing. As displayed in Figure C-113, the melt is composed of smooth ceramic grains exhibiting only one metallurgical phase at room temperature, which suggests $(U,Zr)O_2$. The melt evidently absorbed some oxygen from the nearby fuel, because a clearly defined reaction layer was exposed by etching, while only one fuel phase could be perceived adjacent to the melt after etching. This is unlike the two-phase fuel structure elsewhere on Particle 6D. Figure C-133 further illustrates that interfacial fuel experienced somewhat higher temperatures than the rest of Particle 6D, because individual pores collected at grain boundaries have interlinked here to form connected pathways and because grain sizes are somewhat enlarged. These findings infer that the $(U,Zr)O_2$ was a metallic melt at the time of fuel contact and that it was subsequently oxidized in place until solidified. Moreover, the metallic melt was apparently superheated well above its melting point, because considerable heat was transferred to the adjacent fuel by conduction.

These preliminary deductions were later confirmed by quantitative SAS measurements that are presented in Figure C-114. Oxygen concentration values over the six points are consistently close to 66 atom%, in complete agreement with metallographic indications that this region is composed of UO_2 and $(U,Zr)O_2$. Because these SAS measurements were taken under identical conditions to those elsewhere on Particle 6D, the SAS agreement with metallography lends additional credence to the 71 atom% oxygen concentration result for regions not reduced by metallic melt contact.

The lower portion of Figure C-114 represents continuous O, U, and Zr information along the band through the middle of the SAS micrograph. These line scans were significantly perturbed by sample porosity. For example, the oxygen profile should appear flat over most of the scan length, but instead falls off noticeably over the porous fuel region. Note also that all three profiles display conspicuous depressions at two particularly porous places. These places are poorly imaged on the SAS micrograph, unfortunately. In any case, the Zr line scan provides an accurate measure of the diffusion bond width (approximately 50 μm), which could be very valuable for time-at-temperature estimates. Consequently, this continuous line scan approach is recommended for further development. This is especially recommended where state-of-the-art SAS devices can be employed to compensate automatically for variations in sample topography, to produce quantitative line scan output, and to provide high quality micrographs.

Particle 6E

Particle 6E appears to be a piece of zircaloy with layers of ZrO_2 on both sides. SEM and SAS measurements were not performed on this particle. Figure C-115 is the photomacrograph and Figure C-116 is a close up of a ZrO_2 layer unetched. See Figure B-27 for the particle macro-photograph.

Particle 6F

Particle 6F (Figure B-28) was originally selected for detailed characterization after it was found to be partially ferromagnetic. Despite the complicated overall appearance in Figure C-117, the source of the ferromagnetic nature of Particle 6F was readily identified as the three large metallic ingots. These ingots were determined by EDS to be 96-wt% Ni and 4-wt% Fe, with a small additional amount of Sn.

The process whereby Inconel-718 (initially 52-wt% Ni) was "refined" to nearly pure Ni is not definitely known but is probably related to higher oxygen affinity for the Fe and Cr constituents. Because of the low extent of oxidation, the Ni rich melt presumably contacted the remainder of

Particle 6F late in its evolution, penetrating along large pores and solidifying from heat losses to a cooler matrix. Thus, the temperature of the oxidized portions of this particle was almost certainly well below 1725 K (the melting point of Ni) when the Ni-rich melt arrived.

In addition to the ingots, Particle 6F consists of roughly equal amounts of porous and solid (U,Zr,O) materials at the cross-sectional orientation studied. The granular, relatively pore-free structure evidently solidified before contact with the porous melt. The metallographic appearances and etching behavior of both types of (U,Zr,O) material suggest a high degree of oxidation.

The backscattered electron micrograph at the base of Figure C-118 illustrates major differences in average atomic number of Particle 6F. The composition of the solid-grained structure was determined by EDS to be approximately 32-wt% U and 68-wt% Zr (neglecting oxygen), while the porous heterogeneous melt ranged between 50- and 60-wt% U and 45- to 35-wt% Zr, with the remaining 5-wt% composed of varying amounts of Fe, Cr, Ni, and Al.[a] Therefore, most of the gray-level contrast between the solid-grained and porous structures in Figure C-118 is due to a marked difference in U content. However, the porous melt could conceivably be less oxidized, because oxygen concentrations were not measured by SAS.

The large solid grains are almost definitely $(U,Zr)O_2$. The mixed oxide contains no detectable alloying impurities, as with comparable pore-free $(U,Zr)O_2$ in Particles 1H and 6D, and unlike the adherent mixed oxide in Particle 1E. The preponderance of shrinkage pores and the absence of grains in the bright, irregularly shaped melt confirms solidification on cooling.

Figure C-118 also shows several bright regions lacking both shrinkage pores and grain structure. These regions represent diffusion bonding between the solid $(U,Zr)O_2$ and the partially liquid heterogeneous melt.

---

a. Fe and Cr tend to dominate the impurities, which suggests prior interaction with stainless steel.

Much of this diffusional interaction was caused by melt-solid contact outside the plane of study, because the interfacial area at this orientation is quite small. One such bonding region is shown in closer detail at the right of Figure C-118. Note the absence of diffusional exchange with the Ni ingots, which confirms that the heterogeneous melt had cooled and solidified before the Ni-rich melt arrived. Note also that the heterogeneous melt has not attacked the $(U,Zr)O_2$ grain boundaries.

Figure C-119 provides close-up views of the room-temperature heterogeneous melt microstructure. Metallic ingots present during initial metallography were evidently dislodged or dissolved by etching, so the small inclusions only appear in the upper-left image. Two phases are apparent on the lower backscattered electron micrograph: the (U,Zr,O) matrix and the dark-gray stringers. The matrix composition at this position is approximately 57-wt% U, 38-wt% Zr, 4-wt% Fe, and 1-wt% Ni (plus a substantial concentration of oxygen), while the stringers here are composed of 34-wt% Cr, 33-wt% Fe, 17-wt% Al, and 16-wt% Ni.

Based on the metallographic appearance and immunity to etchants, the matrix seems to be mostly $(U,Zr)O_2$. Much of this mixed oxide would have been in the form of $(U,Zr)O_{2-x}$ at temperature, so the metallic inclusions could conceivably be (U,Zr) alloy that emerged as the $(U,Zr)O_{2-x}$ dissociated upon cooling. However, it is more likely that the inclusions were relatively inert metals like Sn or Ni whose low oxygen affinity prevented incorporation within the matrix.

Despite incomplete understanding of the melt structure, the makeup of Particle 6F resembles Particle 1H in that a porous melt has contacted previously solified $(U,Zr)O_2$. Nevertheless, the melt-solid interactions in these two cases are very different. In Particle 6F the two materials have bonded by diffusion, whereas in Particle 1H the melt has dissolved substantial amounts of the $(U,Zr)O_2$. The heterogeneous melt composition is quite similar in the two particles, although the U content of the mixed oxide is lower in Particle 6F. Therefore, the major distinction between the two situations seems to be the melt temperature. The heterogeneous

melt in Particle 1H was apparently liquefied and superheated above the $(U,Zr)O_2$ melting point, thus accounting for the extensive grain boundary penetration and dissolution of the solid mixed oxide. By comparison, the heterogeneous melt in Particle 6F was evidently a viscous slurry at a temperature well below 2810 K, so only diffusional interactions occurred where the two materials were in contact.

Particle 7A

On a macro scale, Particle 7A (Figure B-33) appears to be a relatively homogeneous particle with many large (~300 μm) round and irregular shaped pores and small (~10 μm) irregular shaped pores as shown in Figure C-120. On closer examination a second phase and metallic inclusions appear uniformly throughout the particle. The base material is U and Zr with a trace of Fe. The second phase contains Cr, Fe, Ni and some Al; the metallic inclusions are mostly Ni with a Cr, Fe phase that occurs around the inclusions (see Table C-9 for compositions). See Figures C-121 through C-130 for typical optical and SEM images of Particle 7A.

Particle 7B

In Particle 7B (Figures B-34) as shown in Figure C-131 there is an outside layer of ZrO_2 followed by layers of alpha-zircaloy, prior molten zircaloy mixed with uranium, and a region of UO_2 fuel, respectively. See Table C-10 for elemental identification and Figures C-132 and C-133 for 100x montages of two regions of the particle. The section for this particle appears to be longitudinal rather than a cross section based on the large radius of curvature. The prior molten material seen in Figures C-134 and 135 apparently flowed down from above and filled a 0.35 mm gap. This is four times the radial gap as fabricated; therefore, there was probably ballooning at this point in the fuel rod. It was determined that the prior molten Zr,U material flowed in from another location by the clear interface with the original cladding and from the known dimensions of the original cladding. There is very little Zr

penetration into the fuel at this point, so most of the U in the prior molten U,Zr material came from above. See Figures C-136 through C-141 for typical optical and SEM images.

Particle 7E

All of Particle 7E (Figure B-37) is shown in Figure C-142 and an edge and central region is shown in Figure C-143 after etching. The central portion of this particle is UO_2 fuel which has experienced grain growth (from ~10 to ~28 μm) and void formation. Some loss of individual grains of UO_2 occurred in this region when etched. All around the edge of this particle is $(U,Zr)O_{2+x}$ with Al-Cr-Fe-Ni second phase material and high Ni/low Sn inclusions. Along one edge there is a cluster of high Ni/low Fe inclusions with Cr and Fe in the base material and Al-Cr-Fe-Ni in a second phase. The amount of Zr in the base material and the amount of second phase material decreases with position toward the central region of this particle. See Table C-11 for more detailed chemical composition and Figures C-144 though C-152 for typical optical and SEM images.

Particle 8A

Particle 8A (Figures B-46) is relatively homogeneous with many irregular shaped pores of various sizes as shown in Figure C-153. The surfaces of the pores tend to be rounded. See Figure C-154 for an example of rounded pore surfaces and the slight effect of etching. Note that some of the pores could be caused by pull out of grains. This particle is predominately $(U,Zr)O_2$ with slight variations in the U,Zr ratio, and there is an Al-Cr-Fe-Ni material in some of the voids and grain boundaries. See Table C-12 for chemical composition data. See Figures C-155 through C-165 for typical optical and SEM images.

Particle 8C

Particle 8C (Figure B-48) can be divided into three regions based on void morphology and elemental distribution as shown in Figure C-166. In all three regions the base material is $(U,Zr)O_{2-x}$ with an Al-Cr-Fe-Ni

material at grain boundaries and in voids. See Table C-13 for composition data. Region 1 contains irregular shaped pores and grains with nonuniform chemical composition. Figures C-167 and C-168 show two different areas within Region I at two different contrast settings of the SEM, so that the variation of U and Zr composition within the grain can be separated from the Al-Cr-Fe-Ni grain boundary phase. The effect of etching can be seen in Figure C-169 which seems to be mainly on the grain boundary material. Region 2 contains large round pores and somewhat more uniform grain composition. Region 3 contains elongated grains and fairly uniform grain compositions. See Figures C-170 through C-176 for more SEM and optical images.

Particle 8E

Particle 8E (Figure B-50) can be divided into five regions based on void morphology and chemical composition. The five regions are shown in Figure C-177, and the chemical composition in the five regions is given in Table C-14. Region 4 which is the narrow band of many small voids running across the lower part of the particle provides a distinct boundary between Regions 3 and 5. The other boundaries are not as visible but can be detected on the SEM. The base material in all five regions is $(U,Zr)O_{2+x}$ with variations in U to Zr ratios from region to region. The grain boundary phase brought out by etching shown in Figures C-178 through C-180 is much higher in Zr than the base material and contains a small amount of Fe with a trace of Cr and Ni. There are also Ni-Sn inclusions and Cr-Fe and Cr-Fe-Ni materials found in and around voids. Figures C-181 through C-189 show typical optical and SEM images.

Particle 8H

Particle 8H (Figure B-52) consists of a ceramic material mechanically bonded to a Ag metallic material. The ceramic material consists of U with some Zr and a trace of Fe. It contains many irregular shaped pores of various sizes and generally rounded surfaces. It can be divided into three regions as shown in Figure C-190 based on the Zr-U ratios. See Table C-15 for elemental identification.

The central region has the lowest Zr content with some increase toward other regions. A Cr, Fe, Ni material occurs in some grain boundaries and voids particularly in Region 3 which has the highest Zr content.

The silver metallic material is pore free with round nickel-low Sn inclusions occurring around the edge. This can be seen in Figure C-191 which shows the results of a spontaneous galvanic etch that occurred in the polisher. See Figures C-192 through C-204 for typical optical and SEM images of Particle 8H.

Particle 9D

Particle 9D (Figure B-61) consists of a Ag metallic material mechanically bonded to several small pieces of U-Zr ceramic material as shown in Figure C-205. The Ag metallic material has round inclusions containing Ni, Sn and traces of Fe (see Figure C-206). The surfaces of the Ag regions are textured with parallel rills which were possibly caused by etching (see Figures C-207 and C-208).

The Zr-U ratios in the ceramic material varies from piece to piece as shown in Table C-16. There are traces of Fe, Ni, and Cr in the ceramic base material, but only the small piece within the large metallic piece contains an Fe-Ni material in grain boundaries and voids. See Figures C-209 through C-219 for typical optical and SEM images.

Particle 9G

Particle 9G (Figure B-64) consists entirely of Ag metallic material with Ni and Sn inclusions. See Figure C-220 for an overall as-polished view, Table C-17 for elemental identification and Figures C-221 through C-232 for typical optical and SEM images.

Particle 10A

Figure C-233 shows Particle 10A (Figure B-71) before and after a five minute immersion etch. Rather than reveal a grain structure, the etch tended to preferentially dissolve material around clusters of small pores. This particle was later repolished so the large void seen in Figure C-233 disappeared as shown in the SEM macro in Figure C-234.

This particle is composed entirely of $(U,Zr)O_2$ with no grain boundary or other phases and practically no inclusions. There are three different zirconium contents within this particle. The high zirconium content material is about 7 atom% Zr and is generally found around cracks, edges, and voids. This material tends to be almost pore free and contains a trace of iron (Fe). The middle zirconium content material is about 1-1/2 atom% Zr and is found throughout most of the particle. This material contains many small (<10 μm) voids. Figure C-235 shows these two materials. The low zirconium content material is about 0.5% to no zirconium and is found in a small central region (see Figure C-233). This was the only material in this particle to exhibit a grain structure; the grain size is approximately 28 μm. Figure C-236 shows this material. See Table C-18 for composition data and Figure C-237 through C-247 for typical optical and SEM images.

Particle 10E

Particle 10E (Figure B-75) appears to be two pieces of fuel stuck together by some prior molten material. Figure C-248 shows the overall mounted particle and a closeup of the upper piece which appears to have broken off during the mounting process. This figure also shows the severe effect of the etch on the fuel regions and the negligible effect on the prior molten material.

The fuel regions contain UO_2 only, and according to the average of nine SAS readings is slightly hypostoichiometric. See Table C-19 for composition data. The fuel grain size is 10 μm indicating essentially no

grain growth from as-fabricated fuel. The adherent prior molten material is composed of $(UZr)O_{2+x}$ with Ni, Sn, and Ag inclusions. The Zr/U ratio decreases with position moving from the outer edge toward the fuel. See Figures C-249 through C-260 for typical optical and SEM images.

Particle 10F

Particle 10F (Figure B-76) is composed of two distinct regions as shown in Figure C-261. Figure C-262 is a closeup of the region interface before and after etching. Region 1 contains many small irregular shaped pores and is composed of $(U,Zr)O_{2+x}$ with a trace of Fe. There is very little grain boundary or second phase material in this region. Region 2 which cuts across Region 1 contains large round pores and is also composed of $(U,Zr)O_{2+x}$ with a trace of Fe. The Zr to U ratio is slightly higher in Region 2 and there is an extensive amount of grain boundary phases containing Cr, Fe, and Ni. There is also a fine grained second phase material found in Region 2 that contains the same constituents as the base material but with more Fe, slightly more Zr and less oxygen. The second phase material is hypostoichiometric while the base material is hyperstoichiometric as shown in the composition data given in Table C-20. See Figures C-263 through C-270 for typical optical and SEM images of Particle 10F.

Particle 11B

Particle 11B (Figure B-84) is composed of metallic material mechanically bonded to ceramic material as shown in Figure C-271. The metallic material has irregular shaped interior voids and one complex rectangular inclusion. See Figure C-272 and Table C-21. The base metallic material is Ni with some Fe and a trace of Sn. The second phase material is also Ni but with substantial amounts of Sn and small amounts of Fe and Ag. There are also Ag inclusions containing small amounts of Mo, Ni, and Fe throughout the metallic material.

The ceramic material is very porous with generally small irregular pores and with rounded surfaces. The base material is U with low Zr, and there is a grain boundary phase containing Cr and Fe, small amounts of U, and a trace of Al and Zr. Throughout the ceramic material there are Ni and Fe inclusions and blisters (see Figure C-273). The inclusions contain some Sn; the blisters contain some Mo and occasionally some Ag, In, and Cd. See Table C-21 for composition data and Figure C-274 through C-281 for typical optical and SEM images.

Particle 11C

Particle 11C (Figures B-85) originally appeared from its dimensions to be a half section of a fuel pellet. Part of this particle was removed for other analysis so the macros shown in Figure C-282 are not half sections. This particle was ground down further after initial analysis in an attempt to find the surface layer seen in Figure B-85. Figures C-283 and C-284 are a 100X cross-section of the particle showing the relative uniformity of grain size from pellet center to surface. Figure C-285 is a closeup, as polished view of fuel showing the high porosity at the grain boundaries which makes the grains distinct without etching. The grain size is about 10 μm indicating virtually no grain growth. The material adhering to the pellet surface is Zr and U with the amount of Zr decreasing with position toward the fuel. There is a small amount of Zr diffused into the surface fuel grains. See Table C-22 for composition data and Figures C-286 through C-290 for typical optical and SEM images.

TABLE C-1. CHEMICAL COMPOSITION OF SELECTED AREAS OF PARTICLE 18

ID[a]	U	Zr	O	Al	Cr	Fe	Ni	Sn	Miscellaneous	Comments
[illegible]	+	--	--	--	--	--	--	--	--	Central fuel region, see Figure C-9
054	+	--	--	--	--	--	--	--	--	Central fuel region, see Figure C-9
066	+	--	--	--	--	--	--	--	--	Central fuel region, see Figure C-9
037	+	--	--	--	?	?	--	--	--	Near large void, see Figure C-9
061	+	--	--	--	--	--	--	--	--	Base material, see Figure C-9 and C-17
033	+	--	--	--	--	?	--	--	--	Edge of fuel region, see Figure C-9
034	+	--	--	--	--	Tr	--	--	--	Edge of fuel region, see Figure C-9
045	+	--	--	--	--	Tr	--	--	--	Edge of fuel region, see Figure C-9
031	+	--	--	--	--	Tr	--	--	--	Base material, see Figure C-16
032	+	--	--	--	--	Tr	--	--	Tc(+),Ru(+)	Material in void, see Figure C-16
018	+	--	--	--	--	?	--	--	--	See figure C-19
017	+	0	--	--	--	Tr	--	--	--	Gradient across melt-fuel interface
016	0	+	--	--	--	Tr	--	--	--	
015	0	+	--	--	?	Tr	Tr	--	--	
019	+	0	--	--	--	?	Tr	--	SN(0)--Pa(+)	Inclusion at melt-fuel interface
022	0	+	--	--	Tr	Tr	Tr	--	--	See figure C-20
023	+	+	--	--	Tr	Tr	--	--	--	Gradient across melt-fuel interface
024	+	0	--	--	--	Tr	--	--	--	
025	+	--	--	--	--	Tr	--	--	--	
026	+	0	--	--	--	Tr	Tr	--	Ru(0)	Inclusion at melt-fuel interface
040	--	+	--	--	--	--	--	--	--	See figure C-18
041	--	+	--	--	--	--	--	--	--	Gradient across melt-fuel interface
042	Tr	+	--	--	--	--	--	--	--	
043	+	+	--	--	--	--	--	--	--	
044	+	Tr	--	--	--	--	--	--	--	

a. See figures mentioned in the comments for location of ID numbers.

Quantitative (SAS): Data is in atom percent.

Qualitative (SEM/EDS): ? - uncertain
Tr - trace
0 - minor
+ - major

TABLE C-2. CHEMICAL COMPOSITION OF SELECTED AREAS OF PARTICLE 3L

ID[a]	U	Zr	O	Al	Cr	Fe	Ni	Sn	Miscellaneous	Comments
671	+	+	--	--	--	--	--	--	--	Dark phase (low Z) in Figure C-36
676	+	+	--	--	--	--	--	--	--	Light phase (high Z) in Figure C-36
671/676	10.0	25.0	65.0	--	--	--	--	--	--	Average of two phases
709	8.0	20.0	72.0	--	--	--	--	--	--	Base material, see Figure C-31 and C-35
710	9.0	22.0	69.0	--	--	--	--	--	--	Base material, see Figure C-31 and C-35
677-1	10.0	23.0	67.0	--	--	--	--	--	--	Base material, see Figure C-37
677-2	10.0	22.0	68.0	--	--	--	--	--	--	--
713	8.0	27.0	65.0	--	--	--	--	--	--	Base material, see Figure C-31
691	9.0	23.0	68.0	--	--	--	--	--	--	Base material, see Figure C-31
688	7.0	23.0	70.0	--	--	--	--	--	--	Base material, see Figure C-31
685	8.0	23.5	68.4	--	--	--	--	--	--	Base material, see Figure C-31
699	7.0	23.0	69.6	--	--	--	--	--	--	Base material, see Figure C-31 and C-38
697	+	+	--	--	Tr	Tr	?	--	--	Material in void, see Figure C-38
689-1	13.5	20.0	66.5	--	--	--	--	--	--	Base material above void, see Figure C-31 and C-39
689-2	14.4	15.0	70.4	--	--	--	--	--	--	Base material below void, see Figure C-31 and C-39
700	+	+	--	--	+	+	+	--	--	Material in void, see Figure C-38
704	+	+	--	+	+	+	+	--	--	Grain boundary material, see Figure C-39
706	+	+	--	--	--	Tr	Tr	--	--	Grain boundary material, see Figure C-39
714	+	+	--	--	0	0	0	--	--	Material in void.
715	+	+	--	+	+	+	+	--	--	Grain boundary material, see Figure C-39

a. See figures mentioned in the comments for location of ID numbers.

Quantitative (SAS): Data is in atom percent.

Qualitative (SEM/EDS): ? - uncertain
Tr - trace
0 - minor
+ - major

TABLE C-3. CHEMICAL COMPOSITION OF SELECTED AREAS OF PARTICLE 3M

ID[a]	U	Zr	O	Al	Cr	Fe	Ni	Sn	Miscellaneous	Comments
899	+	--	--	--	--	--	--	--	--	Region 1 Base Material, see Figure C-40
886	+	--	--	--	--	--	--	--	--	Region 1 Base Material, see Figure C-40 and C-44
887	+	--	--	--	--	Tr	0	--	Tc(+)--Ru(+)	Bead in Region 1, see Figure C-44
894	+	--	--	--	--	--	--	--	--	--
907	+	--	--	--	--	--	--	--	--	Region 1 base material, see Figure C-40 and C-44
908	+	--	--	--	--	--	--	--	--	--
895	+	+	--	--	Tr	Tr	?	--	--	Region 1 and 2, Figures C-40, C-46
896	+	0	--	--	Tr	Tr	?	--	--	--
897	+	Tr	--	--	--	Tr	--	--	--	--
898	+	--	--	--	--	--	--	--	--	--
902	+	+	--	--	--	0	--	--	--	Region 2 Material, see Figure C-40 and C-49
903	+	0	--	--	--	Tr	--	--	--	--
912	+	0	--	--	Tr	Tr	--	--	--	Region 2 base material, see Figure C-40 and C-48
913	+	Tr	--	--	?	--	?	--	--	--
916	+	0	--	--	Tr	0	Tr	--	--	--
915	+	Tr	--	--	+	+	+	--	Mo(?)	Material in void, see Figure C-48
919	+	0	--	--	--	0	--	--	--	Region 2 base material, see Figure C-40 and C-49
920	Tr	+	--	--	Tr	Tr	--	--	--	--
921	+	Tr	--	--	--	Tr	--	--	--	--
905	0	--	--	--	+	+	+	+	--	Material in void, see Figure C-47
906	+	+	--	--	+	+	+	--	--	--
924	+	Tr	--	--	--	Tr	--	--	--	Base material, see Figure C-40 and C-47
925	Tr	--	--	--	--	Tr	0	?	Tc(+)--Ru(+)	Material in void, see Figure C-47

a. See figures mentioned in the comments for location of ID numbers.

Quantitative (SAS): Data is in atom percent.

Qualitative (SEM/EDS): ? - uncertain
Tr - trace
0 - minor
+ - major

TABLE C-4. CHEMICAL COMPOSITION OF SELECTED AREAS OF PARTICLE 4A

ID[a]	U	Zr	O	Al	Cr	Fe	Ni	Sn	Miscellaneous	Comments
953	+	0	--	--	--	Tr	--	--	--	Base material, see Figure C-57
954	+	+	--	--	--	+	0	--	Ti(0)	Material in void
957	+	--	--	0	+	+	0	--	--	Material in void
986	+	Tr	--	--	--	Tr	--	--	--	Base material, see Figure C-53
981	Tr	0	--	0	Tr	+	+	0	Ti(0)	Material in void
984	+	+	--	0	0	+	+	+	Ru(+)	Inclusion
985	Tr	--	--	--	--	0	+	0	Ru(+)--Tc(+)	Inclusion
964	+	Tr	--	--	Tr	Tr	--	--	--	Base material, Figures C-52, C-53
967	Tr	--	--	--	--	--	+	+	Ru(Tr) Ag(?)	Inclusion
968	+	0	--	0	+	+	0	--	--	Second phase
963	+	0	--	--	--	Tr	--	--	--	Base material, see Figure C-57
961	Tr	--	--	--	--	--	+	+	Ag(?)	Second phase
969	+	Tr	--	--	--	Tr	--	--	--	U-Zr base material, see Figure C-50
973	+	0	--	--	Tr	Tr	--	--	--	--
975	+	0	--	--	Tr	Tr	--	--	--	--
976	+	0	--	--	--	Tr	--	--	--	--
978	+	Tr	--	--	--	Tr	--	--	--	--
979	+	Tr	--	--	--	Tr	--	--	--	--
980	+	Tr	--	--	--	--	--	--	--	--
970	+	--	--	--	--	?	--	--	--	Base material, see Figure C-50
958	+	--	--	--	--	--	--	--	--	Base material, see Figure C-52
974	+	--	--	--	--	Tr	--	--	--	Base material, see Figure C-58
988	+	--	--	0	+	+	0	--	--	Grain boundary material, Fig. C-56
991	+	0	--	0	0	+	+	--	Ru(?)	Grain boundary material, Fig. C-56

a. See figures mentioned in the comments for location of ID numbers.

Quantitative (SAS): Data is in atom percent.

Qualitative (SEM/EDS): ? - uncertain
Tr - trace
0 - minor
+ - major

TABLE C-5. CHEMICAL COMPOSITION OF SELECTED AREAS OF PARTICLE 4B

ID[a]	U	Zr	O	Al	Cr	Fe	Ni	Sn	Miscellaneous	Comments
725	32.2	--	67.7	--	--	--	--	--	--	Interior base material
	36.4	--	63.5	--	--	--	--	--	--	See Figure C-63
	34.4	--	65.5	--	--	--	--	--	--	--
738	+	--	--	--	--	Tr	--	--	--	Base material, see Figure C-69
[illegible]	33.9	2.7[b]	63.2	--	--	--	--	--	--	--
760	Tr	--	--	--	--	--	+	+	Ru(+)	Bead, see Figure C-61
761	+	--	--	--	--	--	--	--	S(+)	Material in void
762	0	--	--	--	--	0	+	+	Ru(+)	Bead in vicinity of 760
763	0	--	--	--	0	0	0	--	Ru(+)/Tc(+)	Second bead in vicinity of 760
746	32.6	0.9	66.4	--	--	--	--	--	--	Base material, see Figure C-61
748	+	0	--	0	+	+	0	--	--	Material in void
747	31.6	3.0	65.2	--	--	--	--	--	--	Base material
749	27.6	1.8	70.5	--	--	Tr[c]	--	--	--	Base material, see Figure C-66
729	24.1	8.0	67.7	--	--	Tr[c]	--	--	--	--
729-1	31.9	--	61.7	--	3.6	12.7	9.9	--	--	Grain boundary phase near 729
730	+	0	--	--	--	Tr	--	--	--	Material in void
731	+	+	--	Tr	+	+	+	--	--	Base material
732	+	+	--	Tr	+	+	+	--	--	--
733	+	0	--	--	Tr	0	Tr	--	--	--
757	+	Tr	--	--	--	--	--	--	--	Base material, see Figure C-65
753	+	Tr	--	--	--	--	--	--	--	--
752	+	0	--	--	--	--	--	--	--	--
754	--	3.1	--	--	--	--	84.0	1.2	C-11.6	Inclusion
755	9.8	4.9	56.2	--	6.5	11.5	10.7	--	--	Grain boundary material

a. See figures mentioned in the comments for location of ID numbers.

b. Not detected by SEM/EDS.

c. Detected by SEM/EDS and not by SAS.

Quantitative (SAS): Data is in atom percent.

Qualitative (SEM/EDS): ? - uncertain
Tr - trace element
0 - minor constituent
+ - major constituent

TABLE C-6. CHEMICAL COMPOSITION OF SELECTED AREAS OF PARTICLE 4D

ID[a]	U	Zr	O	Al	Cr	Fe	Ni	Sn	Miscellaneous	Comments
747	+	Tr	--	--	--	--	--	--	--	High Z material, see Figure 70
748	+	0	--	--	--	--	--	--	--	--
757	+	0	--	--	--	Tr	--	--	--	--
334	+	0	--	--	--	--	--	--	--	High Z material, see Figure C-85
332	+	+	--	--	--	--	--	--	--	Low Z material, see Figure C-85
333	+	0	--	--	--	--	--	--	--	High Z material, see Figure C-85
335	+	0	--	Tr	+	+	+	--	--	Void material, see Figure C-85
752	+	+	--	--	--	Tr	--	--	--	Low Z material, see Figure C-81
753	+	0	--	--	--	?	--	--	--	High Z material, see Figure C-81
749	+	0	--	--	--	Tr	--	--	--	High Z material, see Figure C-81
323	+	+	--	--	--	Tr	--	--	--	Base material, see Figure C-78
324	+	0	--	--	--	--	--	--	--	--
325	+	0	--	?	+	+	+	--	Ti(?)	Dendritic material, see Figure C-78
327	0	0	--	--	0	+	+	0	Ti(Tr)	Other material in void
755	+	+	--	--	--	Tr	--	--	--	Base material, see Figure C-80
756	+	0	--	--	--	--	--	--	--	--
746	+	0	--	--	--	--	--	--	--	Base material, see Figure C-80
729	+	0	--	--	--	--	--	--	--	Base material, see Figure C-82
728	+	+	--	--	--	--	--	--	--	--
734	+	0	--	--	--	Tr	Tr	--	--	Base material near void
731	Tr	Tr	--	?	+	+	+	0	Ti(Tr)	Material in void
732	+	0	--	--	Tr	Tr	Tr	--	--	--
733	+	0	--	?	+	+	+	--	--	--
735	+	0	--	--	--	Tr	Tr	--	--	Bead in void, see Figure C-83
739	0	0	--	Tr	+	+	+	0	Ti(O)	Material in void
740	+	0	--	?	+	0	0	--	--	--
741	Tr	+	--	--	--	Tr	--	--	Ag(O)	Fragment off sample edge, see Figure C-79
744	+	+	--	--	--	--	--	--	--	Base material, see Figure C-79

a. See figures mentioned in the comments for location of ID numbers.

Quantitative (SAS): Data is in atom percent.

Qualitative (SEM/EDS): ? - uncertain
Tr - trace element
0 - minor constituent
+ - major constituent

TABLE C-7. CHEMICAL COMPOSITION OF SELECTED AREAS OF PARTICLE 5E

ID[a]	U	Zr	O	Al	Cr	Fe	Ni	Sn	Miscellaneous	Comments
866	32.2	2.0	65.6	--	--	Tr[b]	--	--	--	Region 1 base material, see Figure C-87
846	+	0	--	--	--	--	--	--	--	--
862	+	Tr	--	--	--	Tr	--	--	--	--
852	+	0	--	--	--	Tr	--	--	--	--
873	Tr	Tr	--	--	+	+	+	--	--	Grain boundary phase, see Figure C-89
855	+	Tr	--	--	--	Tr	--	--	--	Base material, see Figure C-87 and C-90
853	Tr[b]	--	--	--	--	--	2.1	5.4	Tc-10.2, Pd-13.8, Ru-52.6, Rh-15.6	Inclusion, see Figure C-90
[illegible]	Tr[b]	--	4.5	--	--	--	23.7	5.3	Tc-7.9, Pd-9.8, Ru-34.9, Rh-13.4	Inclusion, see Figure C-90
847	27.5	2.6	69.7	--	--	Tr[b]	--	--	--	Region 2 base material, see Figure C-87
865	+	0	--	--	--	Tr	--	--	--	--
856	Tr	--	--	--	--	Tr	+	--	Ru(+)	Inclusion in region 2, see Figure 93
868	0	--	--	--	+	+	+	--	--	Grain boundary phase, see Figure C-88
860-A	21.0	9.1	69.8	--	--	Tr[b]	--	--	--	Region 3 base material, see Figure C-87
860-B	22.0	8.0	69.8	--	--	--	--	--	--	--
860-C	22.1	8.9	68.8	--	--	--	--	--	--	--
860-D	22.5	9.2	68.1	--	--	--	--	--	--	--
844	25.1	5.9	68.8	--	--	--	--	--	--	--
863	28.3	2.6	69.0	--	--	--	--	--	--	Region 4 base material, see Figure C-87
848	+	0	--	--	--	--	--	--	--	--
861	+	0	--	--	--	?	--	--	--	--
851	+	0	--	--	--	?	--	--	--	--
874	+	0	--	--	+	+	+	--	--	Grain boundary phase, see Figure C-87 and C-95
	3.7	--	40.8	--	2.0	22.5	30.8	--	--	Dark/grain boundary phase similar to 874
	14.7	2.3	54.9	--	--	10.8	17.0	--	--	Light/grain boundary phase similar to 874
850-A	31.0	0.4	68.5	--	--	--	--	--	--	Region 5 base material, see Figure C-87
850-B	30.9	0.6	68.4	--	--	--	--	--	--	--
850-C	30.7	0.9	68.3	--	--	--	--	--	--	--

TABLE C-7. (continued)

ID[a]	U	Zr	O	Al	Cr	Fe	Ni	Sn	Miscellaneous	Comments
864-A	32.9	0.6	66.4	--	--	--	--	--	--	Region 6 base material, see Figure C-87
864-B	27.0	0.0	72.9	--	--	--	--	--	--	--
864-C	24.9	1.0	74.0	--	--	--	--	--	--	--
864-D	31.3	0.0	68.6	--	--	--	--	--	--	--
864-E	32.2	0.5	67.3	--	--	--	--	--	--	--
864-1	26.4	0.5	73.0	--	--	--	--	--	--	Region 7 base material, see Figure C-87
864-2	28.1	1.1	70.6	--	--	--	--	--	--	--
864-3	29.2	1.6	69.0	--	--	--	--	--	--	--

a. See figures mentioned in the comments for location of ID numbers.

b. Detected by SEM/EDS and not by SAS.

Quantitative (SAS): Data is in atom percent.

Qualitative (SEM/EDS): ? - uncertain
Tr - trace element
0 - minor constituent
+ - major constituent

TABLE C-8. CHEMICAL COMPOSITION OF SELECTED AREAS OF PARTICLE 6C

ID[a]	U	Zr	O	Al	Cr	Fe	Ni	Sn	Minor Elements	Comments
630	--	Tr	--	0	+	+	--	--	--	Large inclusion, see Figures C-97, C-106 and C-107
625-1	--	4.4	21.6	--	--	--	36.4	18.9	C-38.5	--
627	--		--	--	--	--	+	+	--	--
628	--	Tr	--	--	--	--	0	+	Ru(+)	--
629	--		--	--	--	Tr	Tr	+	--	--
634	0	+	--	+	--	--	--	--	--	Aluminum bearing phases, see Figure C-108
635	Tr	0	--	+	--	--	--	--	--	--
646	Tr	Tr	--	+	--	--	--	--	--	--
647	0	+	--	+	--	--	--	--	--	--
648	0	+	--	+	--	--	--	--	--	--
637	--	+	--	--	--	--	--	--	--	ZrO_2 layers, see Figure C-100
638	--	30.4	64.6	--	--	--	--	--	C-4.9	--
639	--	+	--	--	--	--	--	--	--	--
642	--	+	--	--	--	--	--	--	--	ZrO_2-$(U,Zr)O_2$ interface, see Figure C-101
644	0	+	--	--	--	--	--	--	--	--
643	Tr[b]	28.8	62.5	--	--	--	--	--	C-8.5	--
650	Tr[b]	28.9	65.6	--	--	--	--	--	C-5.3	ZrO_2 layer, see Figure C-99
651	--	+	--	--	--	--	--	--	--	--
653	--	10.5	25.7	51.1	--	--	--	--	C-12.3	ZrO_2 interface, see Figure C-109
655	--	Tr	--	+	--	--	--	--	--	--
656	--	+	--	--	--	--	--	--	--	--
658	2.2	27.8	2.1	53.7	3.7	8.6	--	1.5	--	ZrO_2 interface, see Figure C-99
659	--	+	--	0	0	0	--	0	--	--
660	--	Tr	--	--	--	--	--	+	--	--
661	--	+	--	+	0	0	--	0	--	--
662	3.2	29.6	67.1	--	--	--	--	--	--	--
622-1	0.8	30.3	68.7	--	--	--	--	--	--	Base material sample center, see Figure C-97
666	--	+	--	--	--	--	--	--	--	Base material sample center, see Figure C-104
667	Tr	+	--	--	--	--	--	--	--	--
668	--	0	--	+	--	--	--	--	--	--

a. See figures mentioned in the comments for location of ID numbers.

b. Detected by SEM/EDS and not by SAS.

Quantitative (SAS): Data is in atom percent.

Qualitative (SEM/EDS): ? - uncertain
Tr - trace element
0 - minor constituent
+ - major constituent

TABLE C-9. CHEMICAL COMPOSITION OF SELECTED AREAS OF PARTICLE 7A

ID[a]	U	Zr	O	Al	Cr	Fe	Ni	Sn	Miscellaneous	Comments
449	+	0	--	--	Tr	Tr	--	--	--	Base material, see Figure C-124
450	+	0	--	0	+	+	0	--	--	Grain boundary phase
451	+	0	--	--	--	Tr	--	--	--	Second phase
452	+	+	--	--	--	0	--	--	--	Inclusion
465	+	0	--	--	--	--	--	--	--	Base material
466	+	0	--	+	+	+	0	--	--	Grain boundary phase
469	+	0	--	--	--	Tr	--	--	--	Second phase
464	+	0	--	+	+	+	0	--	--	Grain boundary material, see Figure C-130
456	+	0	--	--	--	Tr	--	--	--	Base material
457	+	0	--	--	--	Tr	--	--	--	Second phase
461	0	Tr	--	+	+	+	0	--	--	Complex mixture, see Figure C-129
462	+	+	--	--	0	0	Tr	--	--	--
463	+	+	--	--	Tr	0	Tr	--	--	--
555	--	--	--	--	--	0	+	--	--	Inclusion, see Figure C-127

a. See figures mentioned in the comments for location of ID numbers.

Quantitative (SAS): Data is in atom percent.

Qualitative (SEM/EDS): ? - uncertain
Tr - trace element
0 - minor constituent
+ - major constituent

TABLE C-10. CHEMICAL COMPOSITION OF SELECTED AREAS OF PARTICLE 7B

10[a]	U	Zr	O	Al	Cr	Fe	Ni	Sn	Miscellaneous	Comments
975	+	+	--	--	--	Tr	--	--	--	Complex layering, see Figure C-134
976	Tr	+	--	--	--	--	--	--	--	--
977	Tr	+	--	--	--	--	--	Tr	--	--
978	--	+	--	--	--	--	--	--	--	--
980	0	+	--	--	--	--	--	--	--	--
989	--	+	--	--	--	--	--	--	--	--
994	--	+	--	--	--	--	--	--	--	--
998	--	+	--	--	--	--	--	--	--	--
000	--	+	--	--	--	--	--	?	--	--
001	--	+	--	--	--	--	--	--	--	--
002	Tr	+	--	--	Tr	Tr	--	--	--	--
003	Tr	+	--	--	0	0	Tr	--	--	--
004	+	Tr	--	--	--	--	--	--	--	--
981	+	+	--	--	--	--	--	--	--	--
982	--	+	--	--	Tr	0	0	0	--	--
983	--	+	--	--	--	--	--	--	--	--
984	0	+	--	--	Tr	0	0	--	--	--
985	Tr	+	--	--	0	0	0	0	--	--
996	Tr	+	--	--	--	Tr	--	--	--	--
997	--	+	--	--	Tr	0	0	0	--	--
999	--	+	--	--	--	--	--	--	--	--
988	Tr	+	--	--	--	--	--	Tr	--	Complex mixture, see Figure C-135
990	--	+	--	--	--	--	--	--	--	--
991	Tr	+	--	--	Tr	0	0	--	--	--
992	Tr	+	--	--	--	Tr	Tr	--	--	--
993	Tr	+	--	--	--	--	--	--	--	--
006	+	+	--	--	--	--	--	--	--	Base material in crack, see Figure C-138
007	?	+	--	--	--	?	--	--	--	--
964	+	0	--	--	--	--	--	--	--	Material at interface, see Figure C-136
965	+	+	--	--	--	--	--	--	--	--
969	+	+	--	--	Tr	Tr	Tr	--	--	--
966	--	+	--	--	--	?	--	--	--	--
967	--	+	--	--	--	--	?	Tr	--	--
959	?	+	--	--	--	--	--	?	--	Prior molten (U,Zr,O), see Figure C-141
957	?	+	--	--	--	--	--	--	--	--
958	+	+	--	--	Tr	Tr	--	--	--	--
955	+	+	--	--	?	Tr	--	--	--	--
971	--	+	--	--	--	--		?	--	Base material, see Figure C-137
972	--	+	--	--	Tr	Tr	--	--	--	Second phase
973	0	+	--	--	--	--	--	--	--	Second phase

TABLE C-10. (continued)

ID[a]	U	Zr	O	Al	Cr	Fe	Ni	Sn	Miscellaneous	Comments
008	--	+	--	--	--	--	--	--	--	Base material, see Figure C-131
935	--	+	--	--	--	--	--	--	--	--
009	Tr	+	--	--	Tr	Tr	--	--	--	--
934	?	+	--	--	--	--	--	?	--	--
010	+	?	--	--	--	--	--	--	--	--
933	+	--	--	--	--	--	--	--	--	--
936	+	--	--	--	--	--	--	--	--	--

a. See figures mentioned in the comments for location of ID numbers.

Quantitative (SAS): Data is in atom percent.

Qualitative (SEM/EDS): ? - uncertain
Tr - trace element
0 - minor constituent
+ - major constituent

TABLE C-11. CHEMICAL COMPOSITION OF SELECTED AREAS OF PARTICLE 7E

ID[a]	U	Zr	O	Al	Cr	Fe	Ni	Sn	Miscellaneous	Comments
478-A	34.4	--	65.6	--	--	--	--	--	--	Base material in sample center, see Figure C-145
478-B	34.5	--	65.4	--	--	--	--	--	--	--
478-C	35.7	--	64.2	--	--	--	--	--	--	--
507-A	--	--	--	--	--	3.8	92.7	--	C-3.4[b]	Metallic base material, see Figure C-149
507-B	--	--	--	--	--	0.7	84.3	0.4[b]	C-14.5	--
507-C	--	--	0.4	--	--	--	95.9	0.3[b]	C-3.2	--
508-A	25.9	4.6	69.4	--	Tr[c]	Tr[c]	--	--	--	Ceramic base material
508-B	27.4	4.4	68.0	--	Tr[c]	Tr[c]	--	--	--	--
508-C	26.8	3.7	69.3	--	Tr[c]	Tr[c]	--	--	--	--
509[d]	+[c]	Tr[c]	33.8	40.6	9.2	10.4	5.7	--	--	Low Z second phase
511[d]	30.2	4.9	57.8	2[b]	9.6	9.0	8.2	--	--	High Z second phase
534-A	13.8	6.9	79.1	--	--	--	--	--	--	Base material, see Figure C-142
534-B	22.7	5.3	71.8	--	--	--	--	--	--	--
534-C	30.2	--	65.5	--	--	--	--	--	C-4.2	--
535	+	0	--	--	--	--	--	--	--	--
536	+	--	--	--	--	--	--	--	--	--
537	--	--	--	--	--	--	+	0	--	Inclusion, see Figure C-152
538	+	0	--	--	--	--	--	--	--	Base material
545	+	0	--	--	--	--	--	--	--	Base material, see Figure C-152
546	Tr	--	--	0	--	+	--	--	Cd(0), Mo(0), Si-Tr	Void material
550	--	--	--	0	--	+	--	--	Mo(0), Ag(0), Si-Tr	Particle near location 546
552	Tr	--	--	--	--	+	--	--	Cd(0), Mo(0)	Second particle near location 546

a. See figures mentioned in the comments for location of ID numbers.

b. Not detected by SEM/EDS.

c. Detected by SEM/EDS only.

d. SAS examination not coincident with SEM/EDS.

Quantitative (SAS): Data is in atom percent.

Qualitative (SEM/EDS): ? - uncertain
Tr - trace element
0 - minor constituent
+ - major constituent

TABLE C-12. CHEMICAL COMPOSITION OF SELECTED AREAS OF PARTICLE 8A

ID[a]	U	Zr	O	Al	Cr	Fe	Ni	Sn	Miscellaneous	Comments
003-1	24.8	3.6	71.4	--	--	?[b]	--	--	--	Region 1 base material see Figure C-153
003-2	26.9	3.5	69.5	--	--	--	--	--	--	--
003-3	25.8	4.6	69.4	--	--	--	--	--	--	--
003-4	26.6	4.5	68.7	--	--	--	--	--	--	--
003-5	27.4	3.7	68.8	--	--	--	--	--	--	12 consecutive SAS readings with continuous sputter reveals
003-6	26.8	4.6	68.4	--	--	--	--	--	--	a depth profile of about 1 μm; Avg:27.9 U, 4.2 Zr,
003-7	30.5	4.1	65.3	--	--	--	--	--	--	67.8% O
003-8	27.6	4.5	67.7	--	--	--	--	--	--	--
003-9	27.6	4.2	68.0	--	--	--	--	--	--	--
003-10	30.2	4.0	65.7	--	--	--	--	--	--	--
003-11	29.1	4.3	66.5	--	--	--	--	--	--	
003-12	28.7	4.9	66.3	--	--	--	--	--	--	--
020	27.6	3.7	68.5	--	--	--	--	--	--	Region 2 base material, see Figure C-153
044	28.4	4.0	67.5	--	--	--	--	--	--	Region 3 base material, see Figure C-153
007	+	0	--	--	--	--	--	--	--	--
999	+	+	--	+	+	+	+	--	--	Second phase, see Figure C-161
998	+	+	--	--	0	0	0	--	--	Second phase, see Figure C-161
002	+	0	--	--	Tr	Tr	Tr	--	--	Base material, see Figure C-161
15	17.5	7.9	68.1	?	--	3.1	3.1	--	--	Second phase, see Figure C-162
16	21.9	10.9	65.8	--	--	0.7	0.4	--	--	Base material
17	20.2	6.1	73.5	--	--			--	--	Base material
18	5.7	2.9	30.9	47.4	--	4.2	8.6	--	--	Grain boundary phase
012	+	0	--	--	--	?	--	--	--	Base material, see Figure C-158
014	+	+	--	+	0	0	0	--	--	Second phase, see Figure C-158
018	+	0	--	--	--	--	--	--	--	Base material, see Figure C-158
016	0	+	--	--	0	0	0	--	--	Suface material, see Figure C-158
025	+	0	--	--	--	?	--	--	--	Base material, see Figure C-165
022	+	--	--	--	0	0	0	+	Mo(+)	Inclusion, see Figure C-165
030	+	+	--	+	+	+	+	--	--	Grain boundary phase see Figure C-163
031	+	+	--	--	--	Tr	--	--	--	Base material, see Figure C-163
034	Tr	+	--	--	0	0	0	--	--	Surface material, see Figure C-163
038	+	0	--	--	--	--	--	--	--	Base material, see Figure C-164
039	+	+	--	+	+	+	+	--	--	Void material, see Figure C-164
042	+	0	--	+	+	+	+	--	--	Void material, see Figure C-164

a. See figures mentioned in the comments for location of ID numbers.

b. Detected by SEM/EDS only.

Quantitative (SAS): Data is in atom percent.

Qualitative (SEM/EDS): ? - uncertain
Tr - trace element
0 - minor constituent
+ - major constituent

TABLE C-13. CHEMICAL COMPOSITION OF SELECTED AREAS OF PARTICLE 8C

ID[a]	U	Zr	O	Al	Cr	Fe	Ni	Sn	Miscellaneous	Comments
175	25.3	10.1	64.4	--	Tr[b]	Tr[b]	--	--	--	Base material Region 1, see Figure C-167
176	+	+	--	+	+	+	0	--	--	Grain boundary material Region 1
177	3.7	4.1	33.3	46.2	3.9	7.0	1.4	--	--	[illegible] phase Region 1
180	3.4	2.5	36.1	45.0	4.0	8.0	Tr[b]	--	--	Average eutectic Region 1
181	+	+	--	--	--	Tr	--	--	--	Second phase Region 1
182	26.6	6.7	66.6	--	--	--	--	--	--	Base material Region 1
183	Tr	Tr	--	--	--	--	--	--	Ag(+) S(0)	Bead in void Region 1
231A	+	0	--	--	--	--	--	--	--	High contrast Region 1 material, see Figure C-168
232	+	+	--	--	--	Tr	--	--	--	Medium contrast Region 1 material
233	+	+	--	--	Tr	Tr	--	--	--	Low contrast Region 1 material
201	+	0	--	--	--	?	--	--	--	Base material Region 2, see Figure C-172
224	0	0	--	+	+	+	0	--	--	Dark phase Region 2, see Figure C-172
225	+	+	--	+	+	+	0	--	--	Dendritic material Region 2, see Figure C-172
226	+	+	--	--	Tr	Tr	--	--	--	Light phase Region 2, see Figure C-172
227-1	25.1	11.4	63.3	--	--	--	--	--	--	Region 2 base material, see Figure C-172
227-2	27.9	11.2	60.8	--	--	--	--	--	--	--
227-3	27.0	10.3	62.5	--	--	--	--	--	--	Nine consectuive SAS readings with continue sputter reveals
227-4	30.0	7.0	62.8	--	--	--	--	--	--	a depth profile of about 1 μm
227-5	29.9	8.5	61.4	--	--	--	--	--	--	--
227-6	30.3	7.4	62.2	--	--	--	--	--	--	--
227-7	31.8	7.6	60.4	--	--	--	--	--	--	--
227-8	31.4	6.8	61.6	--	--	--	--	--	--	--
227-9	30.8	7.3	61.7	--	--	--	--	--	--	--
227-10	27.3	7.4	65.1	--	--	--	--	--	--	Edge of 227 grain
227-11	28.7	7.3	63.9	--	--	--	--	--	--	--
227-12	21.9	10.6	67.4	--	--	--	--	--	--	Dark grain near 227
227-13	24.0	7.7	68.2	--	--	--	--	--	--	Light grain near 227
195	+	0	--	--	--	Tr	--	--	--	Region 2 base material, see Figure C-171
229	+	0	--	--	--	--	--	--	--	Region 2 base material, see Figure C-174
235	+	0	--	--	--	--	--	--	--	Region 2 base material, see Figure C-171
238	+	0	--	--	--	Tr	--	--	--	Region 2 base material, see Figure C-174
185	+	+	--	+	+	+	0	--	--	Second phase Region 3 material, see Figure C-176
186-1	24.4	7.9	67.5	--	--	Tr[b]	--	--	--	Base material Region 3 material
186-2	26.5	8.3	65.1	--	--	--	--	--	--	Base material near 186 Region 3
187	+	+	--	0	0	0	--	--	--	gb material Region 3
189	Tr	+	--	--	Tr	0	0	--	Ag(+)	Surface material Region 3
191	Tr	+	--	--	0	0	0	--	Ag(0)	Surface material Region 3

TABLE C-13. (continued)

ID[a]	U	Zr	O	Al	Cr	Fe	Ni	Sn	Miscellaneous	Comments
192	+	+	--	--	Tr	--	--	--	--	Region 3 base material, see Figure C-175

a. See figures mentioned in the comments for location of ID numbers.

b. Detected by SEM/EDS only.

Quantitative (SAS): Data is in atom percent.

Qualitative (SEM/EDS): ? - uncertain
Tr - trace element
O - minor constituent
+ - major constituent

TABLE C-14. CHEMICAL COMPOSITION OF SELECTED AREAS OF PARTICLE 8E

ID[a]	U	Zr	O	Al	Cr	Fe	Ni	Sn	Miscellaneous	Comments
830	16.6	13.3	70.0	--	--	--	--	--	--	Region 1 base material, see Figure C-177
812	17.6	10.7	71.5	--	--	Tr[b]	--	--	--	Region 2 base material
834	15.6	13.7	70.6	--	--	Tr[b]	--	--	--	Region 3 base material
784	12.2	17.3	70.3	--	--	Tr[b]	--	--	--	Region 4 base material
835	14.9	15.3	69.7	--	--	Tr[b]	--	--	--	Region 5 base material
803	•	•	--	--	--	--	--	--	--	Base Region 1 material, see Figure C-179
804	•	•	--	--	--	Tr	--	--	--	Grain boundary Region 1 material
807	12.8	26.6	60.5	--	--	Tr[b]	--	--	--	Grain boundary Region 1 material
808	6.7	25.3	63.8	--	Tr[b]	4.0	Tr[b]	--	--	Grain boundary Region 1 material
832	•	•	--	--	--	0	--	--	--	Grain boundary Region 1 material, see Figure C-180
810	•	•	--	--	--	Tr	--	--	--	Base Region 1 material, see Figure C-182
770	•	•	--	--	0	0	--	--	--	Light phase Region 3 material, see Figure C-184
771	0	0	--	--	•	•	--	--	--	Dark phase Region 3 material
774	--	--	--	--	--	Tr[b]	76.6	19.3	C-4.0	Inclusion Region 3 material
769-A	5.9	6.7	51.6	--	12.5	23.0	--	--	--	Dark phase Region 3 material, see Figure C-183
769-B	4.3	22.4	60.4	--	--	12.6	--	--	--	Light phase Region 3 material
769-C	--	3.4	44.7	--	3.7	14.2	--	--	C-33.8	Average of A and B Region 3 material
768-A	12.6	19.4	67.8	--	--	--	--	--	--	gb material Region 3 material
779	--	--	--	--	--	0	•	•	Ru(0)	Inclusion Region 3 material, see Figure C-187
782	•	•	--	--	--	0	--	--	--	Second phase Region 3 material
783	•	•	--	--	--	?	--	--	--	Base Region 3 material
778	--	--	--	--	--	--	--	--	Si(•)	Particle in void
789	Tr	--	--	--	•	•	0	--	--	Dark phase Region 3 material, see Figure C-185
793	Tr	0	--	--	0	•	0	--	Ti(?)	Dark strip Region 3 material
794	•	•	--	--	•	•	Tr	--	--	Light strip Region 3 material
795	•	•	--	--	--	Tr	--	--	--	Base Region 3 material
796	•	•	--	--	--	Tr	--	--	--	Base in void Region 3 material, see Figure C-189
797	--	--	--	--	--	Tr	•	•	Ru(?)	Base in inclusion Region 3 material
799	--	--	--	--	--	--	•	•	Ru(?)	Other phase Region 3 material
801	Tr	Tr	--	--	--	Tr	•	--	Tc(•)/Ru(•)	Other phase Region 3 material

a. See figures mentioned in the comments for location of ID numbers.

b. Detected by SEM/EDS only.

Quantitative (SAS): Data is in atom percent.

Qualitative (SEM/EDS): ? - uncertain
Tr - trace element
0 - minor constituent
• - major constituent

TABLE C-15. CHEMICAL COMPOSITION OF SELECTED AREAS OF PARTICLE 8H

ID[a]	U	Zr	O	Al	Cr	Fe	Ni	Sn	Miscellaneous	Comments
147	+	0	--	--	--	Tr	--	--	--	Region 1 base material, see Figure C-190
161	+	0	--	--	--	Tr	--	--	--	Region 2 base material
120	+	0	--	--	--	Tr	--	--	--	Region 2 base material
127	+	+	--	--	--	0	--	--	--	Region 3 base material
117	+	0	--	--	--	Tr	--	--	--	Region 1 base material, see Figure C-196
118	+	Tr	--	--	--	Tr	--	--	--	Region 1 base material
168	+	0	--	--	--	Tr	--	--	--	Region 1 base material, see Figure C-201
143	+	0	--	--	--	Tr	--	--	--	Base Region 1 material, see Figure C-195
144	+	0	--	--	--	0	--	--	--	High Z crystals Region 1 material
135	+	0	--	--	--	Tr	--	--	--	Region 1 base, see Figure C-200
137	+	+	--	--	Tr	0	--	--	--	Region 3 base
138			--	--	+	+	0	--	--	Dark grain boundary material
140	+	+	--	--	--	+	0	--	--	Inclusion
141	+	+	--	--	--	0	--	--	--	Light grain boundary material
166	+	+	--	--	--	Tr	--	--	--	Base Region 3 material, see Figure C-203
165	Tr	--	--	--	+	+	0	--	--	Grain boundary Region 3 material
167	0	+	--	--	--	0	0	--	--	Surface material Region 3 material
123	--	--	--	--	--	--	+	Tr	--	Second phase metallic material
124	--	--	--	--	--	--	--	--	Ag(+)	Base metallic material
125	+	0	--	--	--	Tr	--	--	--	High Z bead metallic material

a. See figures mentioned in the comments for location of ID numbers.

Quantitative (SAS): Data is in atom percent.

Qualitative (SEM/EDS): ? - uncertain
Tr - trace element
0 - minor constituent
+ - major constituent

TABLE C-16. CHEMICAL COMPOSITION OF SELECTED AREAS OF PARTICLE 9D

ID[a]	U	Zr	O	Al	Cr	Fe	Ni	Sn	Miscellaneous	Comments
766	--	--	--	--	--	--	--	--	Ag(+)	Base metallic material, see Figure C-207
765	--	--	--	--	--	Tr	+	0	Ag(Tr), Ru(Tr)	Inclusion metallic material
764	+	0	--	--	Tr	Tr	Tr	--	--	Ceramic piece number 1 base material
777	+	+	--	--	?	Tr	Tr	--	--	Ceramic piece number 1 base material
768	--	--	--	--	--	Tr	+	+	Ag(Tr), Ru(Tr)	High Z material in round two-phase inclusions in metallic material
769	--	--	--	--	--	Tr	+	0	Ag(Tr), Ru(Tr)	Low Z material, see Figure C-206
801	--	--	--	--	--	Tr	+	0	Ru(Tr)	Low Z material
802	--	--	--	--	--	Tr	+	+	Ru(Tr)	High Z material
783	+	+	--	--	Tr	Tr	Tr	--	--	Ceramic piece number 2 base material, see Figure C-208
784	+	+	--	--	Tr	Tr	Tr	--	--	Ceramic piece number 2 base material
778	Tr	--	--	--	--	Tr	+	0	Ru(+)	Void material in piece number 1, see Figure C-213
785	+	+	--	--	--	Tr	Tr	--	--	Second phase piece number 2
787	--	--	--	--	--	Tr	+	0	Ag(Tr)	Void material piece number 2
791	+	+	--	--	Tr	Tr	Tr	--	--	Base piece number 3, see Figure C-210
792	+	0	--	--	Tr	Tr	--	--	--	Base piece number 3
793	Tr	--	--	--	--	Tr	+	0	Ru(0)	Void material piece number 3
794	Tr	--	--	--	--	Tr	+	0	Ru(+)	Void material piece number 3
798	+	+	--	--	Tr	Tr	Tr	--	--	Ceramic piece number 4 base material, see Figure C-215
799	+	+	--	--	Tr	Tr	Tr	--	--	Ceramic piece number 4 base material

a. See figures mentioned in the comments for location of ID numbers.

Quantitative (SAS): Data is in atom percent.

Qualitative (SEM/EDS): ? - uncertain
Tr - trace element
0 - minor constituent
+ - major constituent

TABLE C-17. CHEMICAL COMPOSITION OF SELECTED AREAS OF PARTICLE 9G

ID[a]	U	Zr	O	Al	Cr	Fe	Ni	Sn	Miscellaneous	Comments
809	--	--	--	--	--	Tr	+	0	Ru(Tr), Ag(Tr)	Inclusion Area D, see Figure 224
810	--	--	--	--	--	--	--	--	Ag(+)	Base Area D, see Figure 224
811	--	--	--	--	Tr	Tr	Tr	--	Ag(+), Cu(Tr), Mo(O)	Surface bead Area D, see Figure 232
832	--	--	--	--	--	--	--	--	Ag(+), S(Tr)	Surface lump Area D
833	--	--	--	Tr	--	Tr	Tr	--	Ag(+), Cu(Tr), S(Tr)	Void material Area D
836	--	--	--	0	--	Tr	0	--	Ag(+), S(Tr)	Void material Area D
837	--	--	--	--	--	--	+	?	Ag(+)	Inclusion second phase Area D, see Figure 227
841	--	--	--	--	--	--	0	--	Ag(+)	Base Area D
842	--	--	--	--	--	--	+	0	--	Inclusion Area D
846	--	--	--	--	--	Tr	+	0	Ag(+), S(O)	Surface bead Area A, see Figure C-221
847	--	--	--	--	--	Tr	+	0	Ag(Tr)	Inclusion Area A
848	--	--	--	--	--	--	--	--	Ag(+)	Base Area A
862	--	--	--	0	Tr	Tr	Tr	--	Ti(+), S(O), Ag(+), Cu(Tr)	Void material Area A, see Figure C-223
864	--	--	--	--	--	--	--	--	Ag(+)	Base Area A
852	--	--	--	--	--	Tr	+	0	Ag(?)	Inclusion Area A, see Figure C-222
853	--	--	--	--	--	Tr	+	+	Ag(O)	Inclusion second phase Area A
854	--	--	--	--	--	Tr	+	+	Ag(+)	Inclusion phase Area A
855	--	--	--	--	--	Tr	+	Tr	Ag(+)	Inclusion phase Area A
856	--	--	--	--	Tr	Tr	Tr	--	Ag(+), Cu(Tr)	Inclusion phase Area A
868	--	--	--	--	--	Tr	+	0	Ag(Tr)	Inclusion Area B, see Figure C-229
867	--	--	--	--	--	--	--	--	Ag(+)	Base Area B
870	--	--	--	0	--	Tr	Tr	--	Ag(+), S(O) Cu(Tr)	Surface bead Area B
871	--	--	--	--	--	--	--	--	Ag(+)	Sample center base material, see Figure C-220 and 230
874	--	--	--	--	--	--	--	--	Ag(+)	Base Area F, see Figure C-226
875	--	--	--	--	--	Tr	+	0	Ag(Tr), Ru(Tr)	Inclusion Area F

a. See figures mentioned in the comments for location of ID numbers.

Quantitative (SAS): Data is in atom percent.

Qualitative (SEM/EDS): ? - uncertain
Tr - trace element
0 - minor constituent
+ - major constituent

TABLE C-18. CHEMICAL COMPOSITION OF SELECTED AREAS OF PARTICLE 10A

ID[a]	U	Zr	O	Al	Cr	Fe	Ni	Sn	Miscellaneous	Comments
272-A	25.8	6.3	67.8	--	--	--	--	--	--	Low Z Region 1 base material, see Figure C-235
272-B	23.2	7.0	69.6	--	--	--	--	--	--	Low Z Region 1 base material
272-C	24.0	7.6	68.2	--	--	--	--	--	--	Low Z Region 1 base material
273-A	32.7	1.2	65.9	--	--	--	--	--	--	High Z Region 1 base material
273-B	32.5	1.5	65.8	--	--	--	--	--	--	High Z Region 1 base material
273-C	32.2	1.8	65.9	--	--	--	--	--	--	High Z Region 1 base material
291-A	31.9	1.9	66.0	--	--	--	--	--	--	Region 2 base material, see Figure C-236
291-B	34.2	0.0	65.7	--	--	--	--	--	--	
291-C	32.5	0.7	66.6	--	--	--	--	--	--	
291-D	30.4	0.3	69.2	--	--	--	--	--	--	
291-E	34.6	0.3	65.0	--	--	--	--	--	--	
291-F	35.2	0.0	64.7	--	--	--	--	--	--	
274	Tr	Tr	--	--	--	--	Tr	--	Tc(+), Ru(+)	Material in voids, see Figure C-247
280	+	--	--	--	--	--	Tr	--	Tc(0), Ru(0)	Material in voids, see Figure C-236
302	0	--	--	Tr	0	0	+	0	Ti(0)	Material in voids, see Figure C-237
313	+	--	--	--	--	--	0	--	Tc(+), Ru(+)	Material in voids, see Figure C-238
286	+	0	--	--	--	Tr	--	--	--	Low Z Region 1 base material, see Figure C-242
287	+	Tr	--	--	--	?	--	--	--	High Z Region 1 base material
309	+	Tr	--	--	--	--	--	--	--	High Z Region 1 base material

a. See figures mentioned in the comments for location of ID numbers.

Quantitative (SAS): Data is in atom percent.

Qualitative (SEM/EDS): ? - uncertain
Tr - trace element
0 - minor constituent
+ - major constituent

TABLE C-19. CHEMICAL COMPOSITION OF SELECTED AREAS OF PARTICLE 10E

ID[a]	U	Zr	O	Al	Cr	Fe	Ni	Sn	Miscellaneous	Comments
062-A	16.5	15.1	68.2	--	--	--	--	--	--	Three scans at location 062, see Figure C-258
062-B	16.0	13.3	70.6	--	--	--	--	--	--	--
062-C	16.2	14.7	69.0	--	--	--	--	--	--	--
063-A	33.1	--	66.8	--	--	--	--	--	--	Four separate fuel grains near 063, see Figure C-258
063-B	35.4	--	64.5	--	--	--	--	--	--	--
063-C	35.9	--	64.0	--	--	--	--	--	--	--
063-E	37.2	--	62.7	--	--	--	--	--	--	--
064-A	37.6	--	62.3	--	--	--	--	--	--	Three separate fuel grains near 064, see Figure C-258
064-B	33.5	--	66.4	--	--	--	--	--	--	--
064-C	34.3	--	65.6	--	--	--	--	--	--	--
061	Tr	--	--	--	--	?	+	+	--	Inclusion, see Figure C-258
097	Tr	Tr	--	--	--	--	0	--	Ag(+), Mo(0)	Material in void, see Figure C-258
101	Tr	--	--	--	--	Tr	0	+	Ag(+), Mo(0)	--
102	Tr	--	--	--	--	--	+	+	Ag(+), Mo(0)	--
078-A	35.0	--	65.0	--	--	--	--	--	--	Three separate grains near 078 (sample center), see Figure 250
078-B	37.0	--	63.0	--	--	--	--	--	--	--
078-C	36.0	--	64.0	--	--	--	--	--	--	--
075-A	23.7	6.7	69.4	--	--	Tr[b]	--	--	--	On Zr band, see Figure C-251
075-B	33.2	--	66.7	--	--	--	--	--	--	Off Zr band
075-C	34.7	--	65.2	--	--	--	--	--	--	Off Zr band
073	+	--	--	--	--	--	--	--	--	Base matrial, see Figure C-257
088	Tr	Tr	--	--	0	0	Tr	--	Ag(+), Mo(0)	Particle in void, see Figure C-256
092	+	+	--	--	+	+	--	--	--	Base material
081	Tr	Tr	--	--	Tr	Tr	+	+	Ag(0), Ru(Tr)	Inclusion, see Figure C-255
083	Tr	Tr	--	--	--	Tr	--	--	Ag(+), Mo(0)	Inclusion
086	+	+	--	--	--	Tr	--	--	--	Base material
084-A	12.4	16.1	71.3	--	--	Tr[b]	--	--	--	Two locations, near 084
084-B	11.8	15.6	72.4	--	--	--	--	--	--	Two locations, near 084
085-A	32.1	3.5	64.2	--	--	Tr[b]	--	--	--	10 μ in from interface
085-B	32.2	1.9	65.7	--	--	--	--	--	--	60 μ in from interface

a. See figures mentioned in the comments for location of ID numbers.

b. Detected by SEM/EDS only.

Quantitative (SAS): Data is in atom percent.

Qualitative (SEM/EDS): ? - uncertain
Tr - trace element
0 - minor constituent
+ - major constituent

TABLE C-20. CHEMICAL COMPOSITION OF SELECTED AREAS OF PARTICLE 10F

ID[a]	U	Cr	U	Al	Cr	Fe	Ni	Sn	Miscellaneous	Comments
911	23.9	3.3	70.8	--	--	Tr[b]	2.0[c]	--	--	Region 1, base material, see Figure C-261
894	23.6	5.9	70.4	--	--	Tr[b]	--	--	--	Region 1, base material
908	25.3	4.7	69.2	--	--	Tr[b]	--	--	--	Region 1, base material
901	19.2	7.7	71.3	--	--	1.6	--	--	--	Region 2, base material
882	26.4	5.8	67.6	--	--	Tr[b]	--	--	--	Base material, see Figure C-264
883	•	0	--	--	--	Tr	--	--	--	Base material
884	•	•	--	--	Tr	0	Tr	--	--	Grain boundary material
885	Tr	--	5.7	--	--	Tr[b]	12.6	--	Tc-5.0[c], Pd-3.4[c], Ru-60.5, Rh-12.5[c]	Inclusion
890	•	0	--	--	--	Tr	--	--	--	Base material, see Figure C-269
891	•	0	--	--	•	•	•	--	--	Grain boundary material
896	•	0	--	--	--	Tr	--	--	--	Base material, see Figure C-270
897	•	0	--	?	•	•	--	--	--	Grain boundary material
895	•	•	--	--	?	0	Tr	--	--	Fine grain material
897-A	4.7	1.4	51.6	--	13.0	17.6	11.4	--	--	Grain boundary material, material similar to point 897 (see Figure C-270) in center of Region 2
897-B	2.6	0.9	53.4	--	15.8	15.5	11.5	--	--	Grain boundary material
898-A	23.1	9.7	63.7	--	--	3.3	--	--	--	Fine grain material, material similar to point 898 (see Figure C-270) in center of Region 2
898-B	23.0	10.8	62.1	--	--	3.9	--	--	--	Fine grain material
905	•	0	--	--	--	Tr	--	--	--	Base, see Figure C-270
906	0	Tr	--	?	•	•	0	--	--	Grain boundary material
907	10.9	3.6	59.5	--	7.7	10.8	7.1	--	--	Average of two eutectic phases
912	--	--	--	--	--	•	--	--	--	Inclusion in void

a. See figures mentioned in the comments for location of ID numbers.

b. Detected by SEM/EDS only.

c. Not detected by SEM/EDS.

Quantitative (SAS): Data is in atom percent.

Qualitative (SEM/EDS): ? - uncertain
Tr - trace element
0 - minor constituent
• - major constituent

TABLE C-21. CHEMICAL COMPOSITION OF SELECTED AREAS OF PARTICLE 11B

ID[a]	U	Zr	O	Al	Cr	Fe	Ni	Sn	Miscellaneous	Comments
566	--	--	--	--	--	+	+	Tr	--	Base, metallic region, see Figure 277
567	--	--	--	--	--	0	+	0	Ag(+)	Second phase, metallic region
568	--	--	--	--	--	0	0	--	Ag(+), Mo(0)	Inclusion, metallic region
574	+	0	--	--	--	0	Tr	--	--	Rectangular inclusion in metallic region,
575	--	--	--	--	+	+	0	--	--	see Figure C-272
576	--	--	--	--	+	+	0	--	Mo(+)	--
577	--	--	--	--	--	+	+	0	--	Mo(0)
578	--	--	--	--	0	+	0	--	Mo(0)	--
579	--	--	--	--	Tr	0	--	--	Ag(+)	--
584	0	Tr	--	Tr	+	+	--	--	--	Other phases, see Figure C-273
585	0	--	--	0	+	+	--	--	--	--
586	+	+	--	0	+	+	--	--	--	--
587	+	+	--	--	+	+	--	--	--	--
588	+	0	--	--	--	--	--	--	--	--
589	+	+	--	--	--	0	--	--	--	--
593	Tr	--	--	--	--	+	+	0	S/Mo(+), In(0)	Material in blister, see Figure C-274
	--	--	--	--	--	--	--	--	Ag(0), Cd(0)	
594	0	--	--	--	--	+	+	--	Mo(+)	Material in blister
599	0	0	--	0	+	+	--	--	--	Other phases, see Figure C-281
600	+	+	--	--	+	+	--	--	--	Other phases
601	--	--	--	--	--	+	+	0	--	Inclusion
602	+	+	--	--	--	0	--	--	--	Other phase

a. See figures mentioned in the comments for location of ID numbers.

Quantitative (SAS): Data is in atom percent.

Qualitative (SEM/EDS): ? - uncertain
Tr - trace element
0 - minor constituent
+ - major constituent

TABLE C-22. CHEMICAL COMPOSITION OF SELECTED AREAS OF PARTICLE 11C

ID[a]	U	Zr	O	Al	Cr	Fe	Ni	Sn	Miscellaneous	Comments
930	+	--	--	--	--	--	--	--	--	Center region (G) base material, see Figure C-290
934	0	+	--	--	--	Tr	--	--	--	Surface, adherent melt, see Figure C-287
933	0	+	--	--	--	--	--	--	--	Interior, adherent melt
931	0	+	--	--	--	--	--	--	--	Interior, adherent melt
935	+	+	--	--	--	--	--	--	--	Interface, adherent melt
936	+	--	--	--	--	--	--	--	--	Base, adherent melt
938	0	+	--	--	Tr	Tr	--	--	--	Surface base material, see Figure C-289
945	+	+	--	--	+	+	--	?	--	Beads and inclusions, surface reaction layer
942	+	0	--	--	--	Tr	--	--	--	Beads and inclusions, surface reaction layer
943	0	+	--	--	+	+	--	0	--	Beads and inclusions, surface reaction layer
944	+	0	--	--	--	Tr	--	--	--	Interior, surface reaction layer
950	--	--	--	--	--	--	--	--	Ag(+)	Inclusion, surface reaction layer

a. See figures mentioned in the comments for location of ID numbers.

Quantitative (SAS): Data is in atom percent.

Qualitative (SEM/EDS): ? - uncertain
Tr - trace element
0 - minor constituent
+ - major constituent

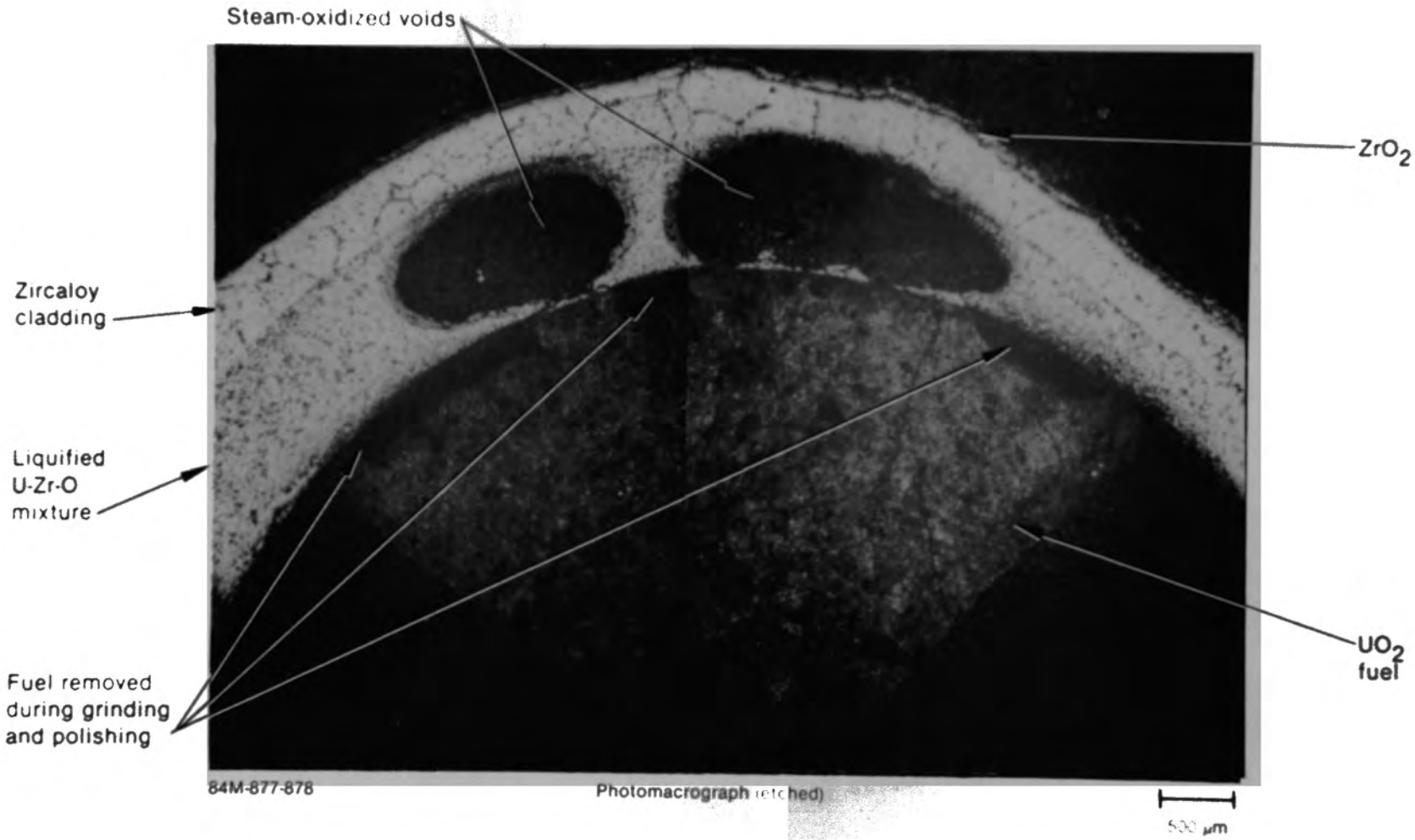

Figure C-1. Photomacrograph of Particle 1A, (H8, surface).

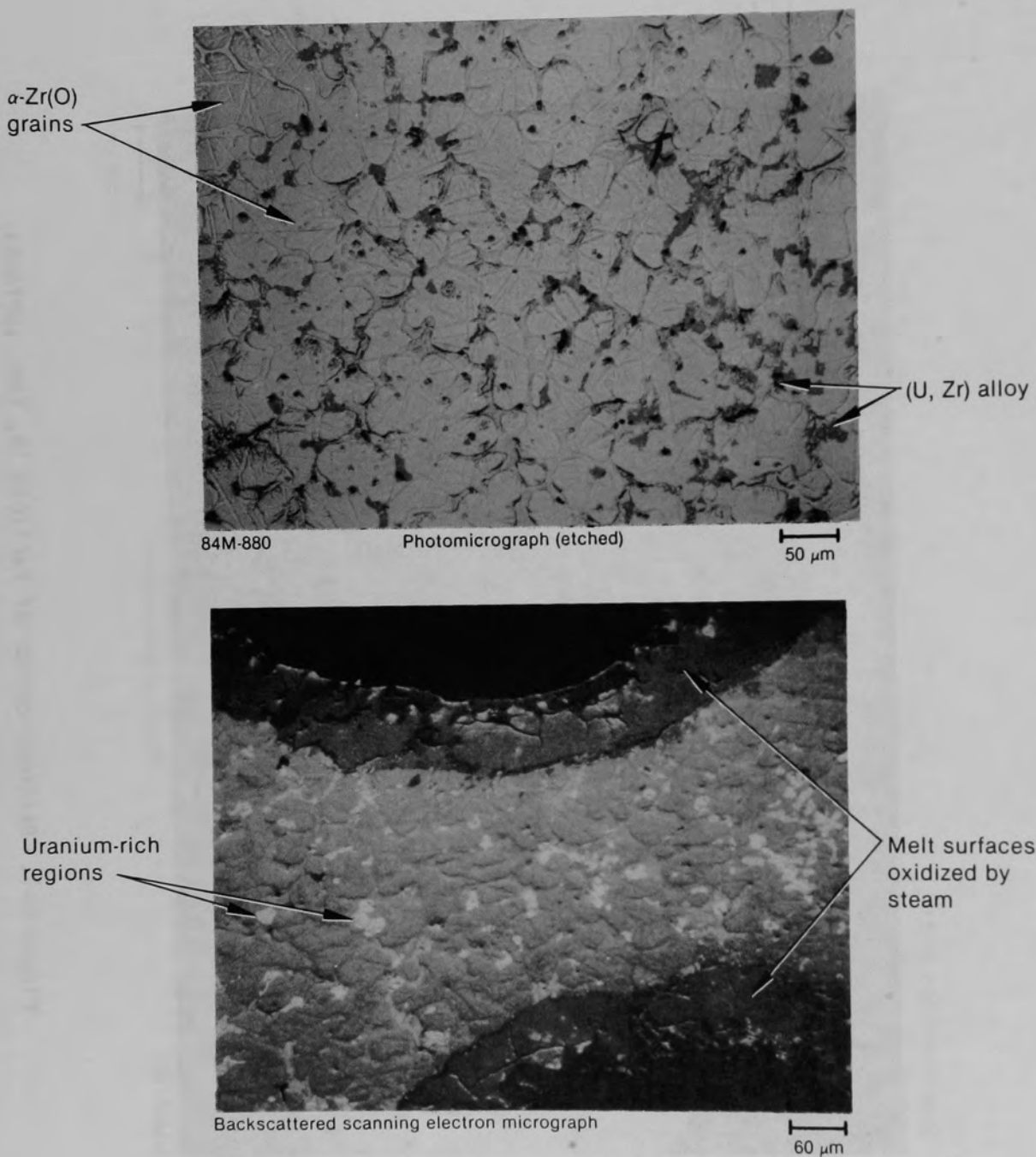

Figure C-2. Metallographic (top) and SEM (bottom) images of liquefied material structures in Particle 1A (H8, surface).

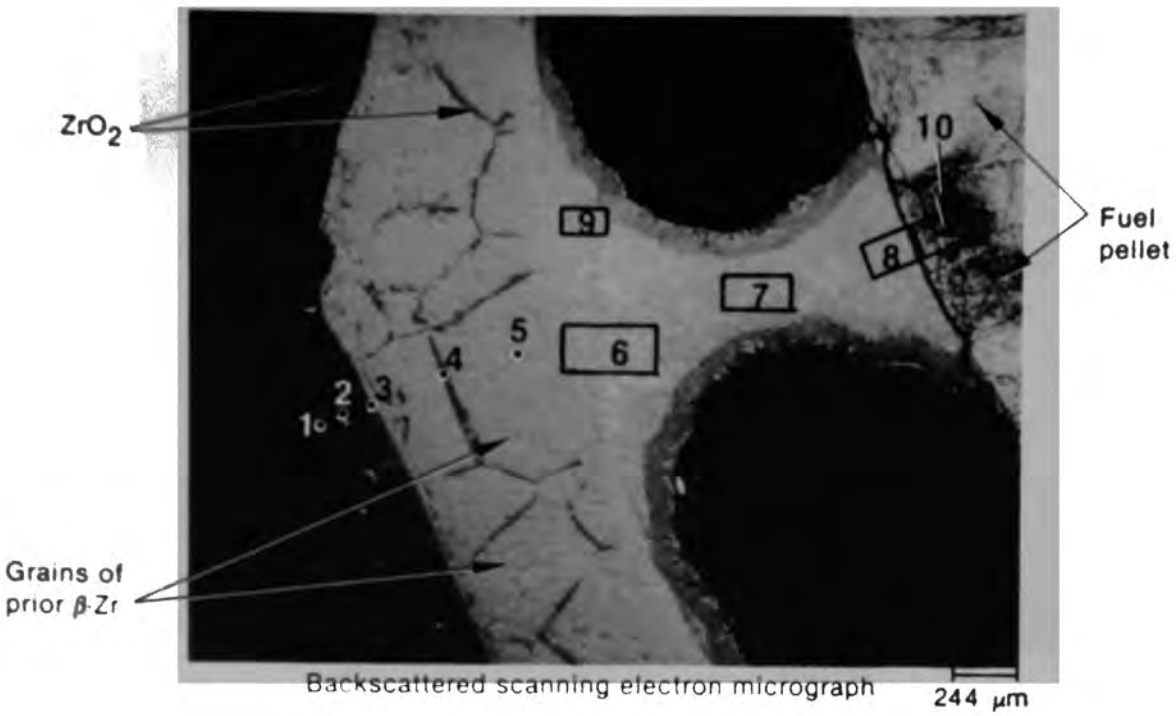

Summary of Particle 1A Composition Data

Point 1: 96.0 weight % Fe, 4.1 weight % Si, trace of Ca
Point 2: 100.0 weight % Zr
Point 3: 100.0 weight % Zr
Point 4: 100.0 weight % Zr
Point 5: 100.0 weight % Zr
Area 6 86.7 weight % Zr, 11.5 weight % U, 1.9 weight % Ni, plus traces of Fe and Cr
Areas 7, 8, 9, and 10 were not quantitively analyzed, but appear similar to Area 6 (see Figures C-4 through C-8).

Figure C-3. Regions of Particle 1A investigated by energy-dispersive X-ray spectroscopy.

Backscattered scanning electron micrograph

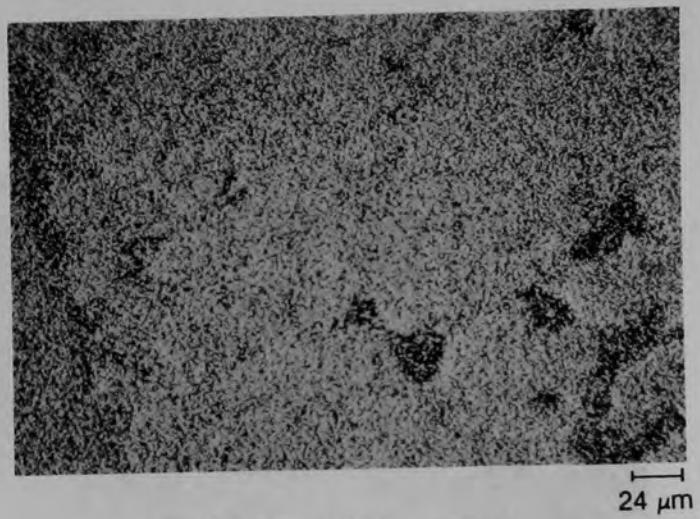

Zr X-ray emission image

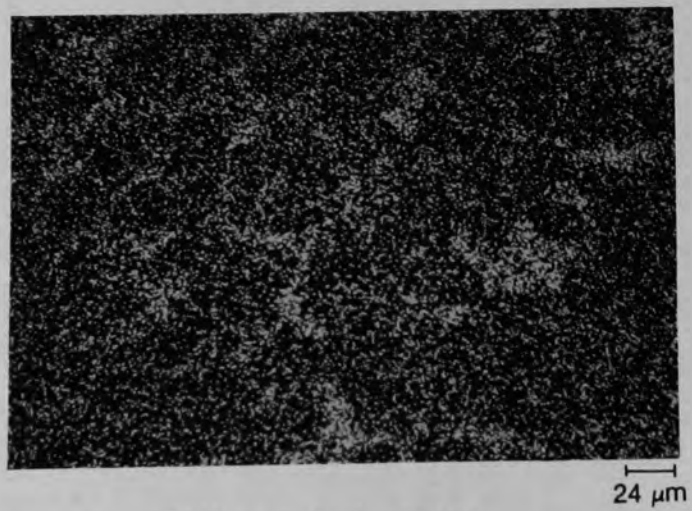

Fe X-ray emission image

U X-ray emission image

Figure C-4. Area 6 of Particle 1A, elemental distributions in melt phases adjacent to zircaloy cladding.

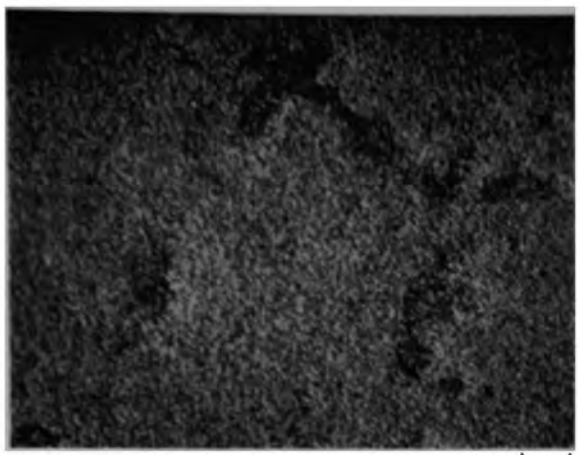

Zr X-ray emission image

Fe X-ray emission image

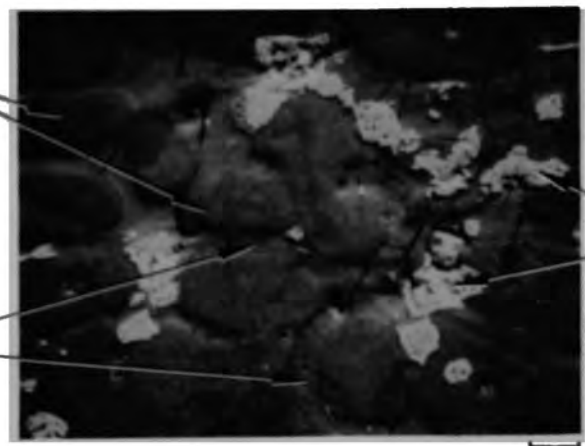

Backscattered scanning electron micrograph

U X-ray emission image

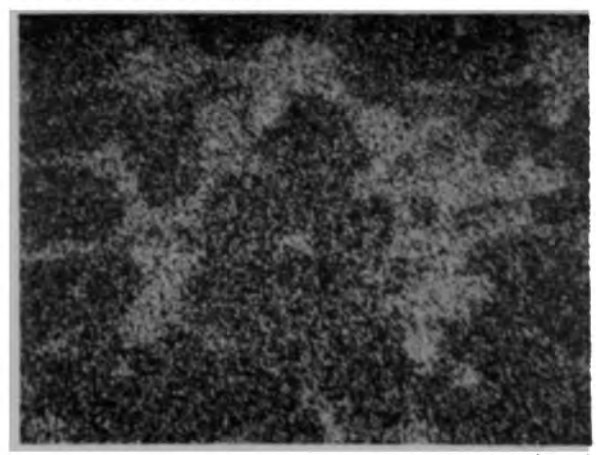

U plus Sn X-ray emission image

Figure C-5. Area 7 of Particle 1A, phase make-up of interior melt region.

Backscattered scanning electron micrograph

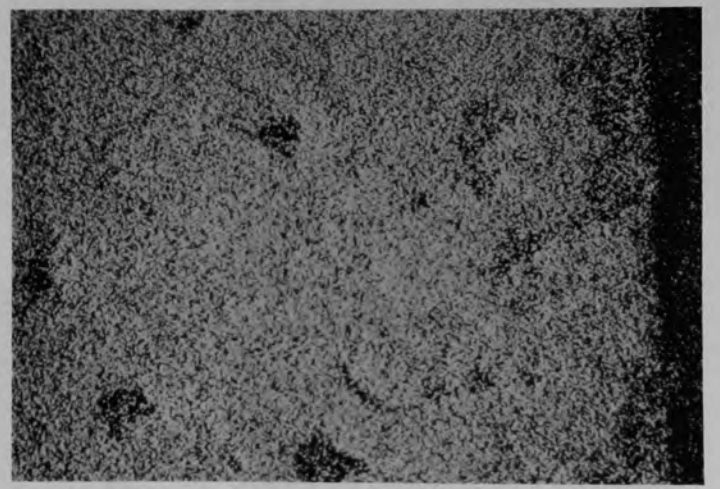

Zr X-ray emission image

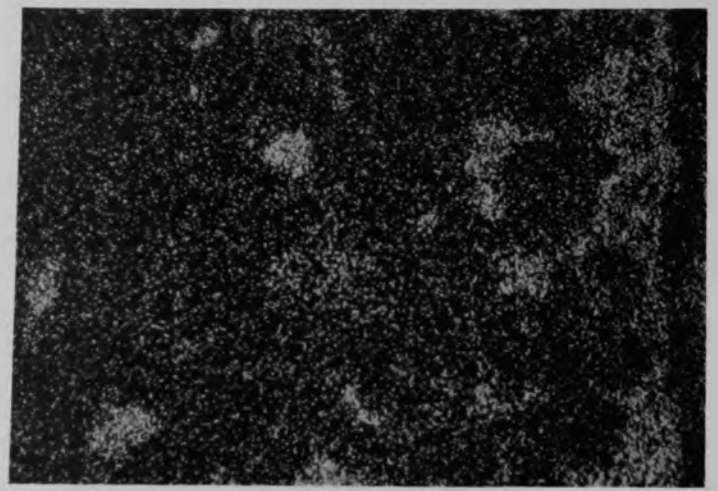

U X-ray emission image

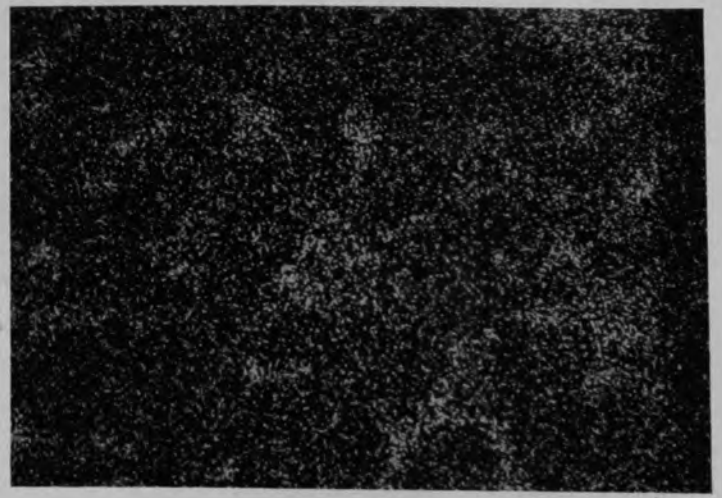

Fe X-ray emission image

Figure C-6. Area 8 of Particle 1A, elemental distributions in melt phases near fuel pellet.

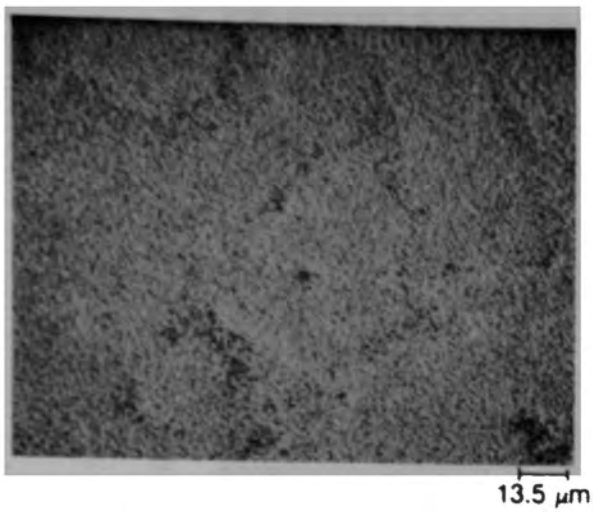

Zr X-ray emission image

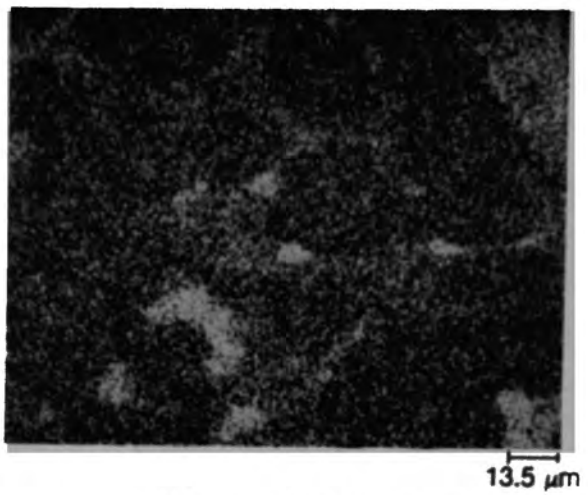

U X-ray emission image

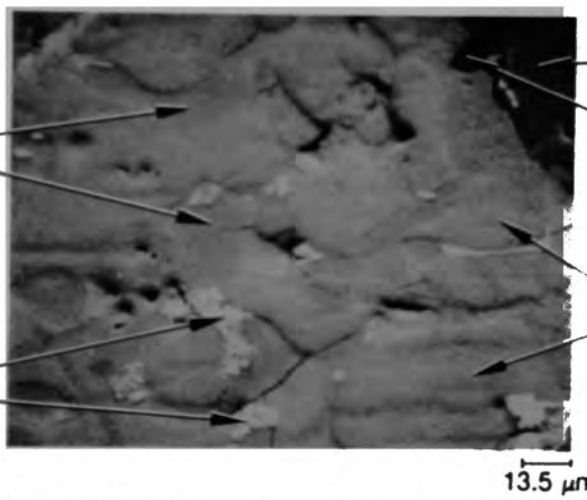

Backscattered scanning electron micrograph

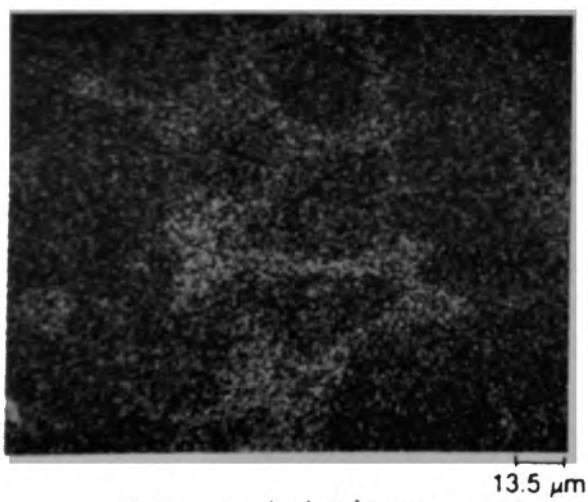

Ni X-ray emission image

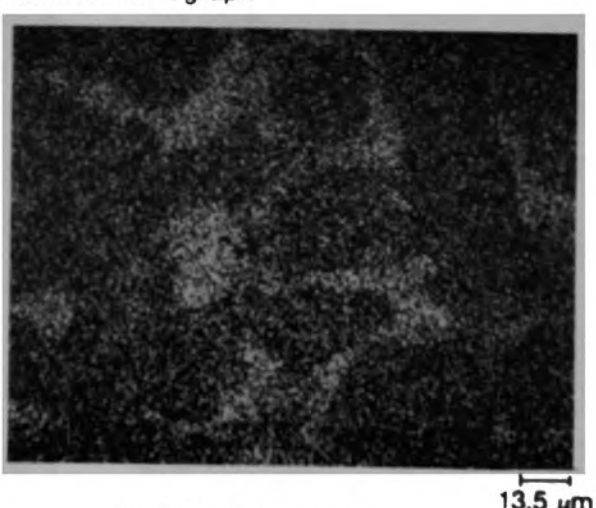

Fe X-ray emission image

Figure C-7. Area 9 of Particle 1A, phase compositions in melt near oxidized pore surface.

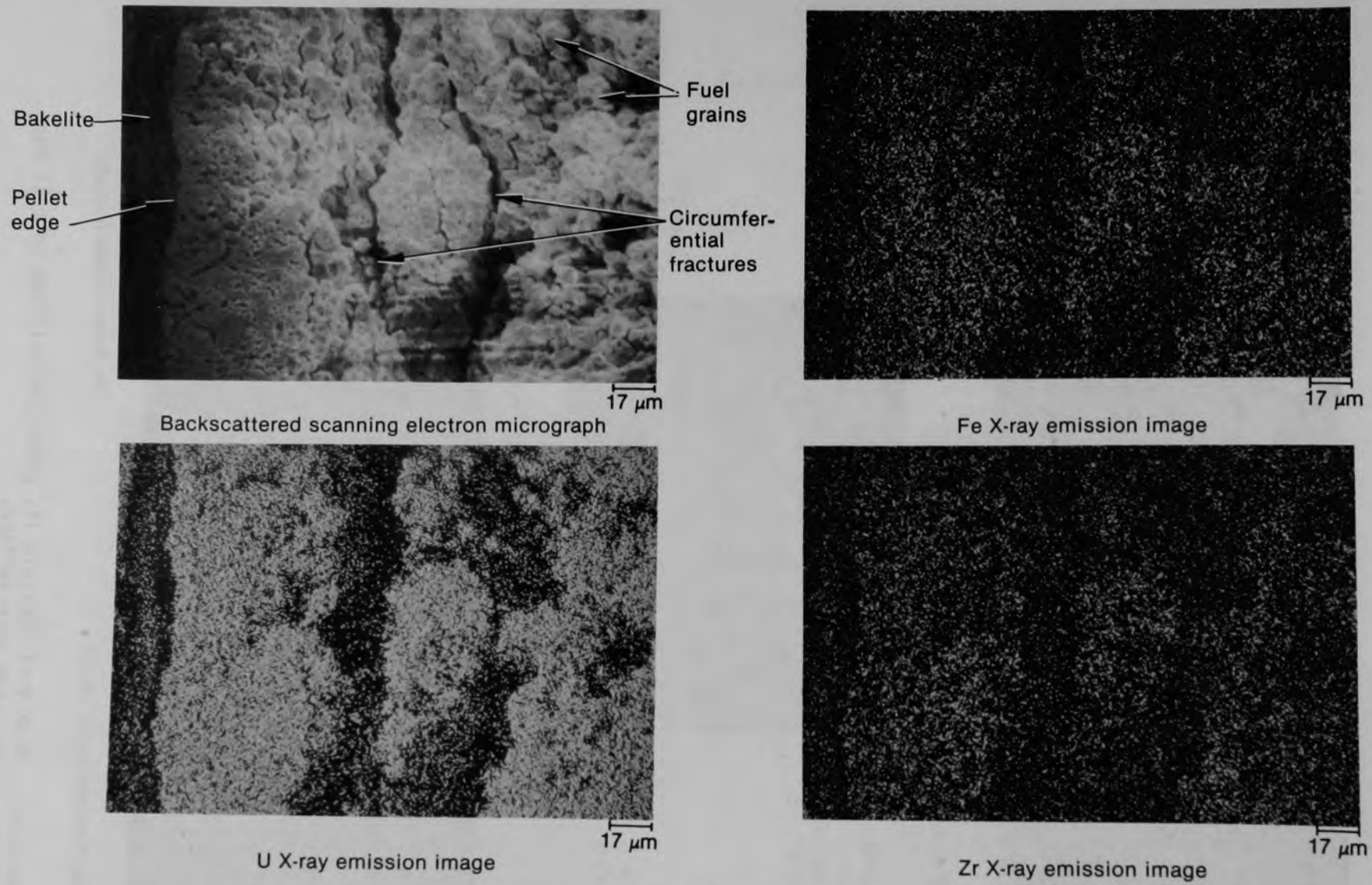

Figure C-8. Area 10 of Particle 1A, periphery of fuel pellet adjacent to homogeneous melt.

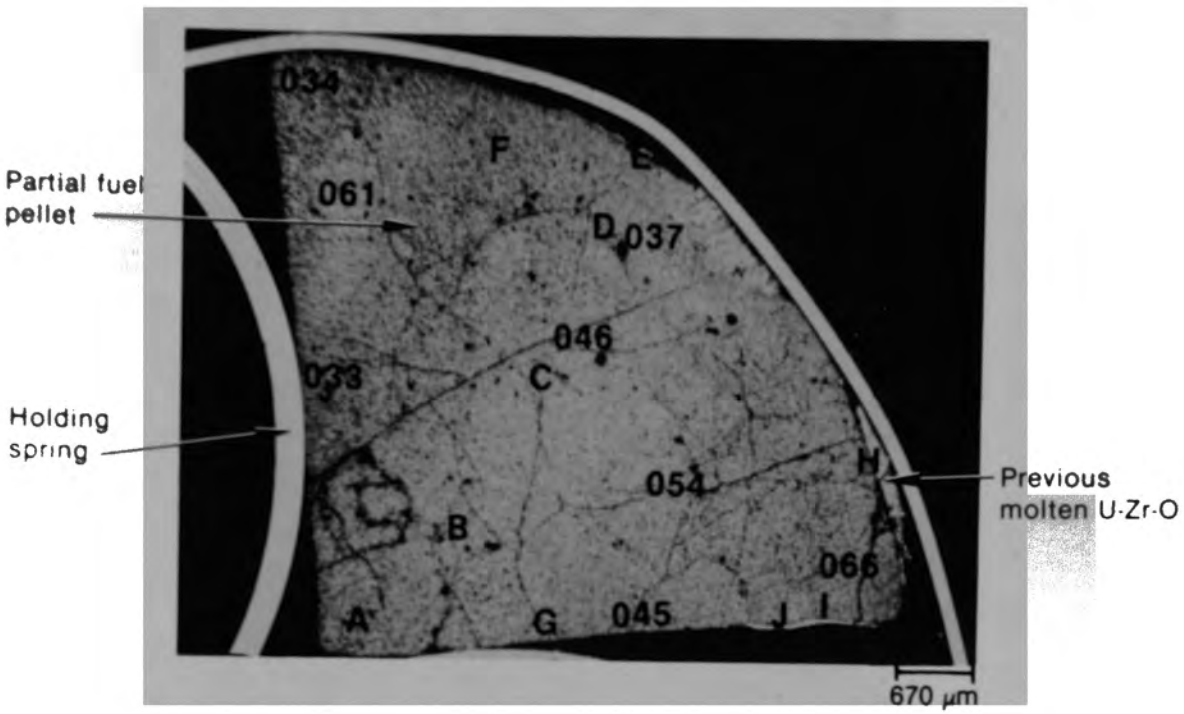

Figure C-9. Photomacrograph of Particle 1b (H8, surface).

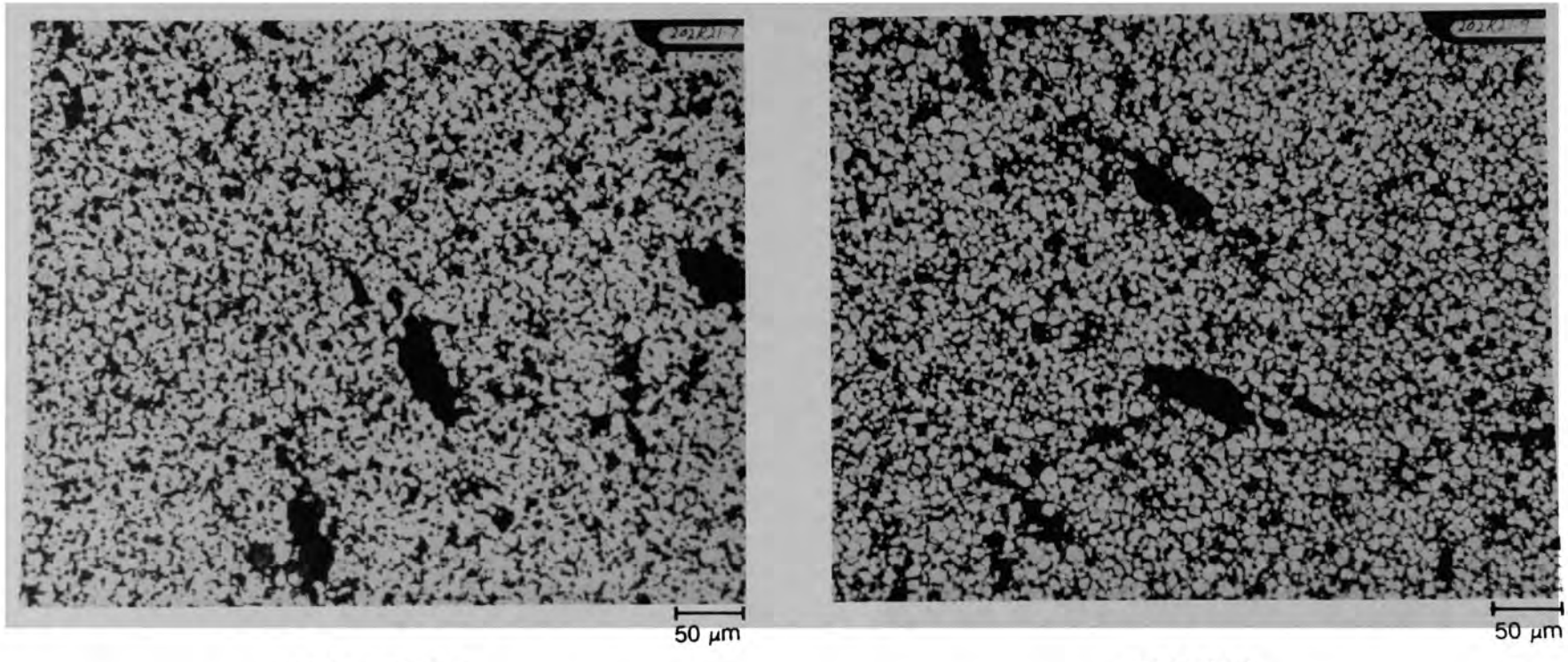

(a) As polished

(b) Etched

Figure C-10. Photomicrographs of Particle 1B (H8, surface) showing fuel grain structure at location A.

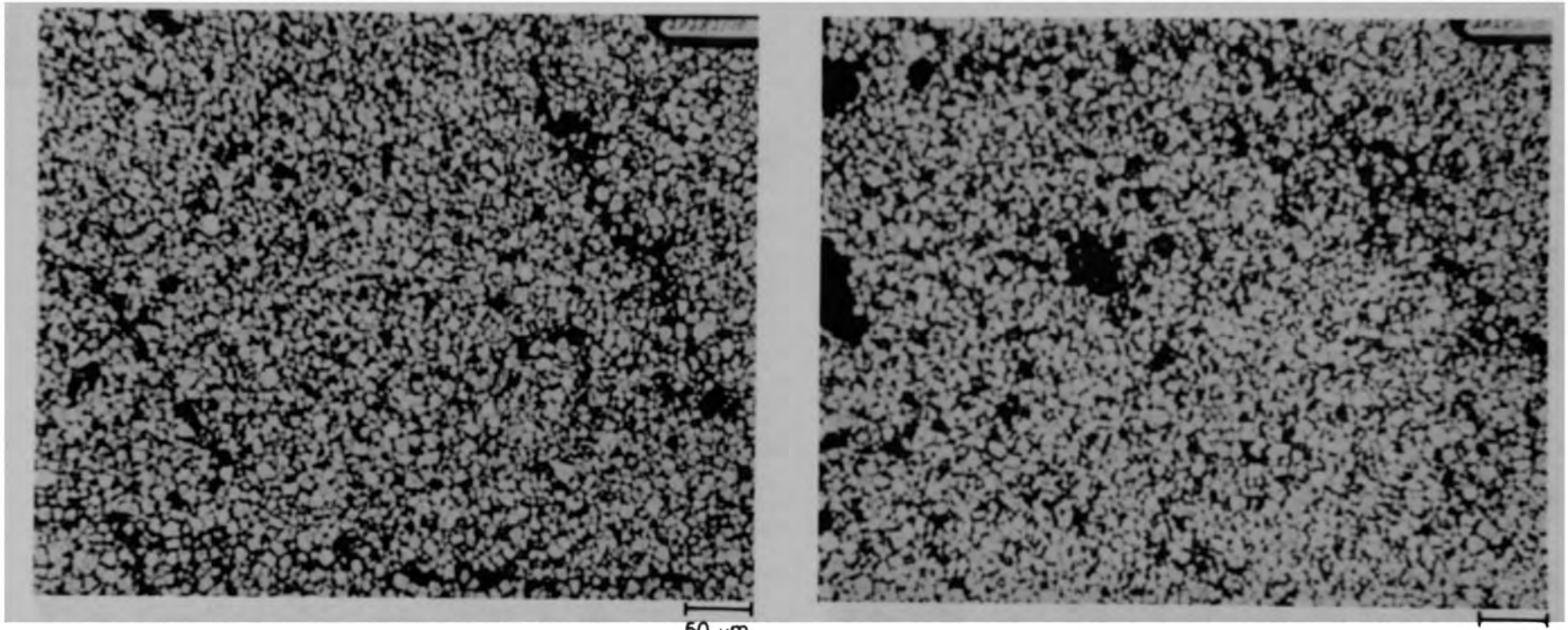

(a) Location B

(b) Location C

Figure C-11. Photomicrographs of Particle 1B (H8, surface) showing etched fuel grain structure.

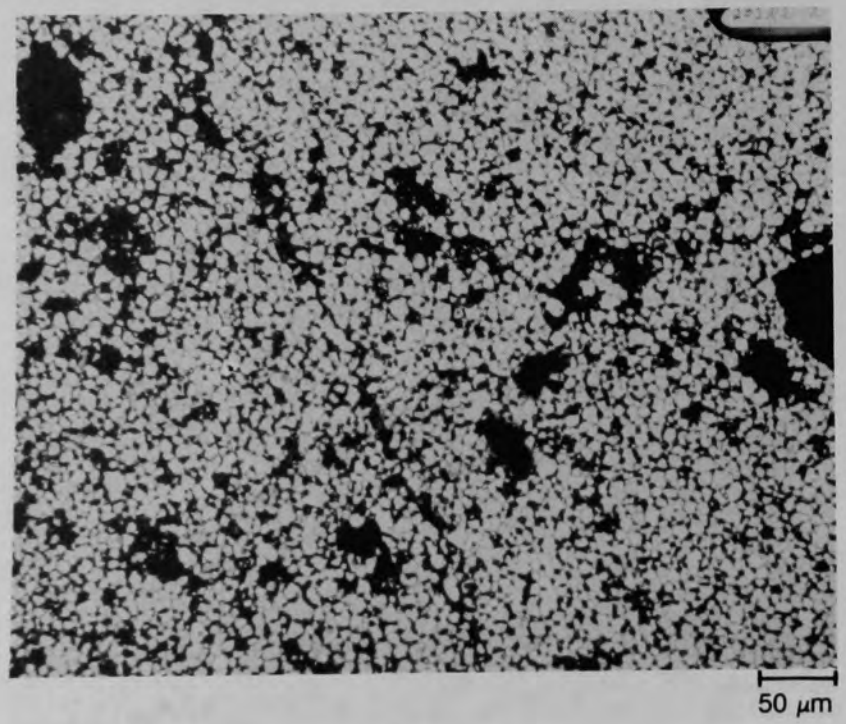

(a) Location D

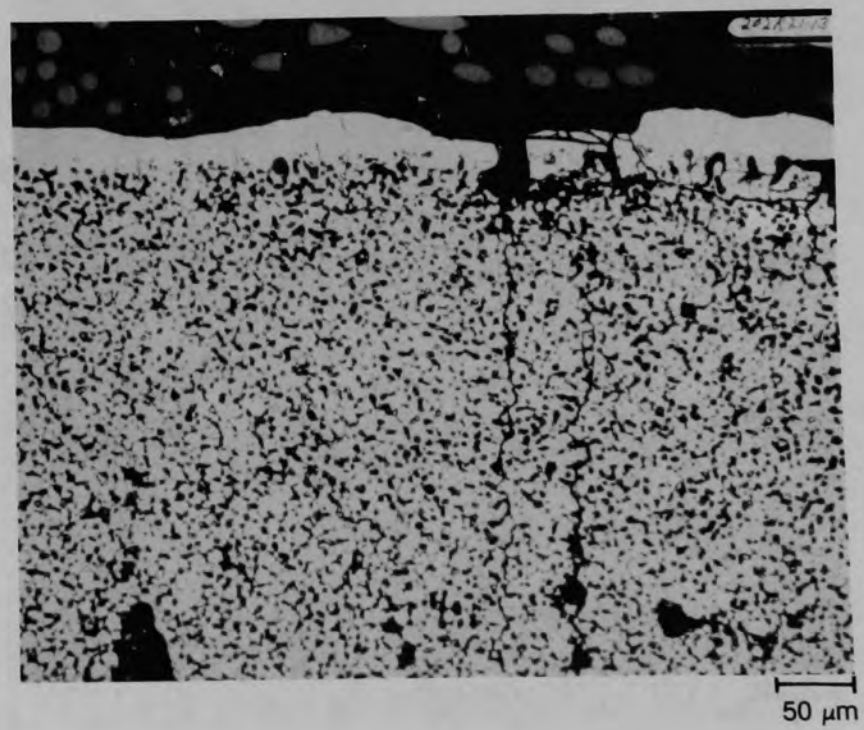

(b) Location E

Figure C-12. Photomicrographs of Particle 1B (H8, surface) showing etched fuel grain structure.

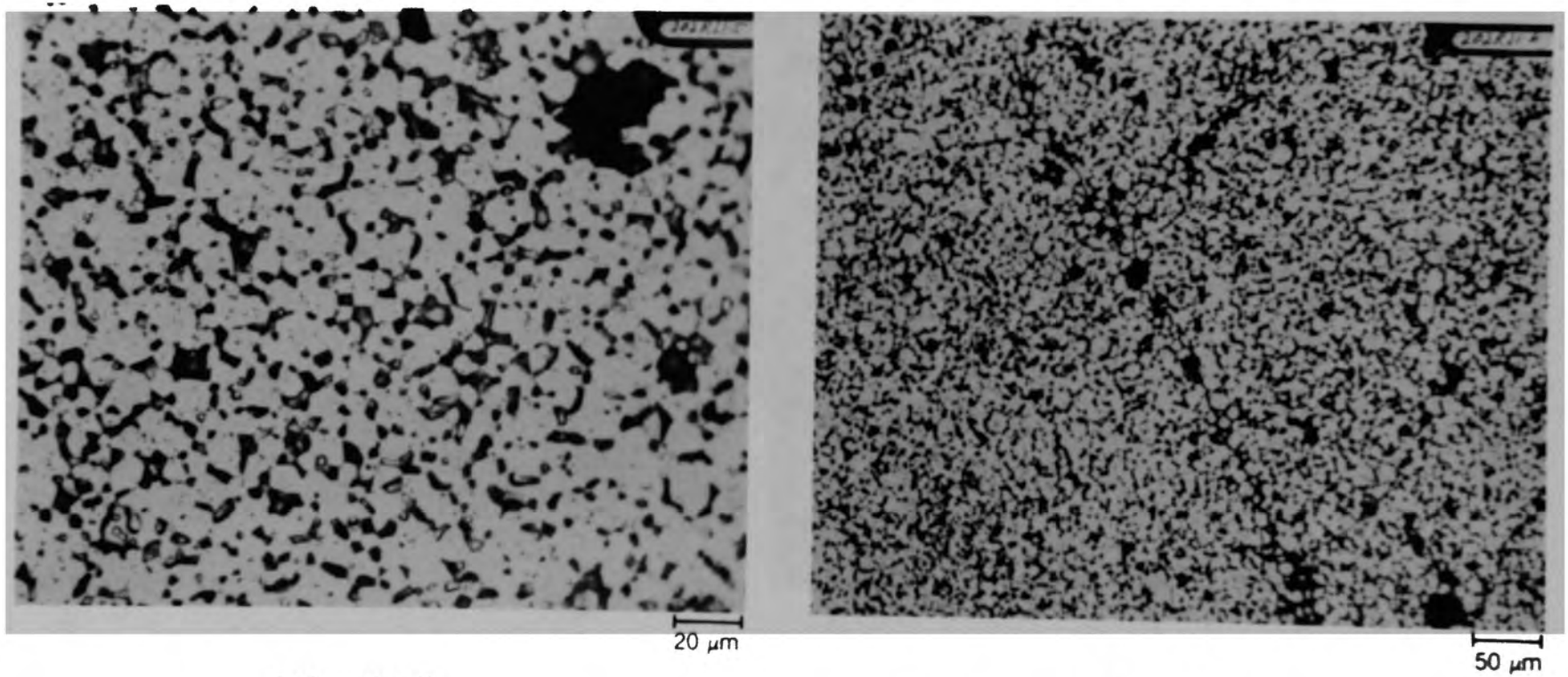

(a) Location F

(b) Location G

Figure C-13. Photomicrographs of Particle 18 (H8, surface) showing etched fuel grain structure.

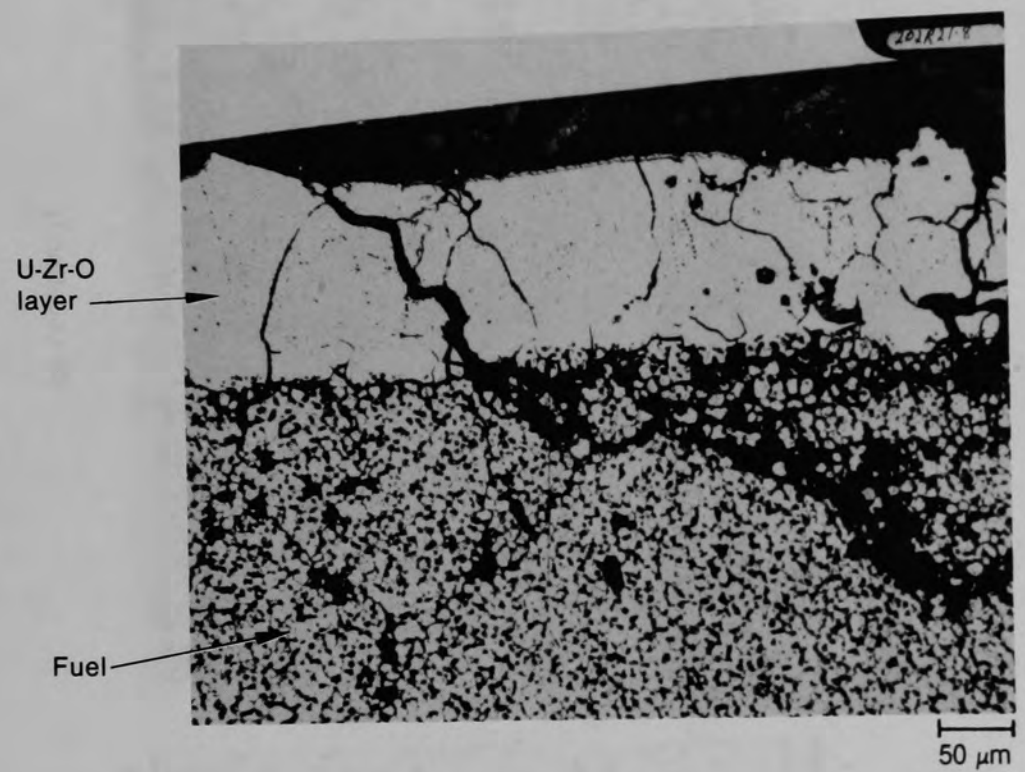

Figure C-14. Photomicrograph of Particle 1B (H8, surface) at Location H.

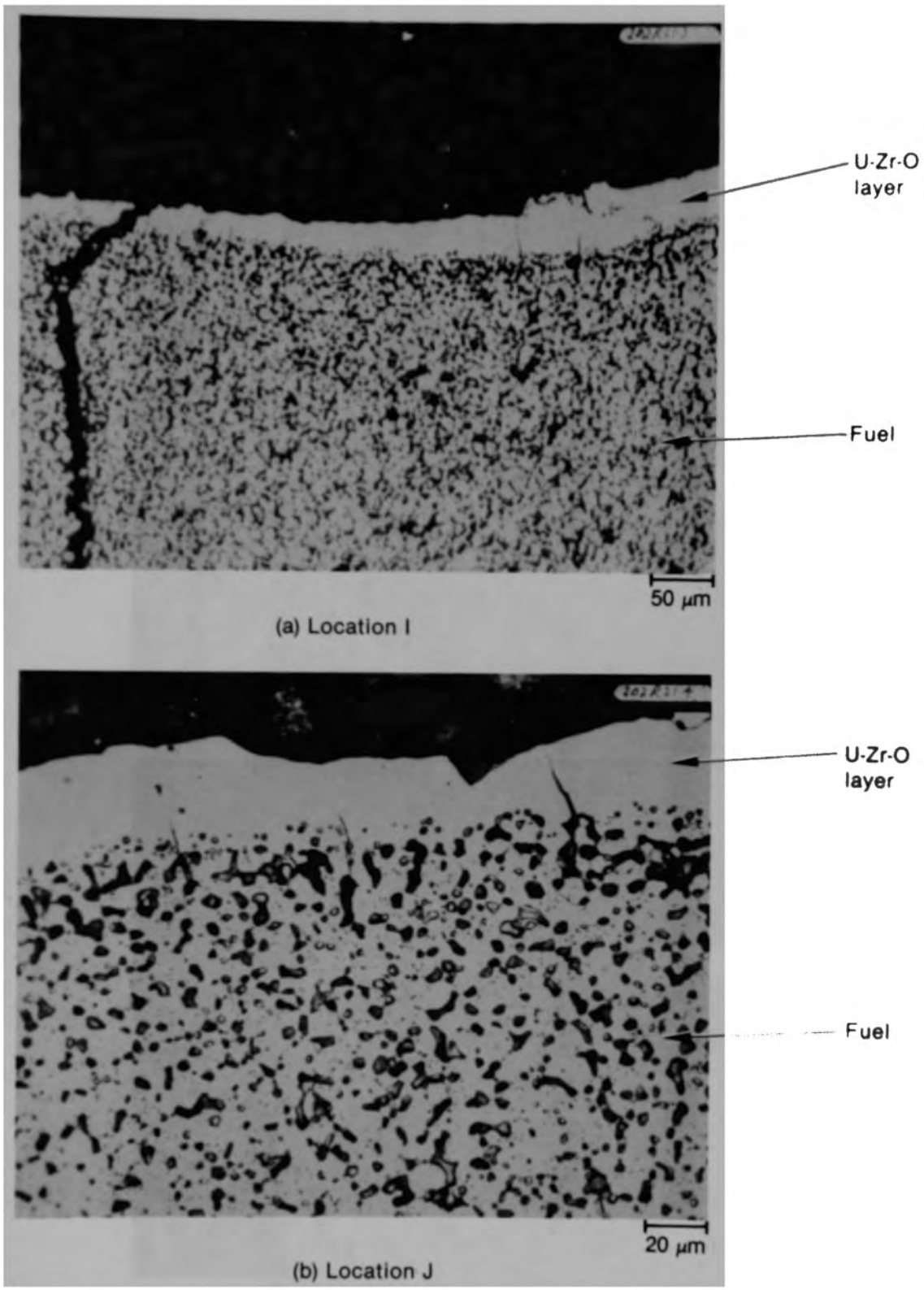

Figure C-15. Photomicrograph of Particle 3B (H8, surface) showing etched fuel grain structure.

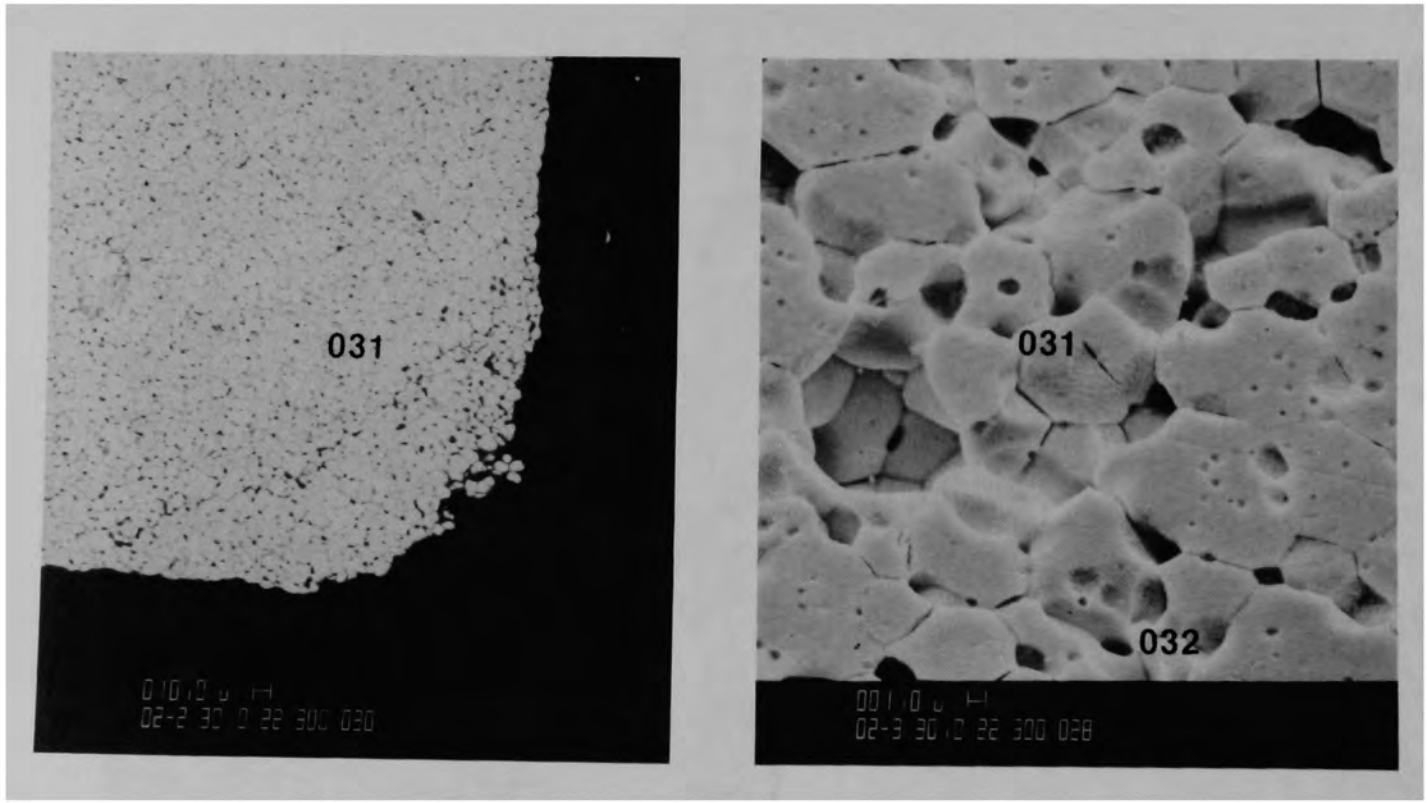

Figure C-16. SEM secondary electron image of fuel from Particle 1B (H8, surface) showing interlinked porosity.

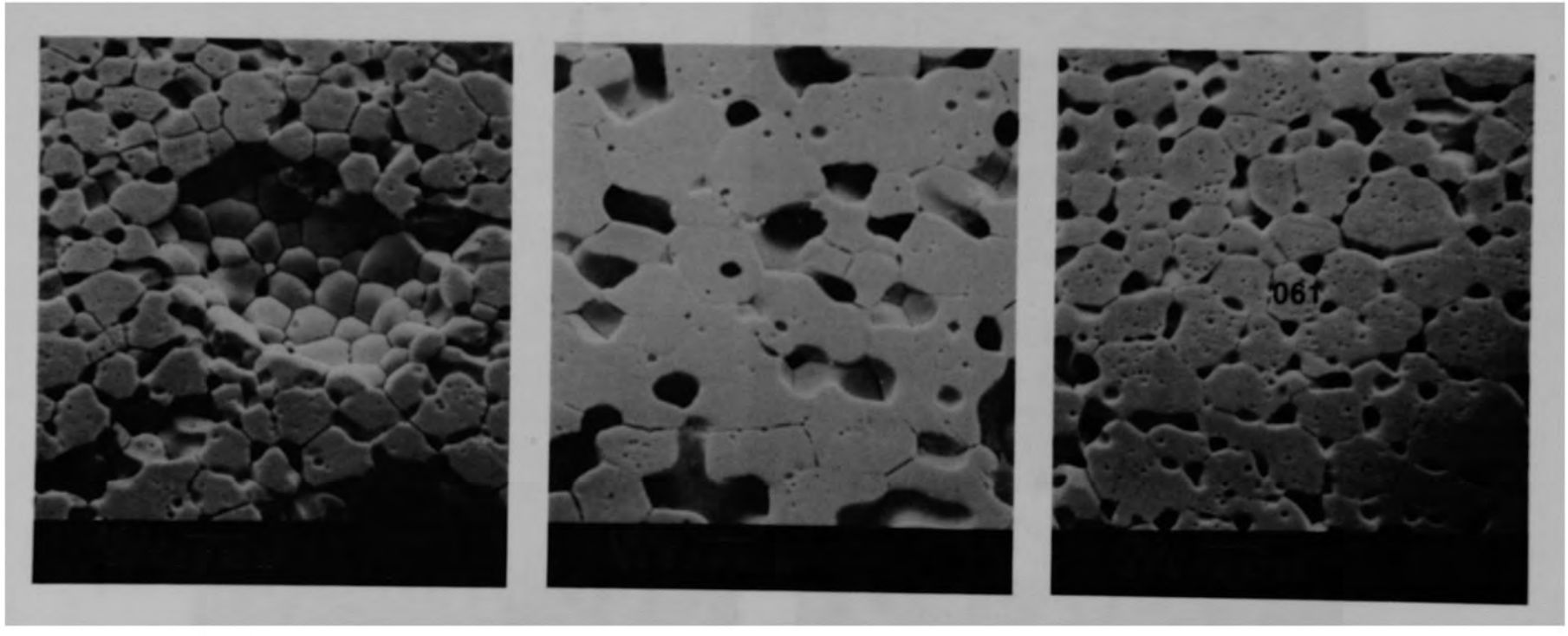

Figure C-17. SEM secondary electron image of fuel from particle 1B (H8, surface) showing interlinked porosity.

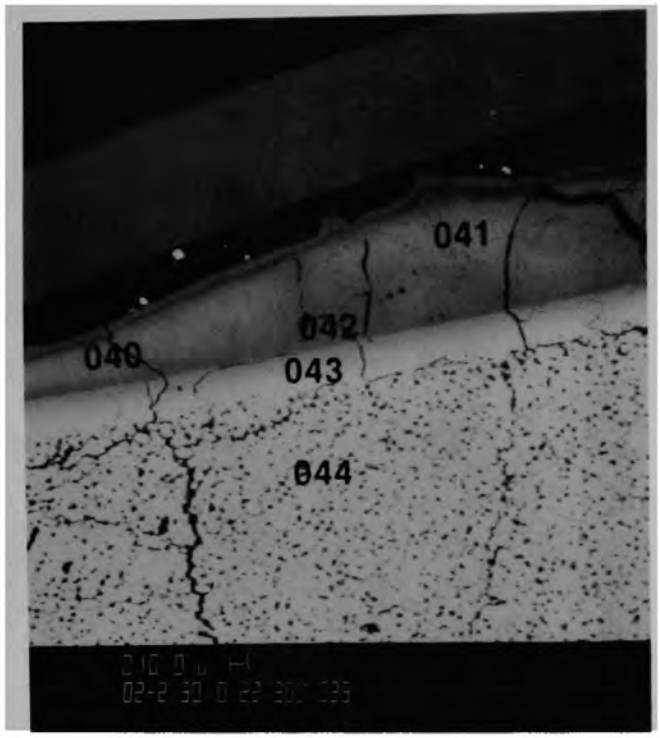

Figure C-18. SEM backscattered electron image of fuel from Particle 1B (H8, surface), corresponding to Figure C-14.

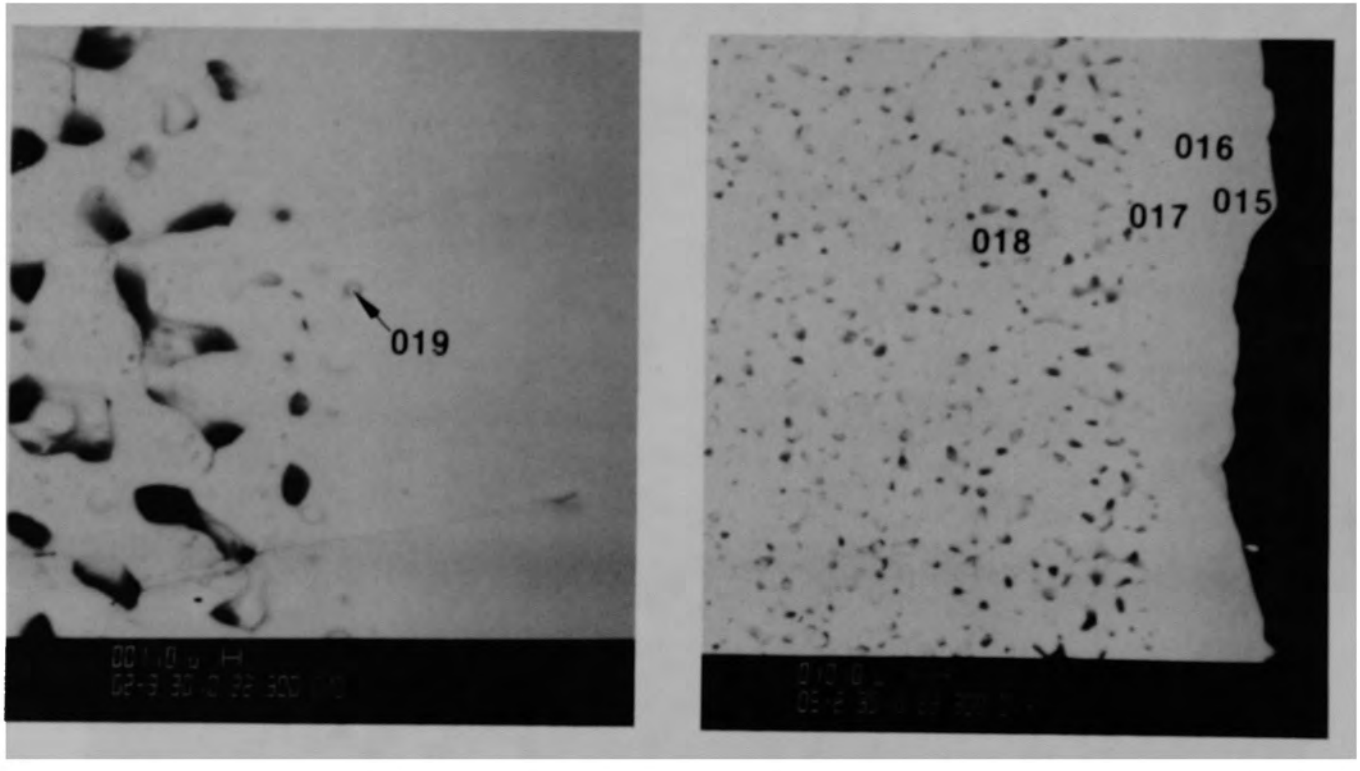

Figure C-19. SEM backscattered electron image of fuel from Particle 1B (H8, surface), corresponding to Figure C-15.

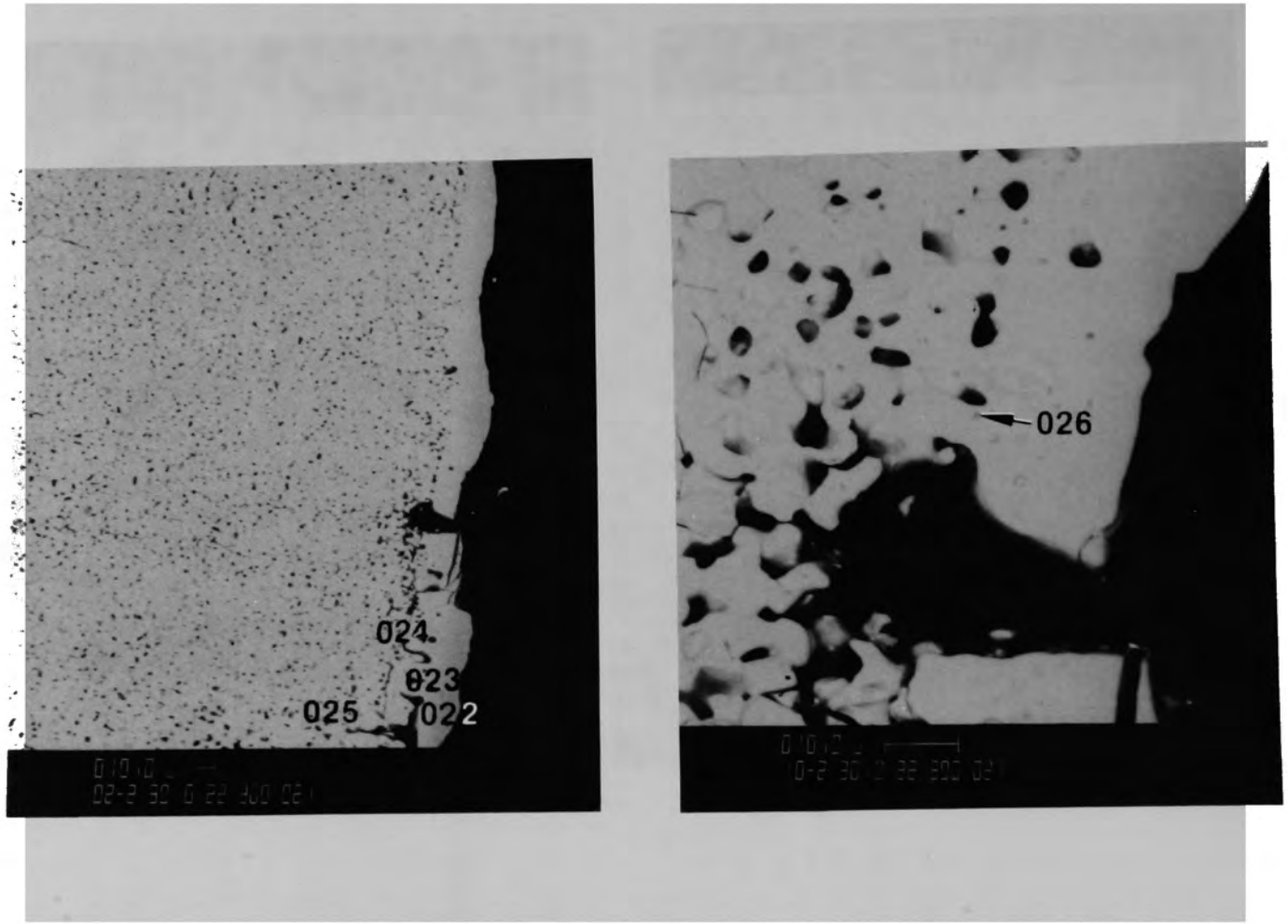

Figure C-20. SEM backscattered electron image of fuel from Particle 1B (H8, surface), corresponding to Figure C-12.

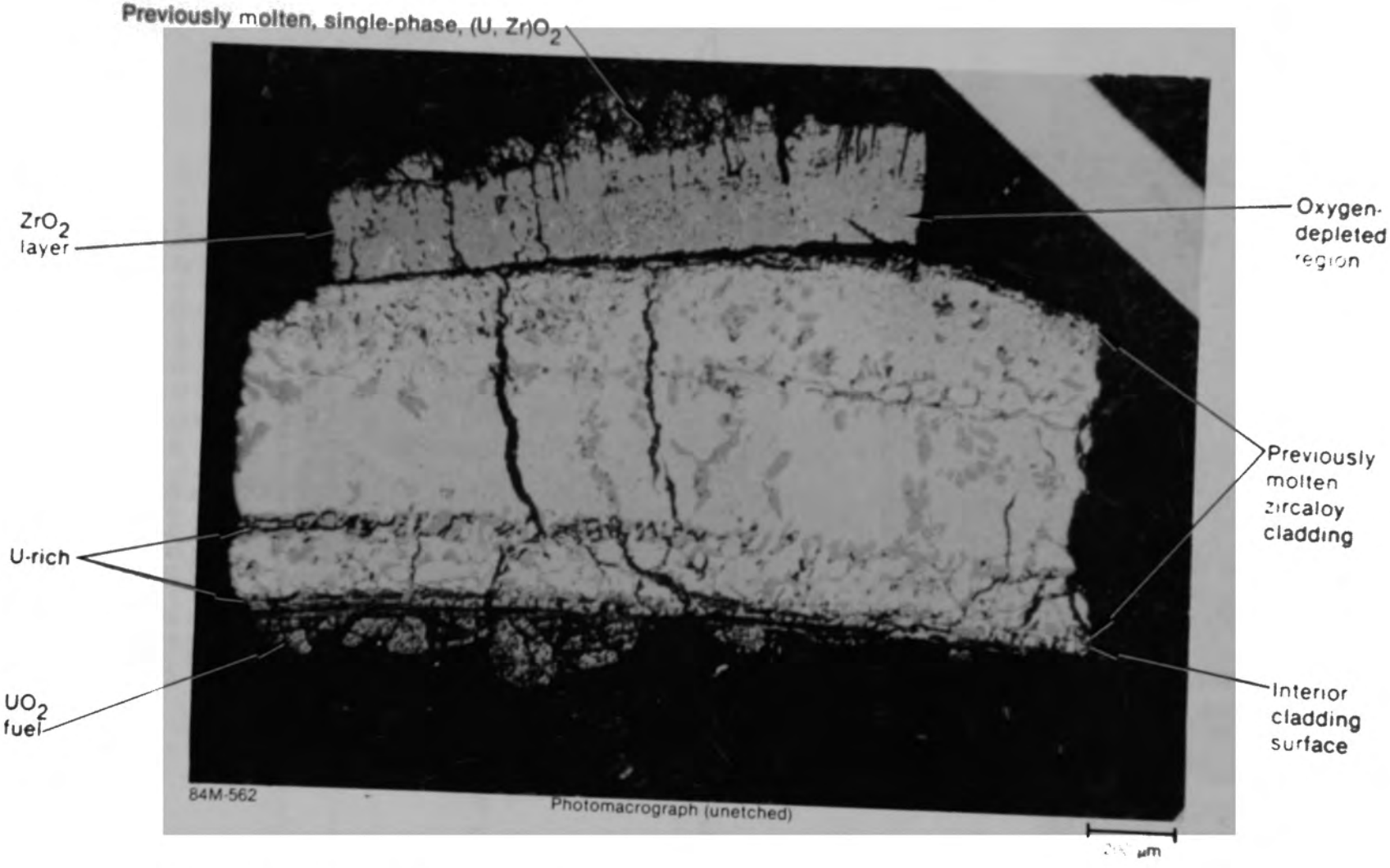

Figure C-21. Photomacrograph of Particle 1E (H8, surface) showing cladding fragment with adherent fuel and once-molten mixed ceramic.

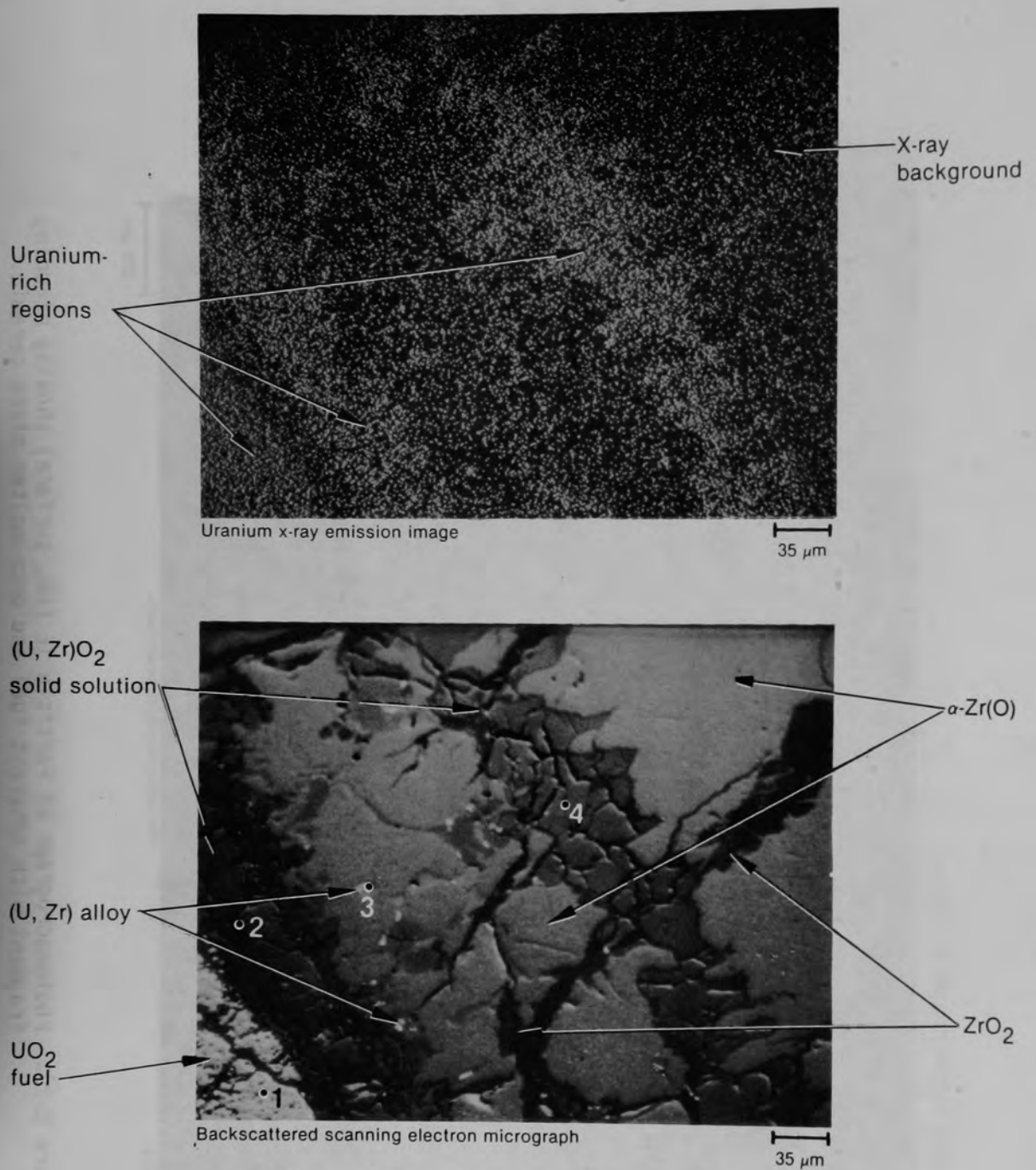

Point 1: 100.0 weight % U
Point 2: 33.0 weight % U, 67.0 weight % Zr
Point 3: 83.0 weight % U, 17.0 weight % Zr
Point 4: 32.1 weight % U, 67.9 weight % Zr

Figure C-22. Uranium and zirconium segregation near the fuel-cladding interface on Particle 1E.

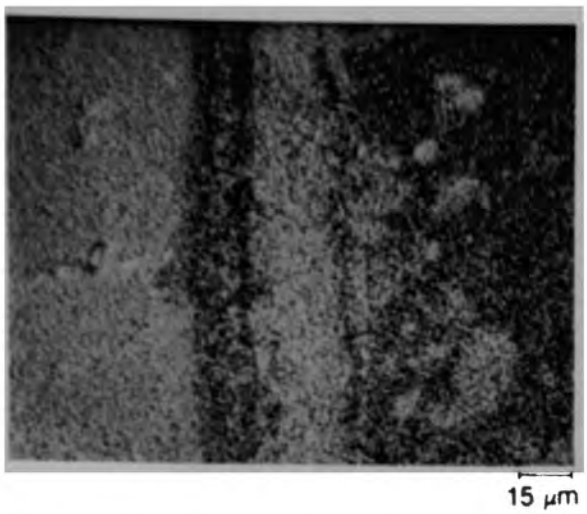

Uranium X-ray emission image

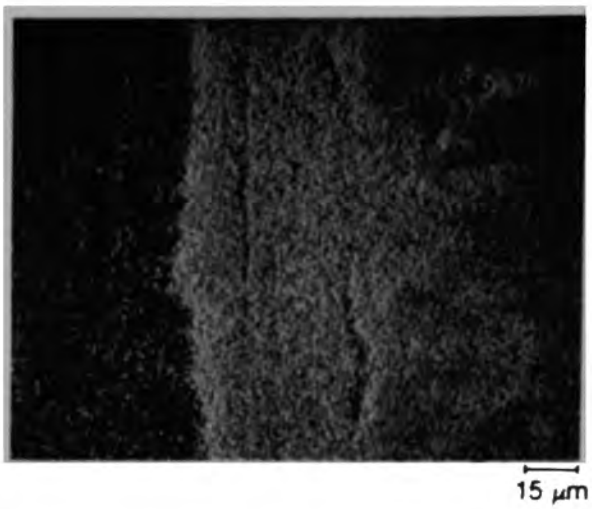

Zirconium X-ray emission image

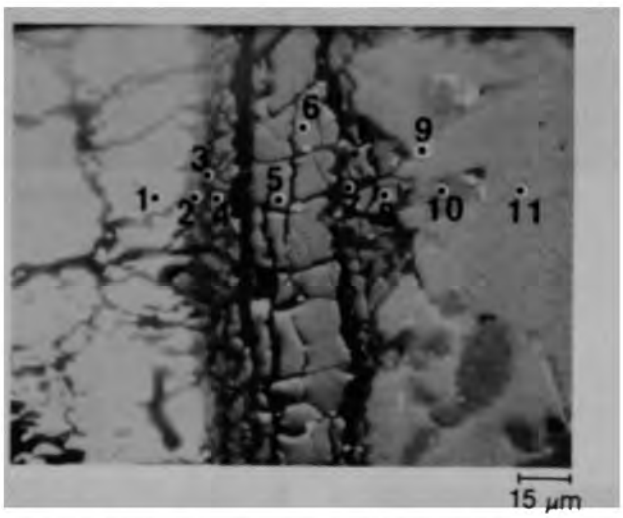

Backscattered scanning electron micrograph

Point 1: 100.0 weight % U
Point 2: 25.8 weight % U, 74.2 weight % Zr
Point 3: 100.0 weight % Zr
Point 4: 19.6 weight % U, 80.5 weight % Zr
Point 5: 37.0 weight % U, 63.1 weight % Zr
Point 6: 67.4 weight % U, 32.7 weight % Zr
Point 7: 3.8 weight % U, 10.6 weight % Cr, 14.0 weight % Fe, 71.7 weight % Zr
Point 8: 32.0 weight % U, 68.1 weight % Zr
Point 9: 84.6 weight % U, 15.5 weight % Zr
Point 10: 32.3 weight % U, 67.8 weight % Zr
Point 11: 7.8 weight % U, 92.3 weight % Zr, plus trace of Fe and Cr

Figure C-23. High magnification elemental composition finding at the pellet-cladding interface on Particle 1E.

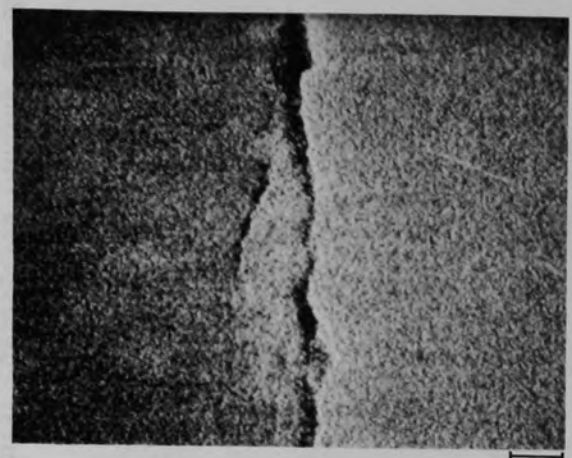

Zirconium X-ray emission image

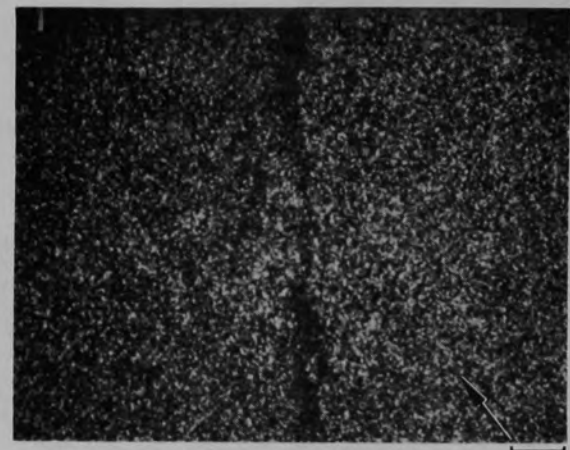

Uranium X-ray emission image

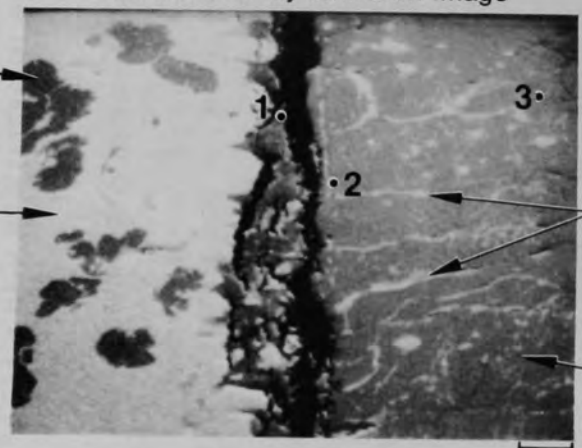

Backscattered scanning electron micrograph

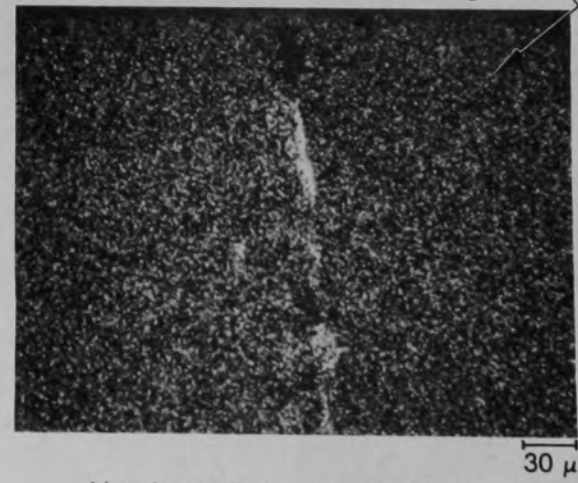

Aluminum X-ray emission image

Point 1: 67.0 weight % Al, 27.2 weight % Zr, 3.0 weight % Fe, 2.8 weight % Cr
Point 2: 100.0 weight % Zr
Point 3: 100.0 weight % Zr

Figure C-24. Phase distributions surrounding the Zr-ZrO_2 interface on Particle 1E.

Backscattered scanning electron micrograph

Point 1: 11.1 weight % U, 89.0 weight % Zr
Point 2: 71.3 weight % Zr, 11.4 weight % Cr, 13.6 weight % Fe, 3.8 weight % Al
Point 3: 80.9 weight % Zr, 10.3 weight % Sn, 4.2 weight % Al, 4.0 weight % Fe, 0.6 weight % Cr
Point 4: 39.9 weight % U, 60.2 weight % Zr
Area average: 10.6 weight % U, 86.0 weight % Zr, 2.0 weight % Fe, 1.1 weight % Cr, 0.4 weight % Al, plus trace of Sn

Figure C-25. Energy-dispersive x-ray spectroscopy measurements within the ZrC_2 layer on Particle 1E.

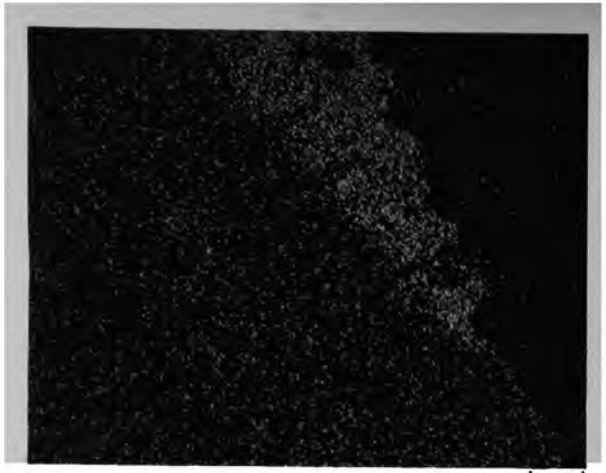

Uranium X-ray emission image 60 μm

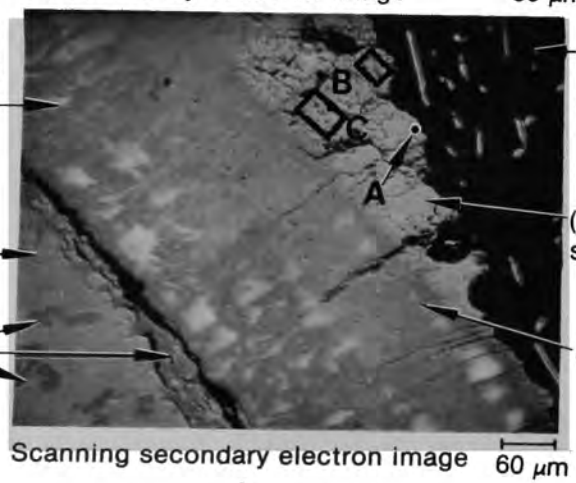

Scanning secondary electron image 60 μm

Energy-dispersive X-ray spectrometer data

Point A: 82.6 weight % U, 17.5 weight % Zr
Area B: 65.8 weight % U, 26.0 weight % Zr, 4.4 weight % Cr, 2.2 weight % Fe, 1.6 weight % Al
Area C: 70.5 weight % U, 26.6 weight % Zr, 0.8 weight % Cr, 0.8 weight % Fe, 1.4 weight % Al

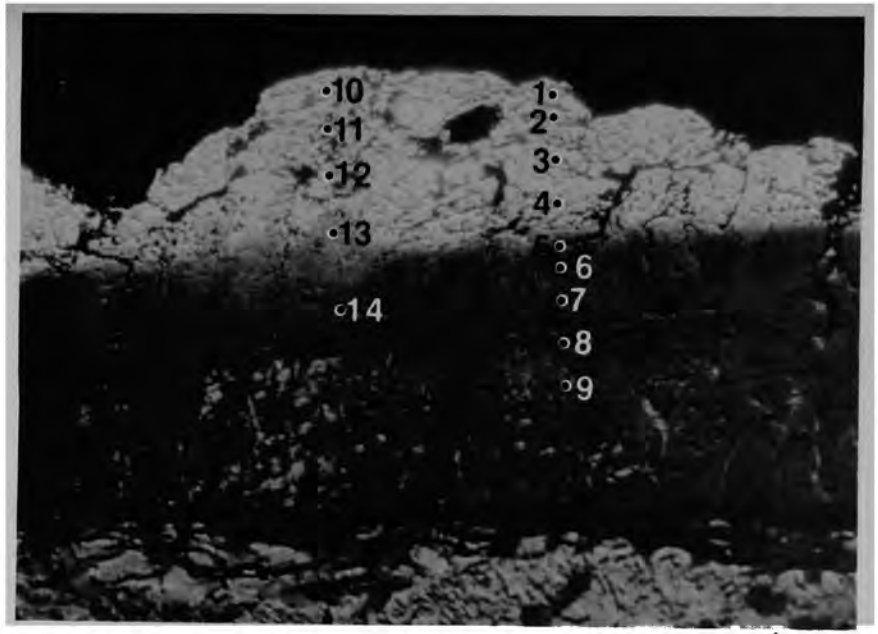

Backscattered scanning electron micrograph 62.5 μm

Auger electron spectroscopy data (15-μm beam size)

Point	U (atom %)	Zr (atom %)	O (atom %)	Trace elements
1	16.7	12.6	70.7	C, Cs
2	18.0	13.8	68.2	Sb, Fe
3	21.0	12.9	66.1	
4	20.9	12.8	66.3	Cr, Al
5	7.1	28.0	64.9	C
6	10.9	23.8	65.3	C, Cr
7	3.2	33.0	63.8	C
8	2.8	33.0	64.2	Fe
9	2.9	35.3	61.8	Fe, C
10	20.2	13.0	66.8	Cr
11	19.0	14.3	66.7	Cr, Fe, C
12	14.1	19.5	66.4	Cr, Fe, C
13	6.7	27.3	66.0	Pr
14	4.7	29.3	66.0	C

Figure C-26. Summary of elemental determinations on and near the adherent, once-molten mixed oxide on Particle 1E.

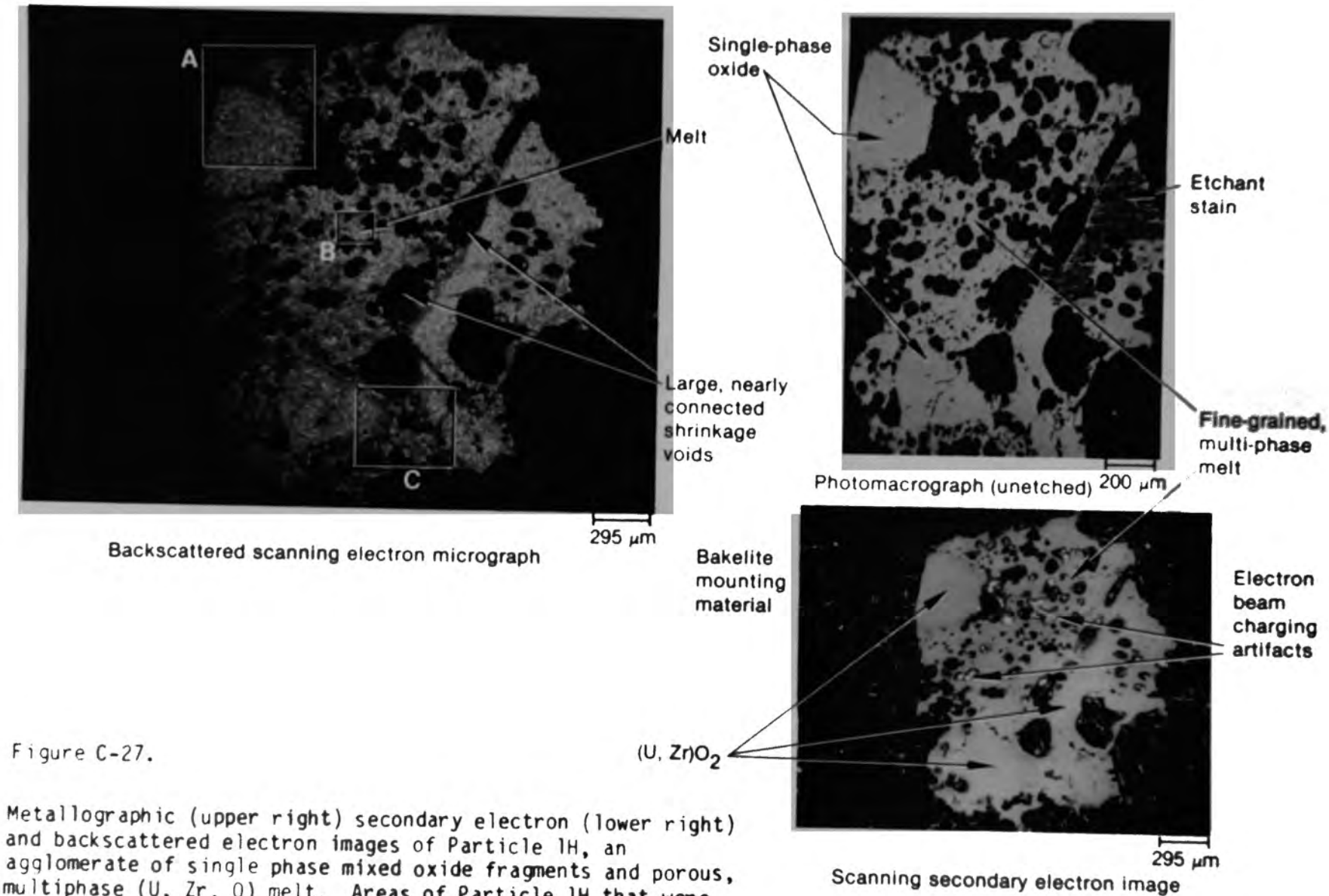

Figure C-27.

Metallographic (upper right) secondary electron (lower right) and backscattered electron images of Particle 1H, an agglomerate of single phase mixed oxide fragments and porous, multiphase (U, Zr, O) melt. Areas of Particle 1H that were investigated in detail are shown on the left.

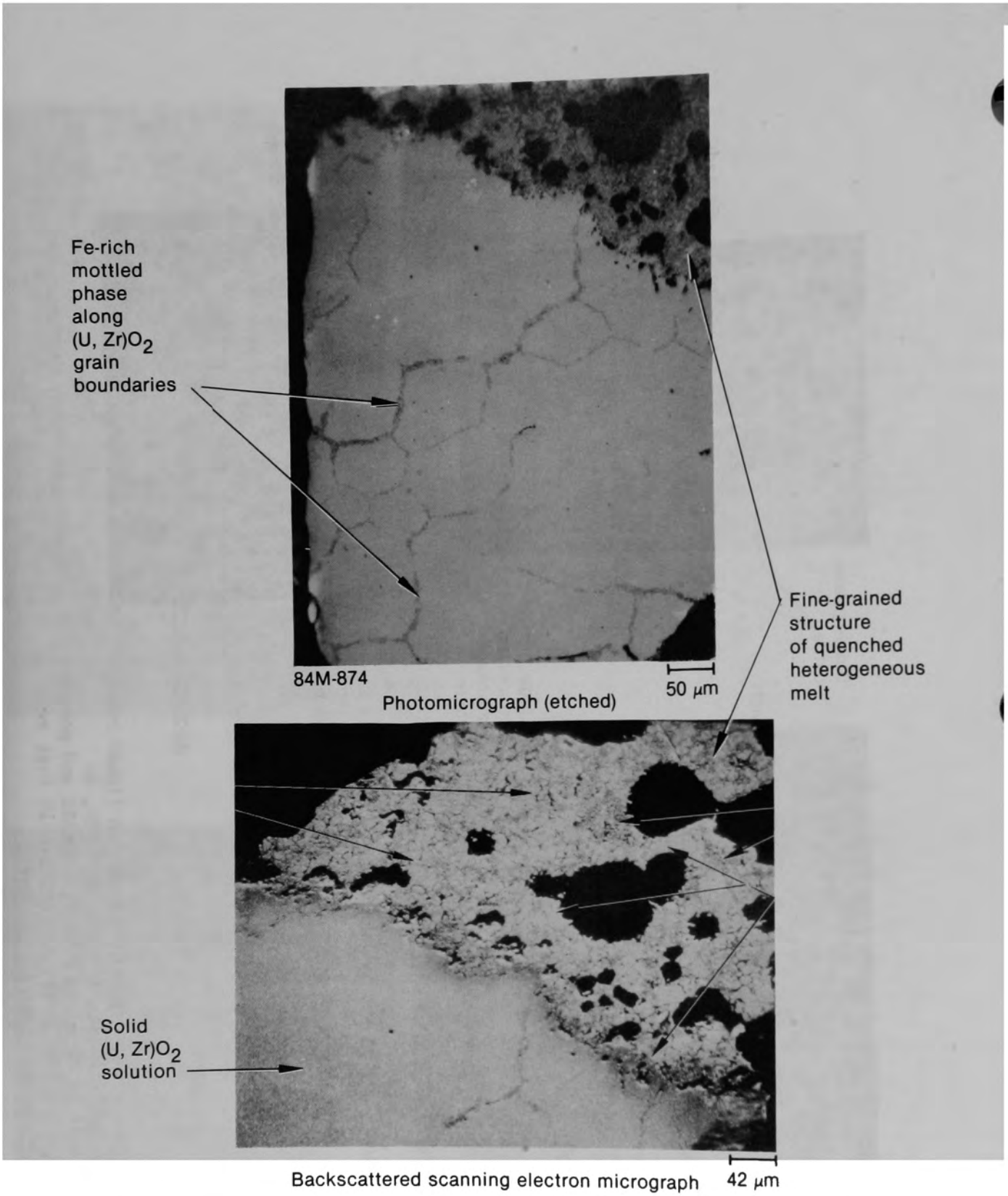

Figure C-28. Metallographic (top) and SEM appearances of (U, Zr) O_2 attack along grain boundaries by an iron rich melt phase, within area A of Particle 1H. Lower image shows locations in which primary composition measurements were made.

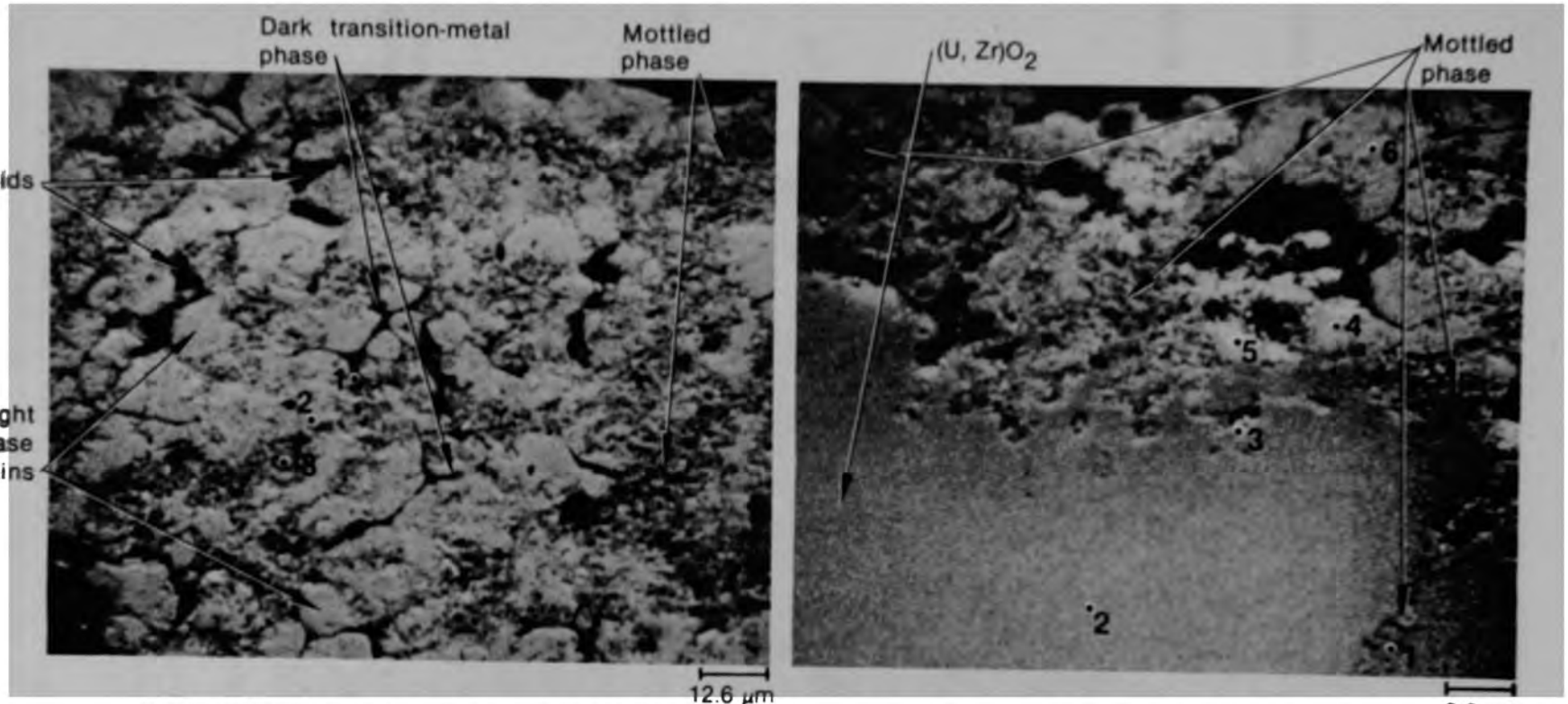

Backscattered scanning electron micrograph

Point 1: 24.6 weight % U, 11.1 weight % Zr, 25.7 weight % Fe, 12.5 weight % Ni, 17.4 weight % Cr, 8.7 weight % Al

Point 2: 70.1 weight % U, 26.0 weight % Zr, 3.9 weight % Fe,

Point 3: 53.6 weight % U, 40.5 weight % Zr, 5.9 weight % Fe,

Area Average (approx.): 68 weight % U, 28 weight % Zr, 4 weight % Fe, plus traces of Ni, Cr, and Al

Backscattered scanning electron micrograph

Point 1: 53.6 weight % U, 42.2 weight % Zr, 4.2 weight % Fe,

Point 2: 58.7 weight % U, 41.3 weight % Zr

Point 3: 43.6 weight % U, 18.4 weight % Zr, 22.4 weight % Fe, 7.3 weight % Ni, 4.4 weight % Al, 3.9 weight % Cr

Point 4: 64.8 weight % U, 31.1 weight % Zr, 4.1 weight % Fe,

Point 5: 50.9 weight % U, 38.4 weight % Zr, 8.0 weight % Fe, 1.7 weight % Ni, 1.0 weight % Cr

Point 6: 66.1 weight % U, 29.5 weight % Zr, 4.4 weight % Fe,

Figure C-29. Melt phase structures away from (left) and adjacent to $(U,Zr)O_2$ fragment in region A of Particle 1H.

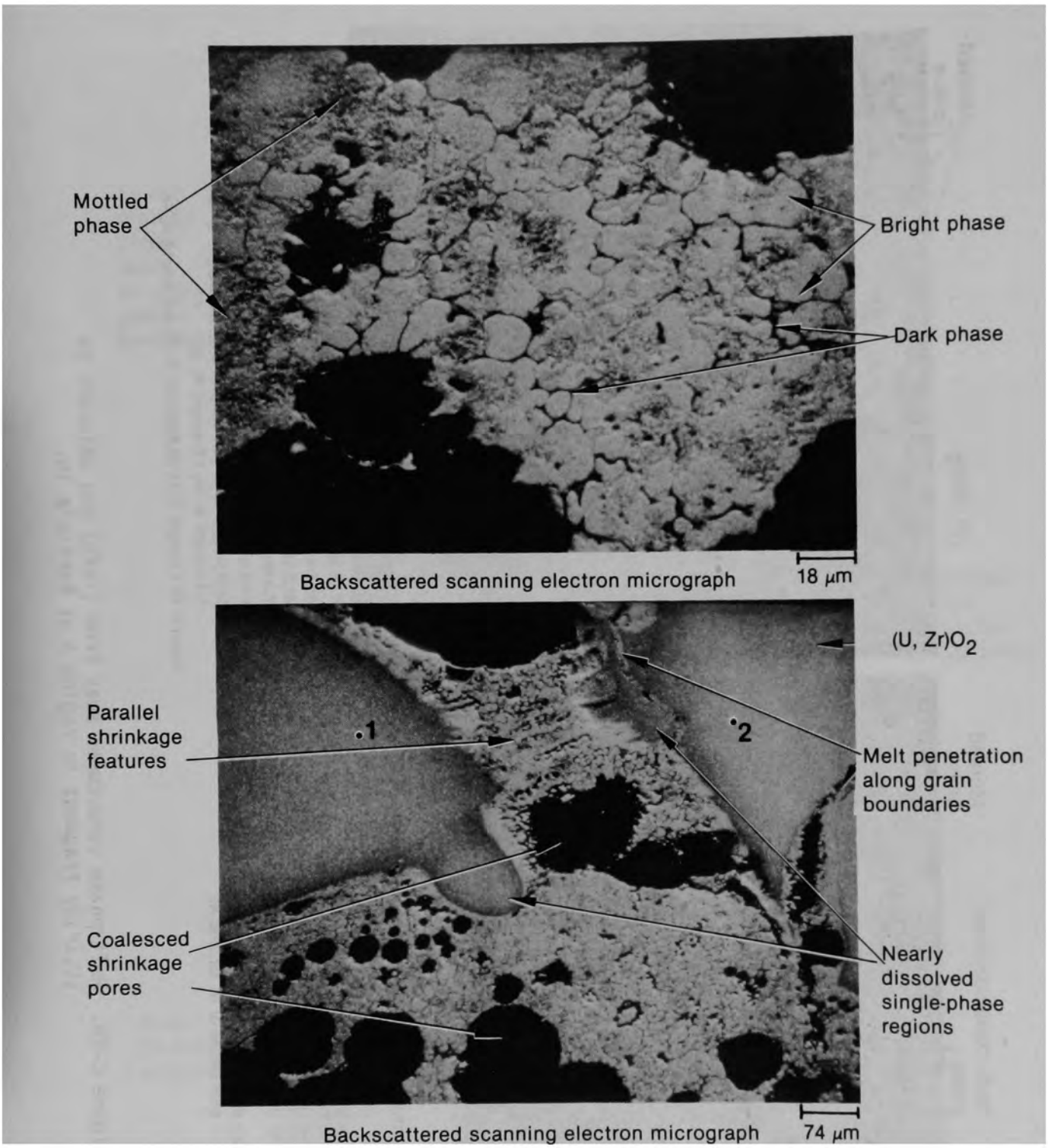

Area B Average (approx.): 68 weight % U, 28 weight % Zr, 4 weight % Fe, plus traces of Ni, Cr, and Al

Point 1 (approx.): 67 weight % U, 33 weight % Zr

Point 2: 67.3 weight % U, 32.7 weight % Zr

Figure C-30. Regions B (upper) and C (lower) of Particle 1H. Note similarities in heterogeneous melt appearance and in wetting of (U, Zr) O_2 fragments to Region A (Figure C-29).

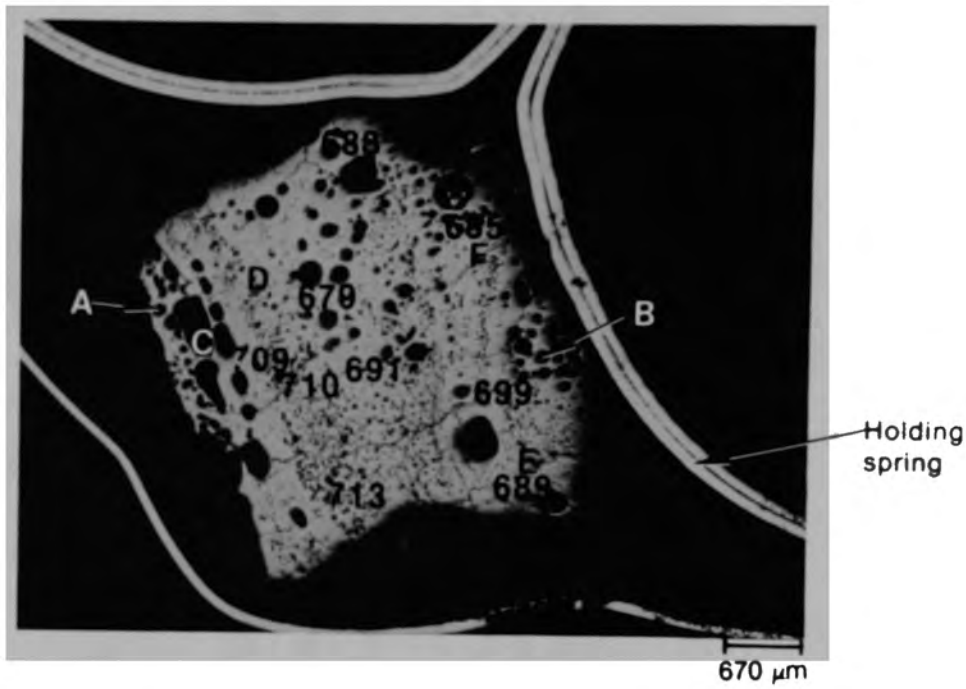

Figure C-31. Photomacrograph of Particle 3L (H8, 56 cm).

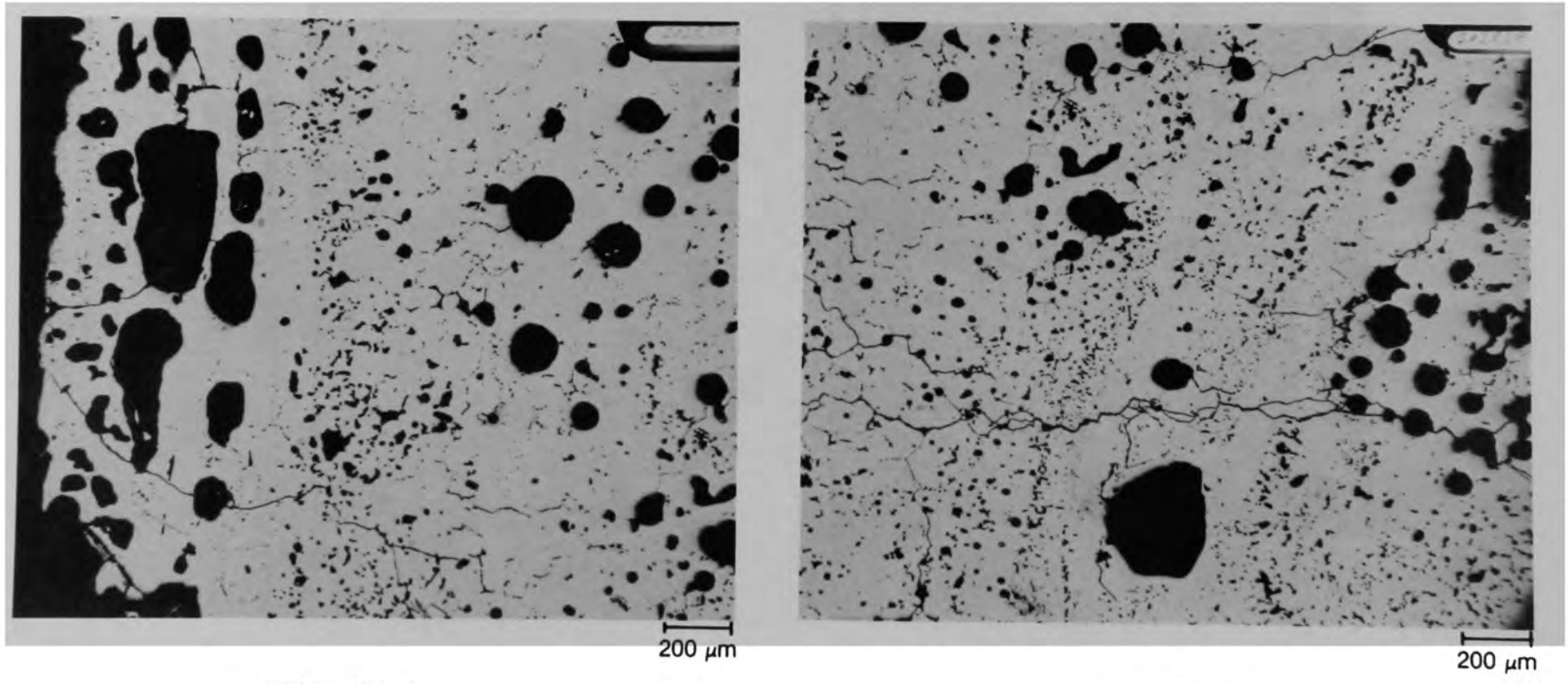

(a) Location A

(b) Location B

Figure C-32. Photomicrograph of Particle 3L (H8, 56 cm) in the unetched condition showing pore morphology.

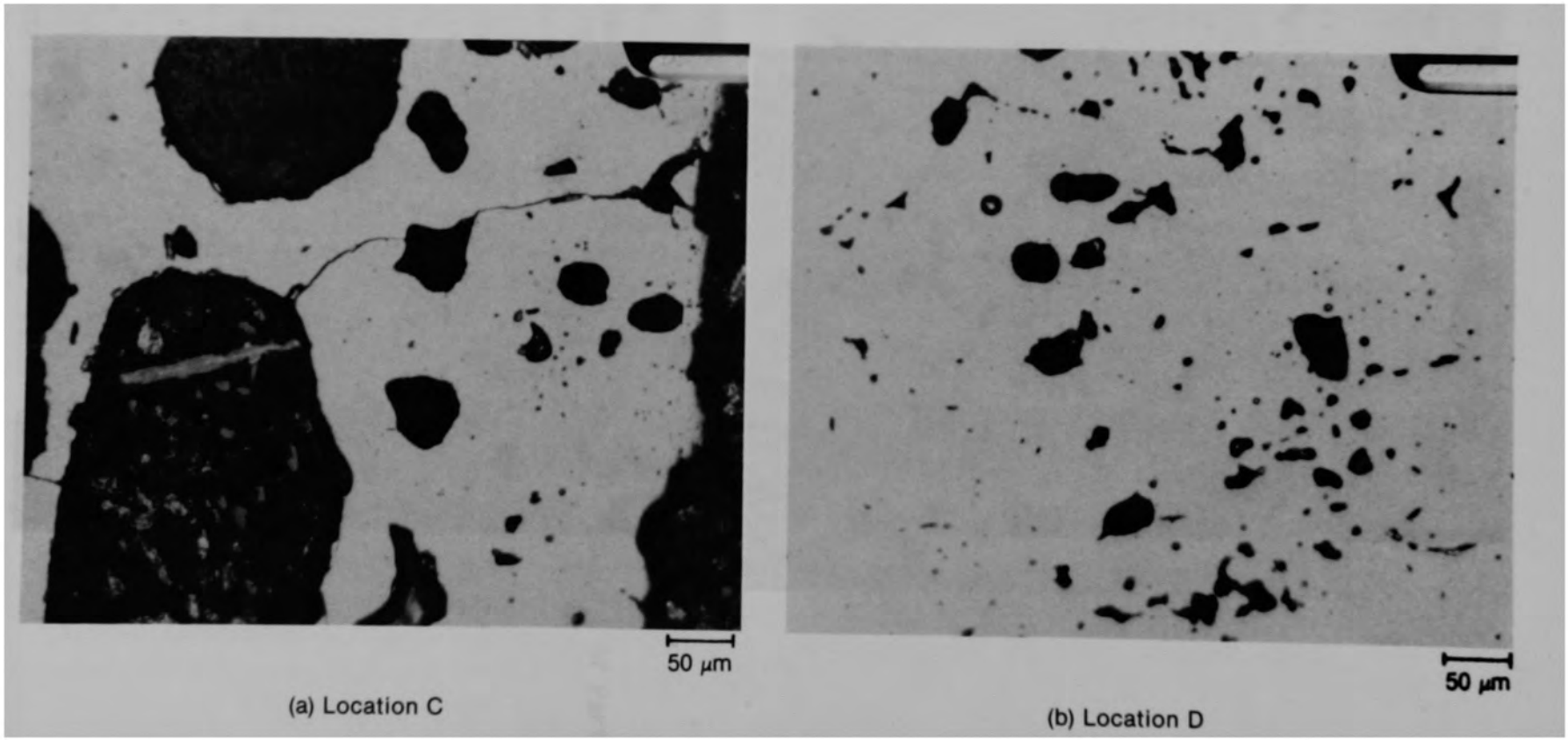

Figure C-33. Photomicrograph of Particle 3L (H8, 56 cm) in the etched condition showing pore morphology.

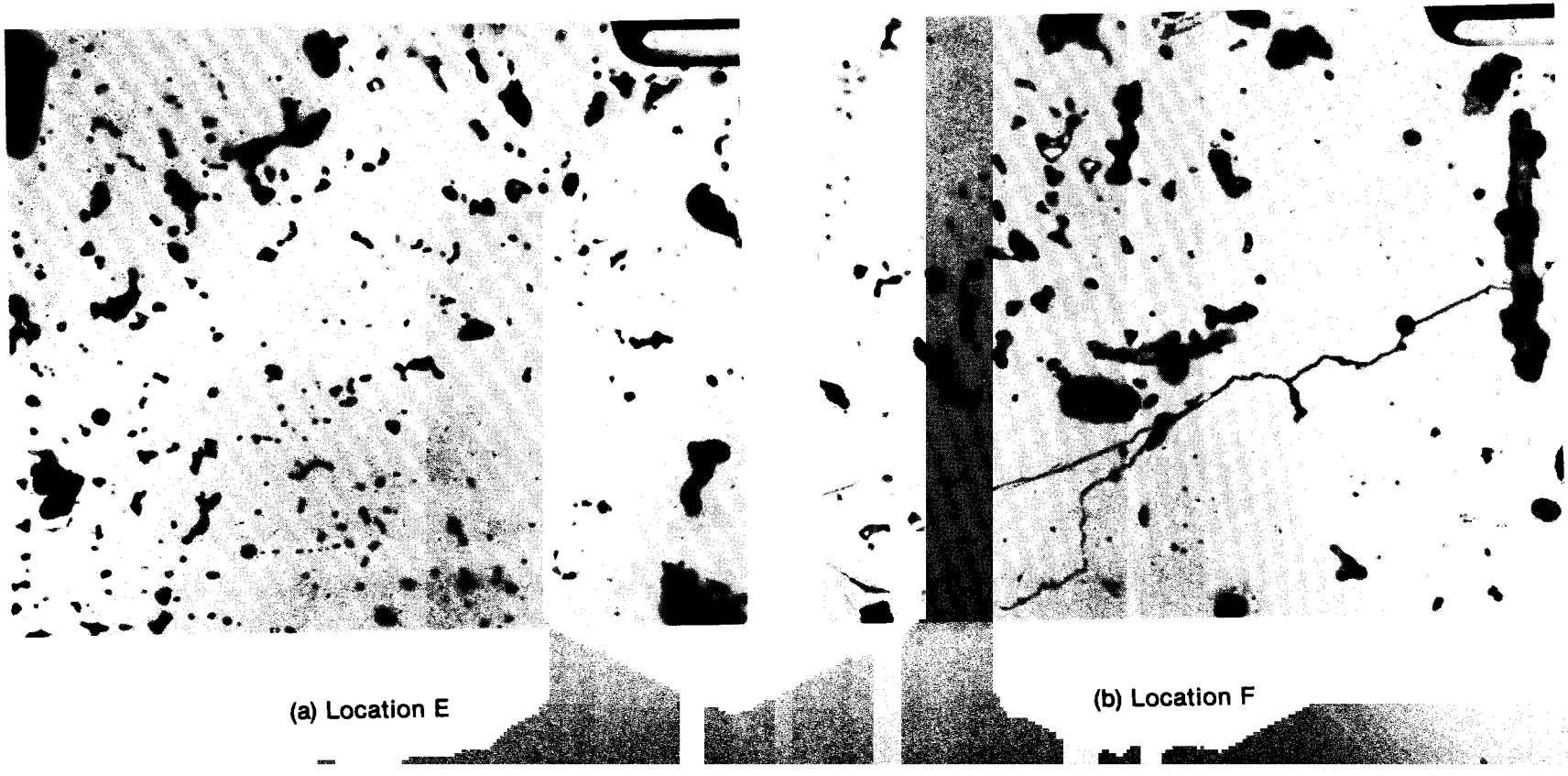

Figure C-34. Photomicrograph of Particle 3L (H8, 56 cm) in the etched condition showing pore morphology.

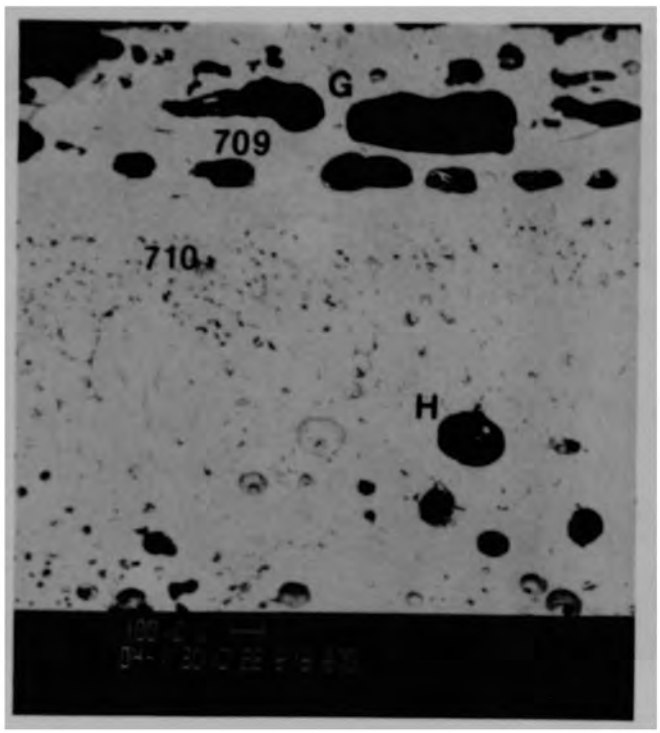

Figure C-35. SEM backscattered electron image at Location C of Particle 3L (H8, 56 cm).

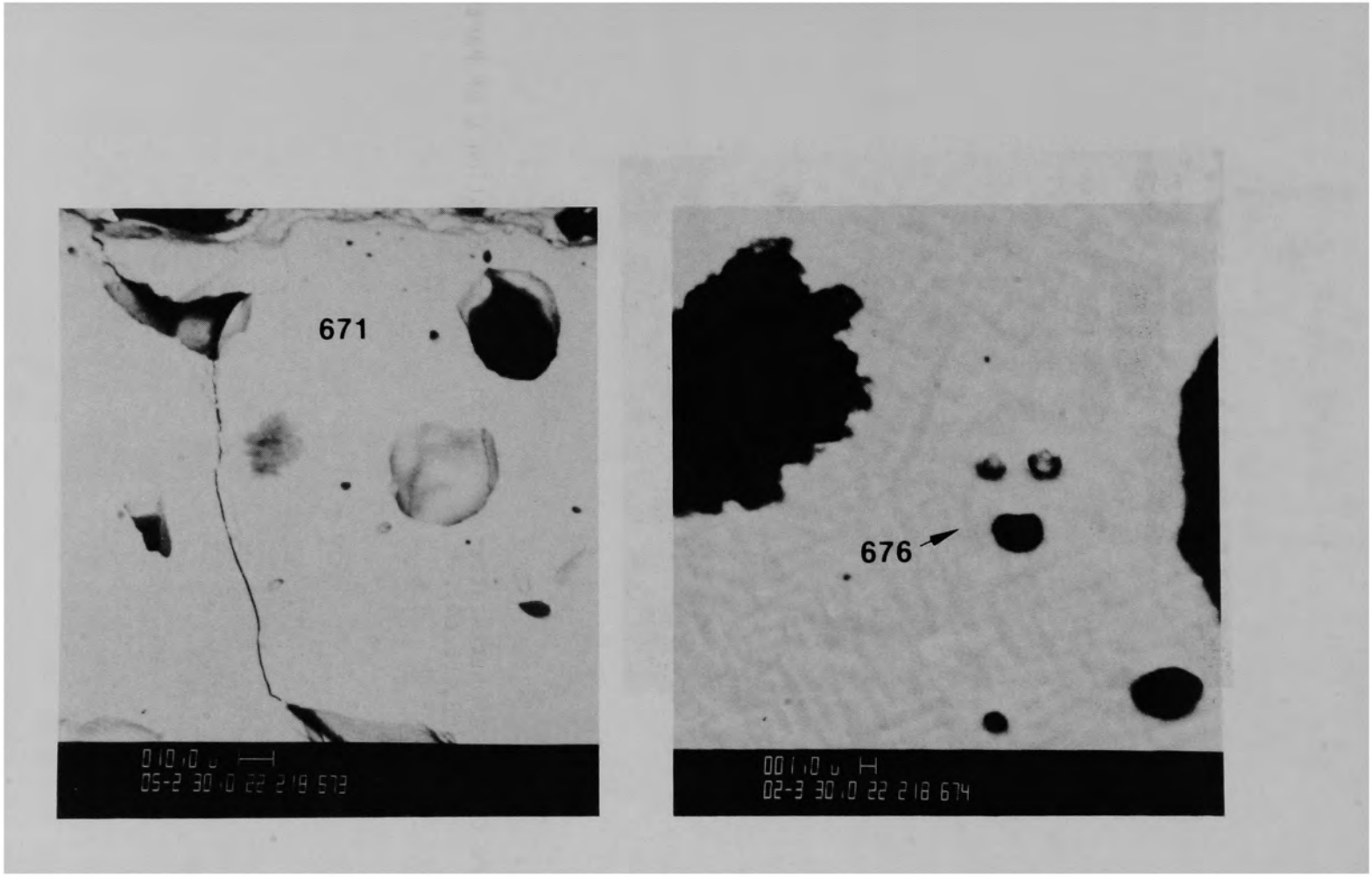

Figure C-36. SEM backscattered electron images of Particle 3L (H8, 56 cm) showing fine grain structure, corresponding to location G on Figure C-35.

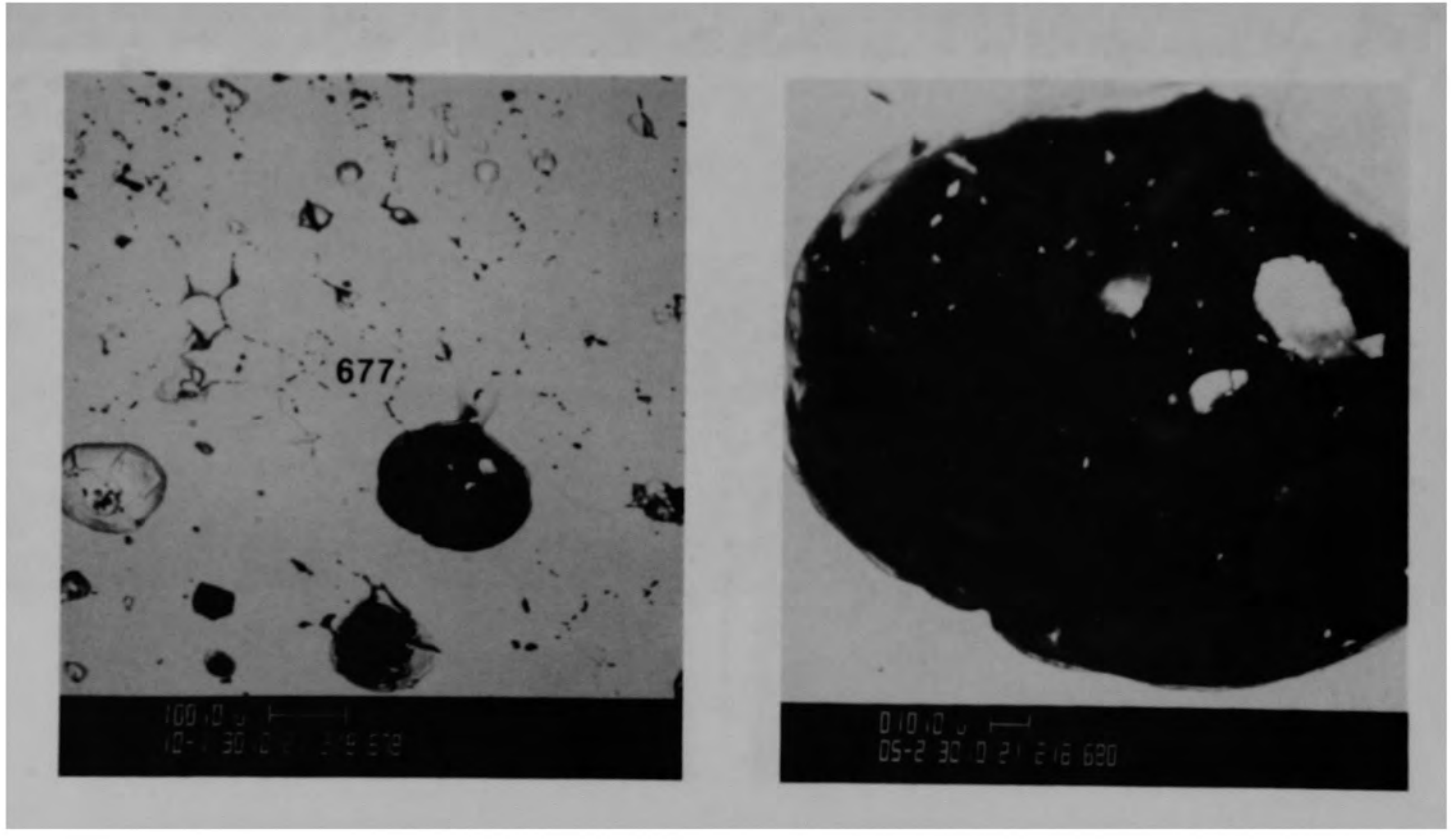

Figure C-37. SEM backscattered electron images of Particle 3L (H8, 56 cm) corresponding to location H on Figure C-35.

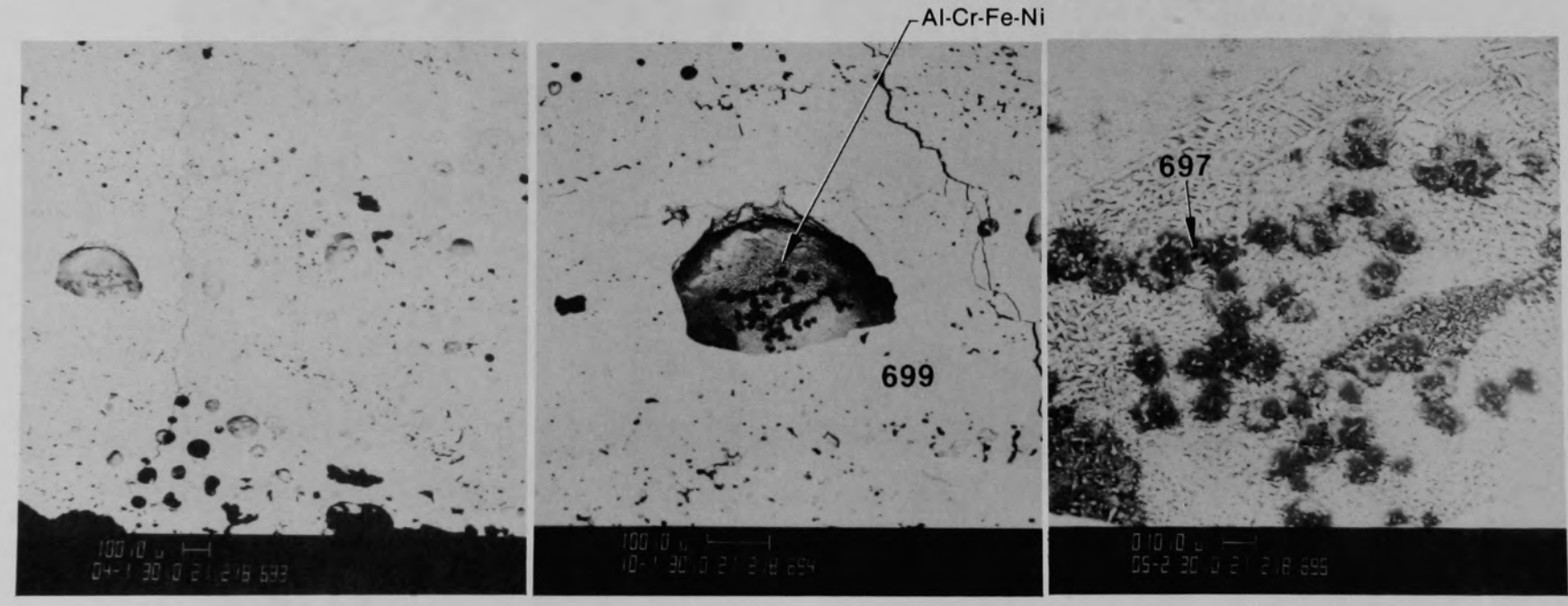

Figure C-38. SEM backscattered electron image of Particle 3L (H8, 56 cm) showing Al-Cr-Fe-Ni phase in large pores.

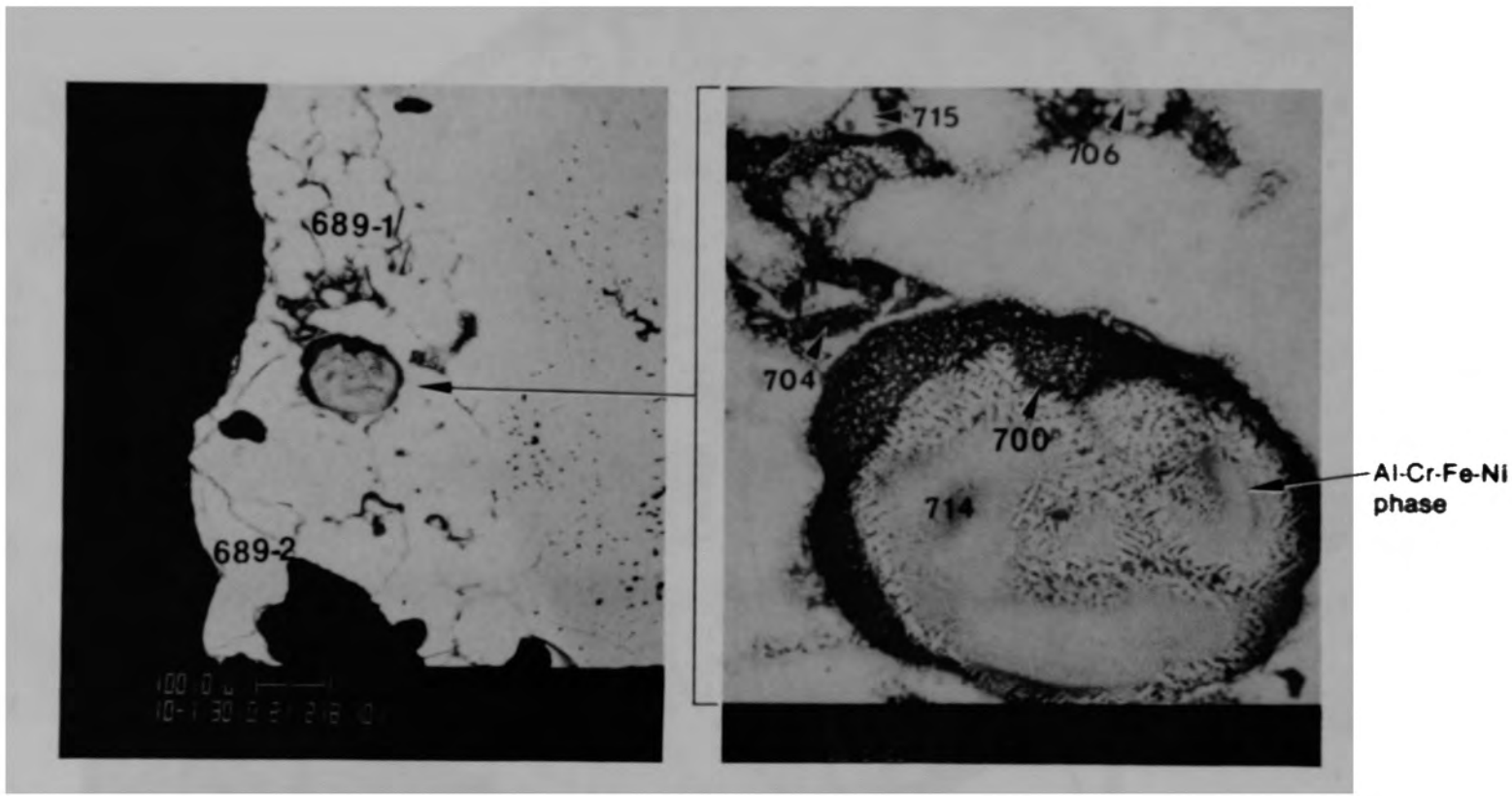

Figure C-39. SEM backscattered electron images of Particle 3L (H8, 56 cm) showing Al-Cr-Fe-Ni phase in large pores.

Figure C-40. Photomacrograph of Particle 3M (H8, 56 cm) showing two regions, Type 1 and 2.

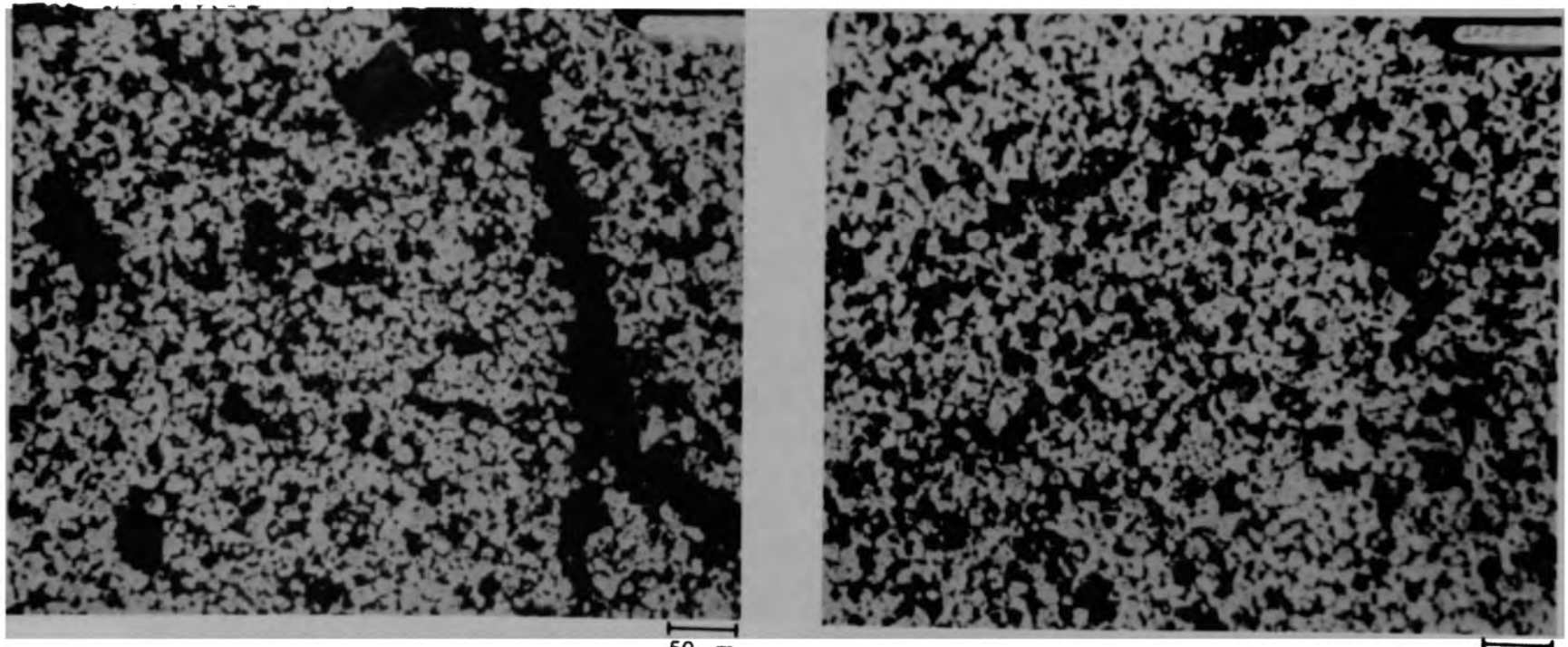

(a) Fuel etch

(b) Unetched

Figure C-41. Photomicrographs of fuel in lower Type 1 region of Particle 3M (H8, 56 cm).

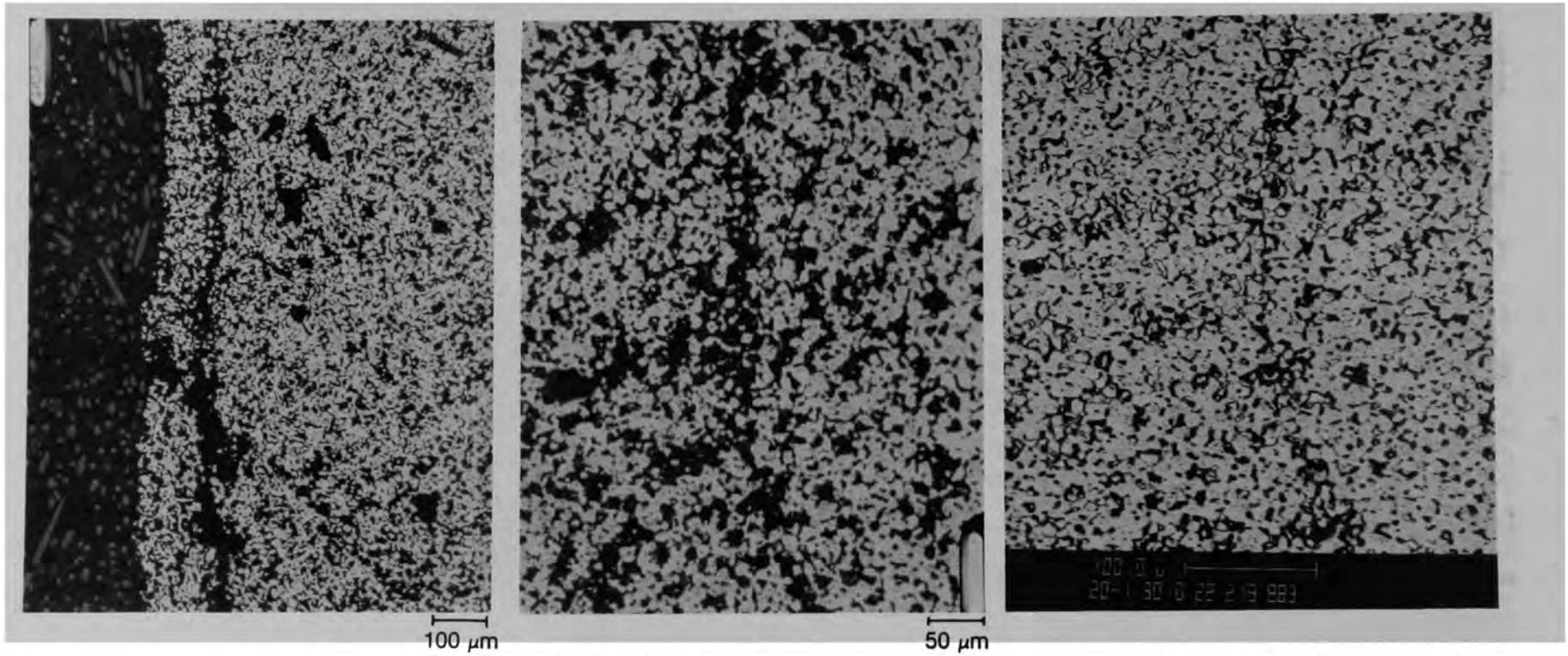

(a) Location A (b) Location B photomicrograph (c) Location B backscattered electron image

Figure C-42. Photomicrographs of the middle type 1 region of Particle 3M (H8, 56 cm).

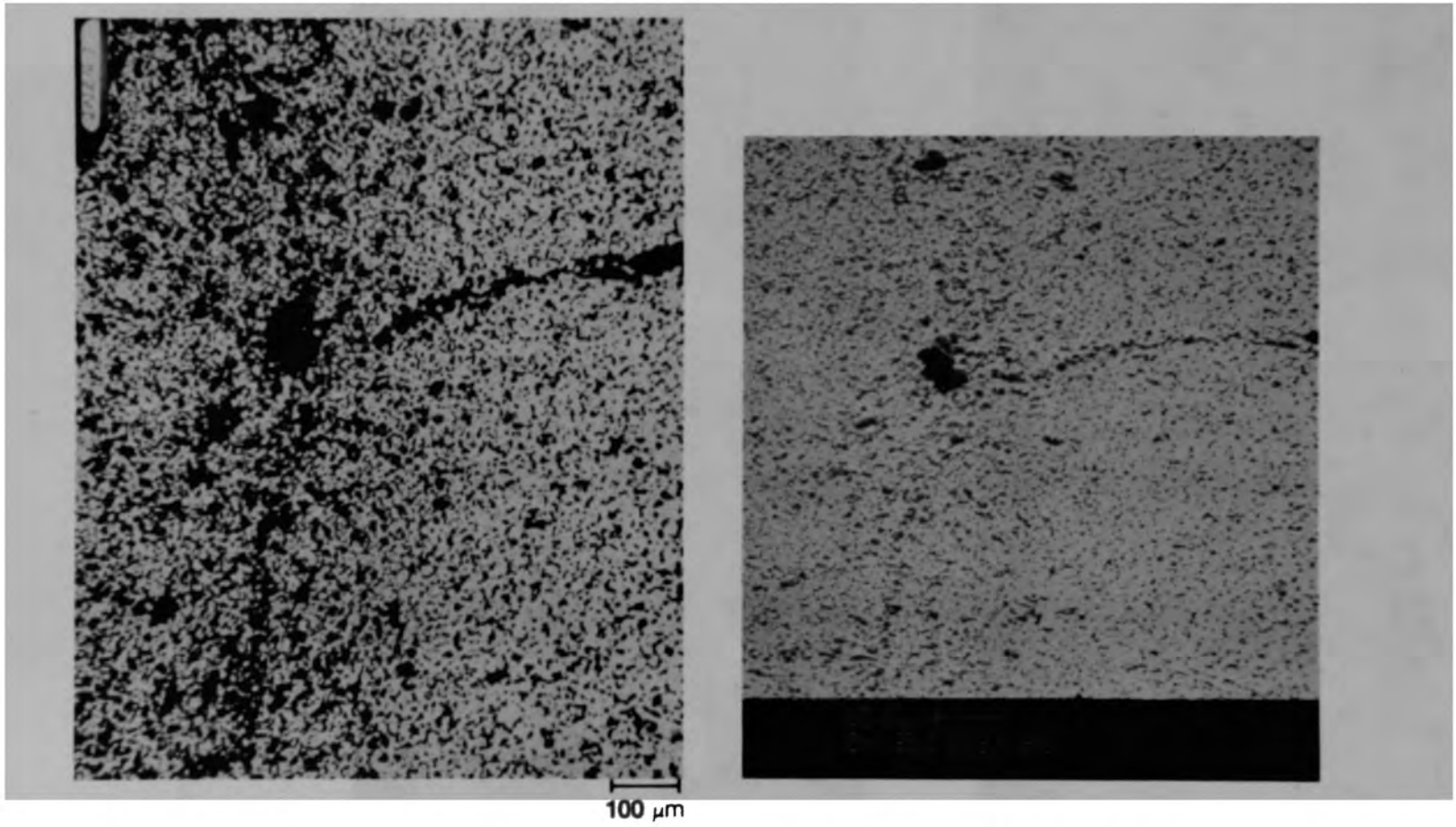

(a) Photomicrograph

(b) Backscattered electron image

Figure C-43. Fuel at location C of Particle 3M (H8, 56 cm).

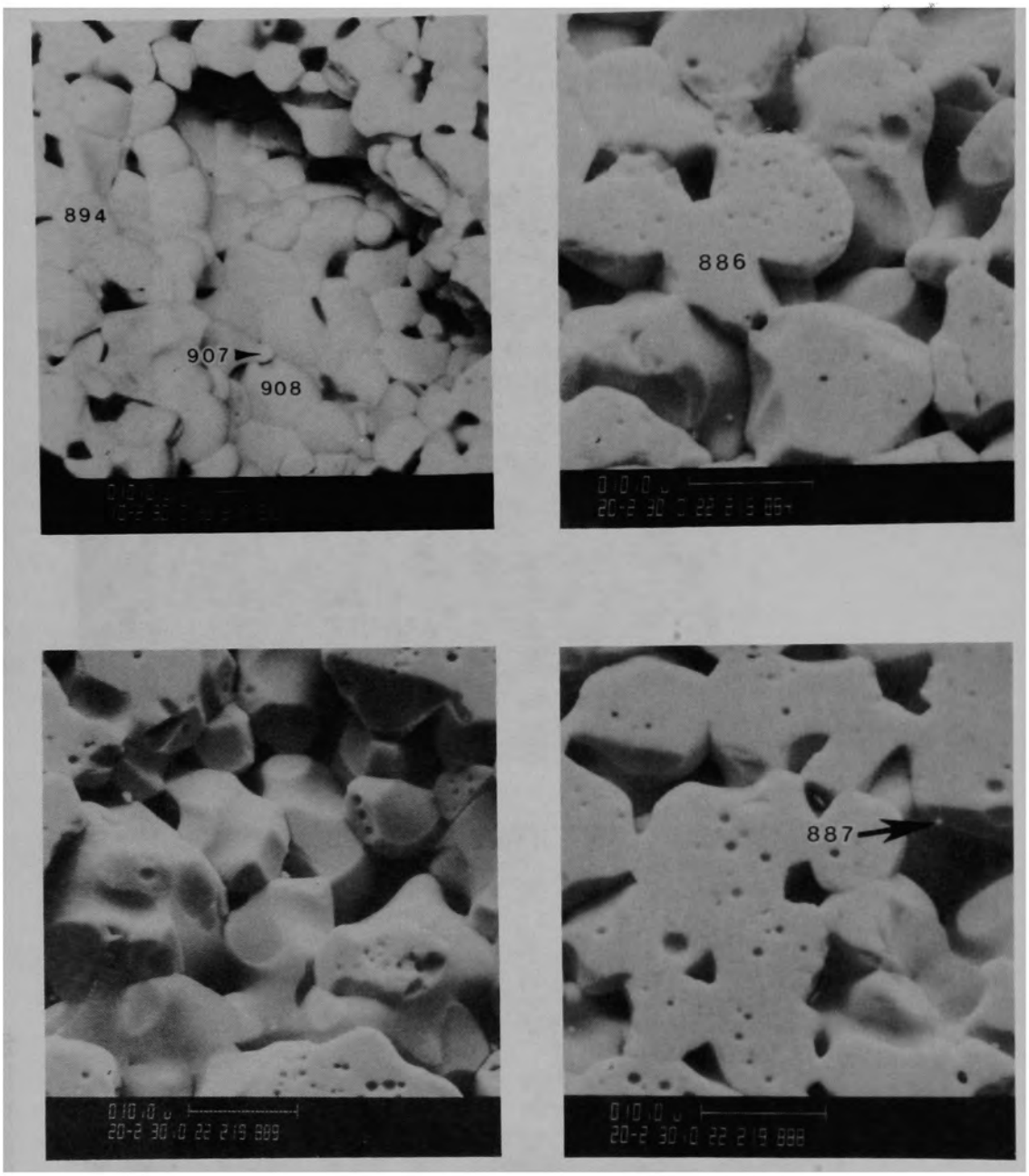

Figure C-44. Backscattered electron images of fuel in Type 1 region of Particle 3M (H8, 56 cm).

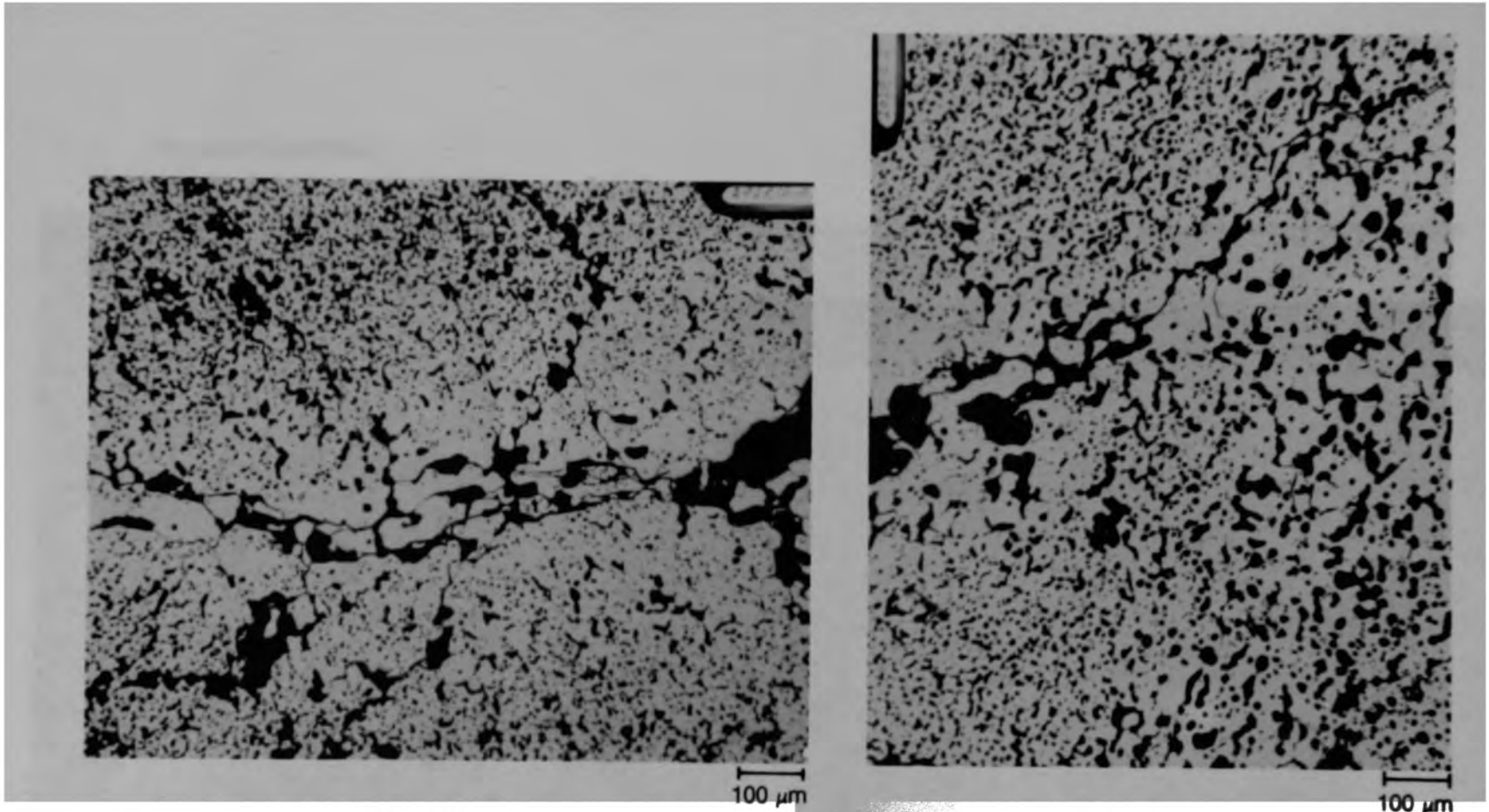

(a) Location D

(b) Location E

Figure C-45. Photomicrographs of material in Type 2 region of Particle 3M (H8, 56 cm).

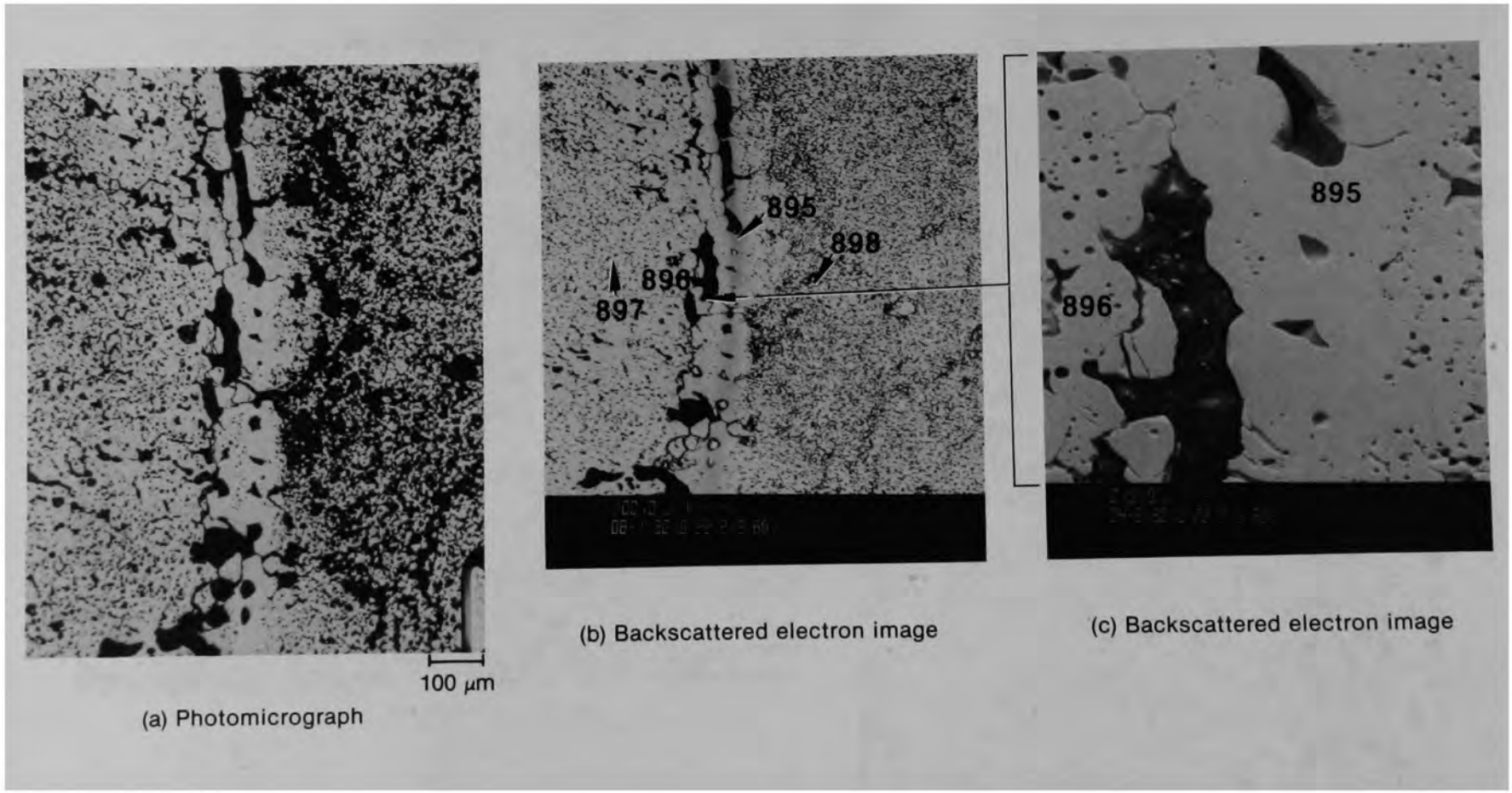

Figure C-46. Material structure from location F in Type 2 region of Particle 3M (H8, 56 cm).

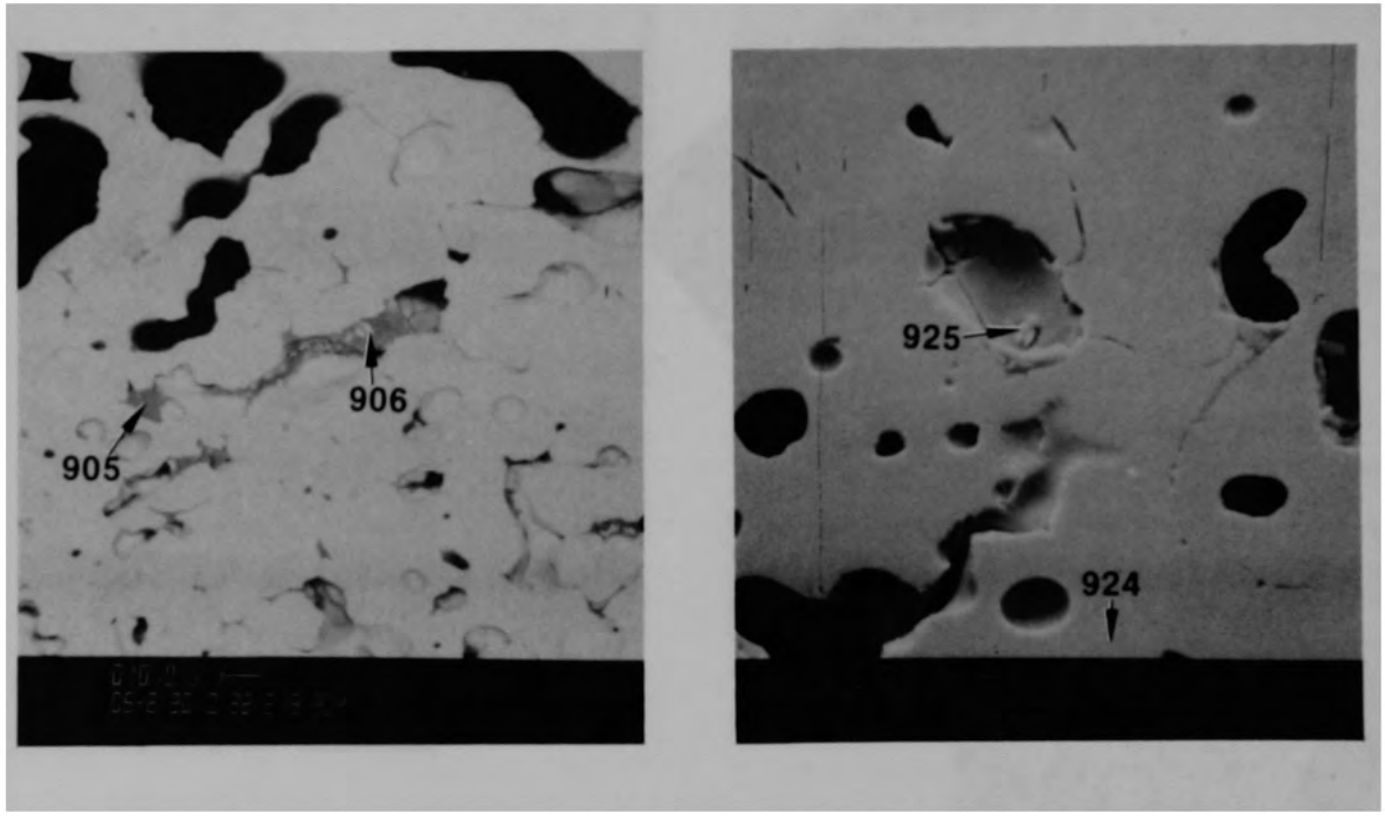

Figure C-47. Backscattered electron images of pore morphology in Type 2 region material of Particle 3M (H8, 56 cm).

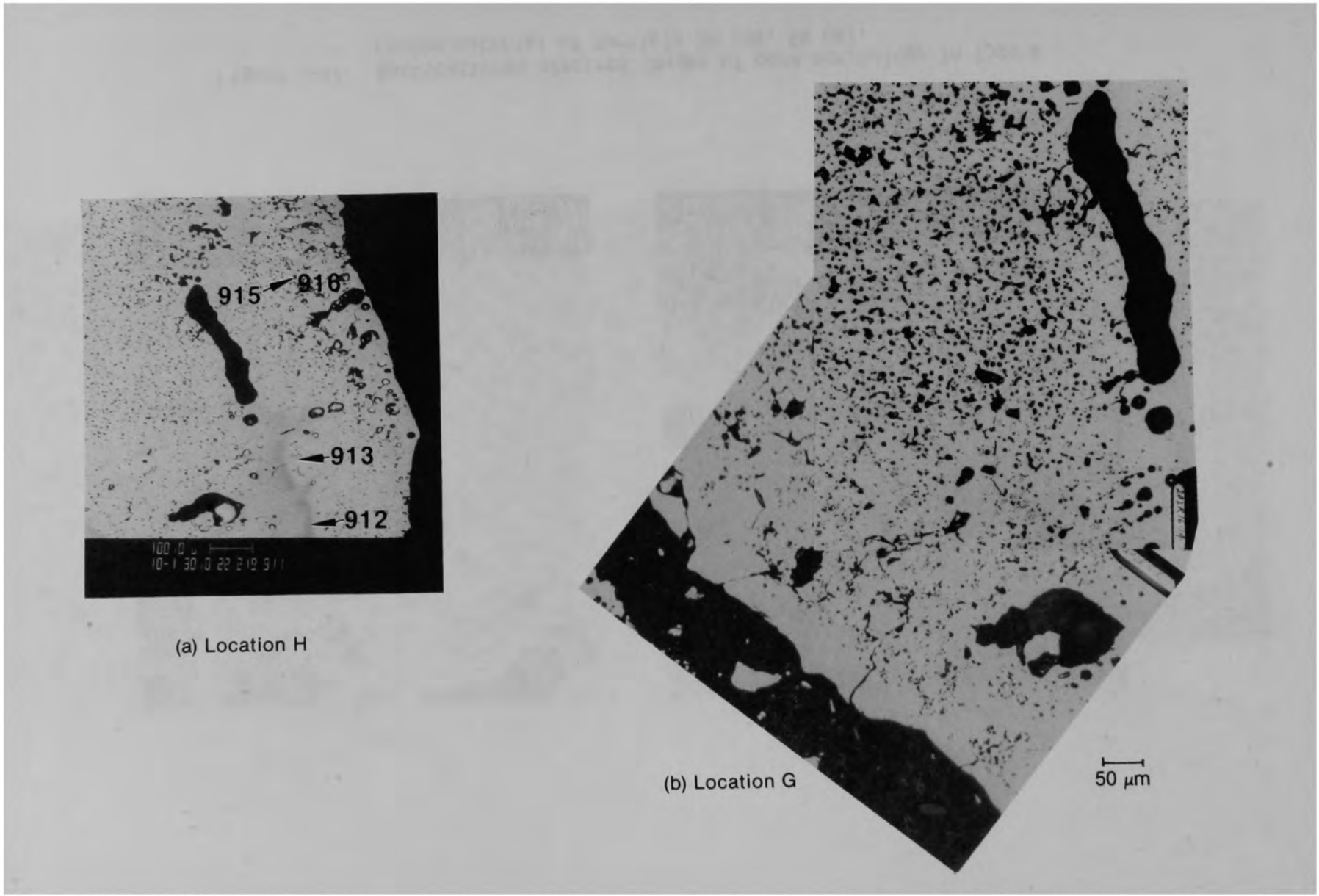

Figure C-48. Material in Type 2 region of Particle 3M (H8, 56 cm).

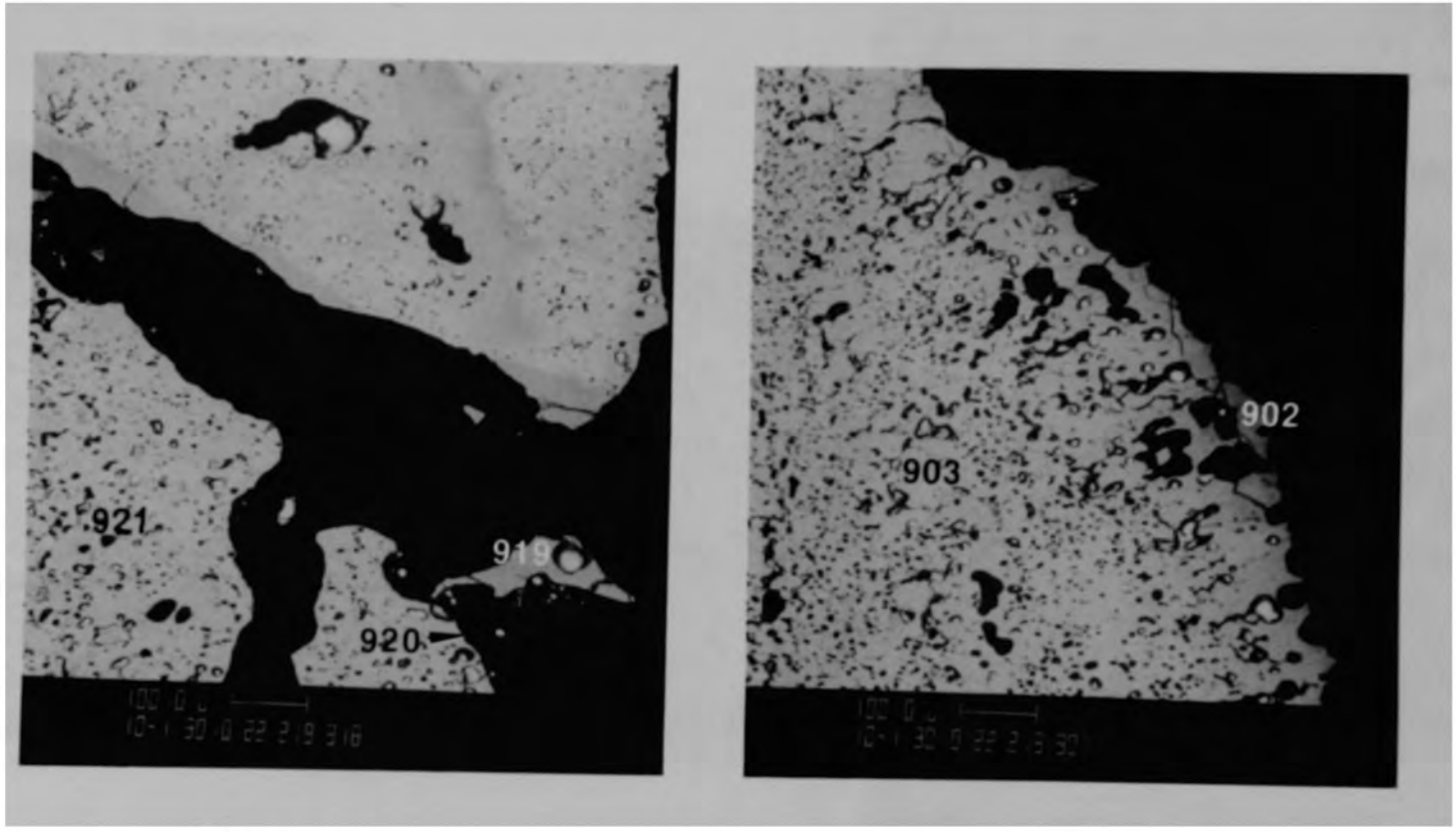

(a) Location J

(b) Location I

Figure C-49. Backscattered electron images of material in Type 2 region of Particle 3M (H8, 56 cm).

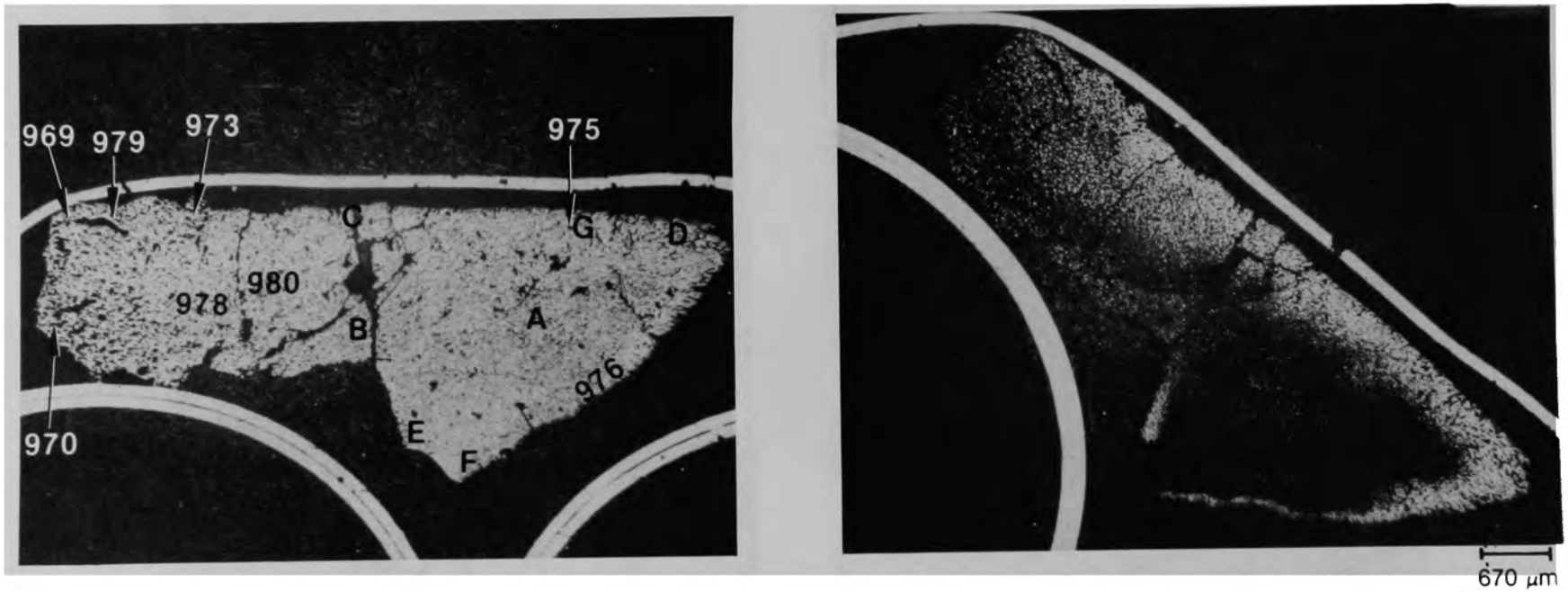

(a) Unetched

(b) Fuel etch

Figure C-50. Photomacrographs of Particle 4A (E9, surface).

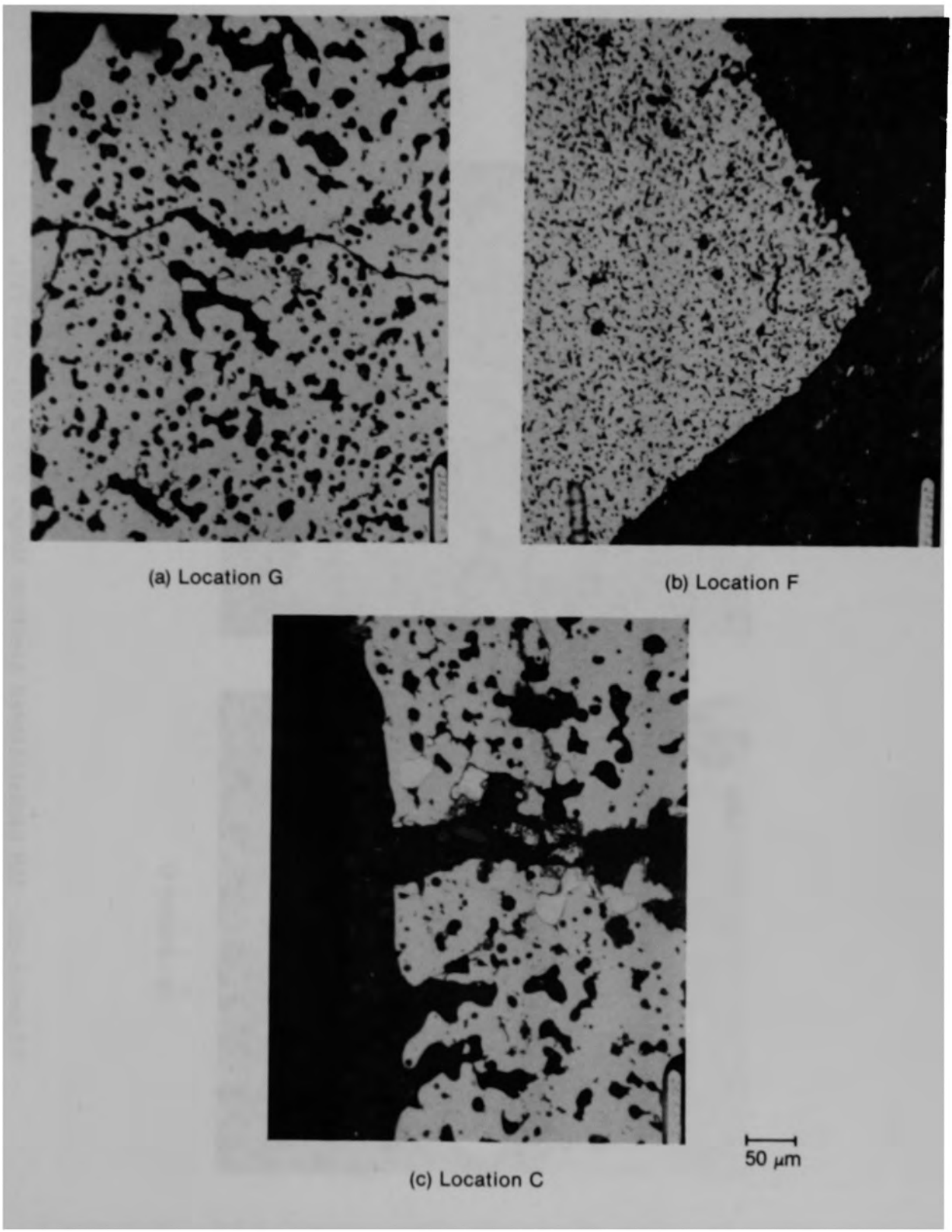

Figure C-51. Photomicrographs of Particle 4A (E9, surface).

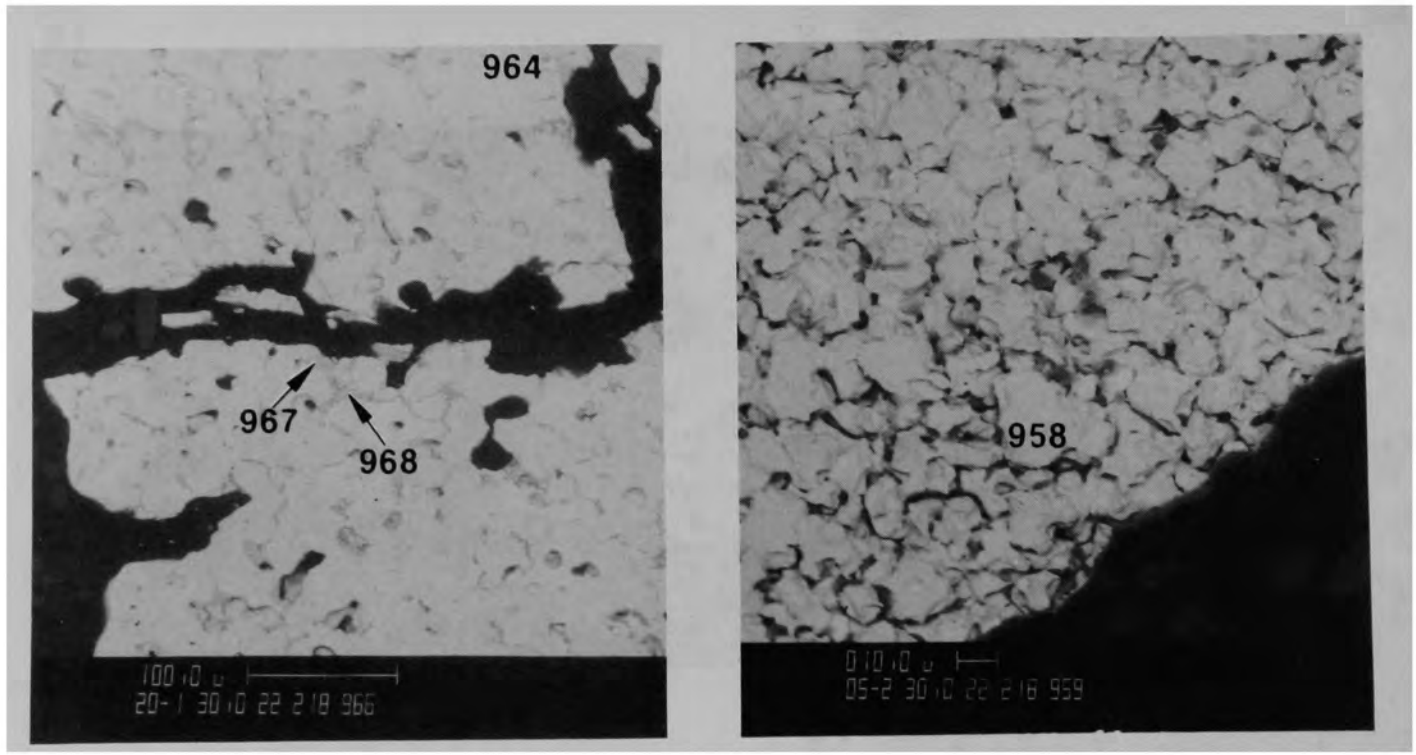

(a) Location C

(b) Location F

Figure C-52. SEM backscattered electron images of Particle 4A (E9, surface).

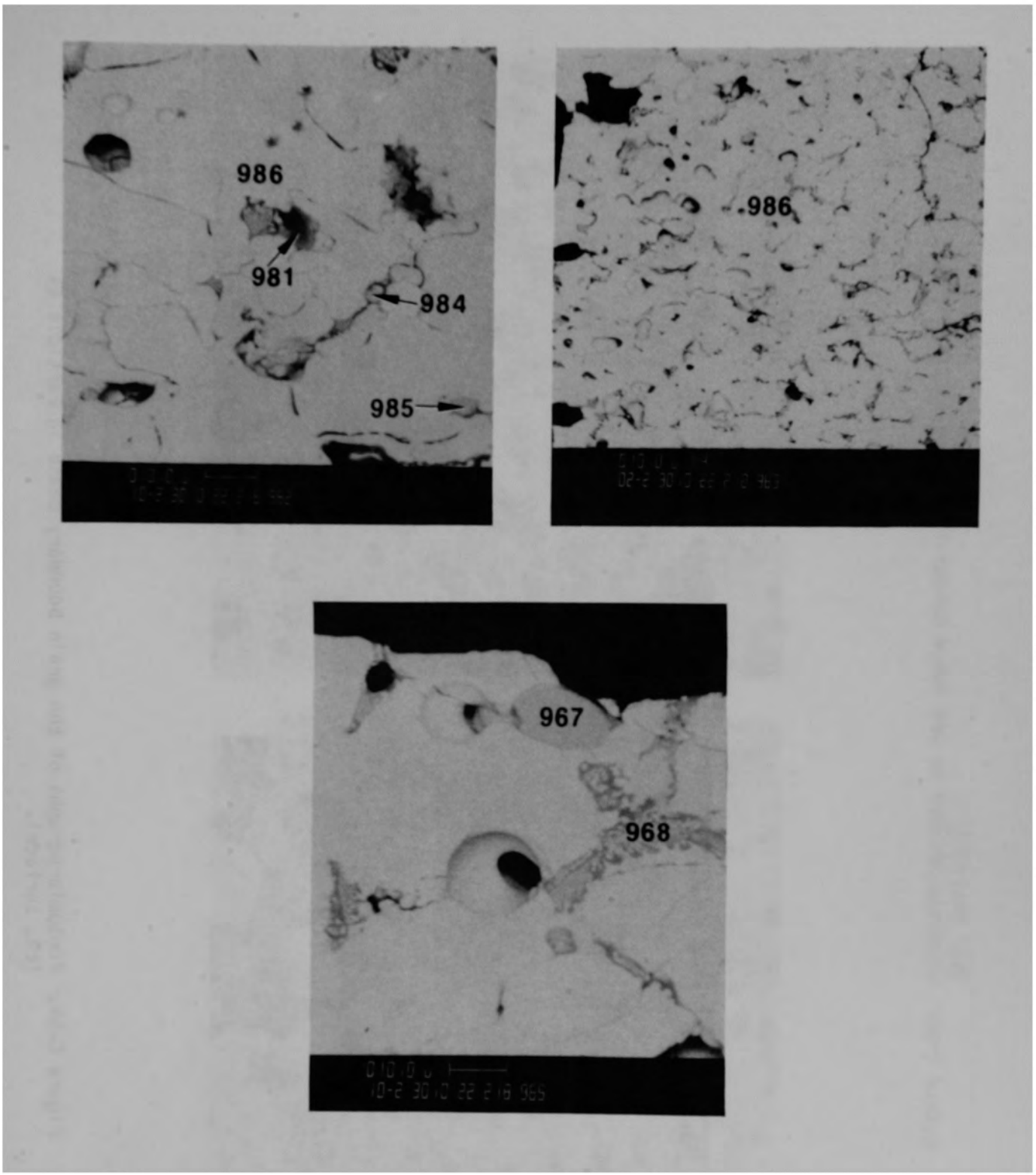

Figure C-53. SEM backscattered electron images showing the grain boundary phase in Particle 4A (E9, surface).

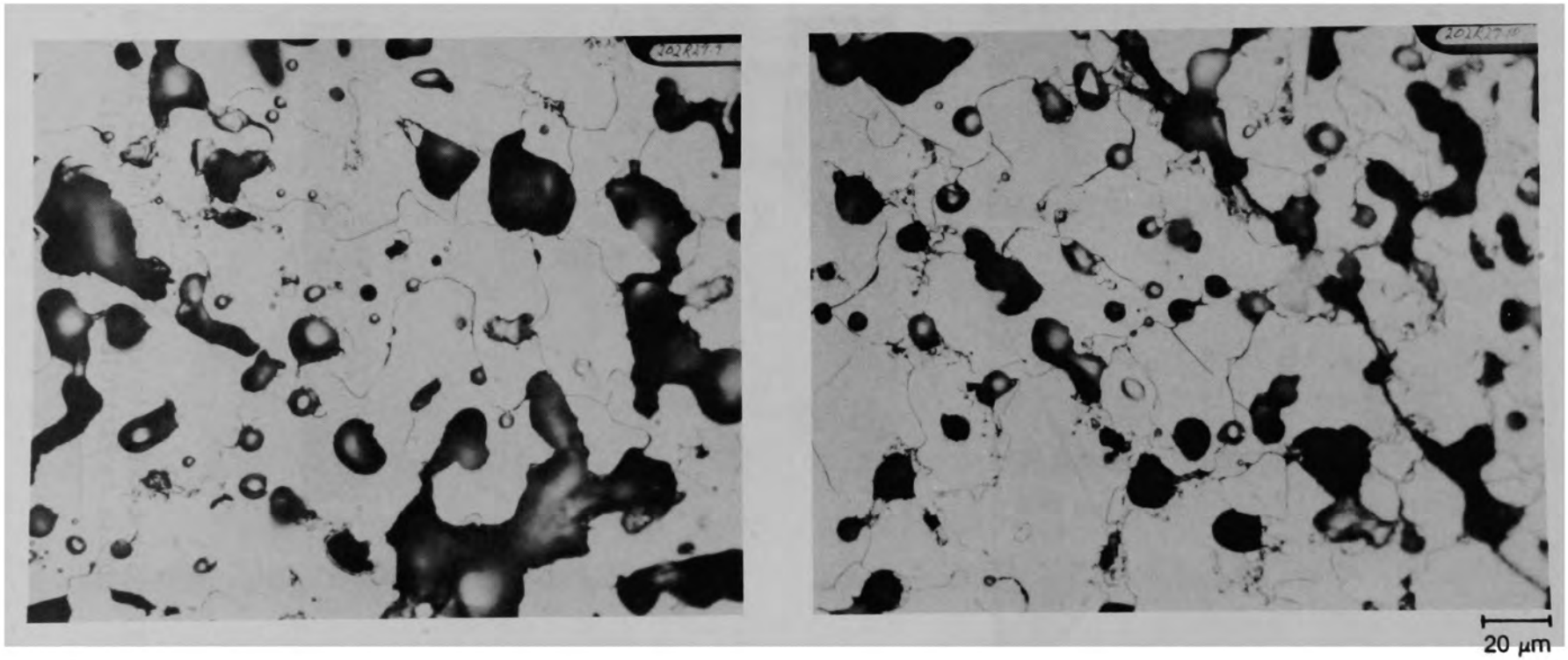

Figure C-54. Photomicrographs of the grain boundary phase in Particle 4A (E9, surface).

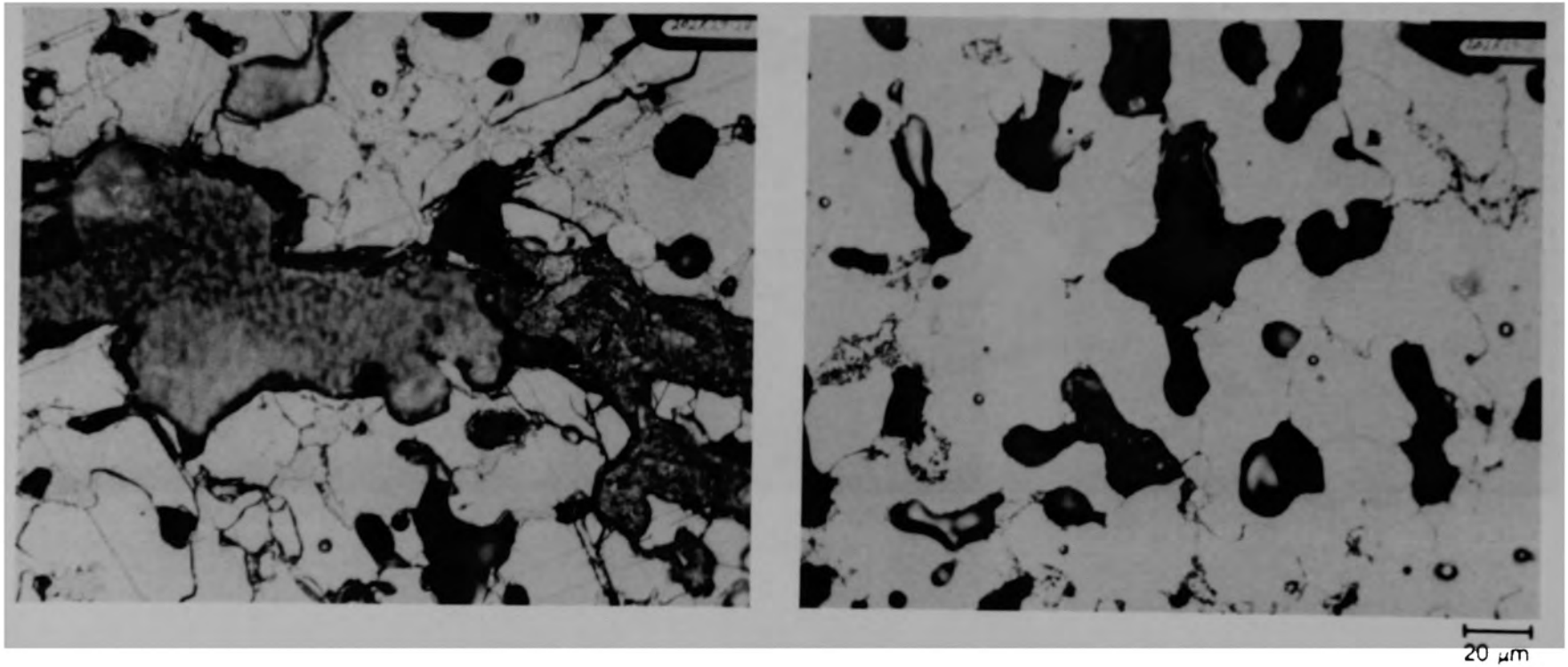

Figure C-55. Photomicrographs of the grain boundary phase in Particle 4A (E9, surface).

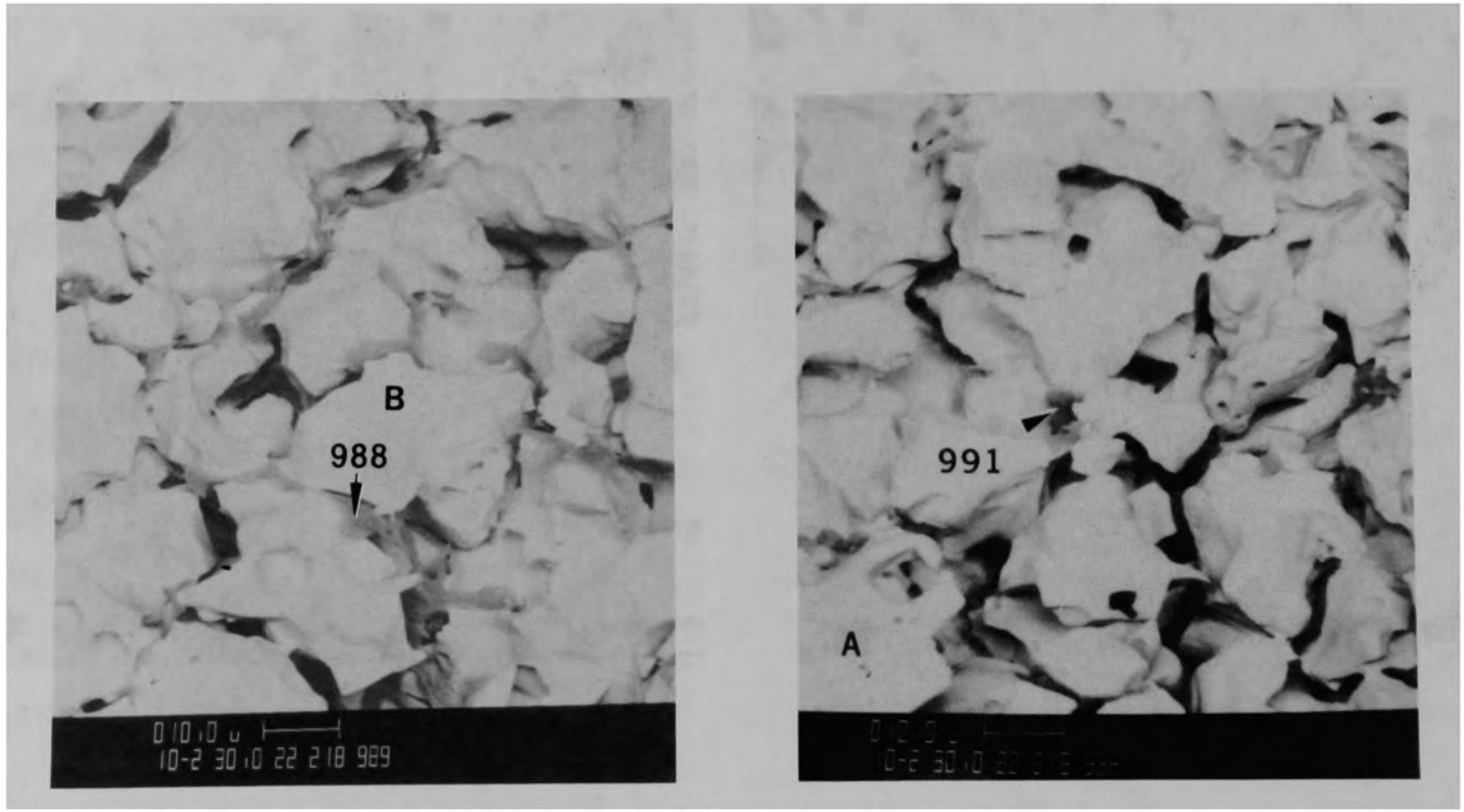

Figure C-56. SEM backscattered electron images showing Al-Cr-Fe-Ni grain boundary phase of Particle 4A (E9, surface).

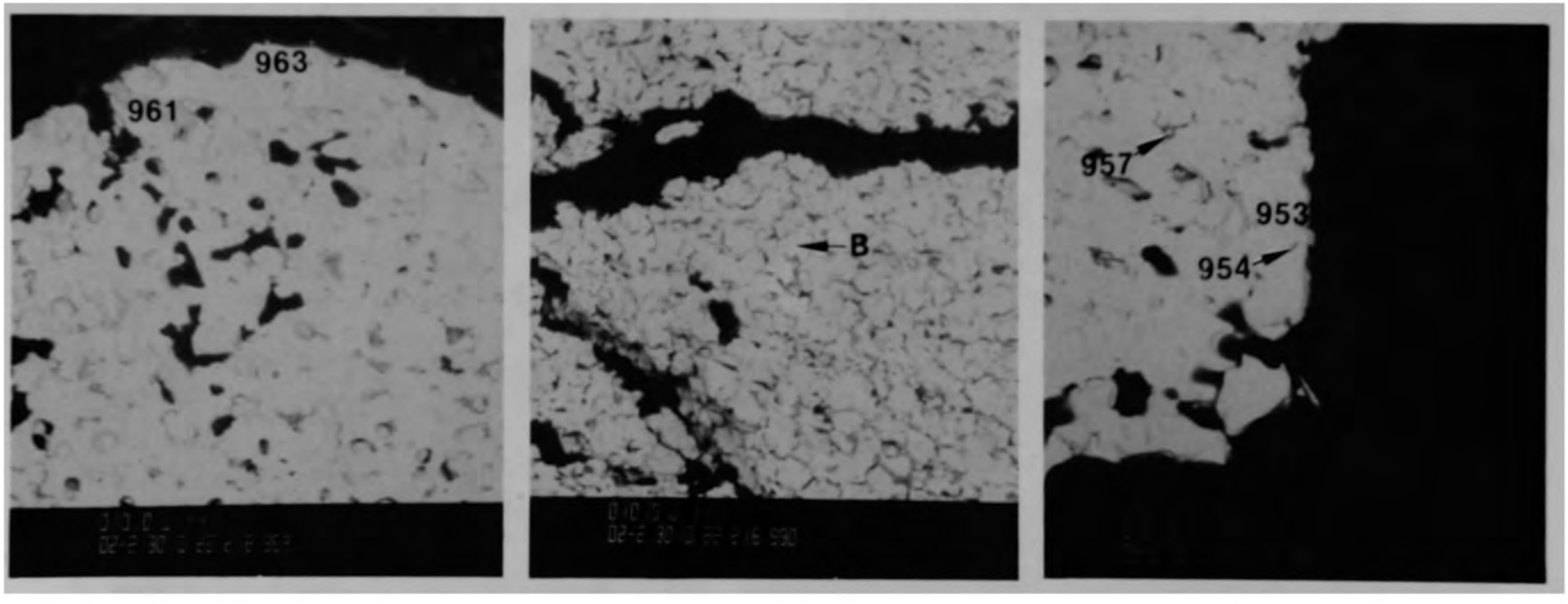

(a) Location D

(b) Location B

(c) Location E

Figure C-57. SEM backscattered electron images of representative material structures for Particle 4A (E9, surface).

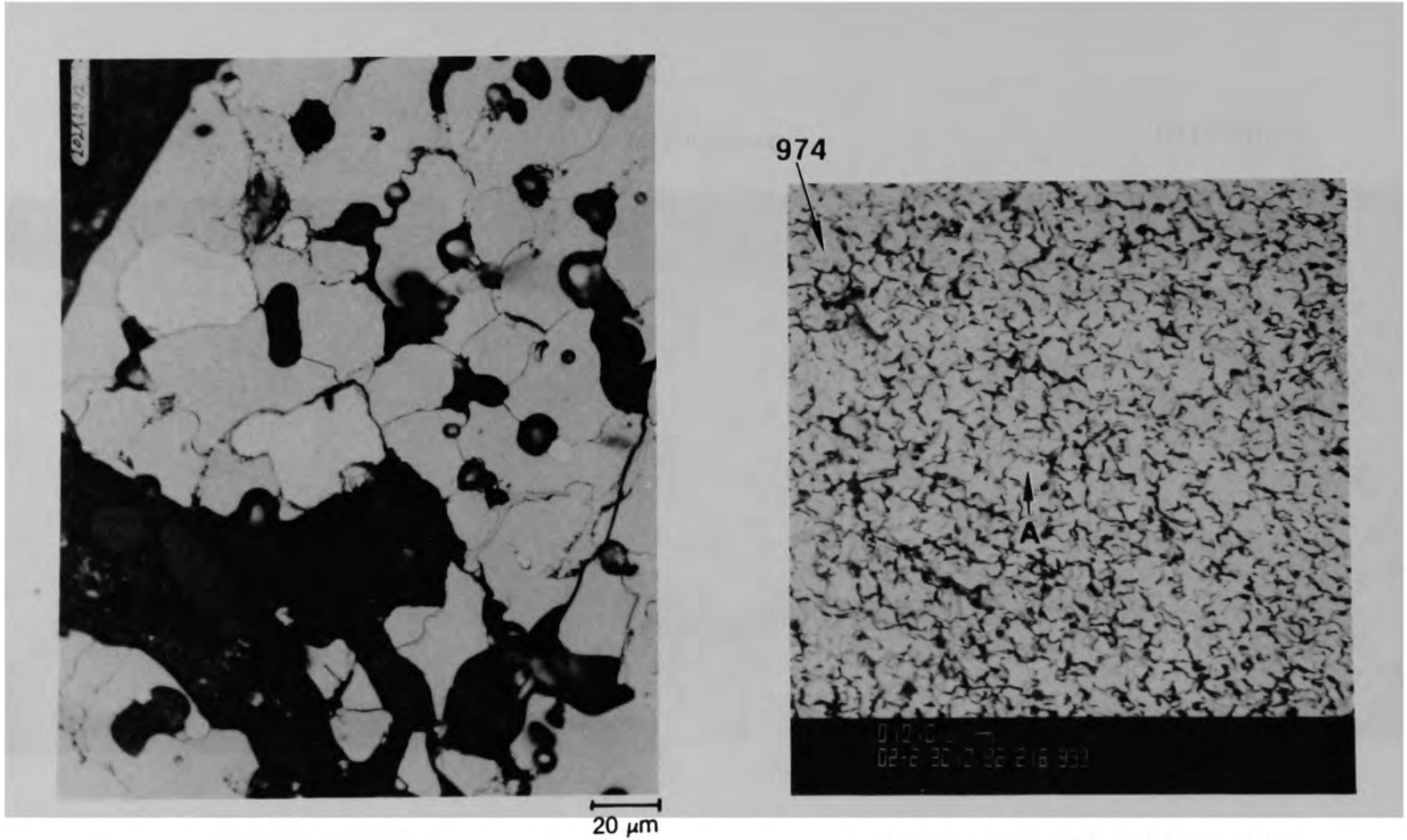

(a) Photomicrograph

(b) SEM backscattered electron image

Figure C-58. Representative material from Particle 4A (E9, surface).

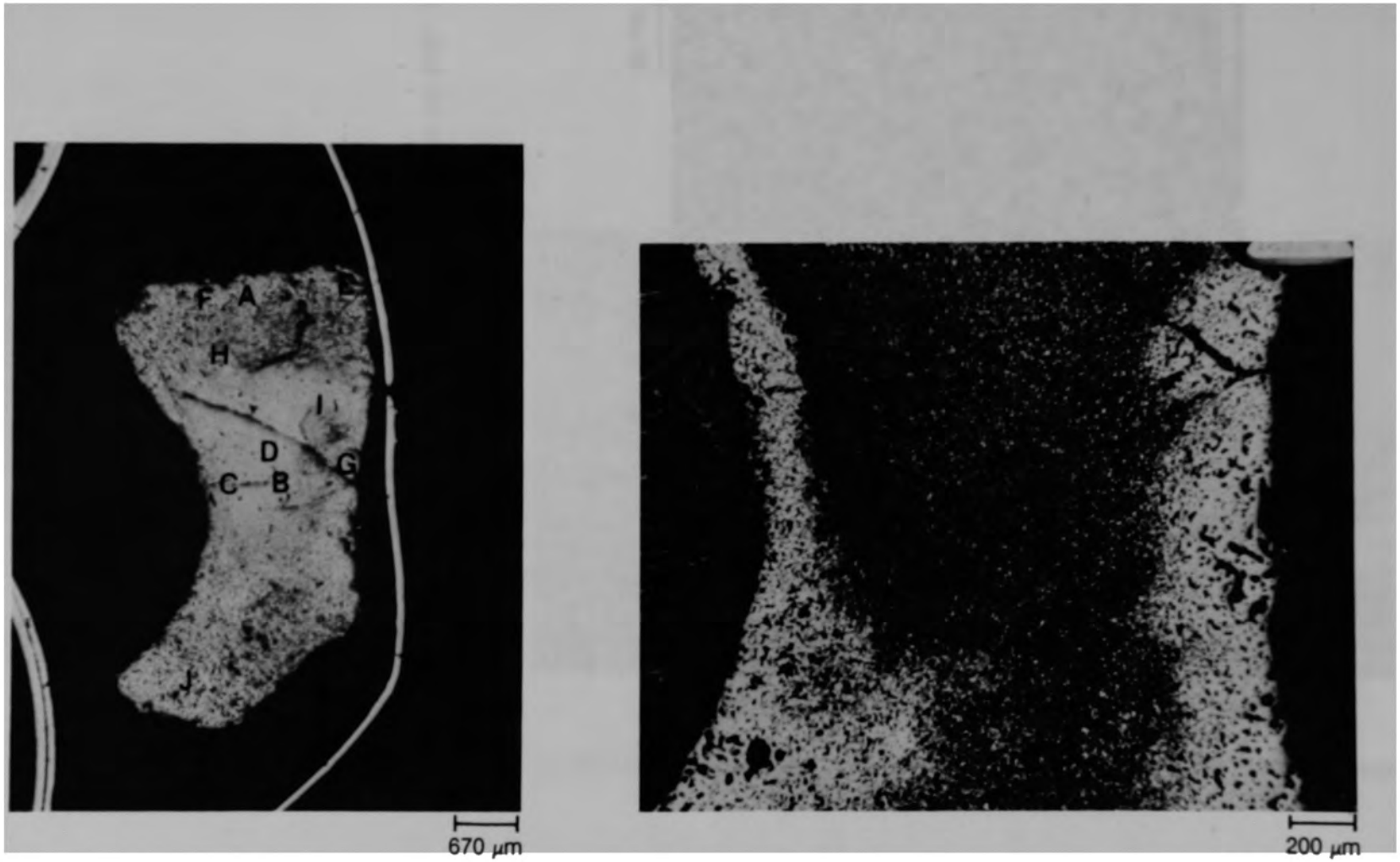

(a) Unetched

(b) Fuel etch

Figure C-59. Photomacrograph of Particle 48 (E9, surface).

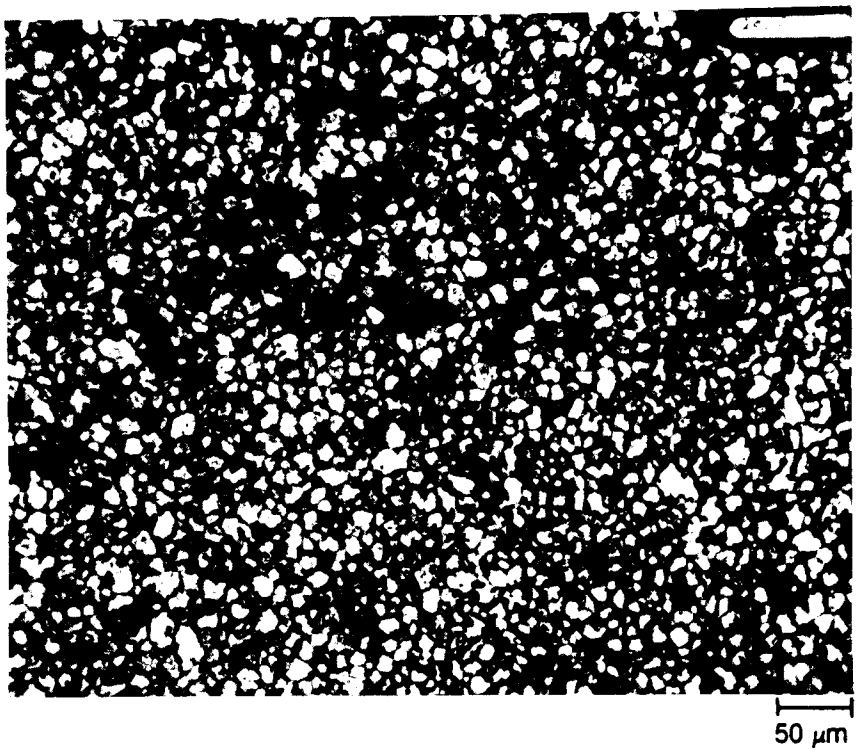

Figure C-60. Photomicrograph of center of Particle 4B (E9, surface) showing fuel pullout.

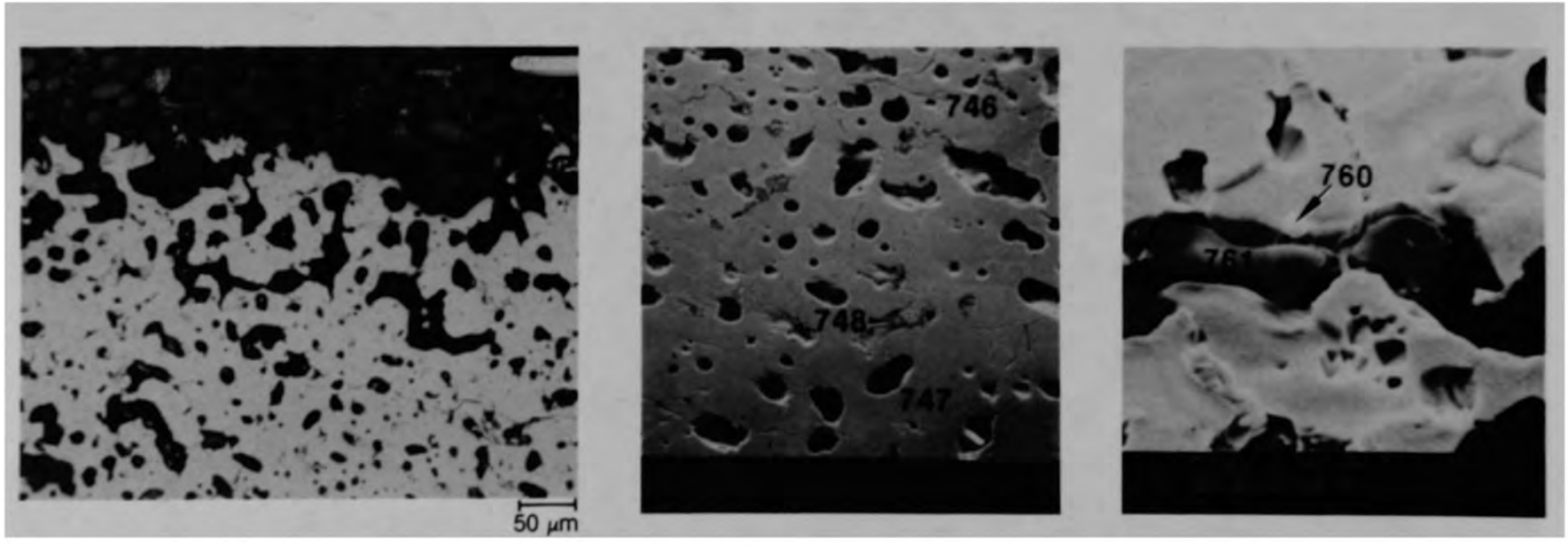

(a) Photomicrograph (b) SEM backscattered electron image (c) SEM backscattered electron image

Figure C-61. Photographs of material from location A (U, low Zr) of Particle 4B (E9, surface).

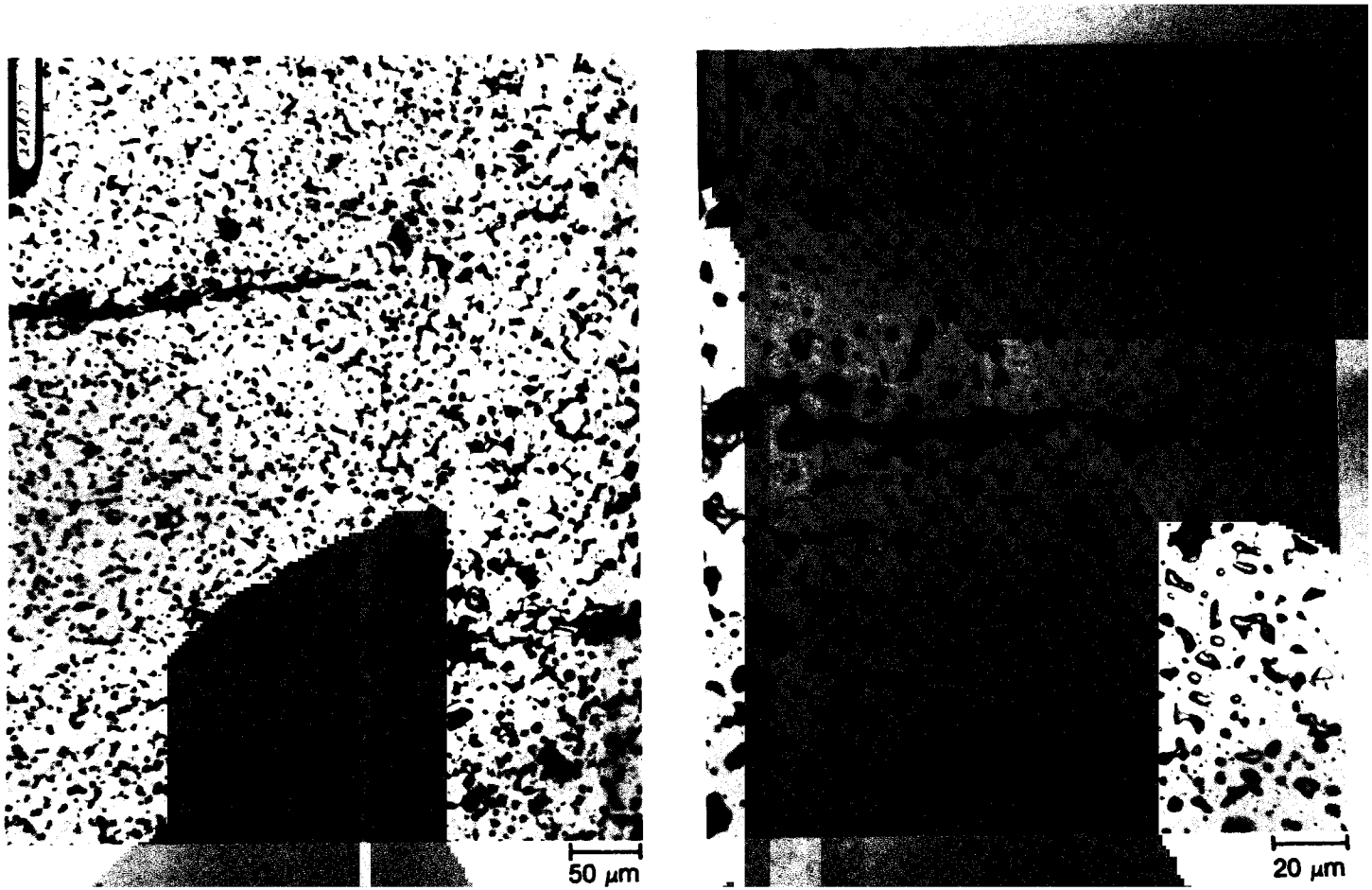

(a) Location B

(b) Location C

Figure C-62. Photomicrographs of material near center of Particle 4B (E9, surface).

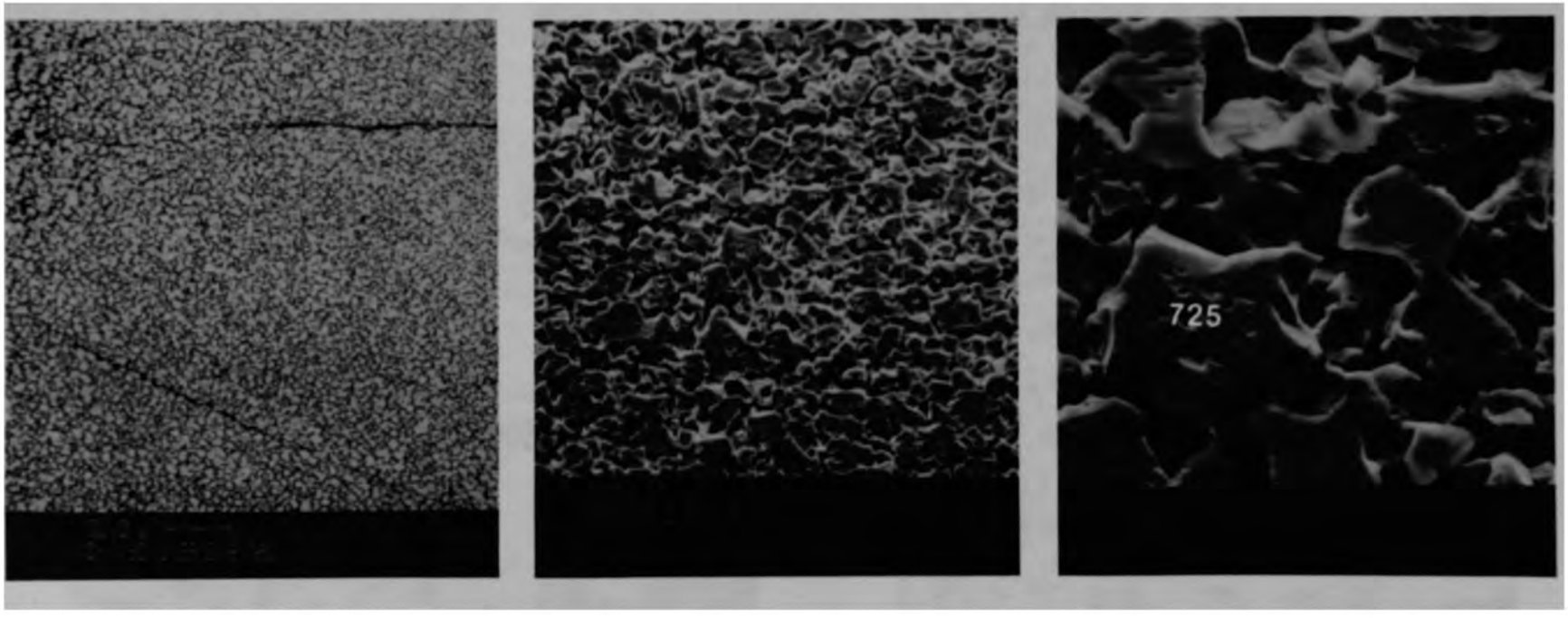

Figure C-63. SEM backscattered electron images from location D of fuel at center of Particle 4B (E9, surface).

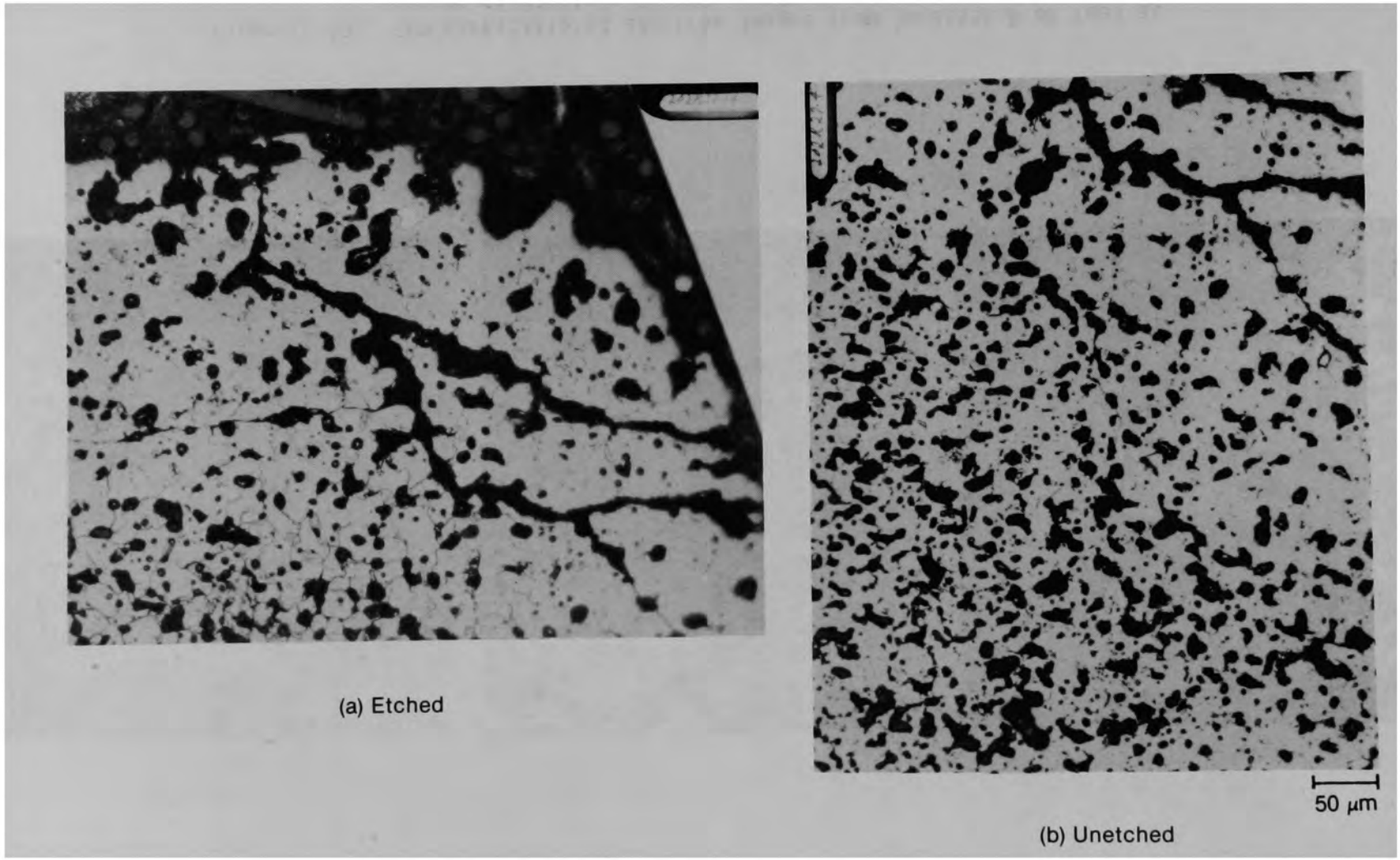

Figure C-64. Photomicrographs of U, low Zr material at location E of Particle 4B (E9, surface).

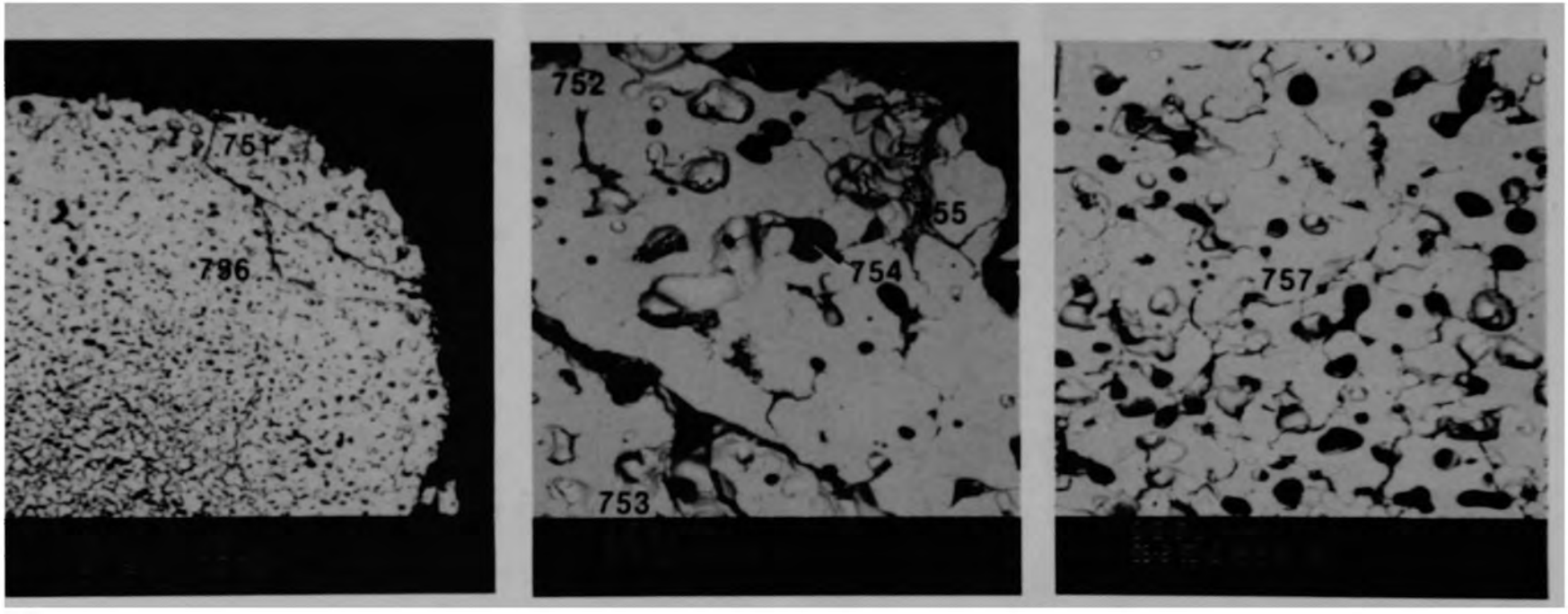

Figure C-65. SEM backscattered electron images of material at location E of Particle 4B (E9, surface).

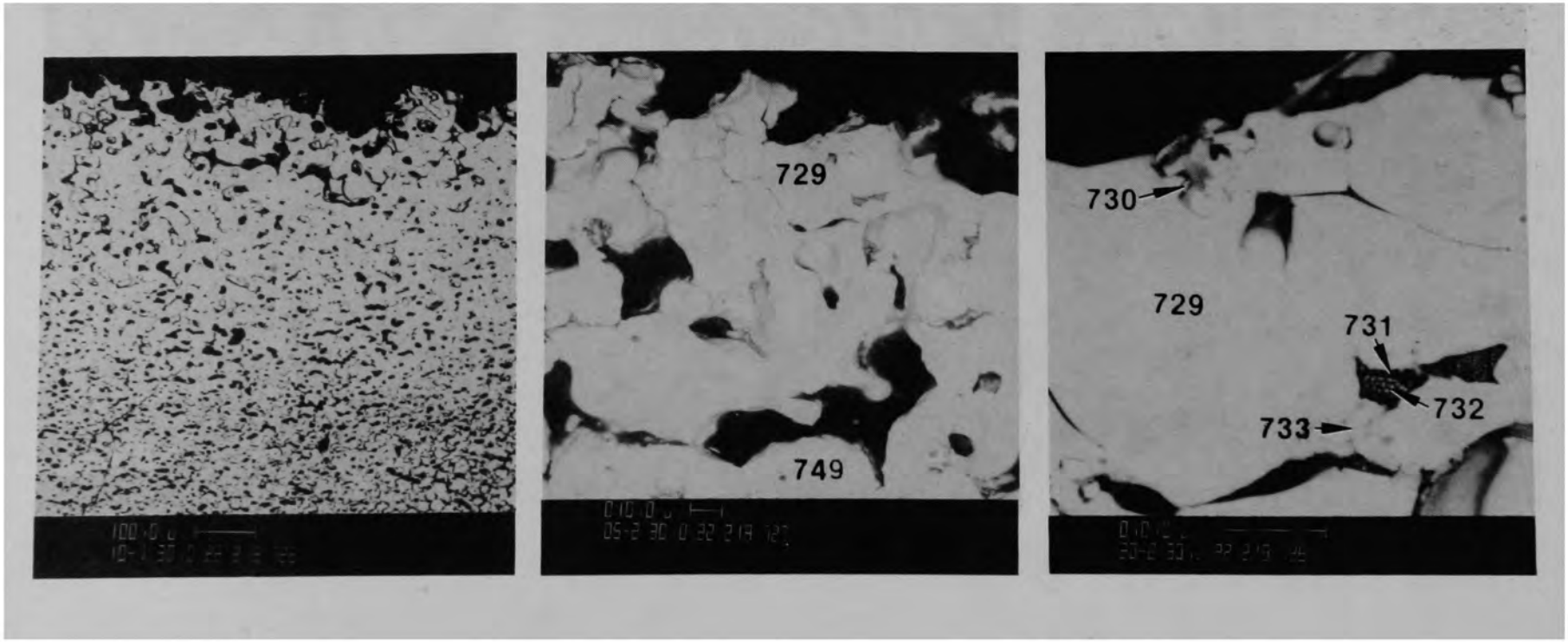

Figure C-66. SEM backscattered electron images from location F of Particle 4B (E9, surface).

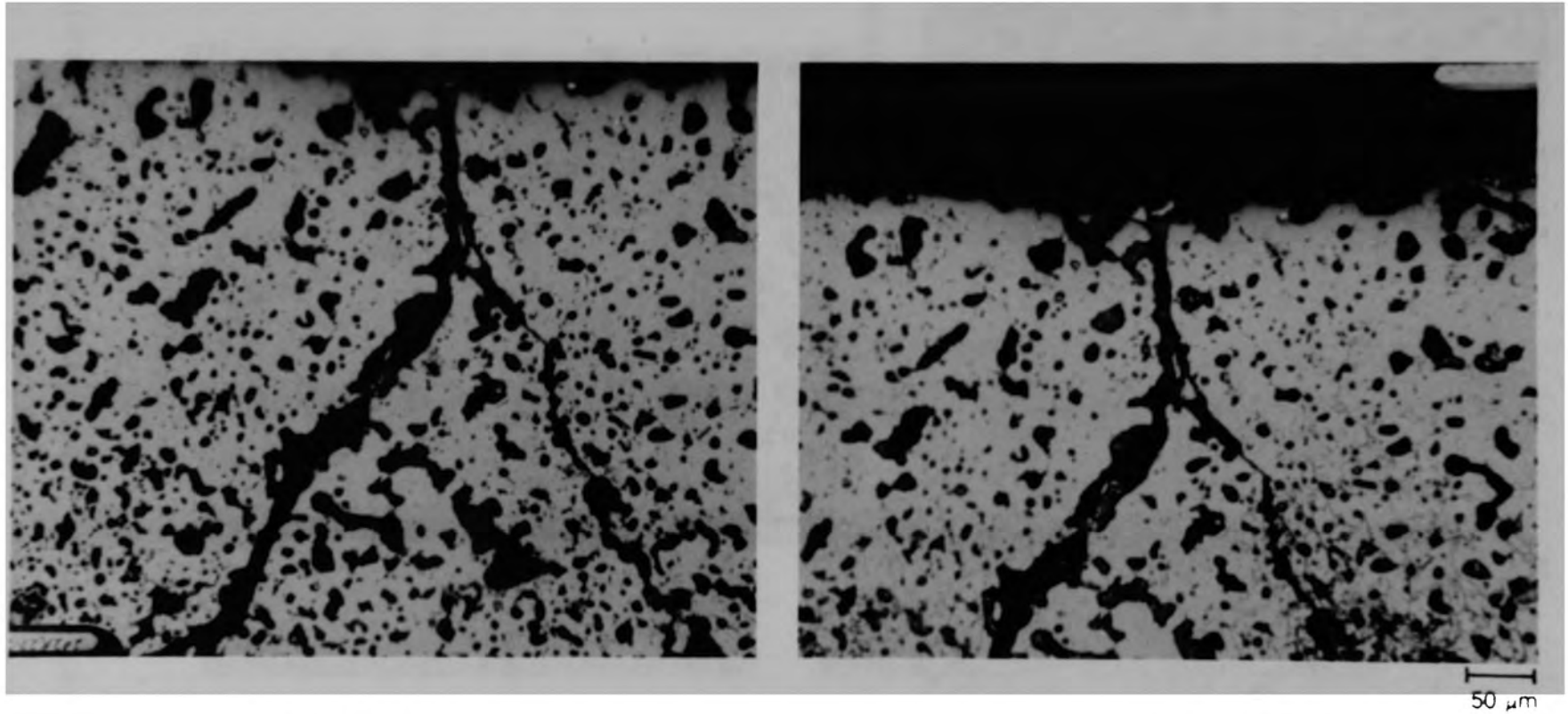

(a) Unetched

(b) Etched

Figure C-67. Photomicrographs from location G of Particle 48 (E9, surface).

(a) Location H

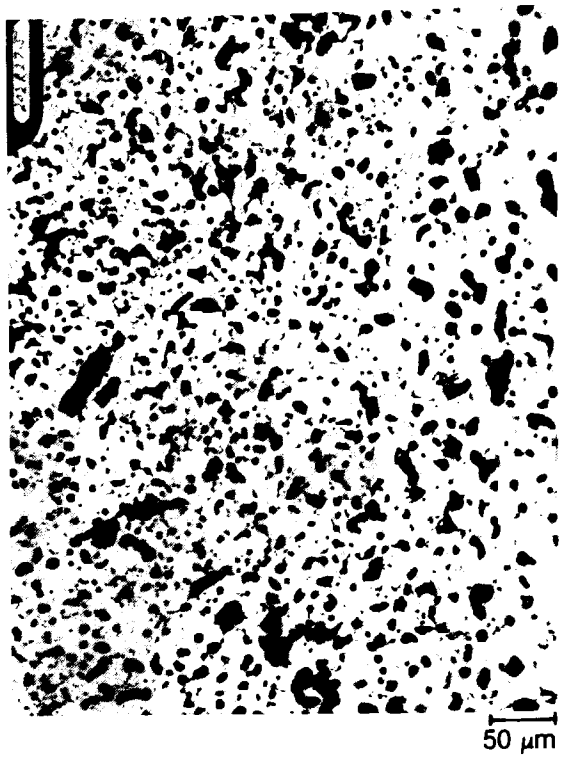

(b) Location I

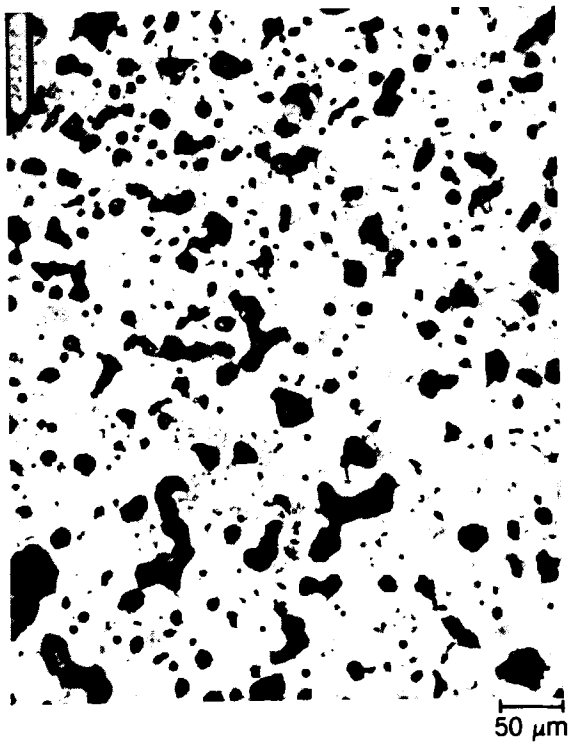

(c) Location J

Figure C-68. Typical structures of material from Particle 4B (E9, surface).

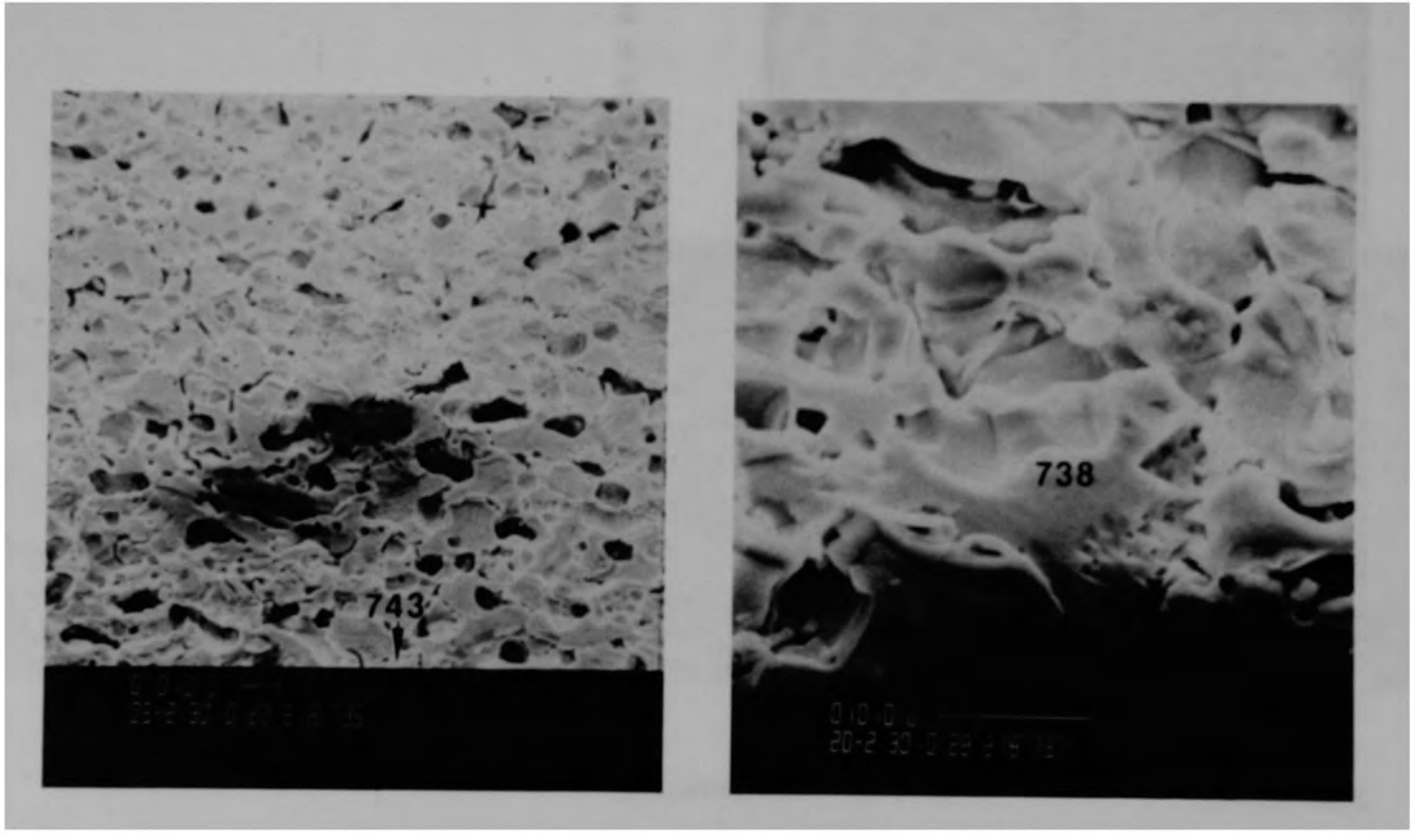

Figure C-69. SEM backscattered electron images of material in outer rim of Particle 4B (E9, surface).

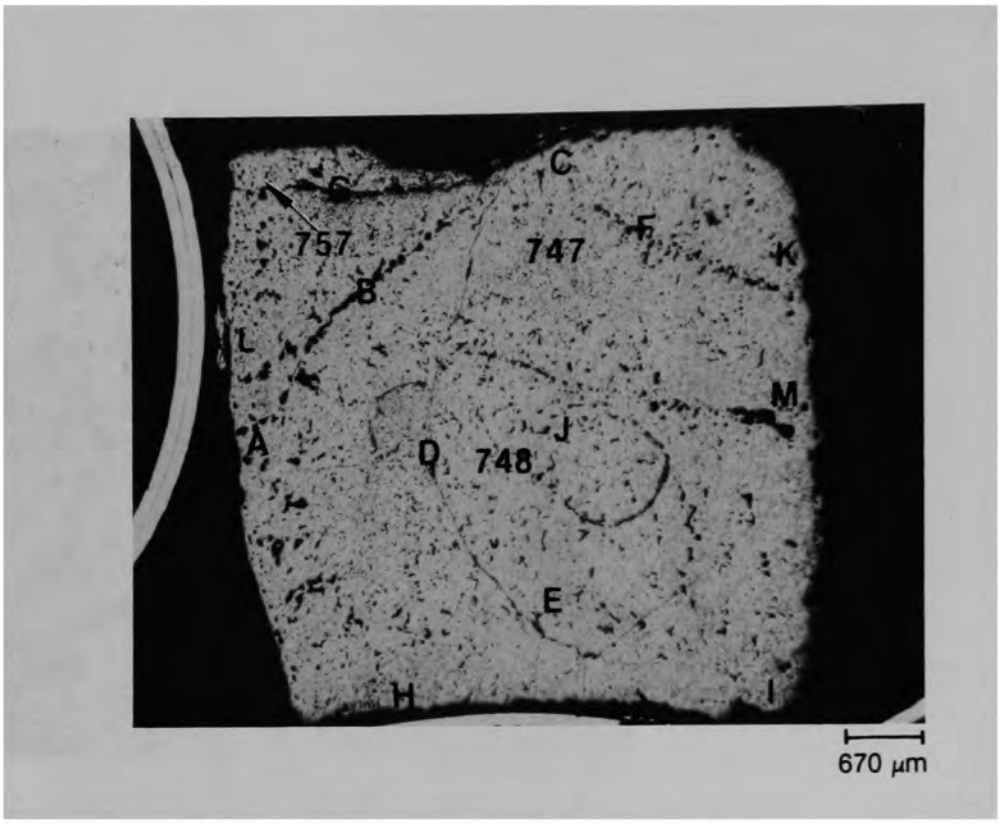

Figure C-70. Photomacrograph of Particle 4D (E9, surface).

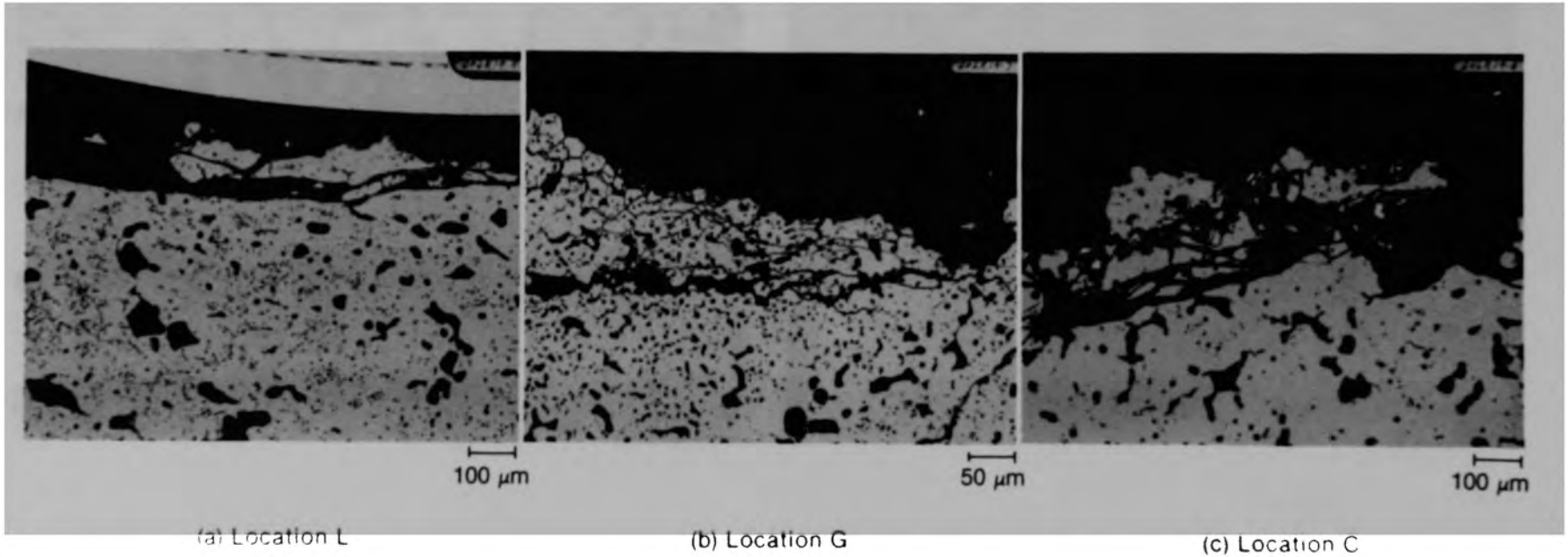

Figure C-71. Photomicrographs of unetched material near the edge of Particle 4D (E9, surface).

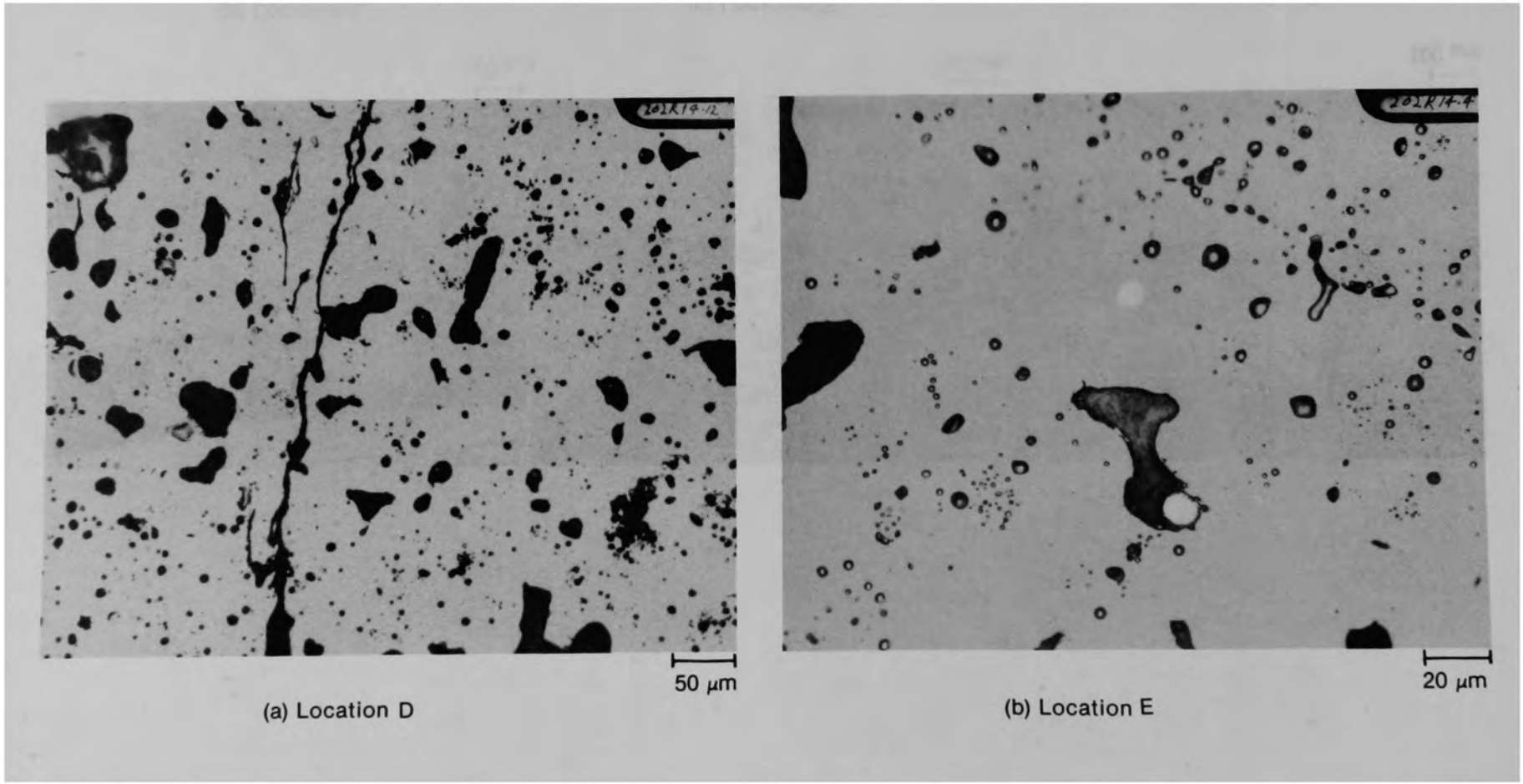

Figure C-72. Photomicrographs of unetched material near the center of Particle 4D (E9, surface).

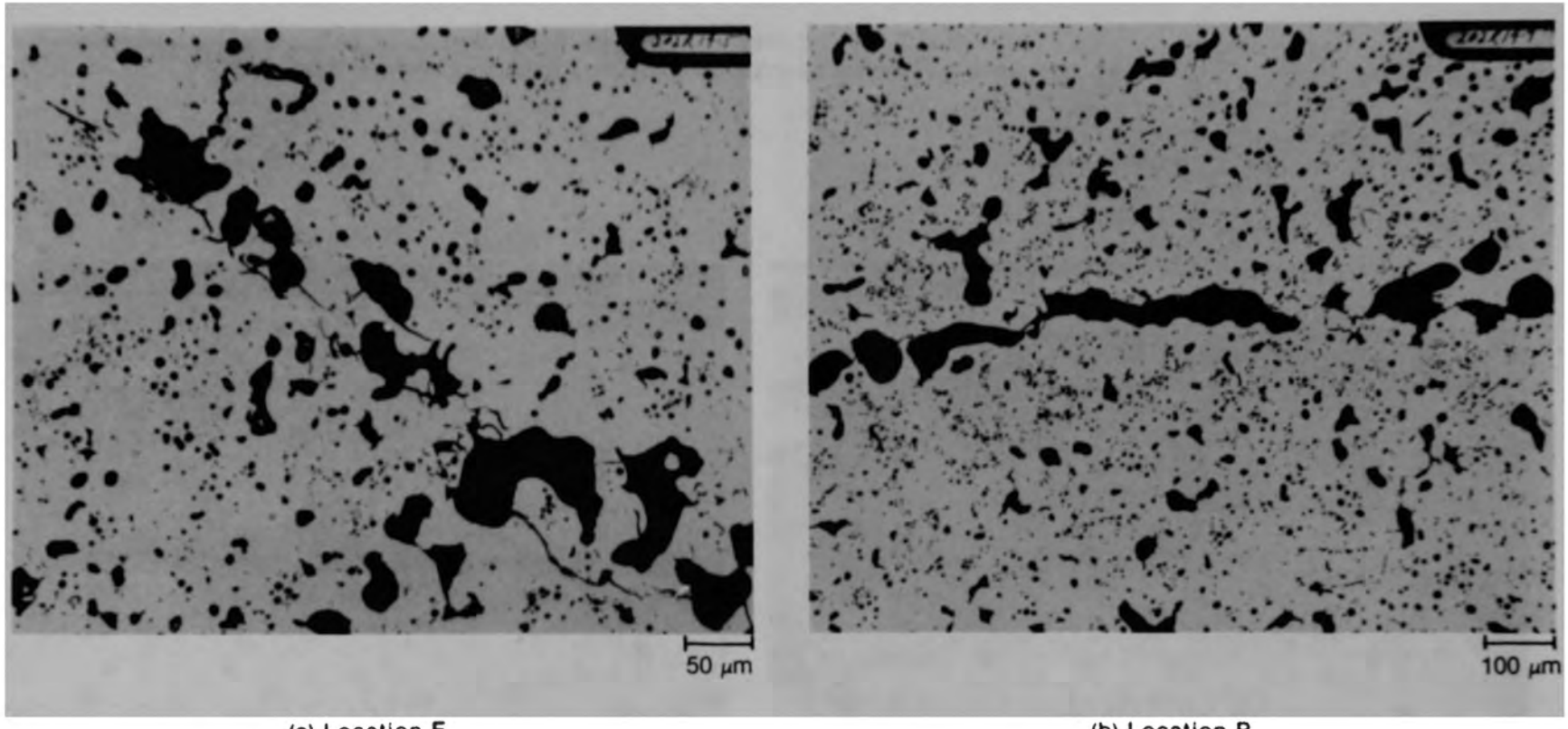

(a) Location F

(b) Location B

Figure C-73. Photomicrographs of unetched material near the mid-radius of Particle 4D (E9, surface).

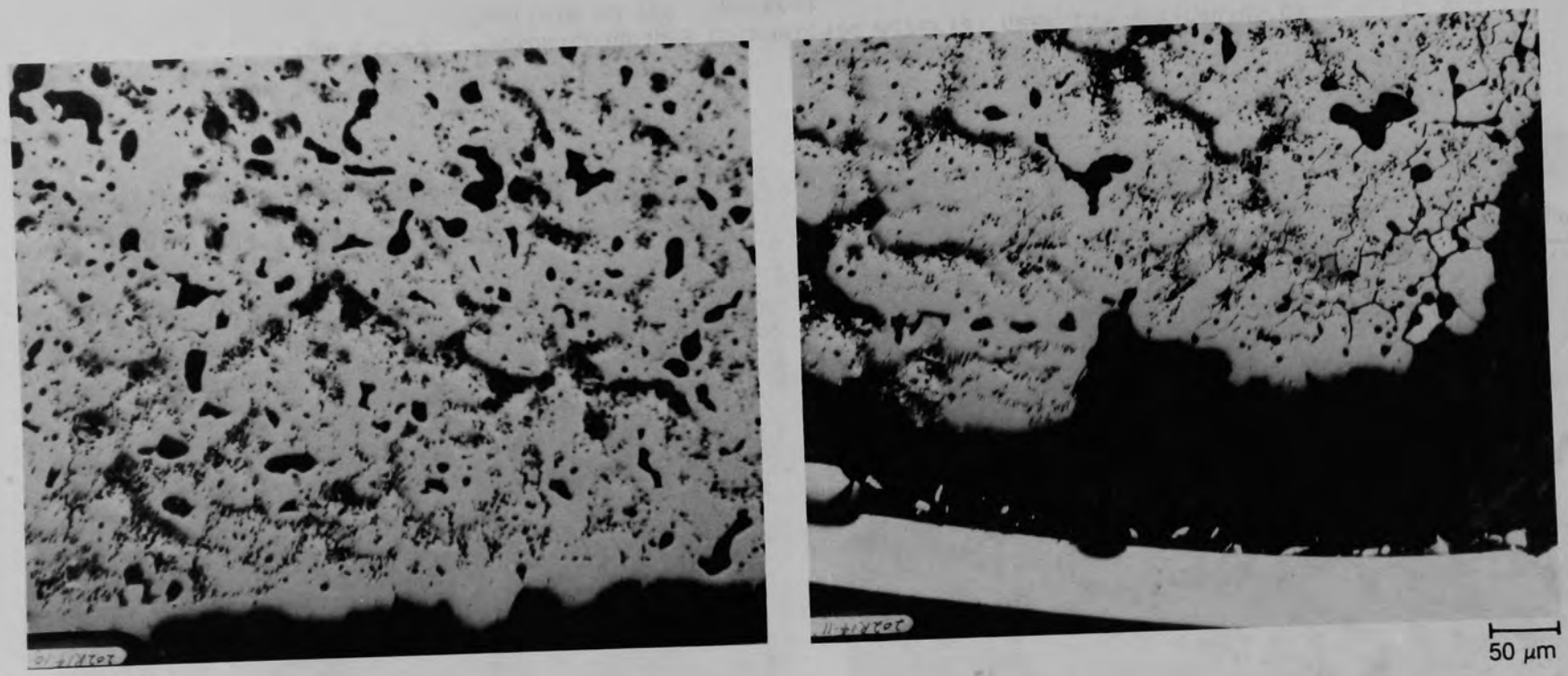

(a) Location H

(b) Location I

Figure C-74. Photomicrographs of etched material near the edge of Particle 4D (E9, surface).

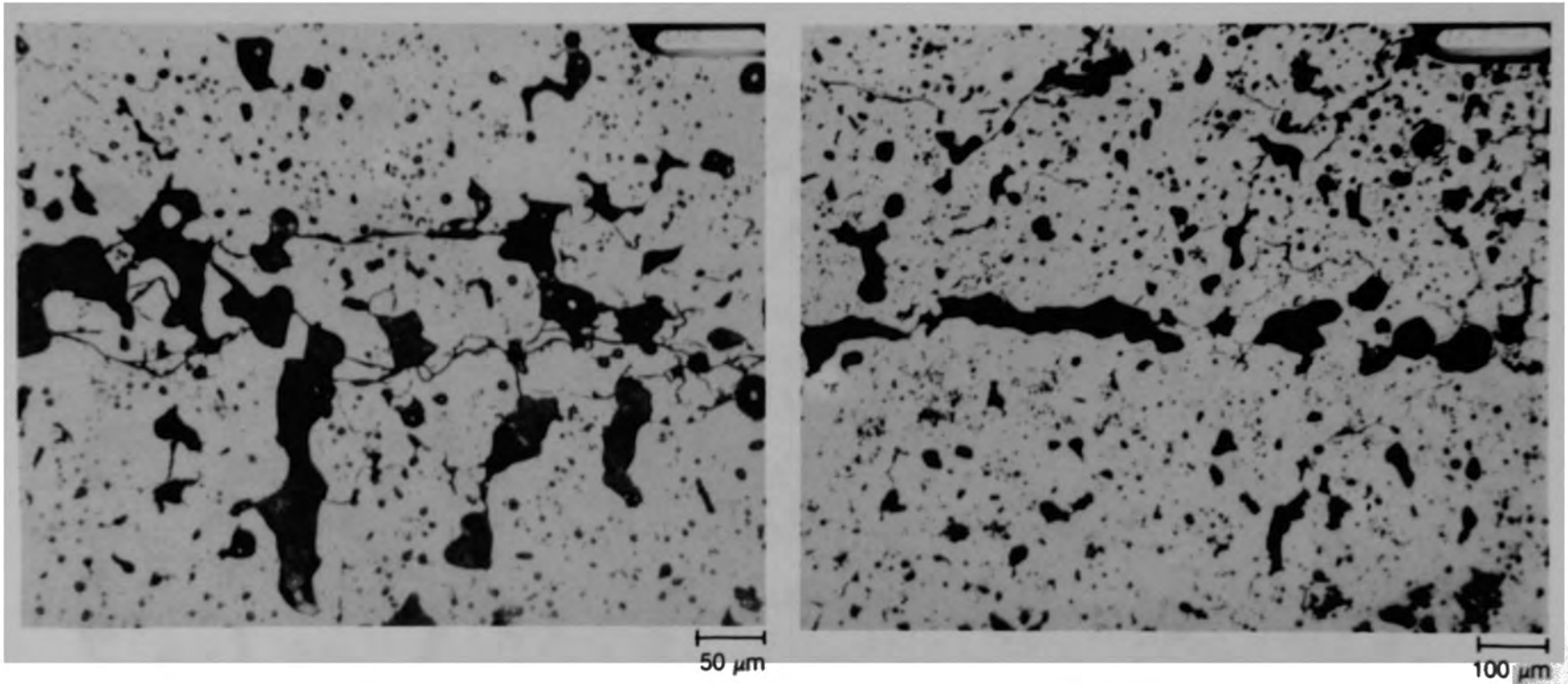

(a) Location F

(b) Location B

Figure C-75. Photomicrographs of etched material near the mid-radius of Particle 4D (E9, surface).

(a) Location E

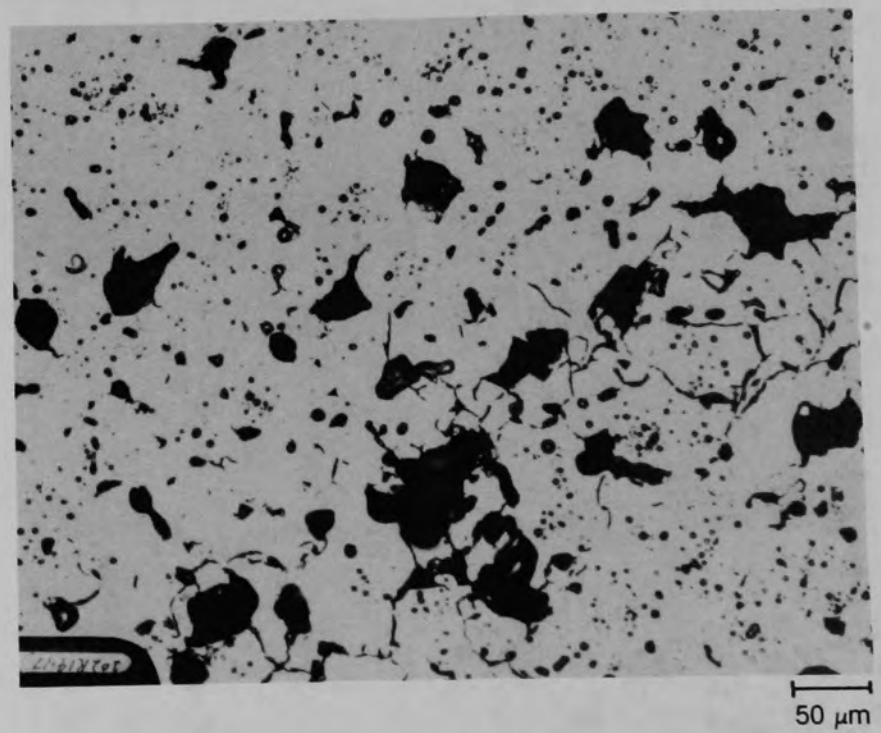

(b) Location J

Figure C-76. Photomicrographs of etched material near the center of Particle 4D (E9, surface).

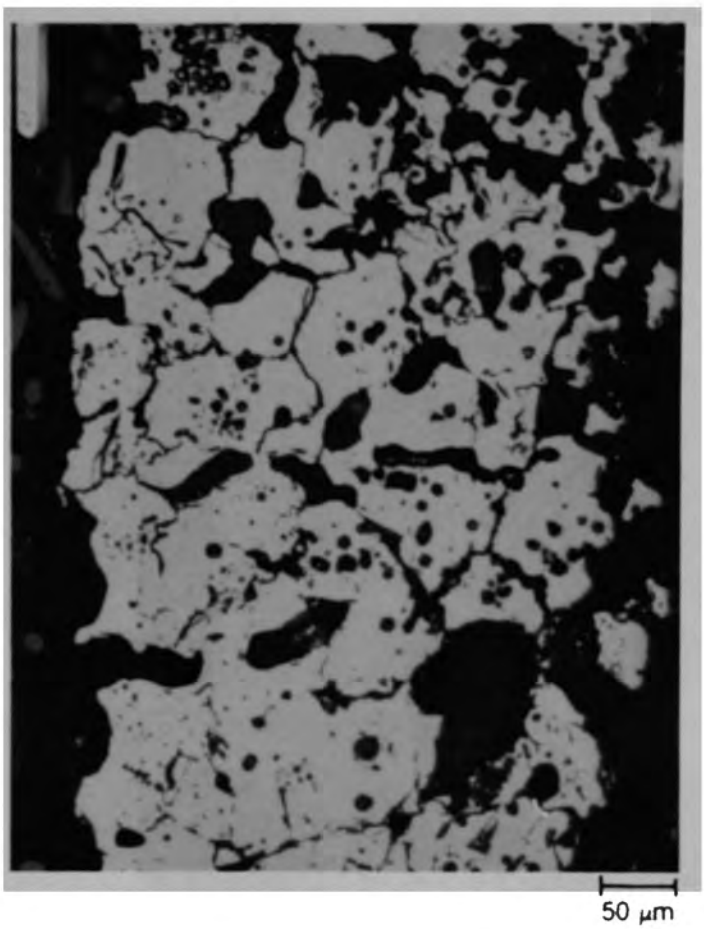

Figure C-77. Photomicrographs of etched material at location G of Particle 4D (E9, surface).

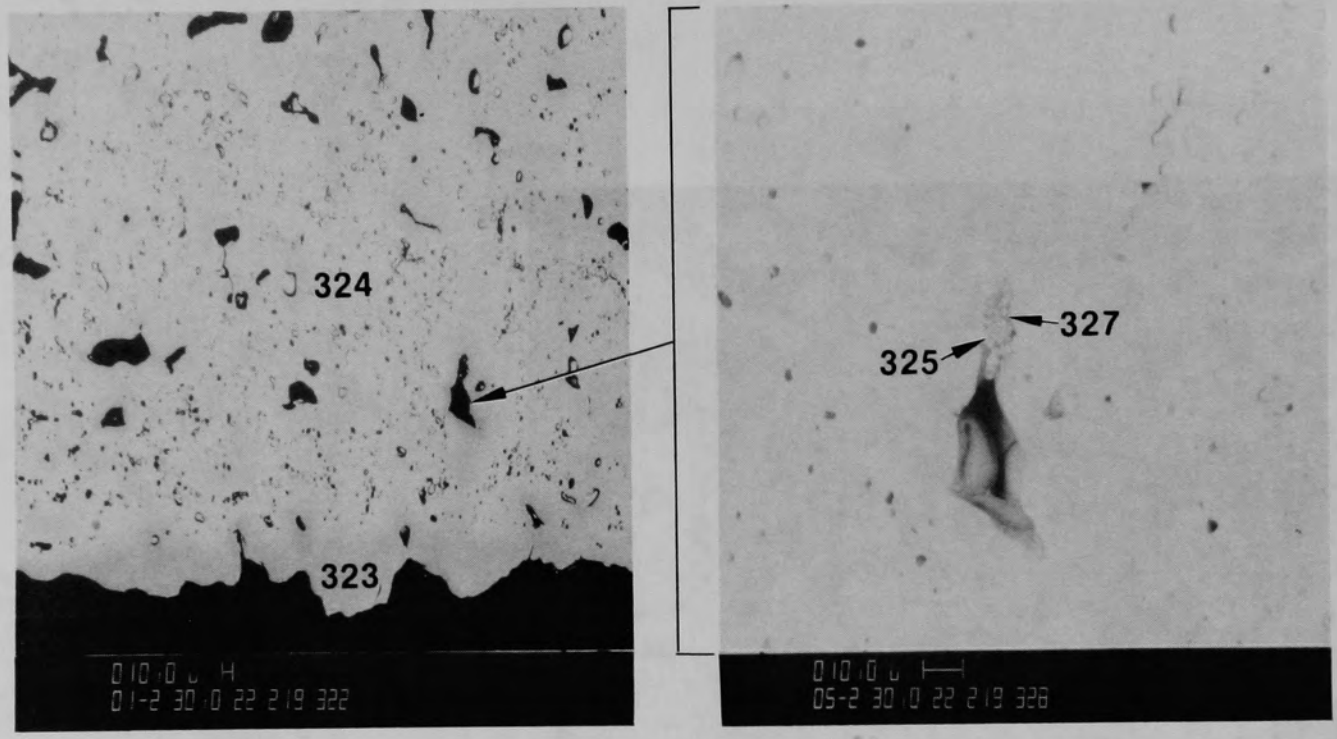

Figure C-78. SEM backscattered electron images of material at edge, location H, of Particle 4D (E9, surface).

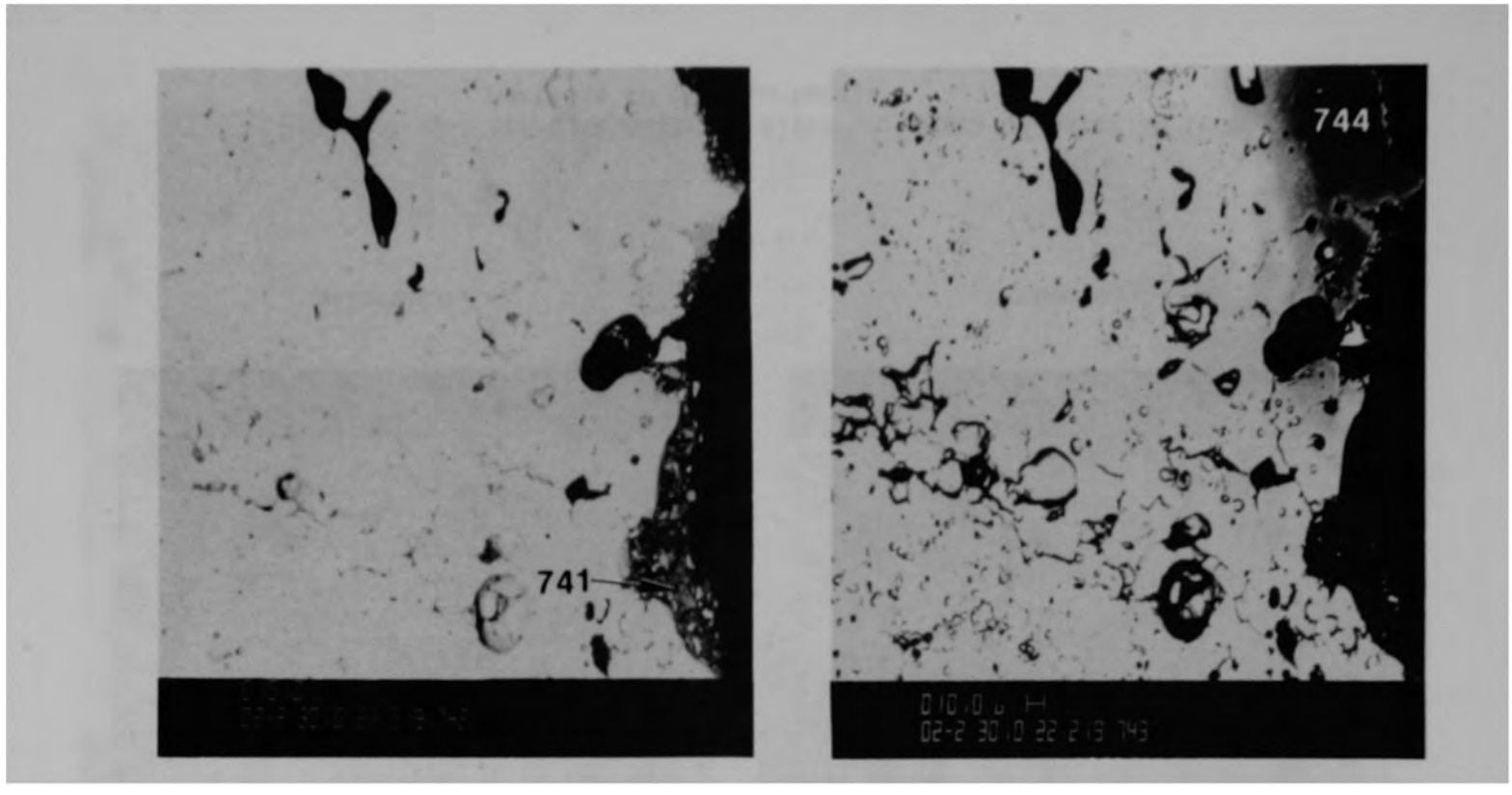

(a) Low contrast

(b) High contrast

Figure C-79. SEM backscattered electron images of location K of Particle 40 (E9, surface).

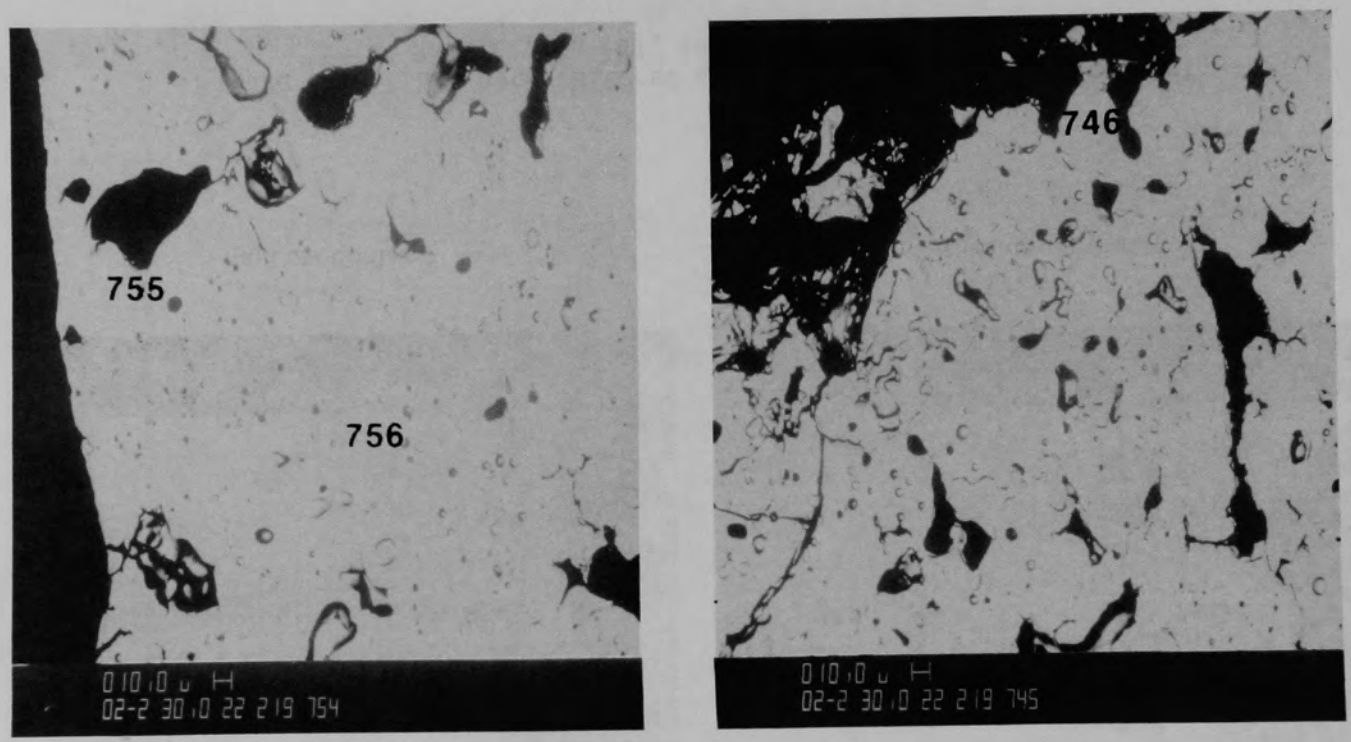

(a) Location A

(b) Location C

Figure C-80. SEM backscattered electron images of material from Particle 4D (E9, surface).

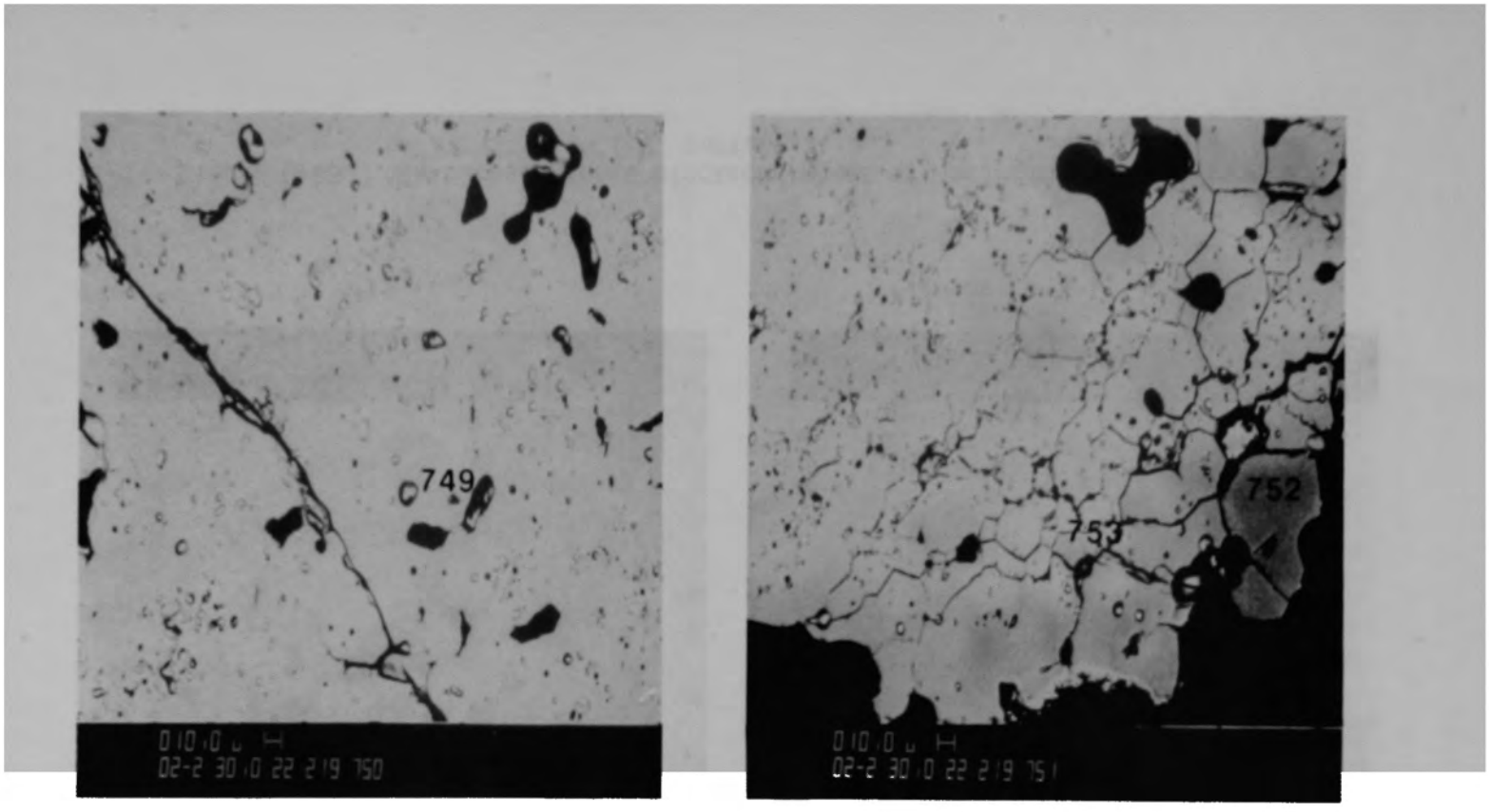

(a) Location E

(b) Location I

Figure C-81. SEM backscattered electron images of material from Particle 40 (E9, surface).

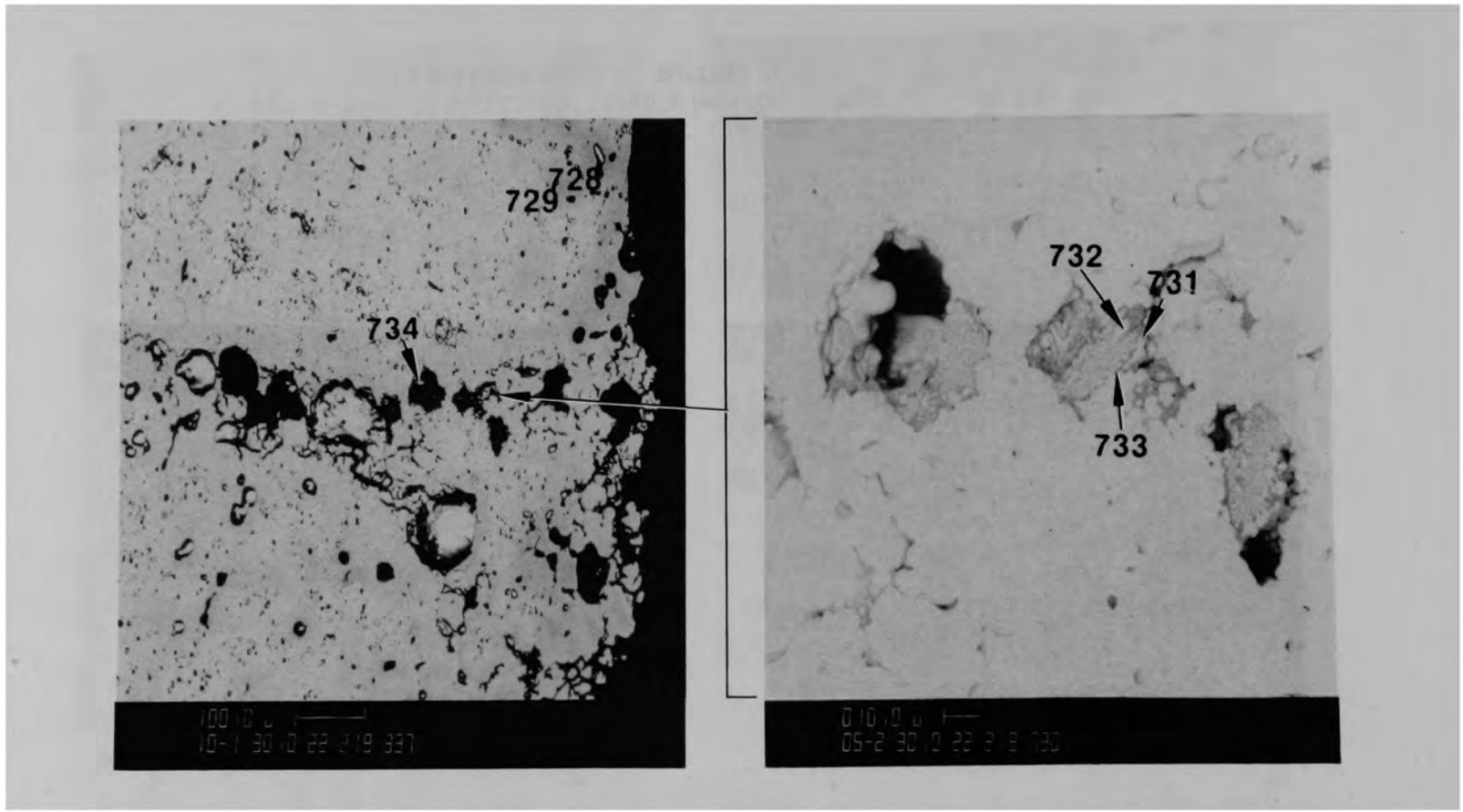

Figure C-82. SEM backscattered electron images of inclusions at location M of Particle 4D (E9, surface).

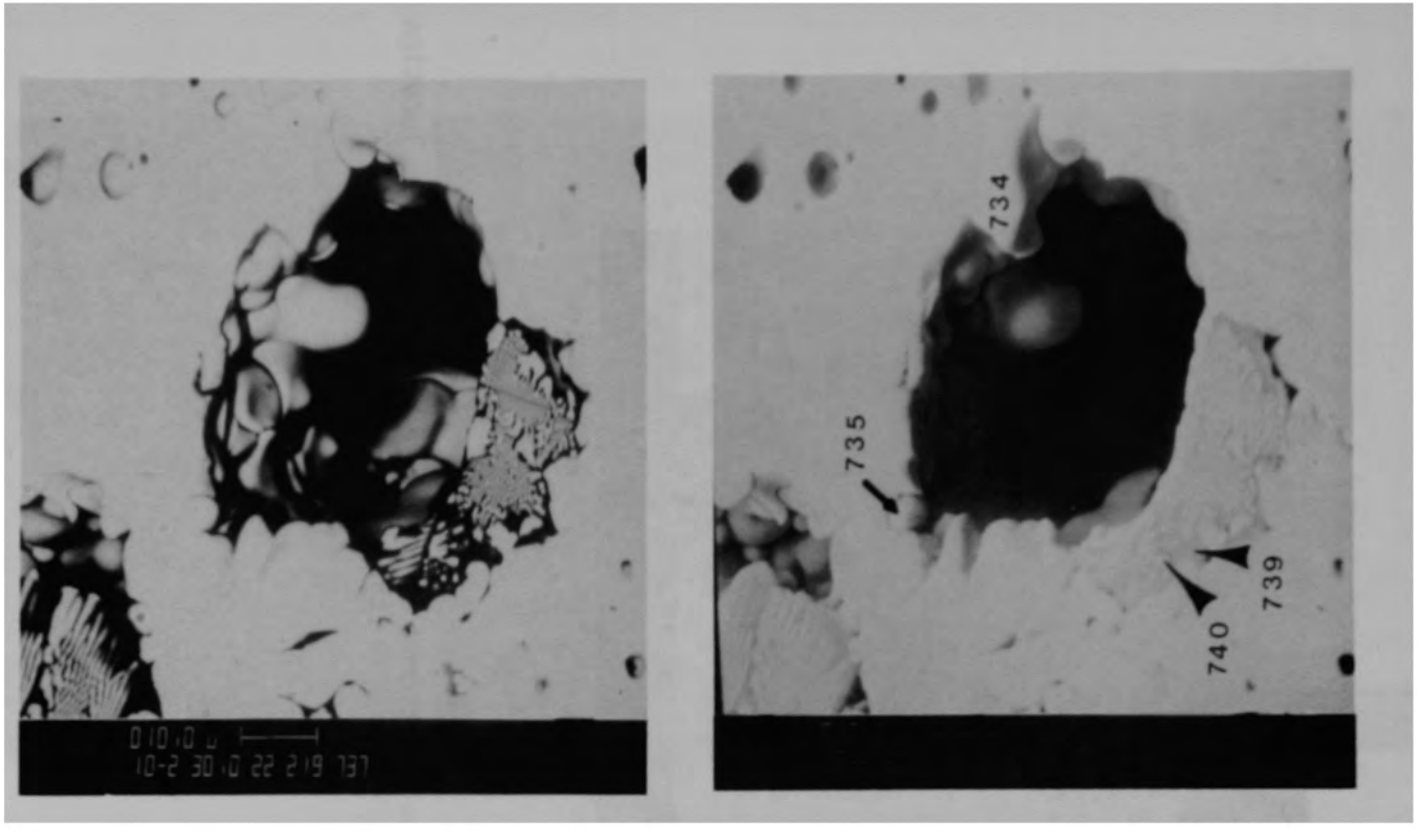

(a) Backscattered electron image

(b) Secondary electron image

Figure C-83. SEM photographs of Location M of Particle 4D (E9, surface).

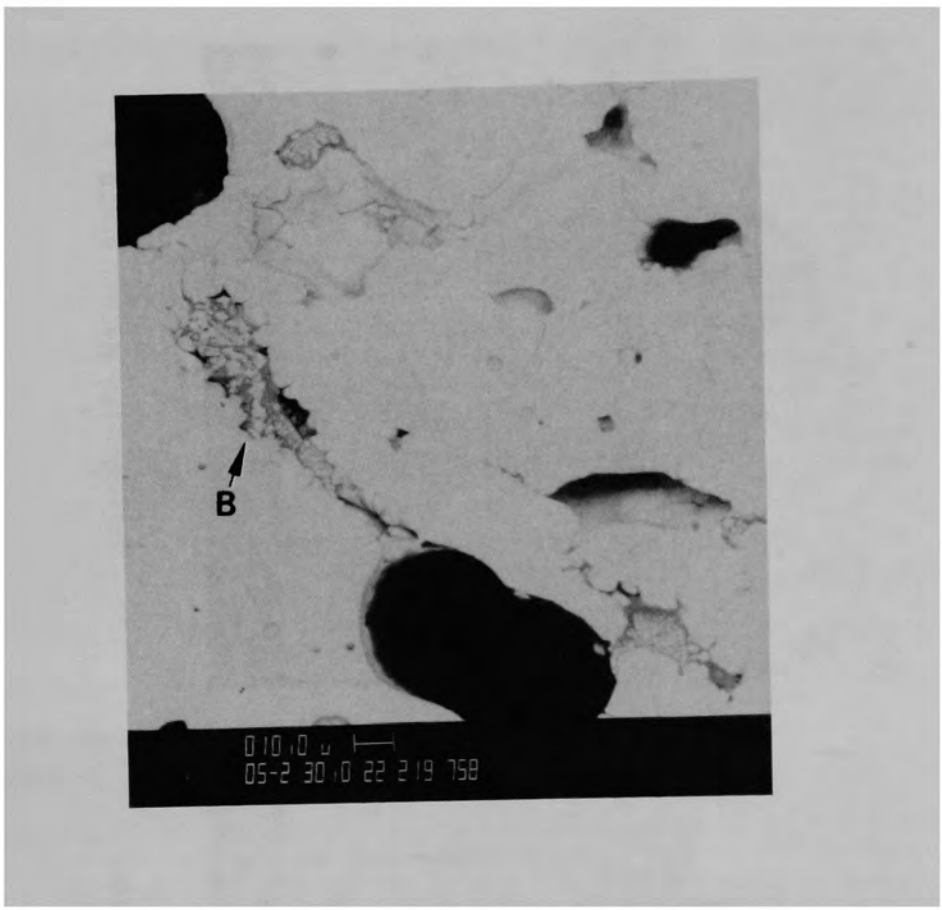

Figure C-84. SEM backscattered electron image of material in location B from Particle 4D (E9, surface).

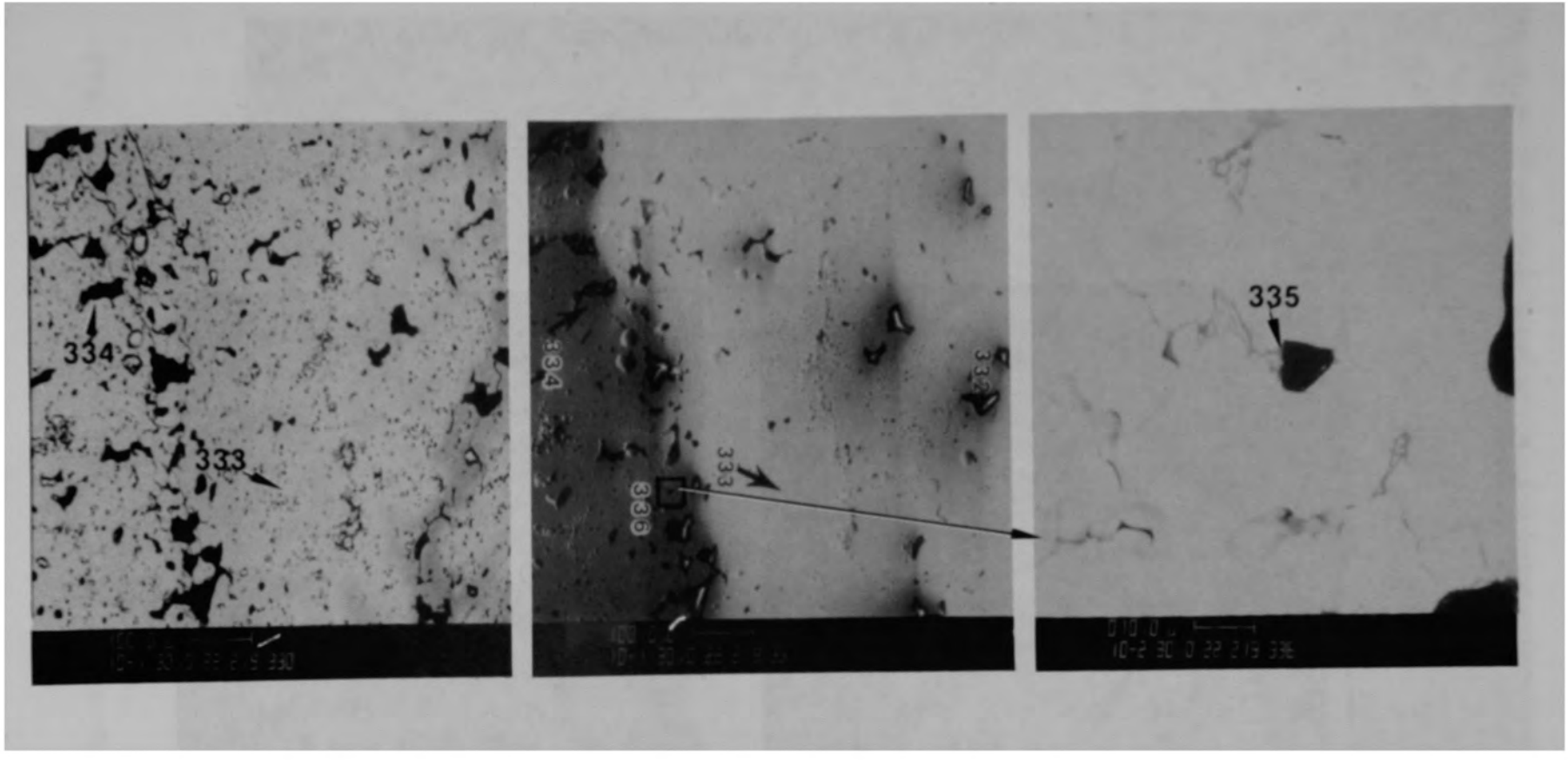

Figure C-85. SEM backscattered electron images of material at location F from Particle 4U (E9, surface).

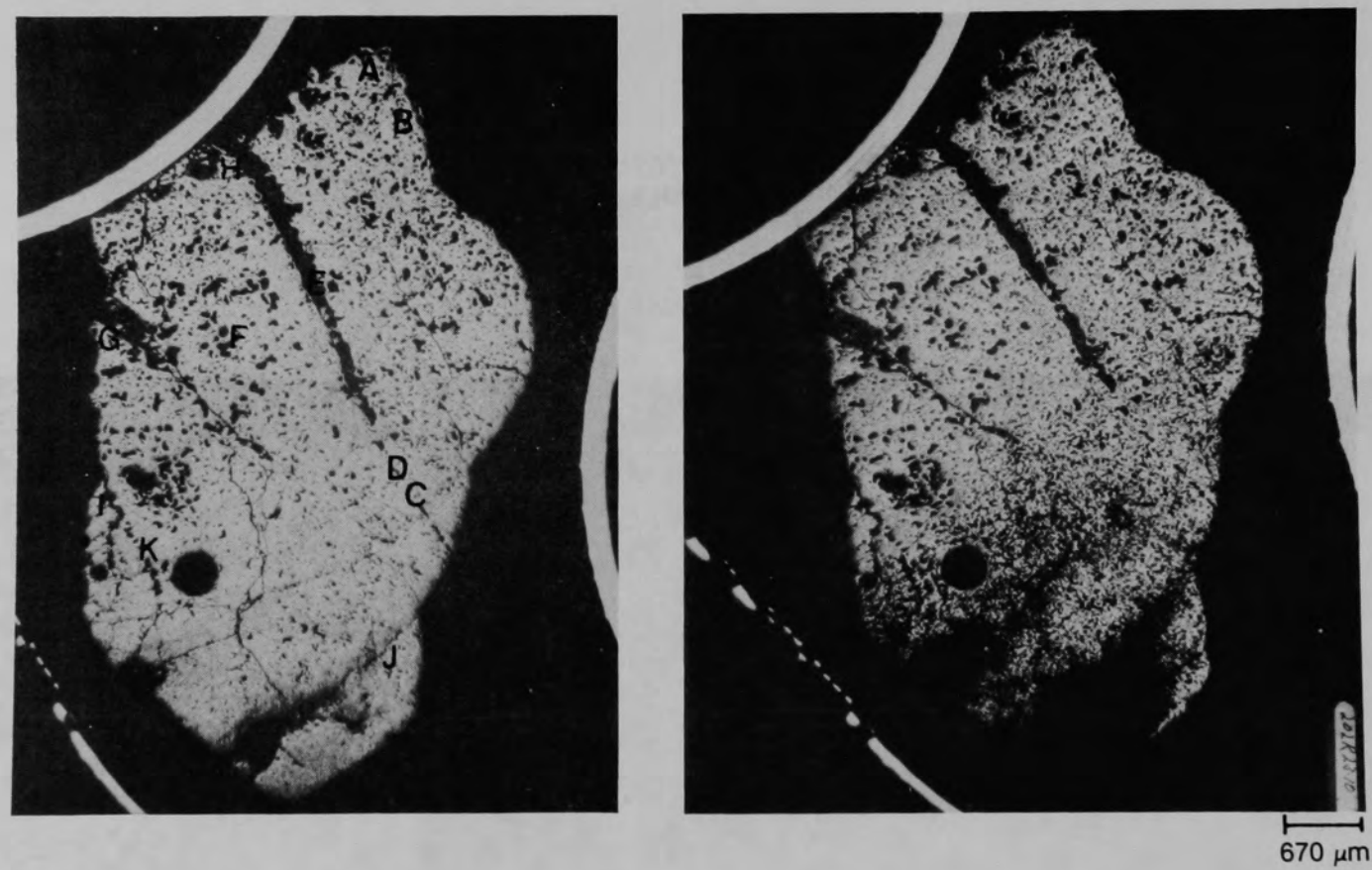

(a) Unetched

(b) Etched

Figure C-86. Photomacrographs of Particle 5E (E9, 8 cm).

Figure C-87. SEM backscattered electron images showing 6 regions of Particle 5E (E9, 8 cm).

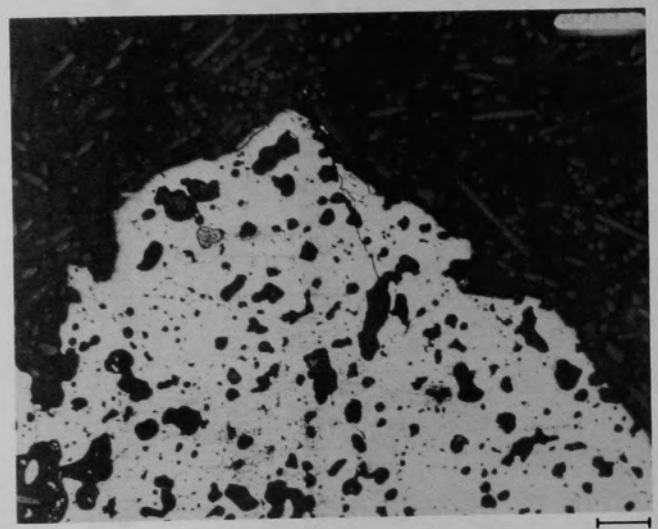

(a) Photomicrograph

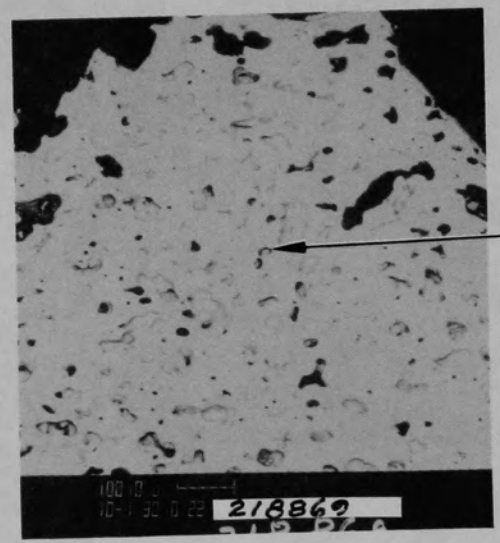

(b) SEM backscattered electron image

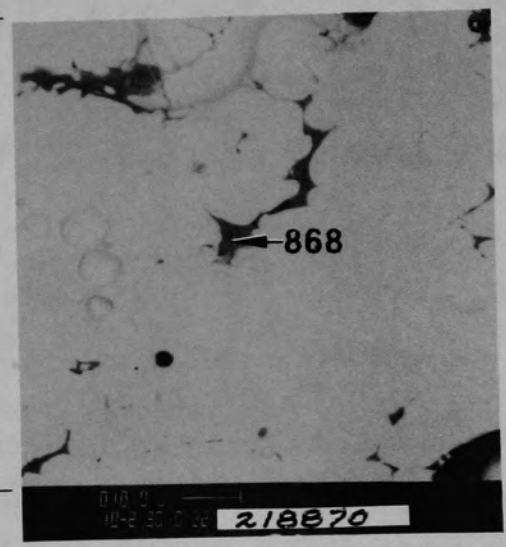

(c) SEM backscattered electron image

Figure C-88. Photographs of material in Region 1, location A, of Particle 5E (E9, 8 cm).

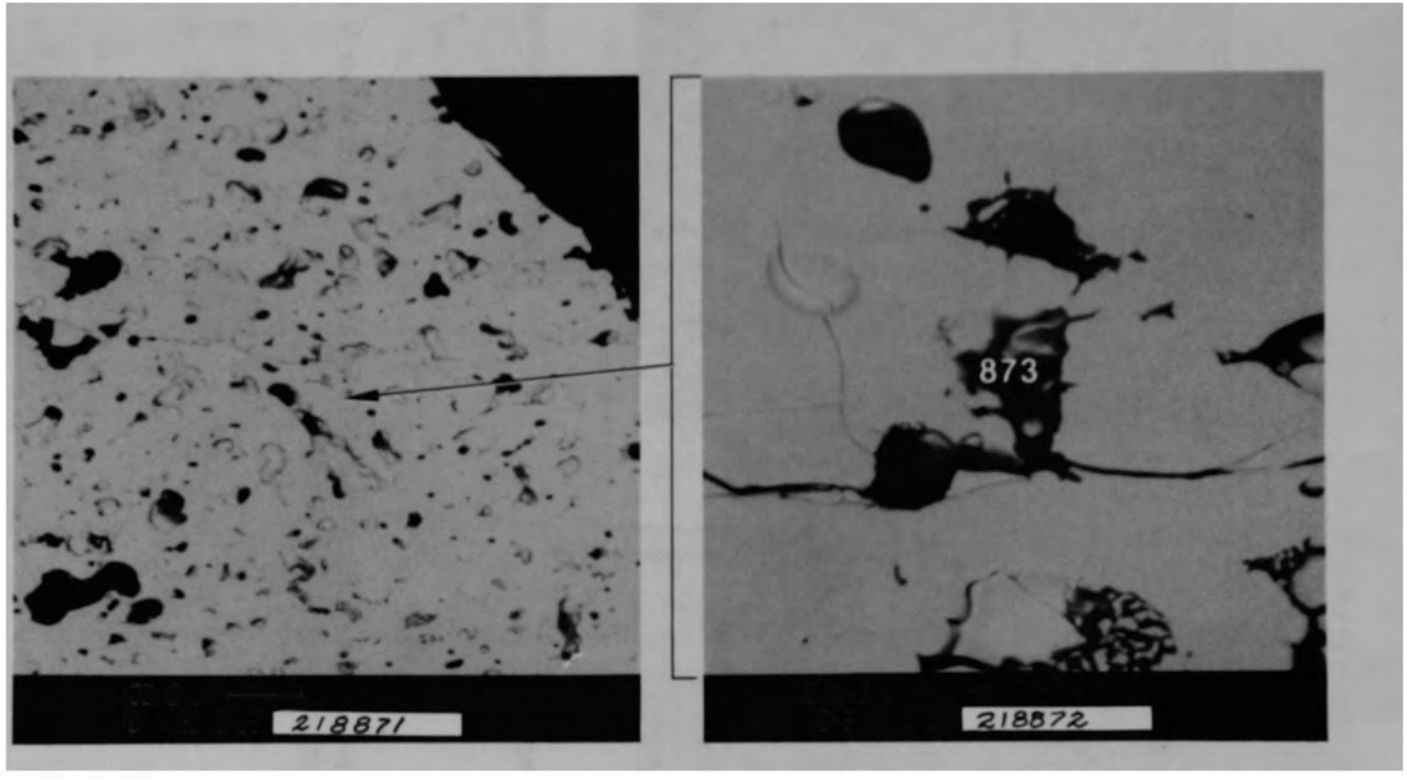

Figure C-89. SEM backscattered electron images of Region 1, location B, of Particle 5E (E9, 8 cm).

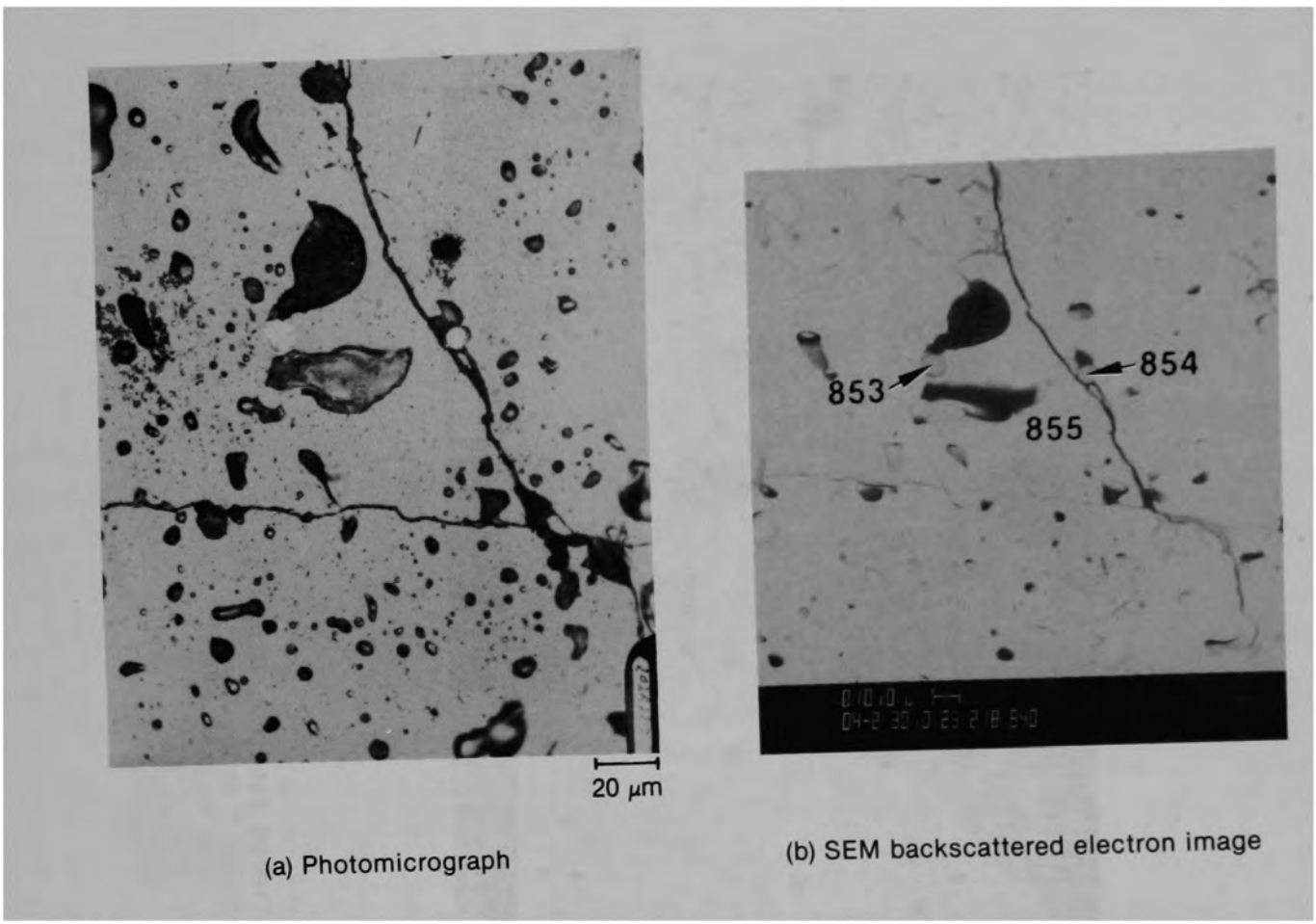

Figure C-90. Photographs of material from Region 1, Location C of Particle 5E (E9, 8 cm).

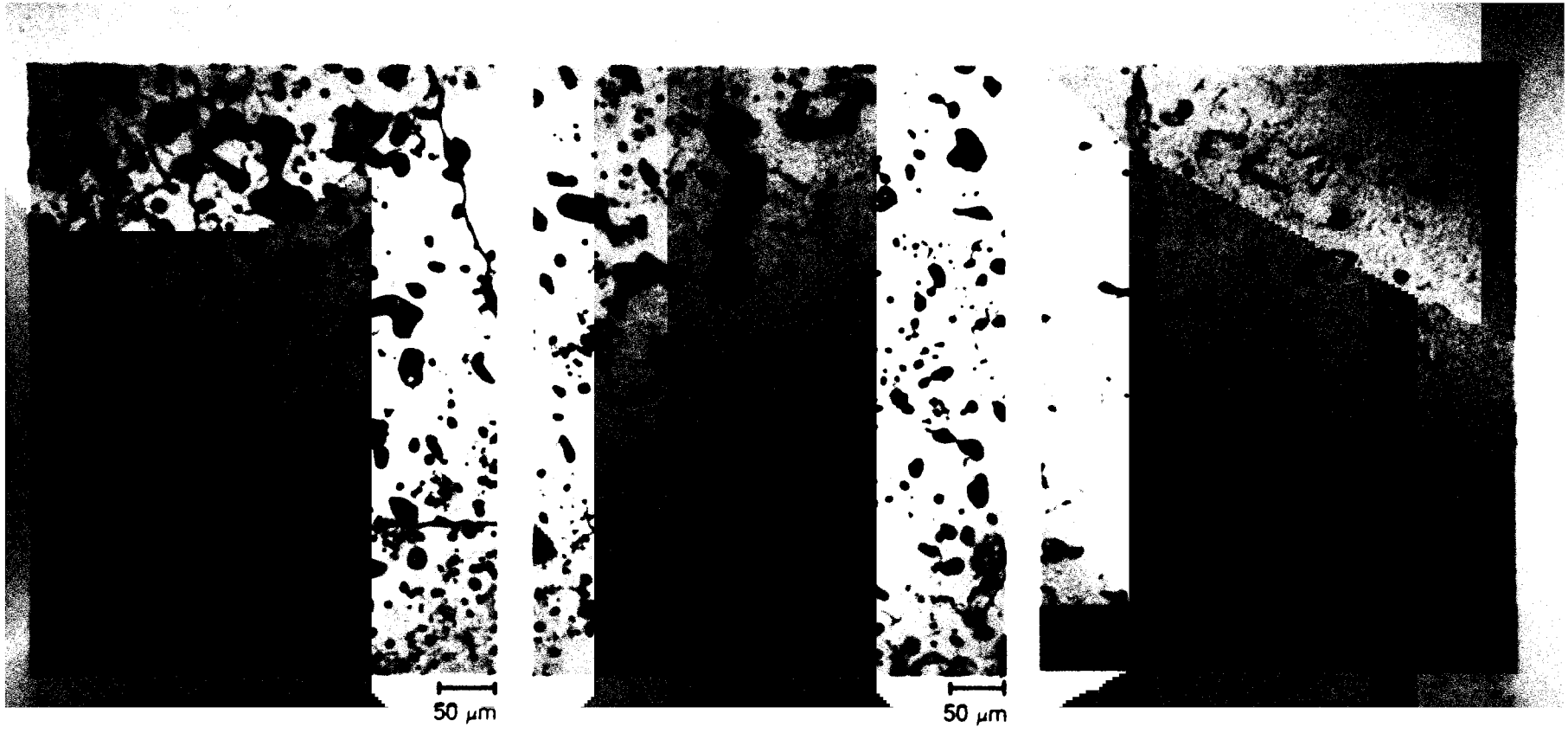

(a) Photomicrograph (b) Photomicrograph (c) SEM backscattered electron image

Figure C-91. Photographs of material from Region 1, Location D, of Particle 5E (E9, 8 cm).

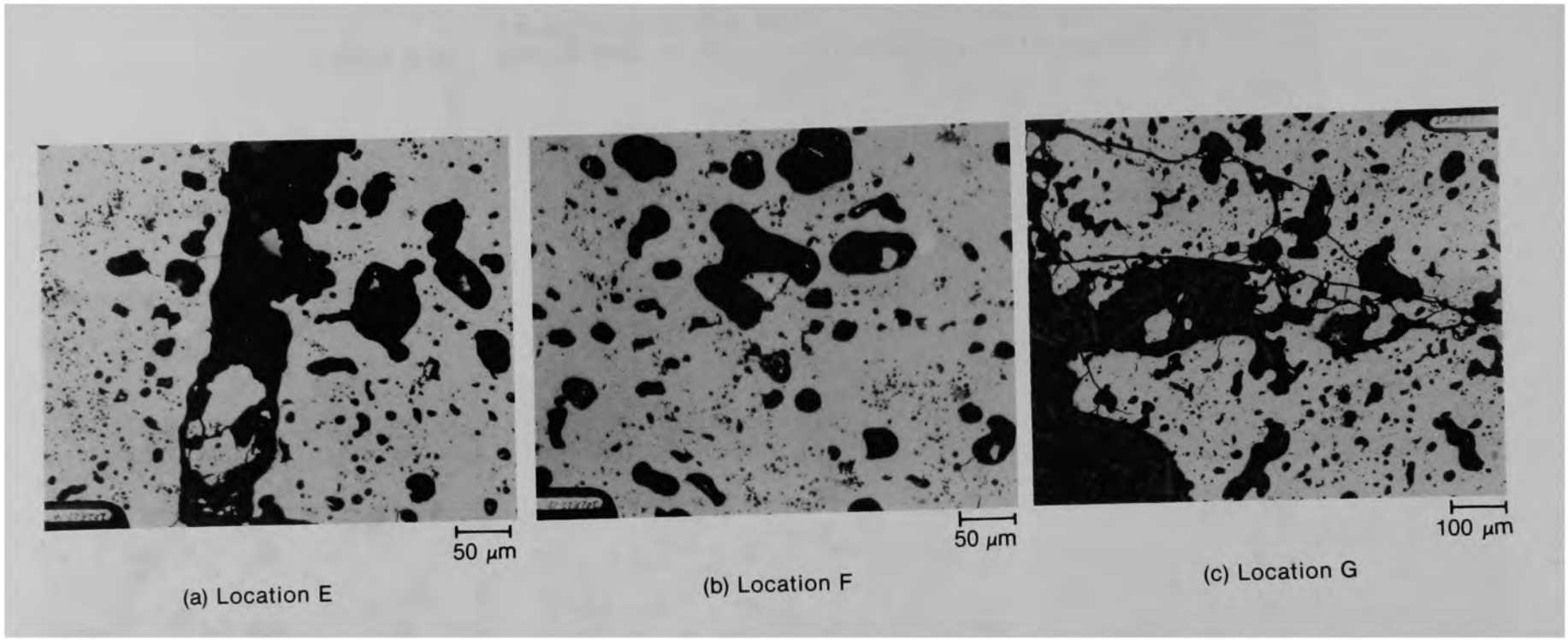

Figure C-92. Photomicrographs of material from Region 2 of Particle 5E (E9, 8 cm).

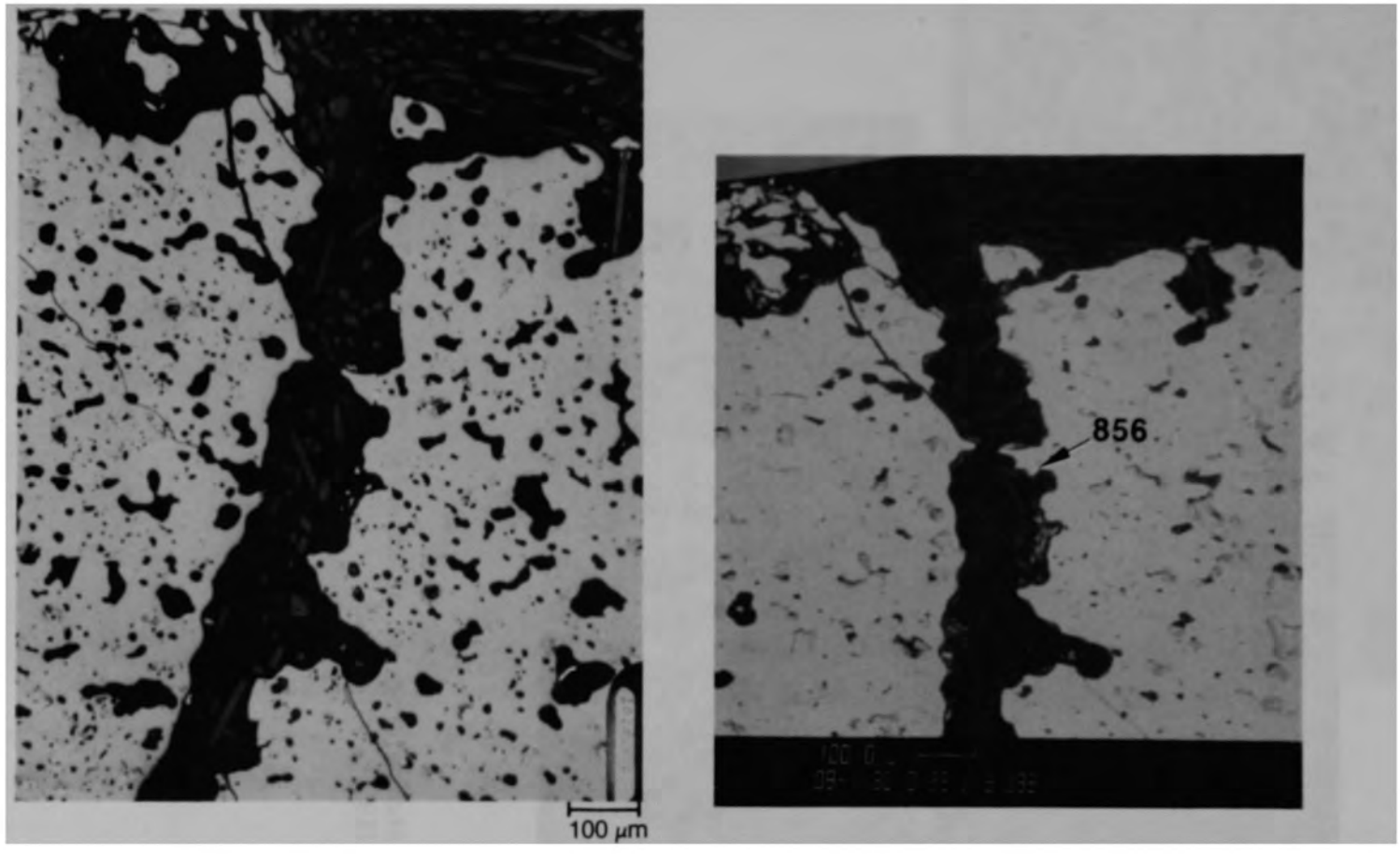

(a) Photomicrograph

(b) SEM backscattered electron image

Figure C-93. Photographs of material from Region 2, Location H, of Particle 5E (E9, 8 cm).

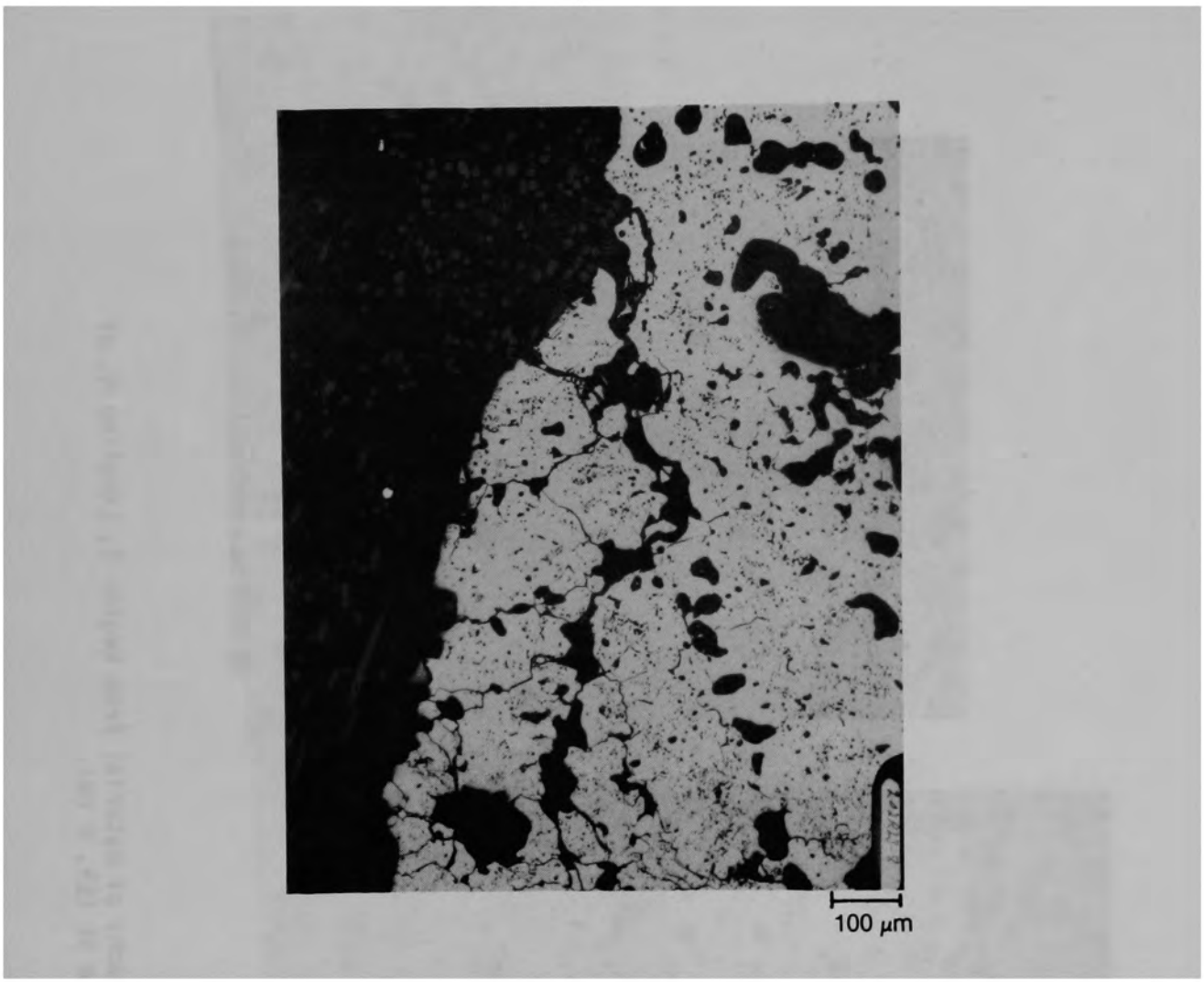

Figure C-94. Photomicrograph of material from Region 3 of Particle 5E (E9, 8 cm).

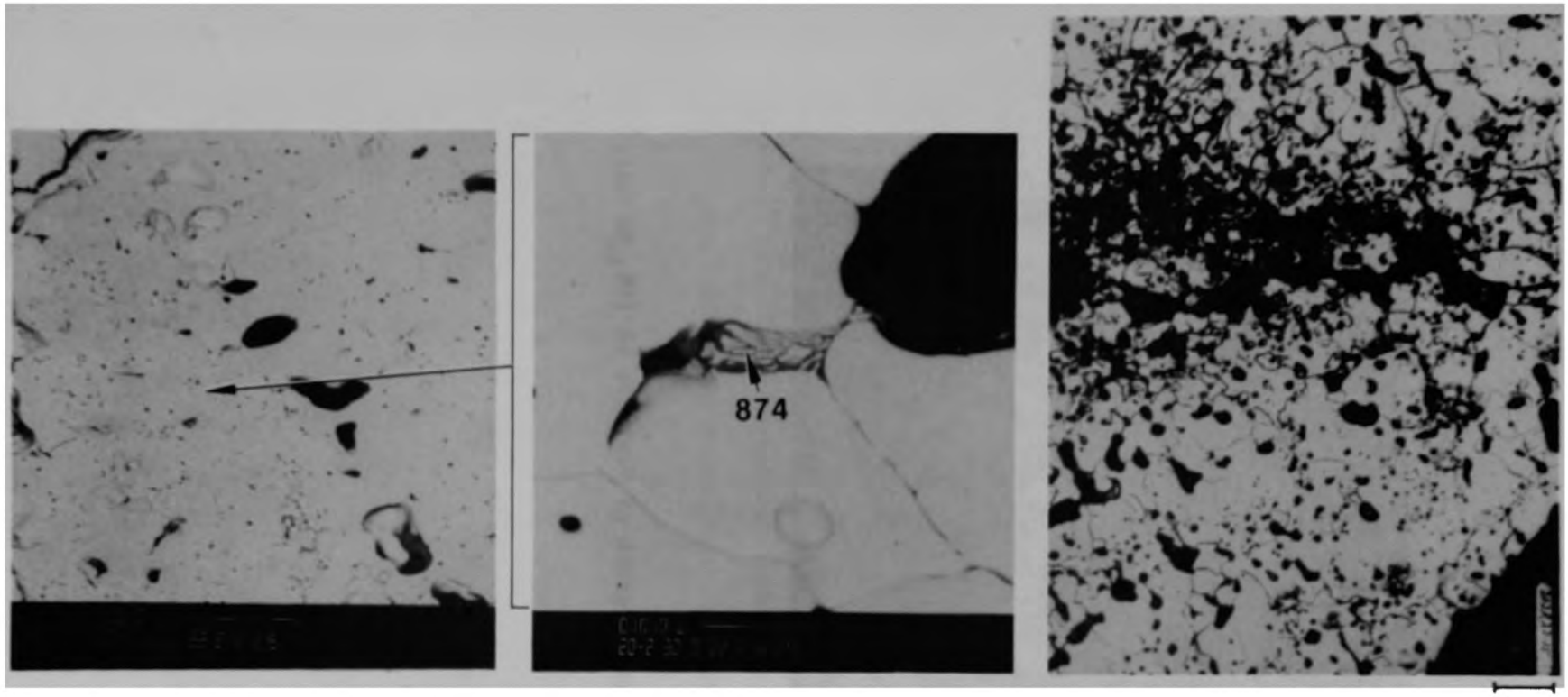

(a) SEM backscattered electron image
Location K

(b) SEM backscattered electron image
Closeup of (a)

(c) Photomicrograph
Location J

Figure C-95. Photographs of material from Region 4 of Particle 5E (E9, 8 cm).

Figure C-96. Photomacrograph of Particle 6B (E9, 56 cm).

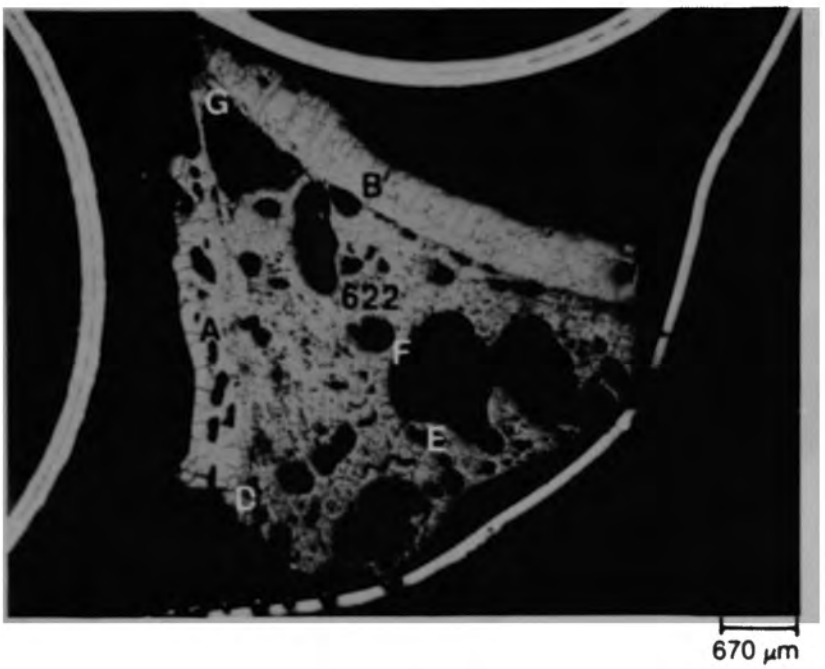

Figure C-97. Photomacrograph of Particle 6C (E9, 56 cm).

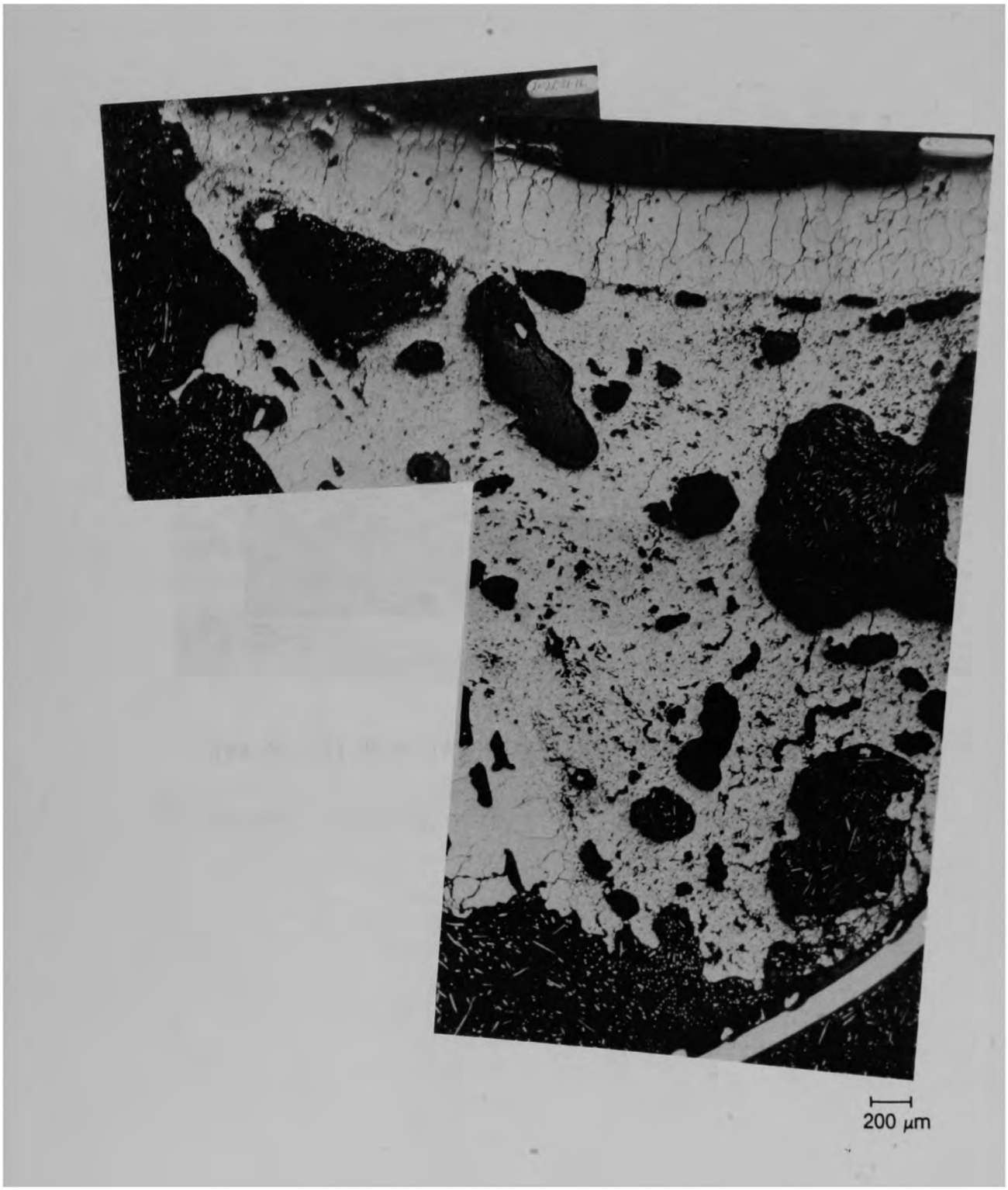

Figure C-98. Photomacrographs of upper region of Particle 6C (E9, 56 cm).

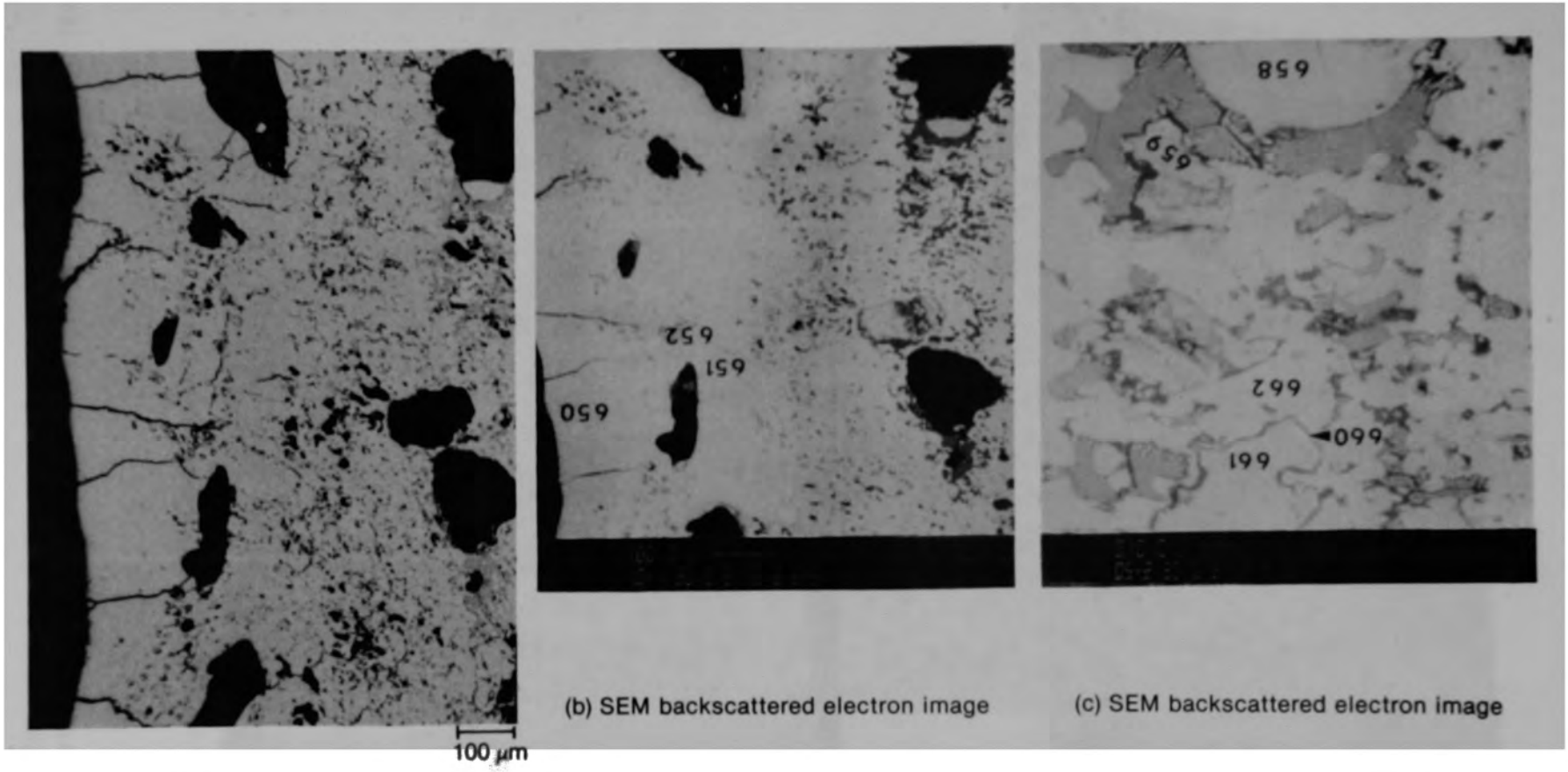

(a) Photomicrograph

Figure C-99. Photographs of material from Location A of Particle 6C (E9, 56 cm) showing cladding-melt interface.

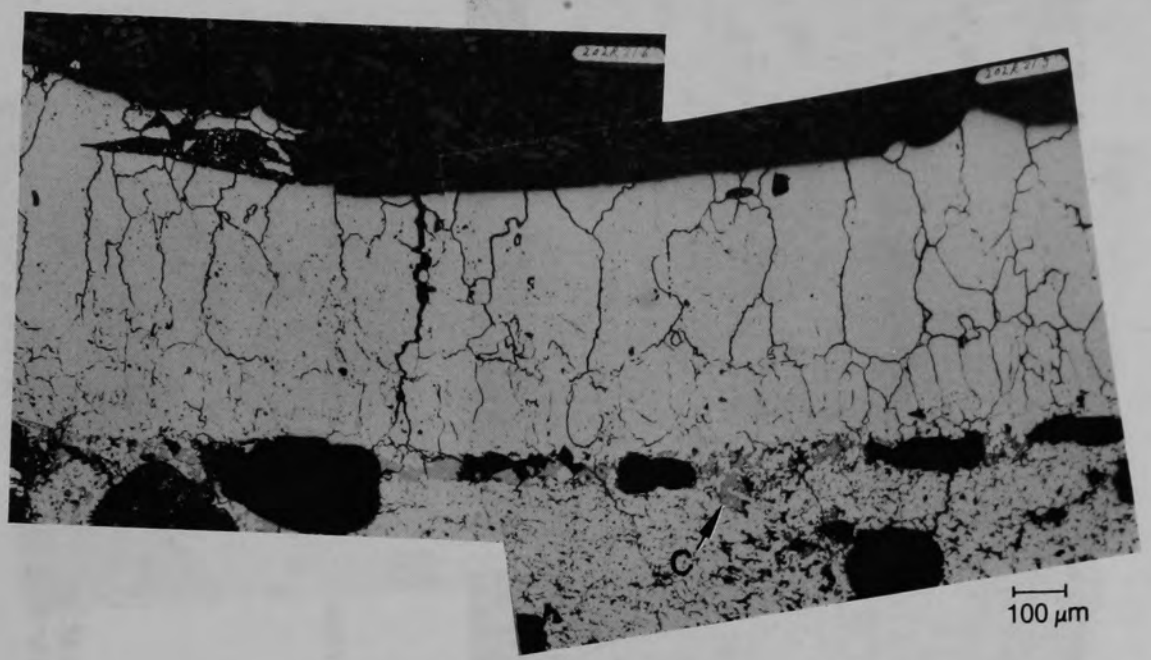

(a) Photomicrograph

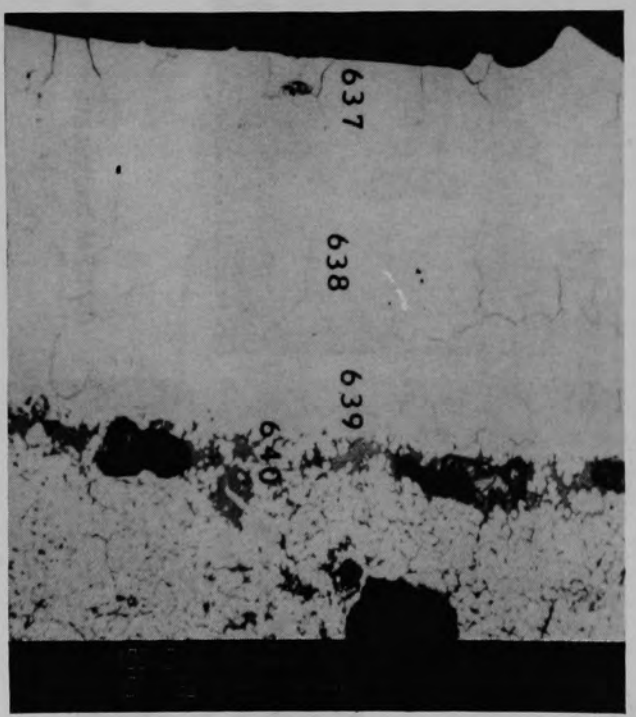

(b) SEM backscattered electron image

Figure C-100. Photographs of material from location B of Particle 6C (E9, 56 cm).

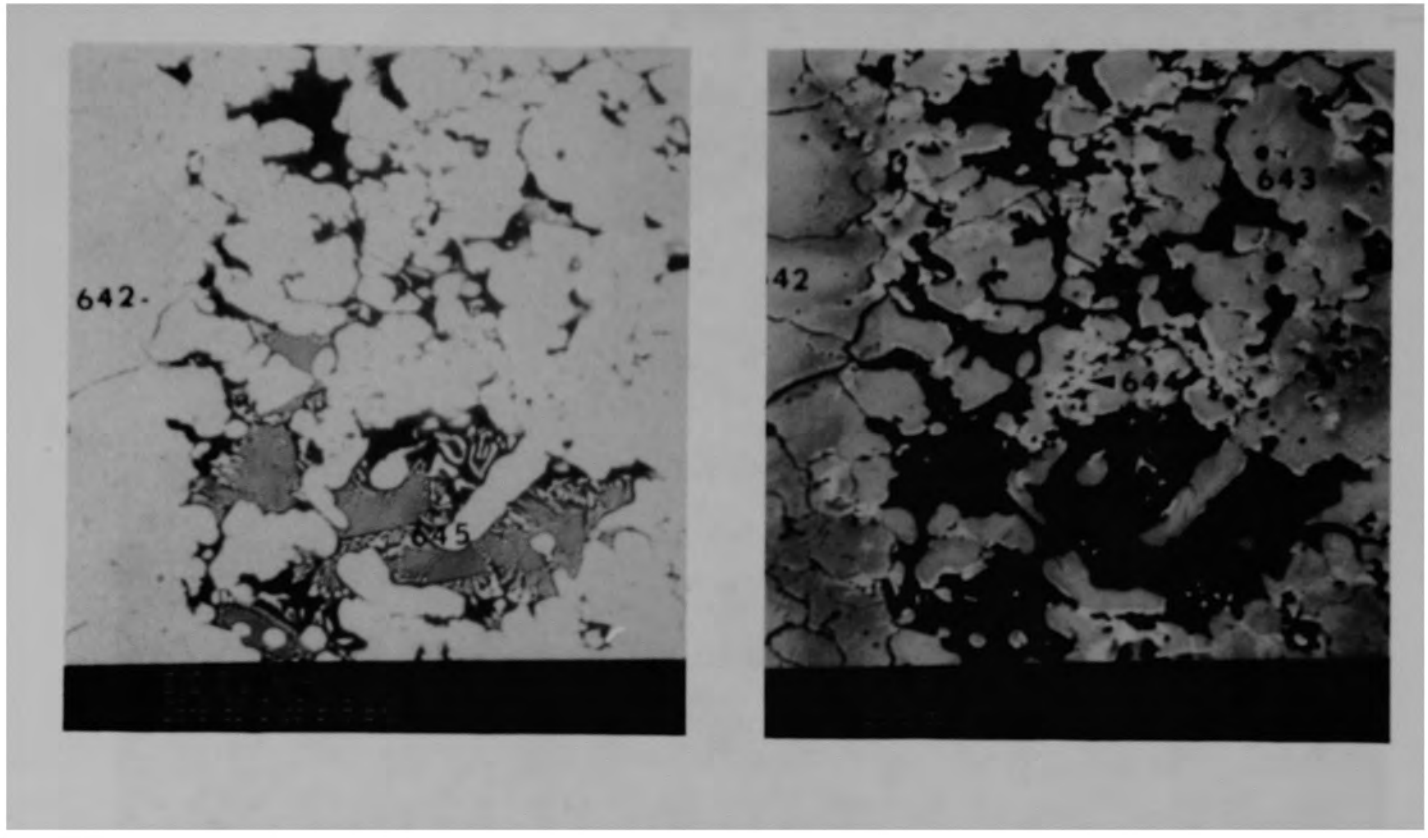

Figure C-101. SEM backscattered electron image of location C (Figure C-100) of Particle 6C (E9, 56 cm).

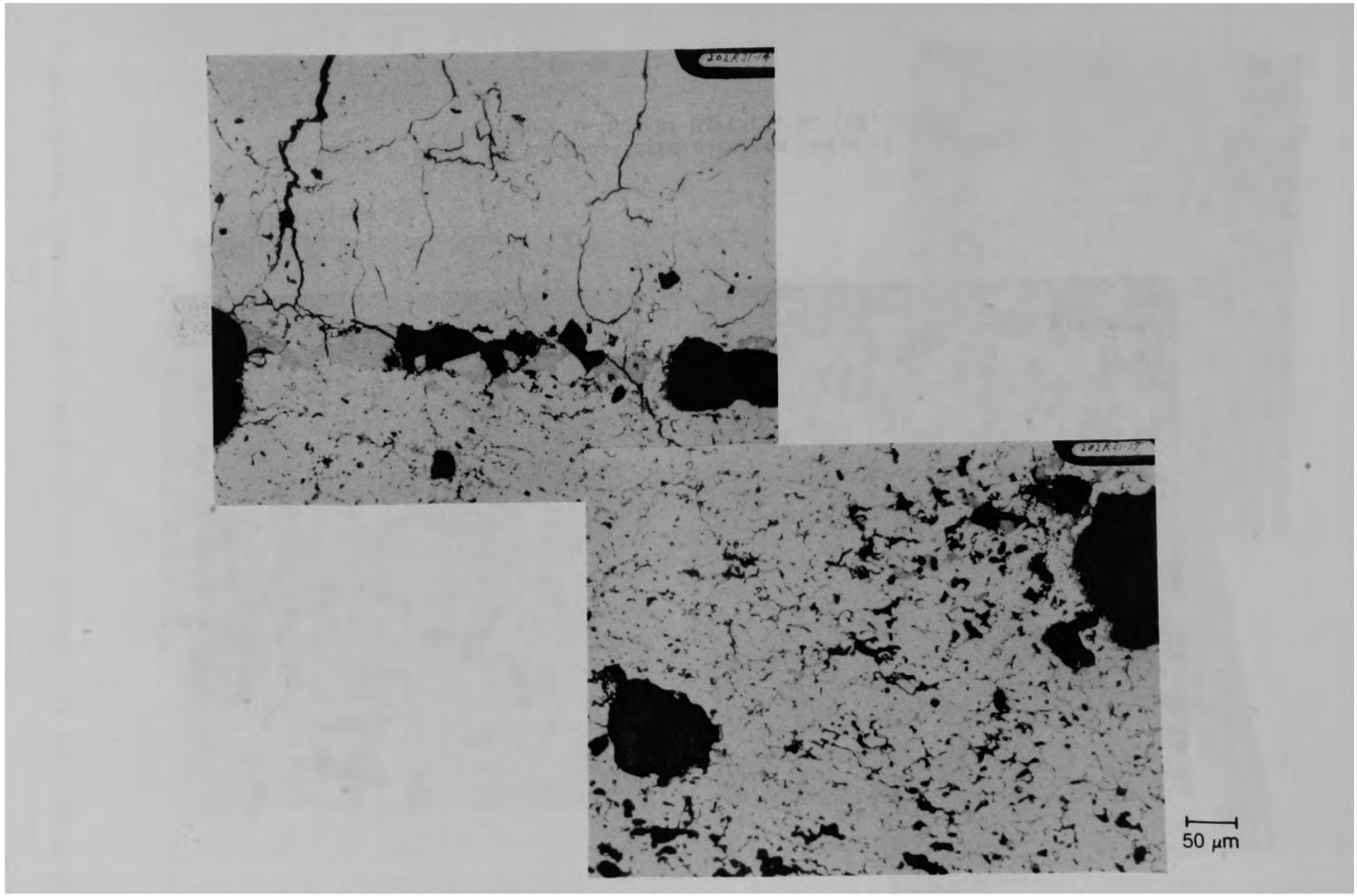

Figure C-102. Photomicrographs of material from location B of Particle 6C (E9, 56 cm).

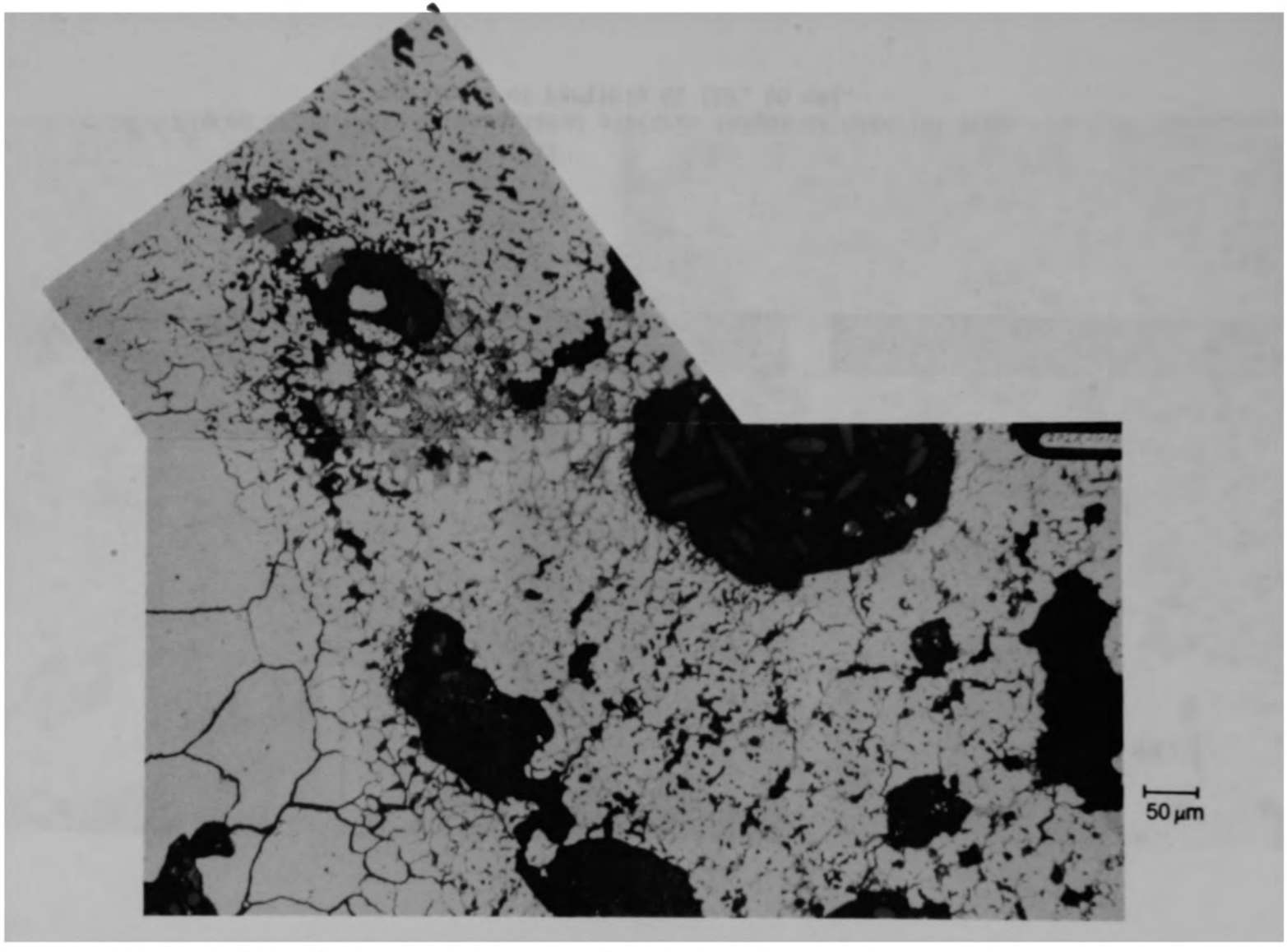

Figure C-103. Photomicrographs of material from location D of Particle 6C (E9, 56 cm).

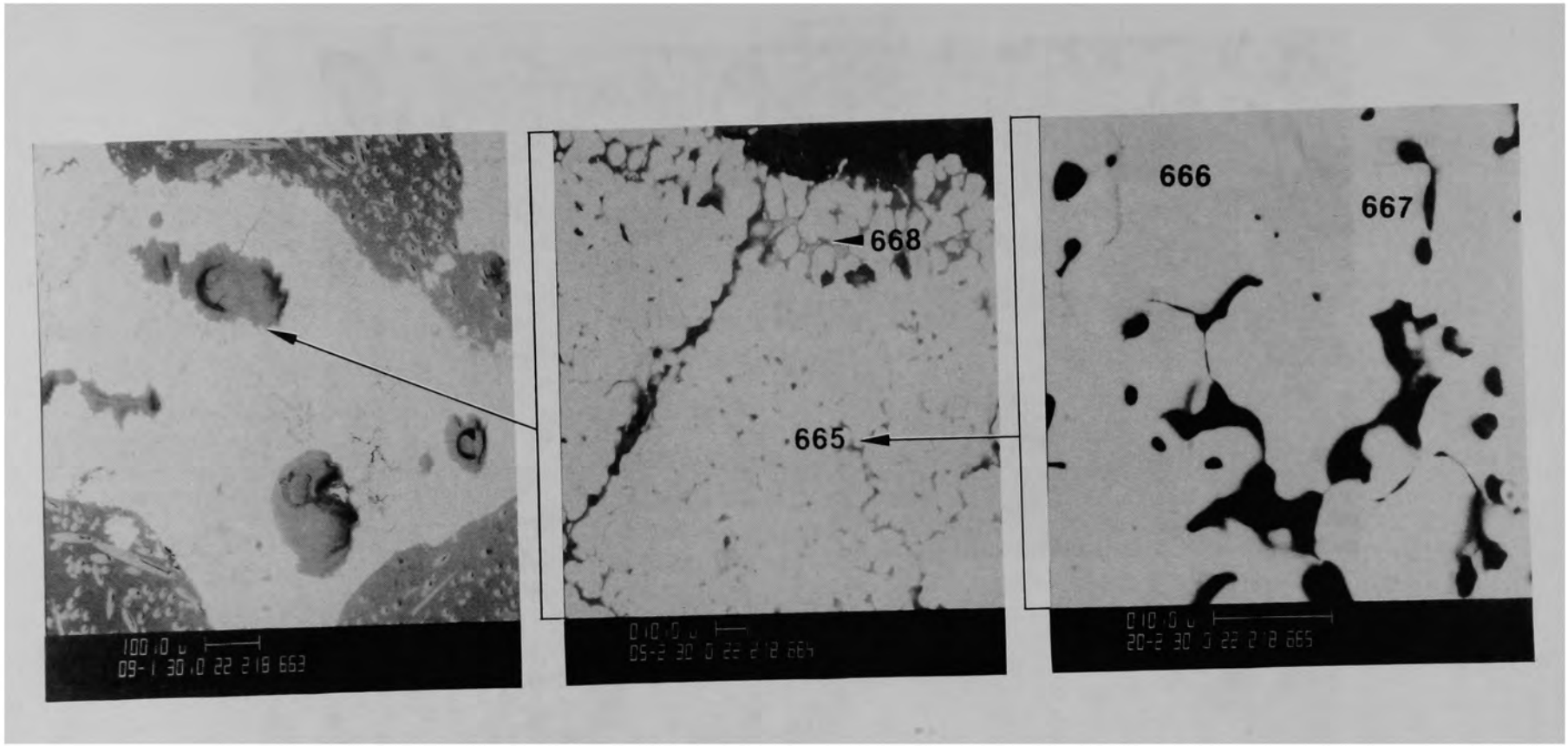

Figure C-104. SEM backscattered electron images of material from location E of Particle 6C (E9, 56 cm).

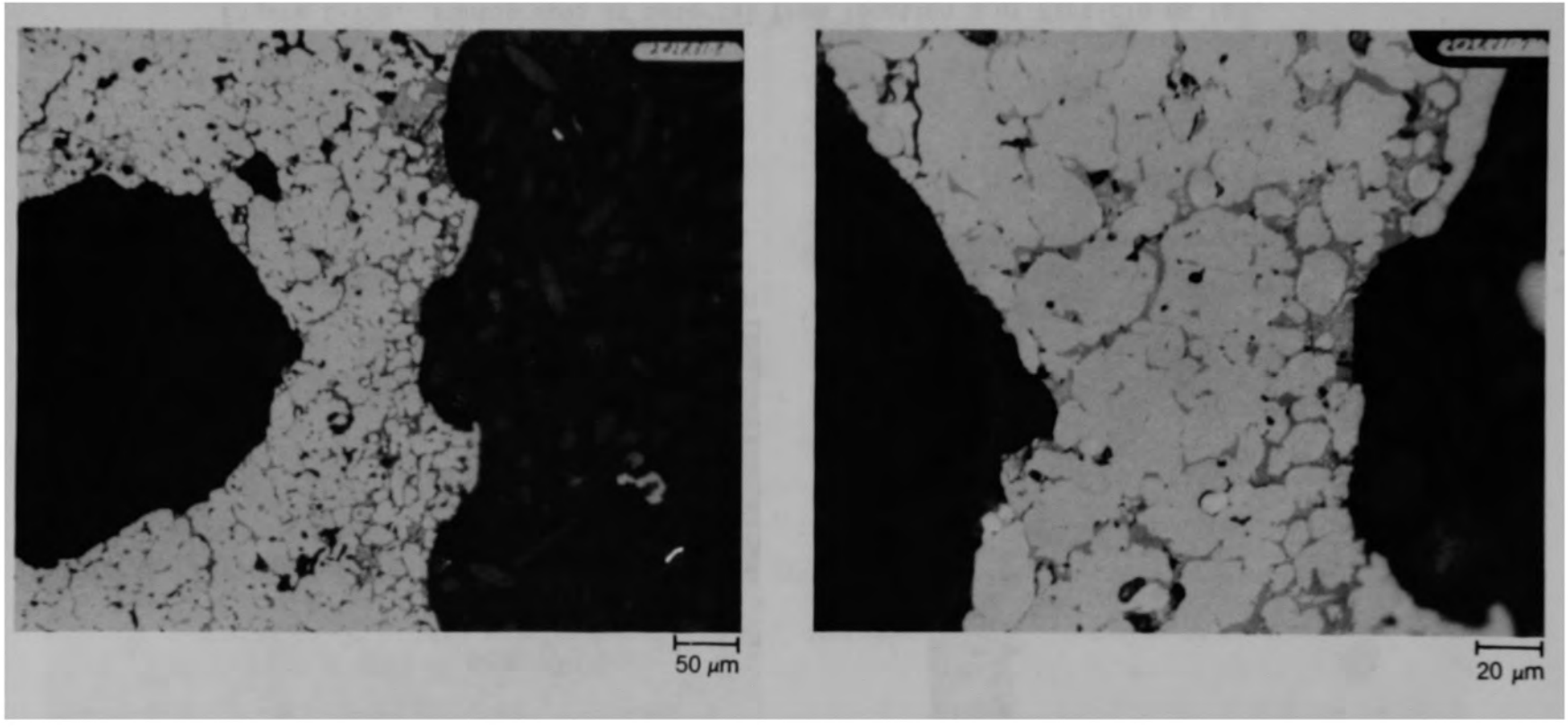

Figure C-105. Photomicrographs of material from location F of Particle 6C (E9, 56 cm).

(a) Photomicrograph

(b) SEM backscattered electron image

Figure C-106. Photographs of material from location G of Particle 6C (E9, 56 cm).

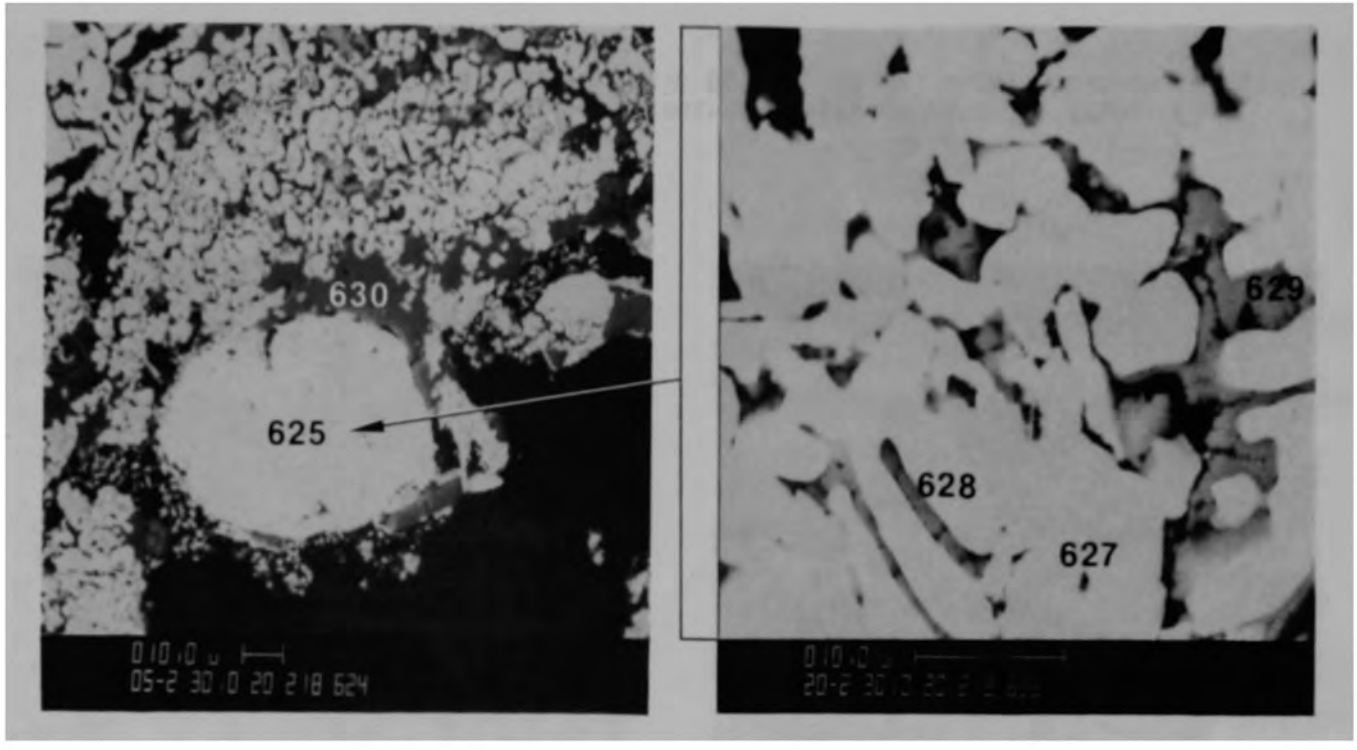

Figure C-107. SEM backscattered electron images of material from location D of Particle 6C (E9, 56 cm).

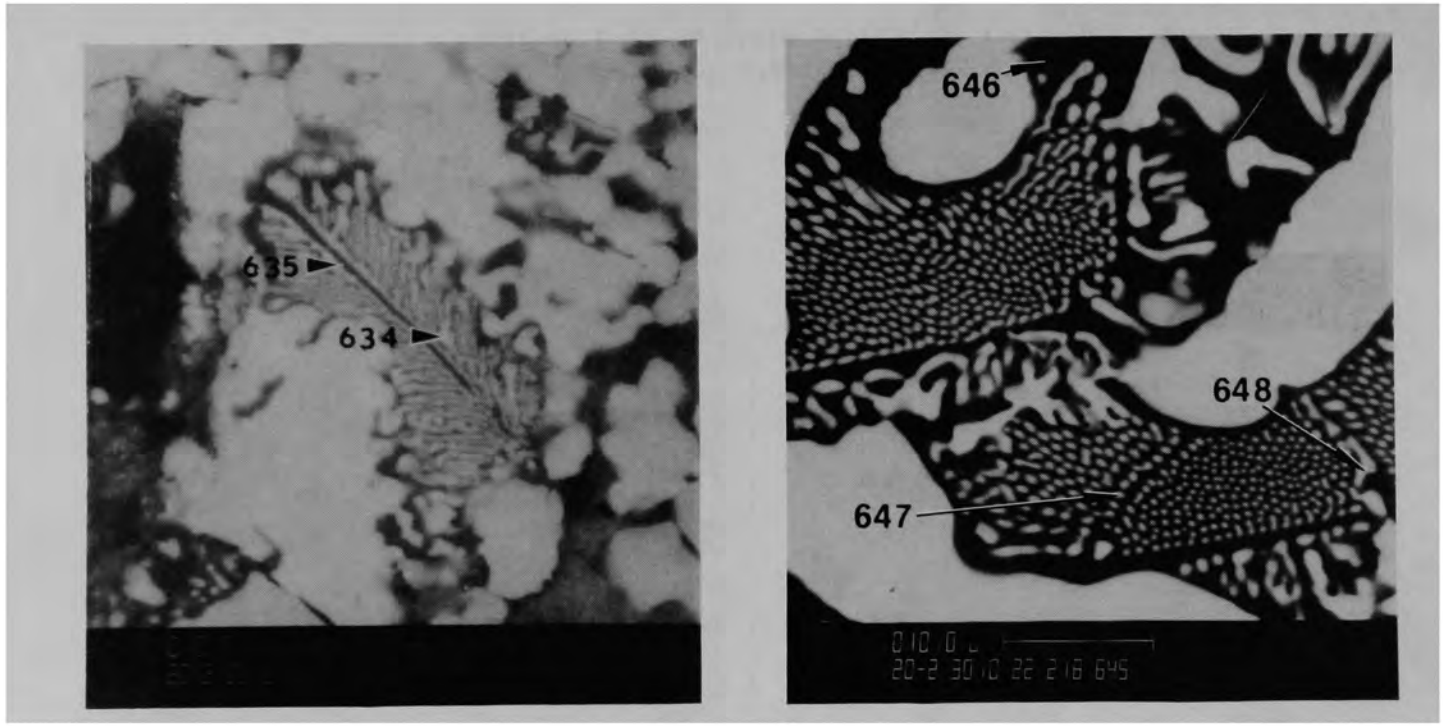

Figure C-108. SEM backscattered electron images of material from location D of Particle 6C (E9, 56 cm) showing two phase structure.

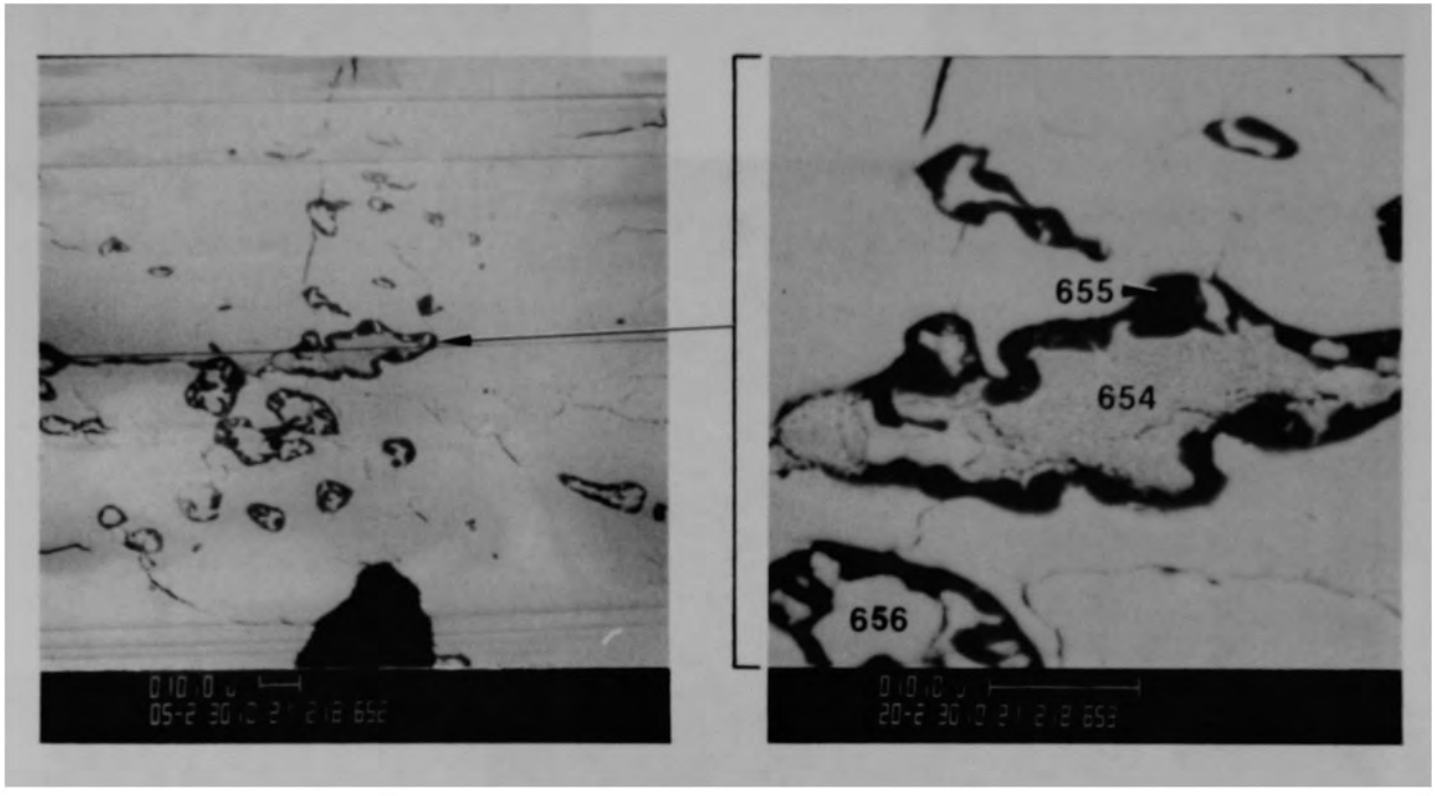

Figure C-109. SEM backscattered electron images of material from location A of Particle 6C (E9, 56 cm).

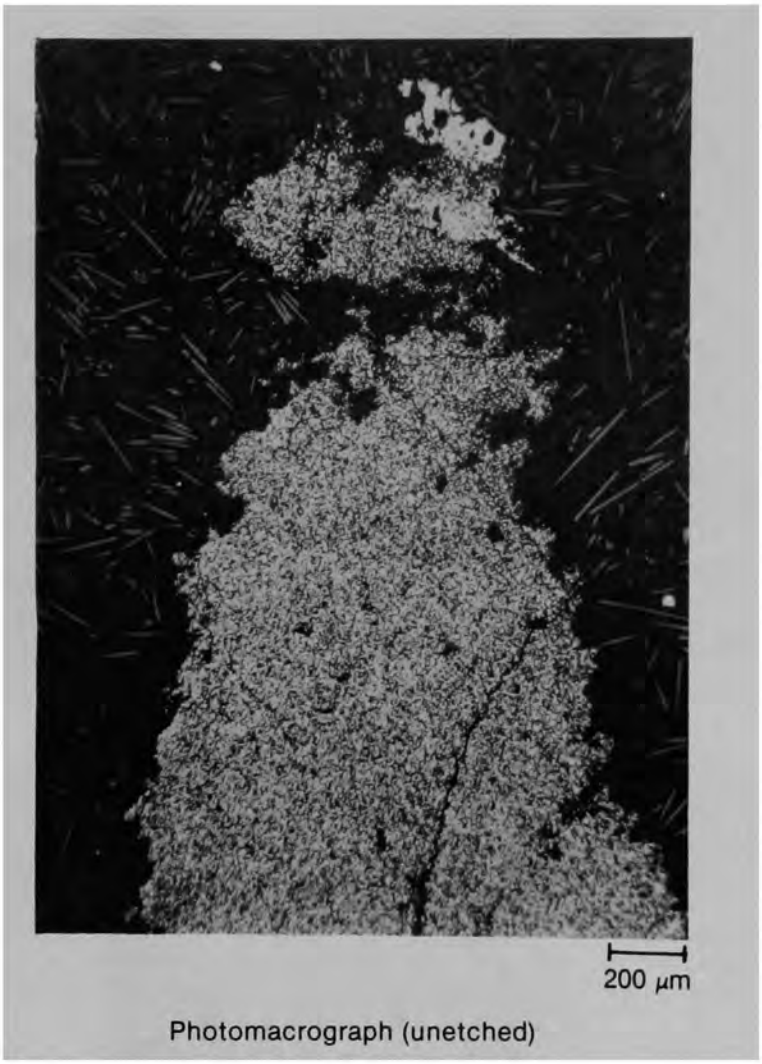

Figure C-110. Upper portion of Particle 6D (E9, 56 cm) showing oxidized fuel with adherent (U, Zr, O) melt.

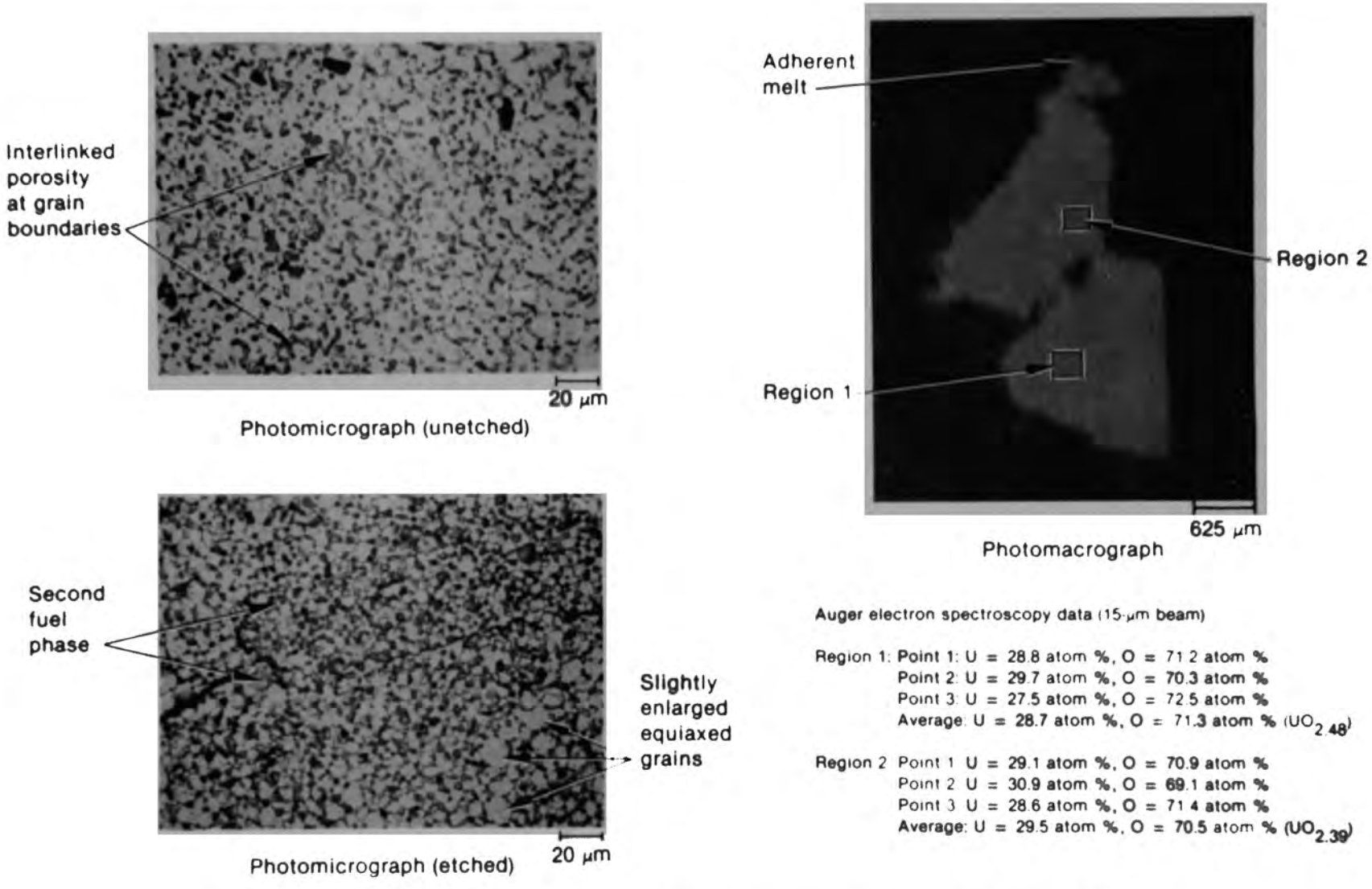

Figure C-111. Typical fuel grain structure of Particle 6D before and after etching (left), plus Auger spectroscopy measurements of elemental composition.

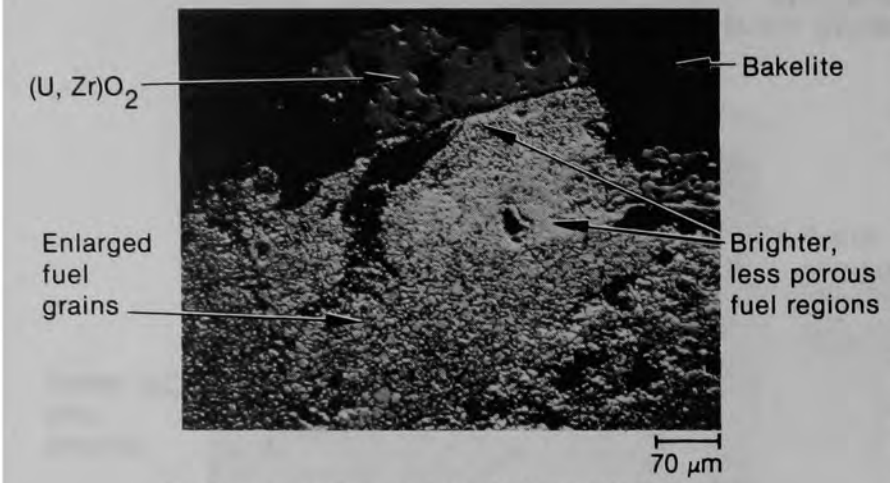

Backscattered scanning electron micrograph

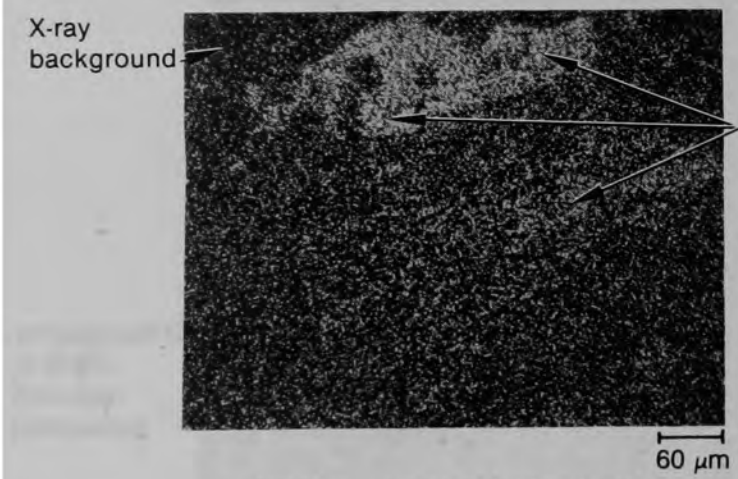

Zirconium x-ray emission image

Backscattered scanning electron micrograph

Energy-dispersive x-ray spectroscopy data

Point 1: 66.3 weight % U, 33.8 weight % Zr
Point 2: 66.3 weight % U, 33.8 weight % Zr
Point 3: 66.5 weight % U, 33.6 weight % Zr
Point 4: 65.8 weight % U, 34.3 weight % Zr
Point 5: 67.3 weight % U, 32.7 weight % Zr
Point 6: 66.8 weight % U, 33.3 weight % Zr
Point 7: 66.2 weight % U, 33.9 weight % Zr
Point 8: 66.3 weight % U, 33.7 weight % Zr
Point 9: 75.3 weight % U, 24.8 weight % Zr
Point 10: 65.7 weight % U, 34.3 weight % Zr
Point 11: 71.1 weight % U, 29.0 weight % Zr
Point 12: 88.8 weight % U, 11.3 weight % Zr
Point 13: 92.5 weight % U, 7.5 weight % Zr
Point 14: 91.0 weight % U, 9.1 weight % Zr
Point 15: 100.0 weight % U

Figure C-112. Energy dispersive x-ray spectroscopy studies of melt-fuel interactions on Particle 6D.

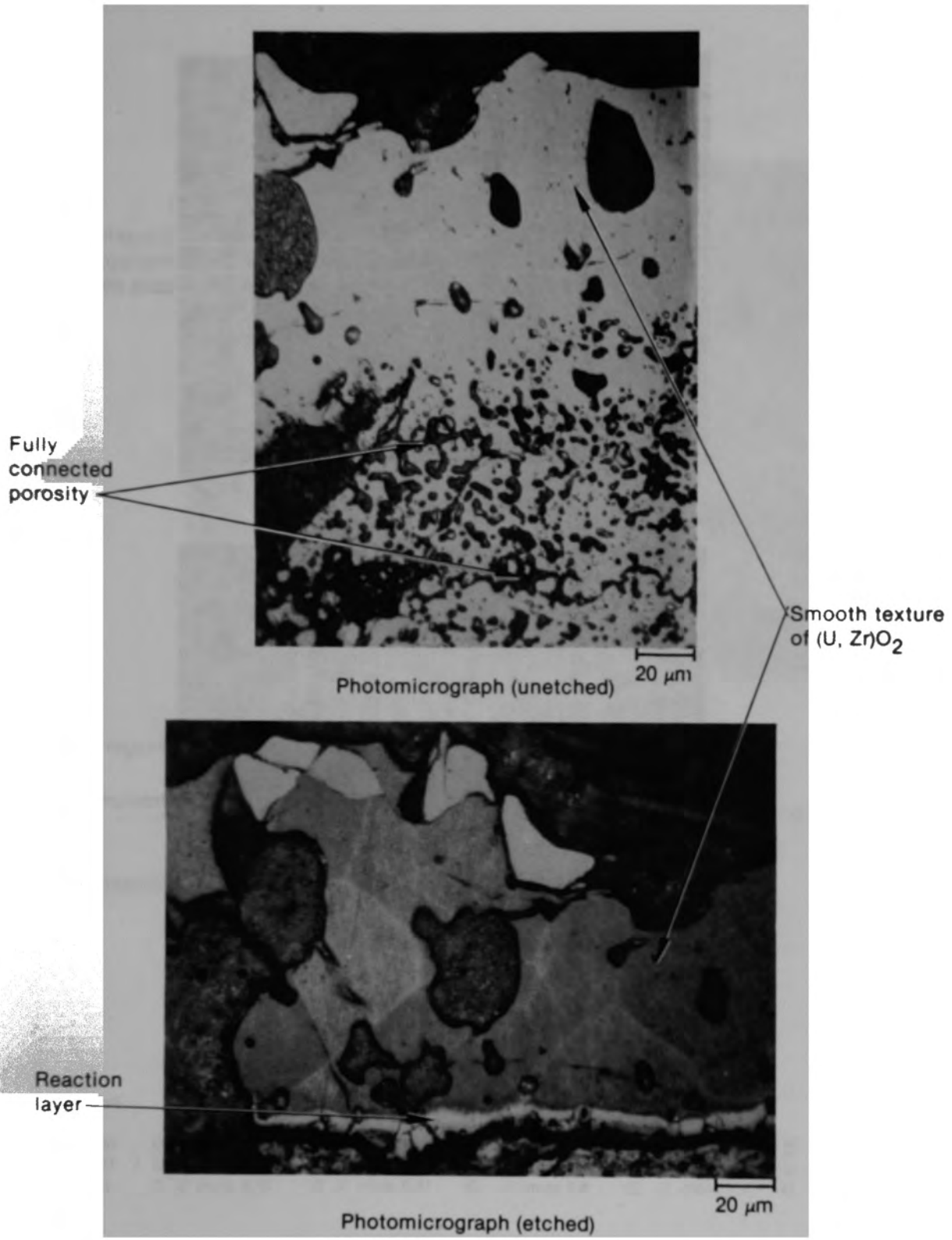

Figure C-113. Highly magnified metallographic images of the melt-fuel interface on Particle 6D.

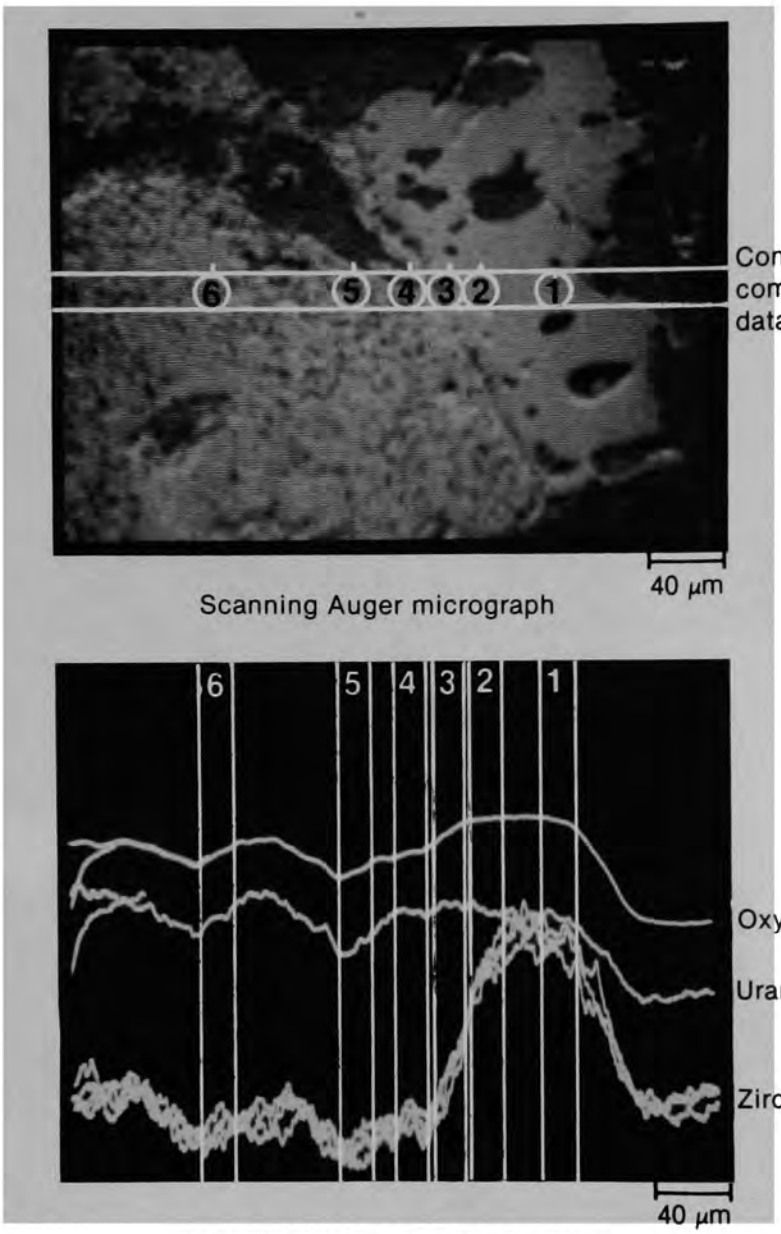

Point 6	Point 5	Point 4	Point 3	Point 2	Point 1
65.9 atom % O	63.8 atom % O	67.2 atom % O	65.6 atom % O	64.6 atom % O	66.5 atom % O
31.1 atom % U	32.1 atom % U	27.6 atom % U	18.9 atom % U	16.0 atom % U	15.4 atom % U
3.0 atom % Zr	4.1 atom % Zr	5.3 atom % Zr	15.5 atom % Zr	19.4 atom % Zr	18.0 atom % Zr

Figure C-114. Scanning Auger microprobe investigations of diffusion bending across the melt-fuel interface on Particle 6D.

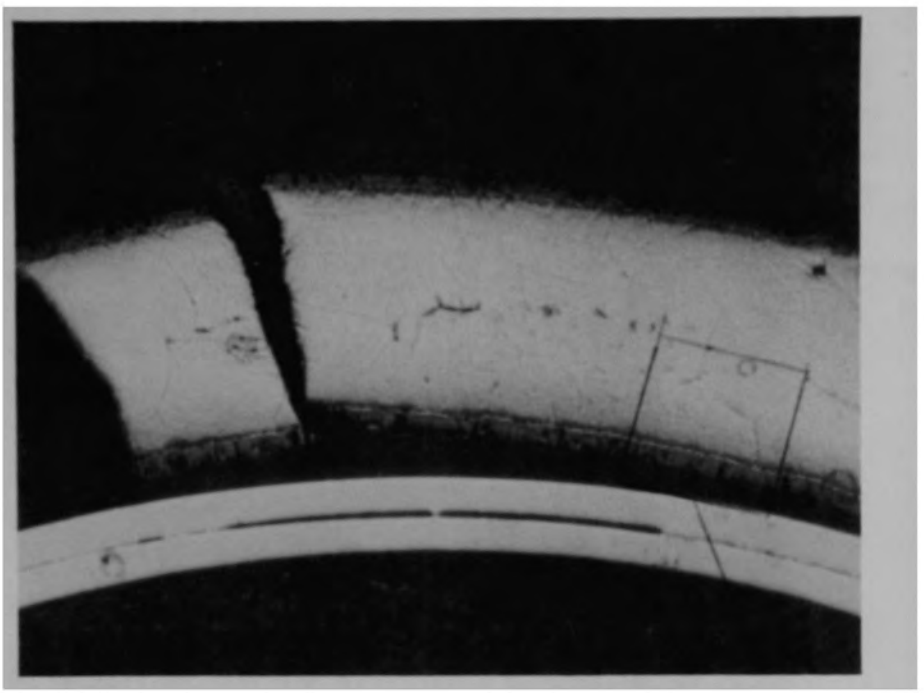

Figure C-115. Photomacrograph of Particle 6E (E9, 56 cm).

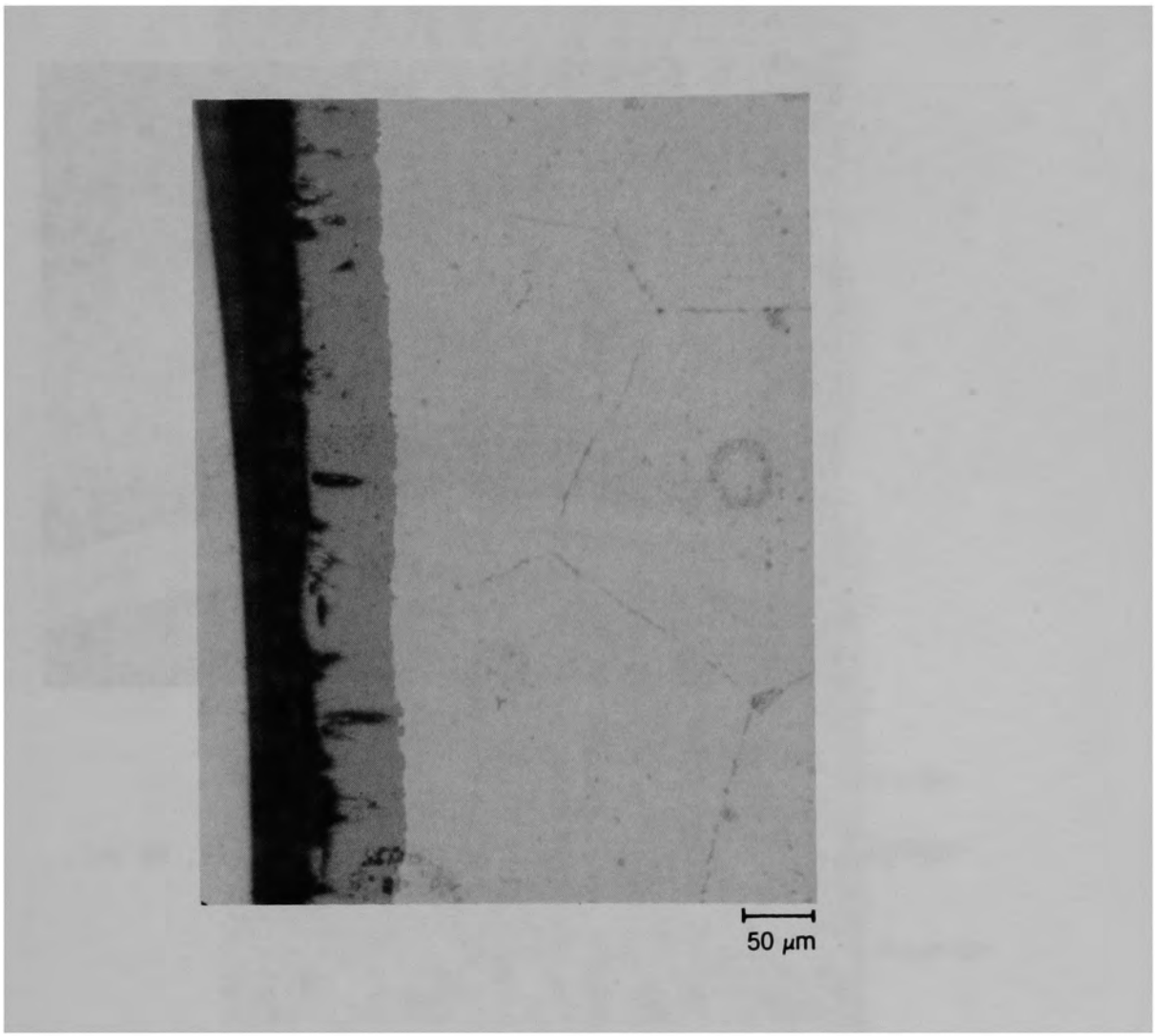

Figure C-116. Photomicrograph of material from area A of Particle 6E (E9, 56 cm).

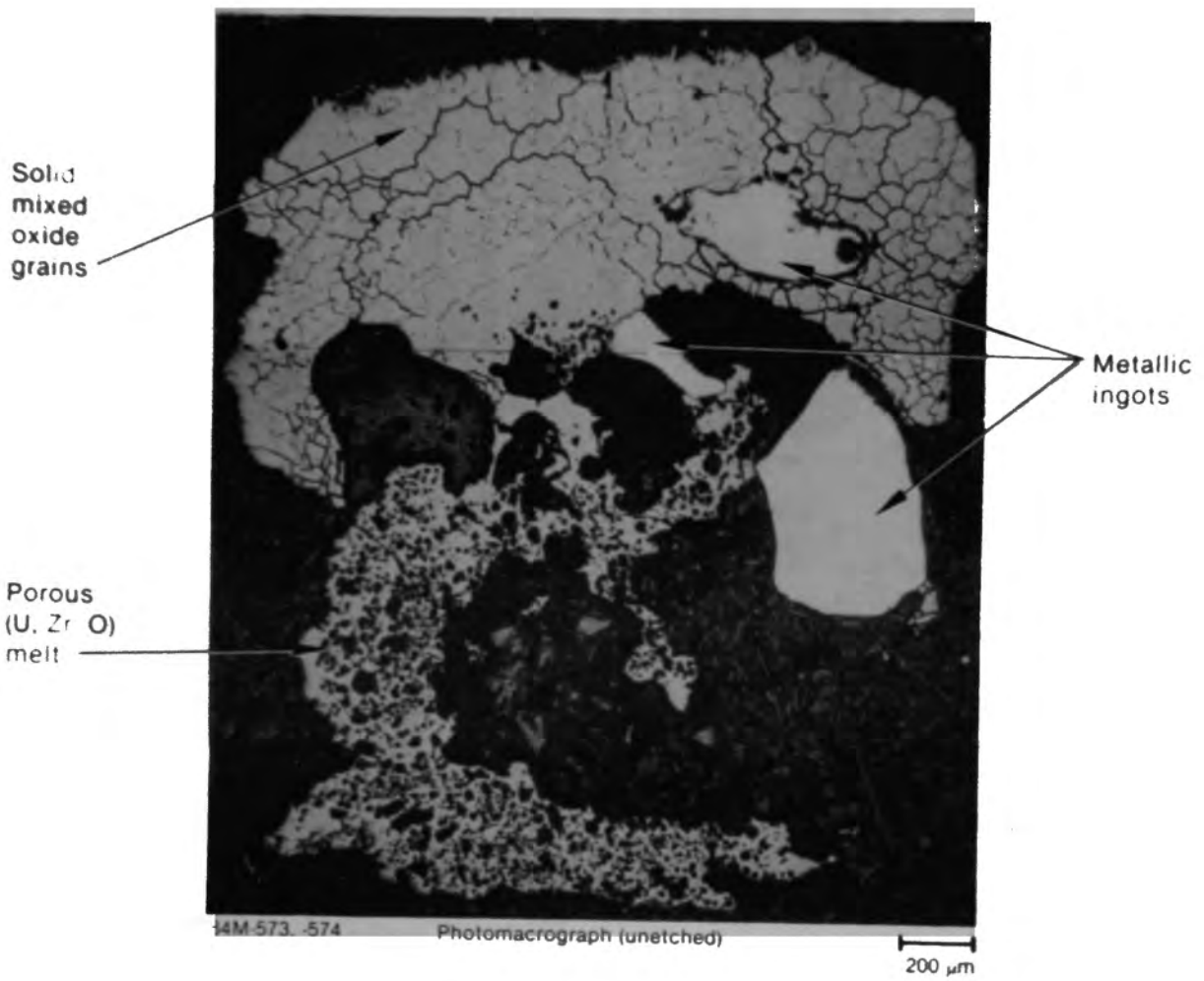

Figure C-117. Particle 6F from 56 cm of E9 position. An agglomerate of porous and solid (U, Zr, O) melts, both highly oxidized and metallic, ferromagnetic ingots.

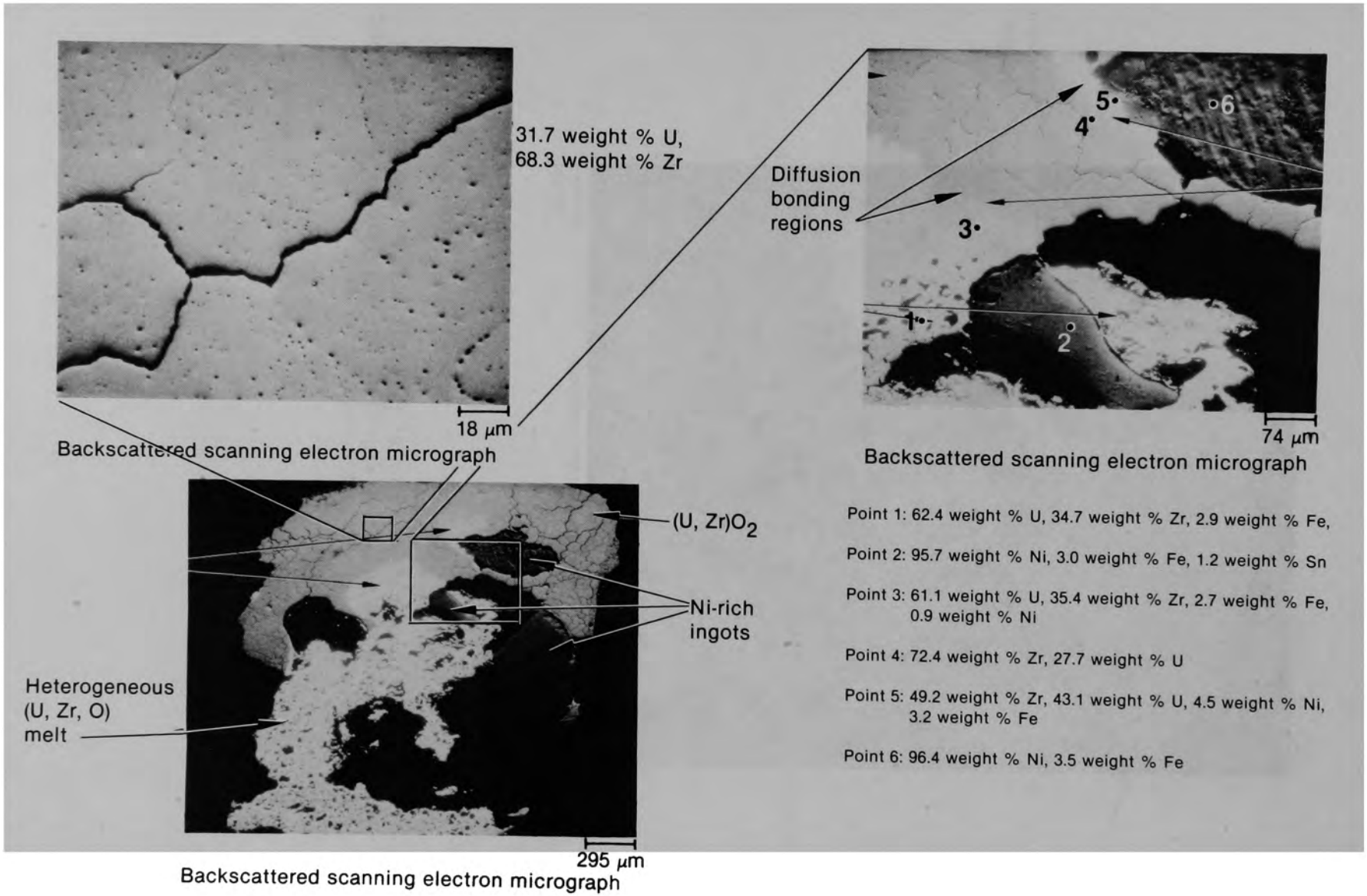

Figure C-118. Energy dispersive x-ray spectroscopy results on upper portion of Particle 6F.

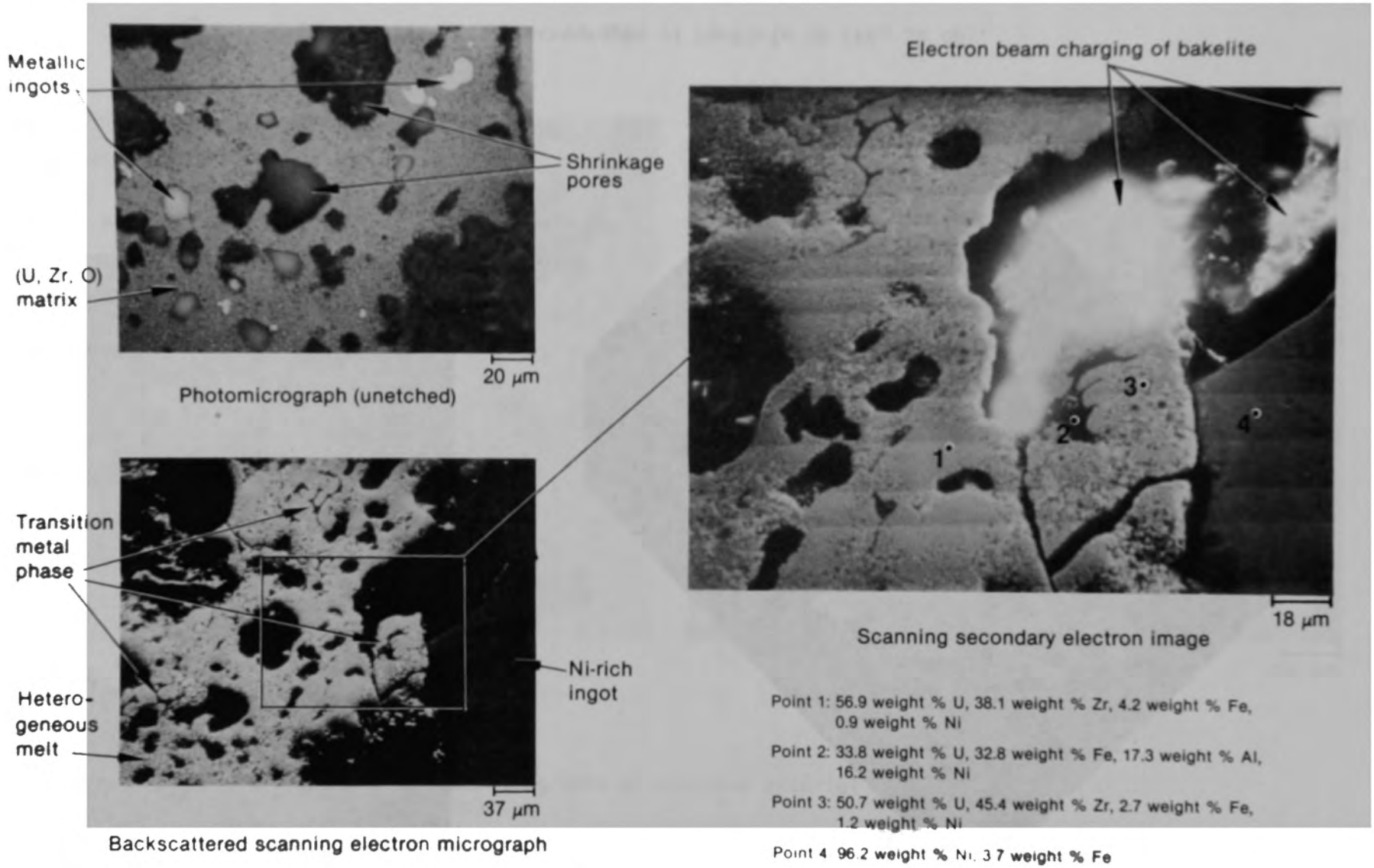

Figure C-119. Energy dispersive x-ray spectroscopy findings on the lower, hetergeneous melt region of Particle 6F.

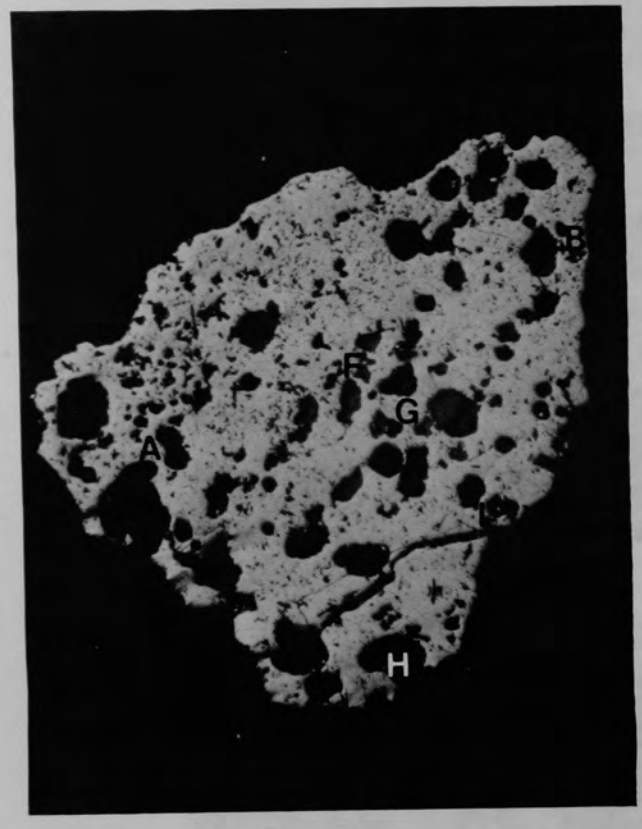

(a) Unetched

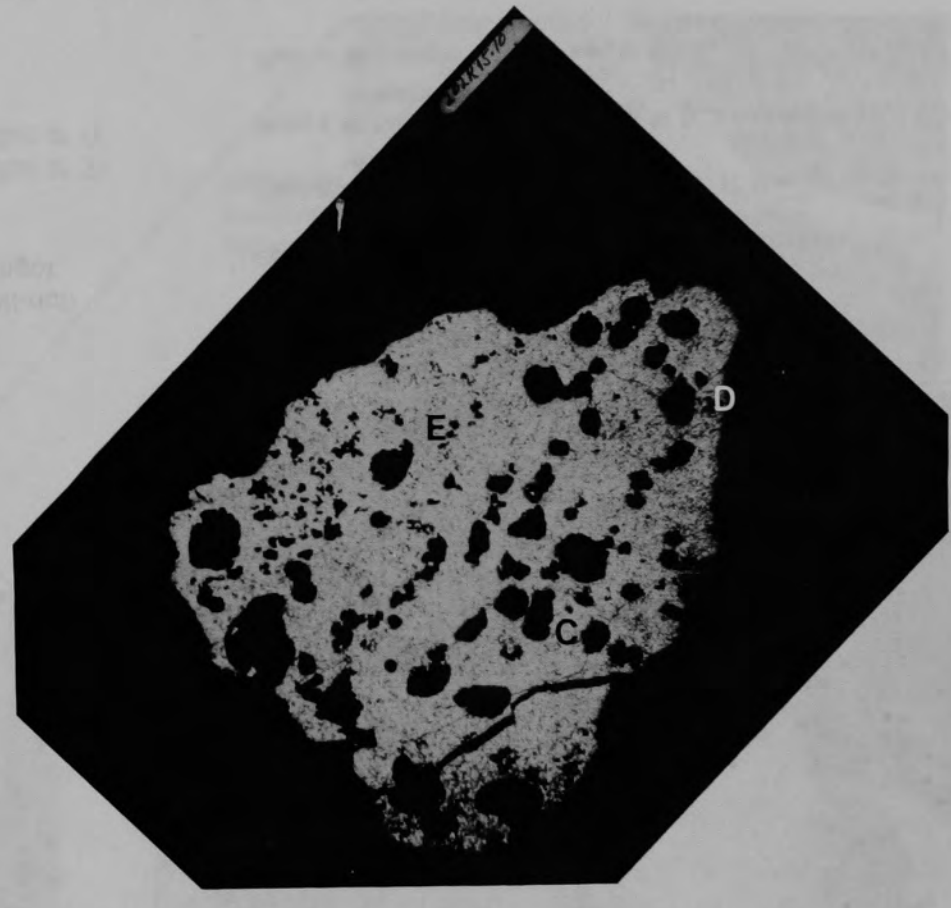

(b) Fuel etch

Figure C-120. Photomacrographs of Particle 7A (H8, 36 cm).

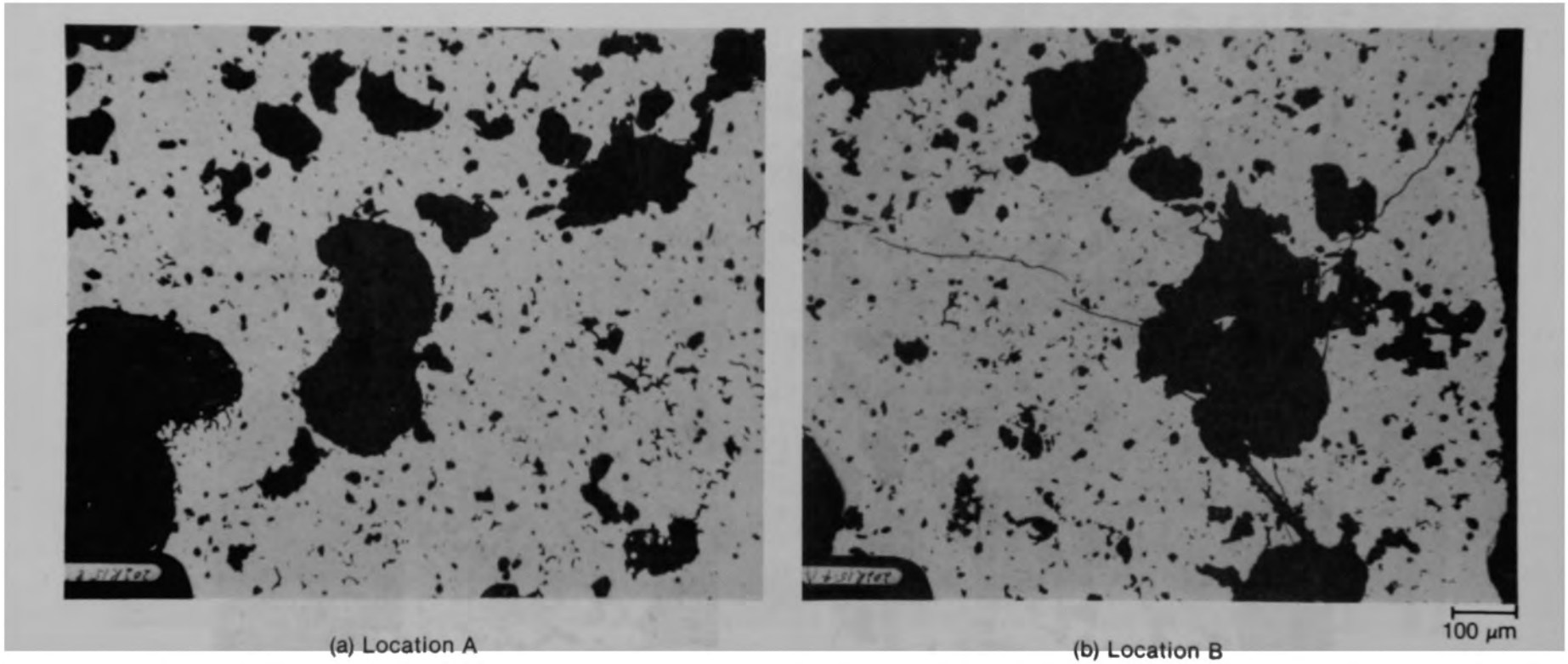

Figure C-121. Photomicrographs of unetched material from Particle 7A (H8, 36 cm).

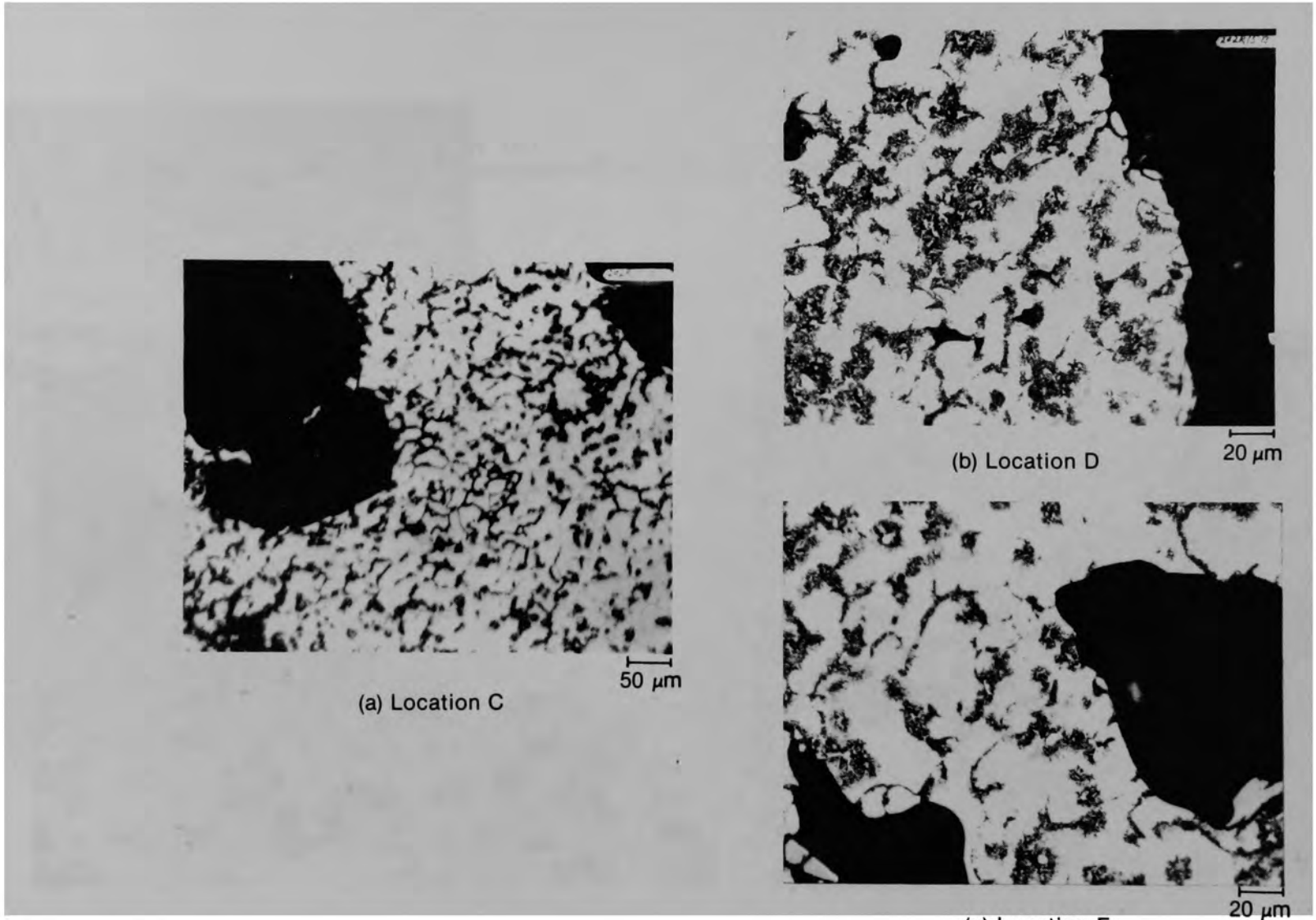

Figure C-122. Photomicrographs of etched material from Particle 7A (H8, 36 cm).

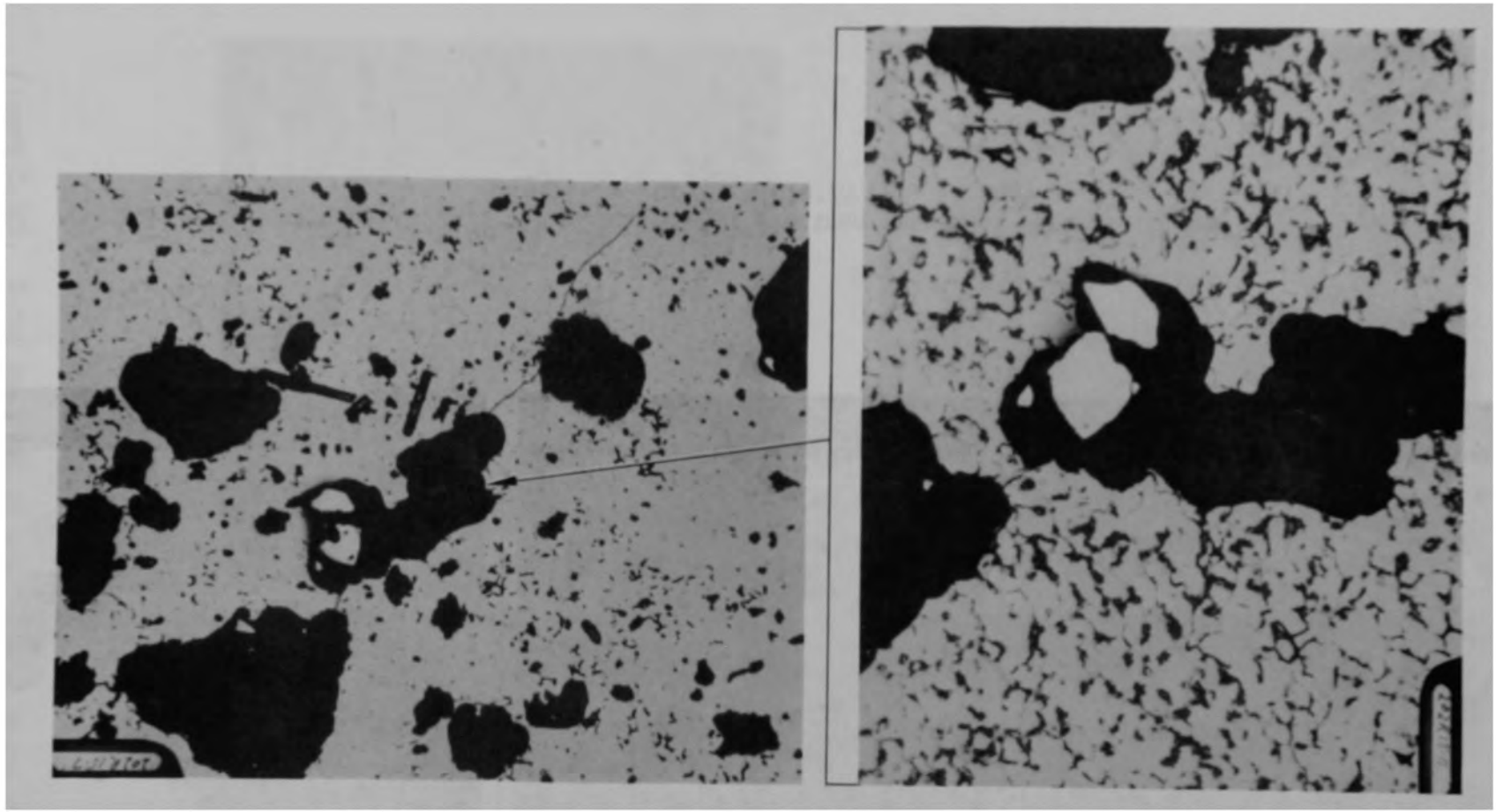

(a) Unetched

(b) Etched

Figure C-123. Photomicrographs of material from Location F of Particle 7A (H8, 36 cm).

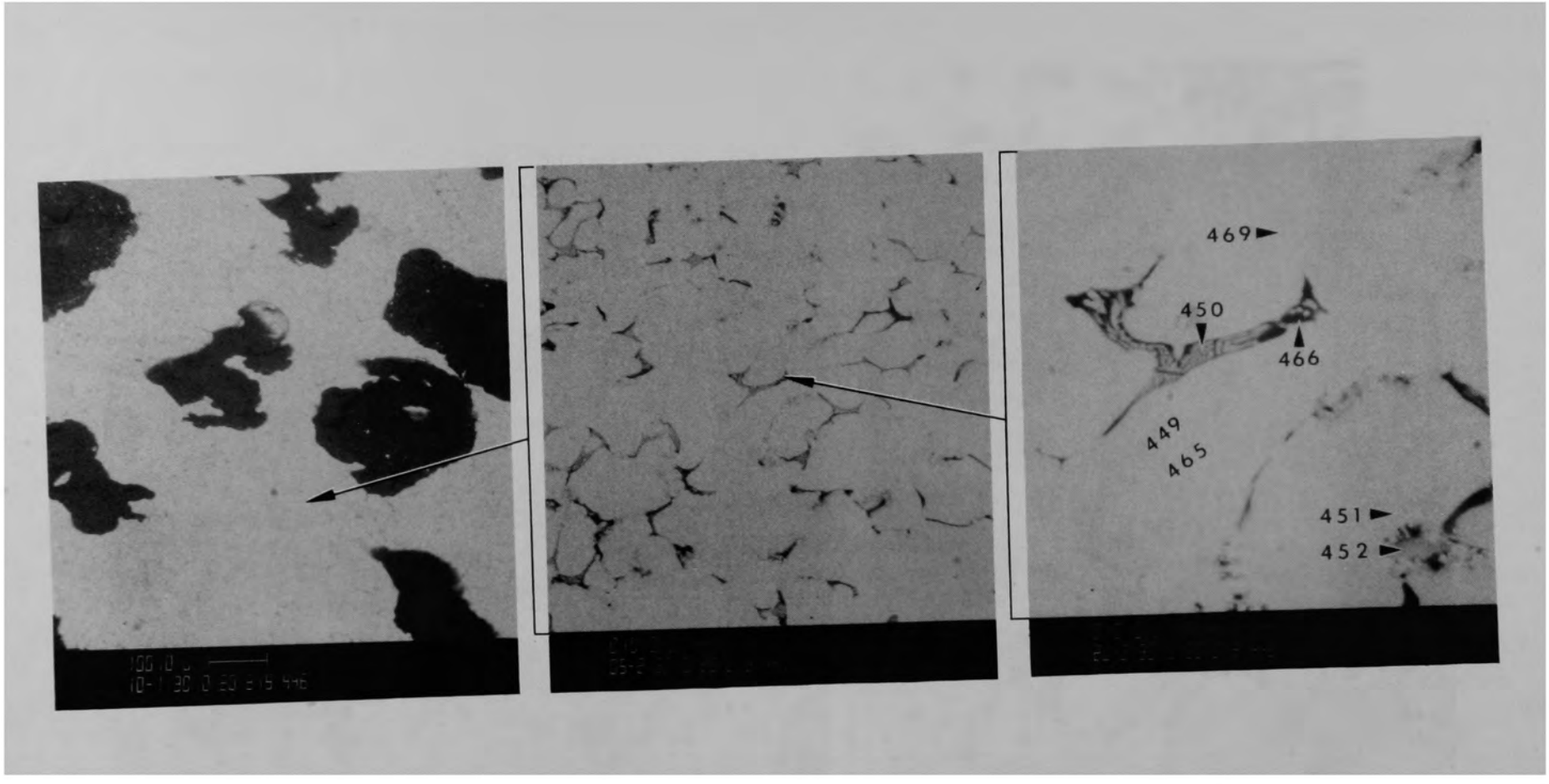

Figure C-124. SEM backscattered electron images of material from location G of Particle 7A (H8, 36 cm).

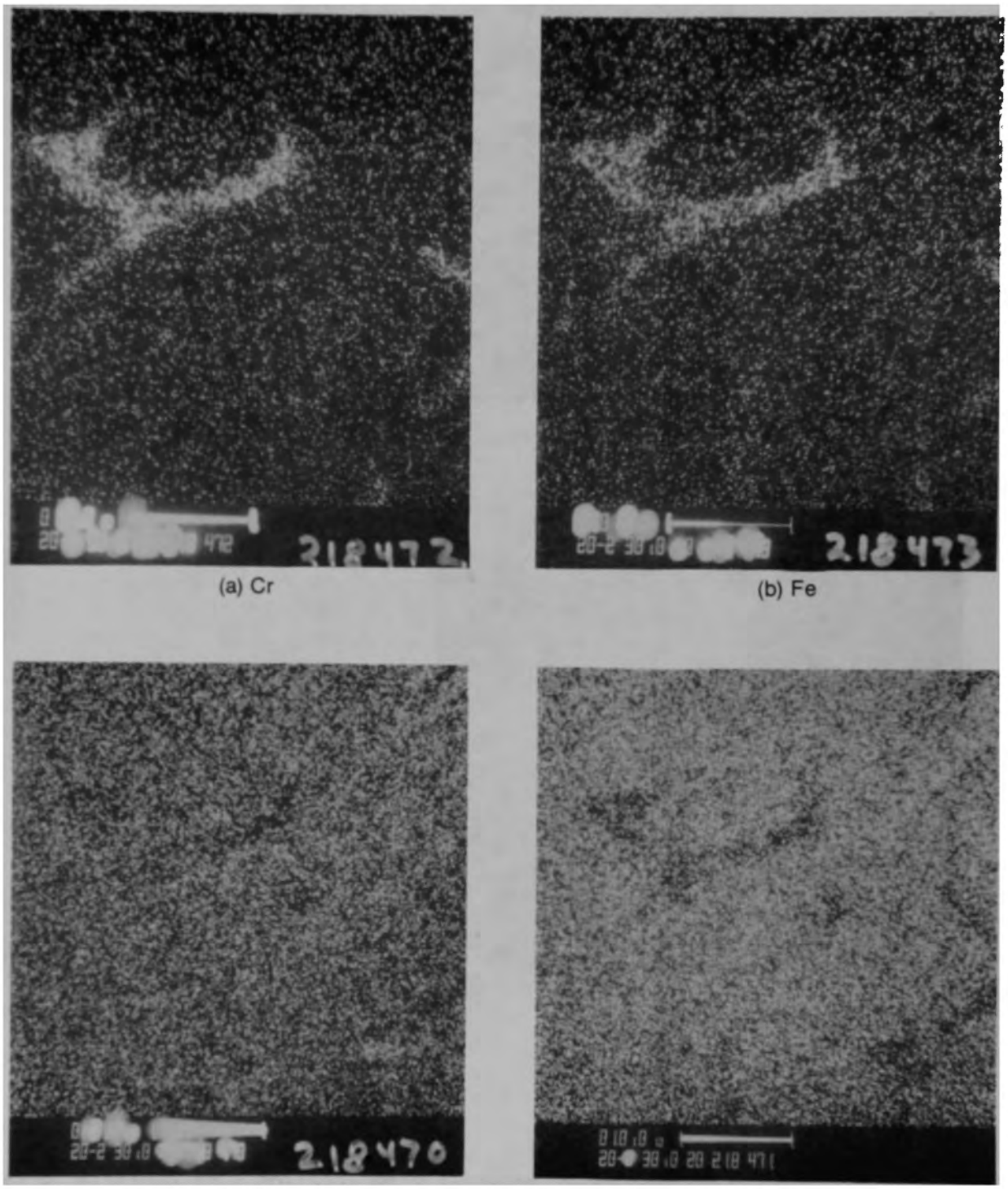

Figure C-125. X-ray dot maps of second phase material in location G of Particle 7A (H8, 36 cm).

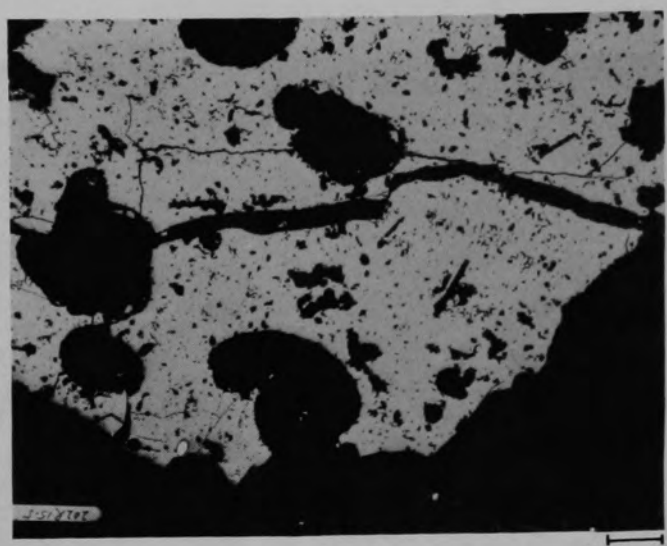

(a) Photomicrograph

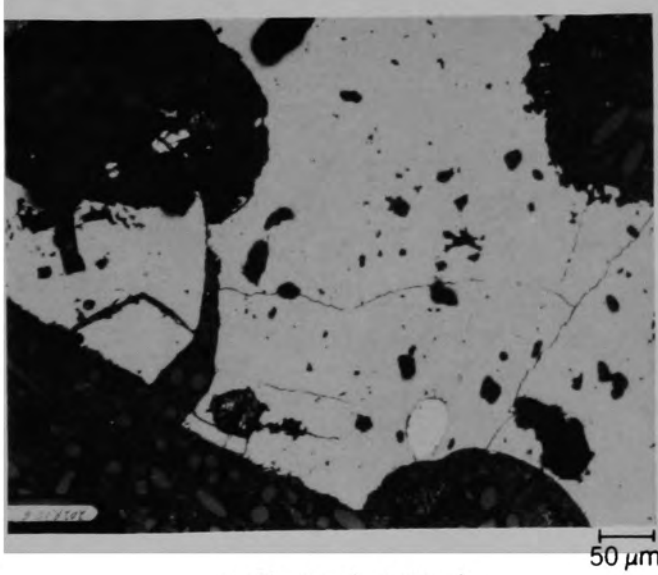

(b) Photomicrograph

(c) SEM backscattered electron image

Figure C-126. Photographs of material from location H of Particle 7A (H8, 36 cm).

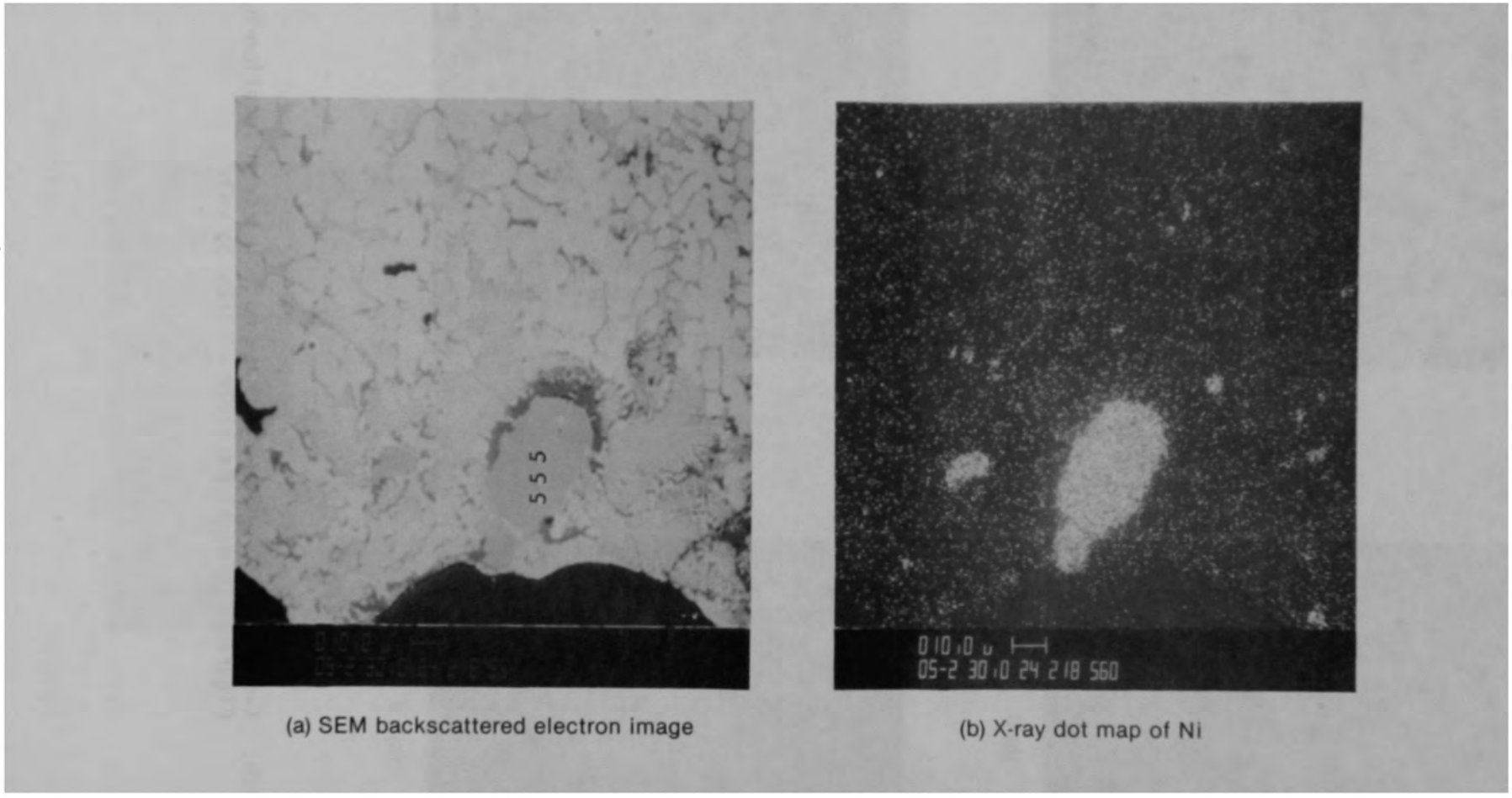

(a) SEM backscattered electron image

(b) X-ray dot map of Ni

Figure C-127. Photographs of material from location H of Particle 7A (H8, 36 cm).

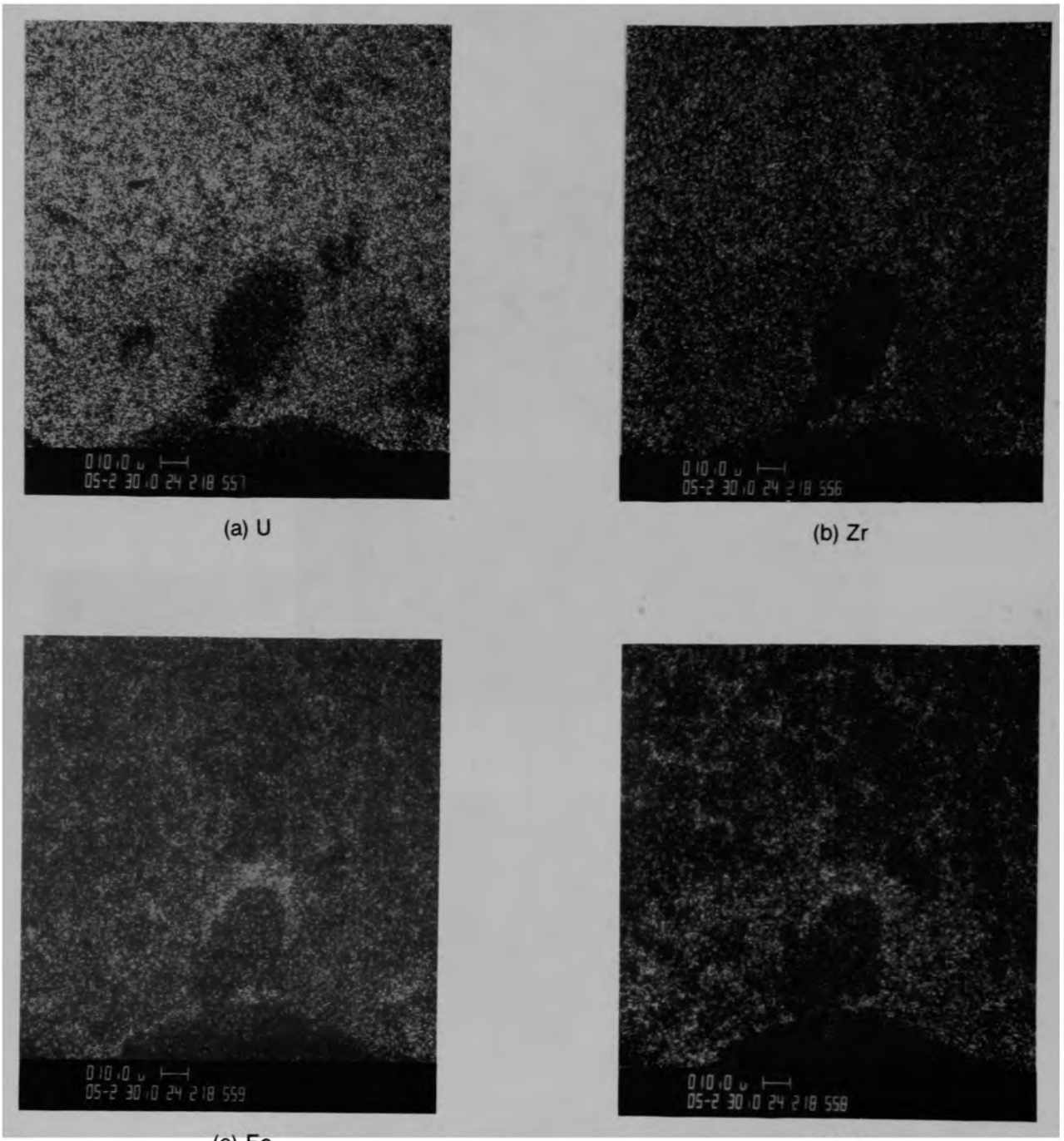

Figure C-128. X-ray dot map of second phase material from location H, Figure C-127a, of Particle 7A (H8, 36 cm).

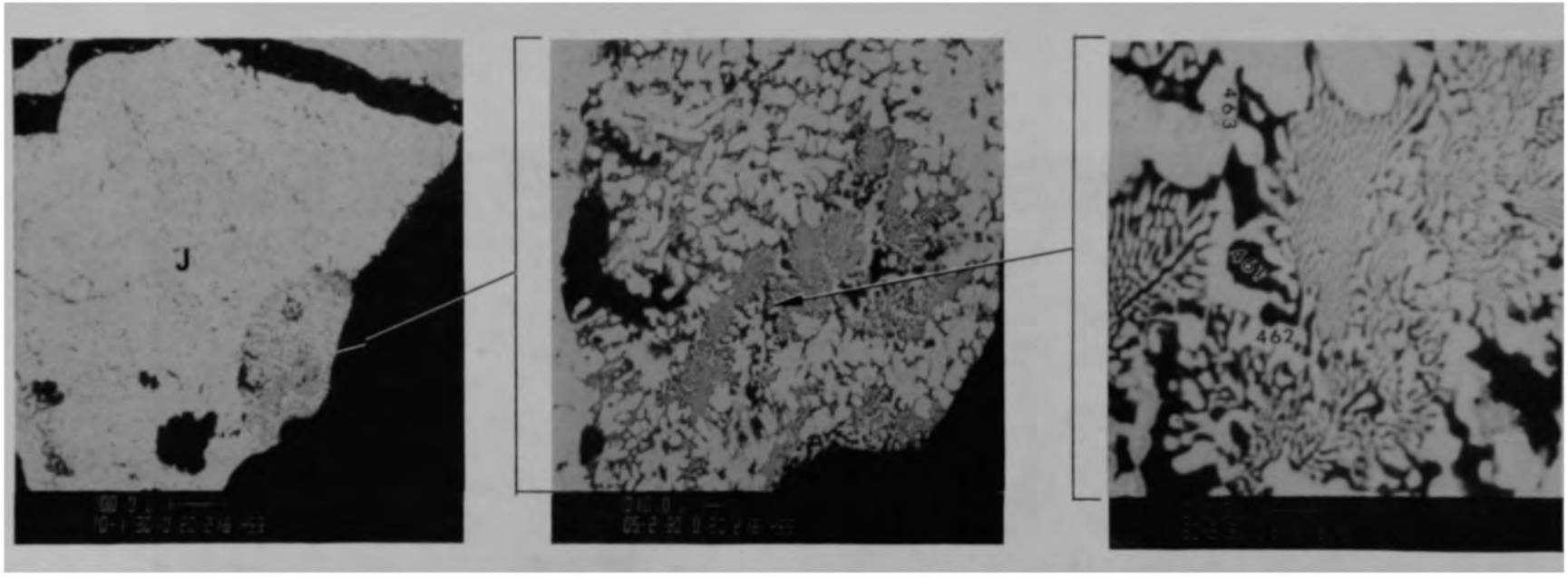

Figure C-129. SEM backscattered electron images of material from location I of Particle 7A (H8, 36 cm).

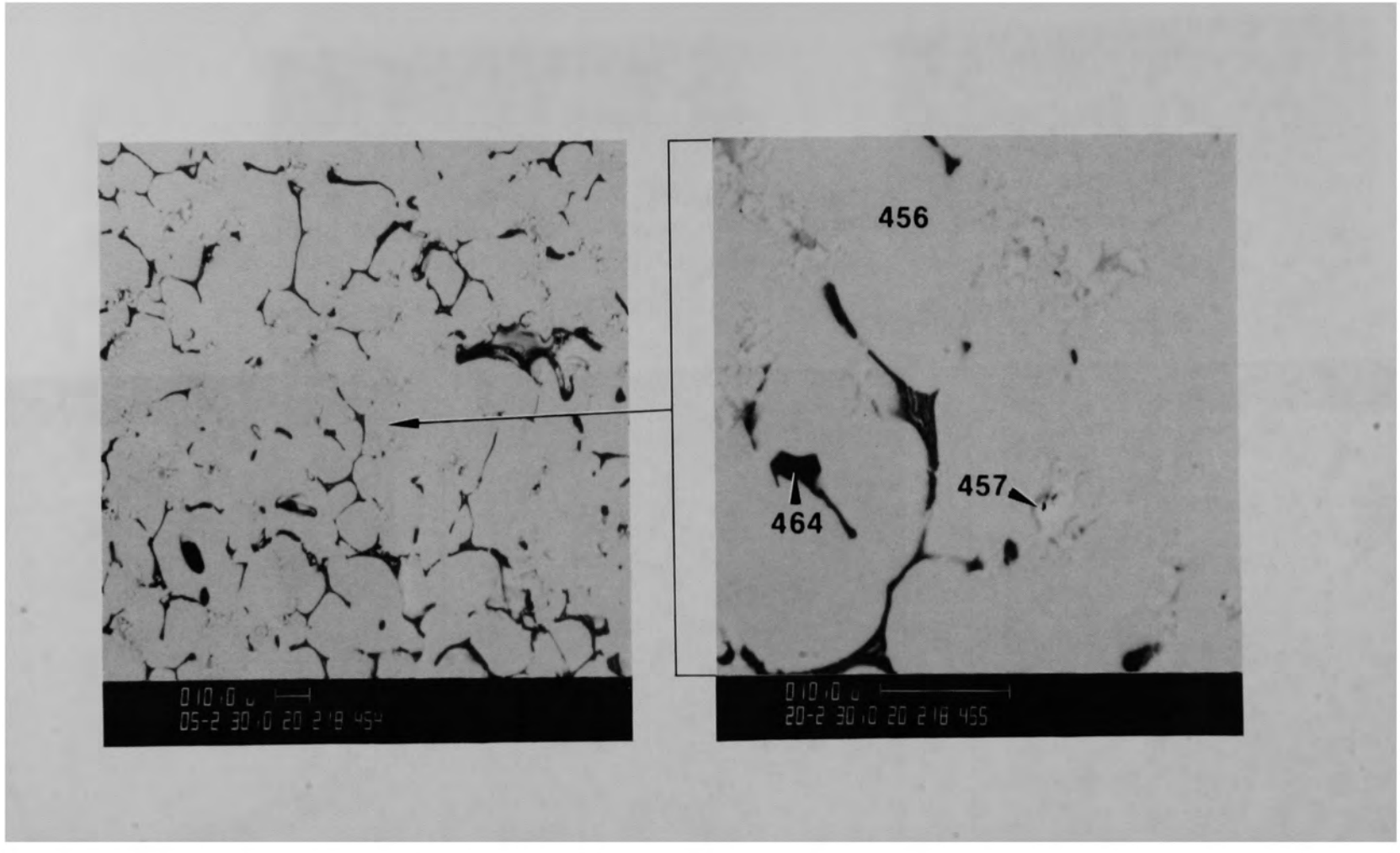

Figure C-130. SEM backscattered electron images of material from location J, Figure C-129, of Particle 7A (H8, 36 cm).

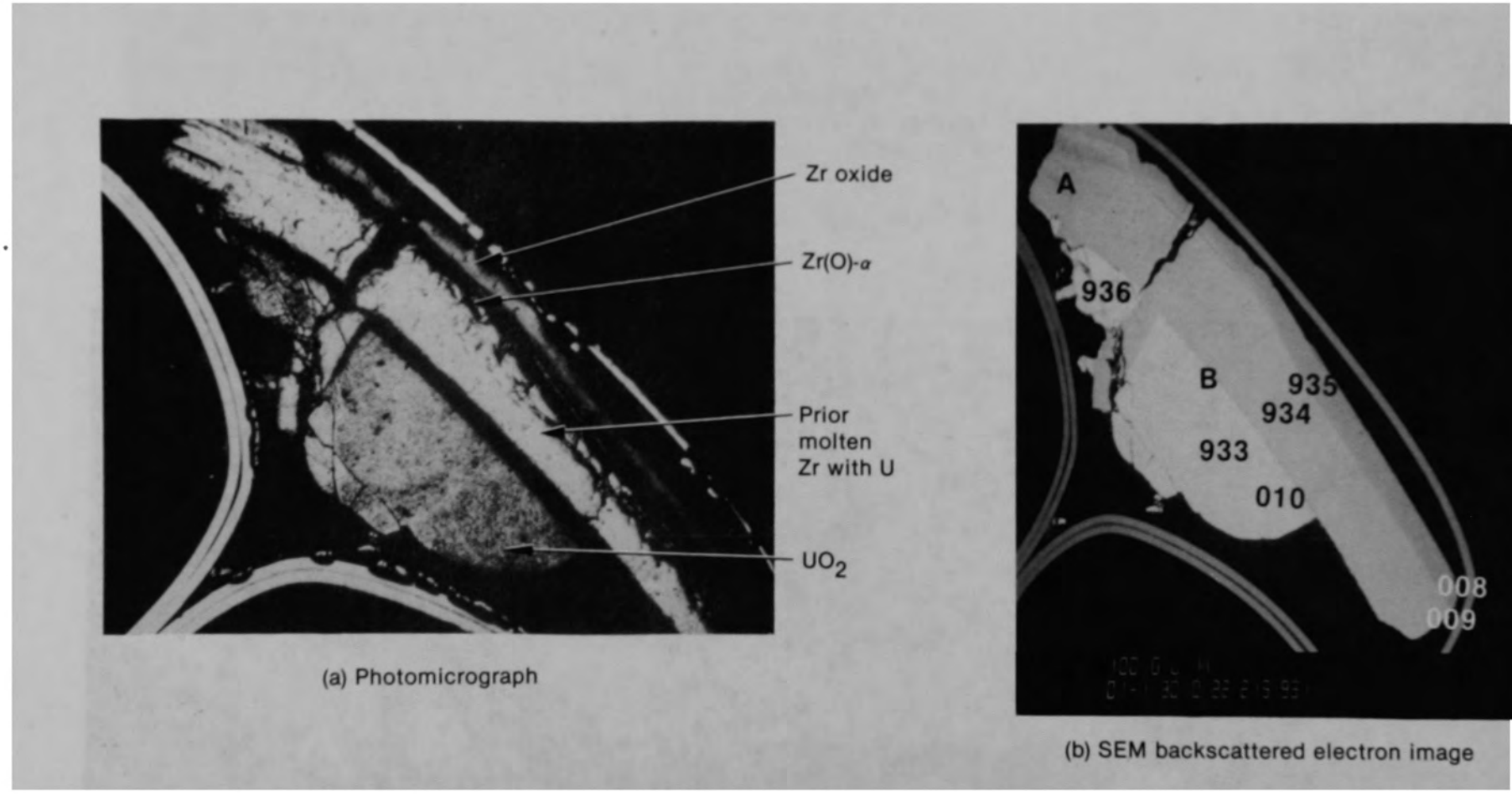

Figure C-131. Photographs of Particle 7B (H8, 36 cm).

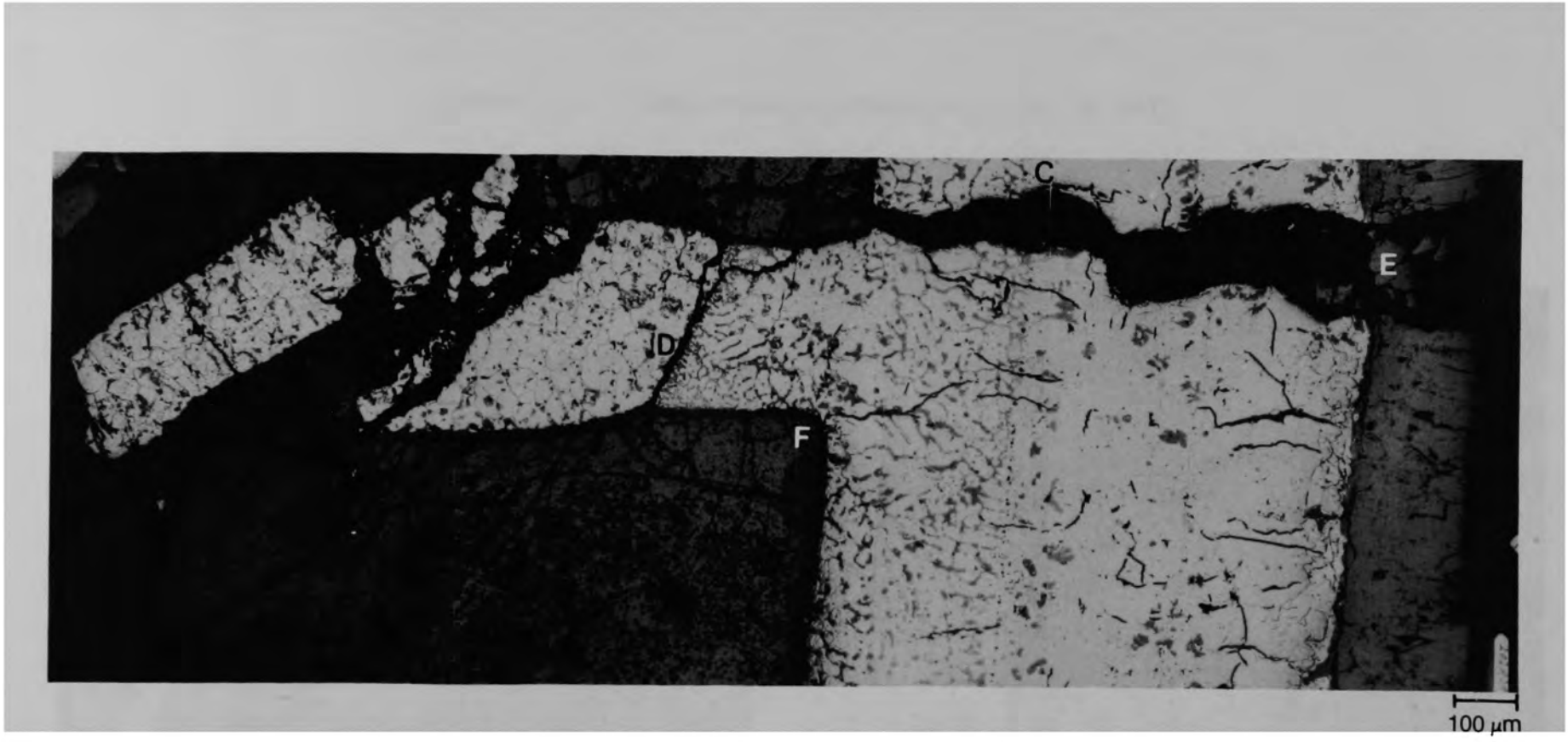

Figure C-132. Photomicrographs of prior molten material in cladding gap and fuel crack of Particle 7B (H8, 36 cm).

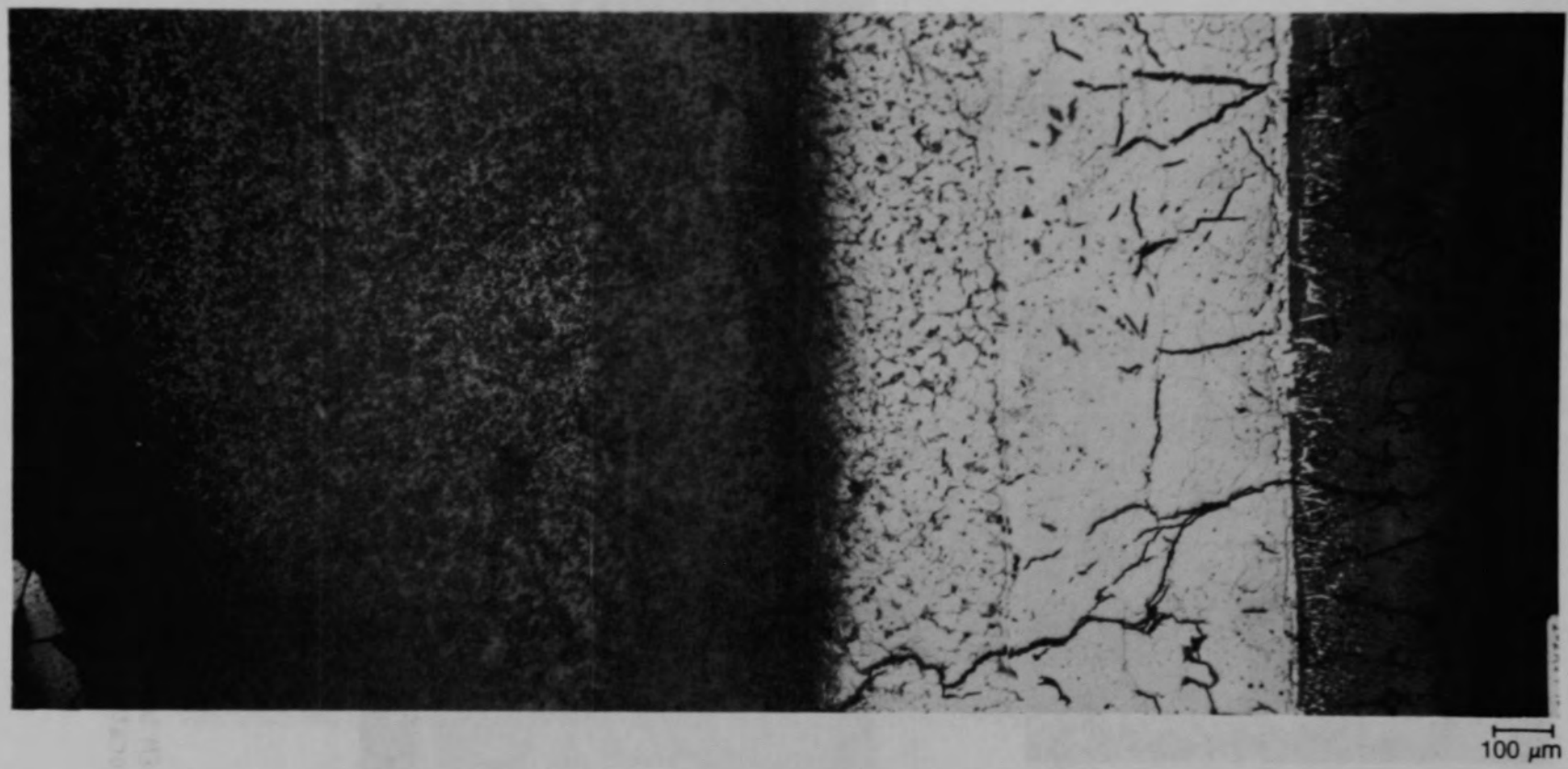

Figure C-133. Photomicrographs of cladding in Particle 7B (H8, 36 cm).

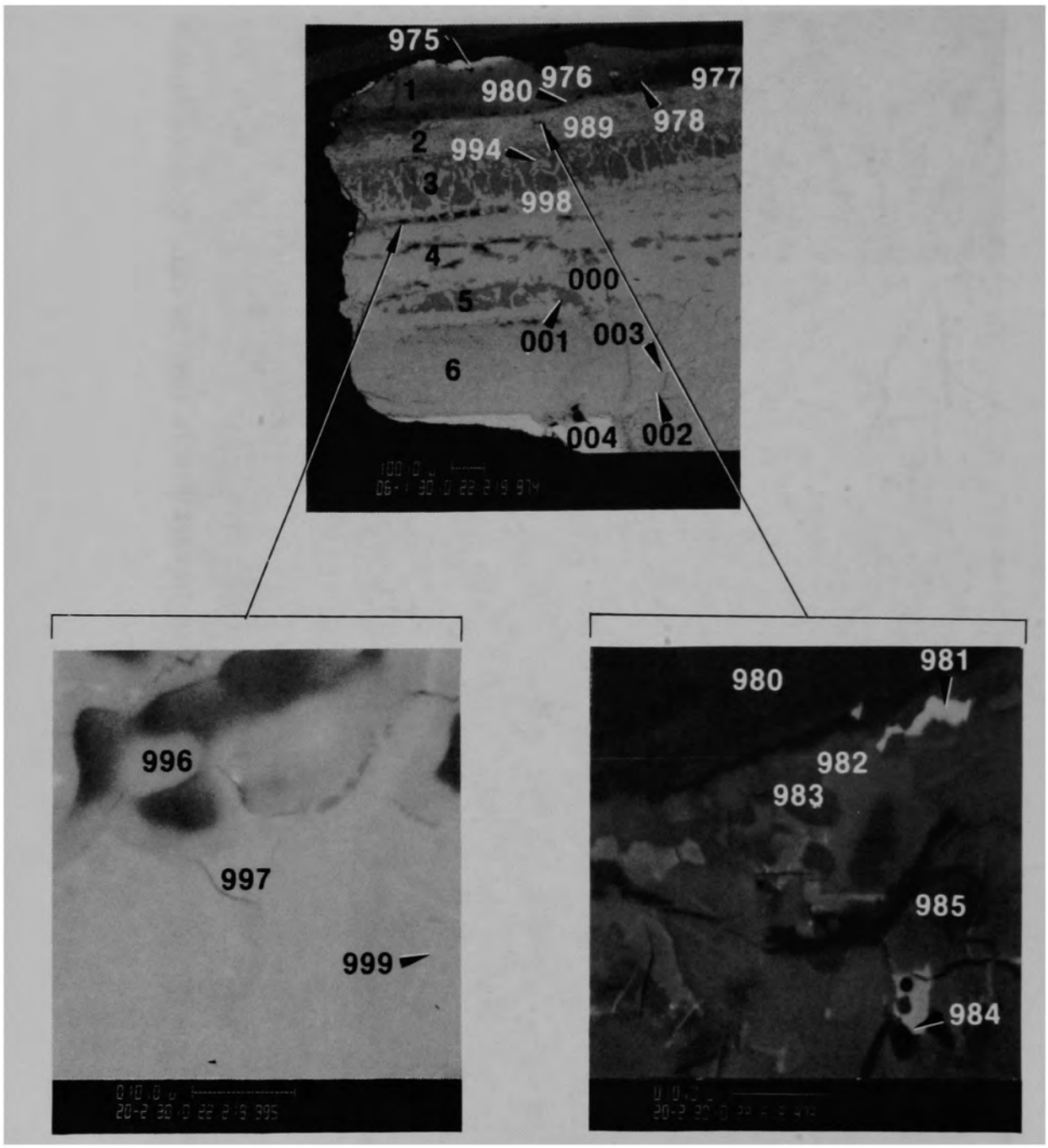

Figure C-134. SEM backscattered electron images of material from location A of Particle 7B (H8, 36 cm).

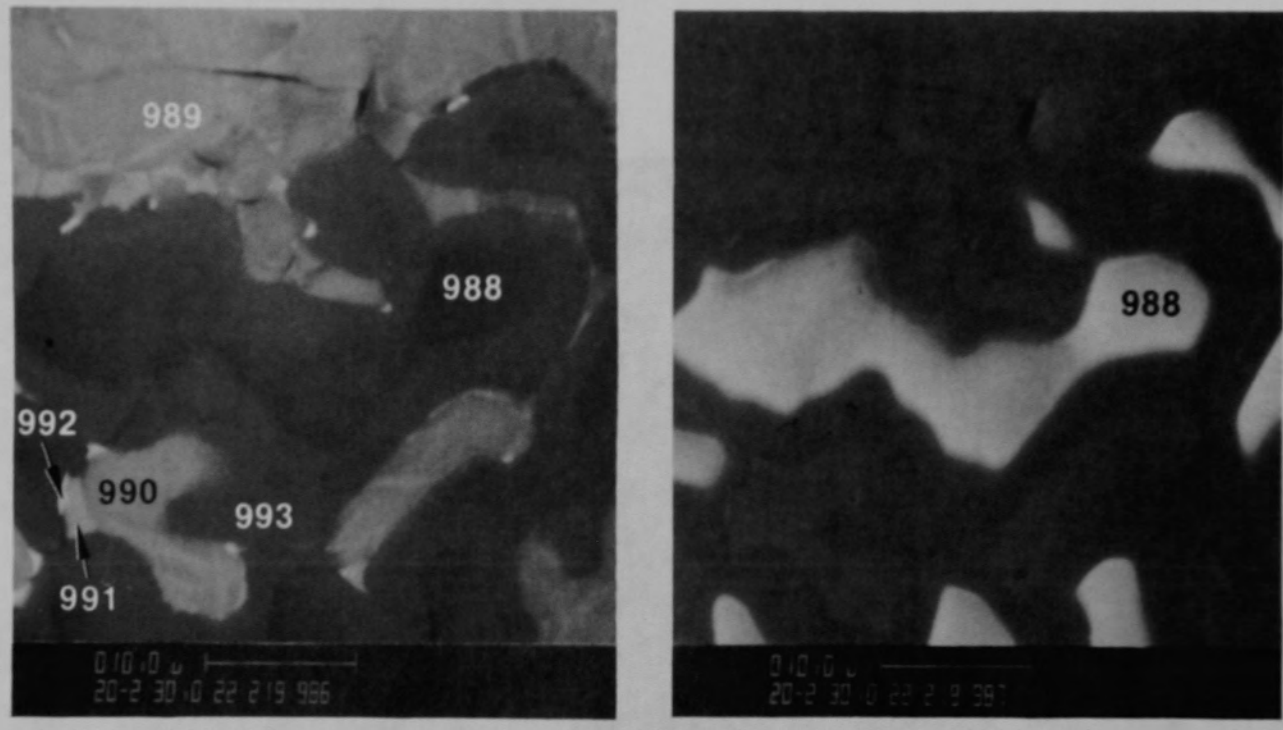

(a) Backscattered electron image

(b) Secondary electron image

Figure C-135. SEM images of interface between first and second layers in location A for Particle 7B (H8, 36 cm).

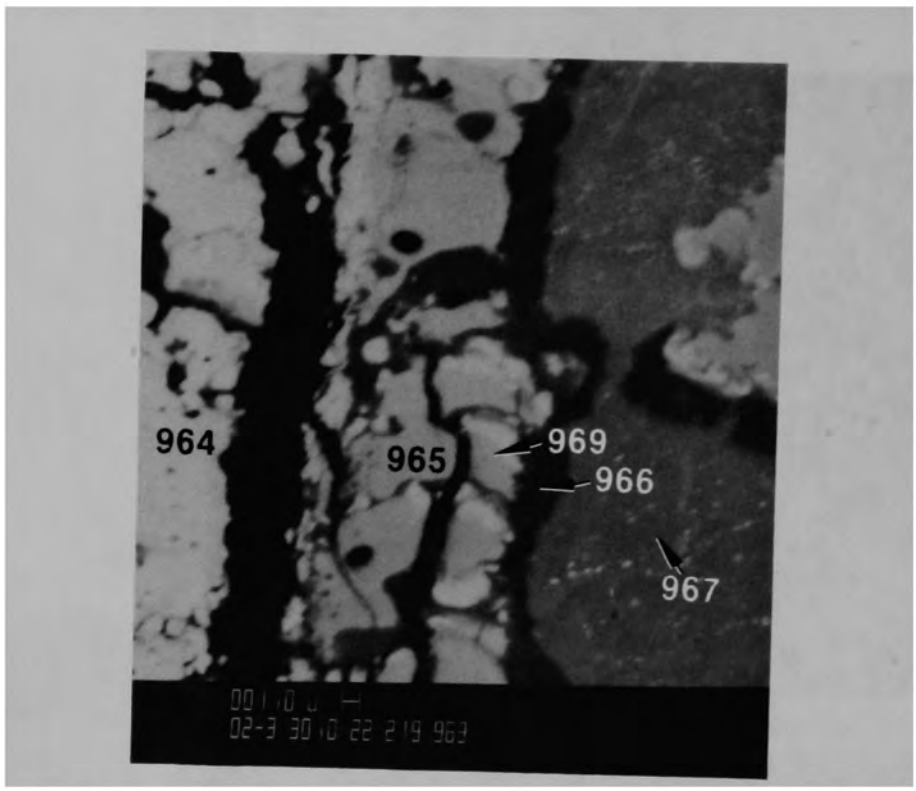

Figure C-136. SEM backscattered electron image of material from location B of Particle 7B (H8, 36 cm).

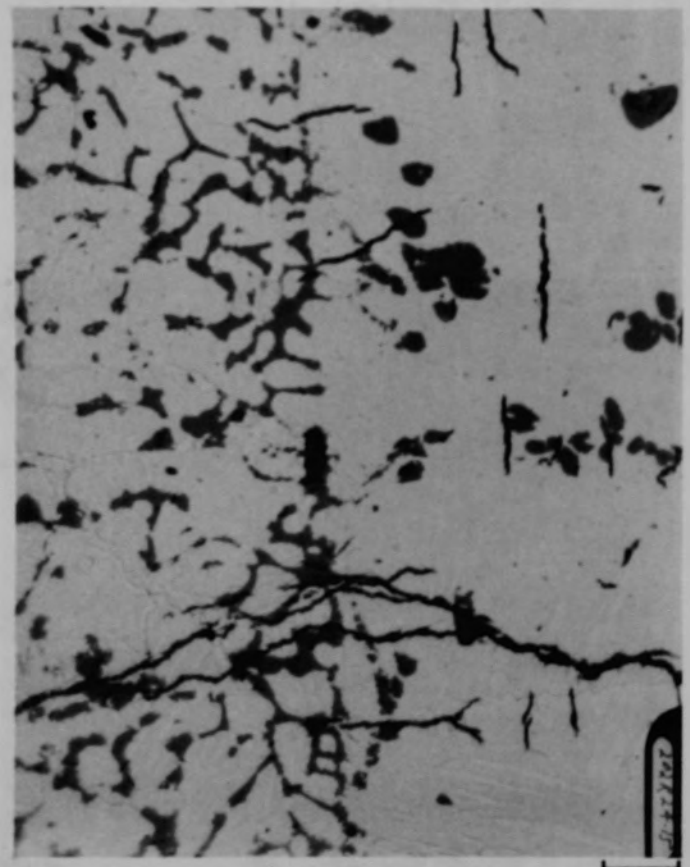

(a) Photomicrograph

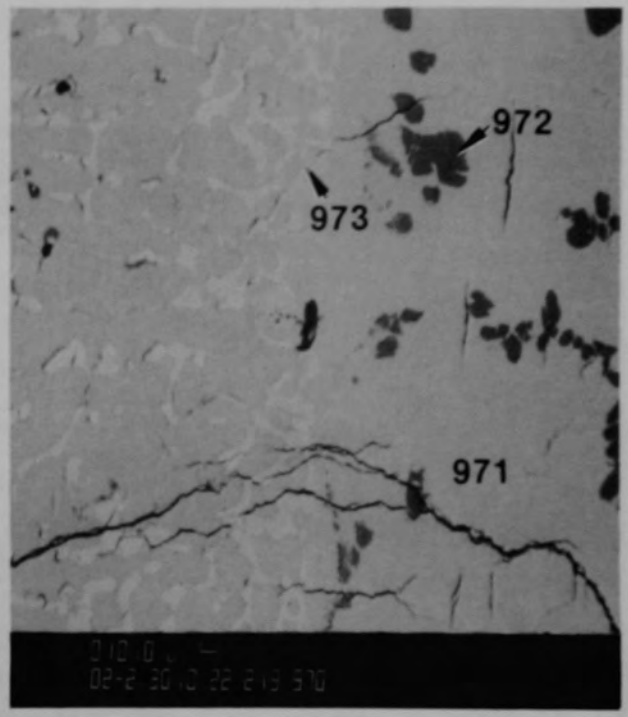

(b) SEM backscattered electron image

Figure C-137. Photographs of material from location C, Figure C-132, of Particle 7B (H8, 36 cm).

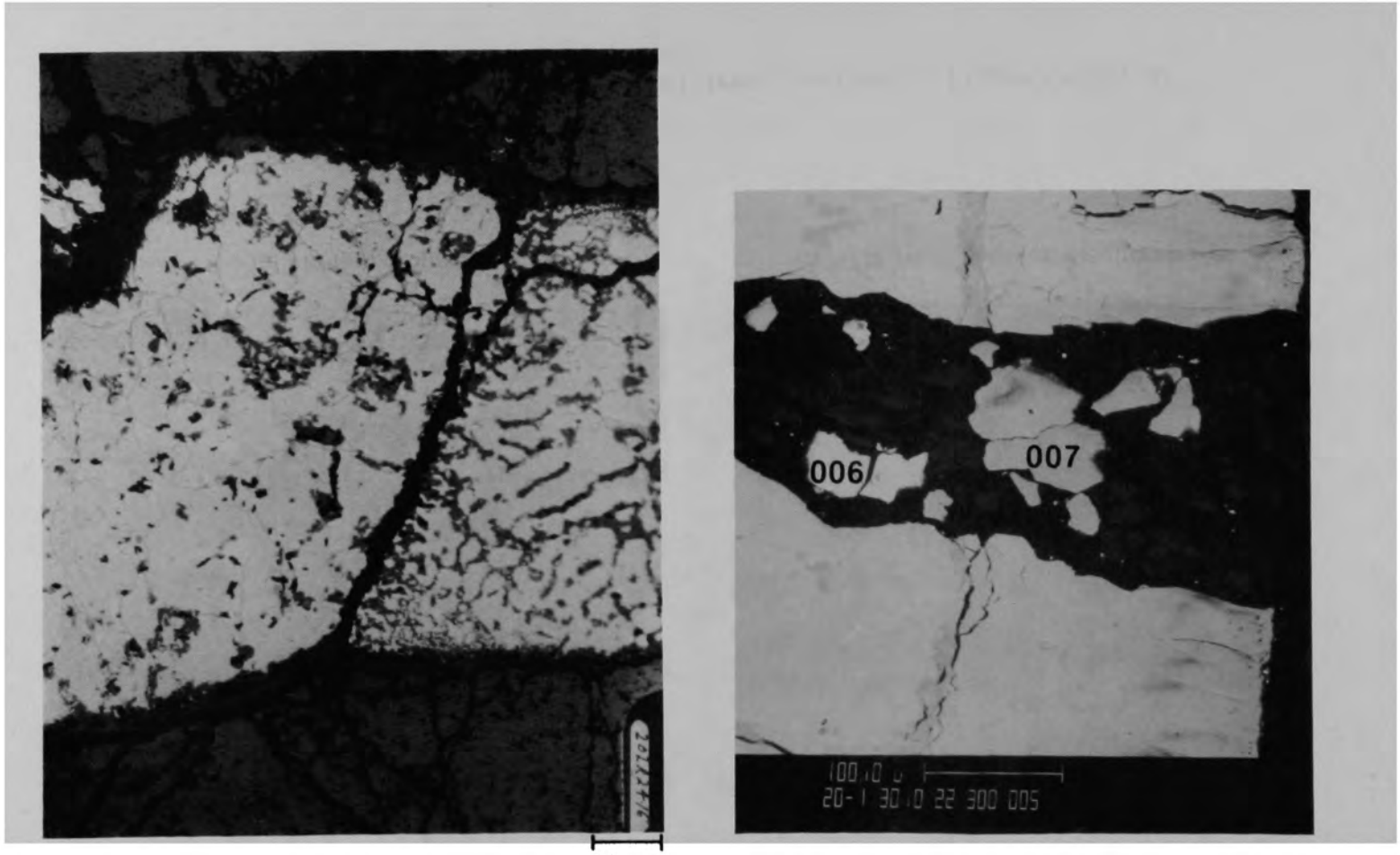

(a) Photomicrograph of location D

(b) SEM backscattered electron image of location E

Figure C-138. Photographs of material in crack shown in Figure C-132 of Particle 7B (H8, 36 cm).

(a) Photomicrograph

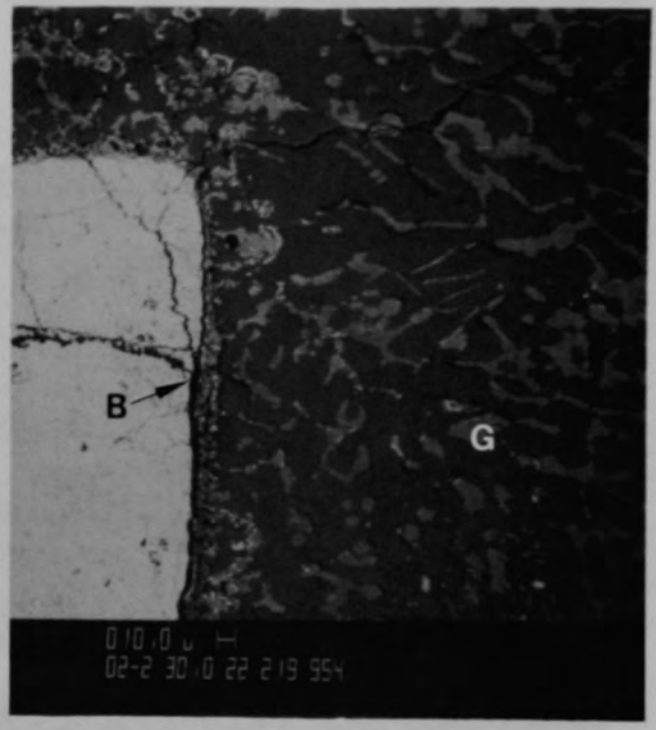

(b) SEM backscattered electron image

Figure C-139. Photographs of material from location F, Figure C-132, of Particle 7B (H8, 36 cm).

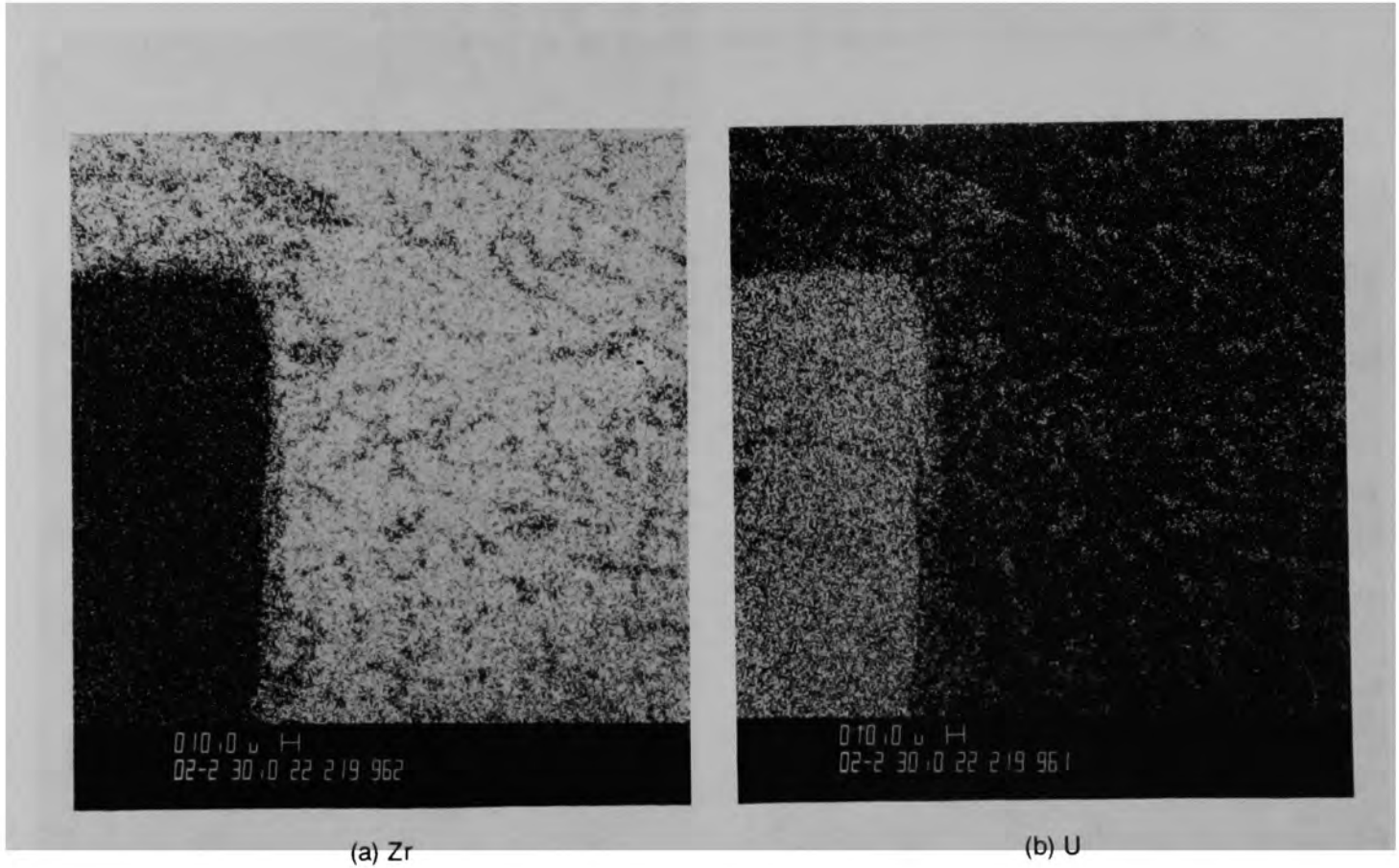

Figure C-140. X-ray dot map of material from location F, Figure C-132, of Particle 7B (H8, 36 cm).

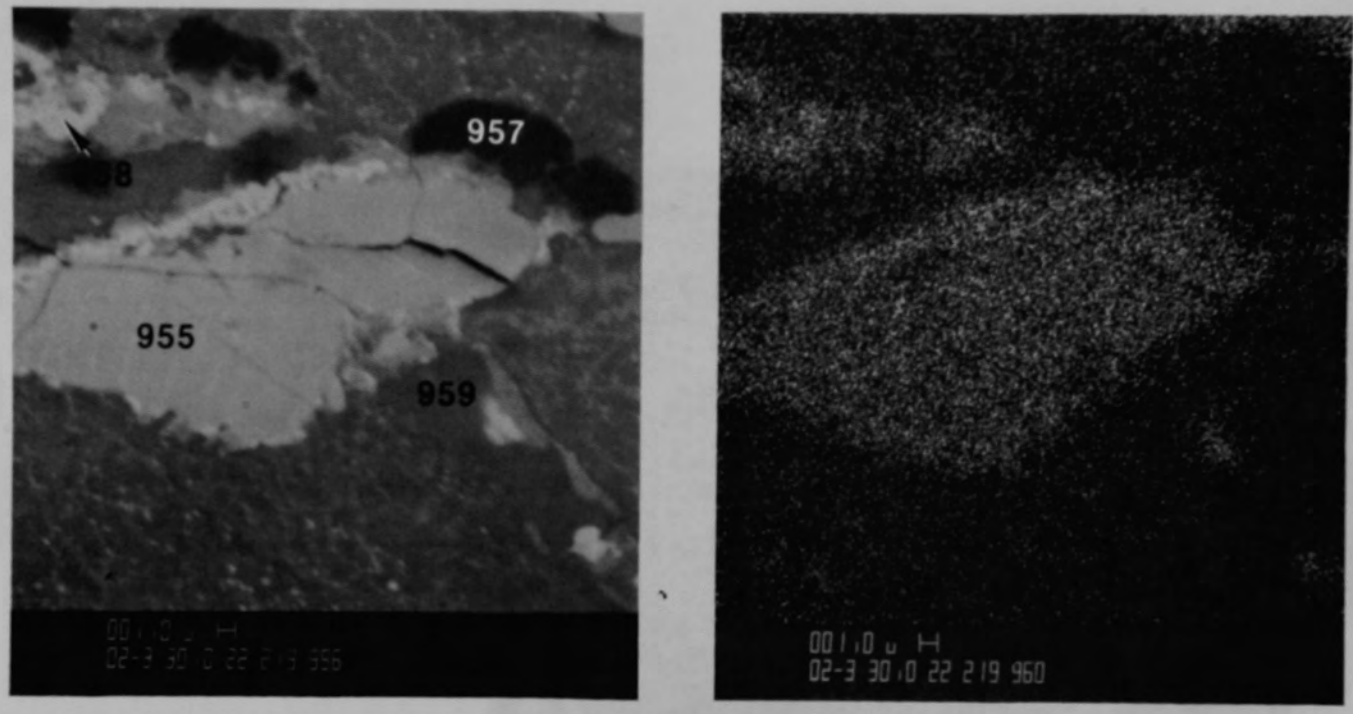

(a) SEM backscattered electron image

(b) X-ray dot map of U

Figure C-141. Photographs of material from location G, Figure C-139, of Particle 7B (H8, 36 cm).

Figure C-142. Photomacrograph of Particle 7E (H8, 36 cm).

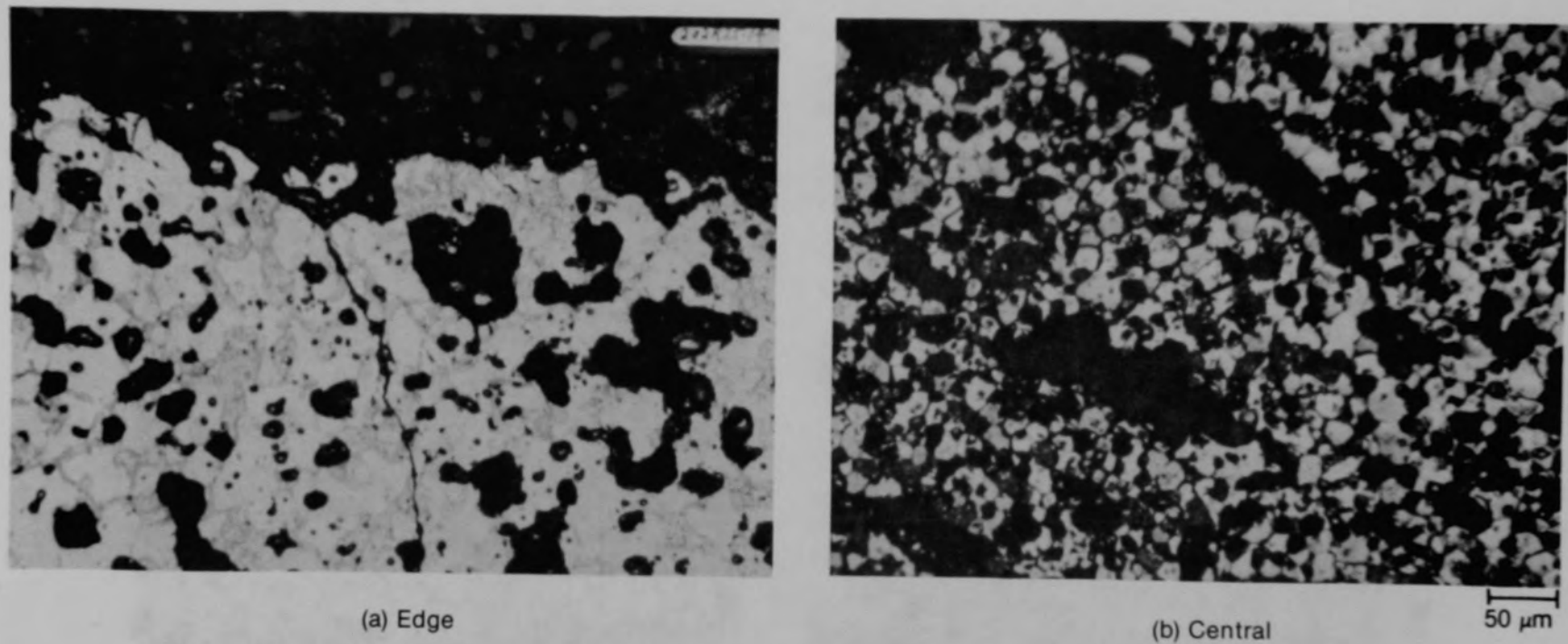

Figure C-143. Photomicrograph of etched material from Particle 7E (H8, 36 cm).

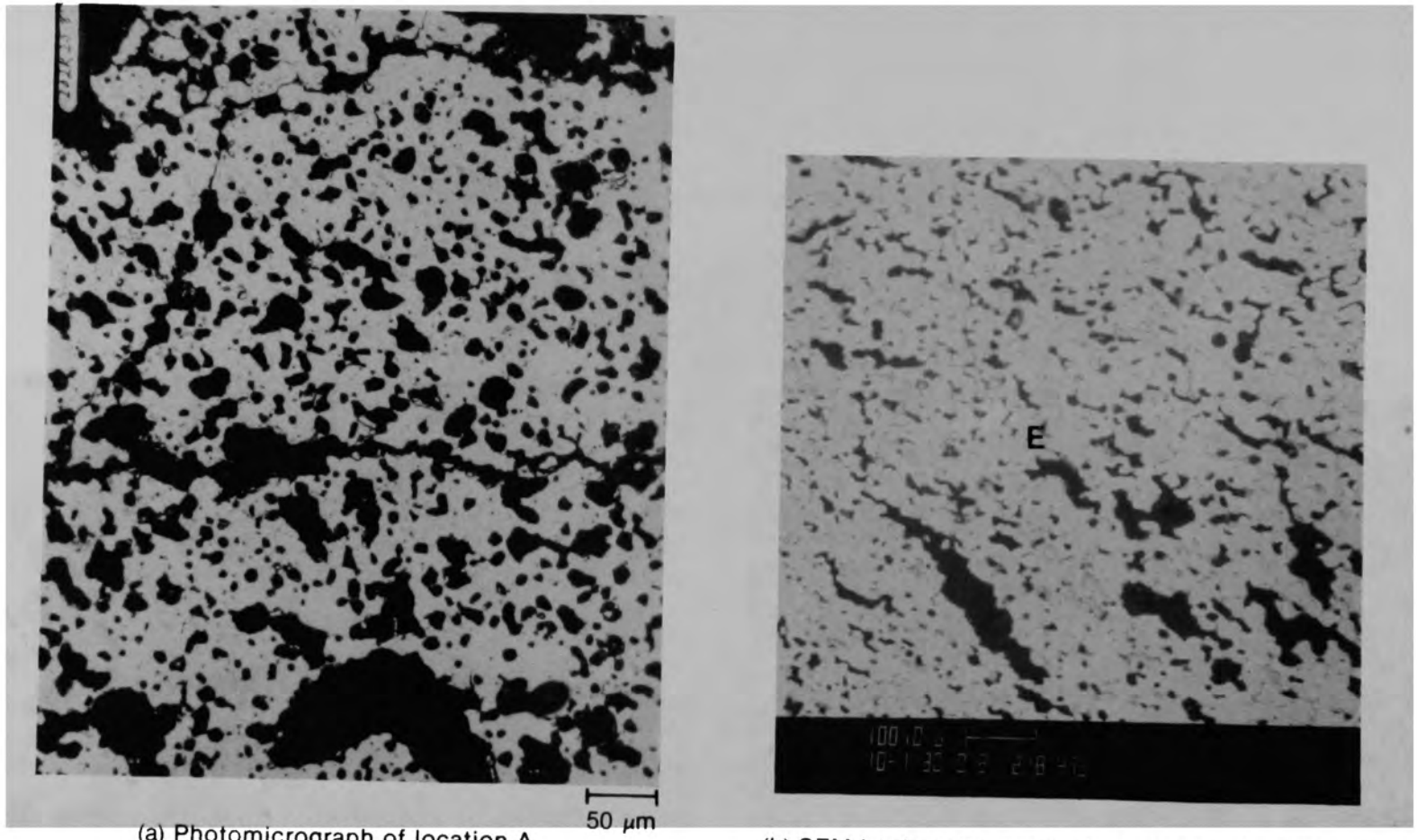

(a) Photomicrograph of location A

(b) SEM backscattered electron image of location B

Figure C-144. Photographs of material near center of Particle 7E (H8, 36 cm).

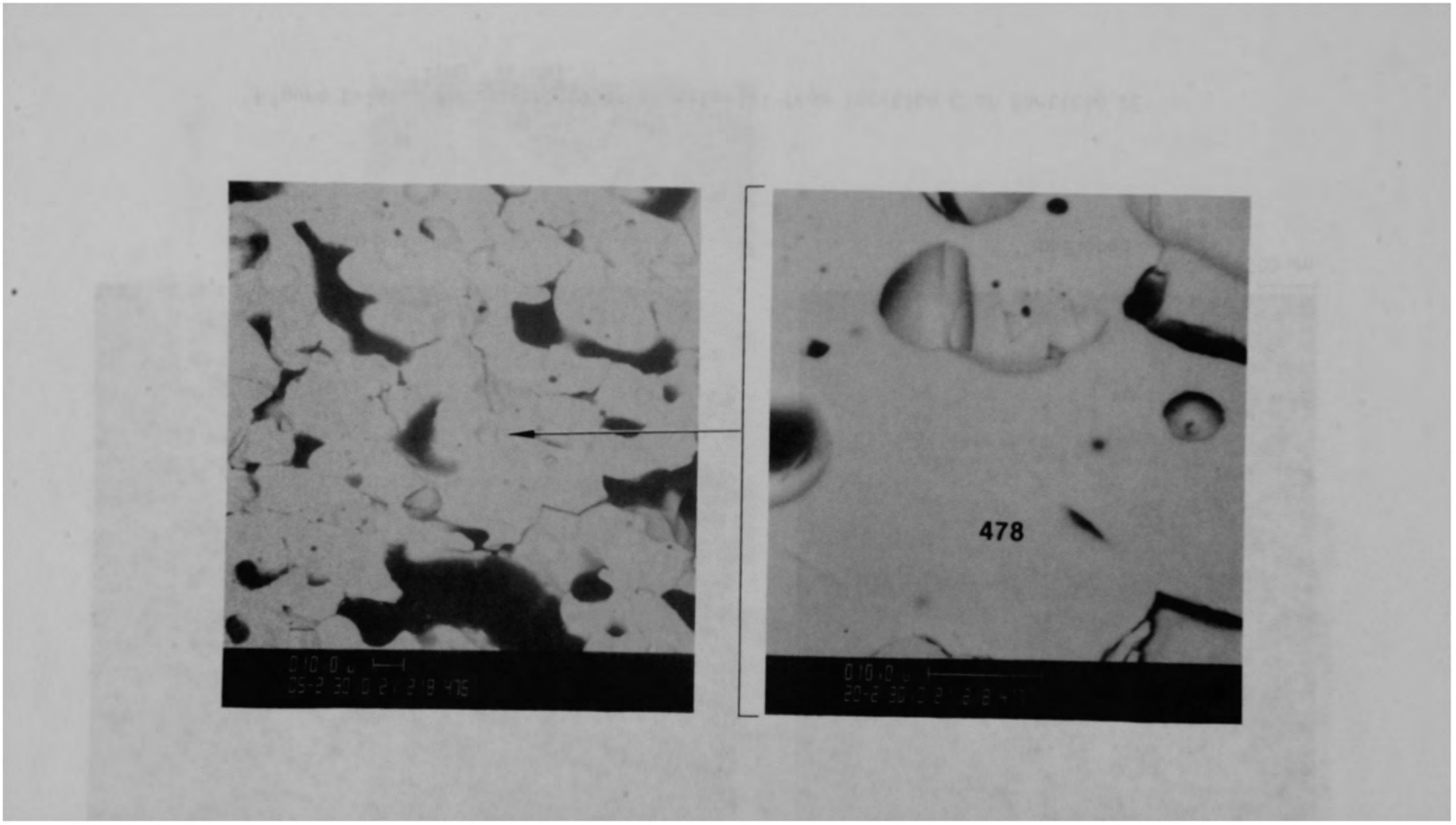

Figure C-145. SEM backscattered electron images of material from location E, Figure C-144, of Particle 7E (H8, 36 cm).

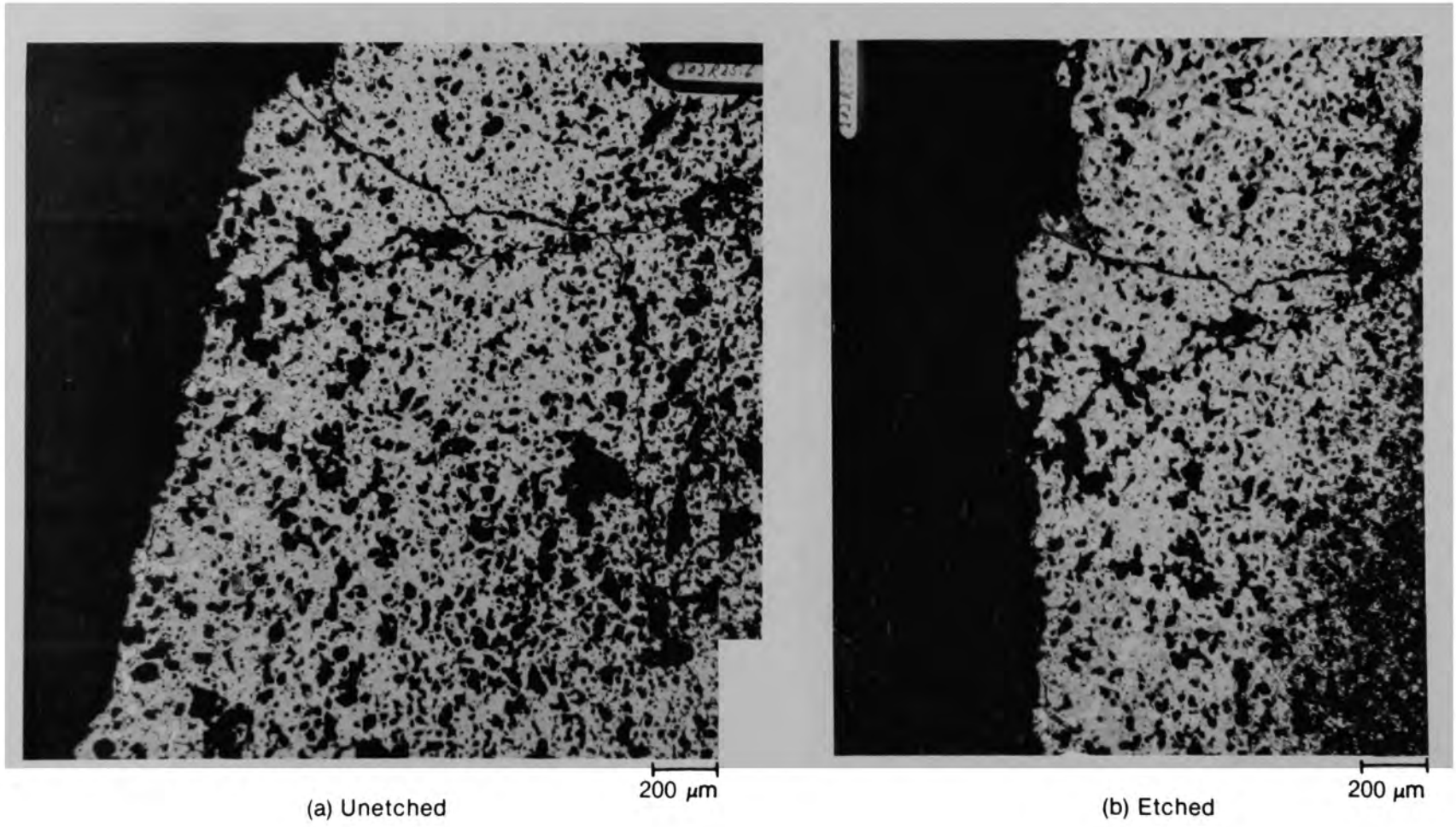

Figure C-146. Photomicrographs of material from location C of Particle 7E (H8, 36 cm).

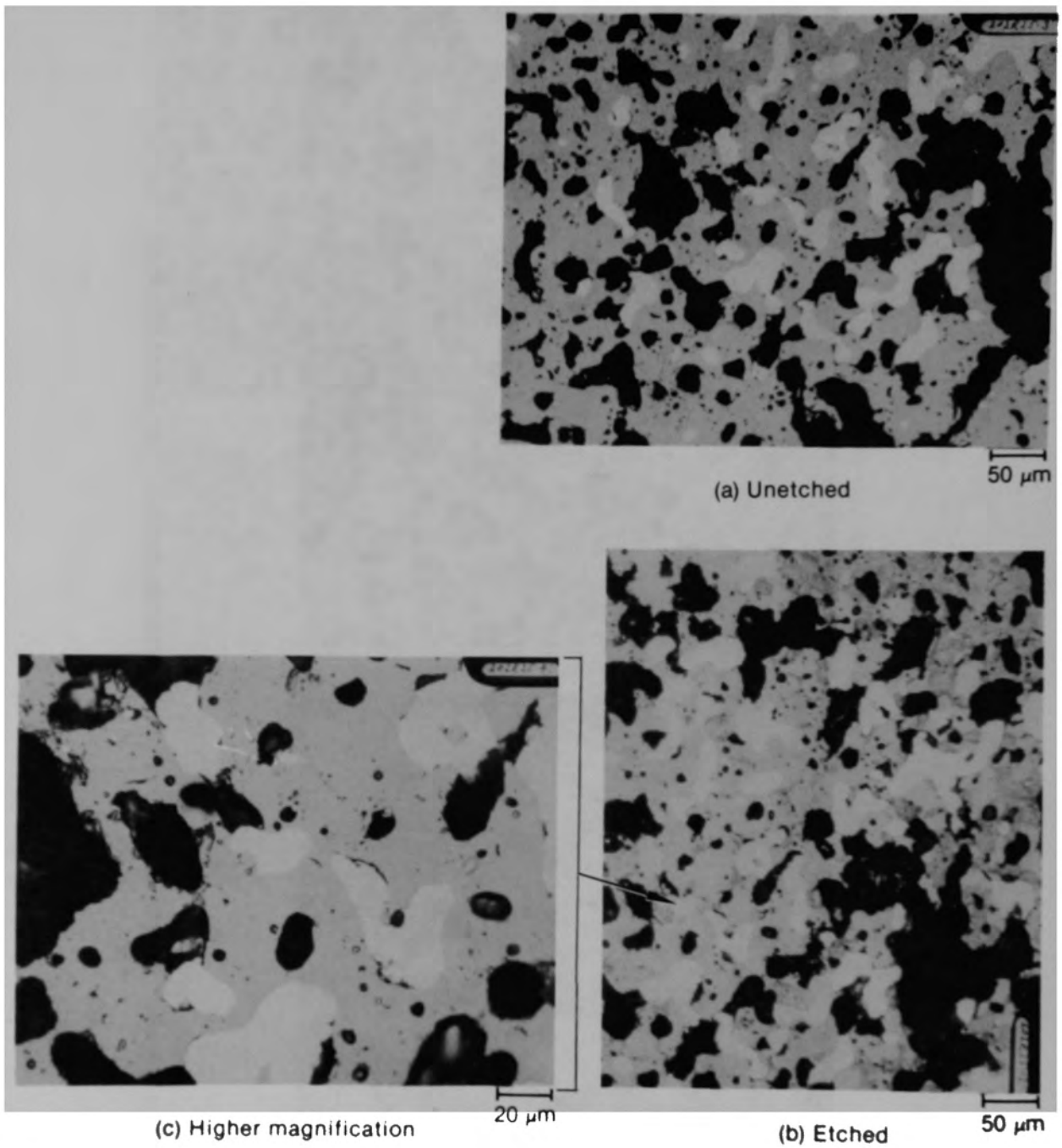

Figure C-147. Photomicrographs of material from location D of Particle 7E (H8, 36 cm).

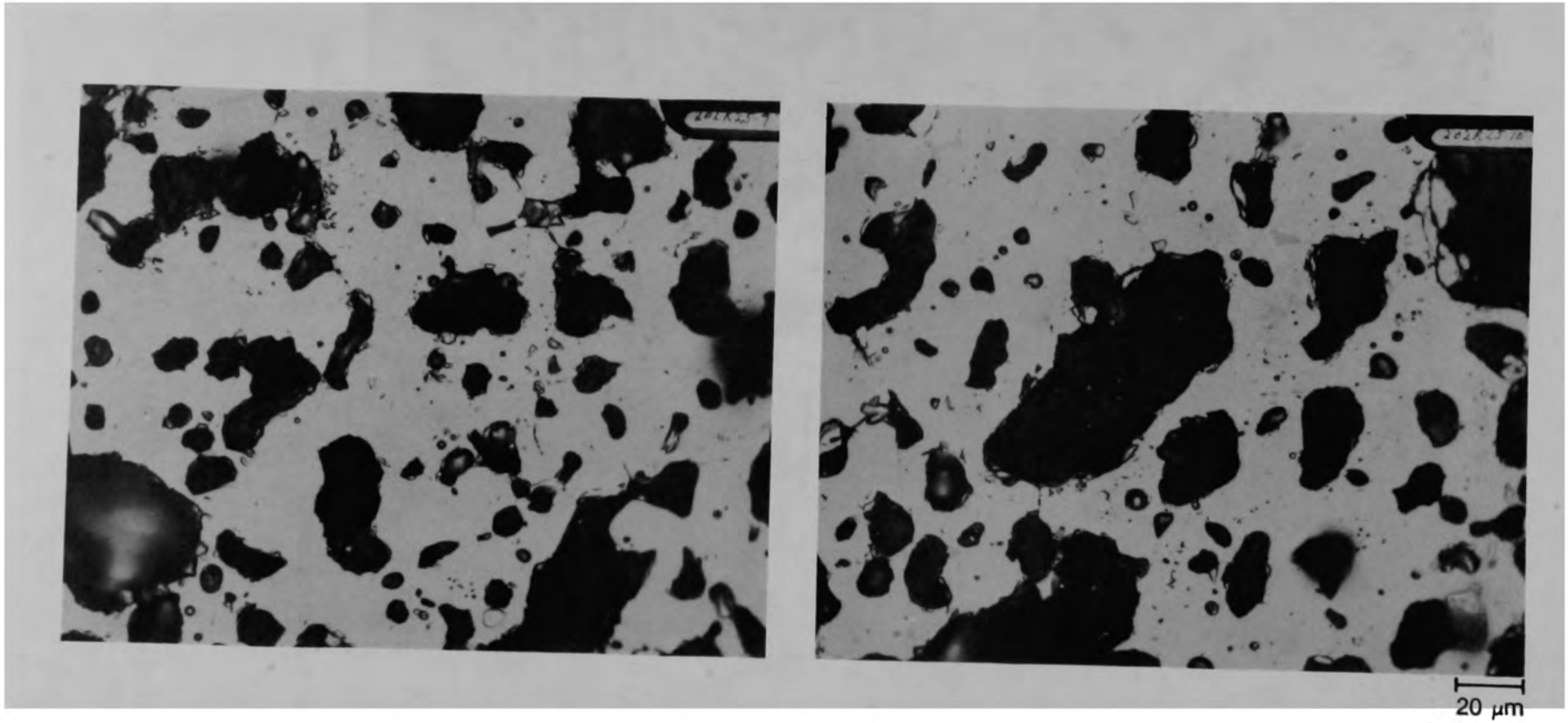

Figure C-148. Photomicrographs of unetched material from location F of Particle 7E (H8, 36 cm).

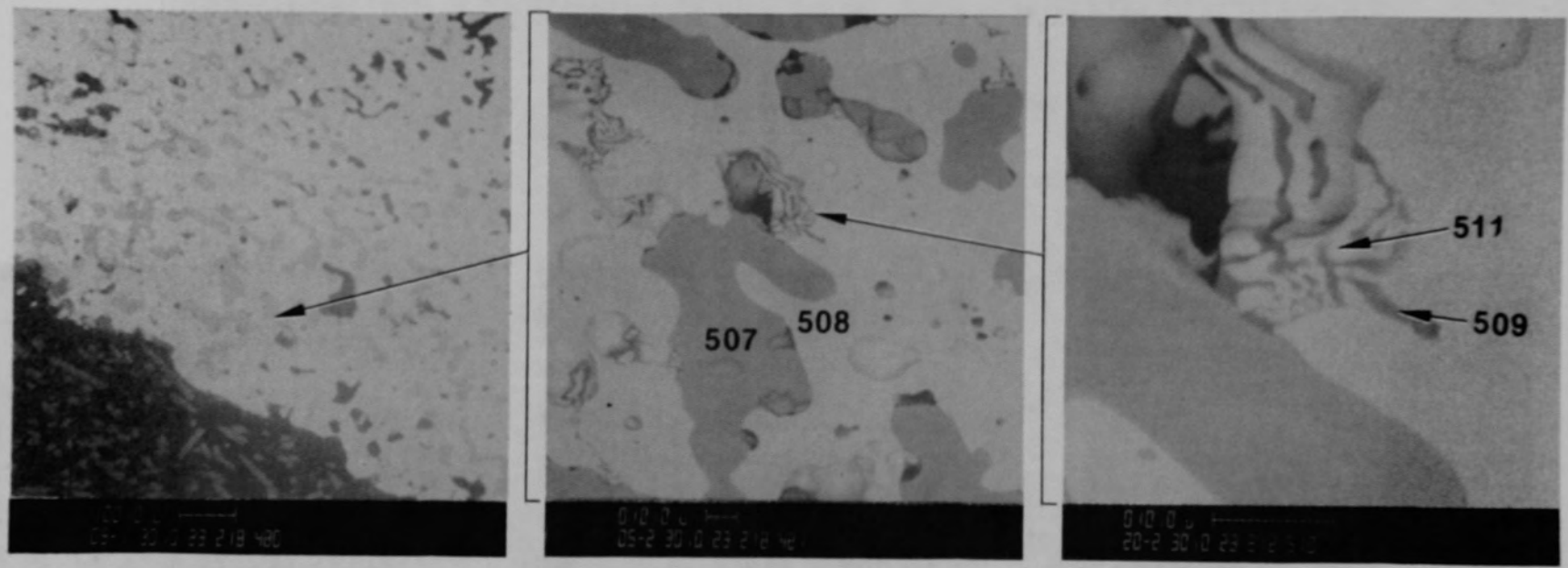

Figure C-149. SEM backscattered electron images of material from location G of Particle 7E (H8, 36 cm).

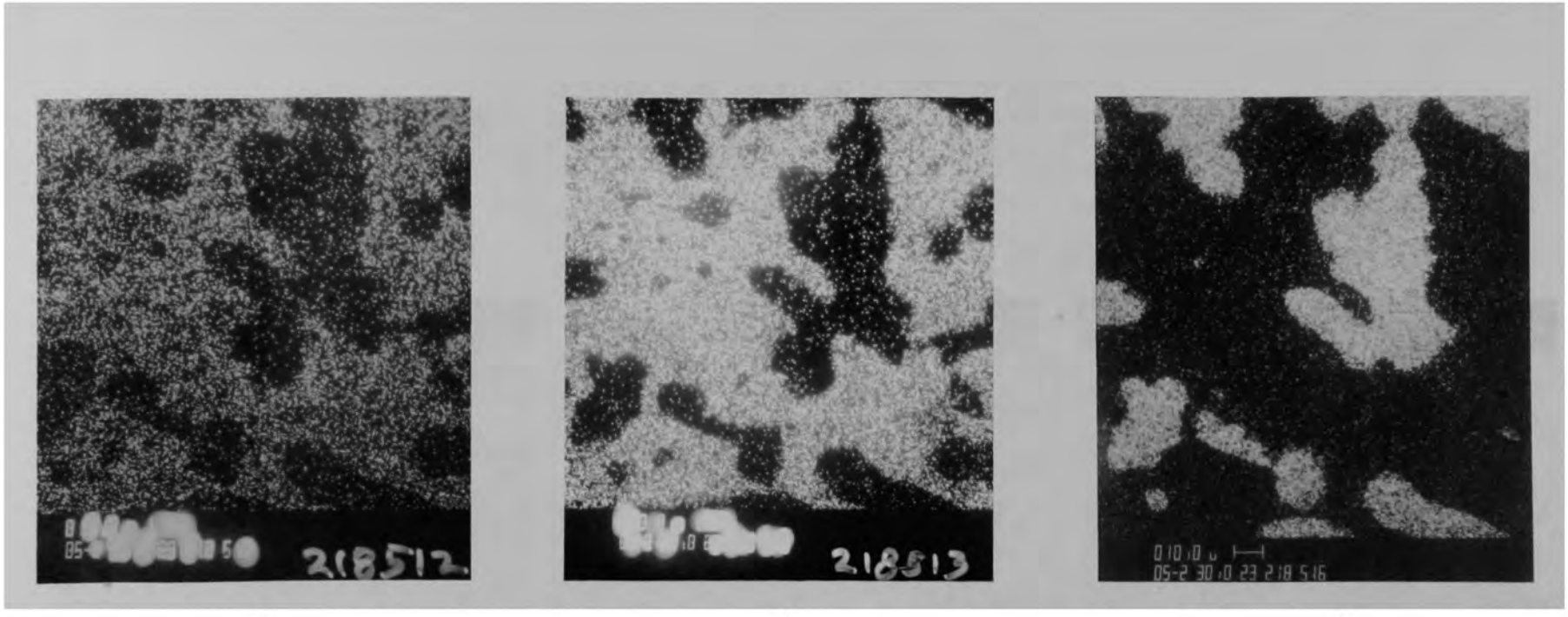

Zr U Ni

Figure C-150. X-ray dot map of material shown in Figure C-149b of Particle 7E (H8, 36 cm).

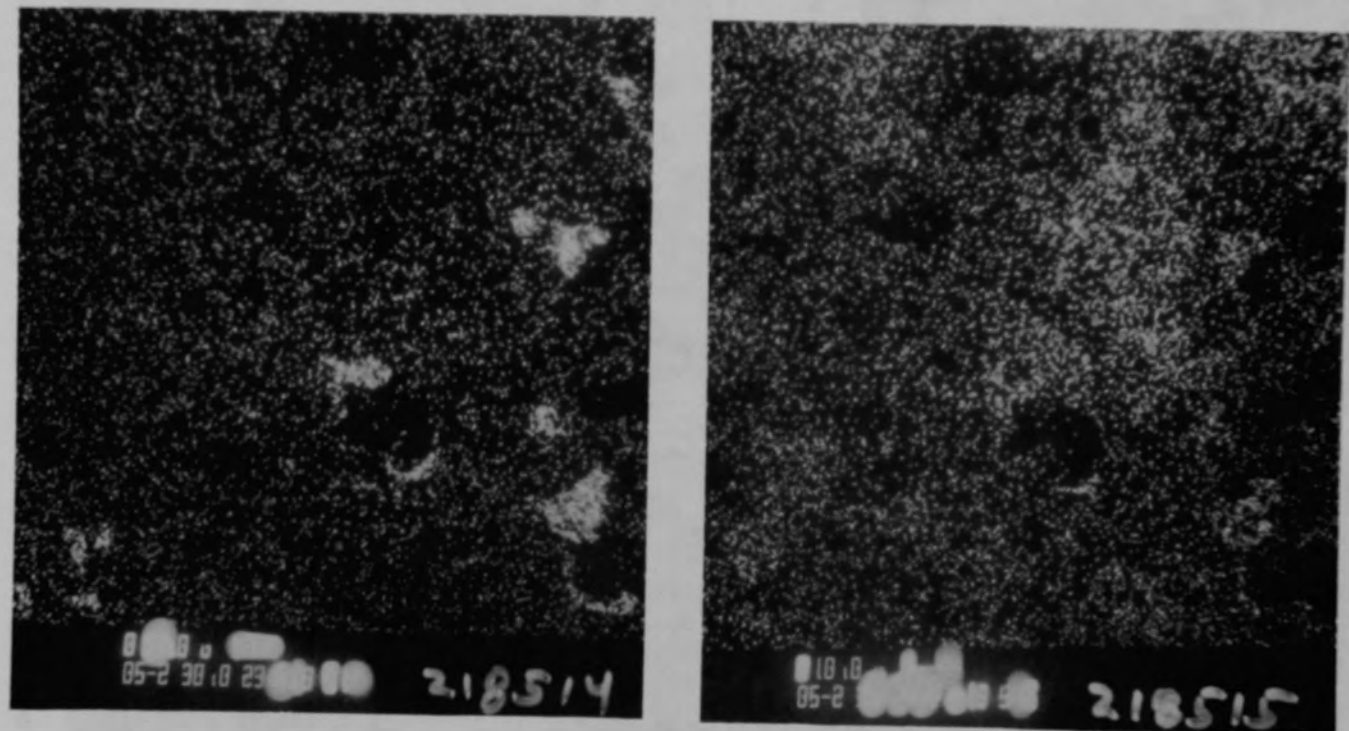

(a) Cr

(b) Fe

Figure C-151. X-ray dot map of material shown in Figure C-149c of Particle 7E (H8, 36 cm).

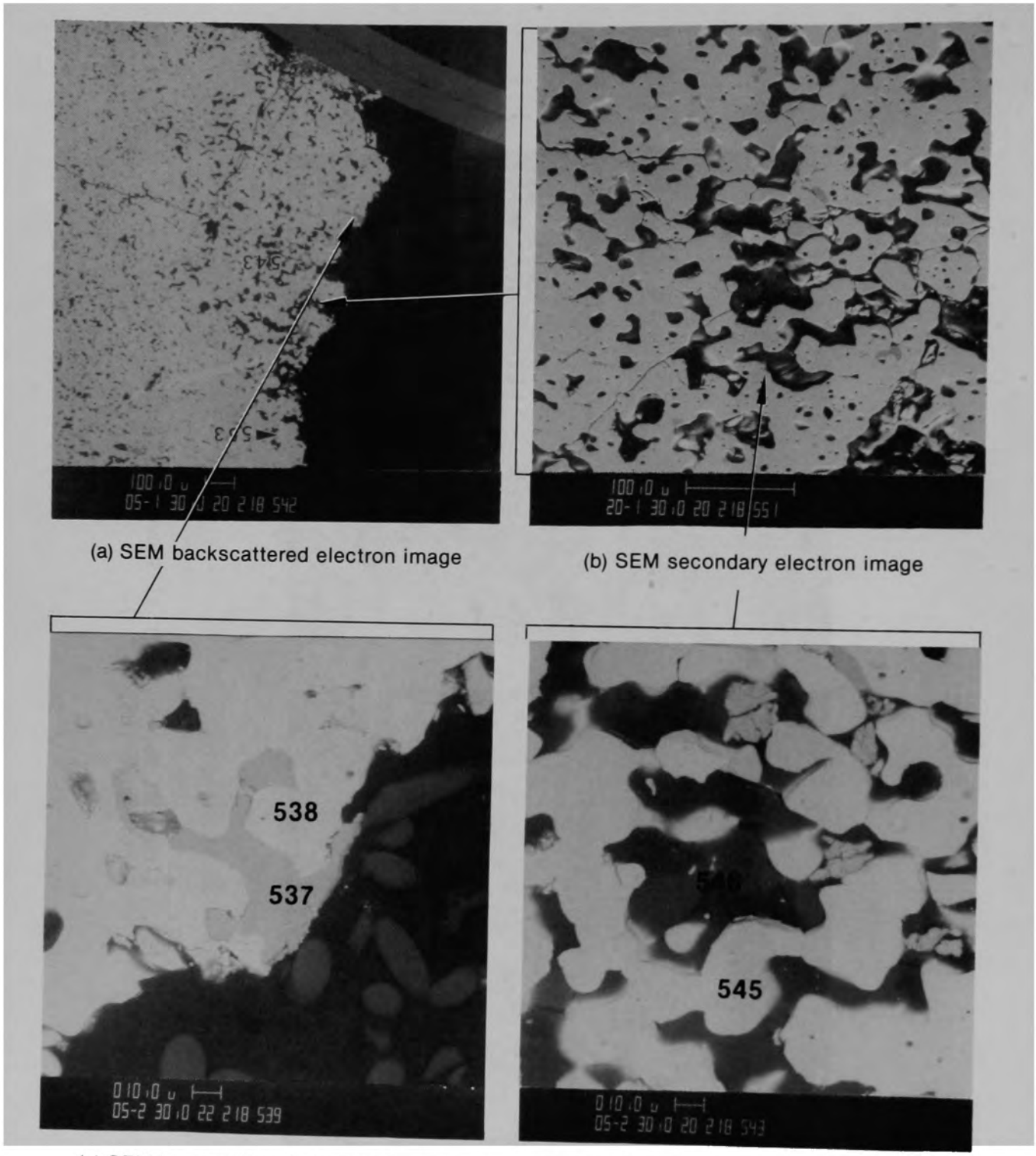

Figure C-152. SEM images of material from location H of Particle 7E (H8, 36 cm).

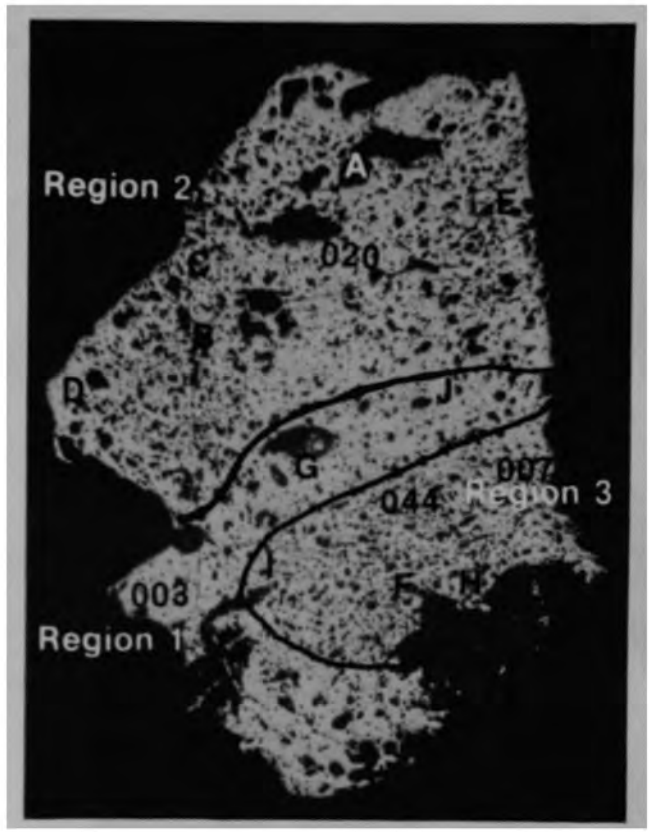

Figure C-153. Photomacrograph of Particle 8A (H8, 70 cm).

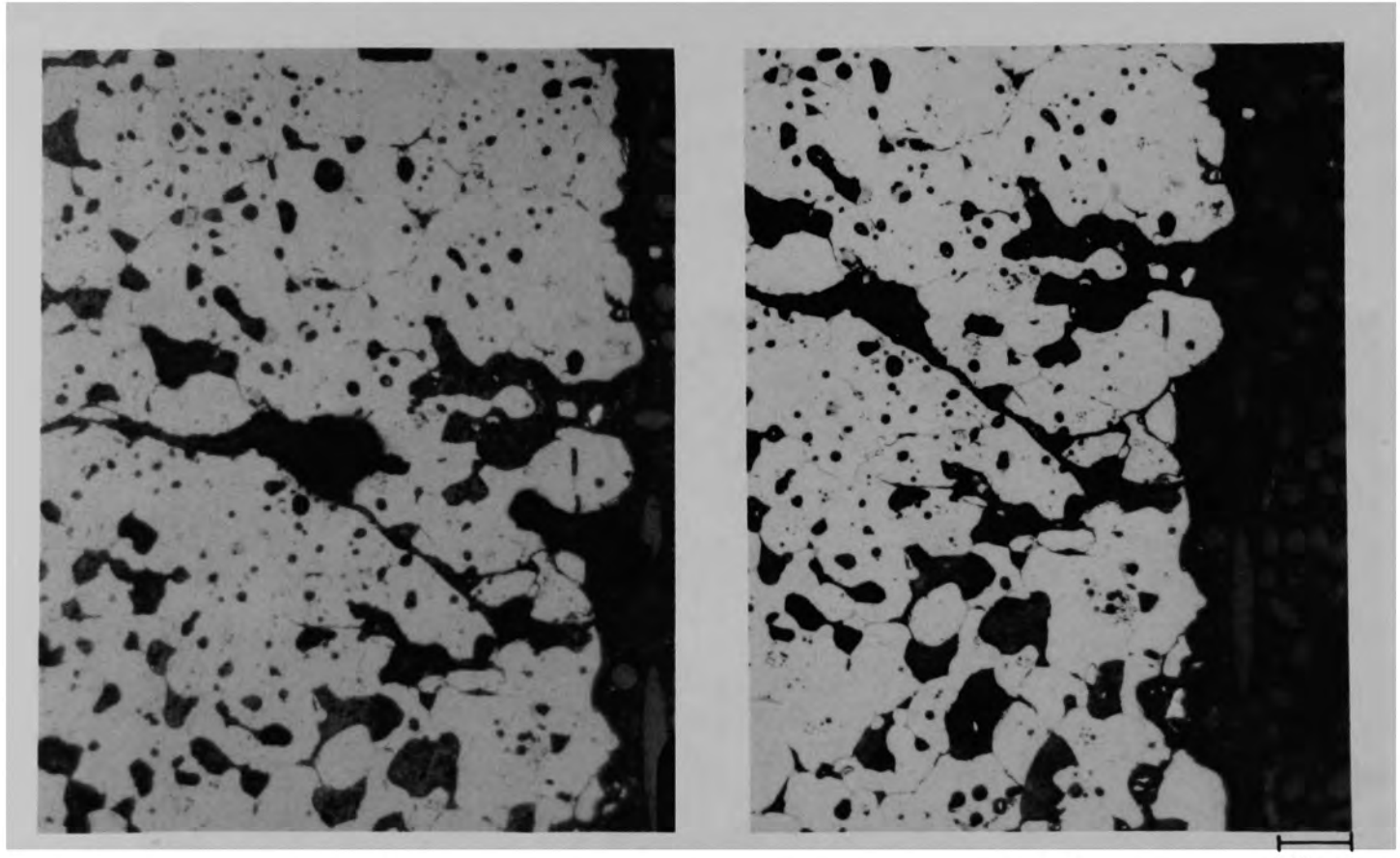

Figure C-154. Photomicrographs of material from location E of Particle 8A (H8, 70 cm) showing rounded pore surfaces and the effect of etching.

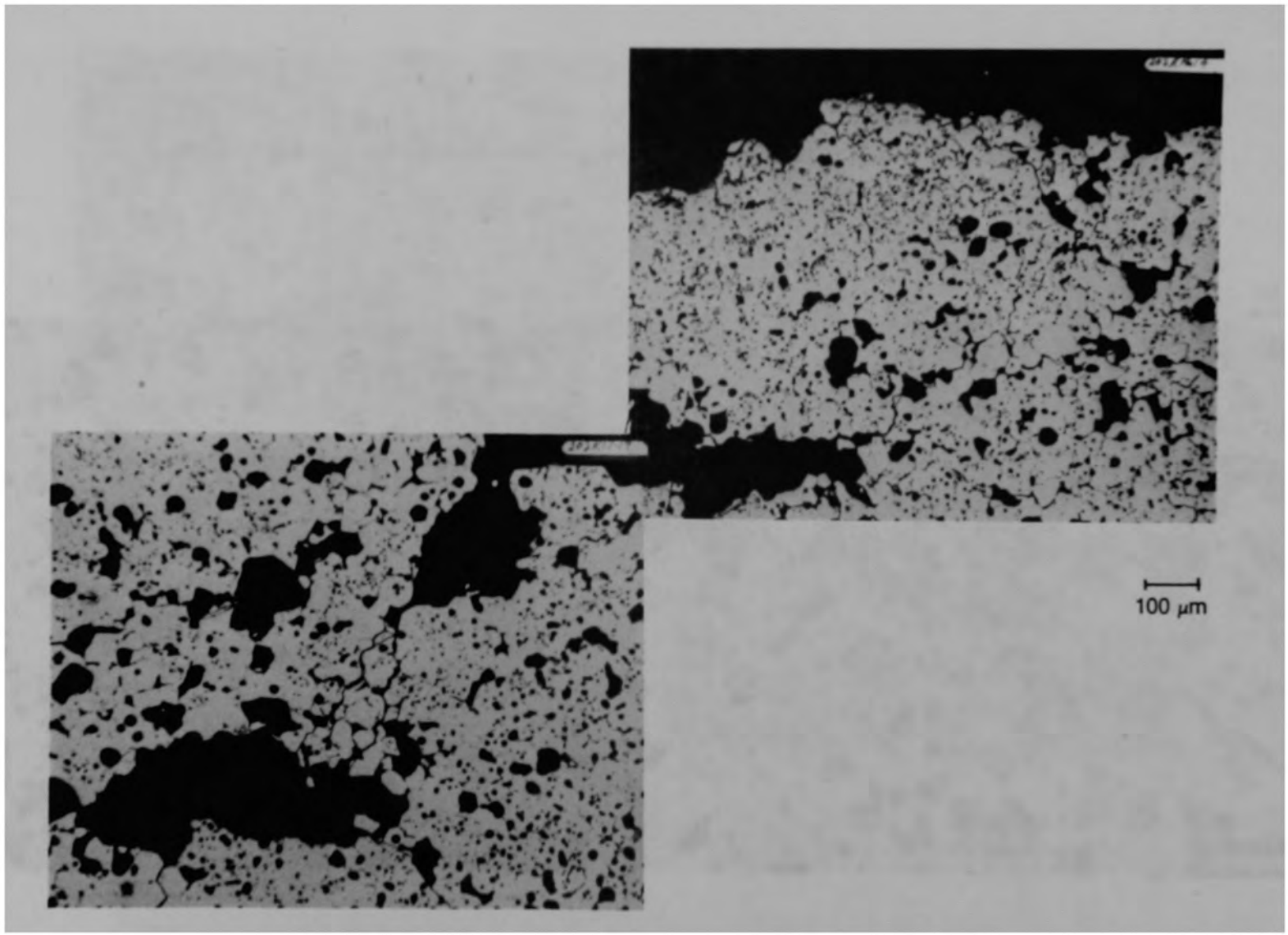

Figure C-155. Photomicrographs of material from location A of Particle 8A (H8, 70 cm).

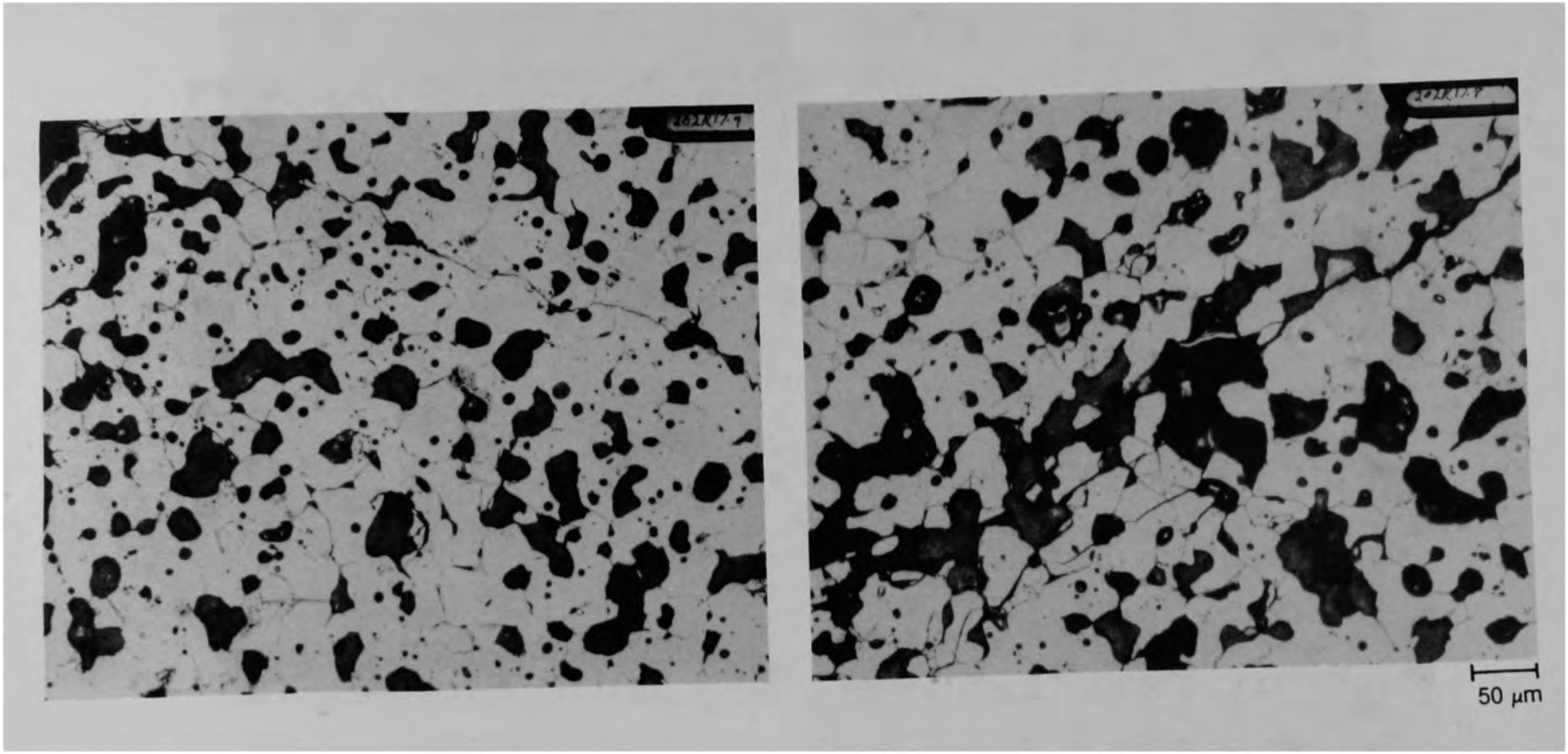

Figure C-156. Photomicrographs of material from location B of Particle 8A (H8, 70 cm).

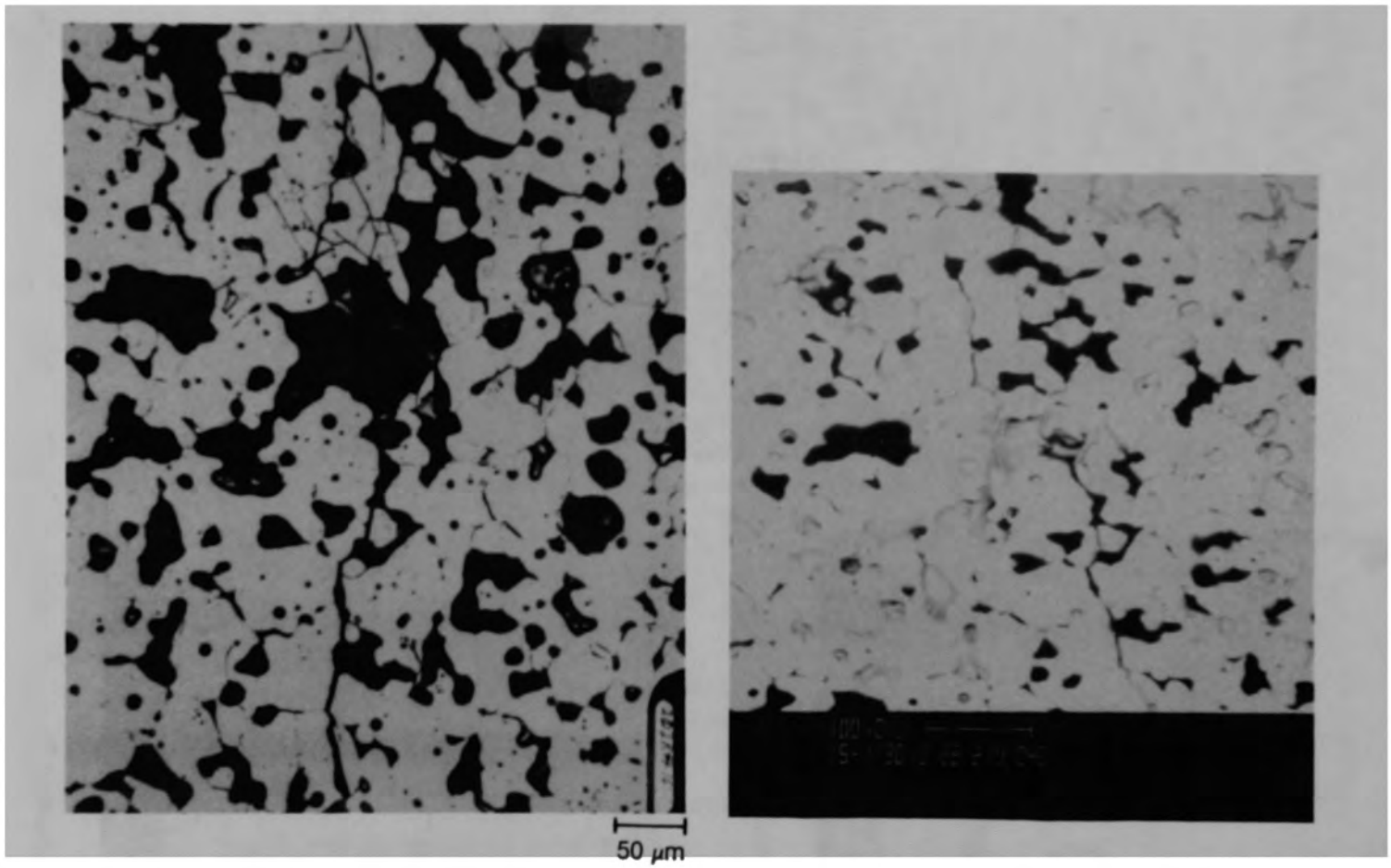

(a) Photomicrograph

(b) SEM backscattered electron image

Figure C-157. Photographs of material from location B of Particle 8A (H8, 70 cm).

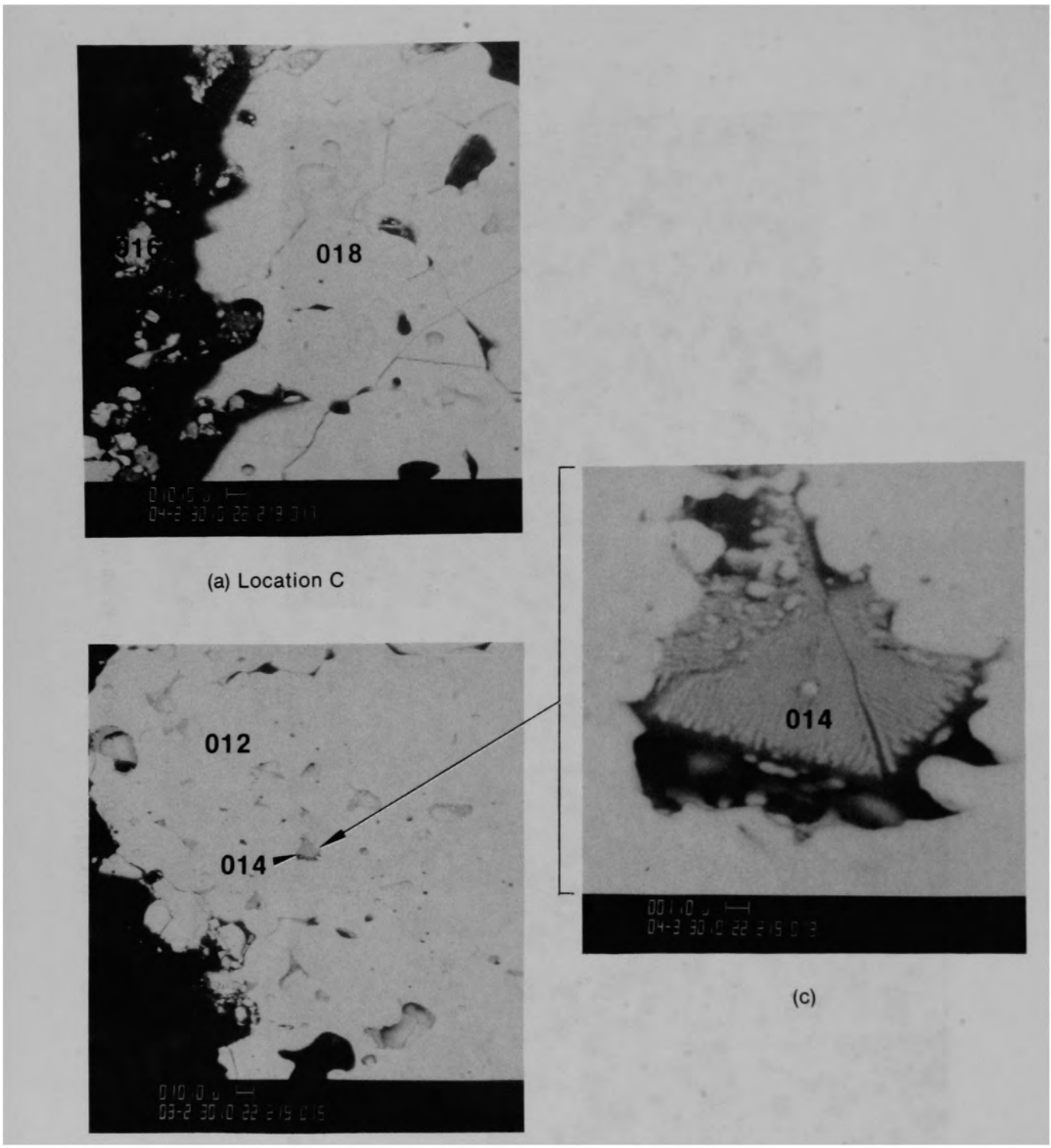

Figure C-158. SEM backscattered electron images of Particle 8A (H8, 70 cm).

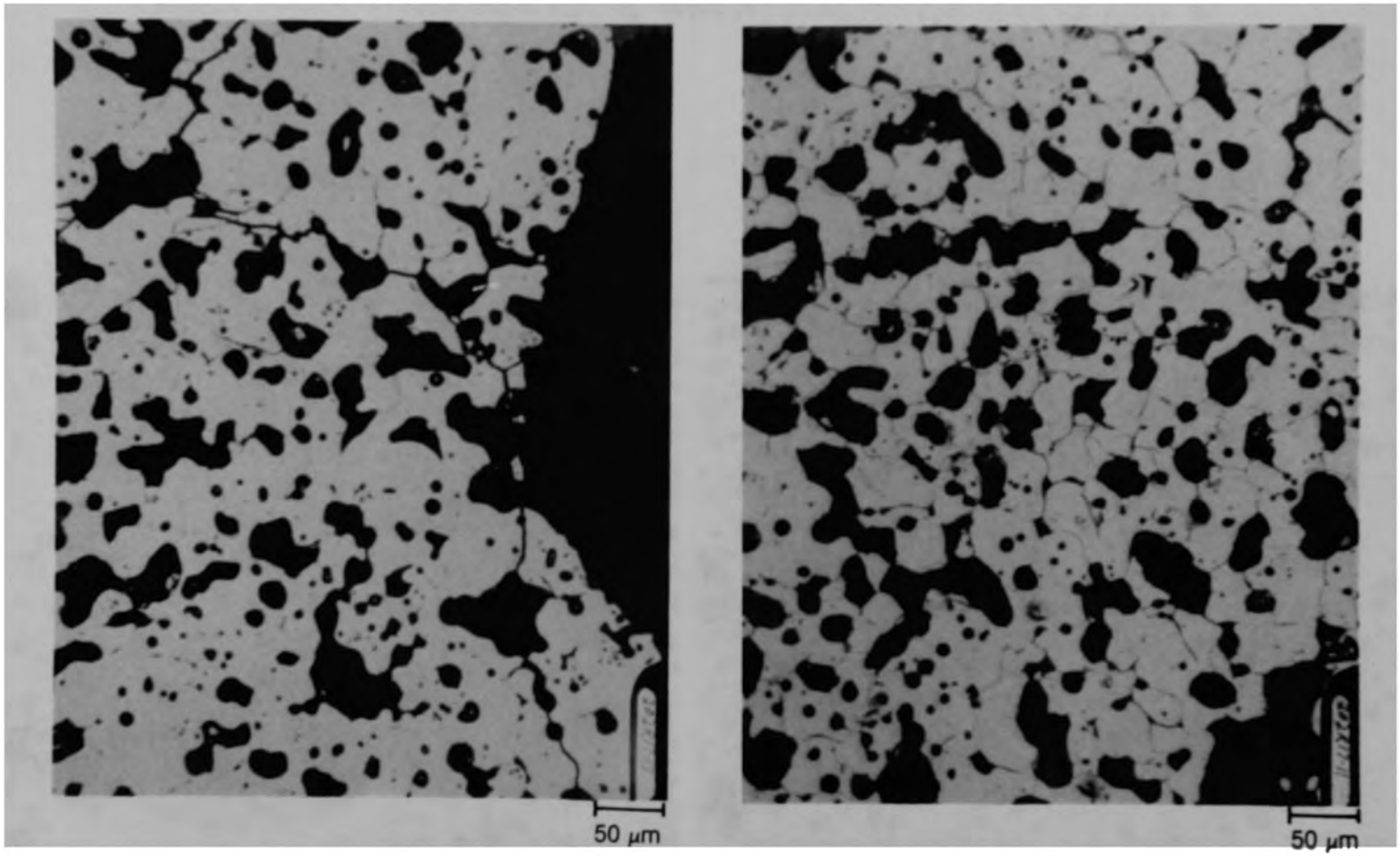

(a) Unetched

(b) Etched

Figure C-159. Photomicrographs of material from location F of Particle 8A (H8, 70 cm).

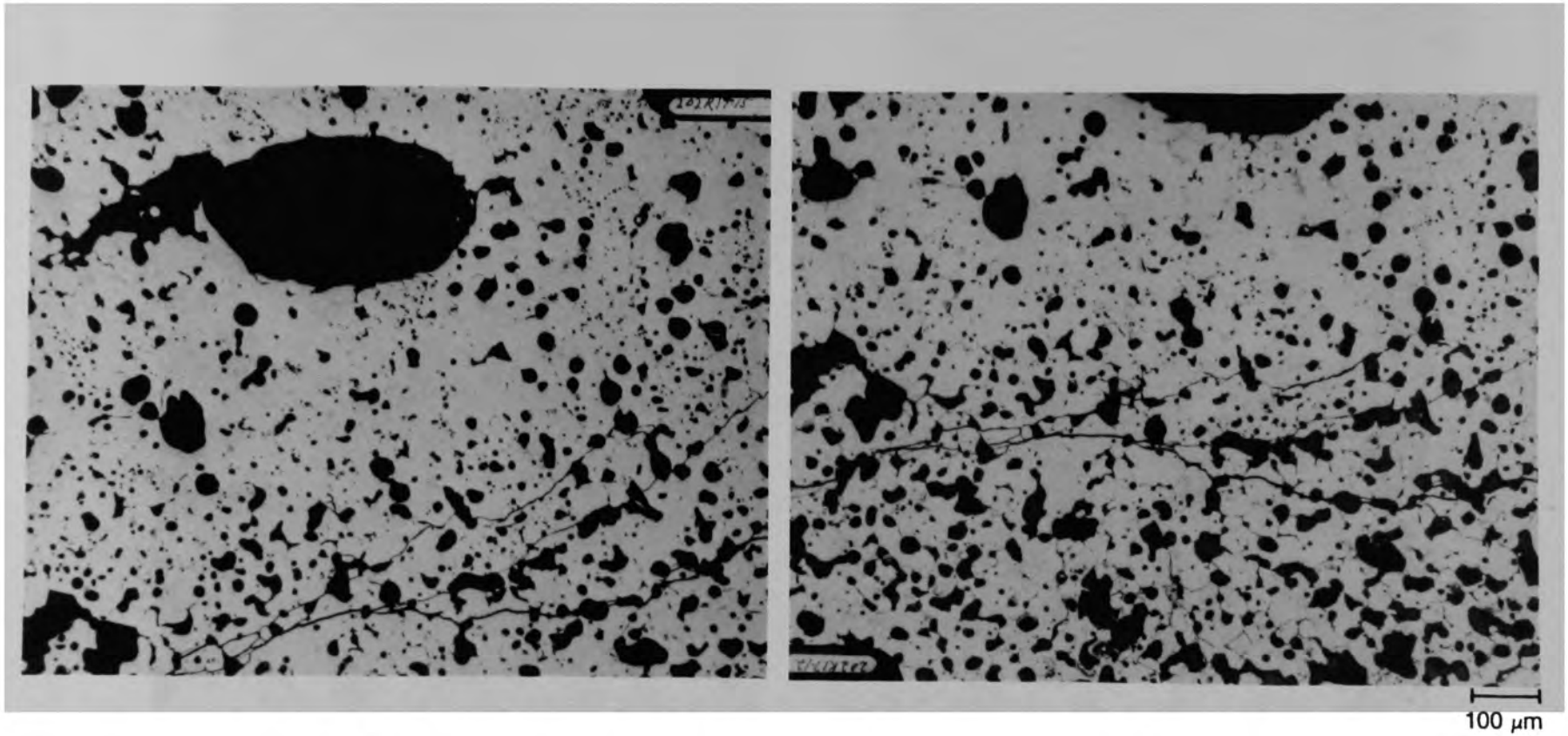

(a) Unetched

(b) Etched

Figure C-160. Photomicrographs of material from location G of Particle 8A (H8, 70 cm).

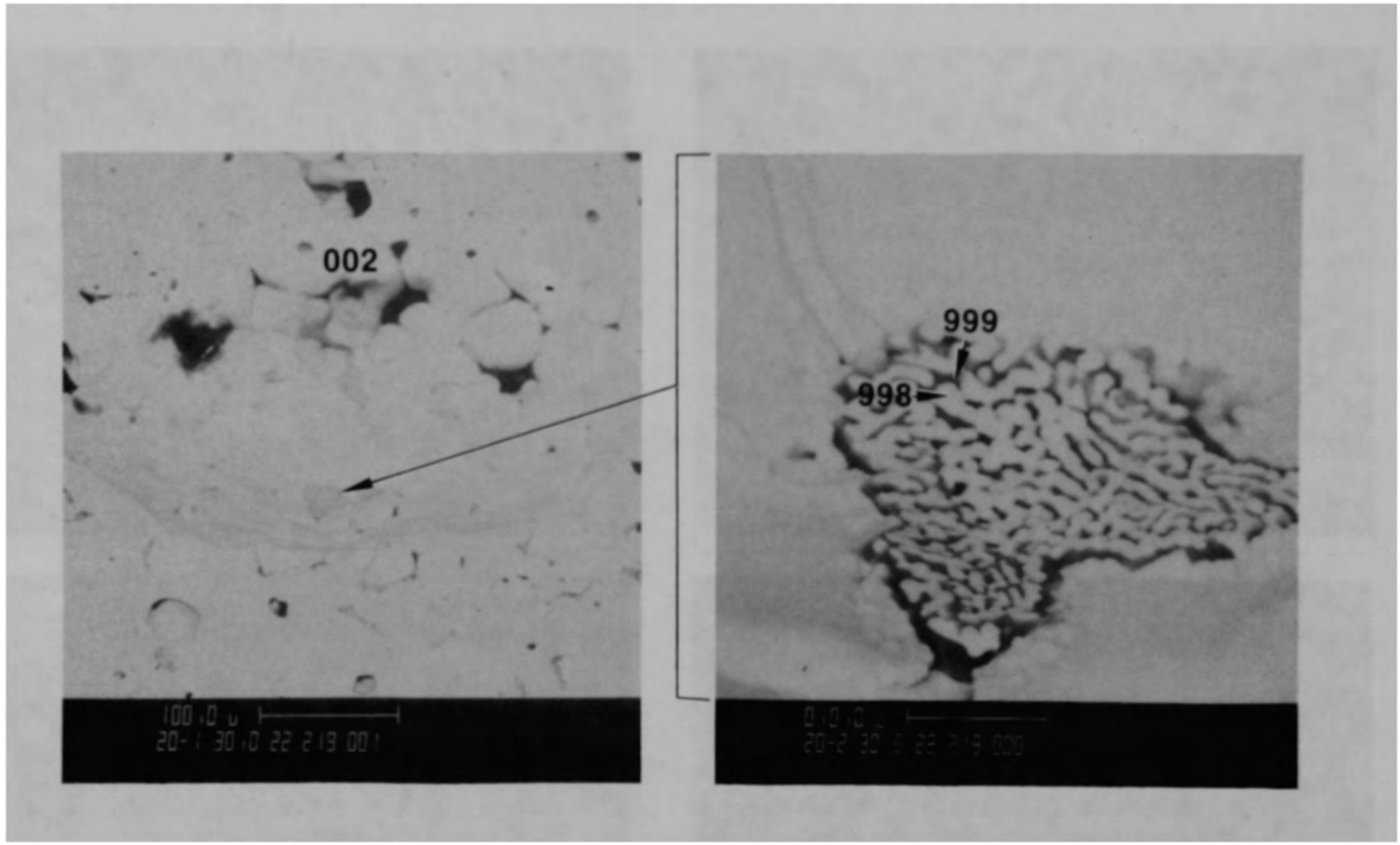

Figure C-161. SEM backscattered electron images of material from location G of Particle 8A (H8, 70 cm).

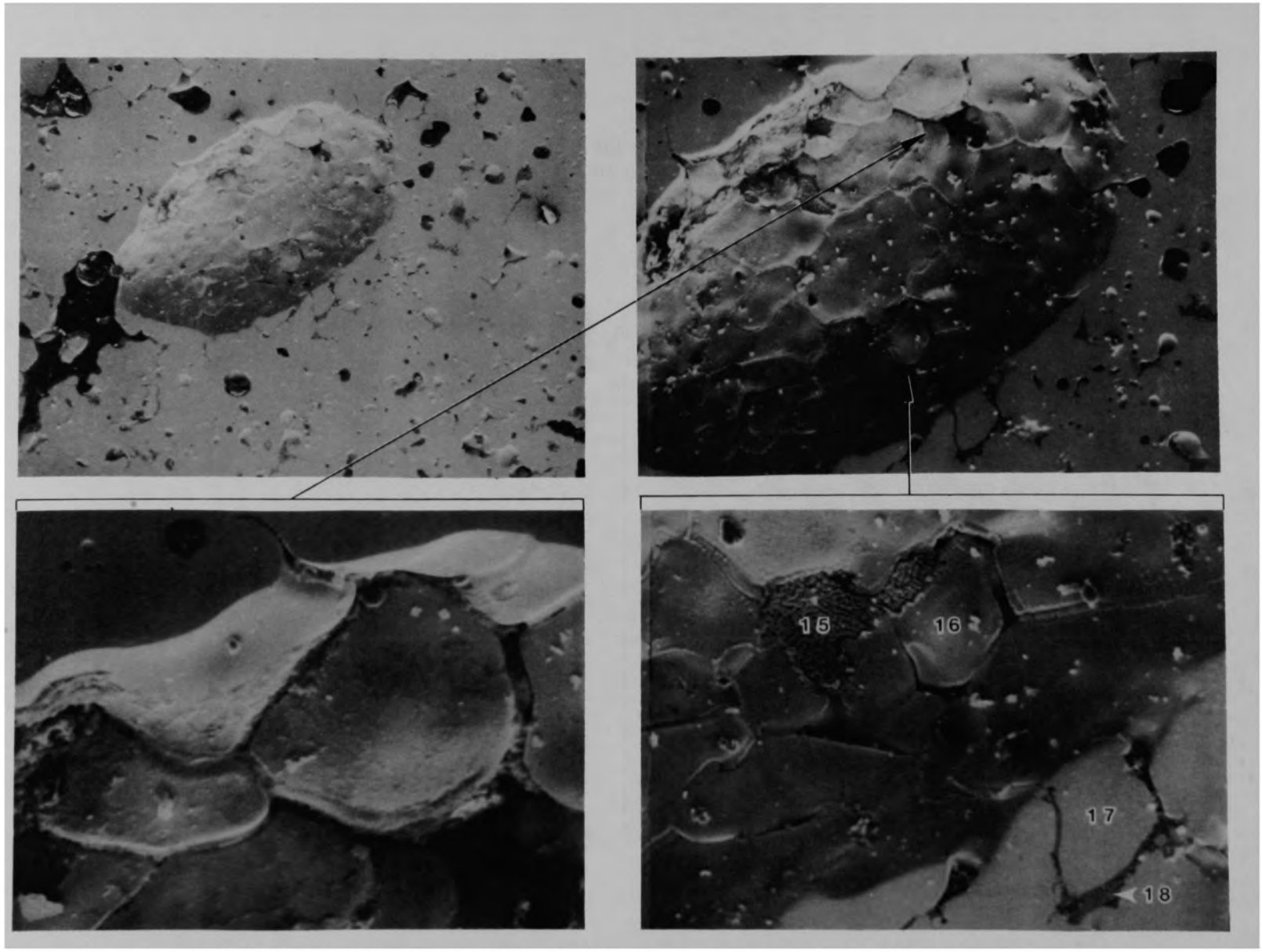

Figure C-162. Auger images of material from location G of Particle 8A (H8, 70 cm).

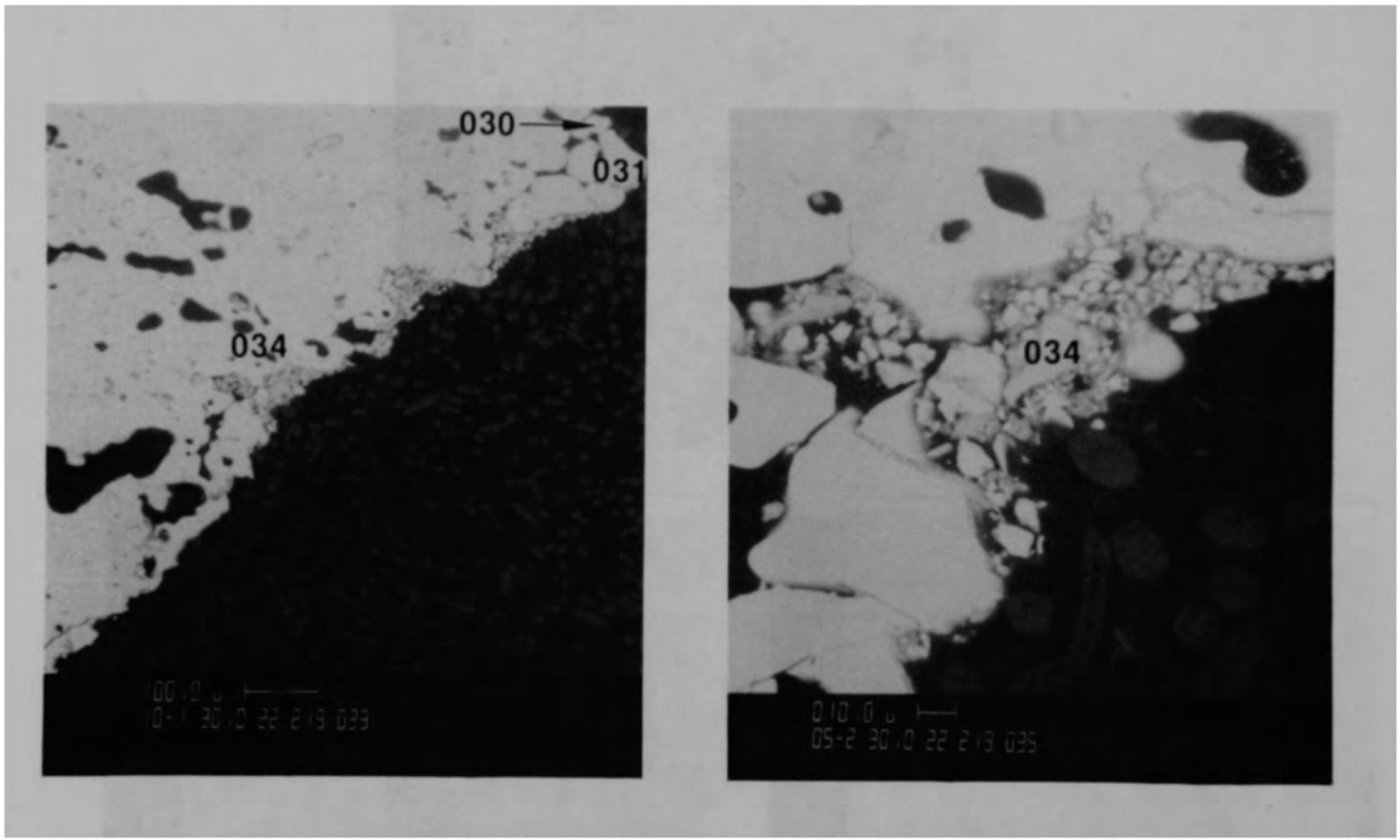

Figure C-163. SEM backscattered electron images of material from location H of Particle 8A (H8, 70 cm).

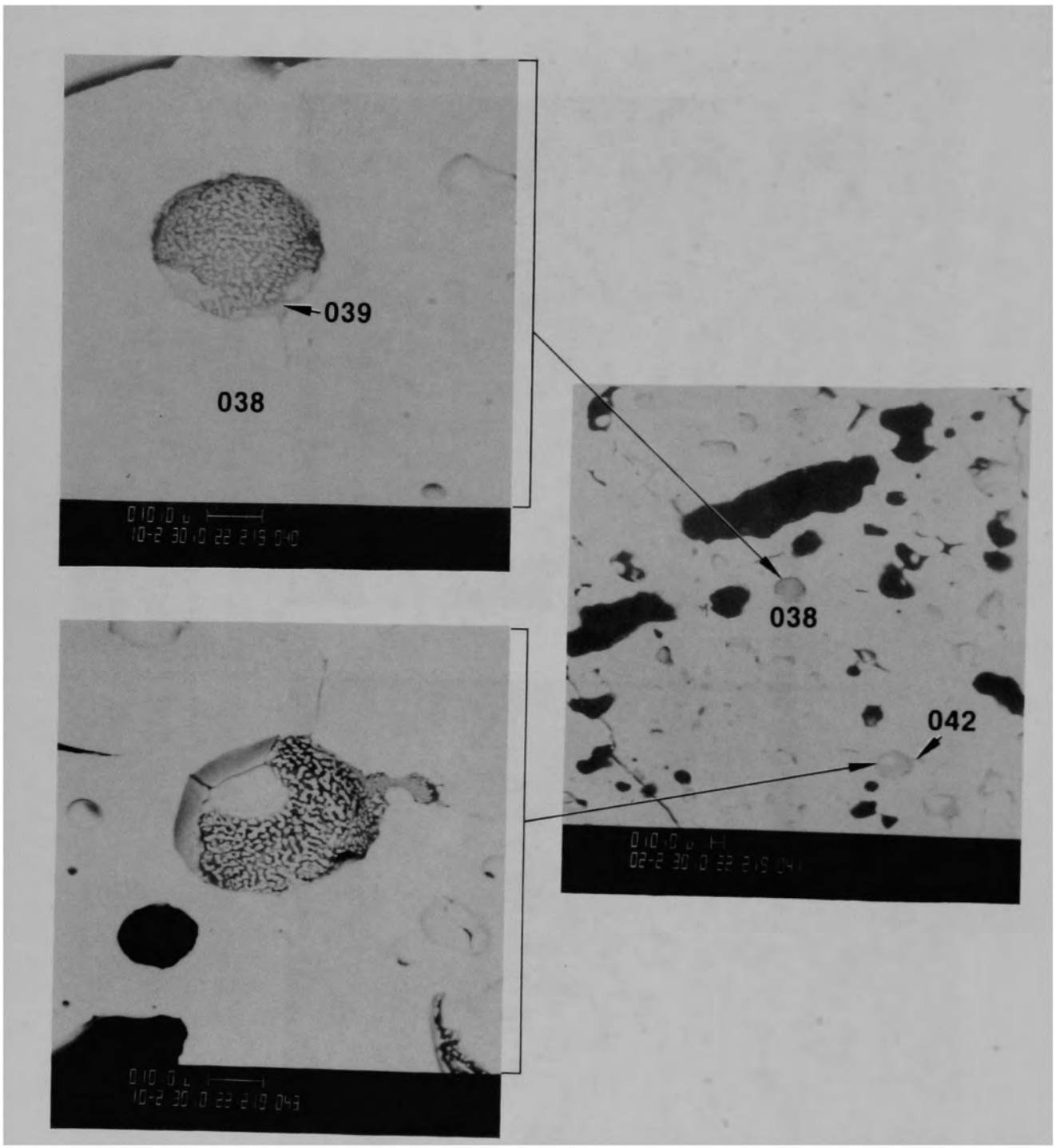

Figure C-164. SEM backscattered electron images of material from location I of Particle 8A (H8, 70 cm).

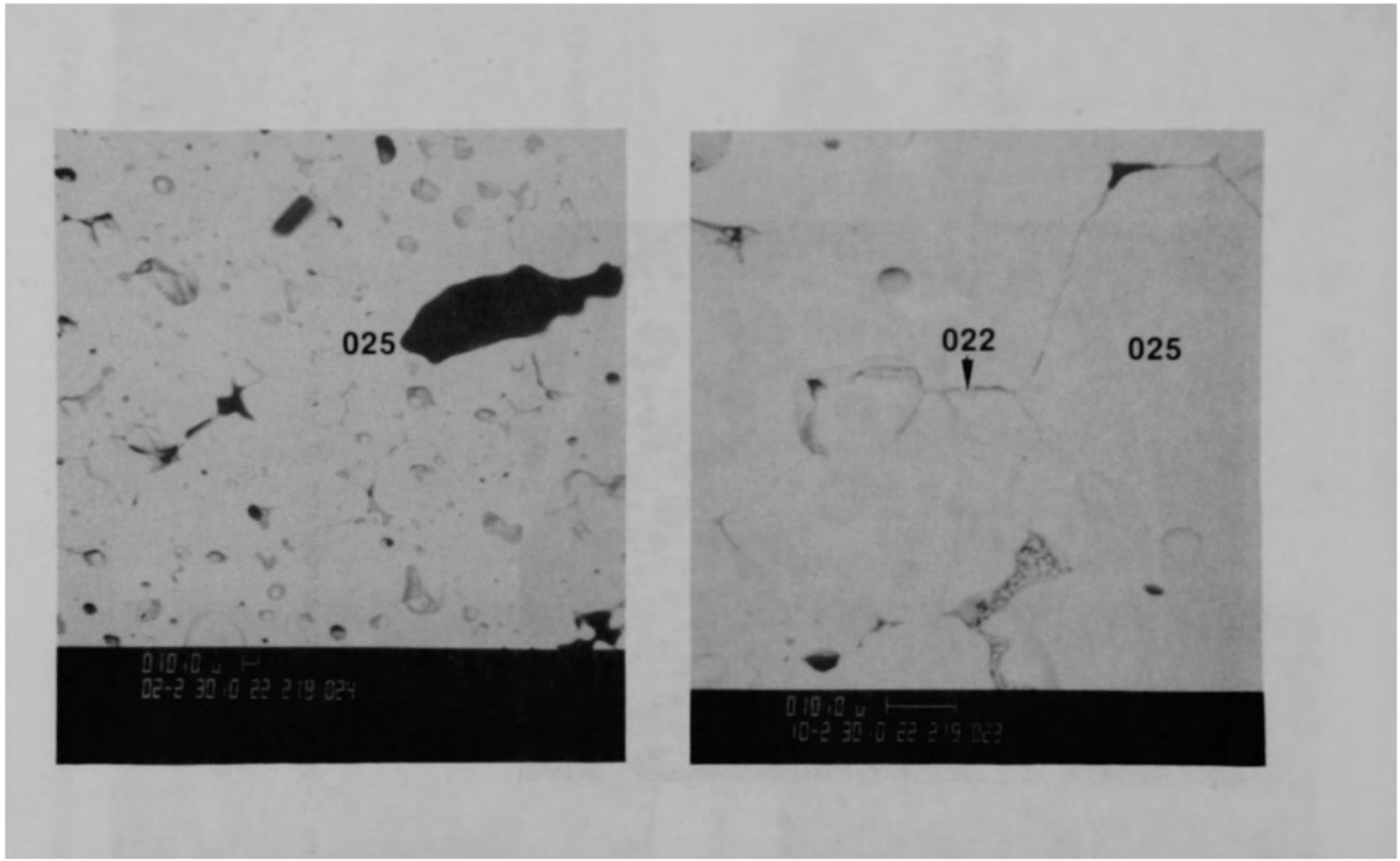

Figure C-165. SEM backscattered electron images of material from location J of Particle 8A (H8, 70 cm).

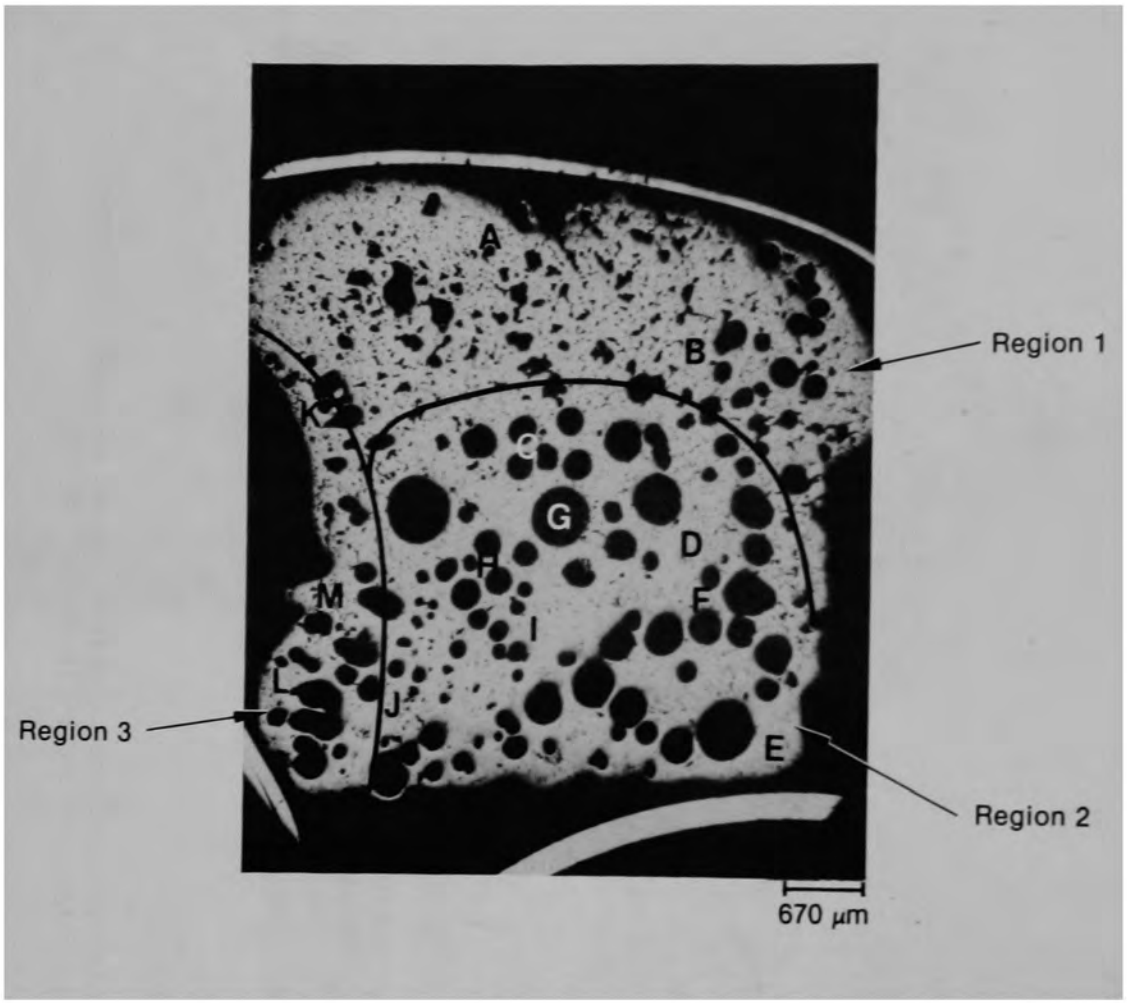

Figure C-166. Photomacrograph of Particle 8C (H8, 70 cm).

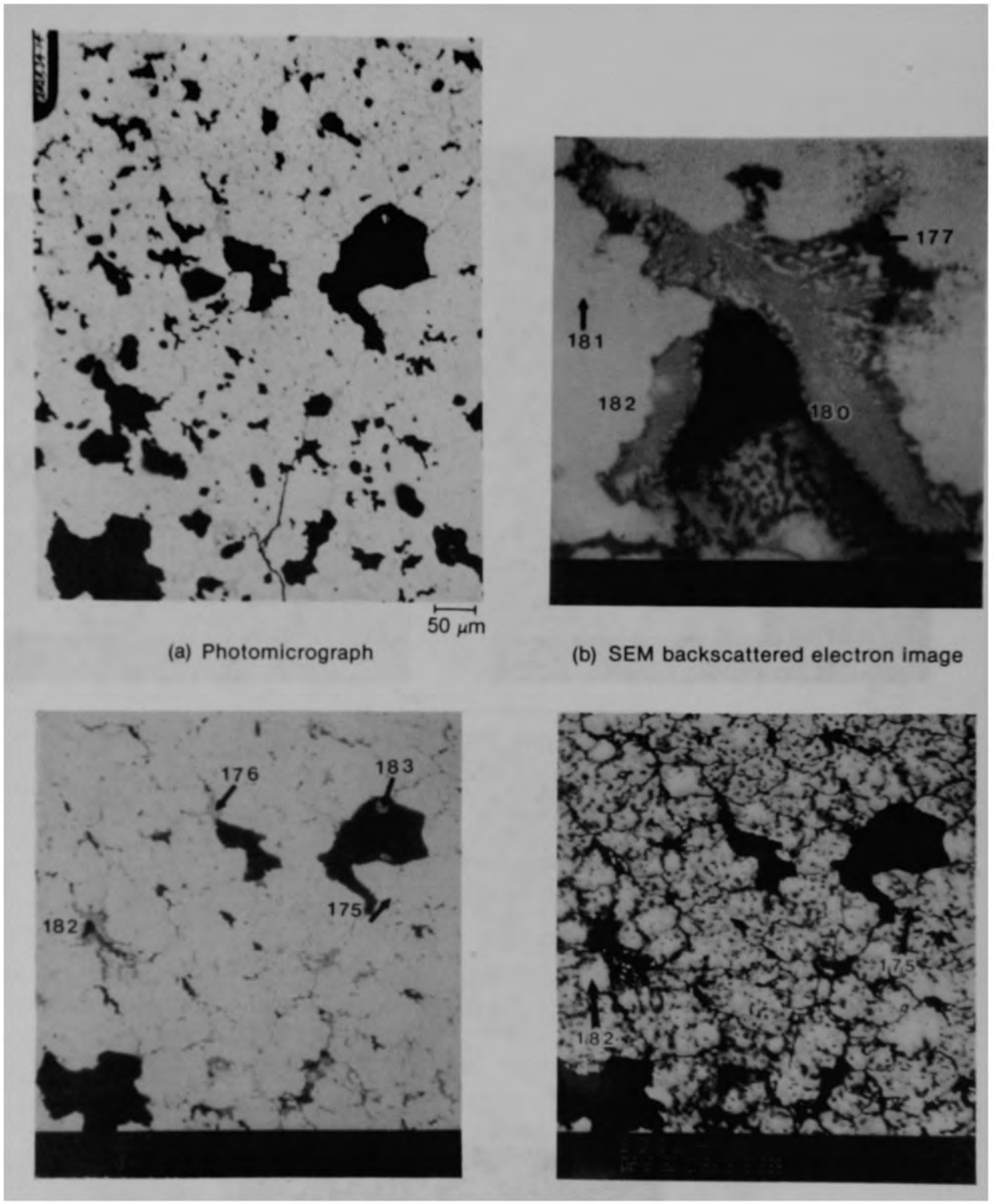

Figure C-167. Photographs of material from Region 1, location A of Particle 8C (H8, 70 cm).

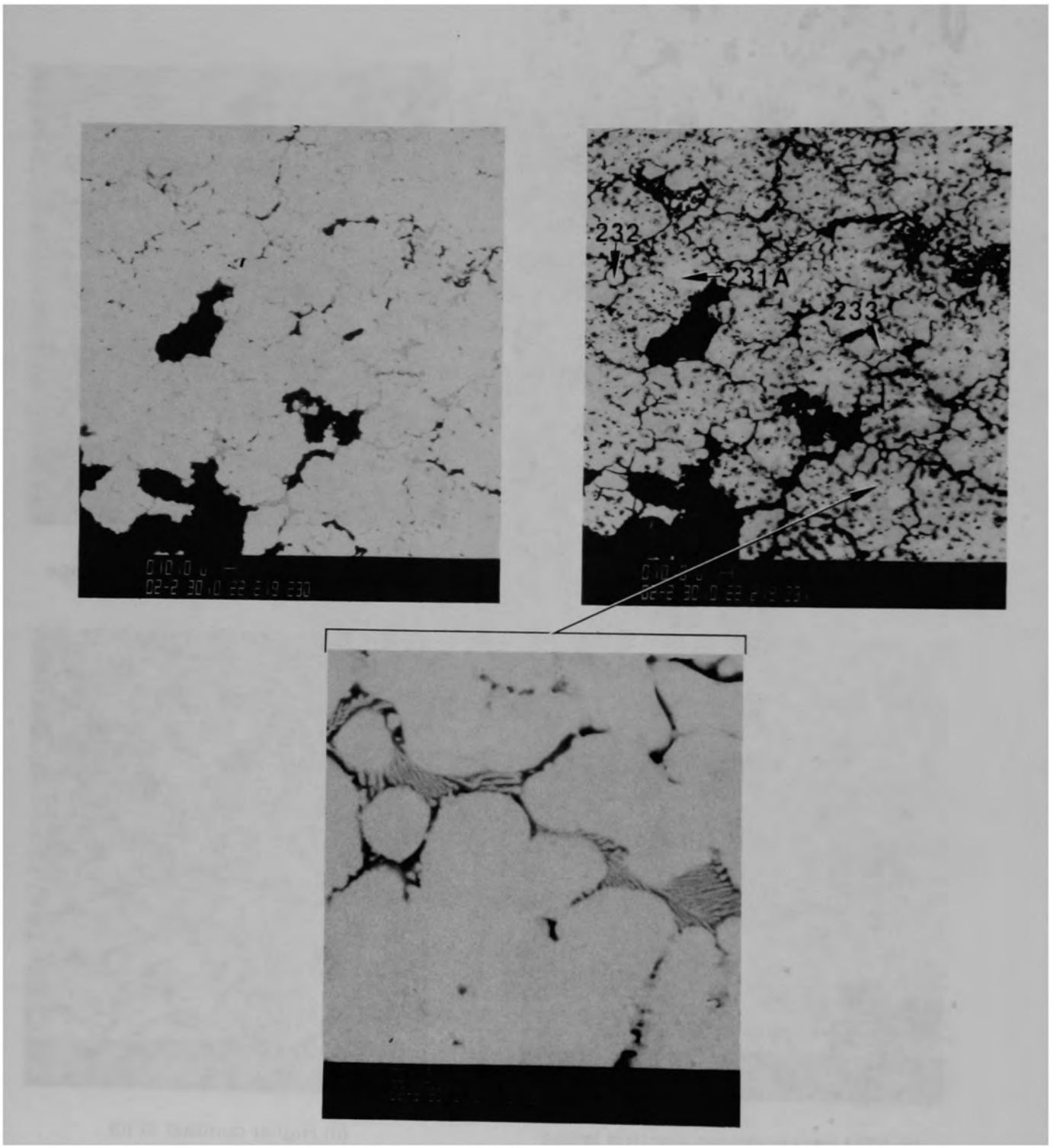

Figure C-168. SEM backscattered electron images of material from Region 1, location B of Particle 8C (H8, 70 cm).

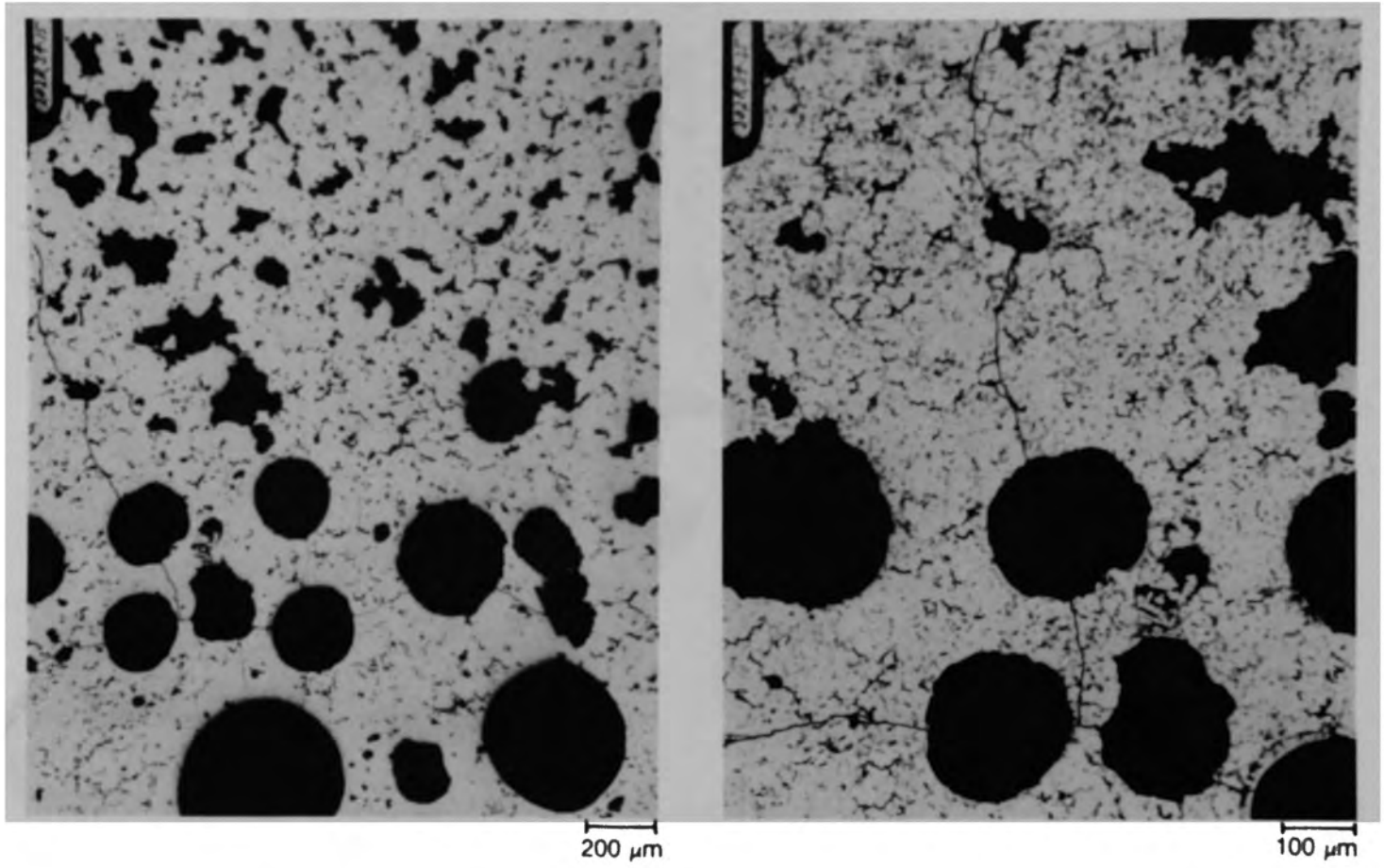

Figure C-169. Photomicrographs of material from Region 2, location F of Particle 8C (H8, 70 cm).

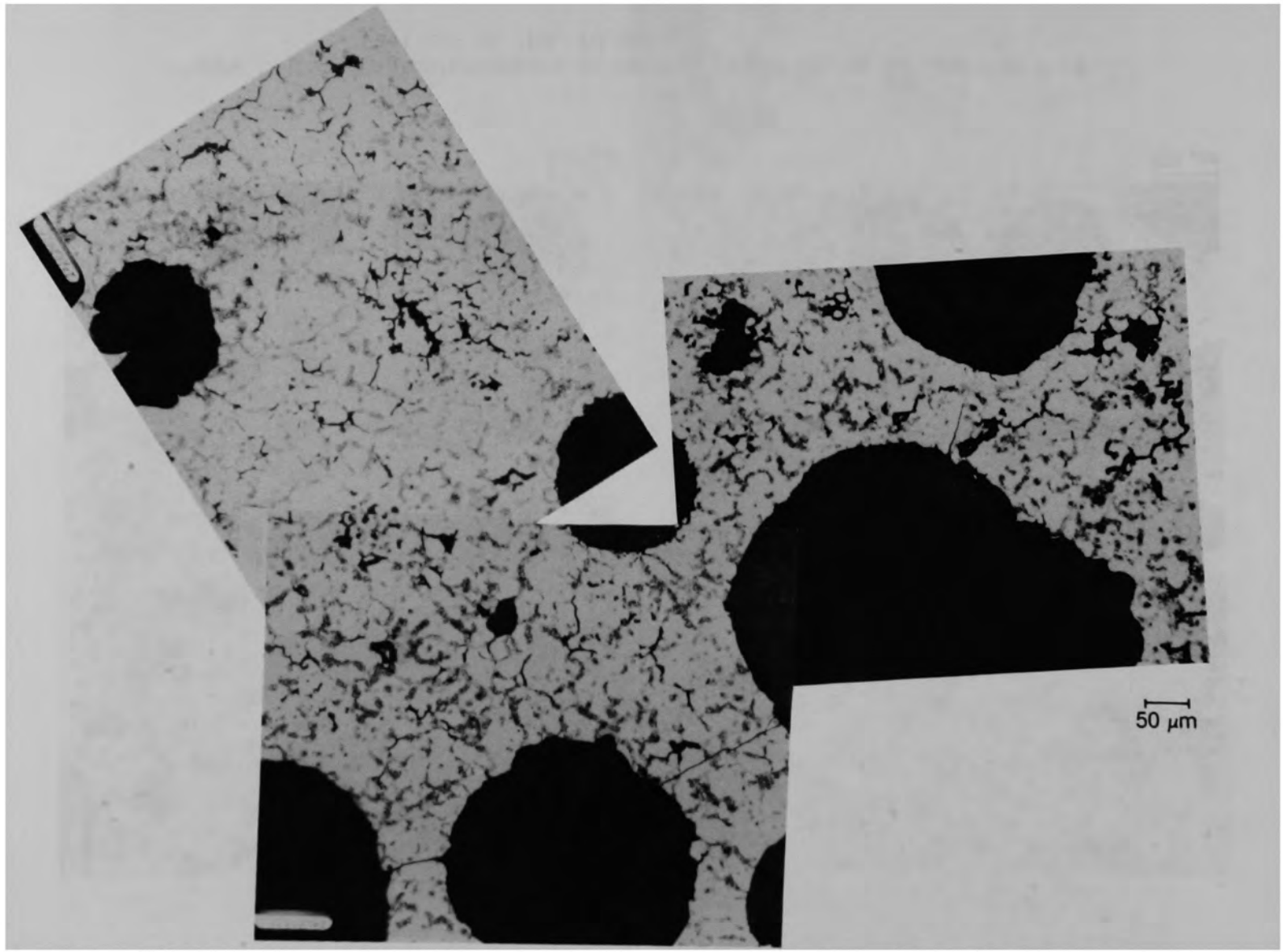

Figure C-170. Etched photomicrographs of material from Region 2, location F of Particle 8C (H8, 70 cm).

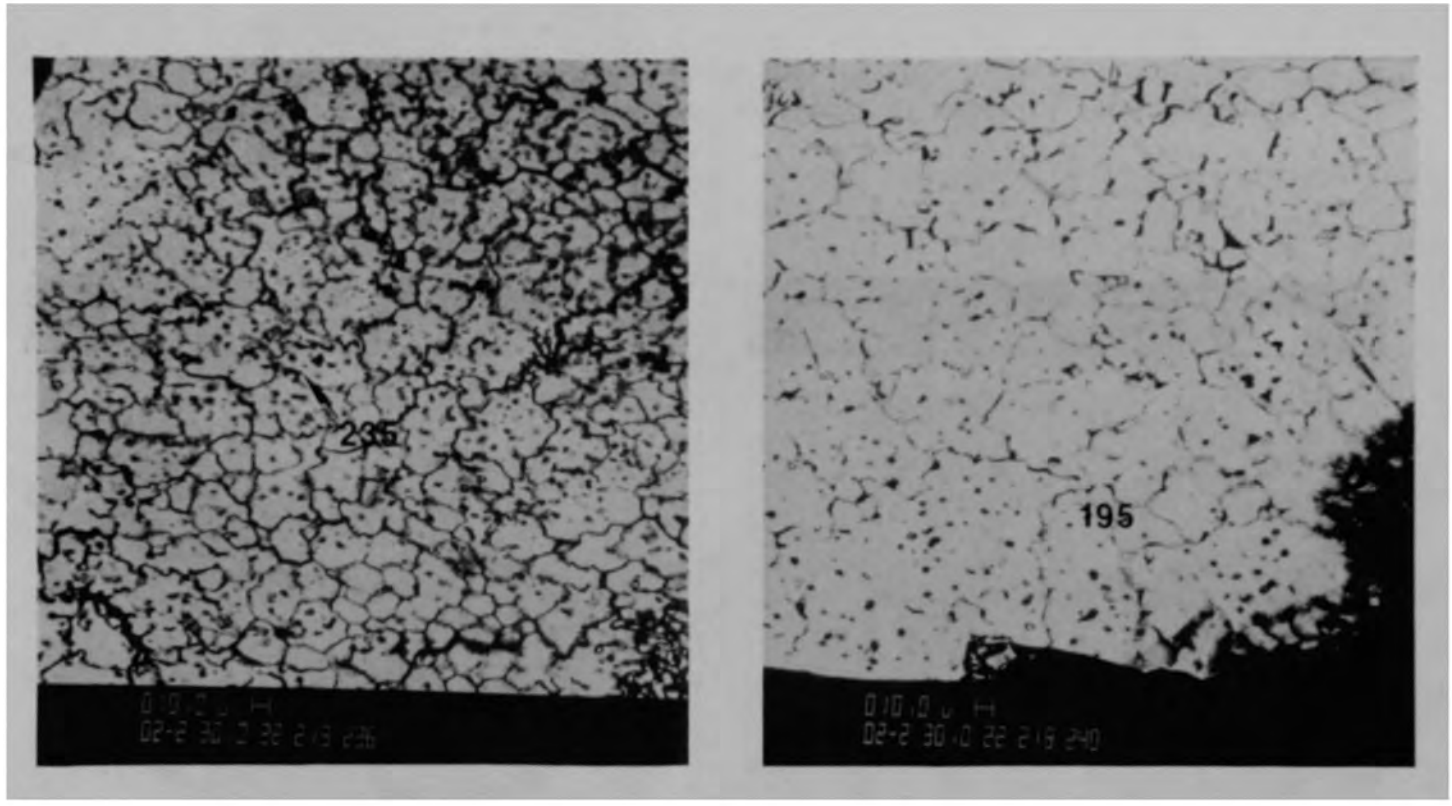

(a) Location D

(b) Location E

Figure C-171. SEM backscattered electron images of material from Region 2 of Particle 8C (H8, 70 cm).

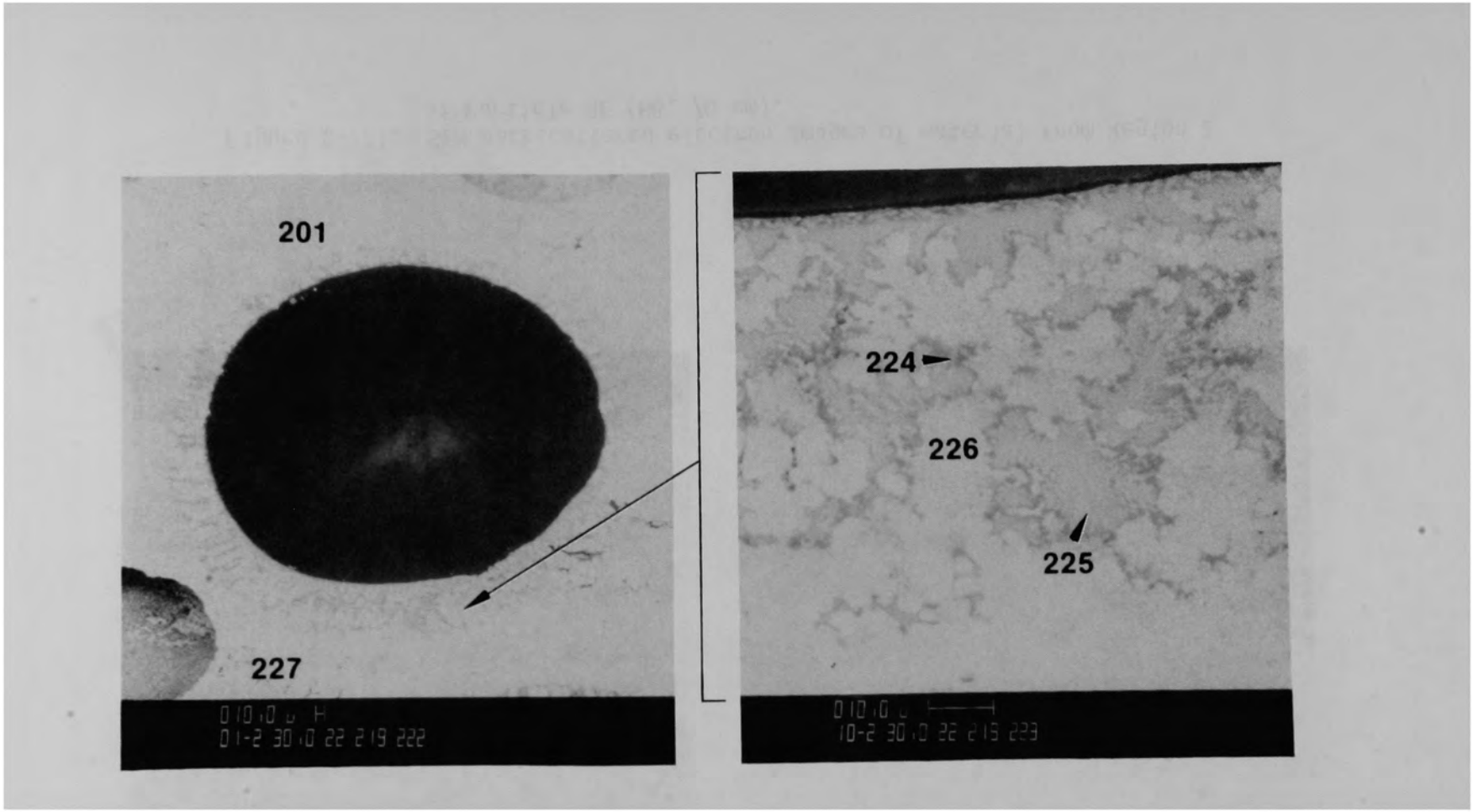

Figure C-172. SEM backscattered electron images of material from Region 2 location G of Particle 8C (H8, 70 cm).

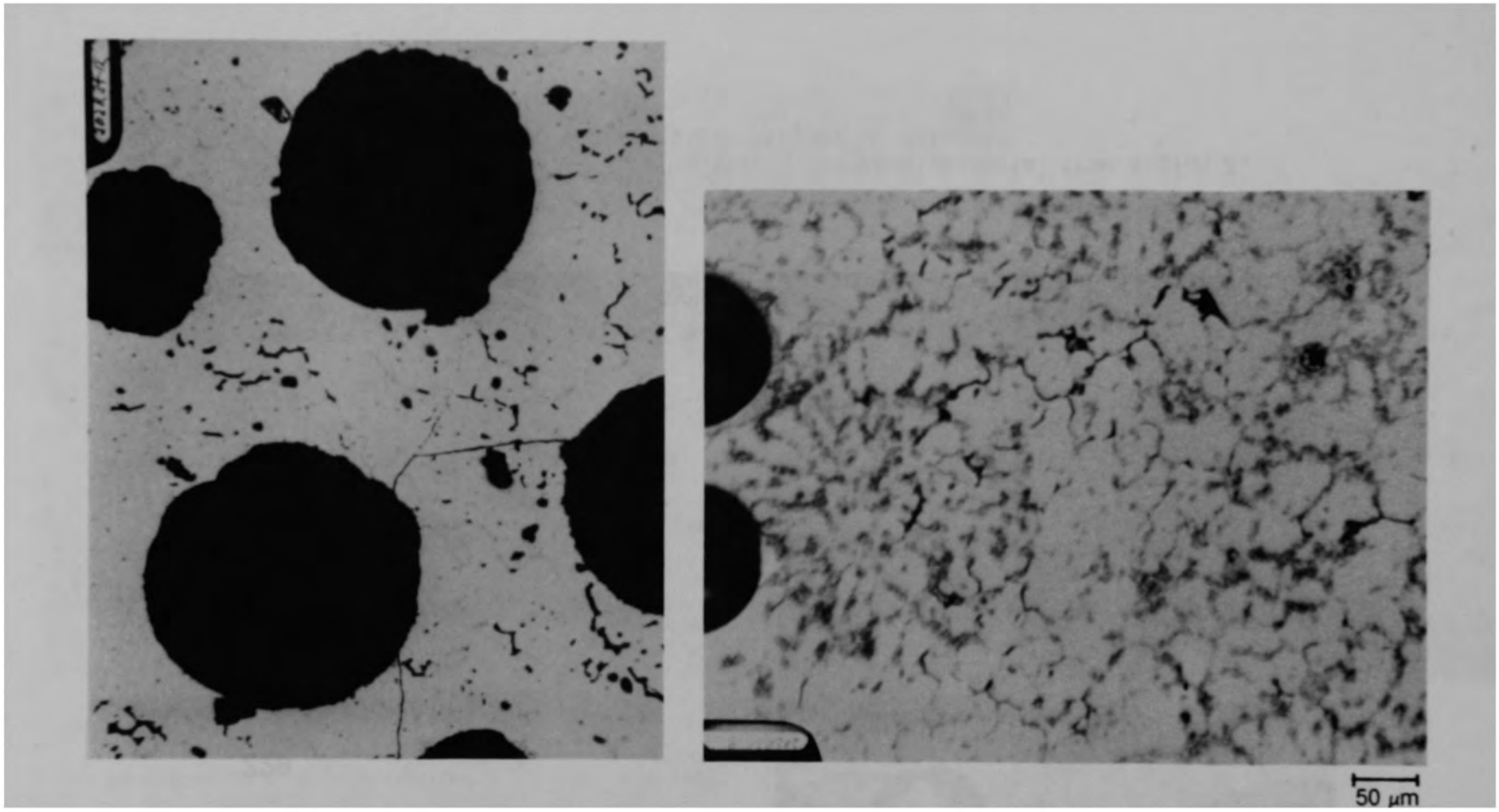

(a) Location H

(b) Location I

Figure C-173. Photomicrographs of material from Region 2 of Particle 8C (H8, 70 cm).

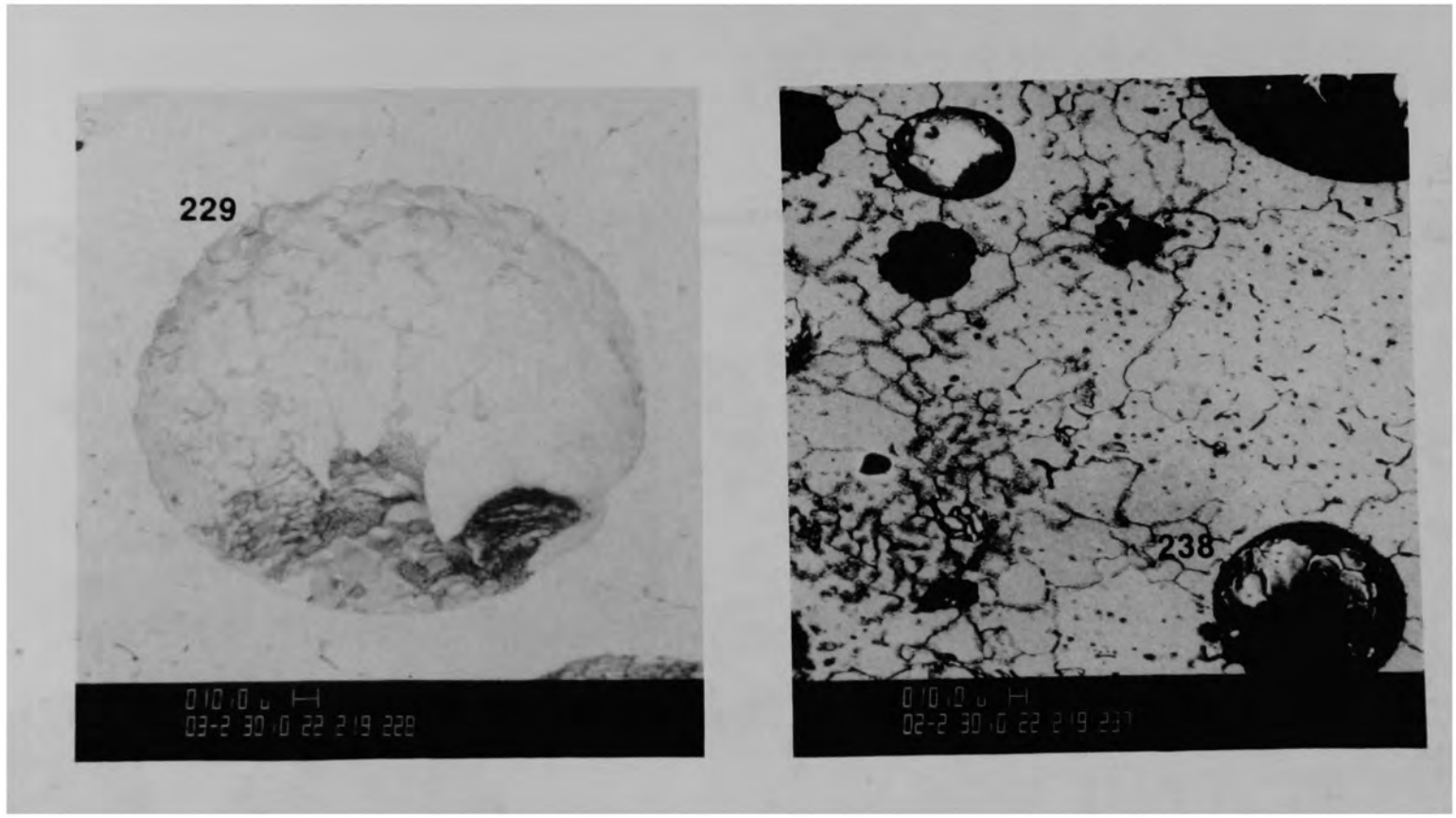

Figure C-174. SEM backscattered electron images of material from Region 2, location H of Particle 8C (H8, 70 cm).

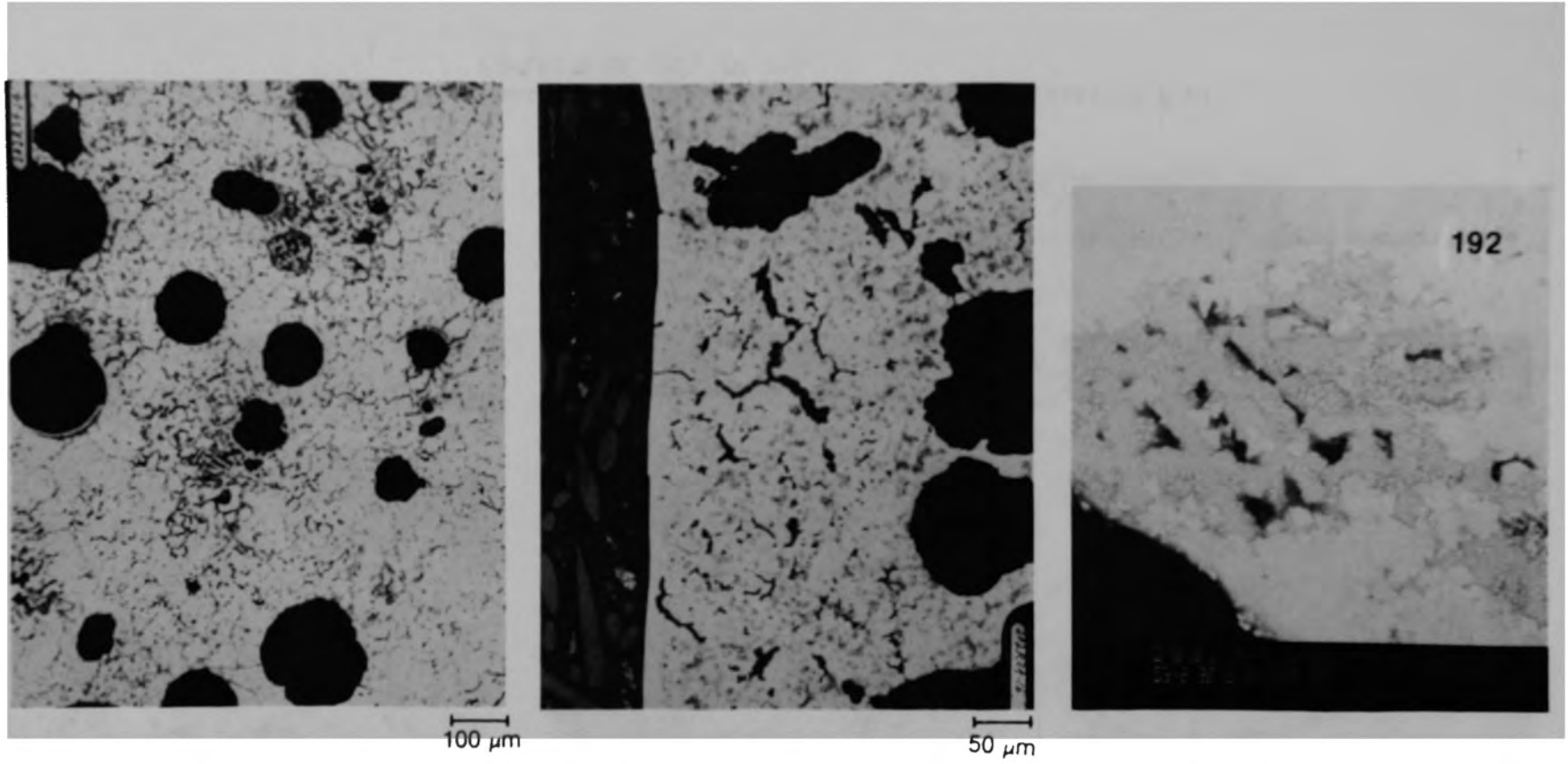

(a) Region2/Region 3, location J

(b) Region 3, location K

(c) Region 3, location L

Figure C-175. Photographs of material from Regions 2 and 3 of Particle 8C (H8, 70 cm).

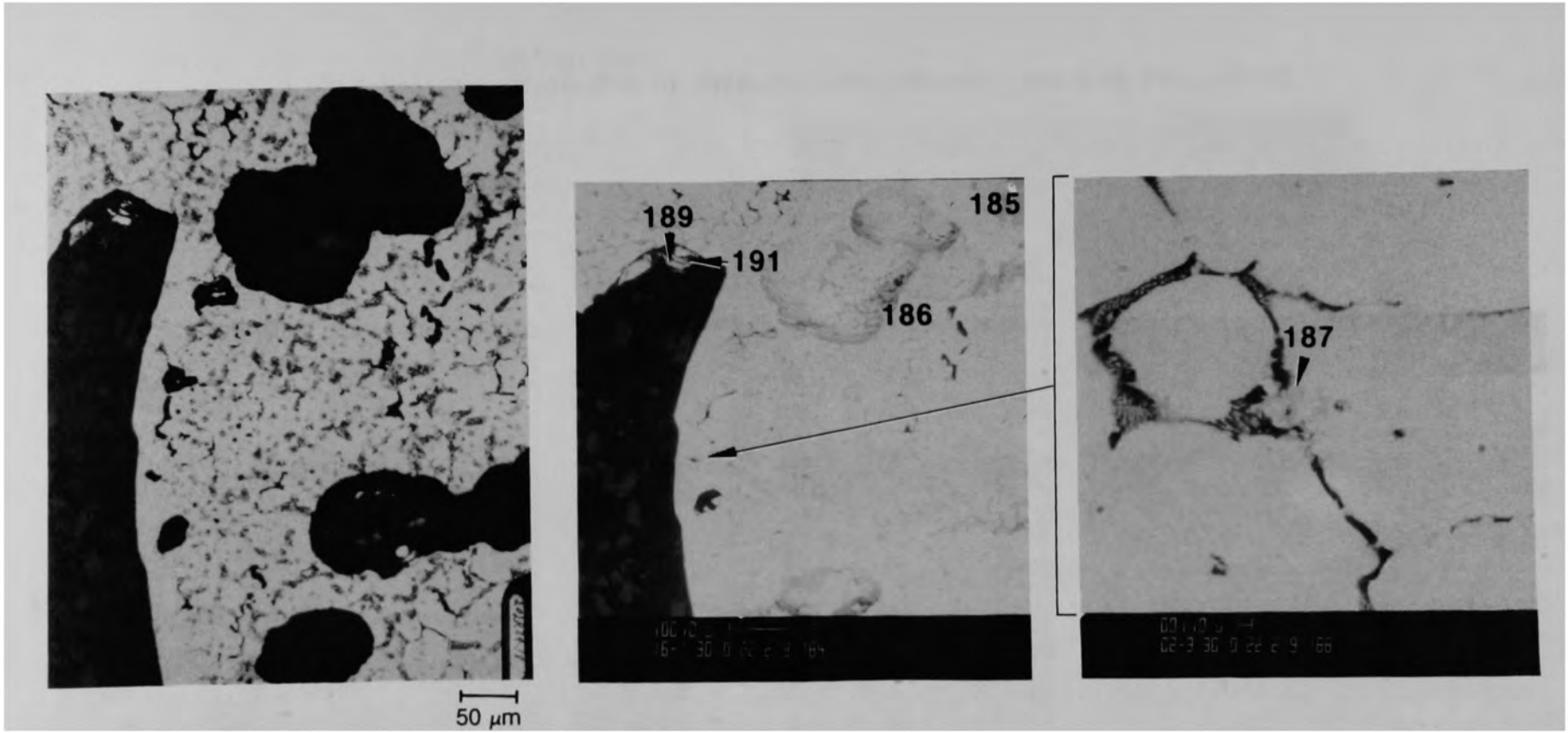

(a) Photomicrograph (b) SEM backscattered electron image (c) SEM backscattered electron image

Figure C-176. Photographs of material from Region 3, location M of Particle 8C (H8, 70 cm).

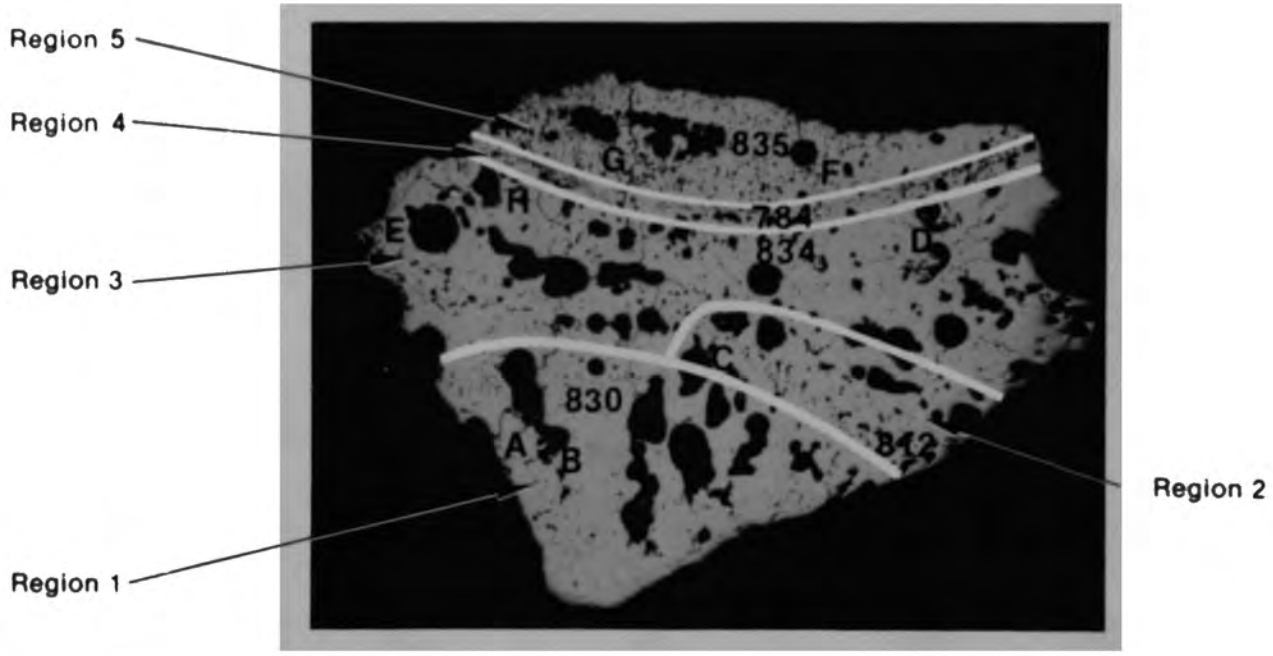

Figure C-177. Photomacrograph of Particle 8E (H8, 70 cm) showing 5 regions based on void morphology and chemical composition.

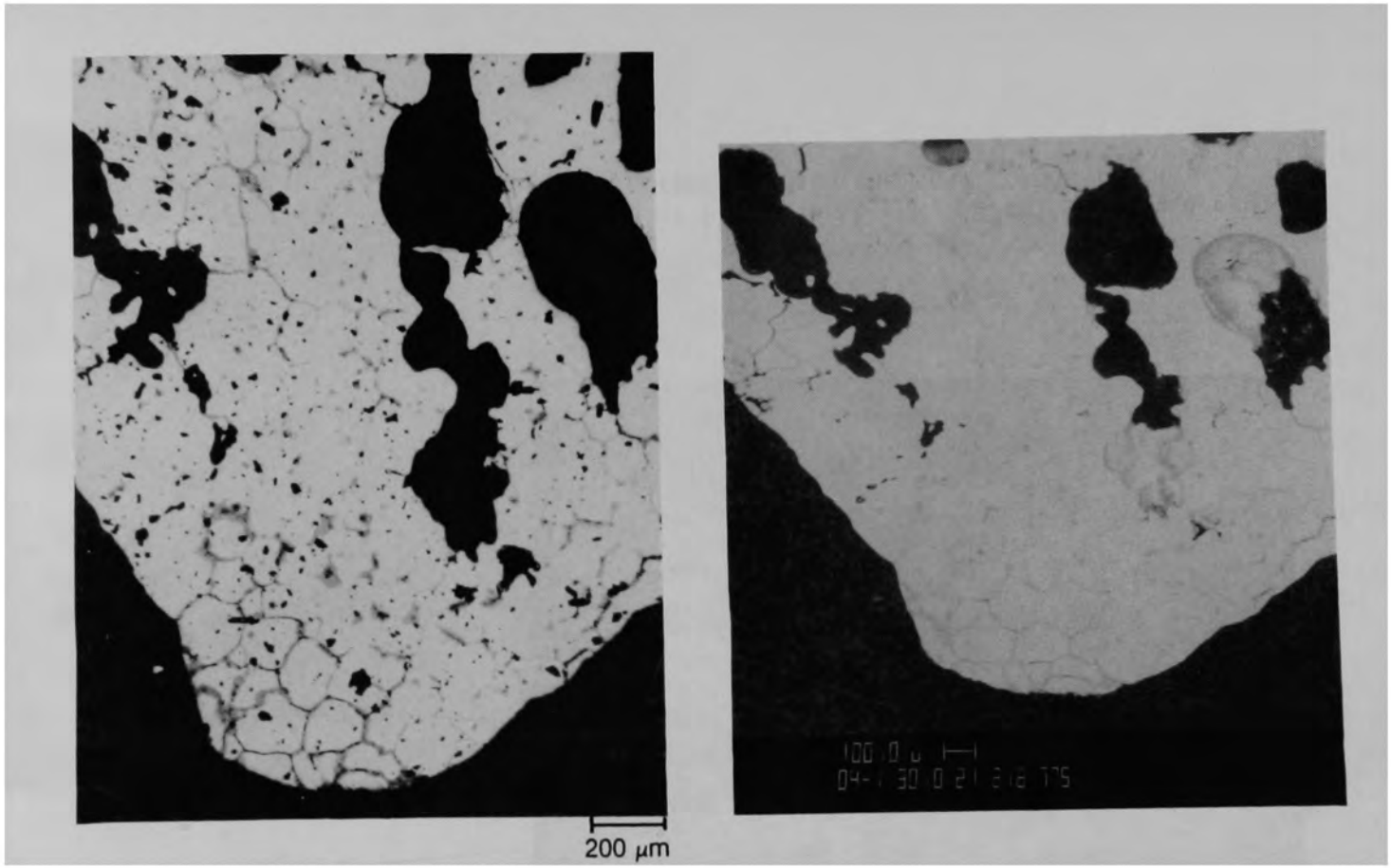

(a) Photomicrograph

(b) SEM backscattered electron image

Figure C-178. Photographs of material from Region 1 of Particle 8E (H8, 70 cm).

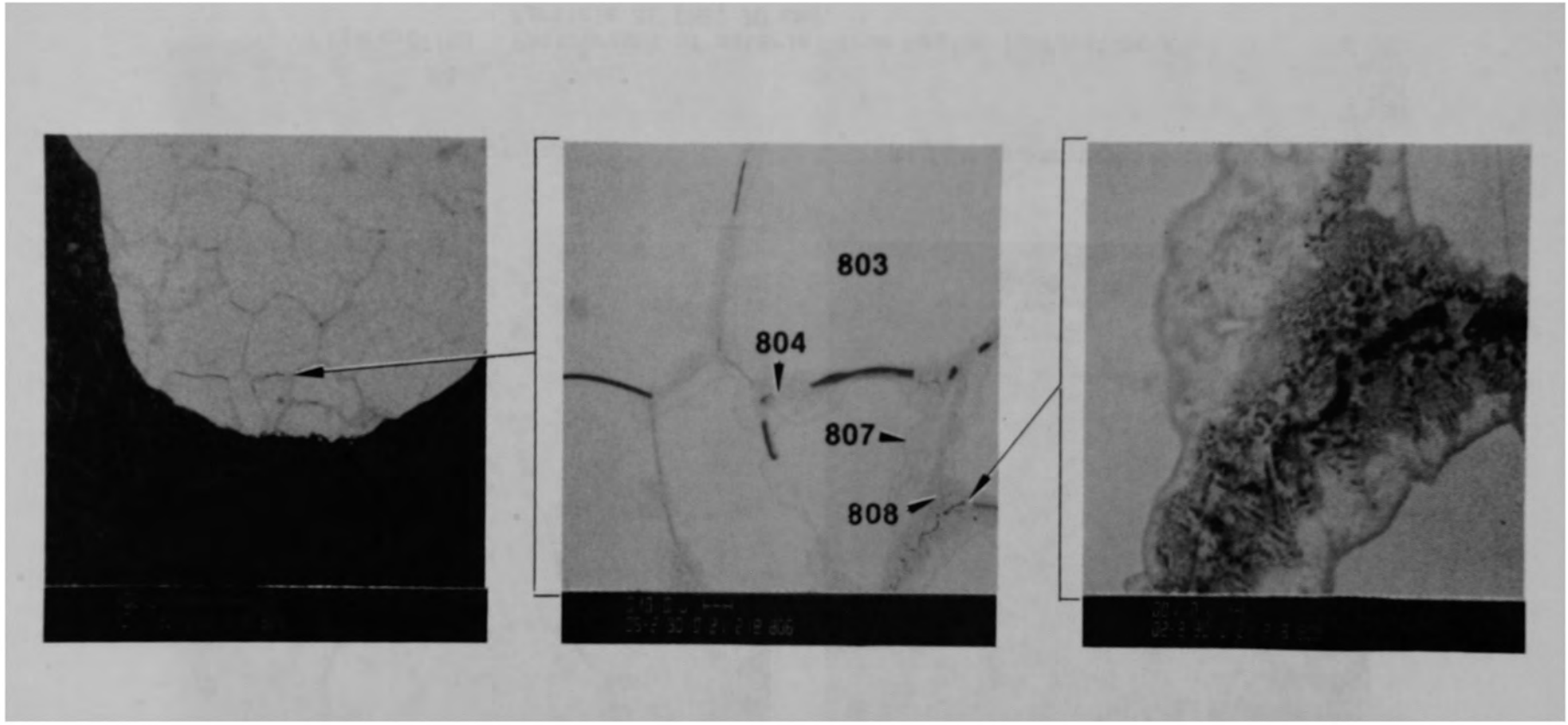

Figure C-179. SEM backscattered electron images of Region 1 of Particle 8E (H8, 70 cm).

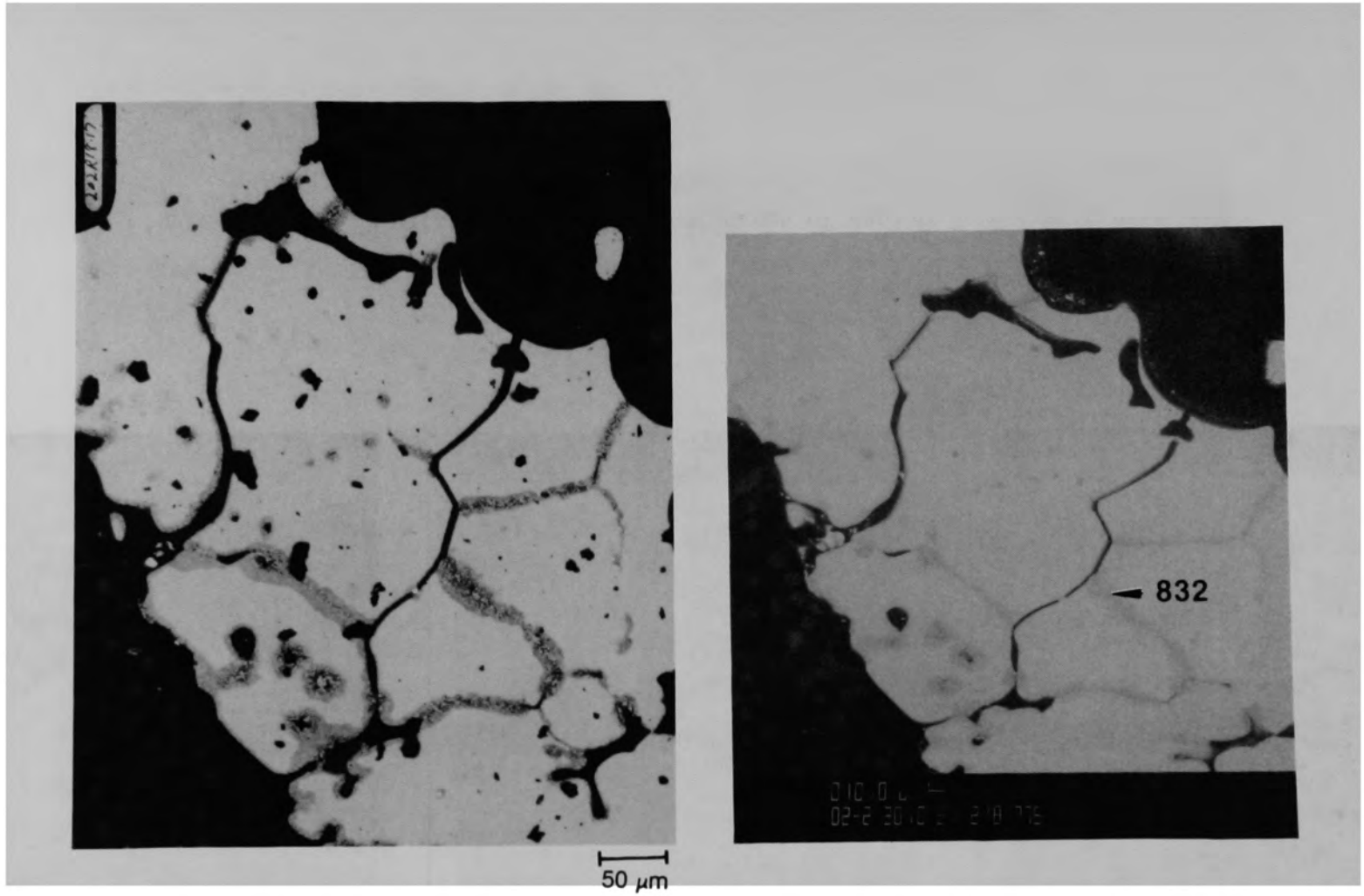

(a) Photomicrograph

(b) SEM backscattered electron image

Figure C-180. Photographs of material from Region 1, location A of Particle 8E (H8, 70 cm).

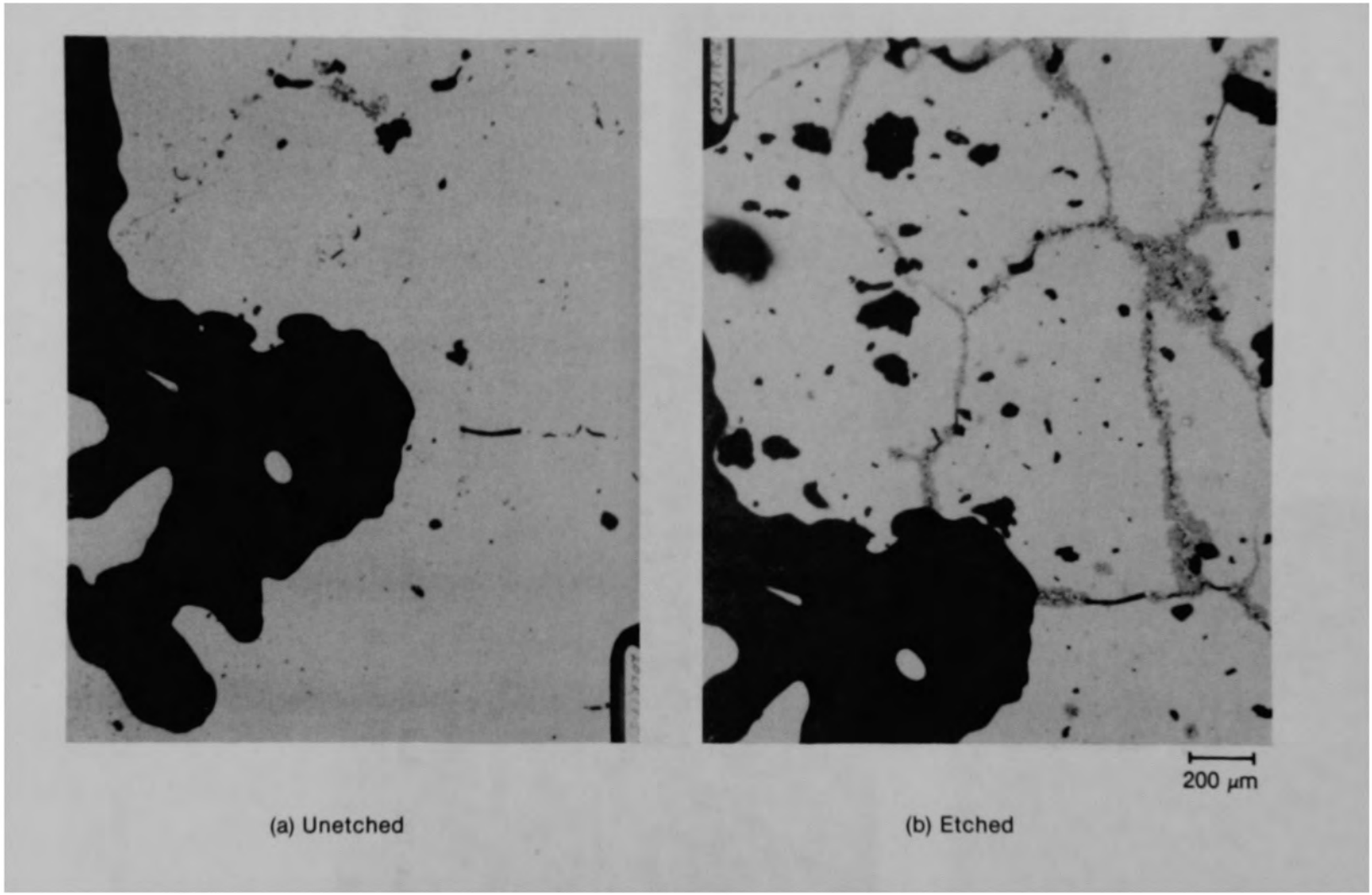

Figure C-181. Photomicrographs of material from Region 1, location B of Particle 8E (H8, 70 cm).

Figure C-182. SEM backscattered electron image of Region 1, location C of Particle 8E (H8, 70 cm).

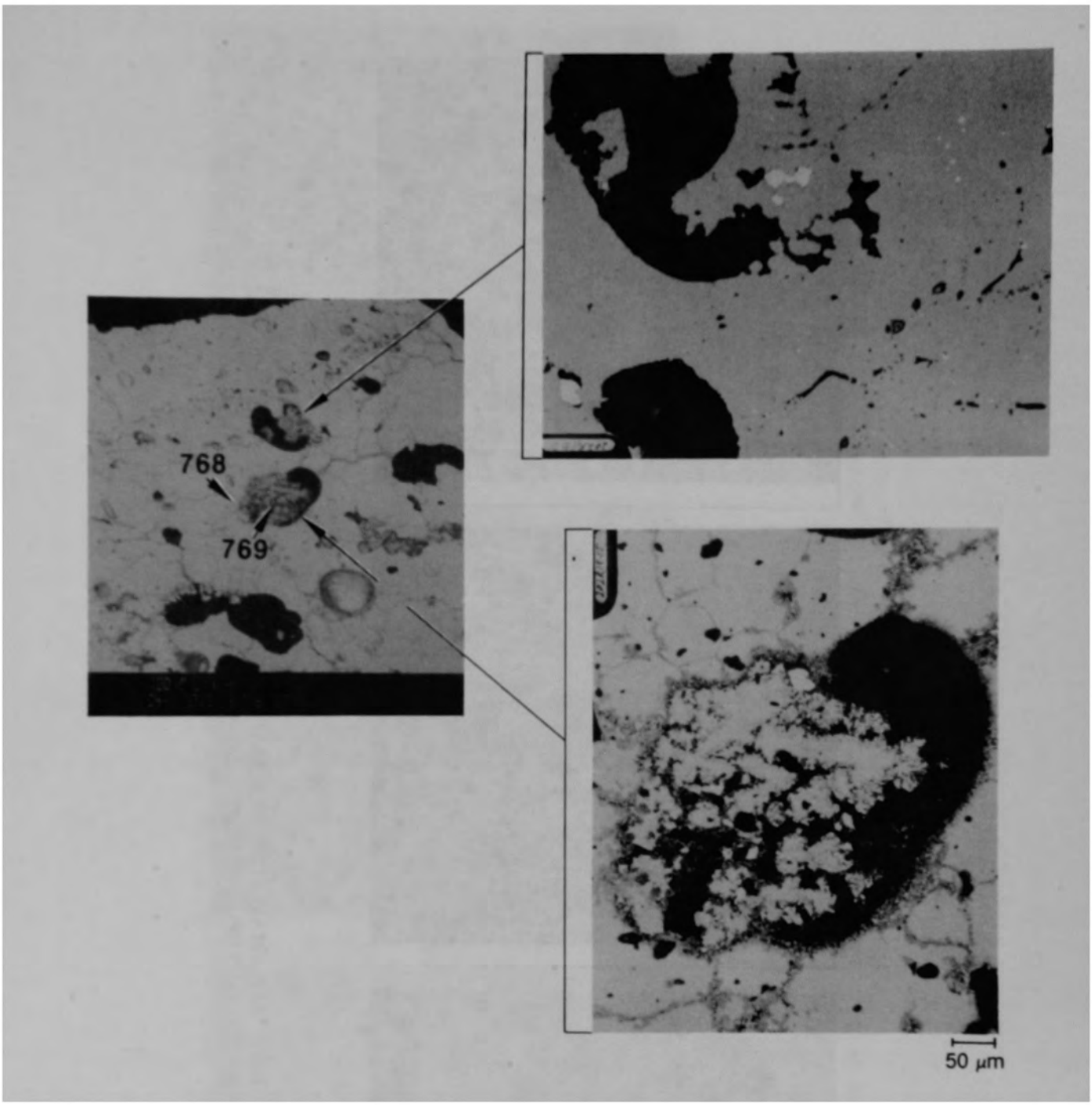

Figure C-183. Photographs of material from Region 3, location D of Particle 8E (H8, 70 cm).

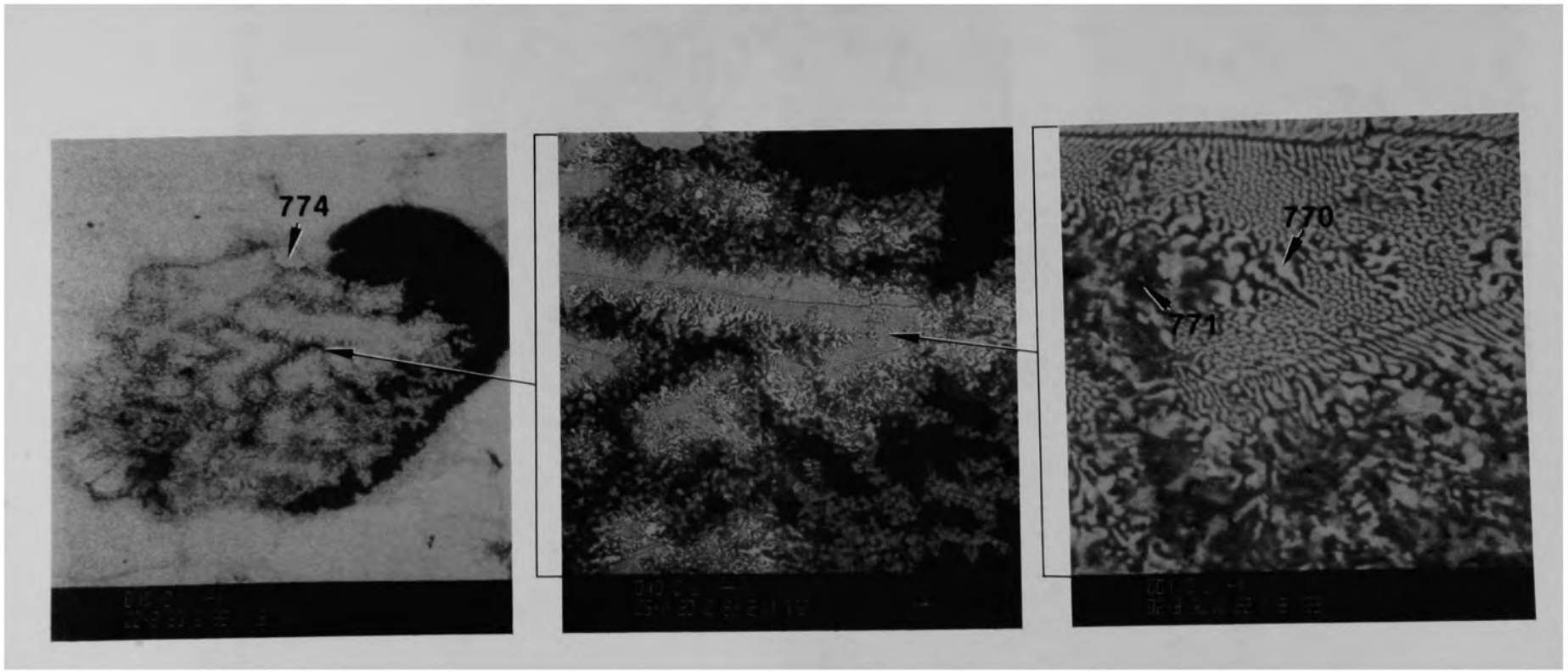

Figure C-184. SEM backscattered electron images of material from Region 3 location D of Particle 8E (H8, 70 cm).

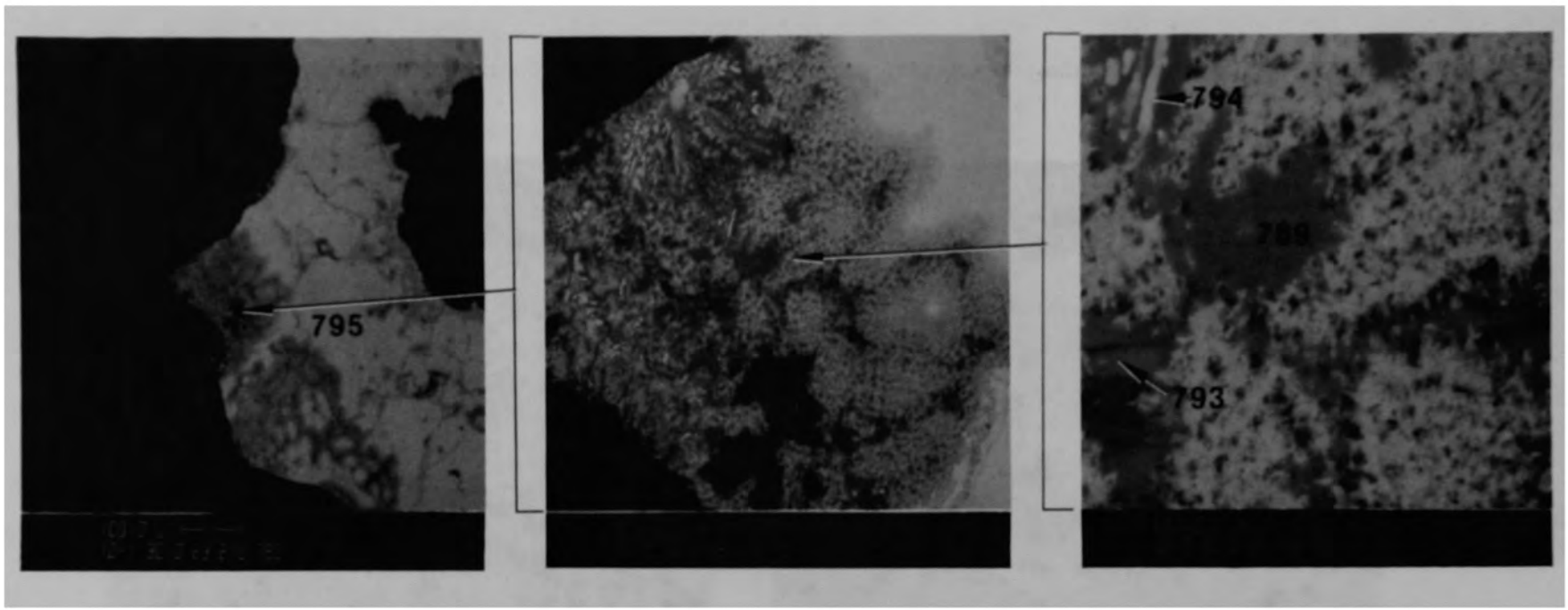

Figure C-185. SEM backscattered electron images of material from Region 3, location E of Particle 8E (H8, 70 cm).

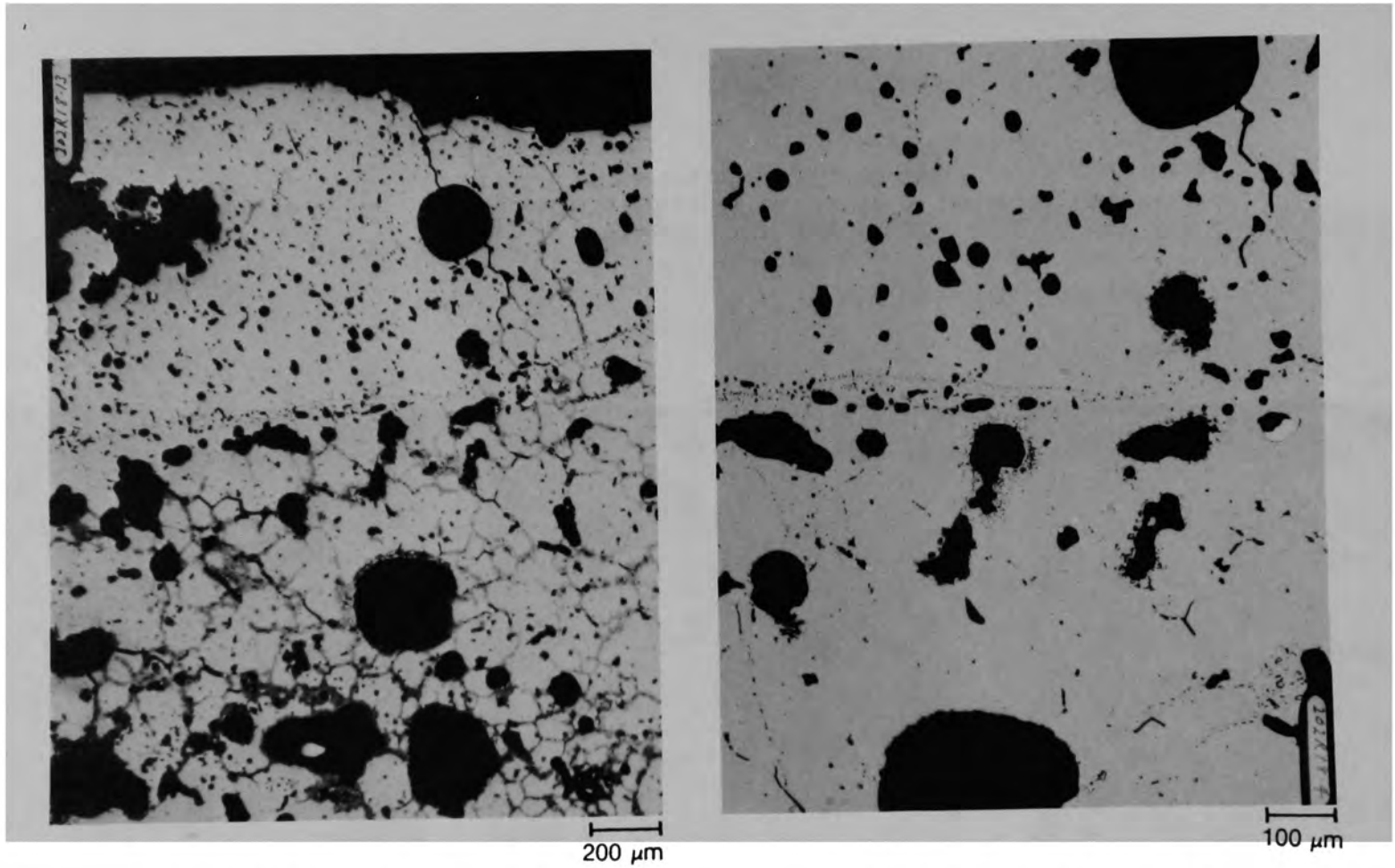

(a) Includes Regions 2 through 5

(b) Includes Regions 3 through 5

Figure C-186. Photomicrographs of region interfaces from location F of Particle 8E (H8, 70 cm).

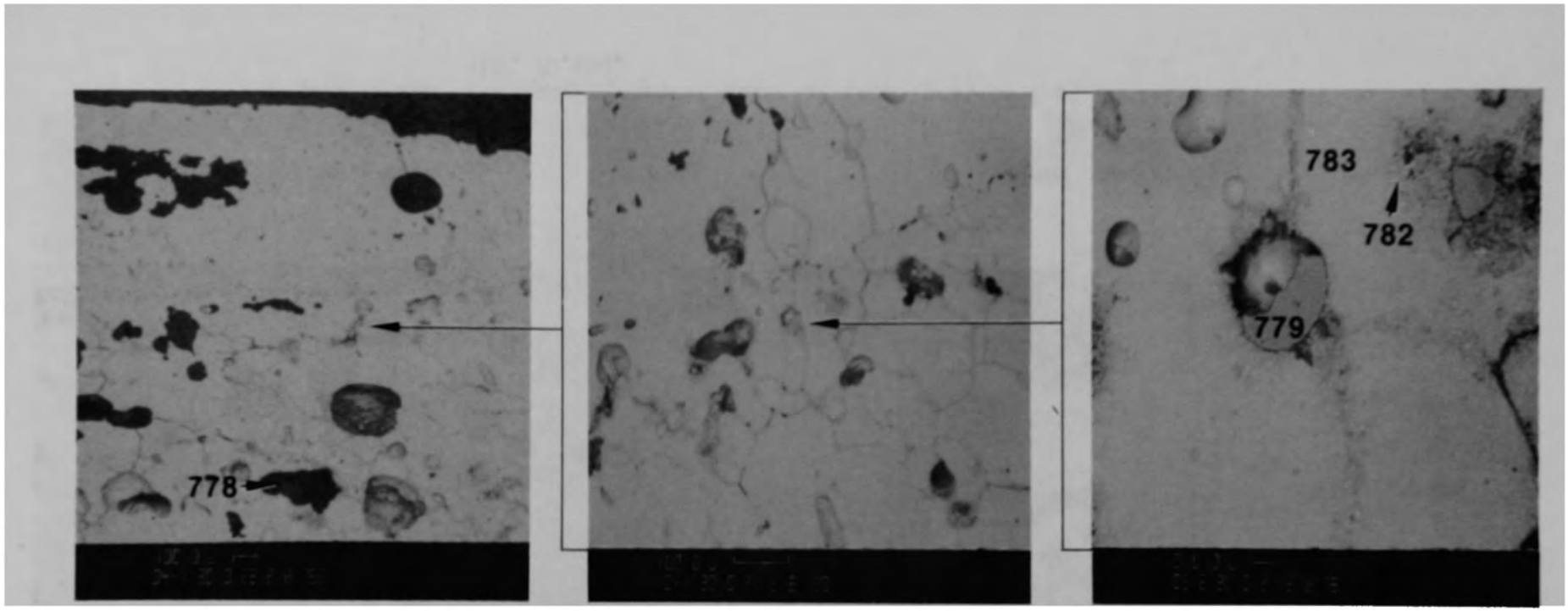

(a) Includes Regions 2 through 5

(b) Includes Regions 3 and 4

(c) Region 4 inclusion

Figure C-187. SEM backscattered electron images of location F region interfaces of Particle 8E (H8, 70 cm).

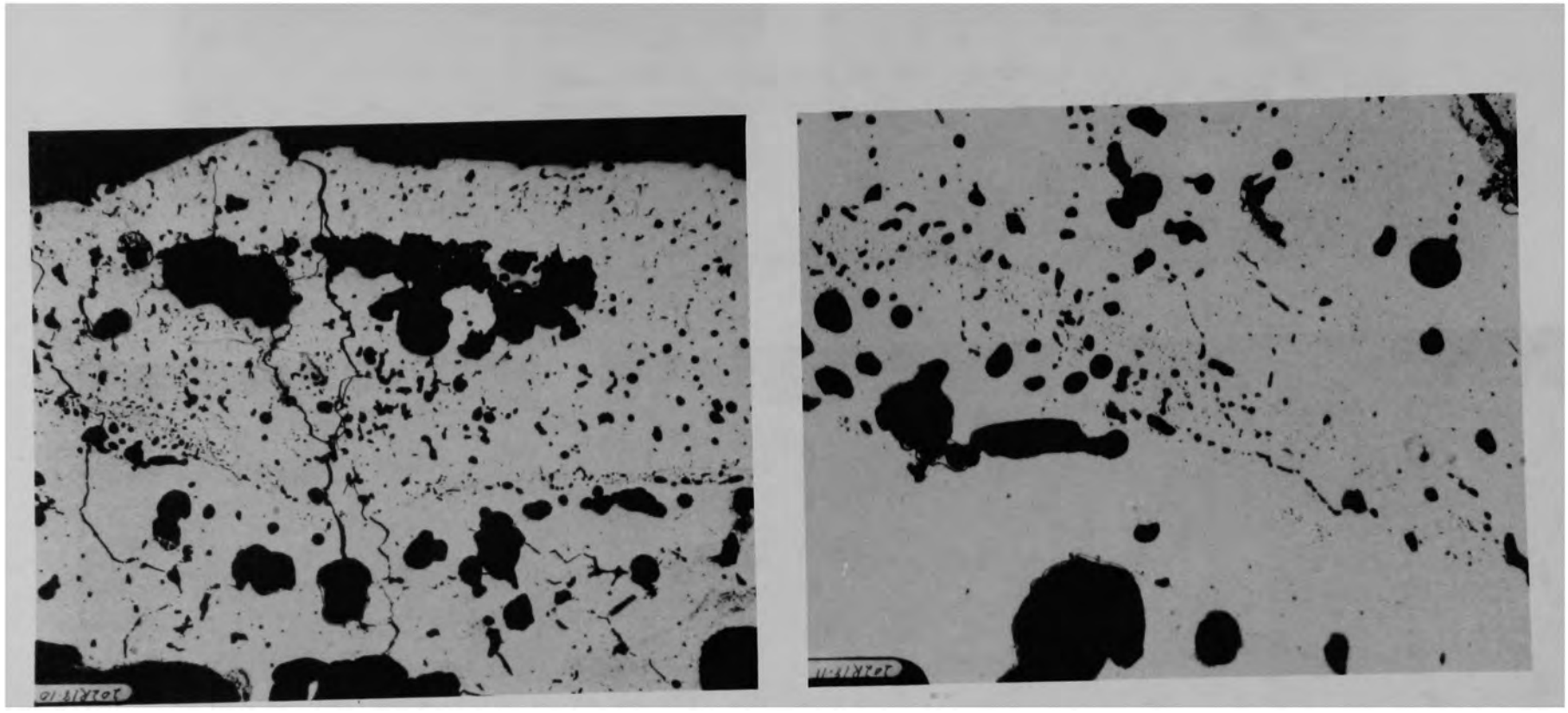

(a) Region 3 through 5

(b) Regions 3 through 5

Figure C-188. Photomicrograph of material from location G of Particle 8E (H8, 70 cm).

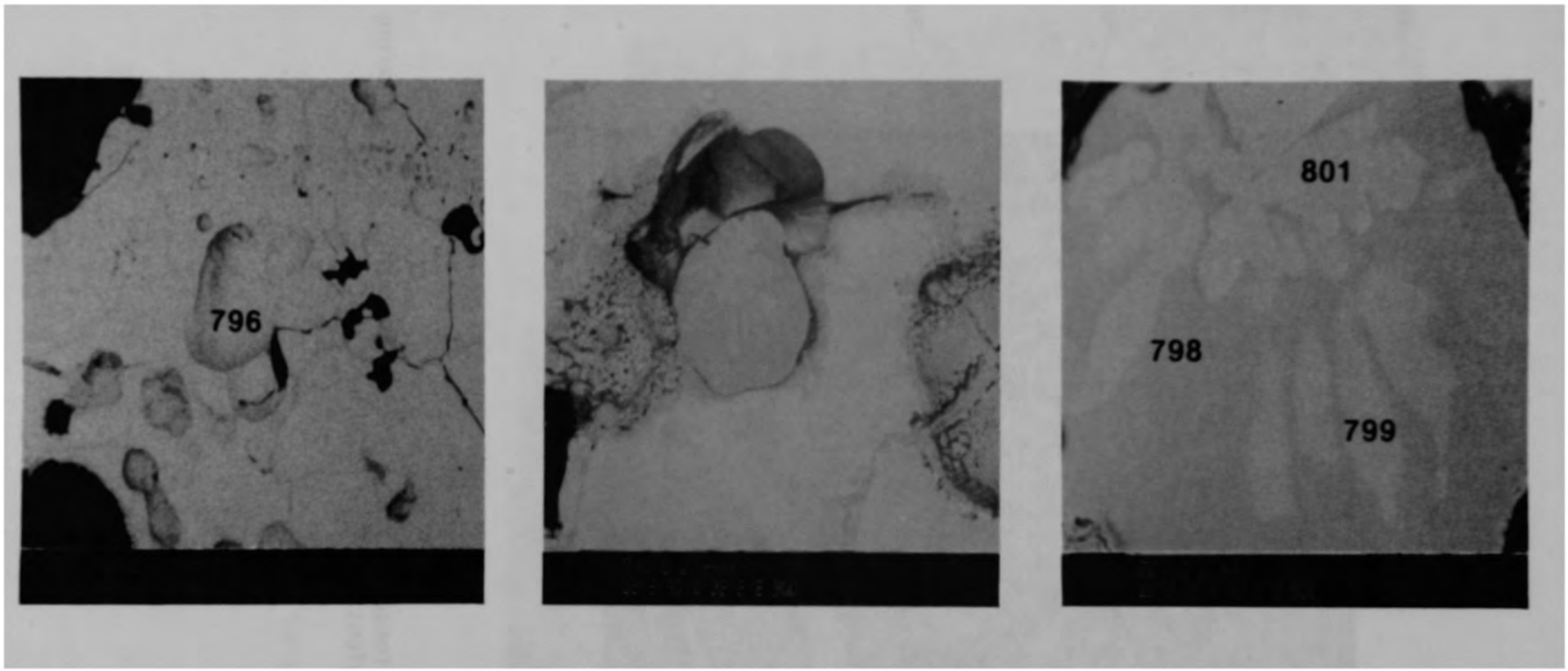

Figure C-189. SEM backscattered electron images of material from Region 3, location H of Particle 8E (H8, 70 cm).

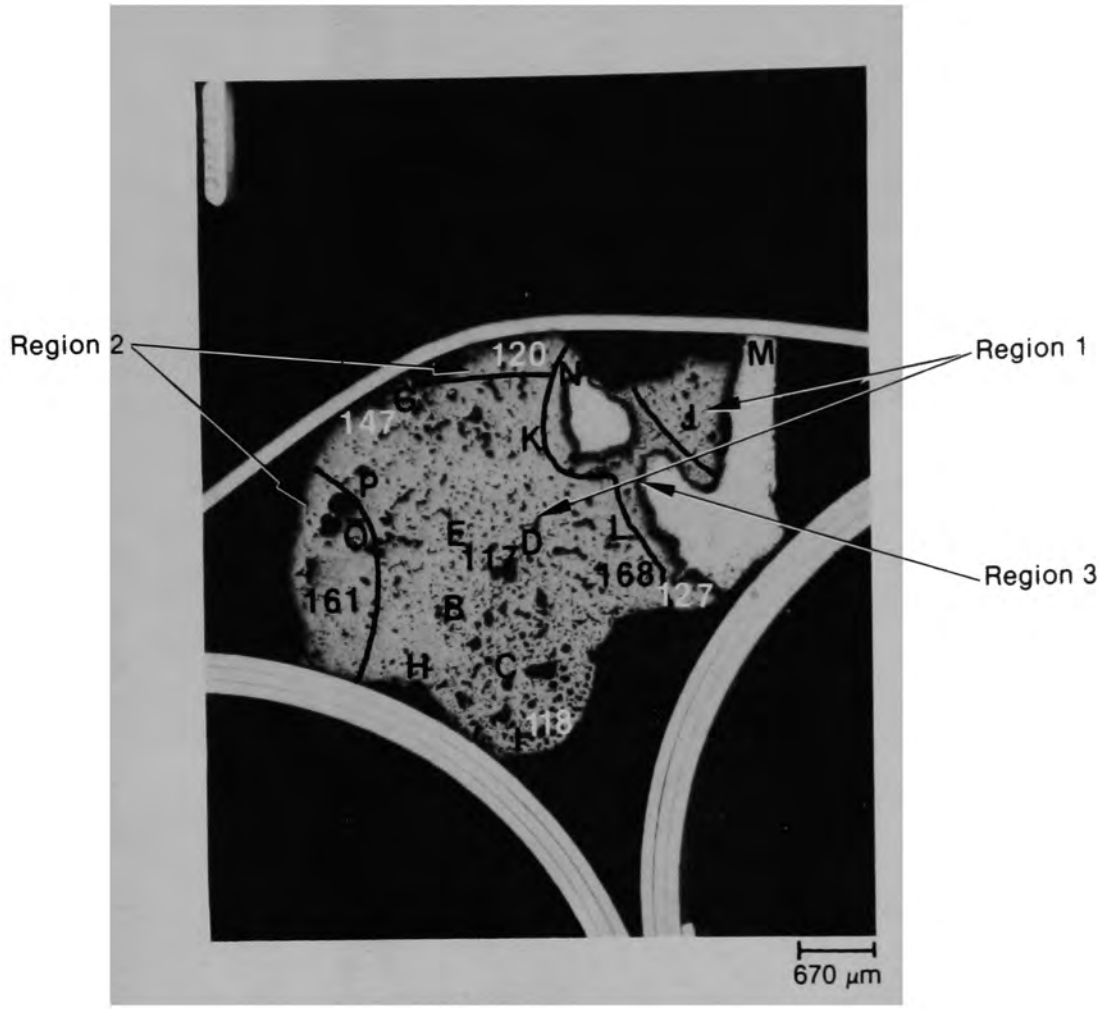

Figure C-190. Photomacrograph of Particle 8H (H8, 70 cm) showing three regions based on Zr,U ratios.

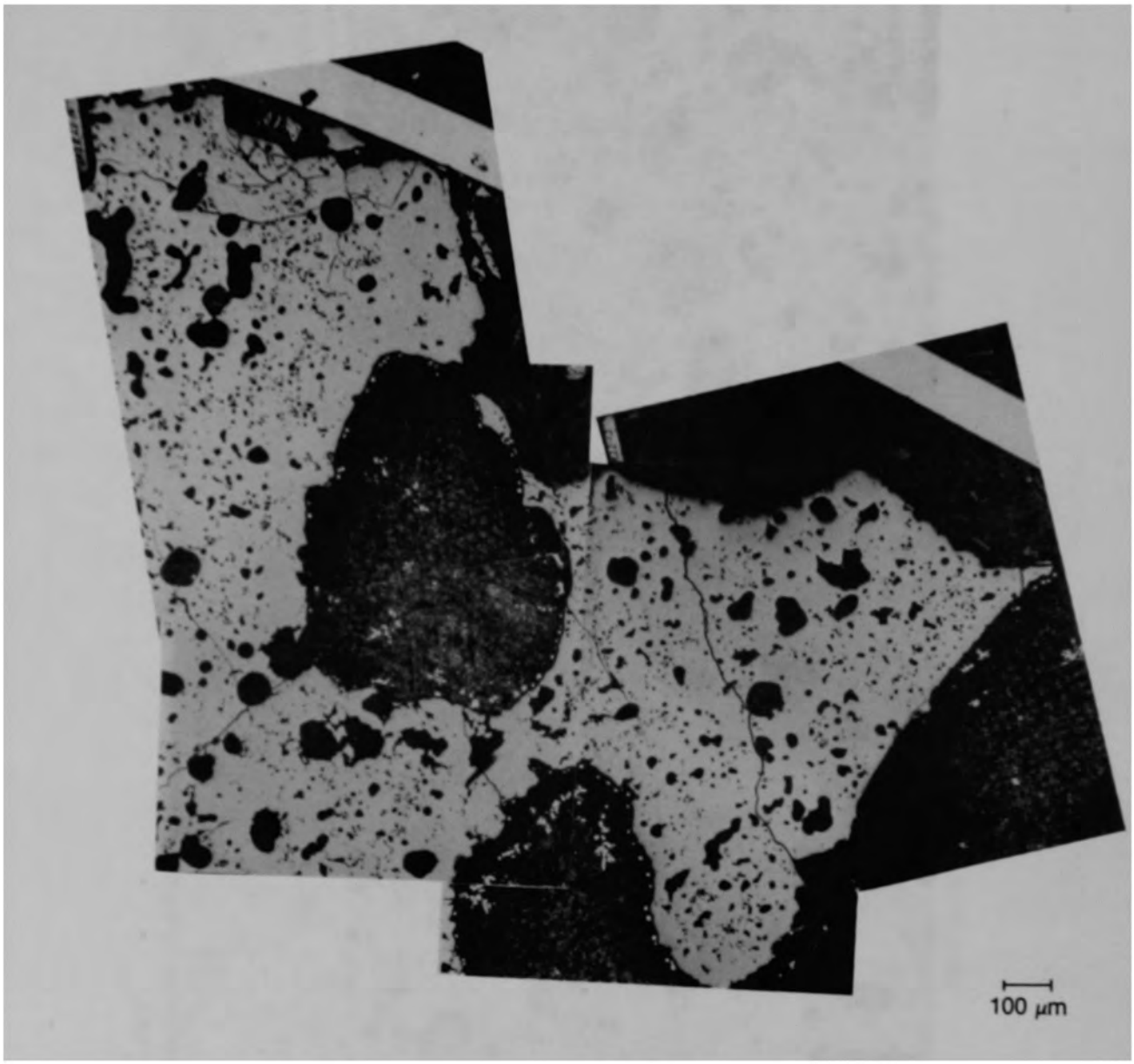

Figure C-191. Photomicrographs of galvanic etch in polisher of Particle 8H (H8, 70 cm).

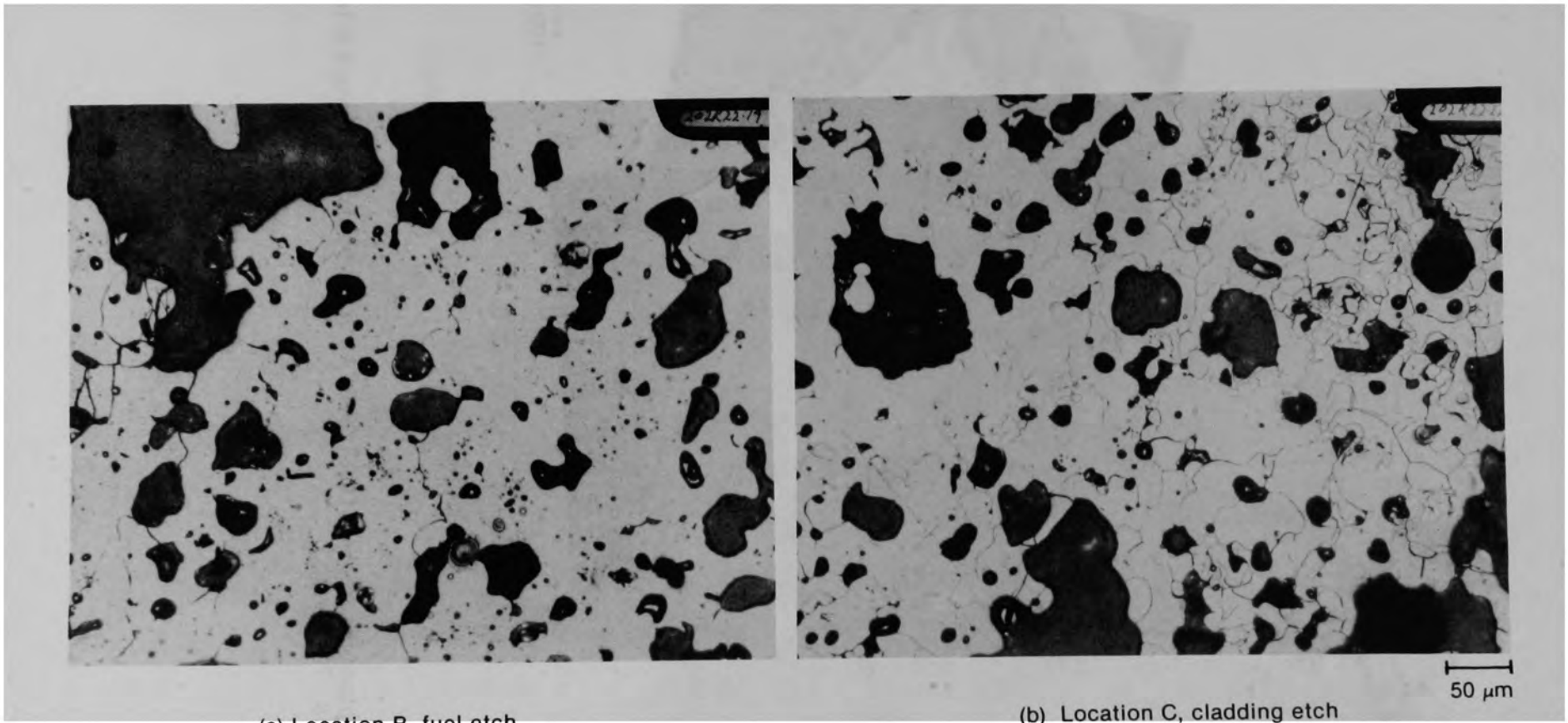

(a) Location B, fuel etch

(b) Location C, cladding etch

Figure C-192. Photomicrographs of material in Region 1 of Particle 8H (H8, 70 cm).

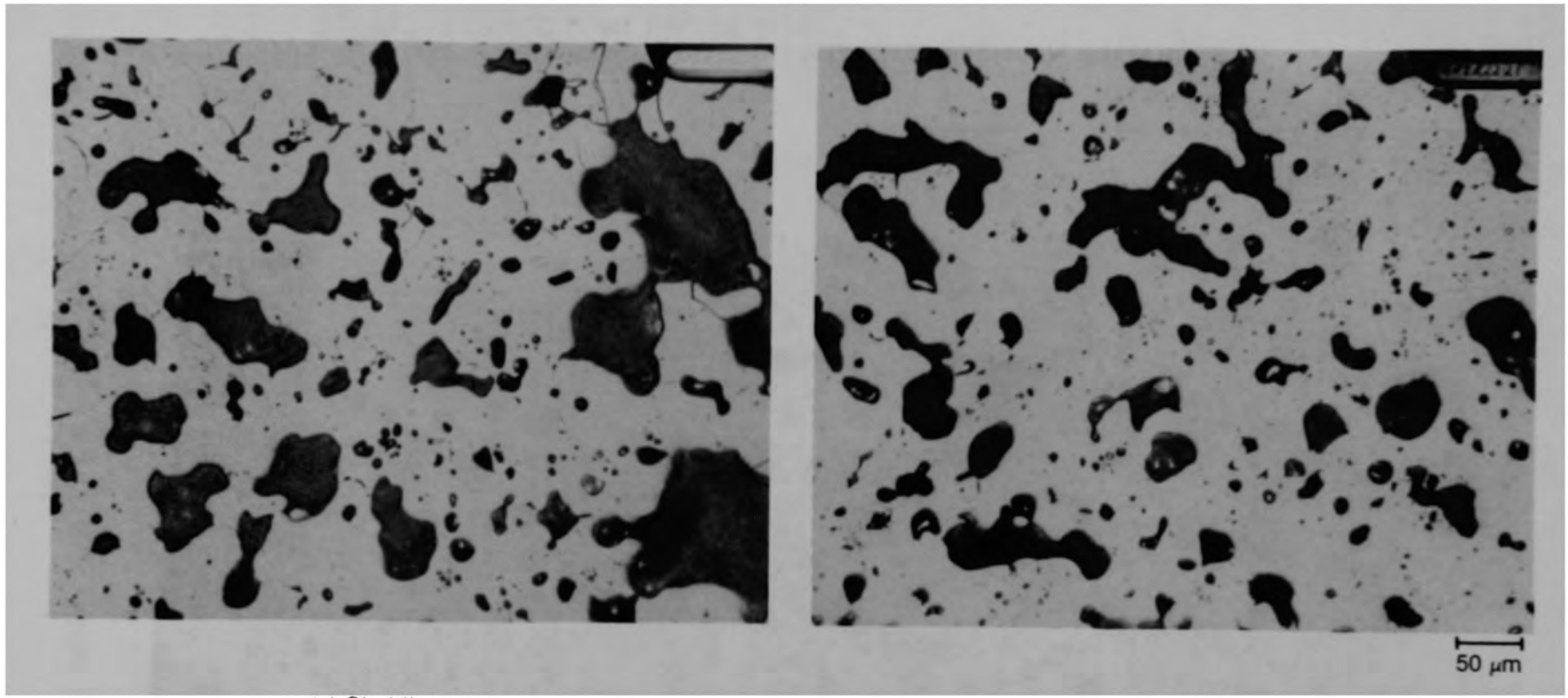

(a) Cladding etch

(b) Fuel etch

Figure C-193. Photomicrographs of material from Region 1, location E of Particle 8H (H8, 70 cm).

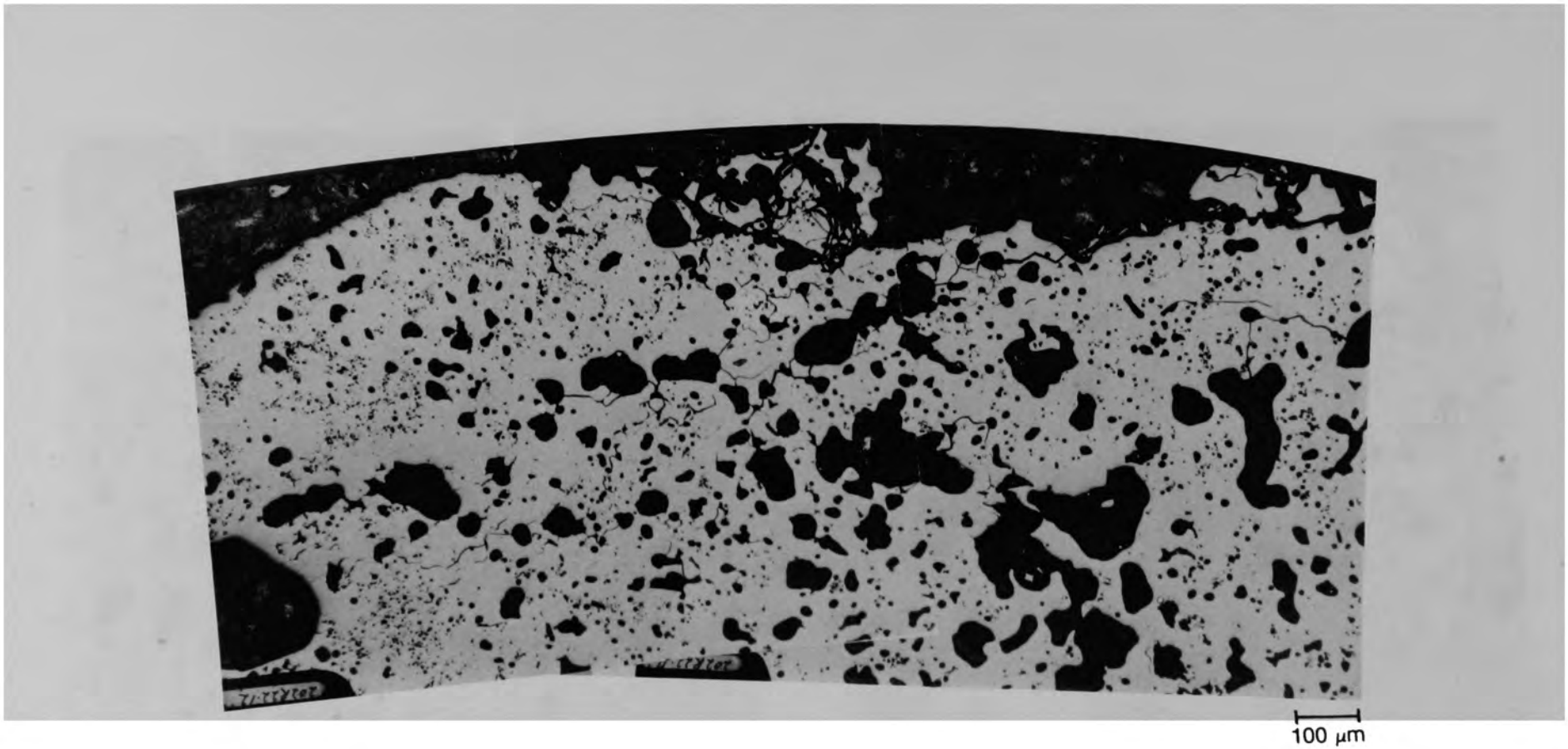

Figure C-194. Photomicrographs of material from Region 1, location G of Particle 8H (H8, 70 cm).

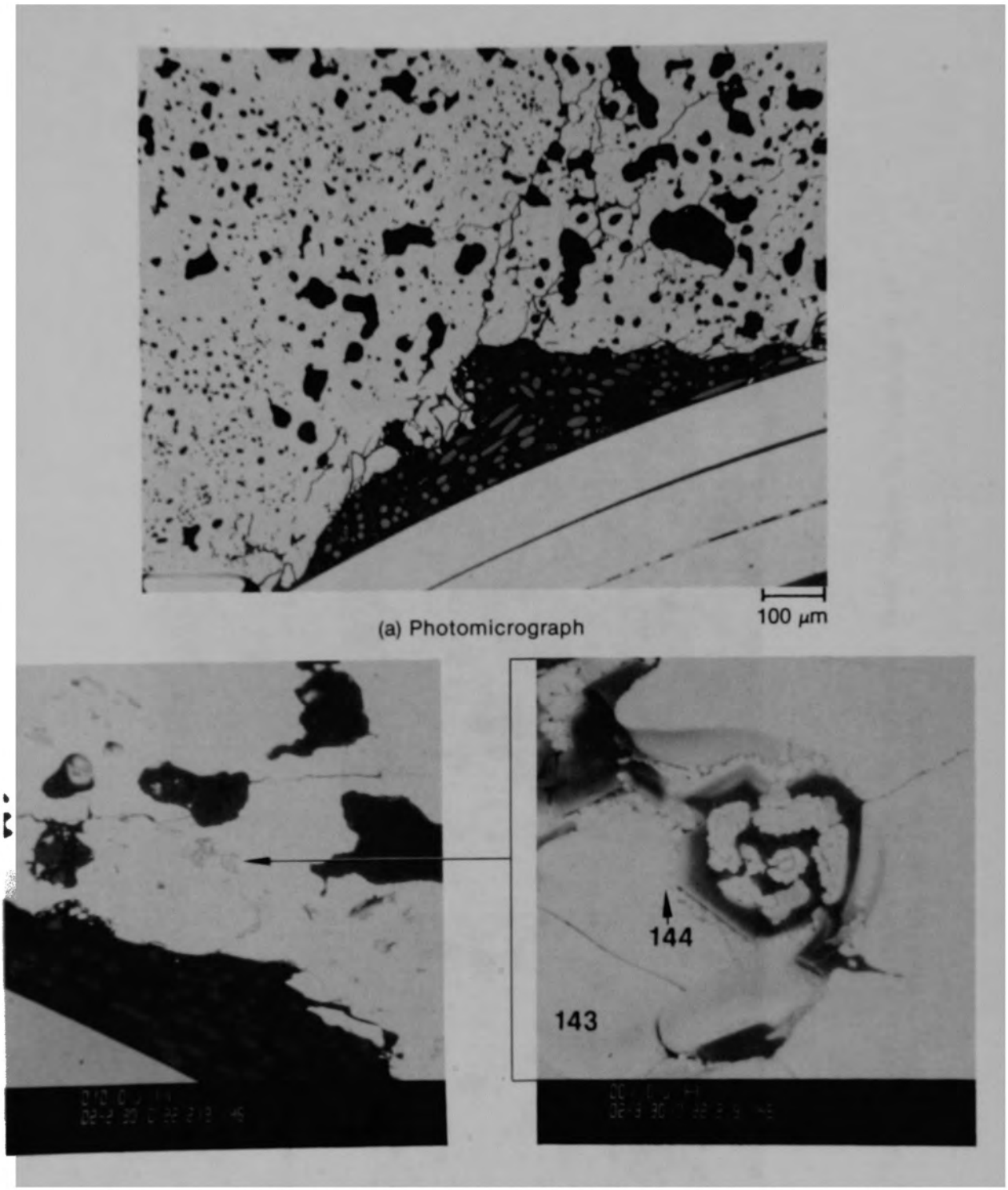

Figure C-195. Photographs of material from Region 1, location H of Particle 8H (H8, 70 cm).

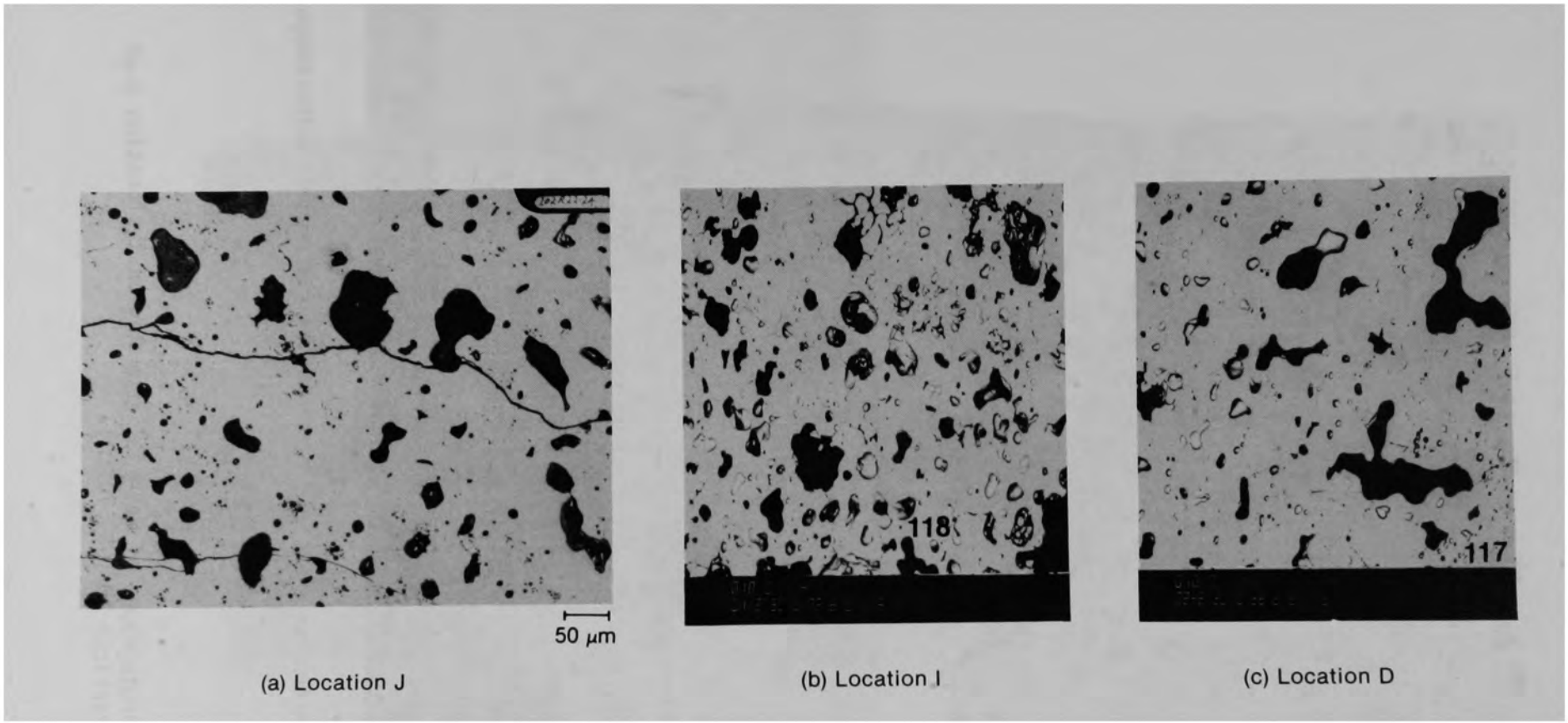

Figure C-196. Photographs of material from Region 1 of Particle 8H (H8, 70 cm).

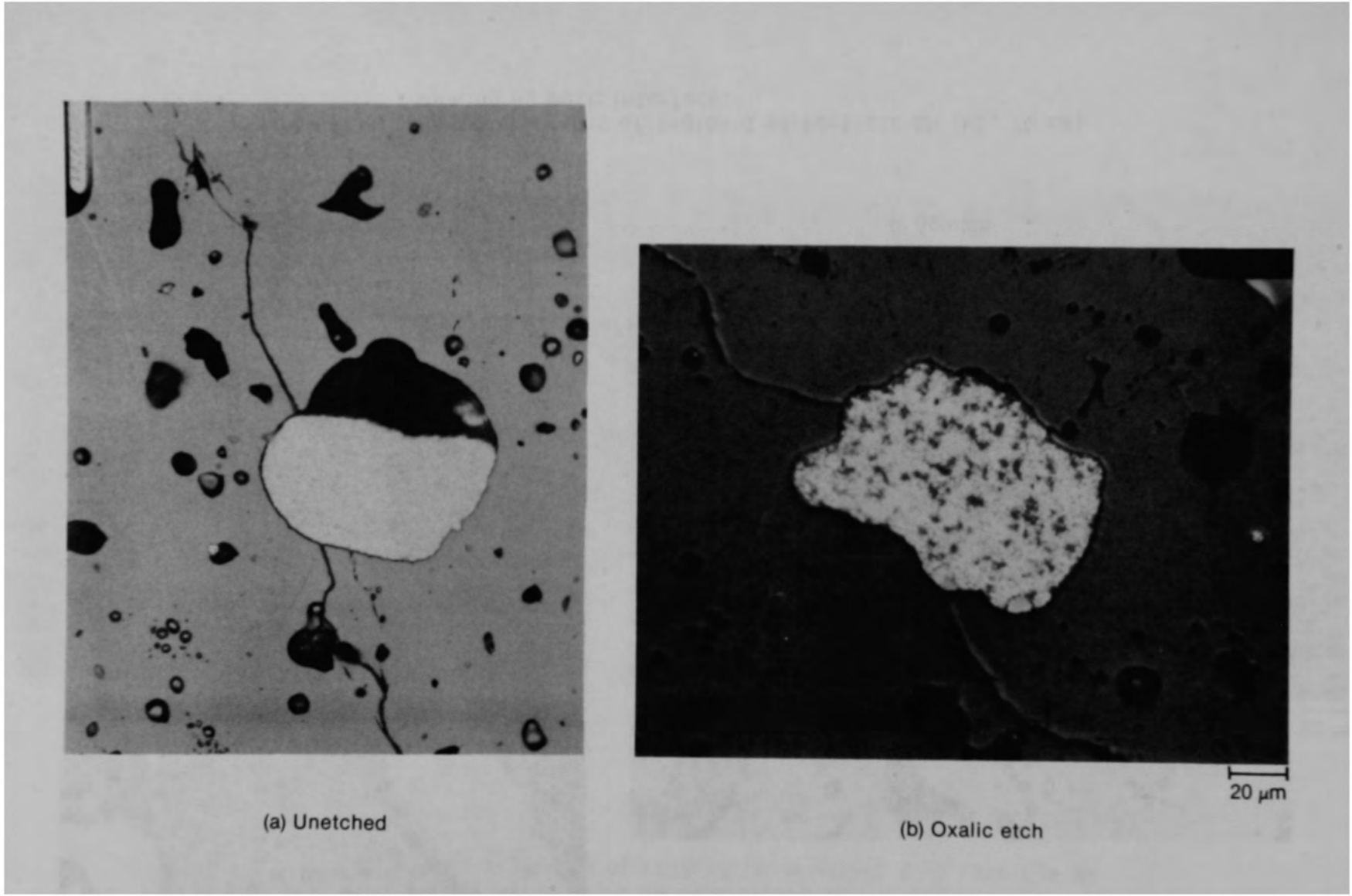

Figure C-197. Photomicrographs of material from Region 1, location K of Particle 8H (H8, 70 cm).

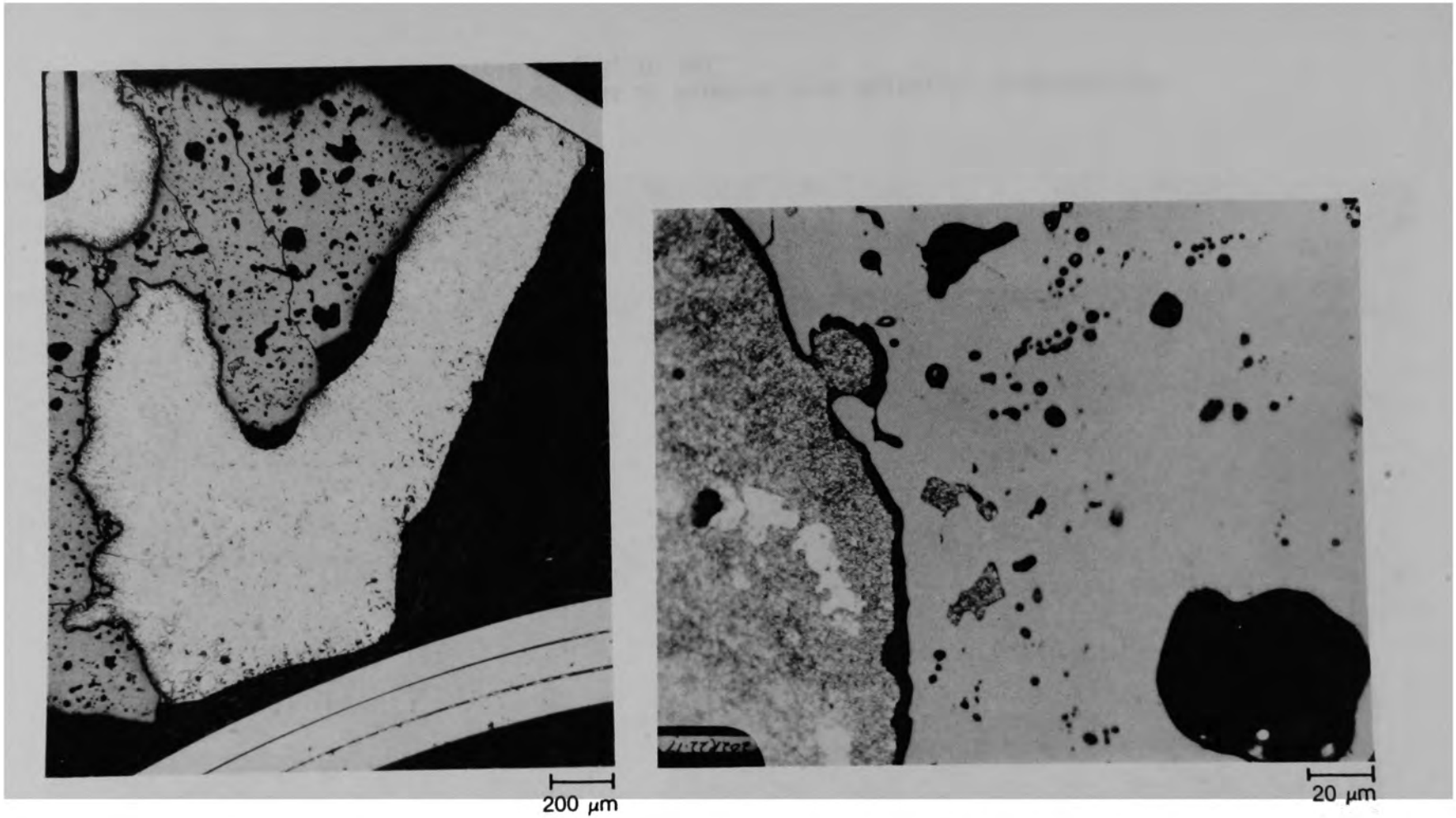

(a) Unetched

(b) Ag etch

Figure C-198. Photomicrographs of Region 3 of Particle 8H (H8, 70 cm) showing Ag melt interface.

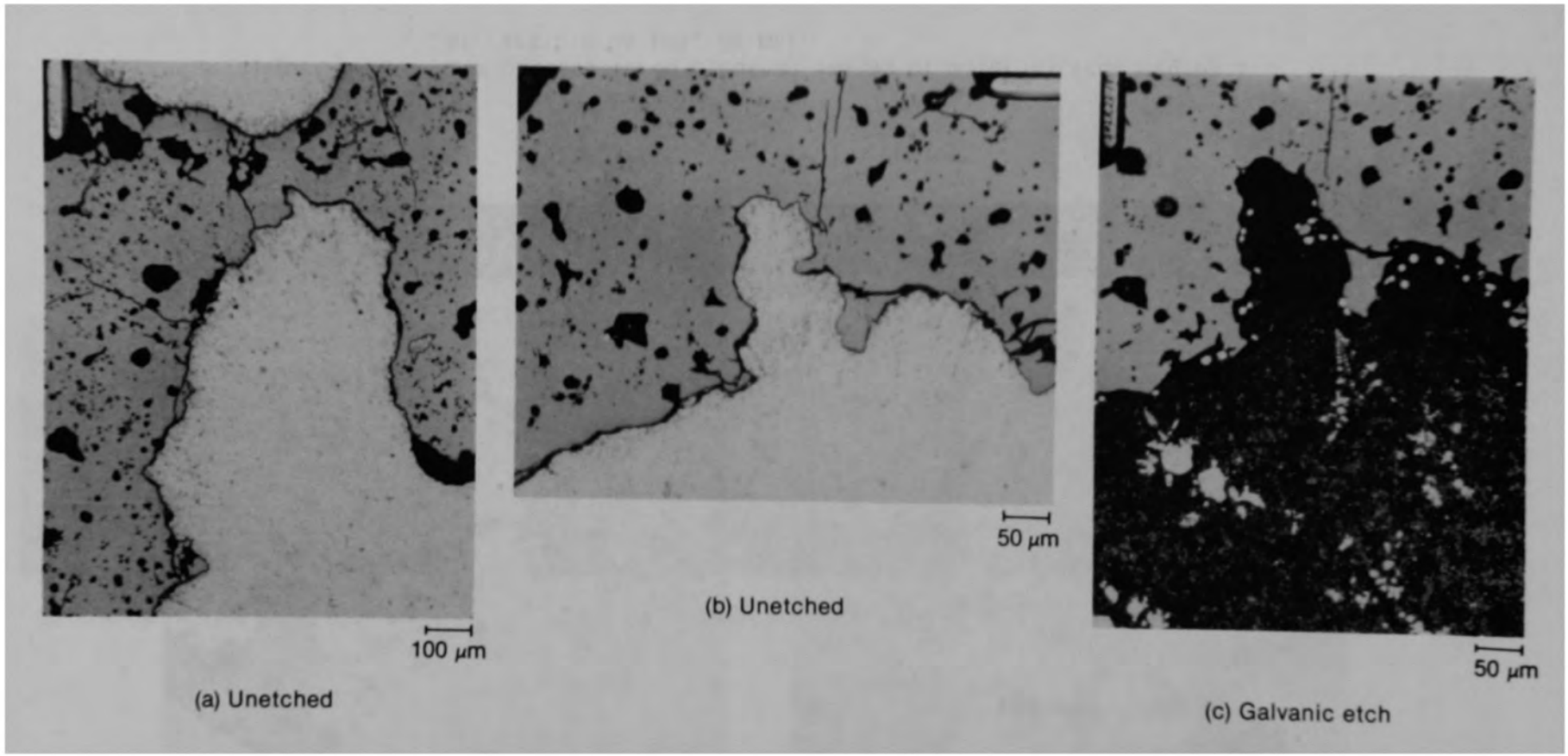

Figure C-199. Photomicrographs of material from Region 3 of Particle 8H (H8, 70 cm) showing Ag melt interface.

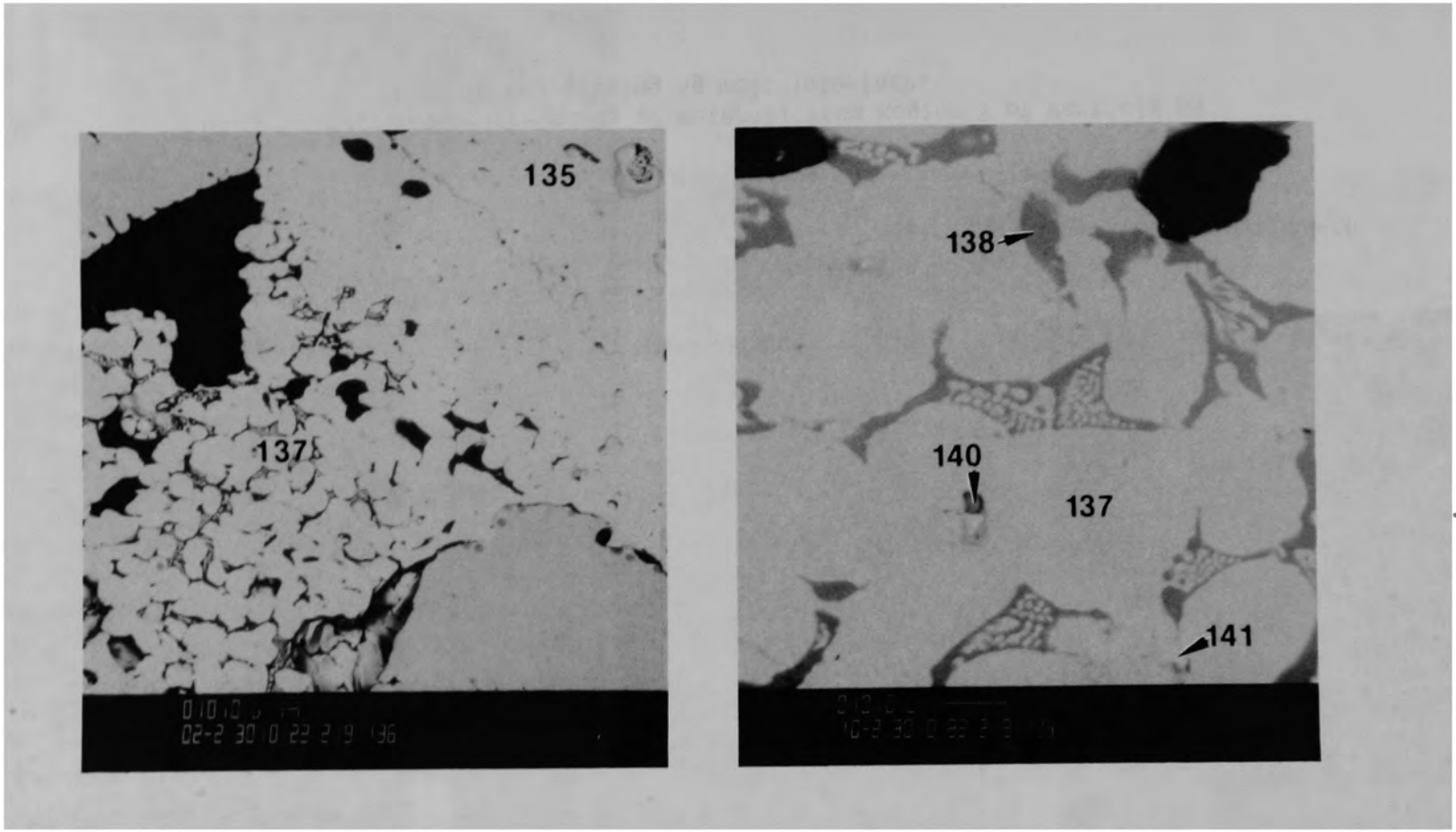

Figure C-200. SEM backscattered electron images of material from Region 3 of Particle 8H (H8, 70 cm).

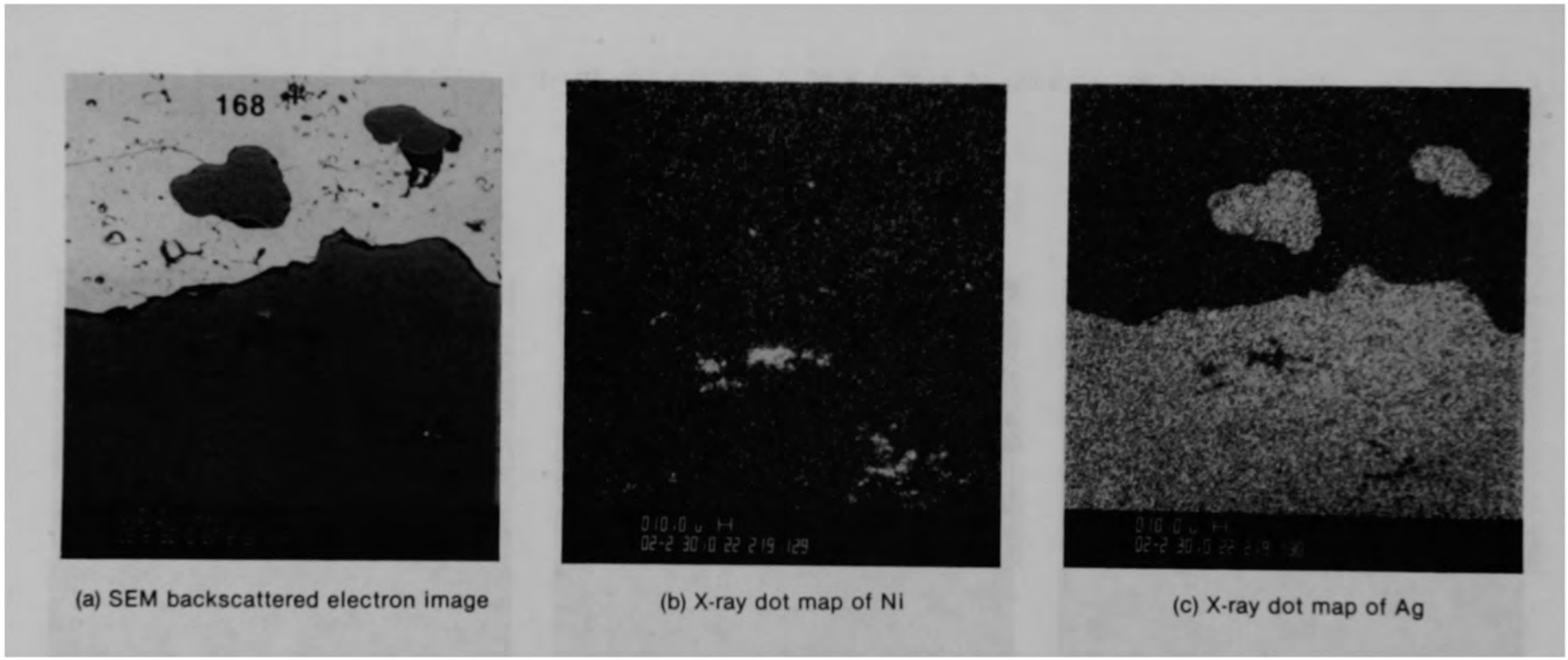

Figure C-201. Photographs of material from Region 1, Region 3 and Ag interface of Particle 8H (H8, 70 cm).

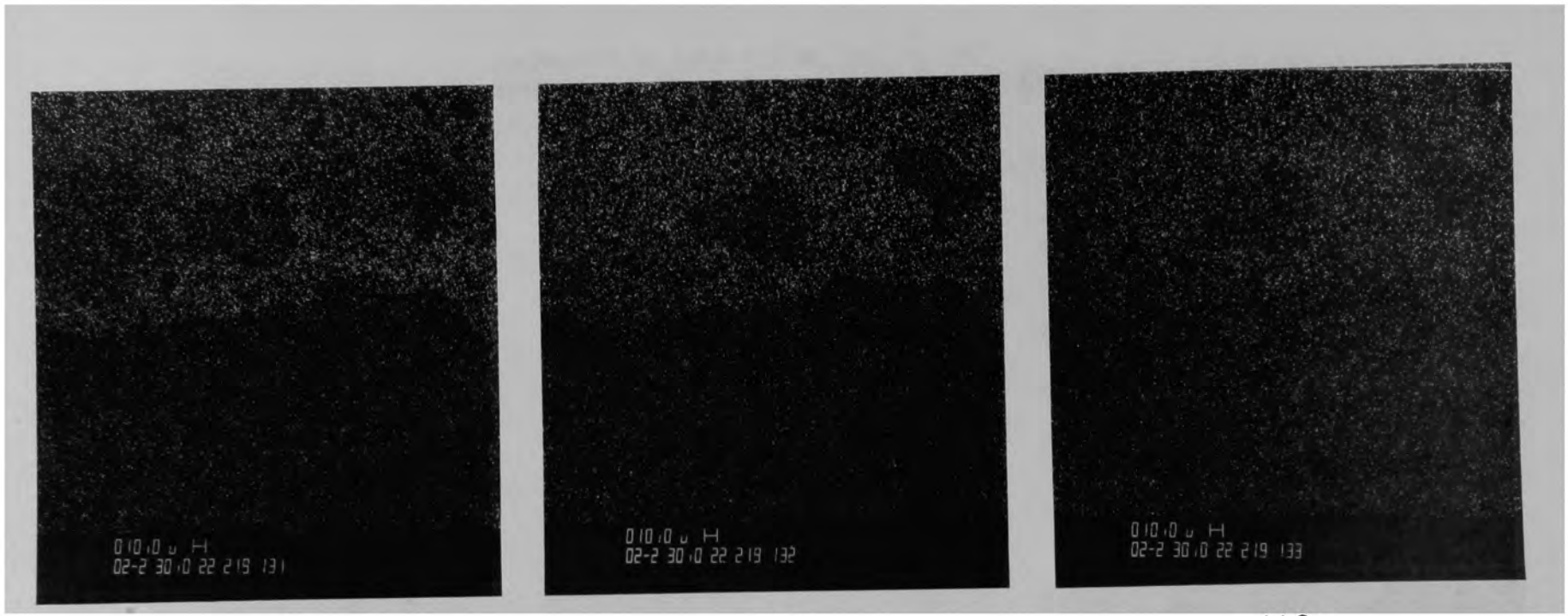

(a) Zr (b) U (c) Sn

Figure C-202. X-ray dot maps of Figure C-201a of Particle 8H (H8, 70 cm).

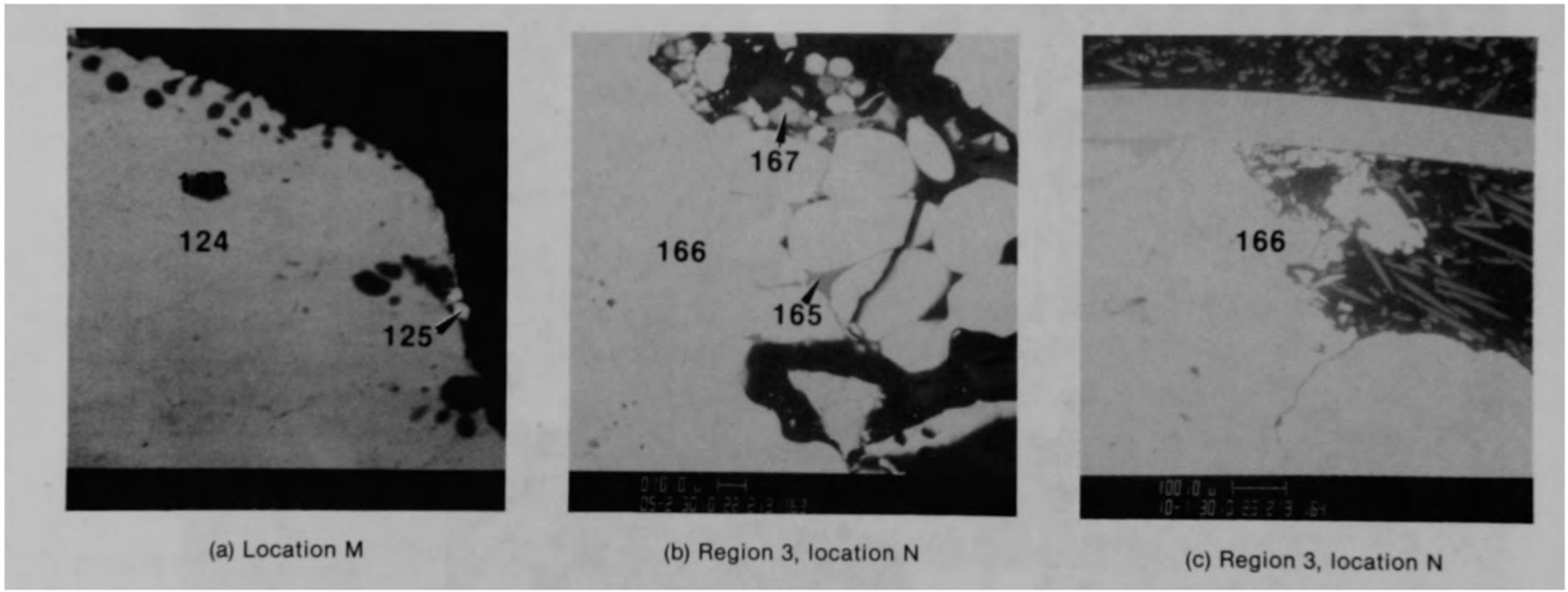

Figure C-203. SEM backscattered electron images of Particle 8H (H8, 70 cm).

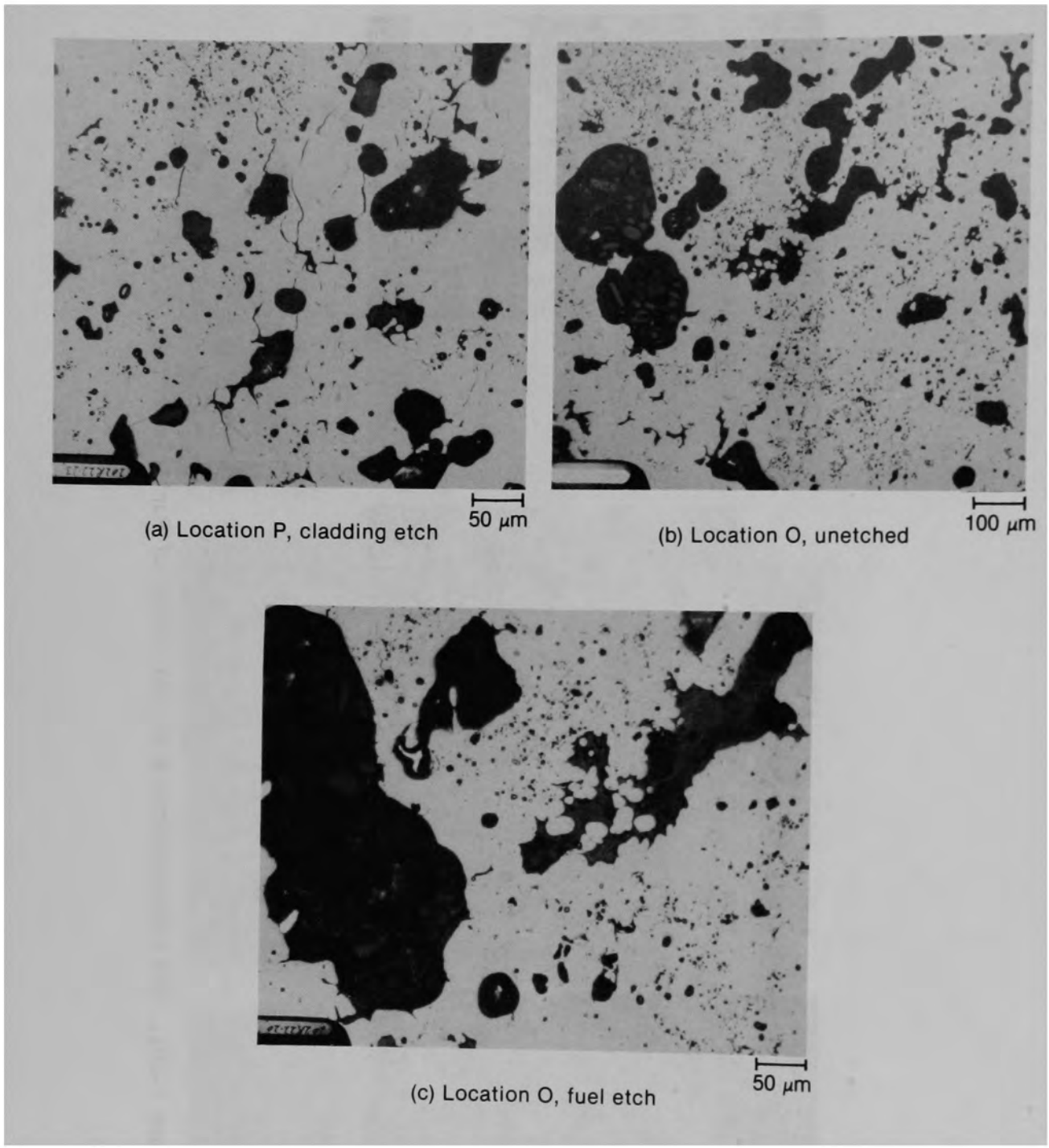

Figure C-204. Photomicrographs of material from Region 1, Region 2 interface of Particle 8H (H8, 70 cm).

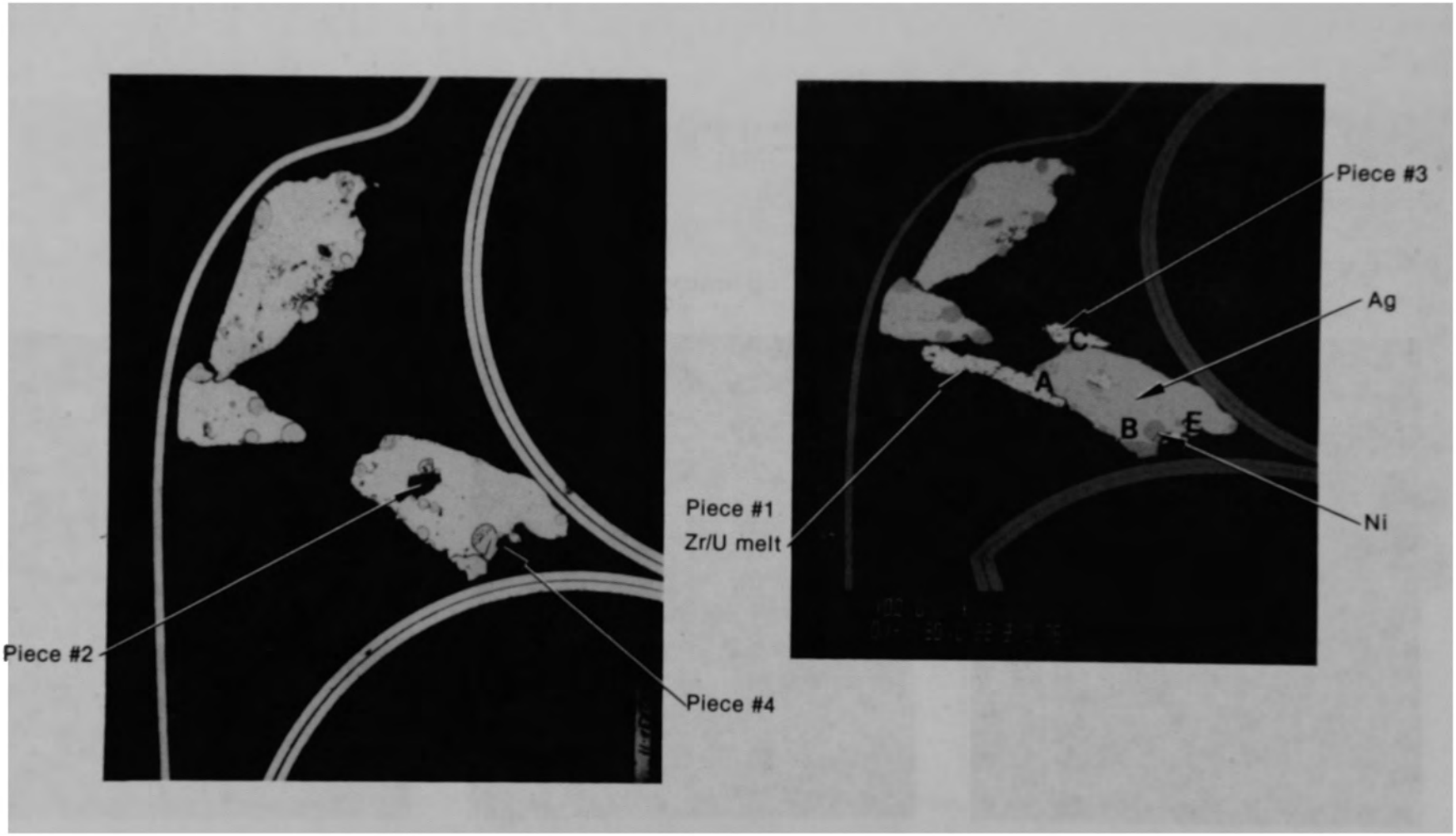

Figure C-205. Photomacrographs of Particle 9D (H8, 77 cm).

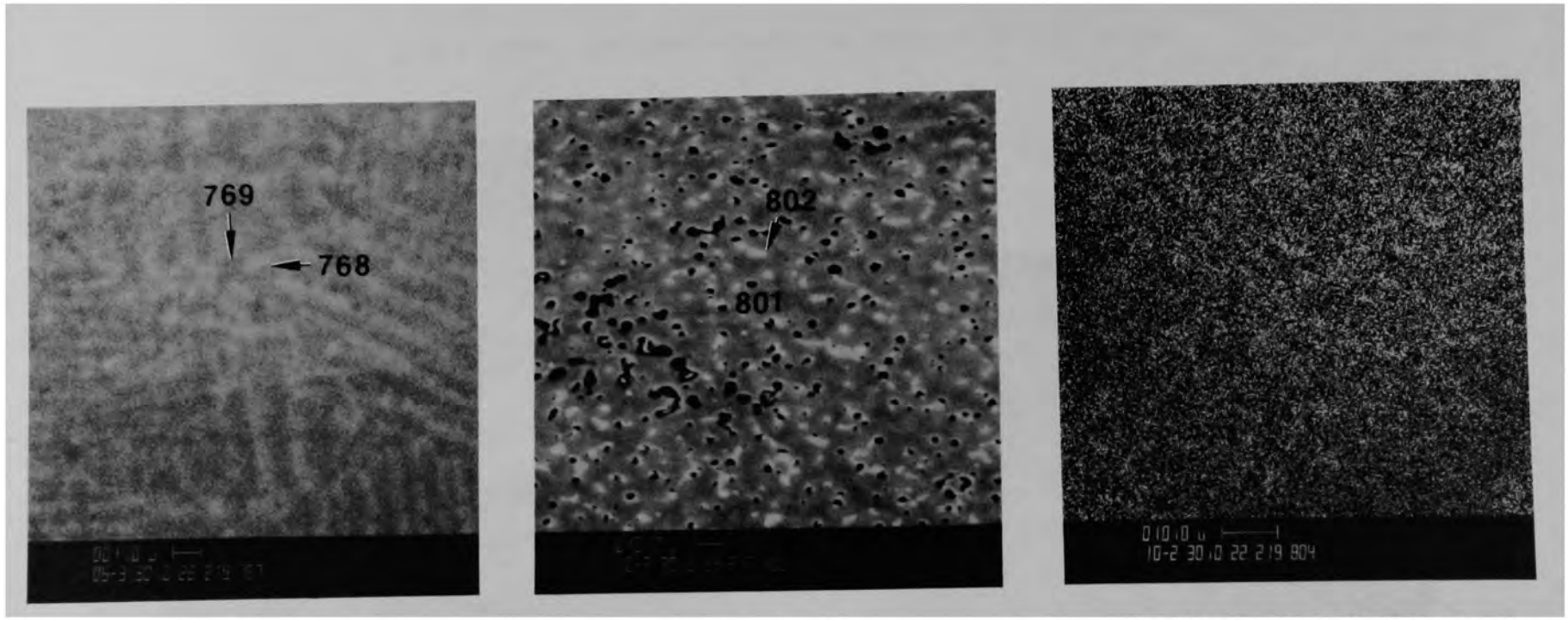

(a) Location A

(b) Location B

(c) X-ray dot map of (b) for Sn

Figure C-206. Photographs of material from Ag region of Particle 9D (H8, 77 cm).

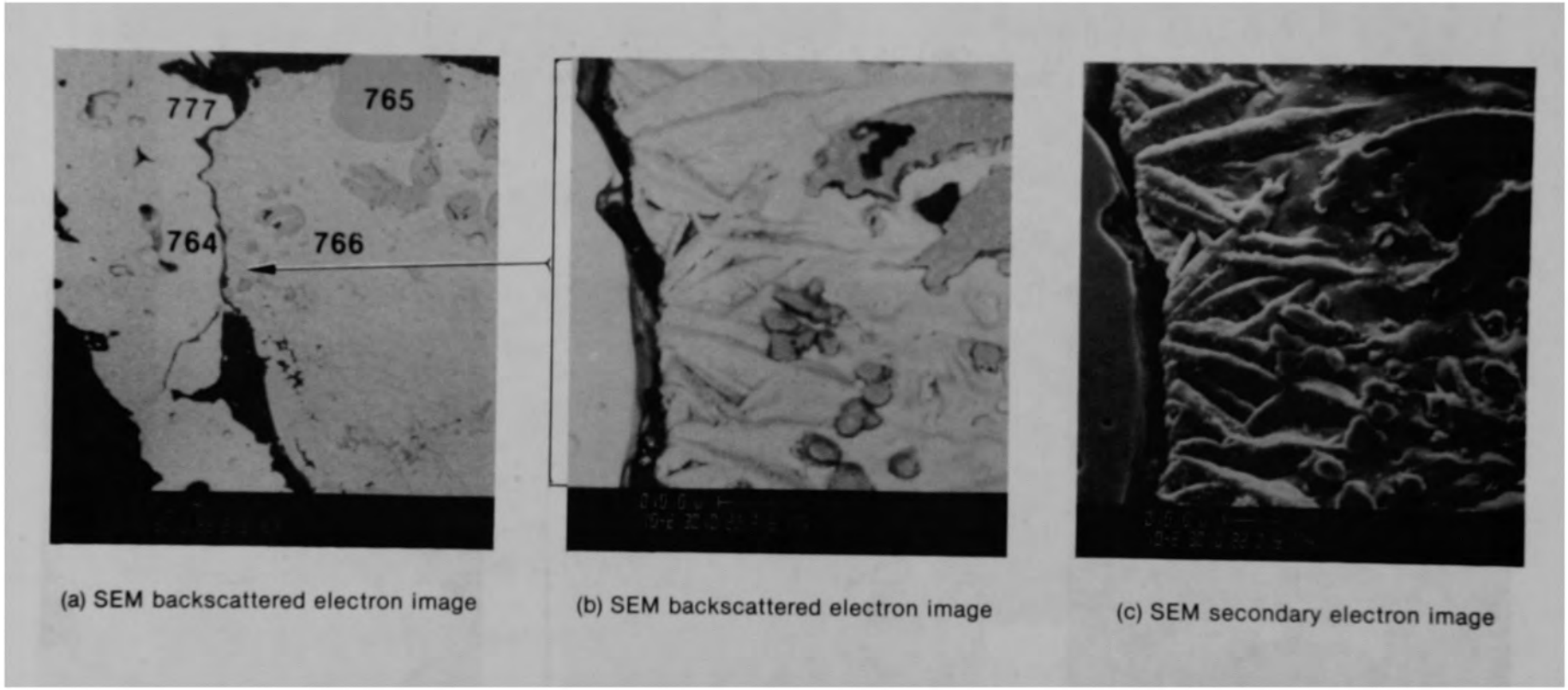

Figure C-207. SEM electron images of material from location A of Particle 9D (H8, 77 cm).

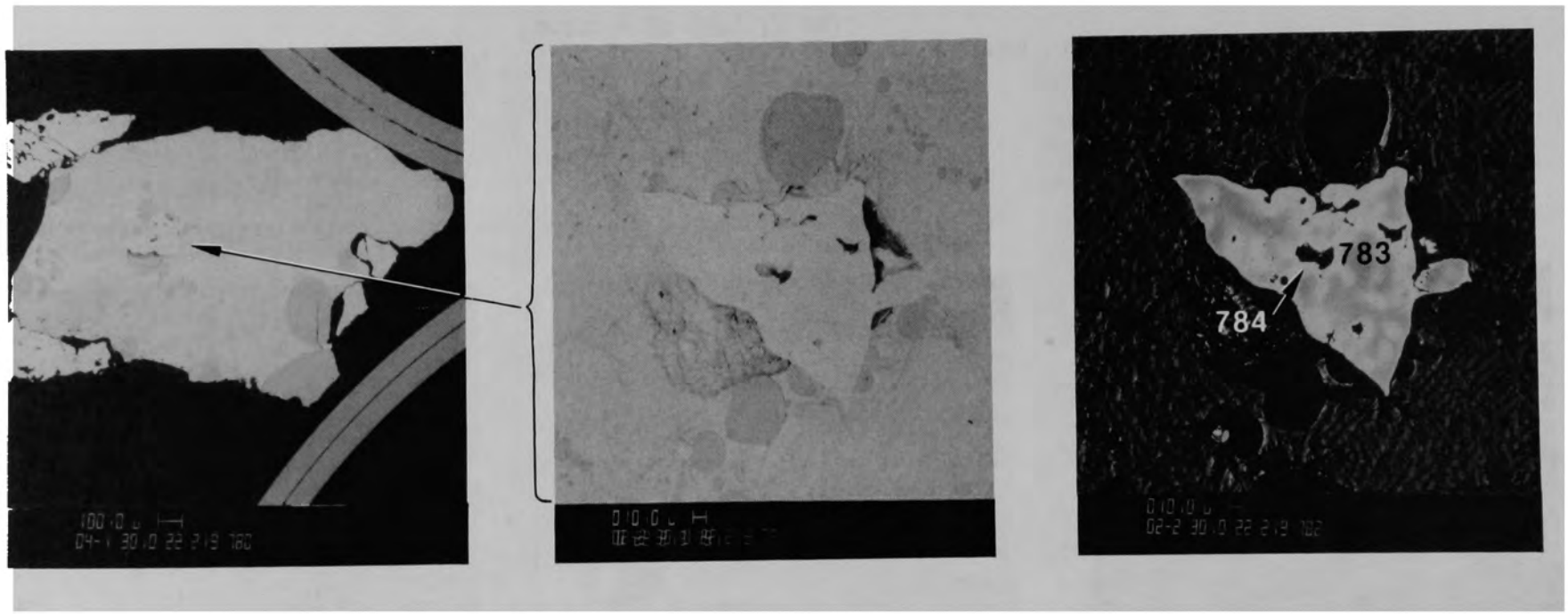

Figure C-208. SEM backscattered electron images of material from lower right Ag region of Particle 9D (H8, 77 cm).

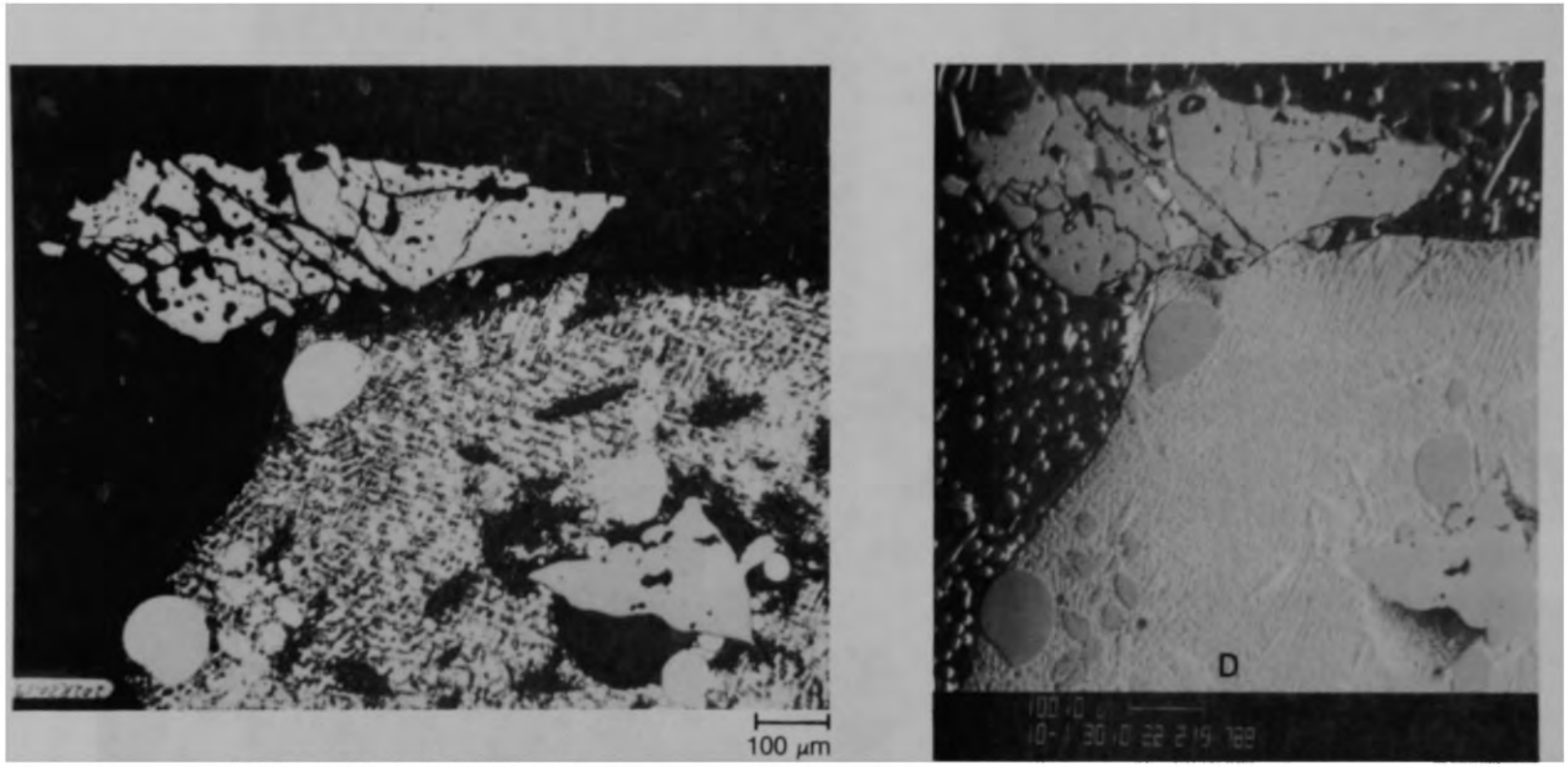

(a) Photomicrograph (etched)

(b) SEM backscattered electron image

Figure C-209. Photographs of material from location C of Particle 9D (H8, 77 cm).

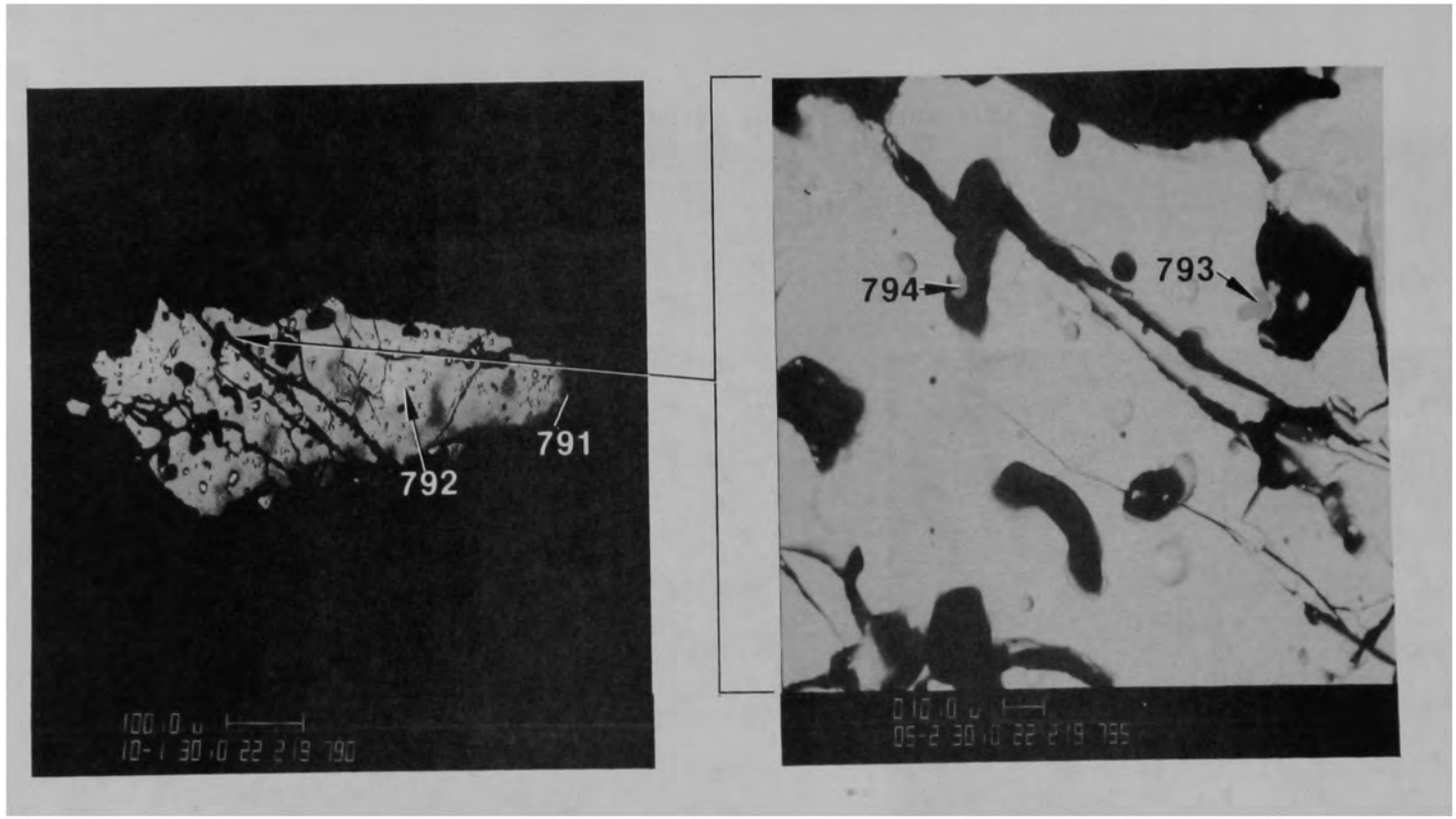

Figure C-210. SEM backscattered electron images of material from location C of Particle 9D (H8, 77 cm).

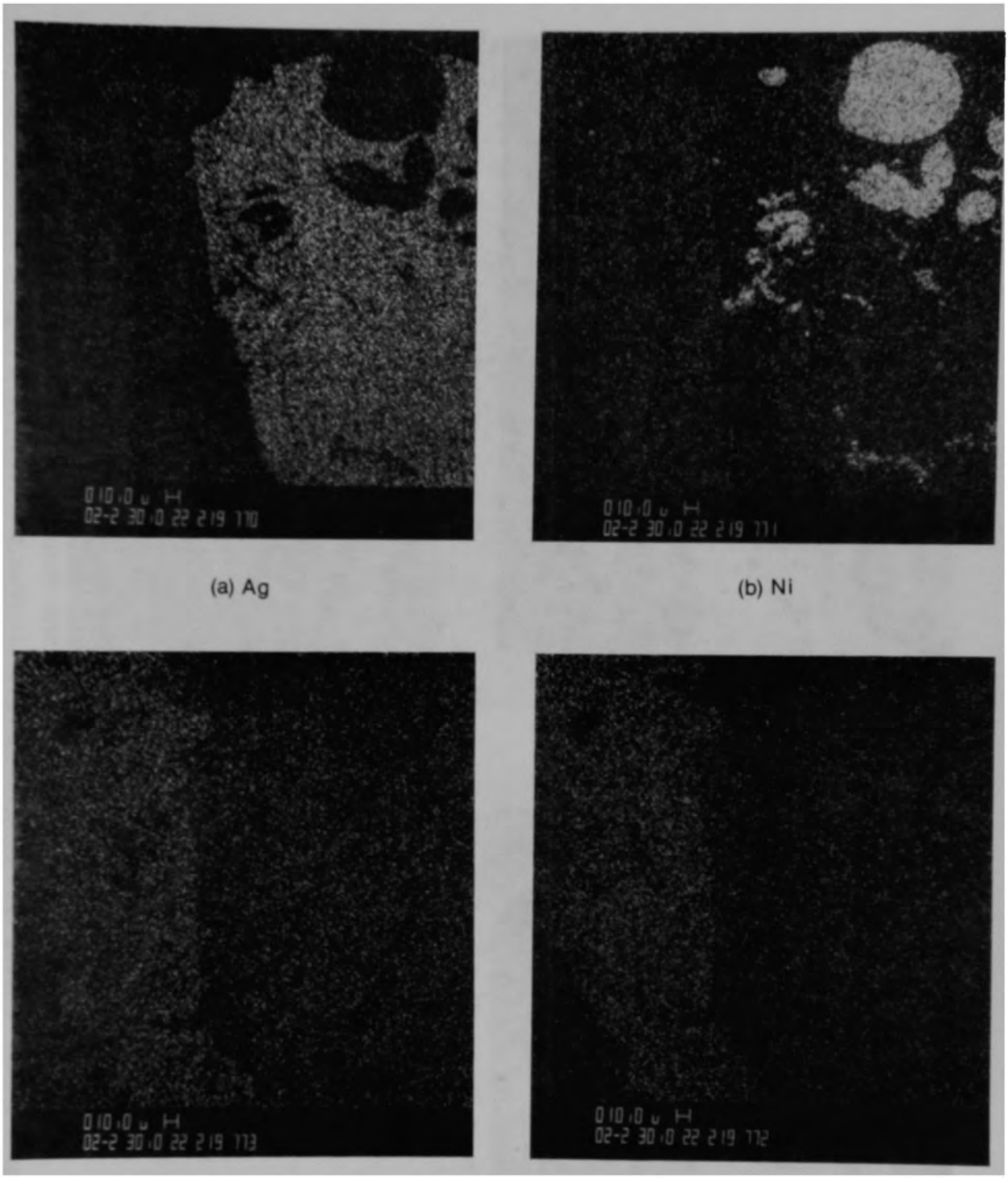

Figure C-211. X-ray dot maps of material from location D, Figure C-210b, of Particle 9D (H8, 77 cm).

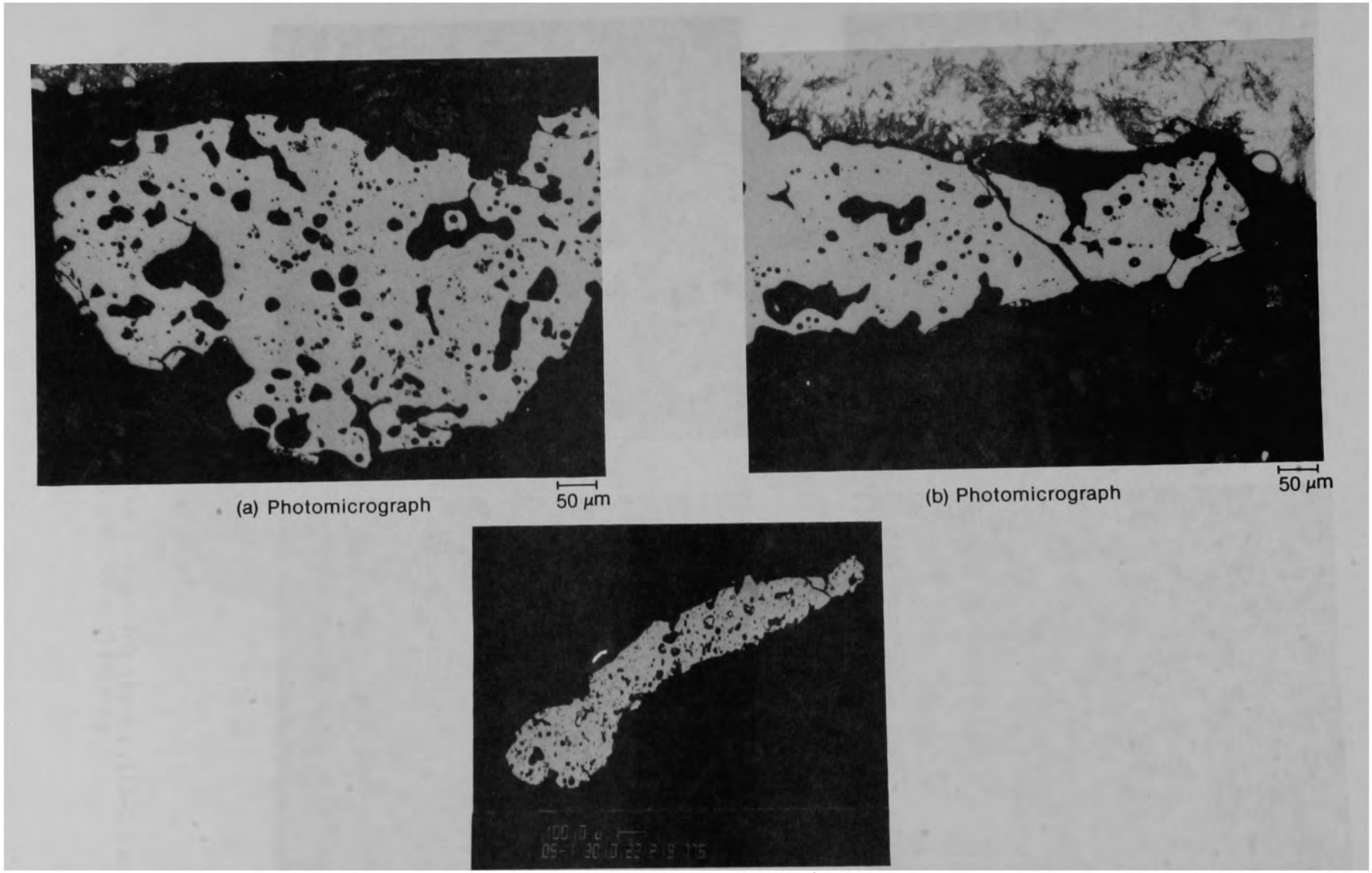

Figure C-212. Photographs of ceramic material from the lower left region of Particle 9D (H8, 77 cm).

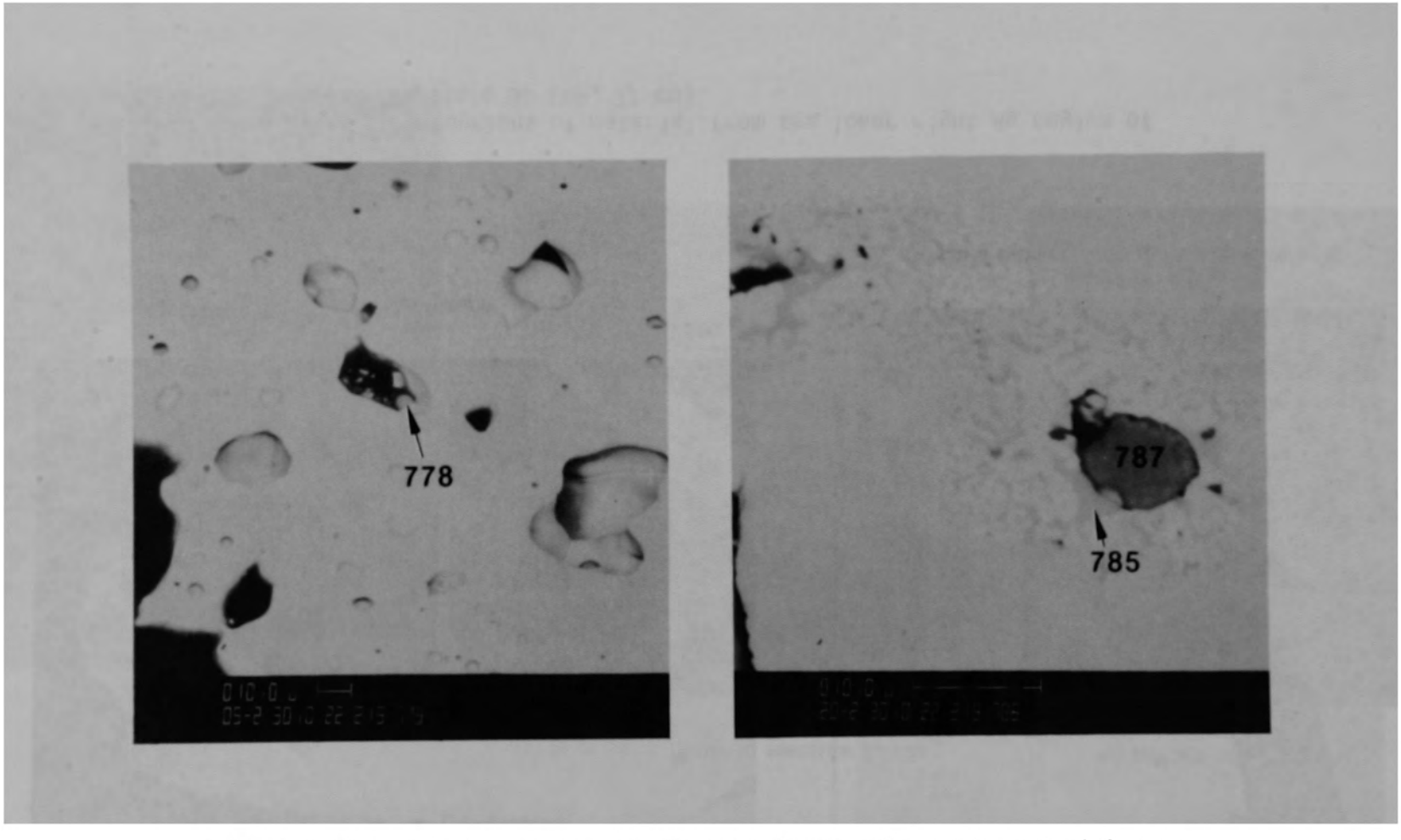

Figure C-213. SEM backscattered electron images of ceramic material from the lower left region of Particle 9D (H8, 77 cm).

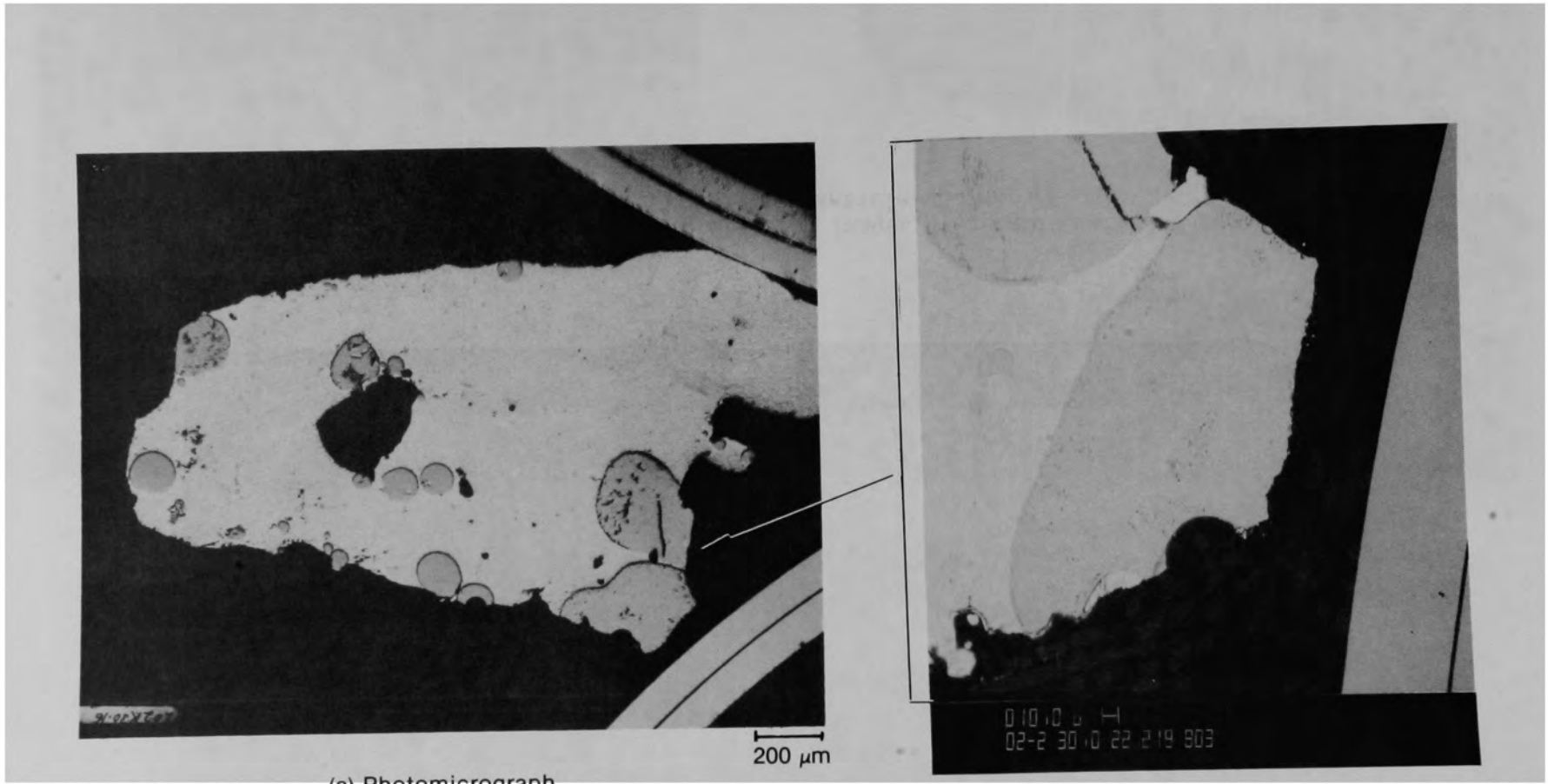

Figure C-214. Photographs of material from the lower right Ag region of Particle 9D (H8, 77 cm).

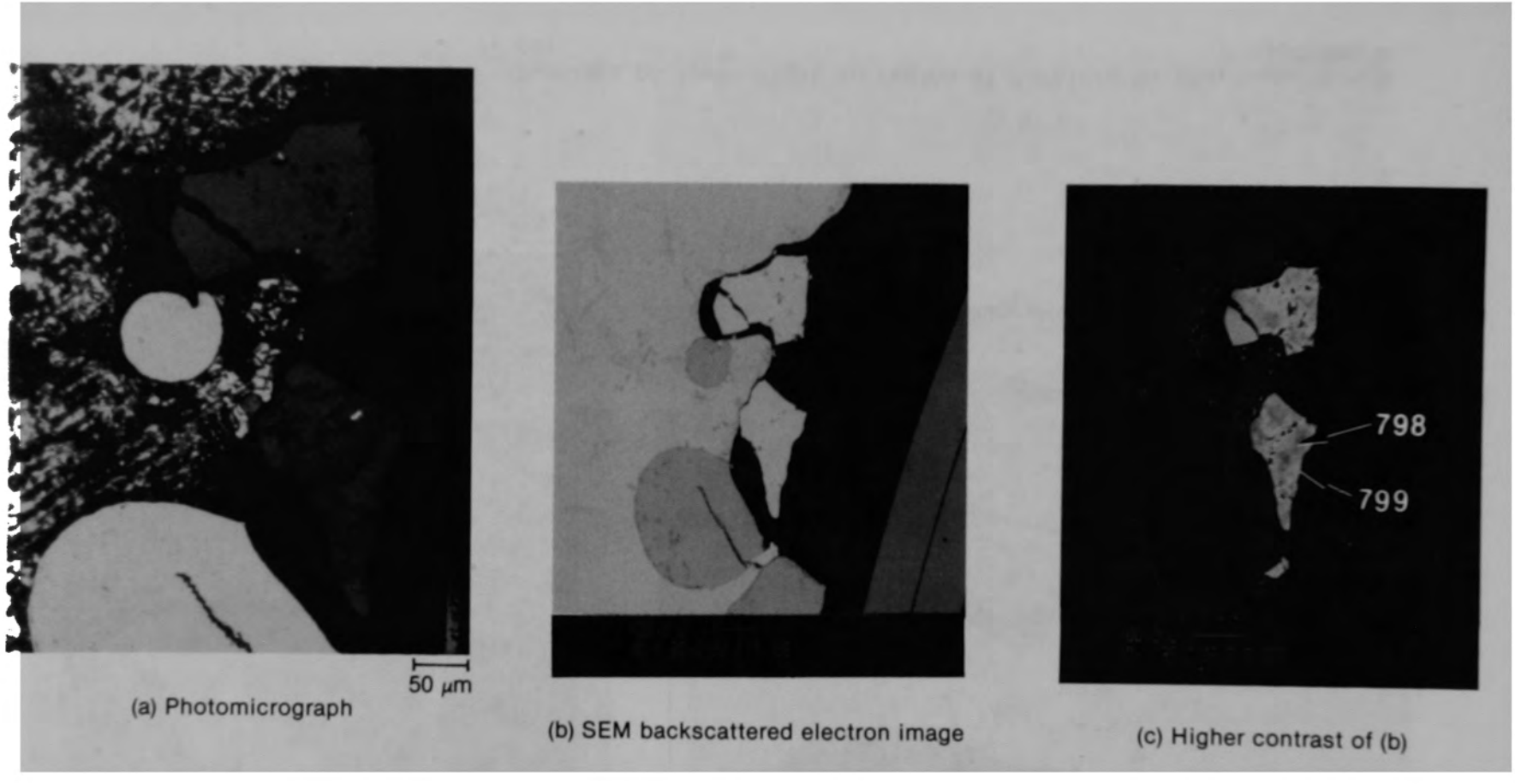

Figure C-215. Photographs of material from location E of Particle 9D (H8, 77 cm).

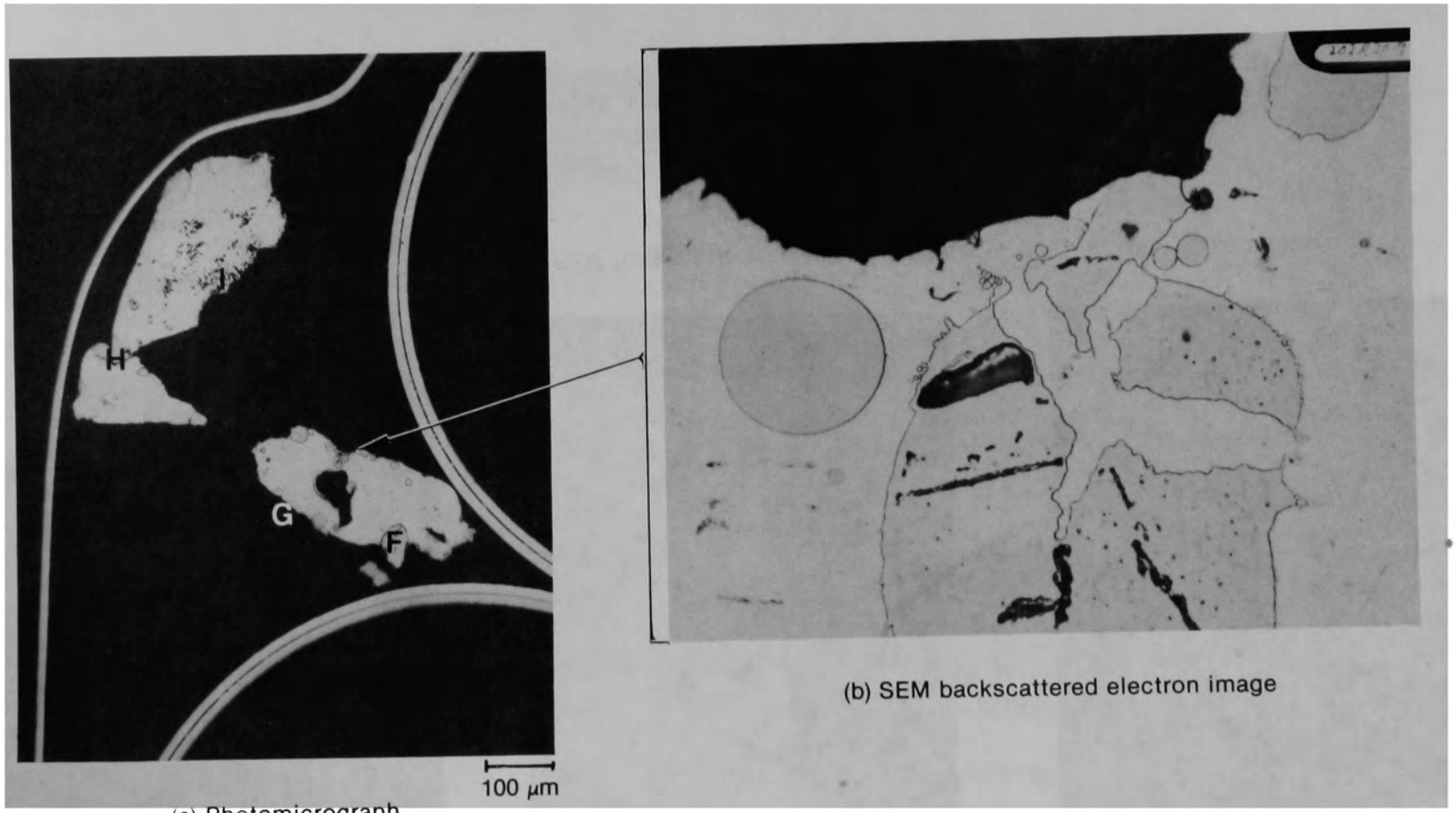

Figure C-216. Photographs of lower right Ag region of Particle 9D (H8, 77 cm).

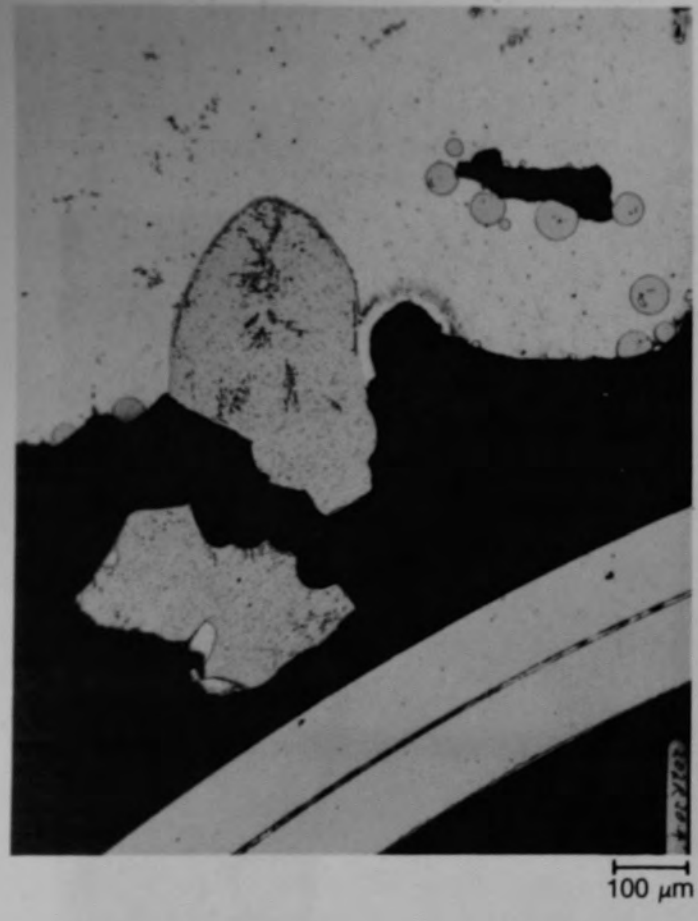

Figure C-217. Photomicrographs of material from location F, Figure C-216a, of Particle 9D (H8, 77 cm).

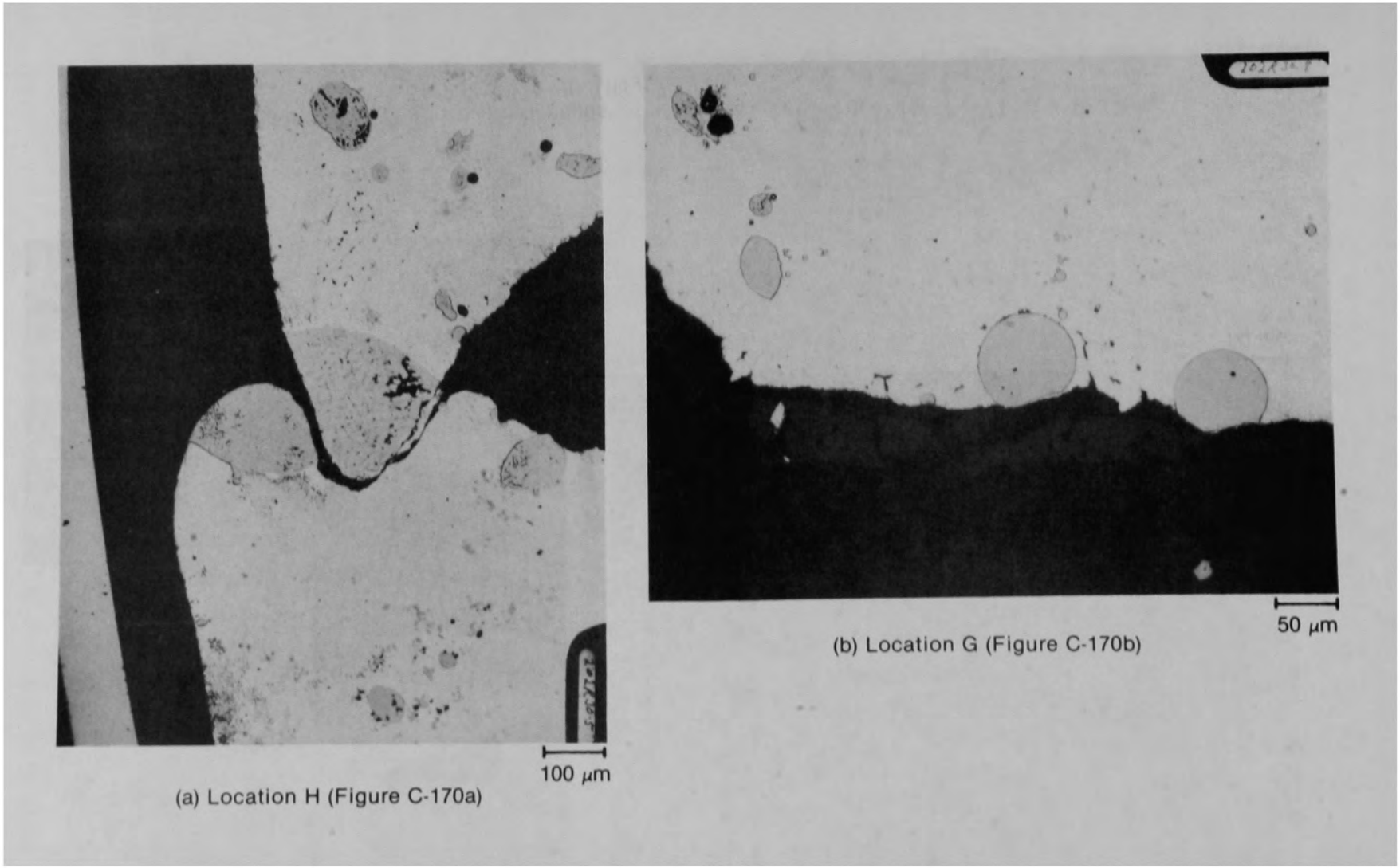

(a) Location H (Figure C-170a)

(b) Location G (Figure C-170b)

Figure C-218. Photomicrographs of Ag regions of Particle 9D (H8, 77 cm).

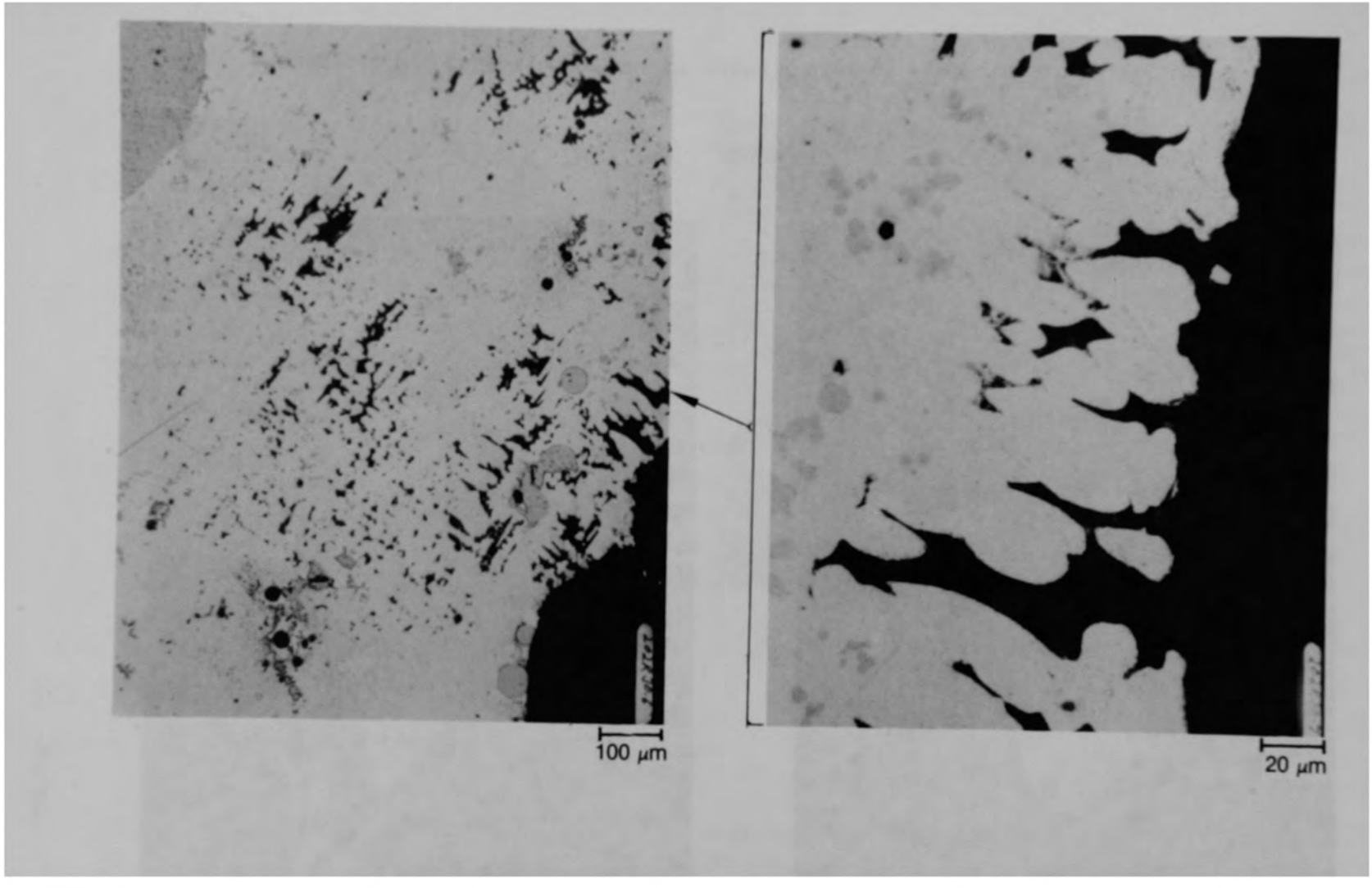

Figure C-219. Photomicrographs of material from location I, Figure C-216a, of Particle 90 (H8, 77 cm).

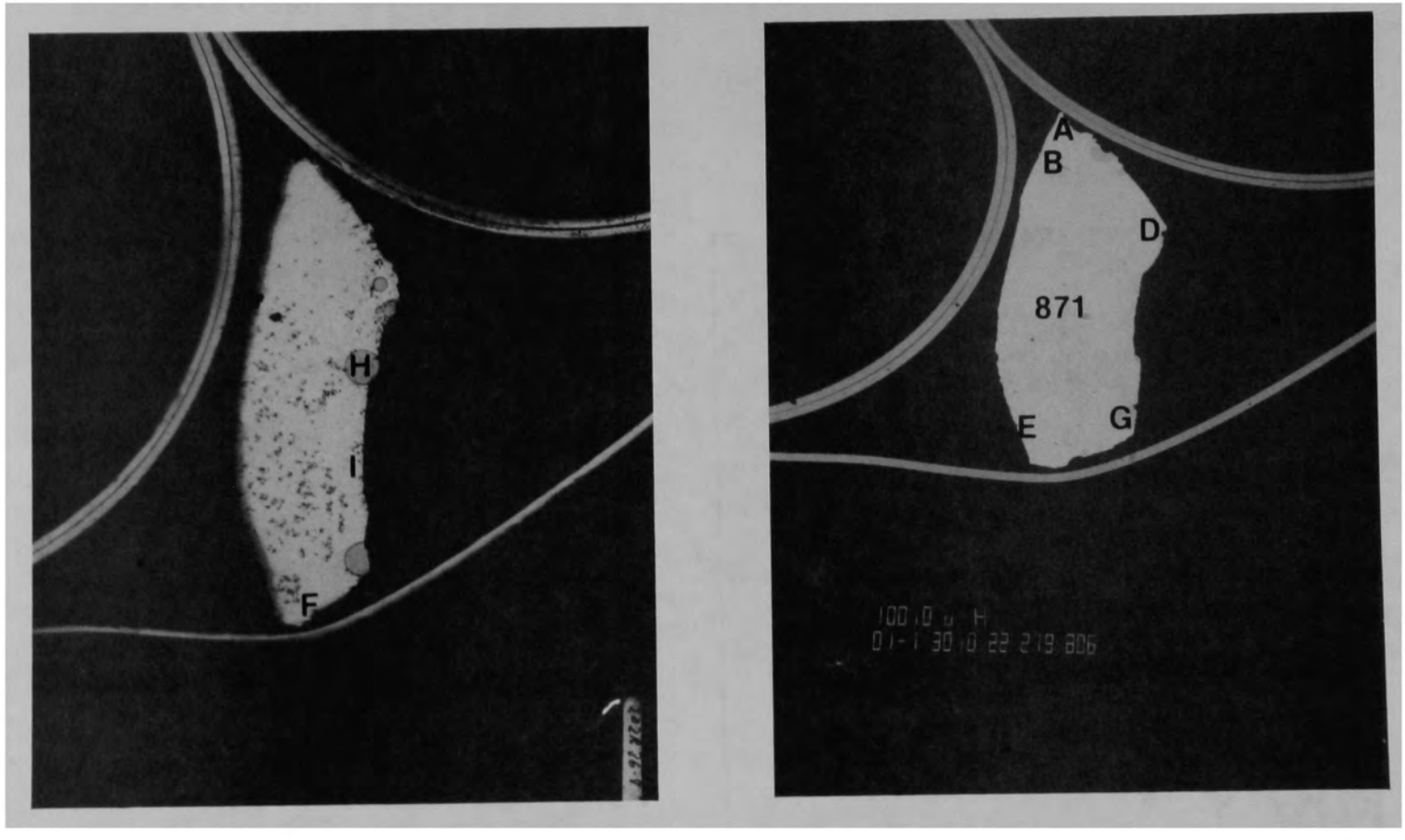

Figure C-220. Photomacrographs of overall view of Particle 9G (H8, 77 cm).

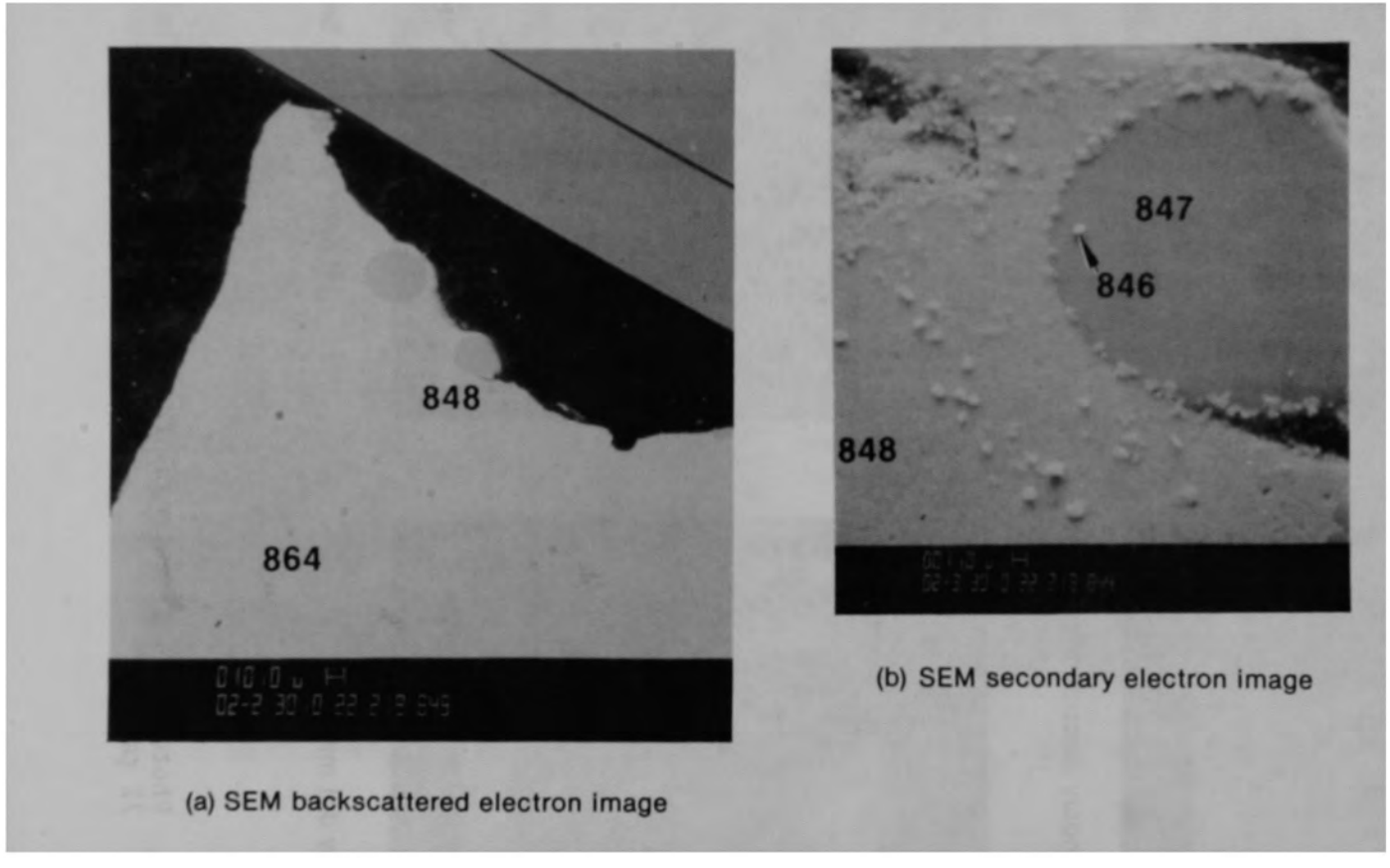

Figure C-221. SEM backscattered electron images of material from location A of Particle 9G (H8, 77 cm).

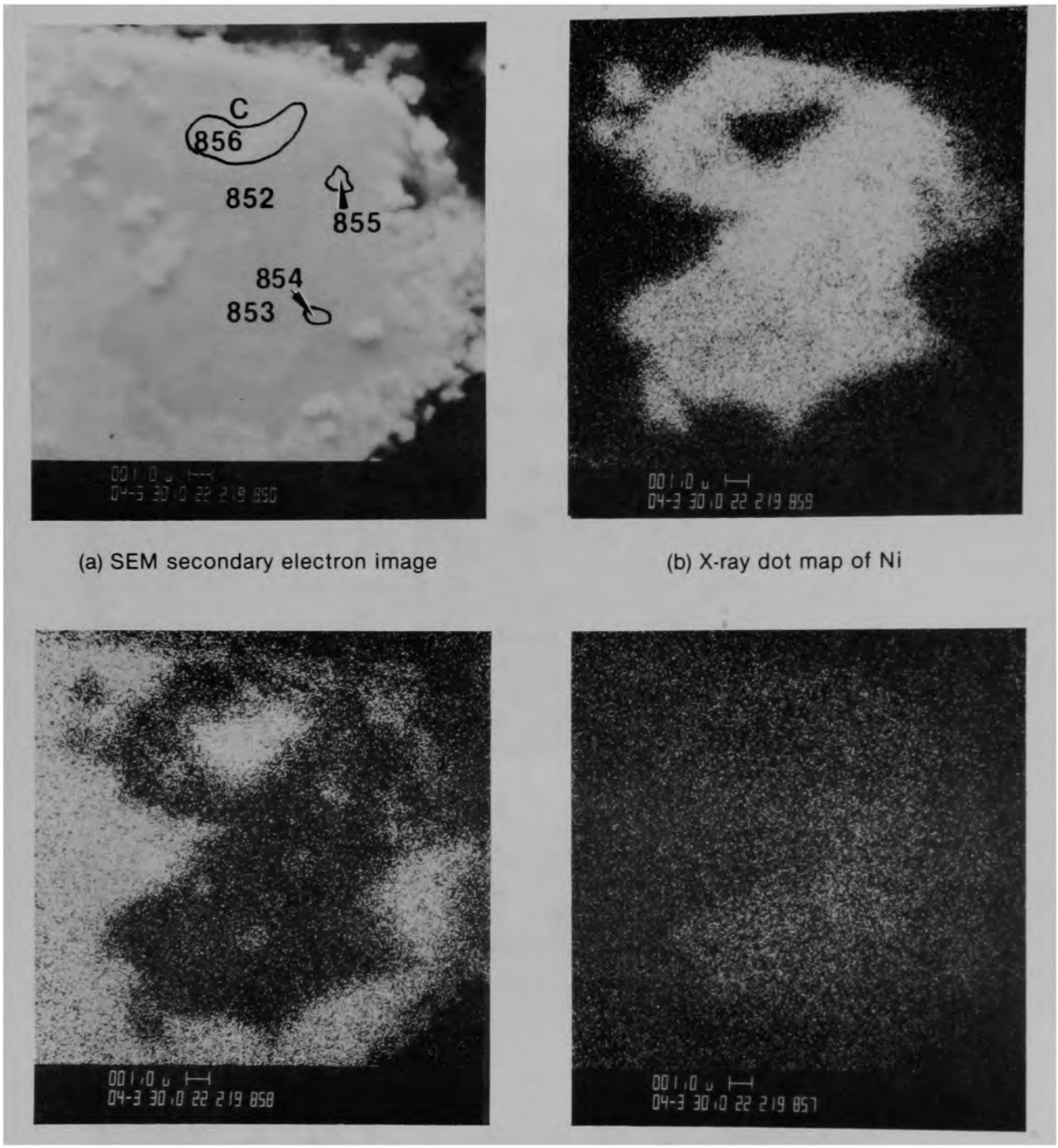

(a) SEM secondary electron image

(b) X-ray dot map of Ni

(c) X-ray dot map of Ag

(d) X-ray dot map of Sn

Figure C-222. Photographs of material from location B of Particle 9G (H8, 77 cm).

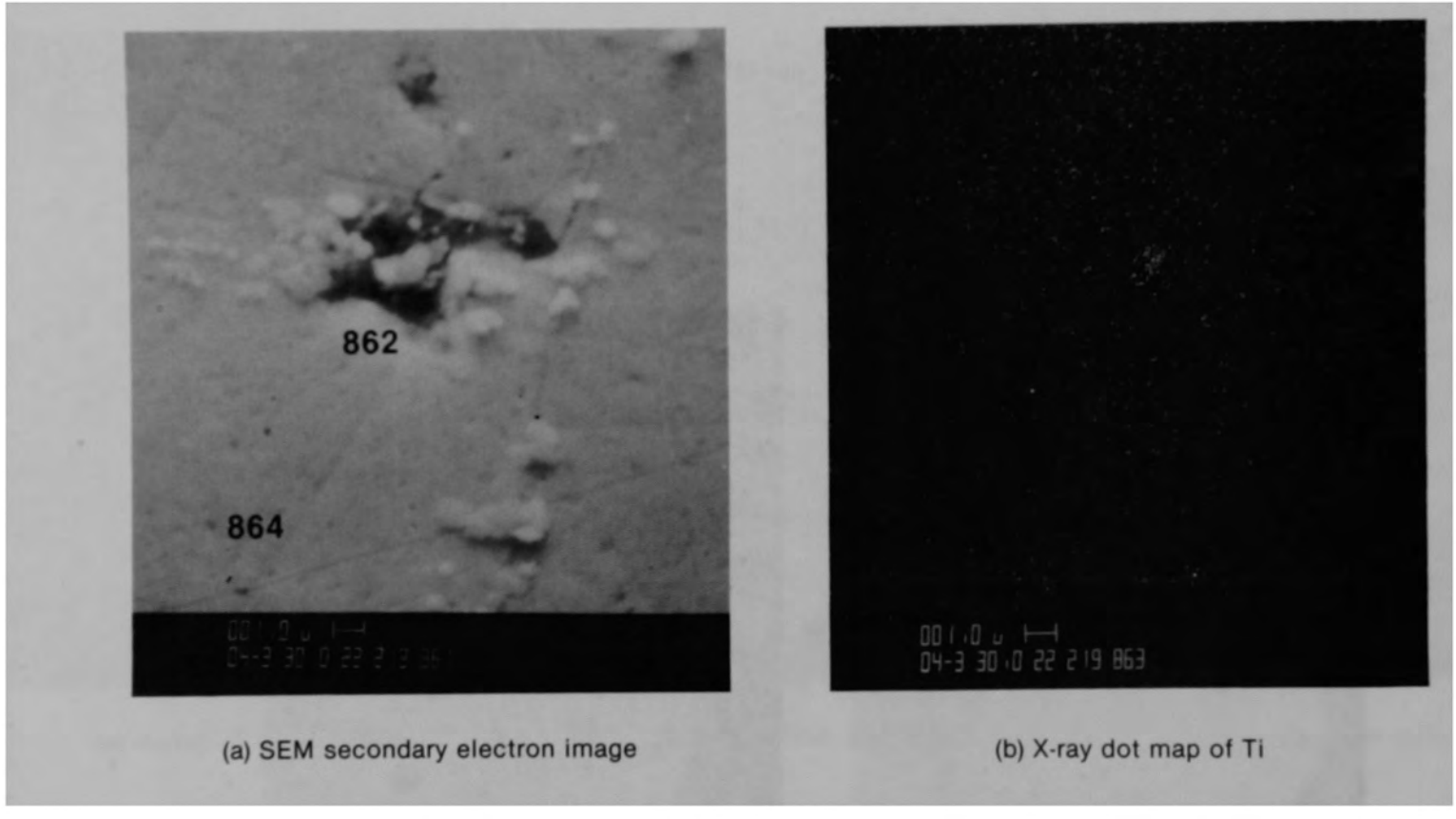

(a) SEM secondary electron image

(b) X-ray dot map of Ti

Figure C-223. Photographs of material from location C, Figure C-222a, of Particle 9G (H8, 77 cm).

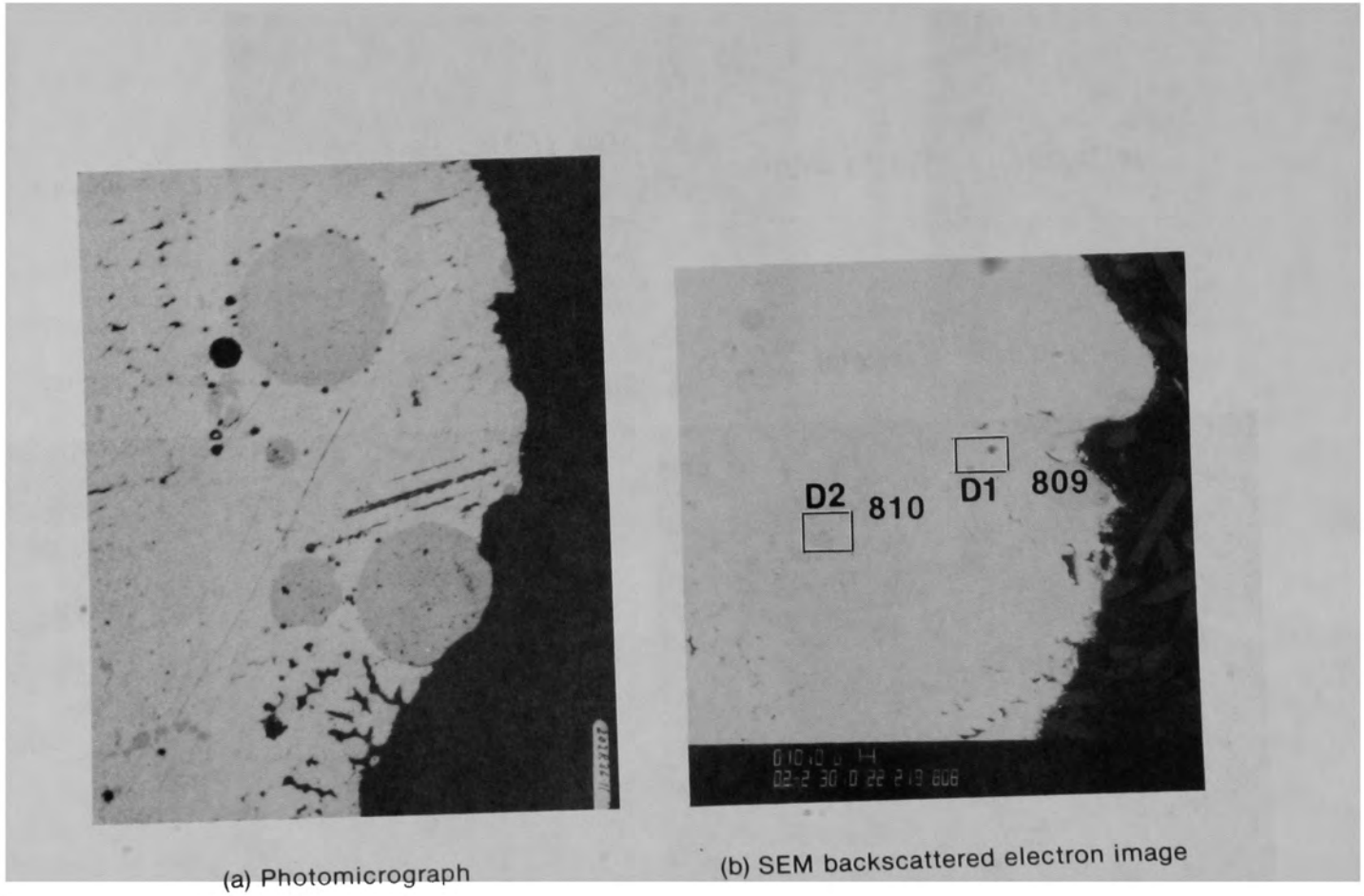

Figure C-224. Photographs of material from location D of Particle 9G (H8, 77 cm).

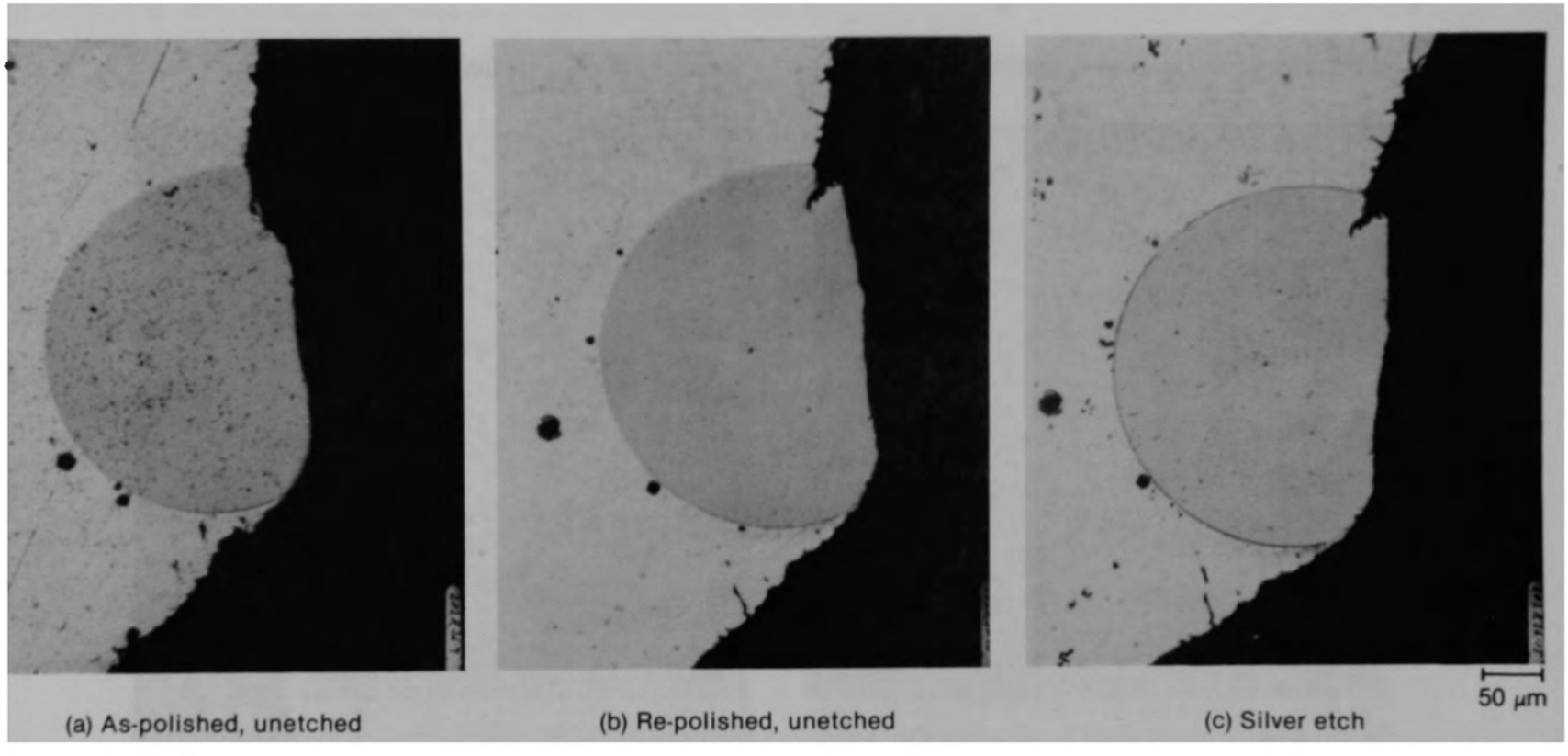

Figure C-225. Photomicrographs of material from location H of Particle 9G (H8, 77 cm).

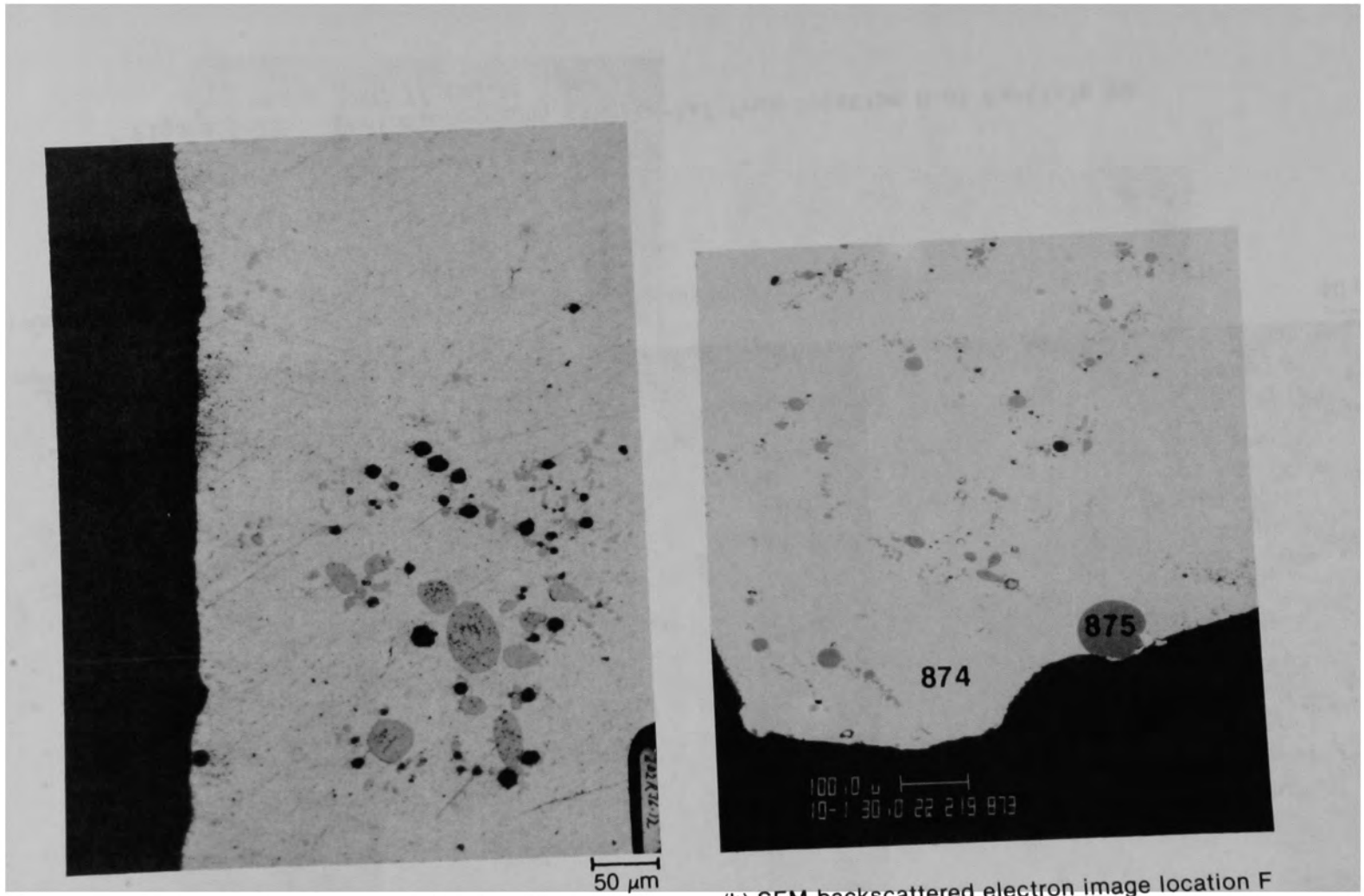

(a) Photomicrograph location E

(b) SEM backscattered electron image location F

Figure C-226. Photographs of Particle 9G (H8, 77 cm).

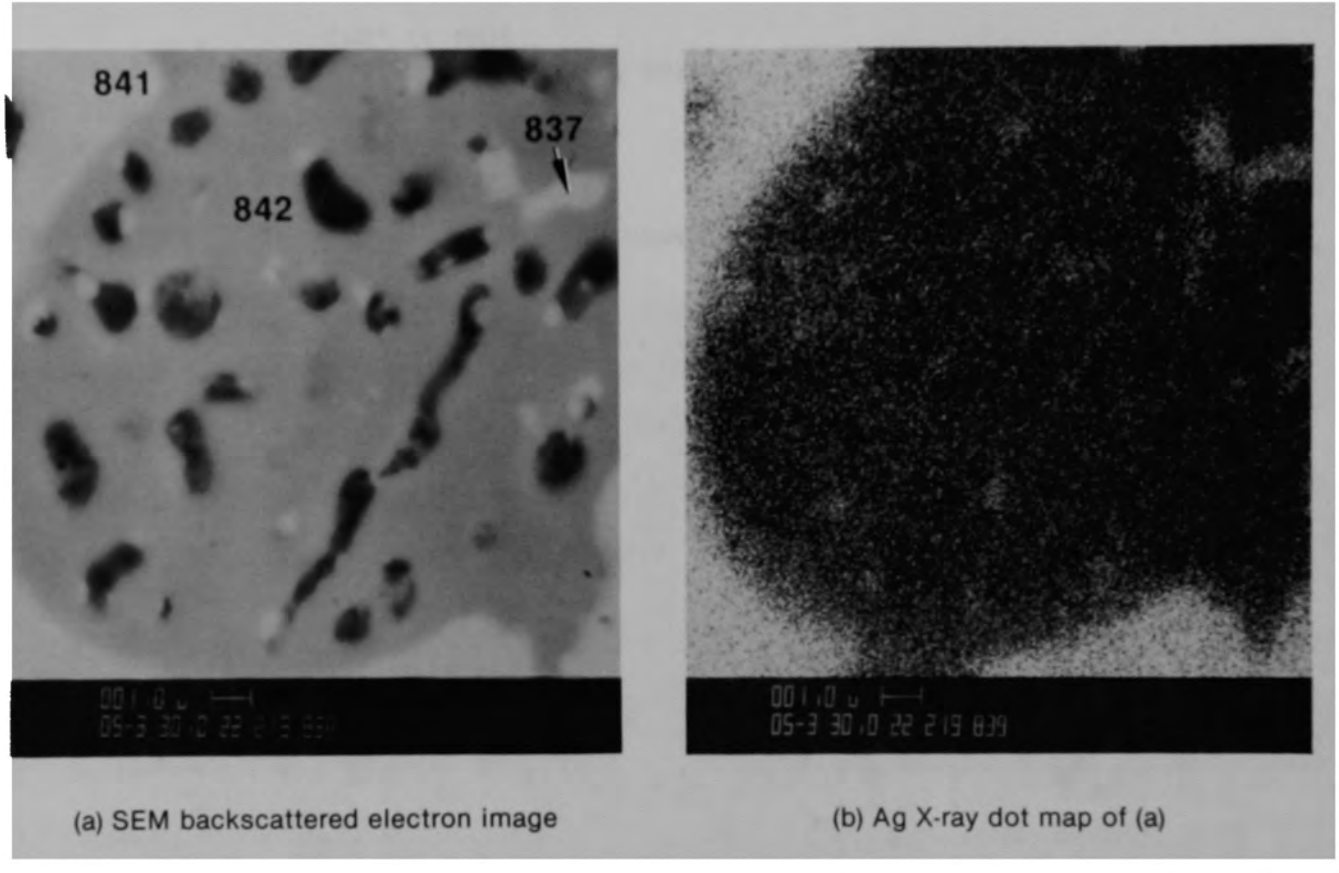

Figure C-227. Photographs of material from location D2, Figure C-224b, of Particle 96 (H8, 77 cm).

Figure C-228. Photomicrographs of material near the center of Particle 9G (H8, 77 cm).

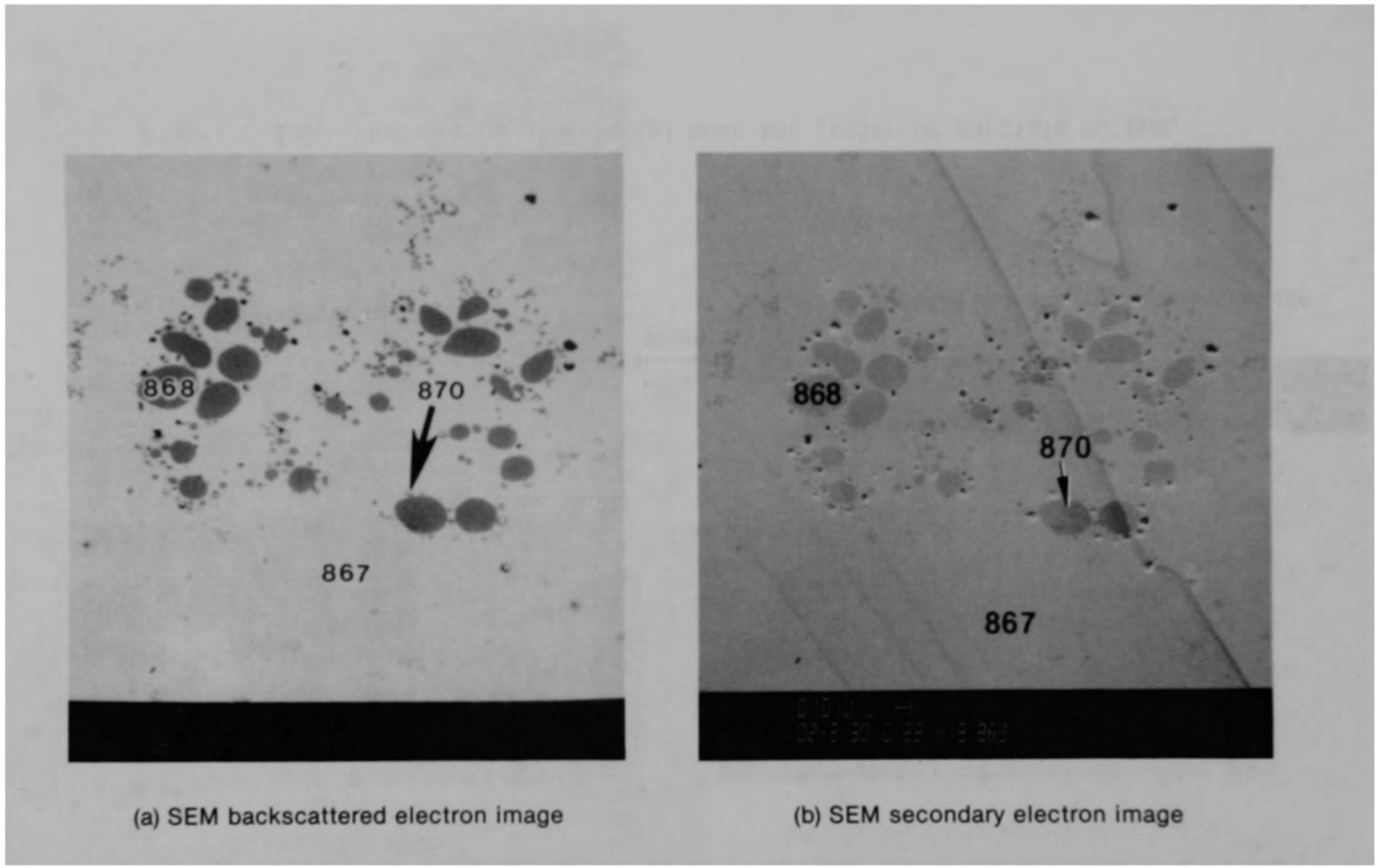

Figure C-229. SEM backscattered electron images of material from location B of Particle 9G (H8, 77 cm).

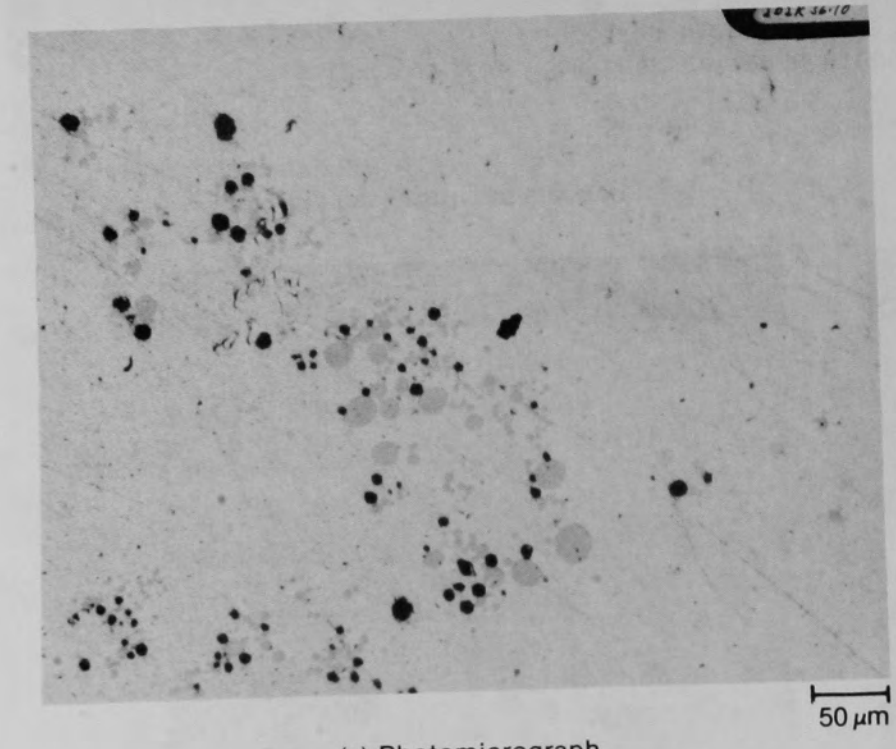

(a) Photomicrograph

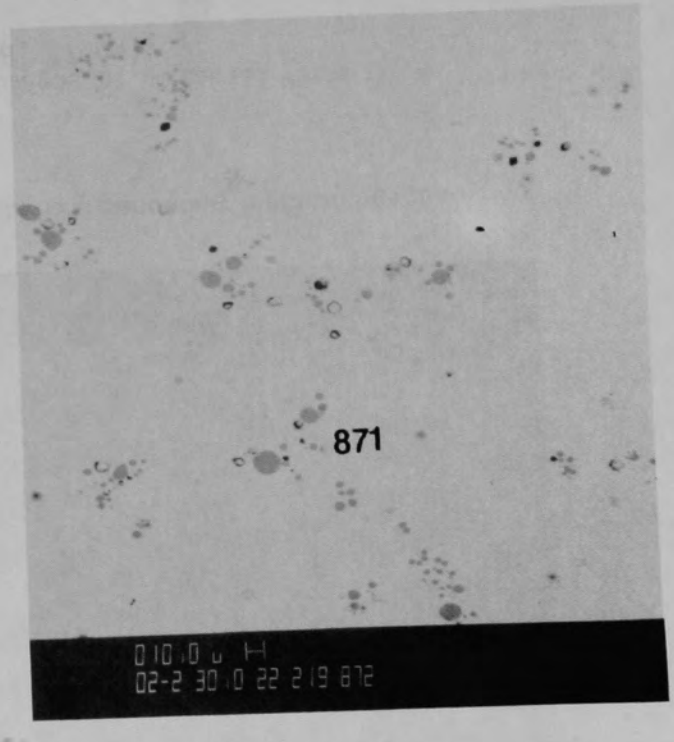

(b) SEM backscattered electron image

Figure C-230. Photographs of material near the center of Particle 9G (H8, 77 cm).

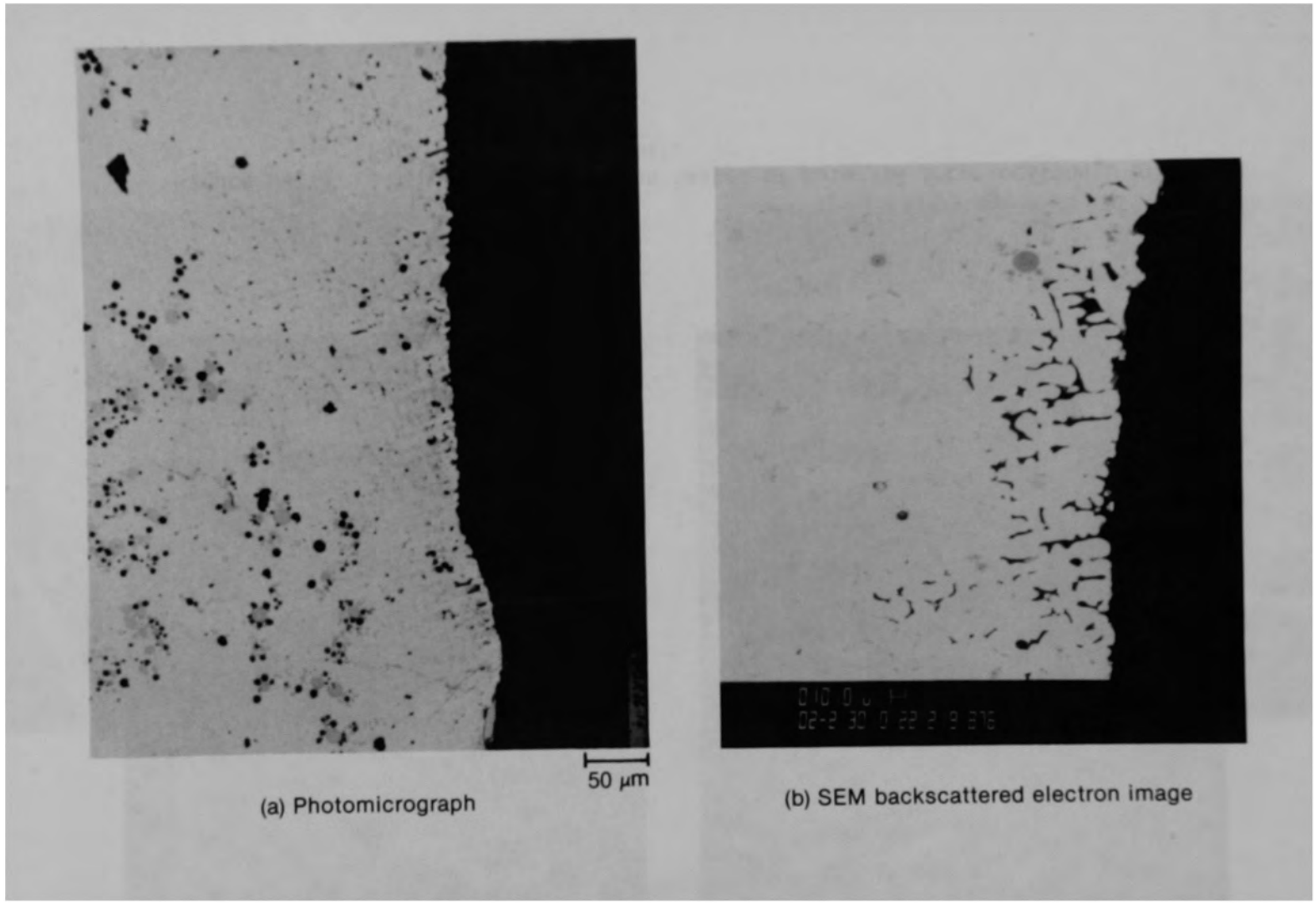

Figure C-231. Photographs of material near location I of Particle 9G (H8, 77 cm).

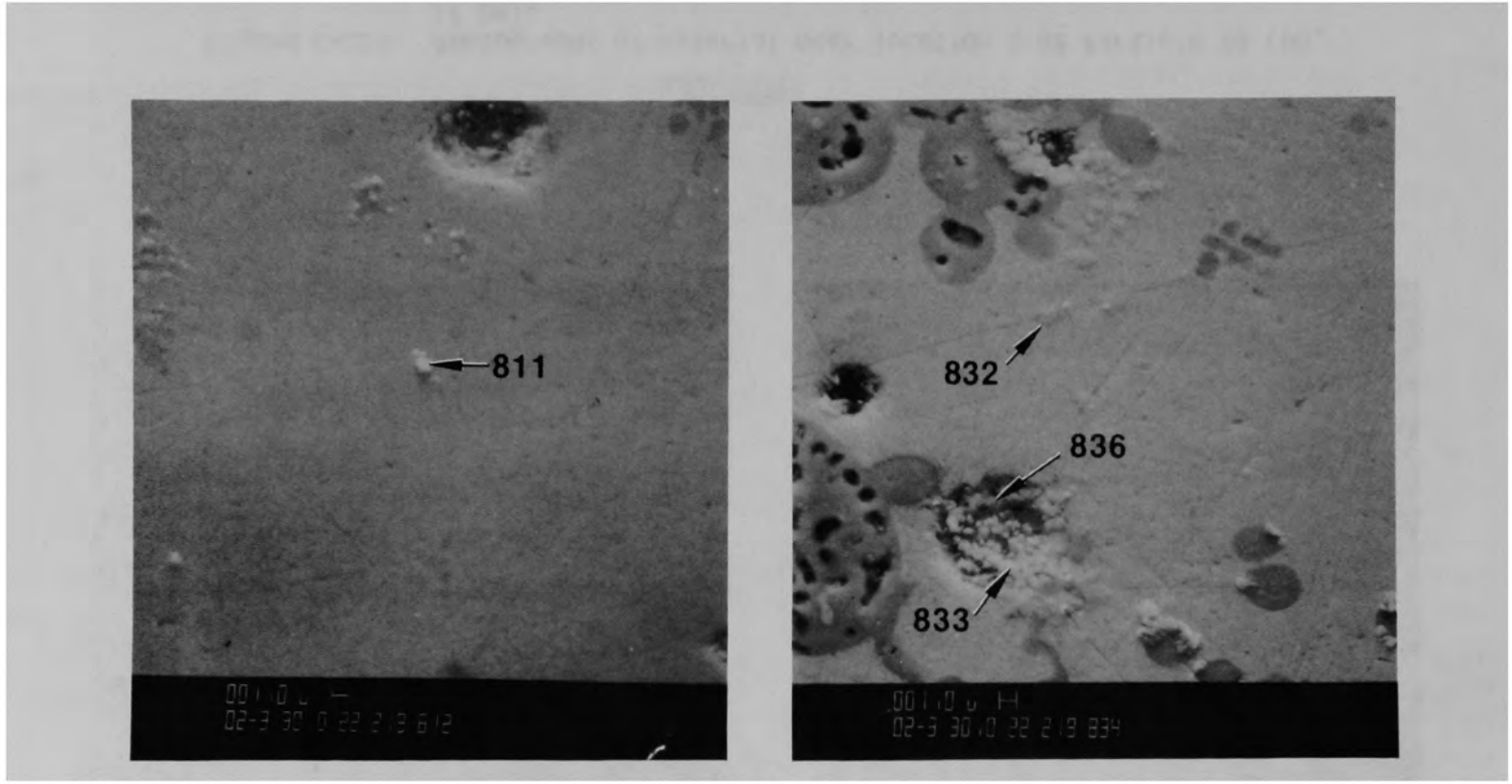

(a) Location D1

(b) Location D2

Figure C-232. SEM secondary electron images of material from location D of Particle 9G (H8, 77 cm).

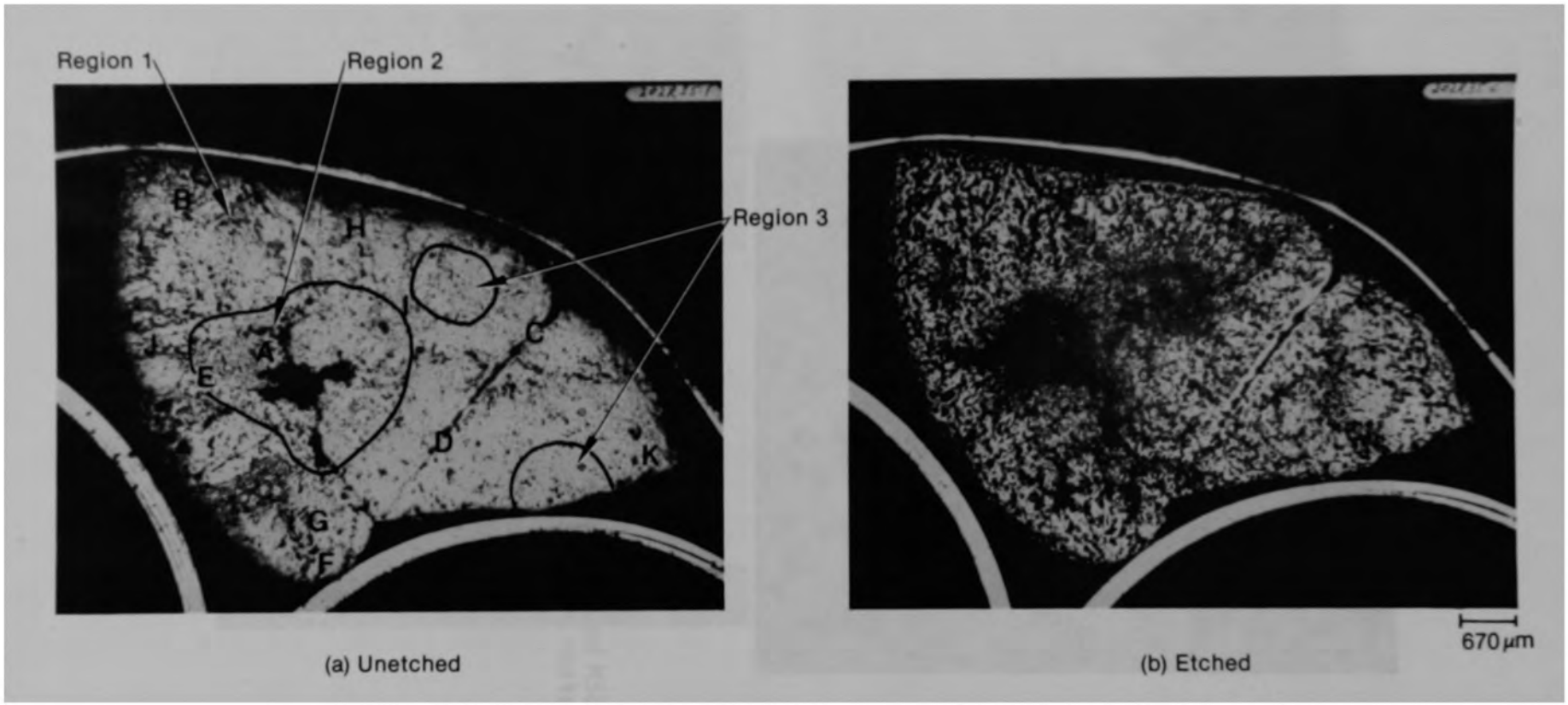

Figure C-233. Photomacrographs of Particle 10A (E9, 74 cm).

Figure C-234. SEM backscattered electron image of Particle 10A (E9, 74 cm) after repolishing.

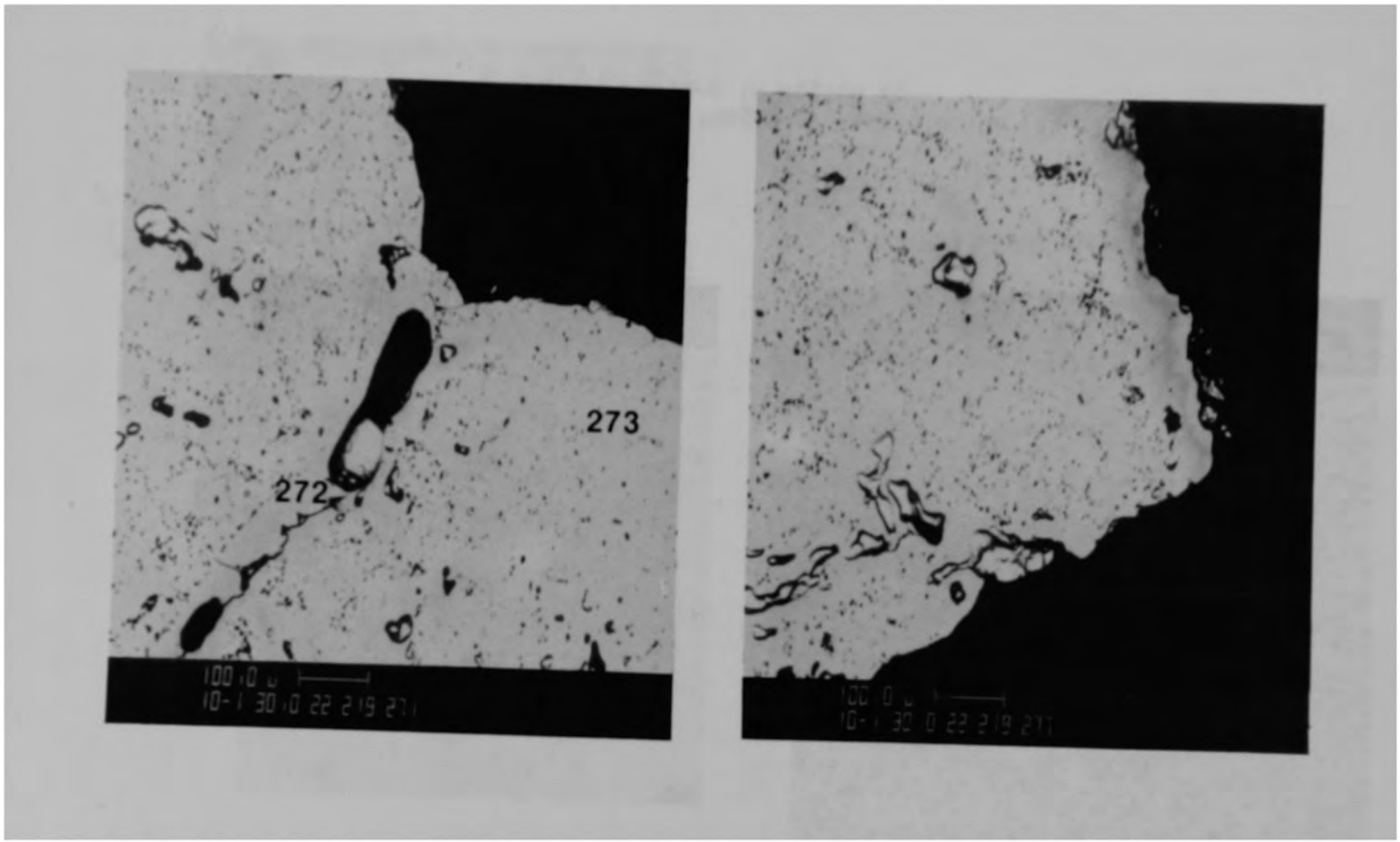

Figure C-235. SEM backscattered electron image of material from Region 1 of Particle 10A (E9, 74 cm).

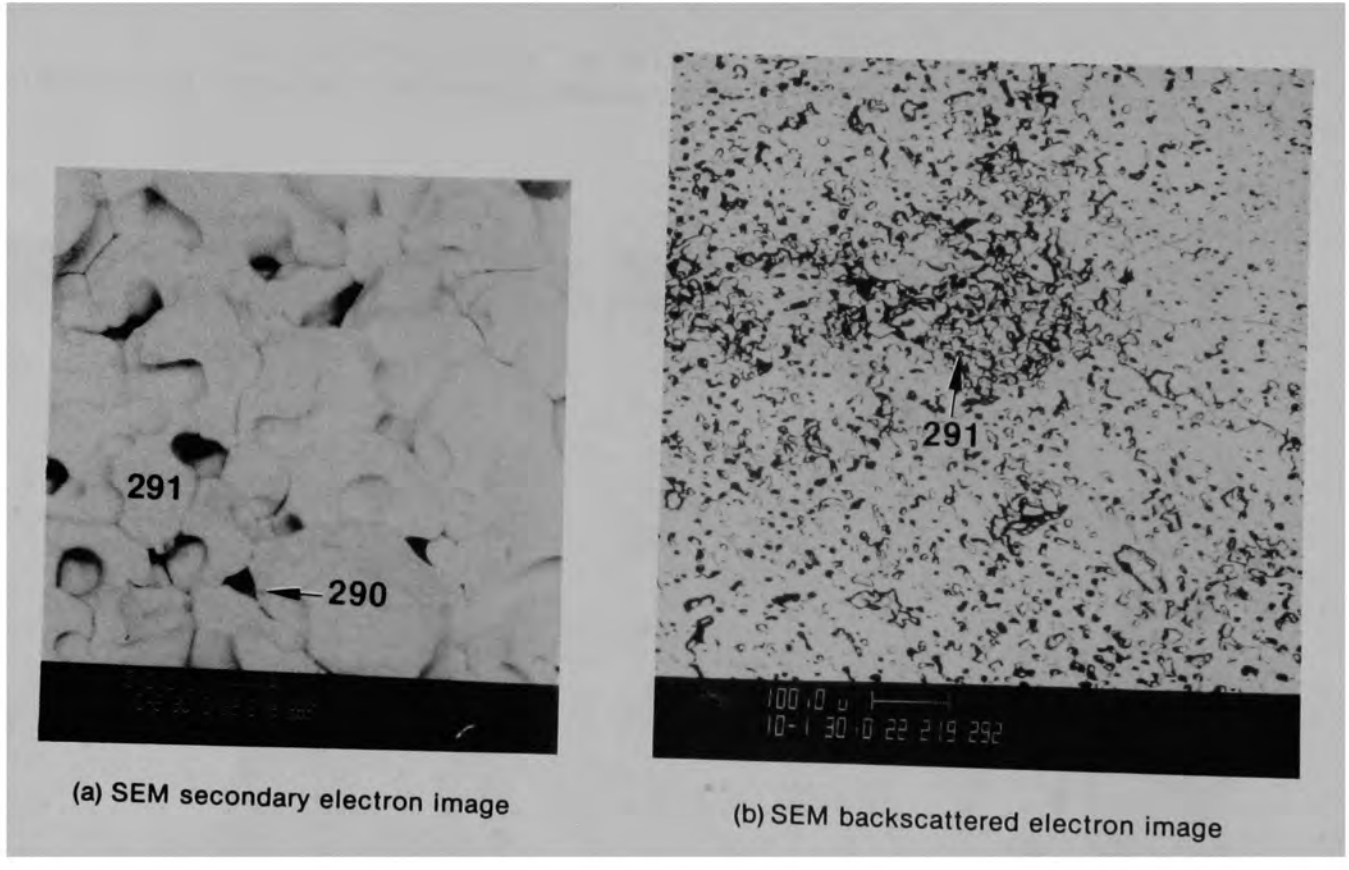

Figure C-236. SEM electron images of Particle 10A (E9, 74 cm) showing a grain structure in Region 2.

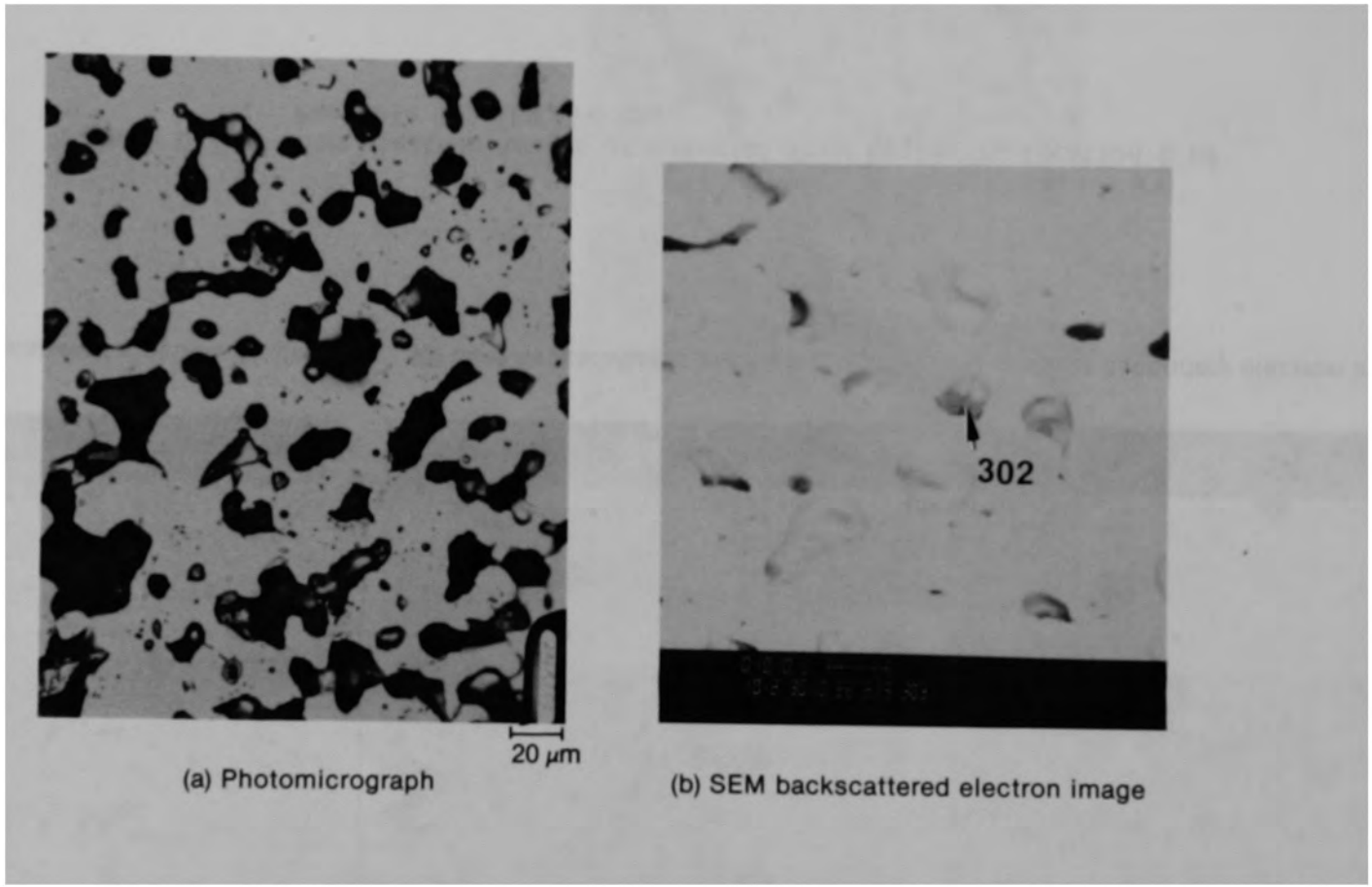

Figure C-237. Photographs of material from Region 2, location A of Particle 10A (E9, 74 cm).

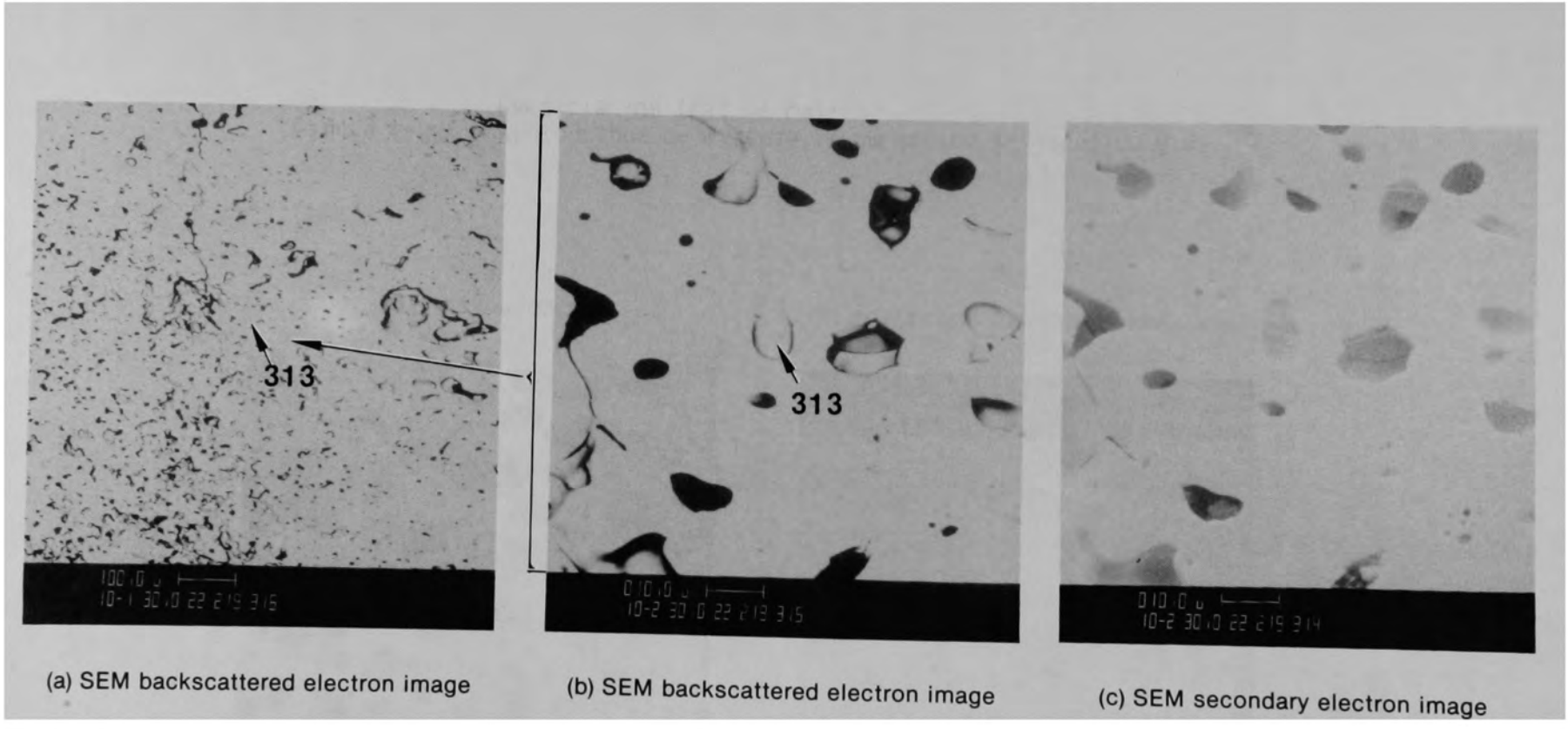

Figure C-238. SEM electron images of material from Region 1, location B of Particle 10A (E9, 74 cm).

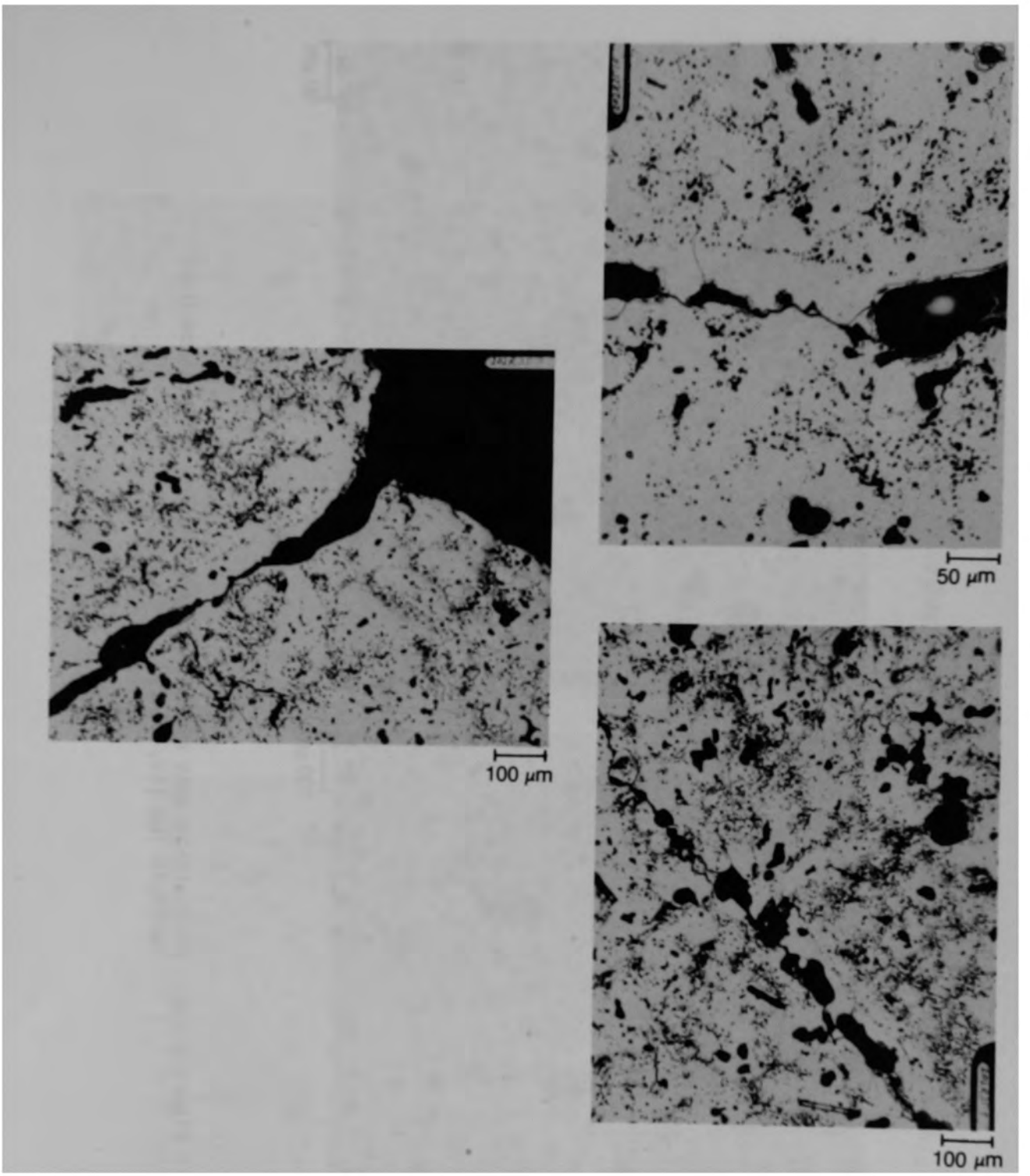

Figure E-239. Photomicrographs of etched material from Region 1, location C of Particle 10A (E9, 74 cm).

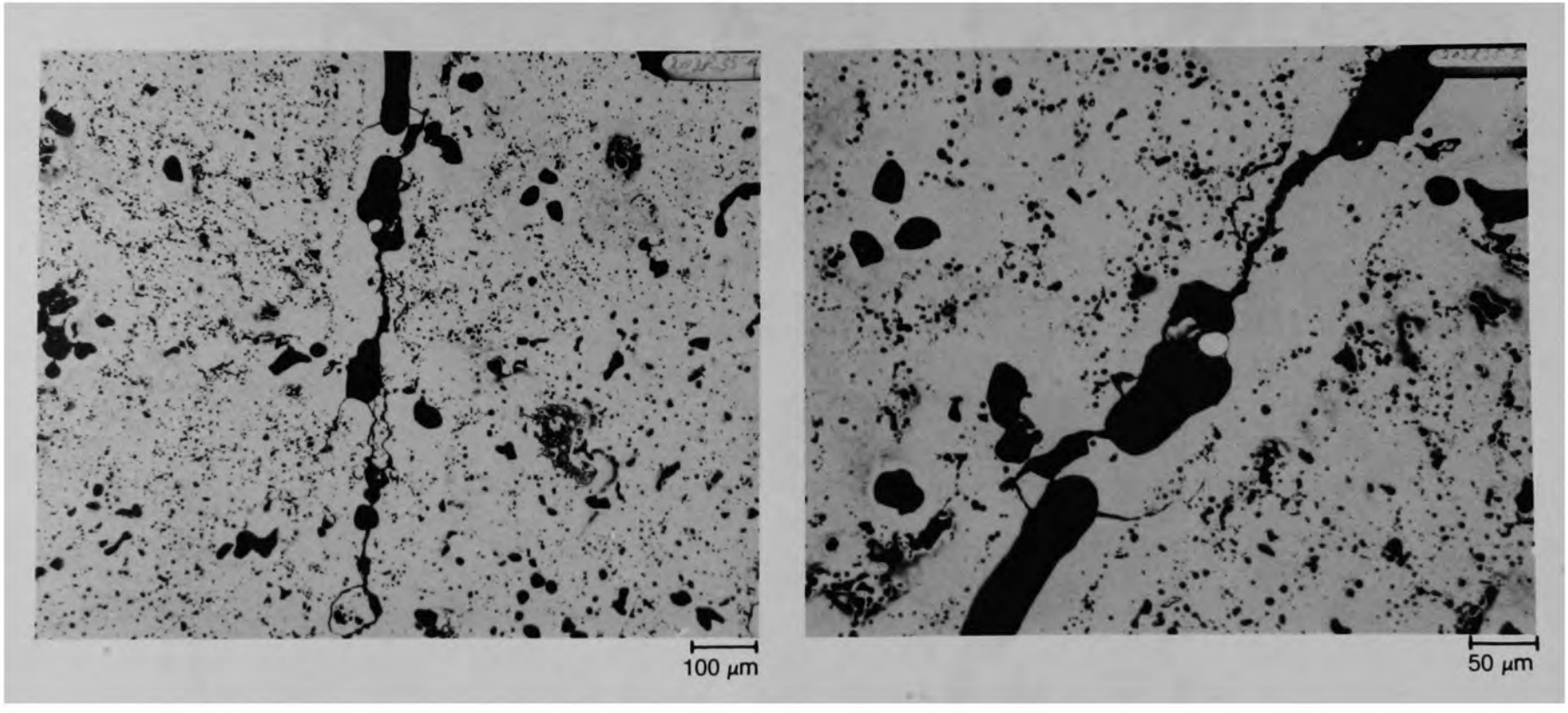

Figure C-240. Photomicrographs of material from Region 1, location D of Particle 10A (E9, 74 cm).

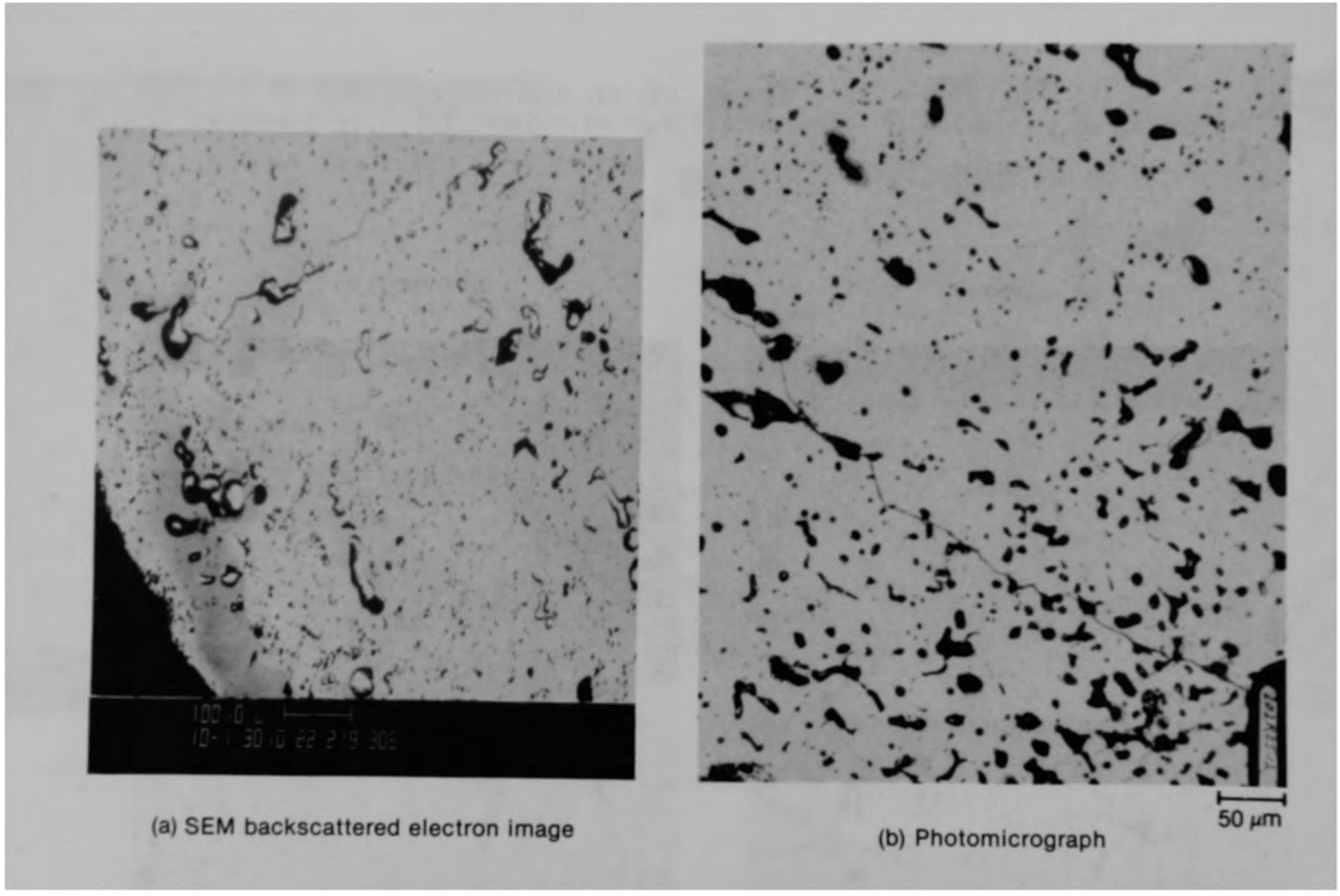

Figure C-241. Photographs of material from Region 2, location E of Particle 10A (E9, 74 cm).

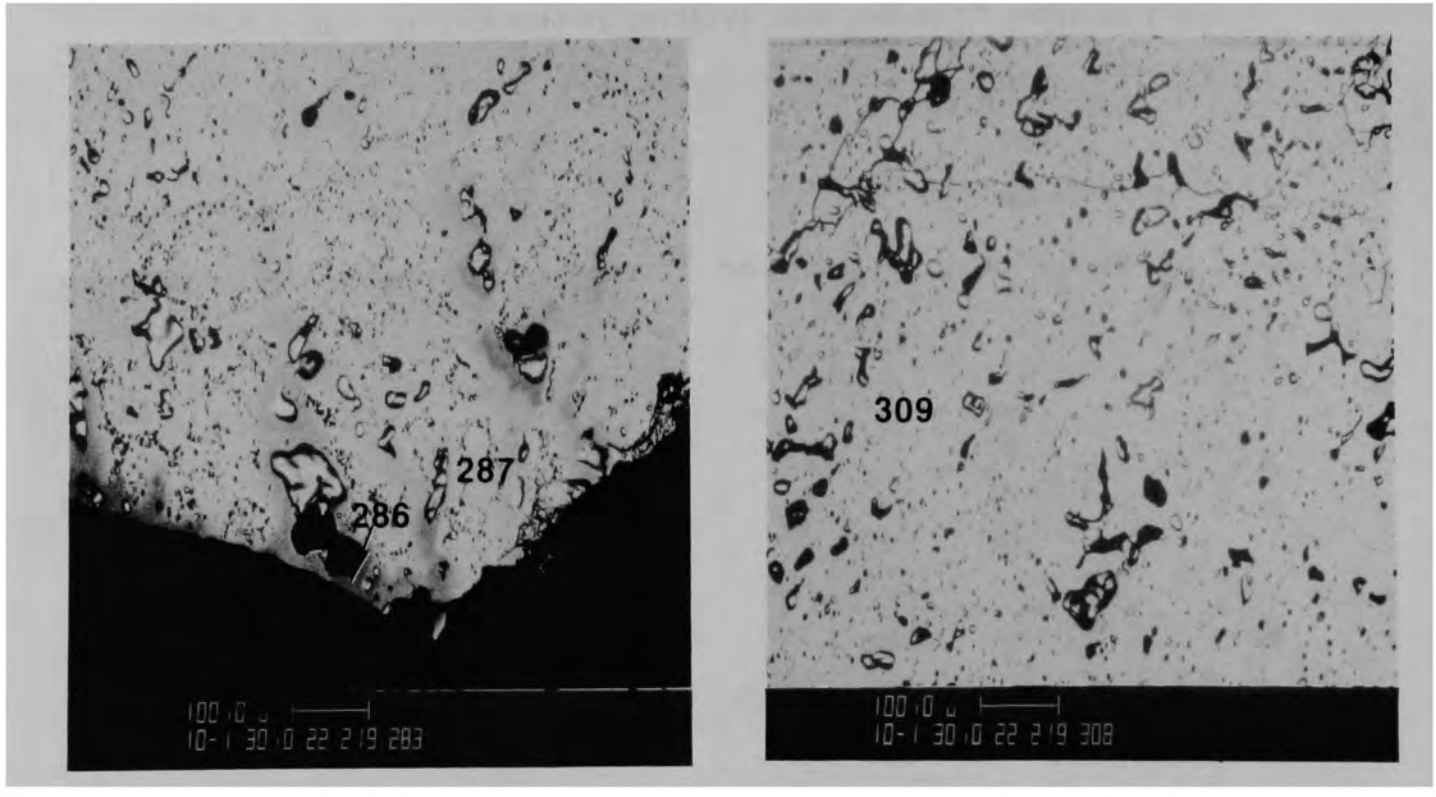

(a) Location F

(b) Location G

Figure C-242. SEM backscattered electron images of material from Region 1 of Particle 10A (E9, 74 cm).

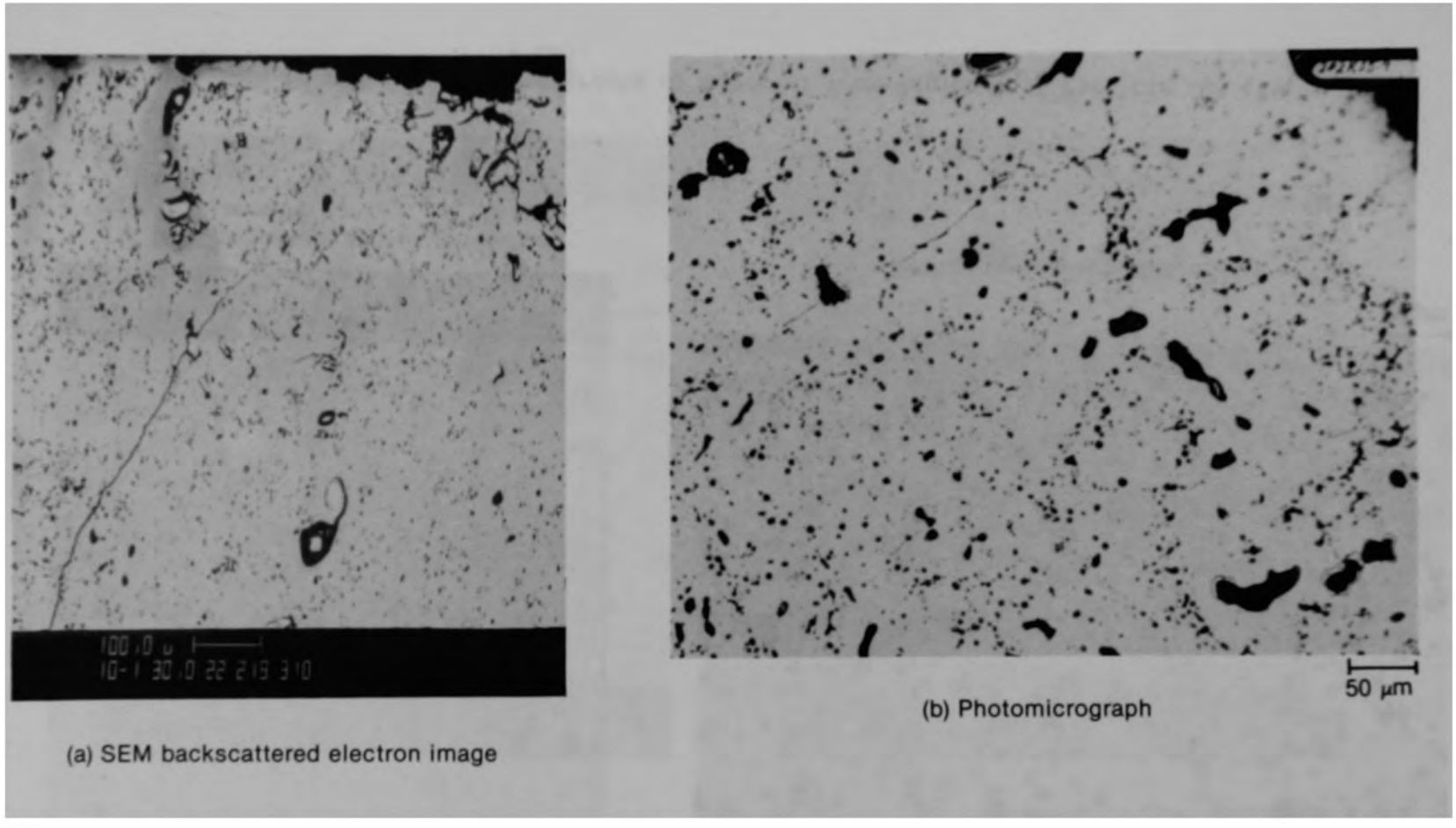

Figure C-243. Photographs of material from Region 1, location B of Particle 10A (E9, 74 cm).

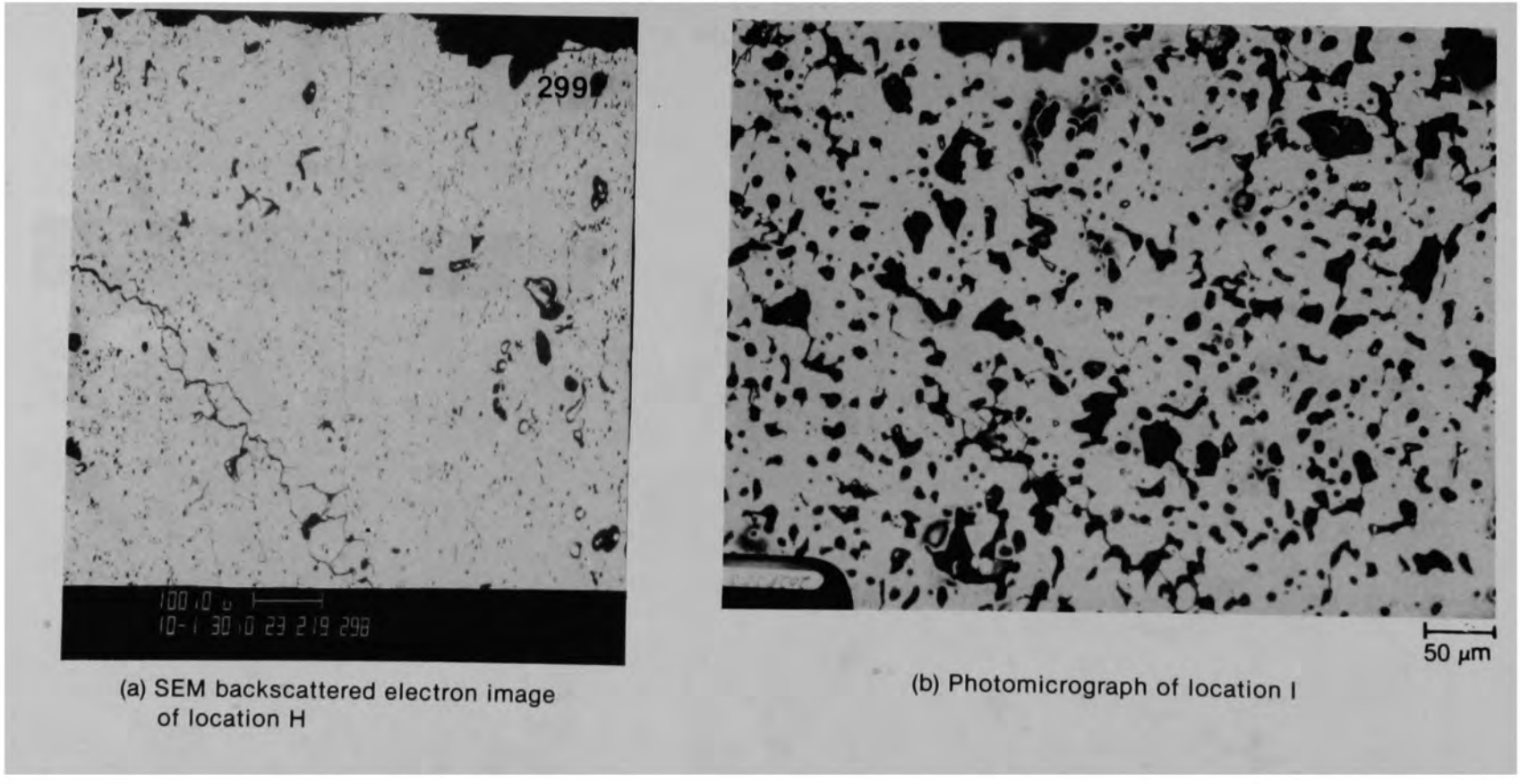

(a) SEM backscattered electron image of location H

(b) Photomicrograph of location I

Figure C-244. Photographs of material from Region 1 of Particle 10A (E9, 74 cm).

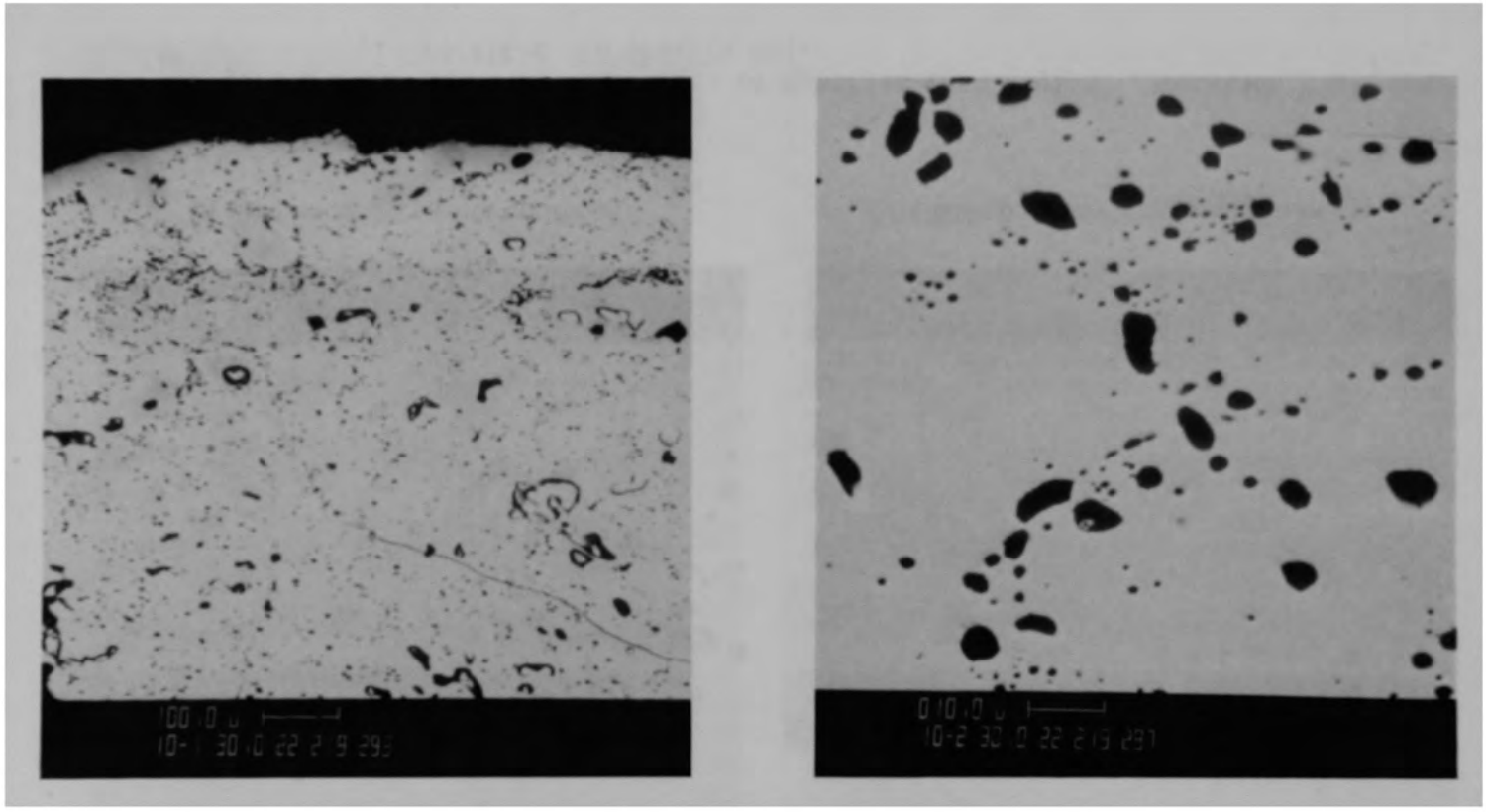

Figure C-245. SEM backscattered electron image of material from Region 1, location J of Particle 10A (E9, 74 cm).

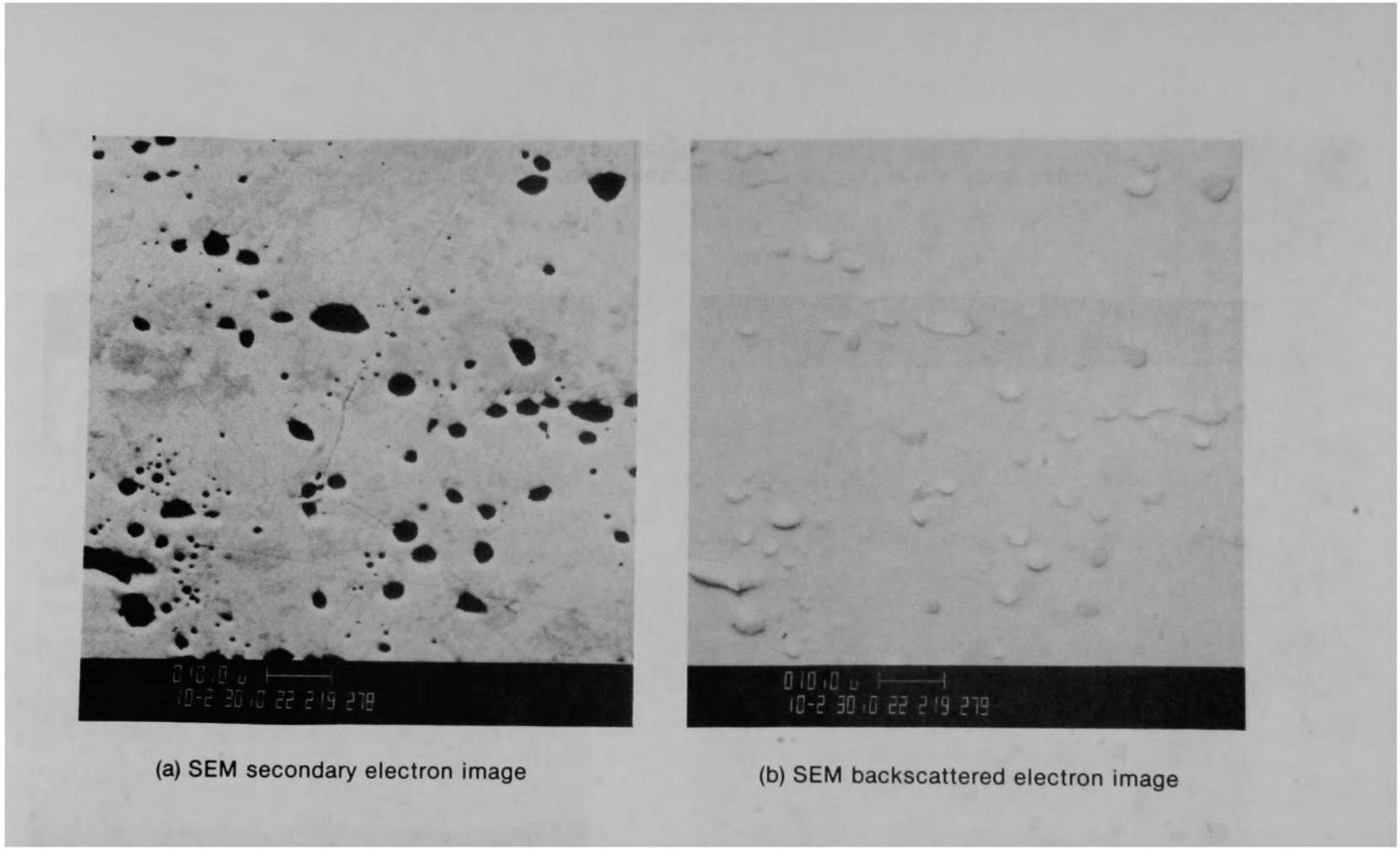

(a) SEM secondary electron image

(b) SEM backscattered electron image

Figure C-246. SEM electron images of material from Region 1, location K of Particle 10A (E9, 74 cm).

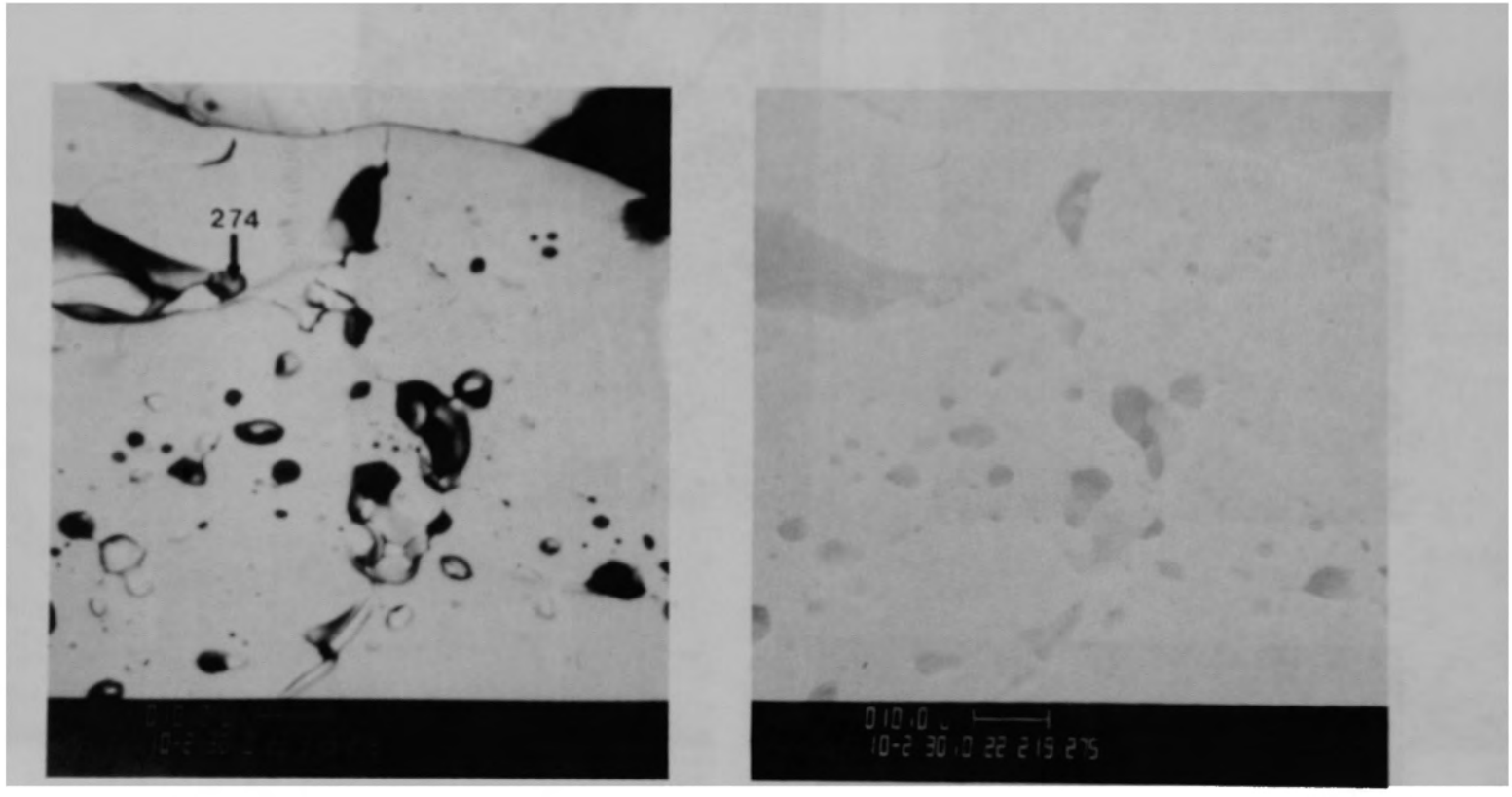

(a) SEM backscattered electron image

(b) SEM secondary electron image

Figure C-247. Photomicrographs of Particle 10E (E9, 74 cm).

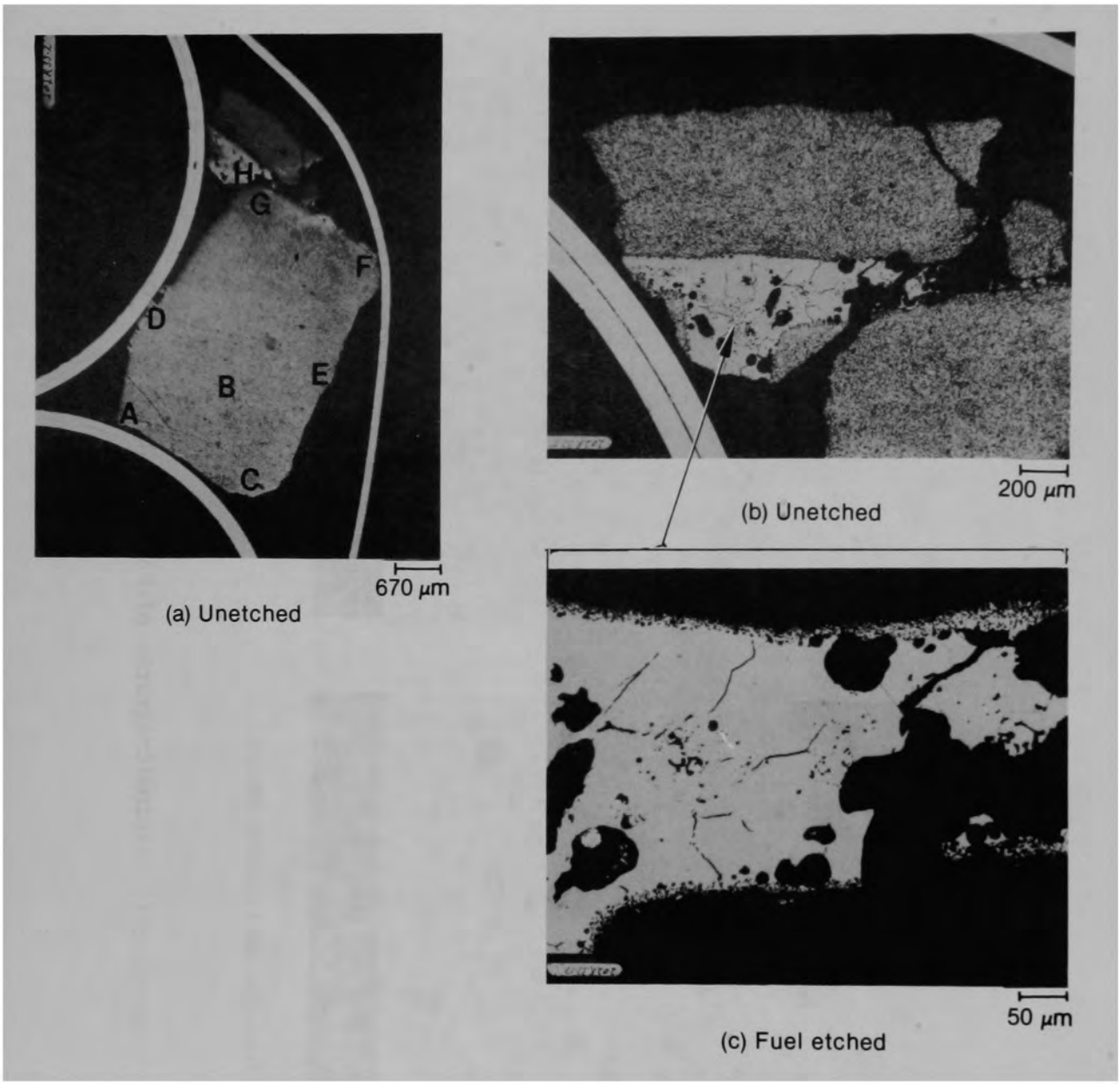

Figure C-248. Photomicrographs of Particle 10E (E9, 74 cm).

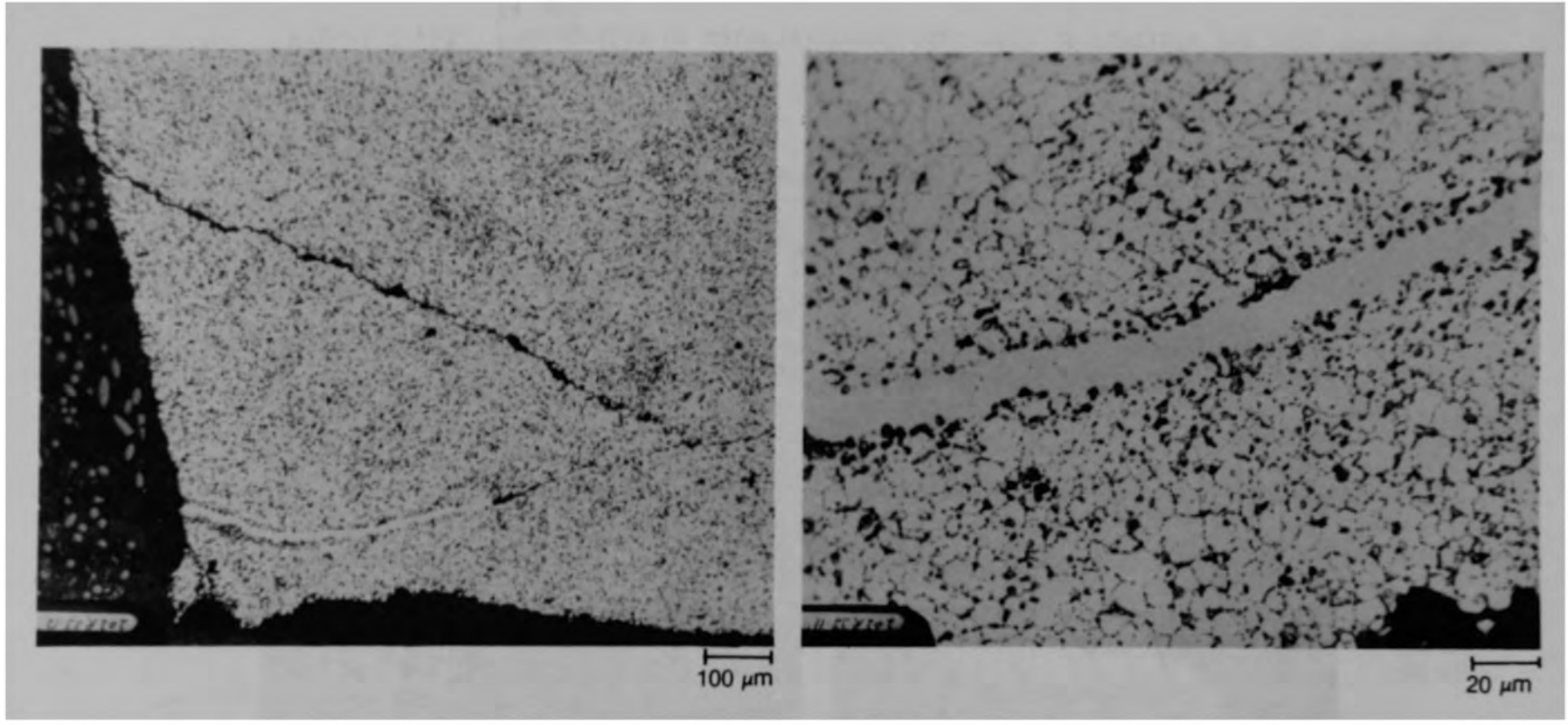

Figure C-249. Photomicrographs of material from location A of Particle 10E (E9, 74 cm).

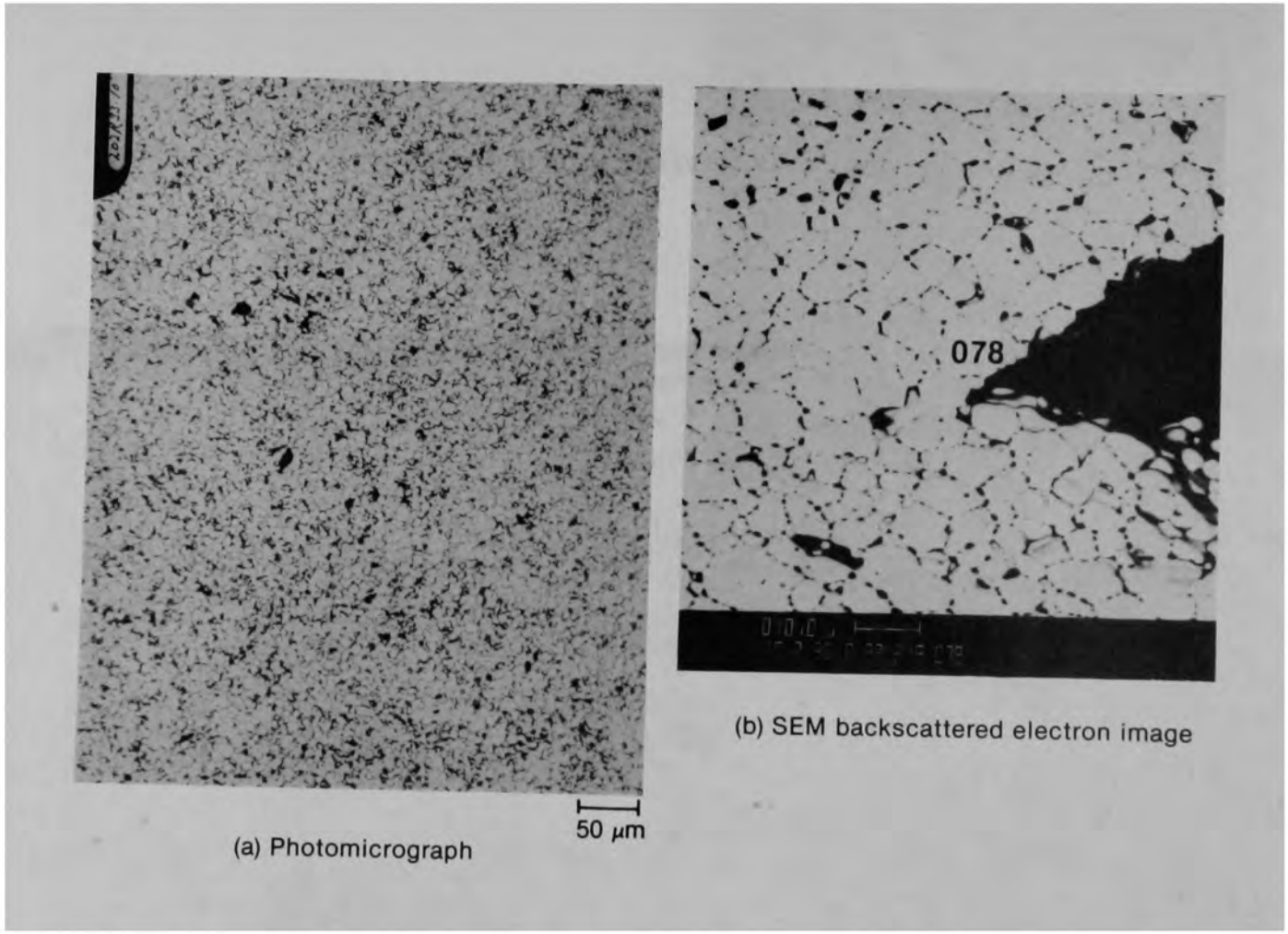

Figure C-250. Photographs of material from location B of Particle 10E (E9, 74 cm).

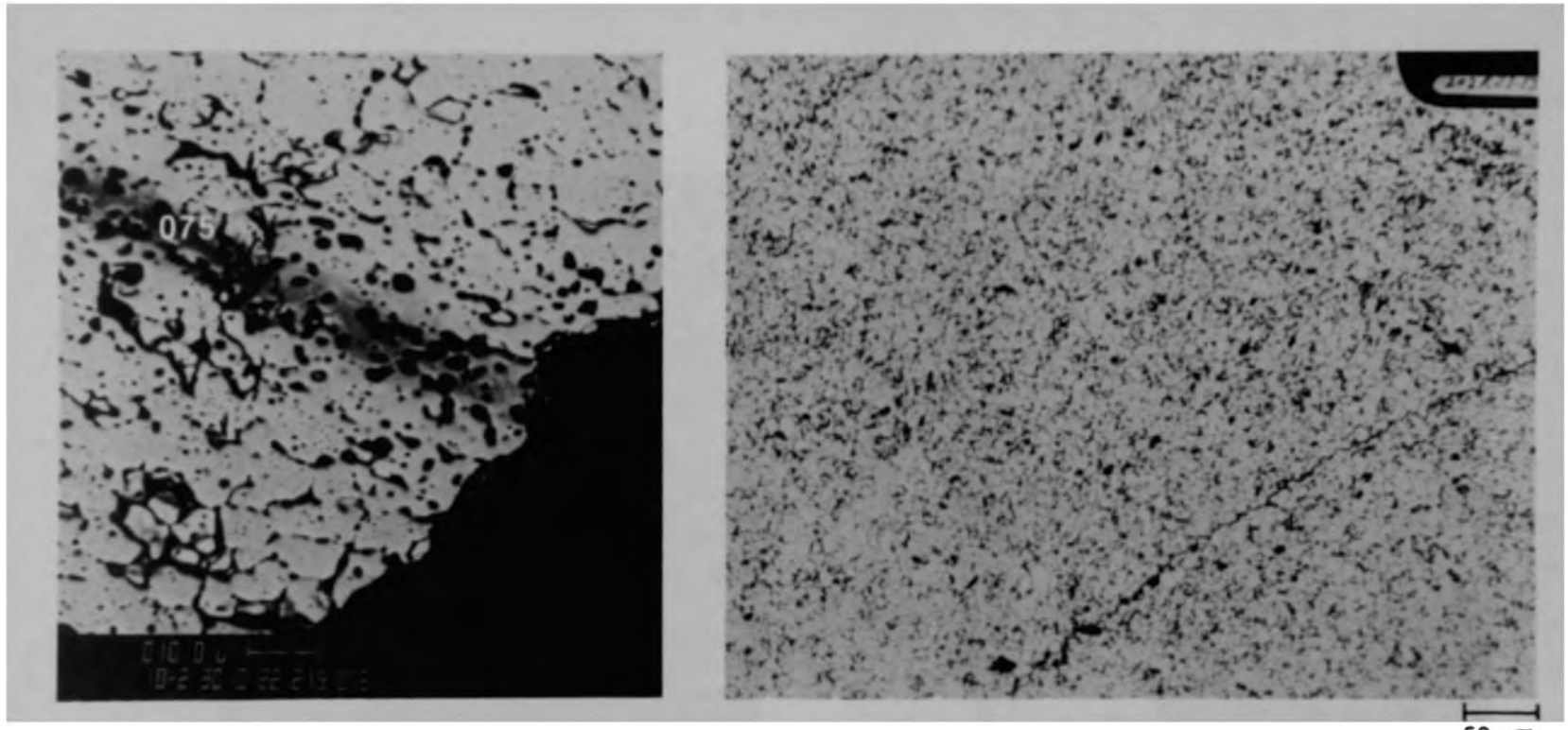

(a) SEM backscattered electron image

(b) Photomicrograph

Figure C-251. Photographs of material from location C of Particle 10E (E9, 74 cm).

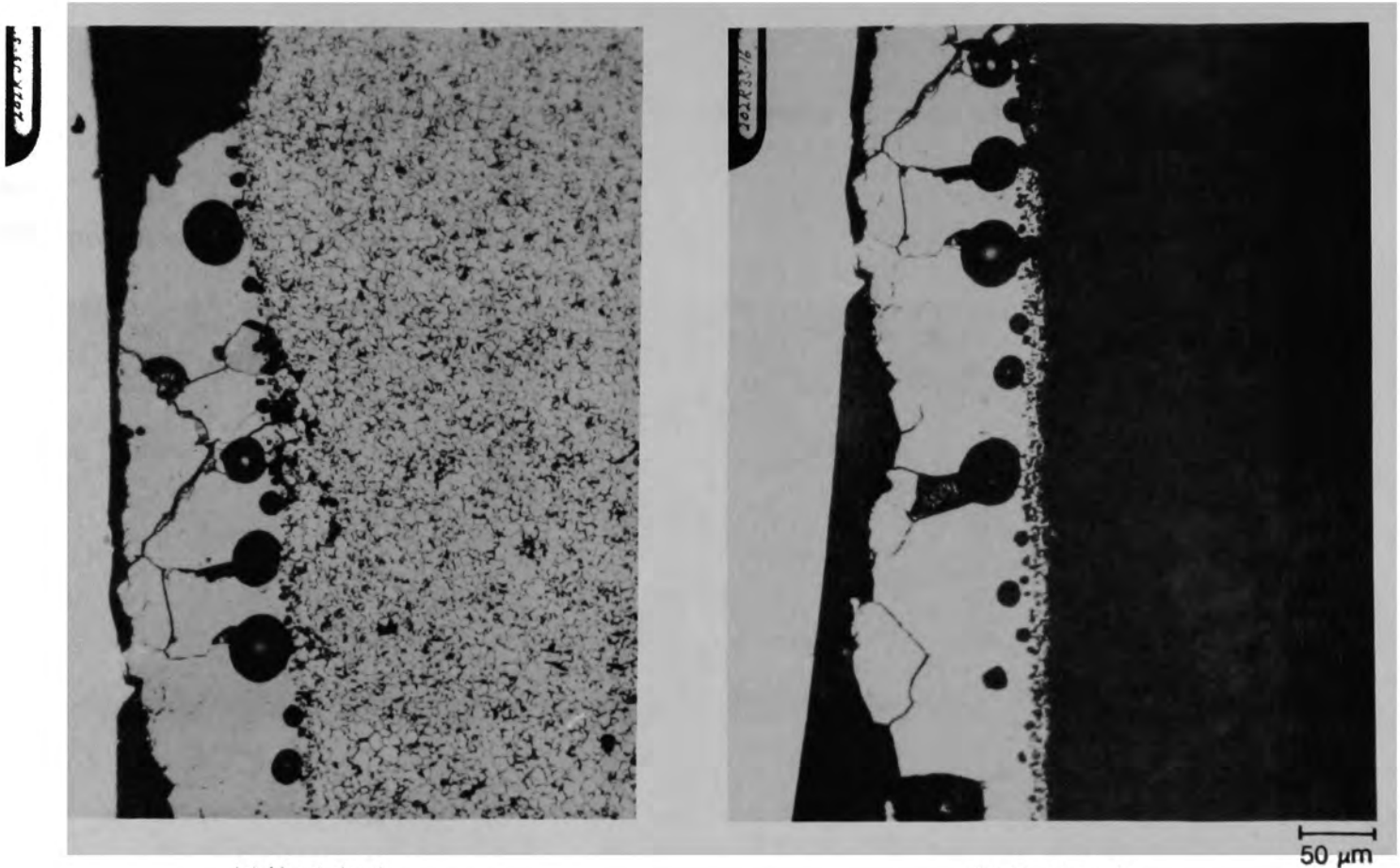

(a) Unetched

(b) Fuel etch

Figure C-252. Photomicrographs of material from location D of Particle 10E (E9, 74 cm).

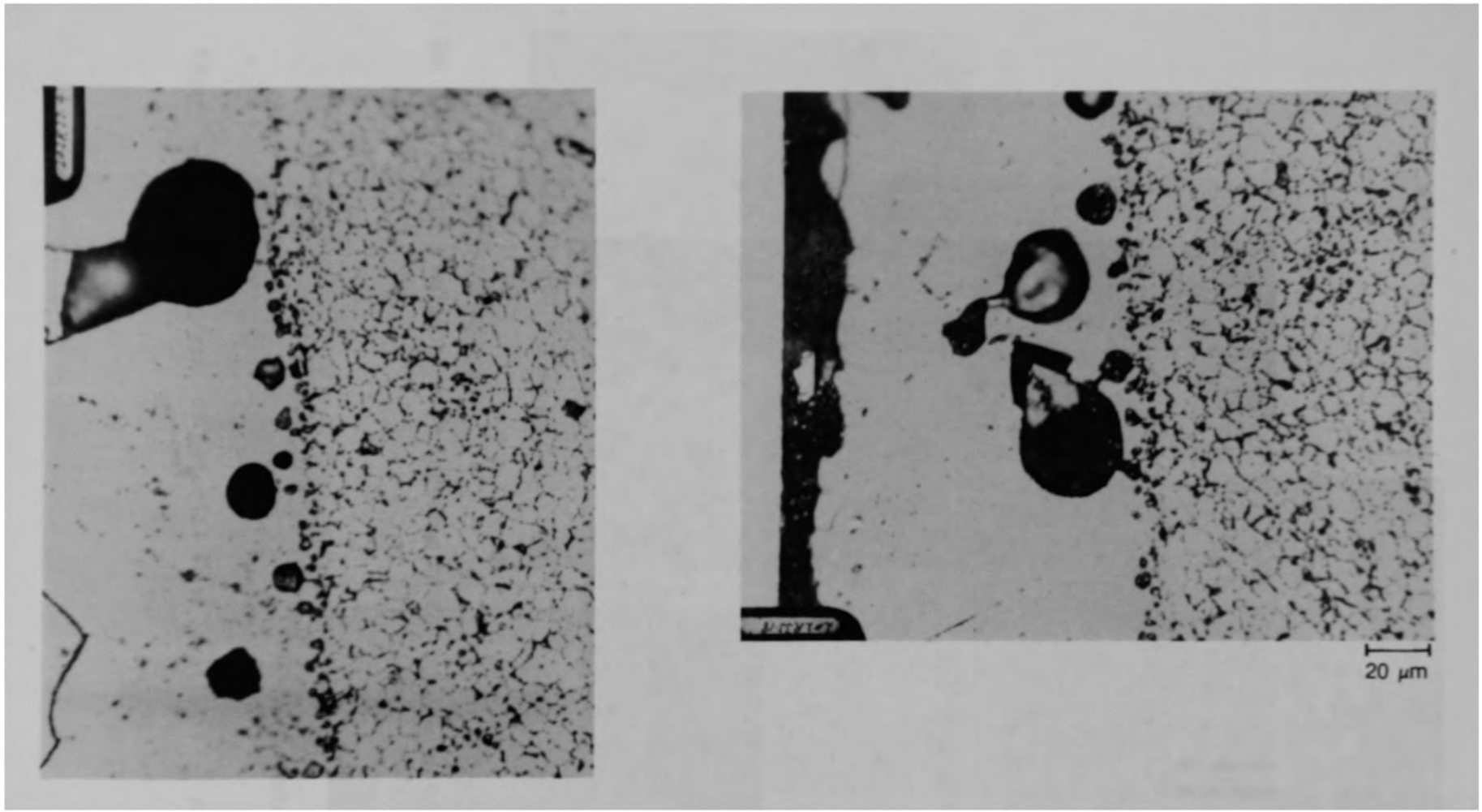

Figure C-253. Photomicrographs of material from location D of Particle 10E (E9, 74 cm).

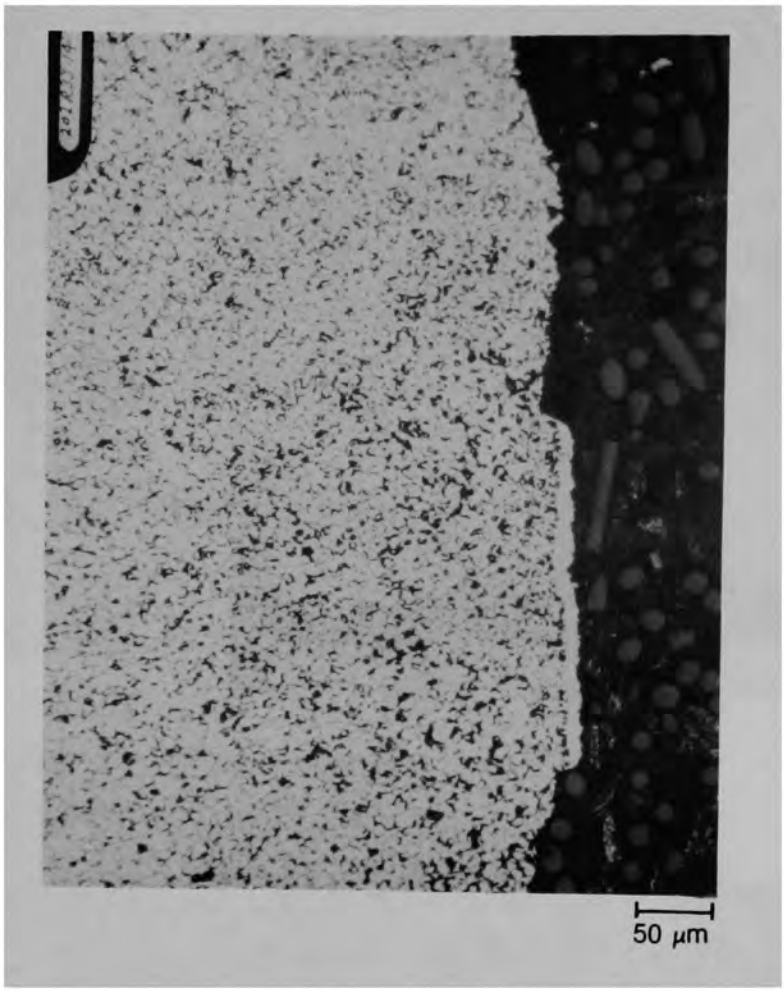

Figure C-254. Photomicrograph of material from location E of Particle 10E (E9, 74 cm).

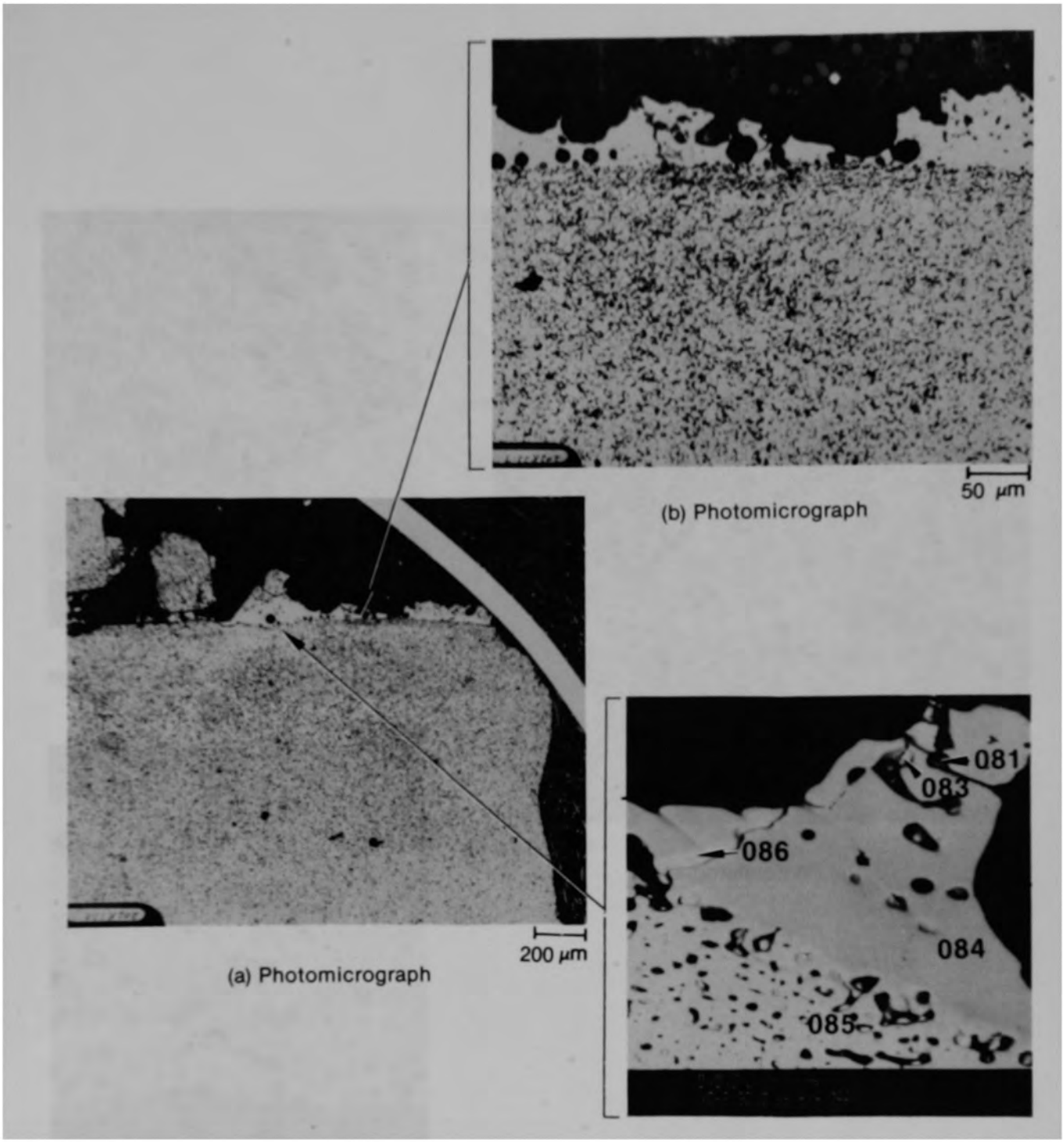

Figure C-255. Photographs of material from location F of Particle 10E (E9, 74 cm).

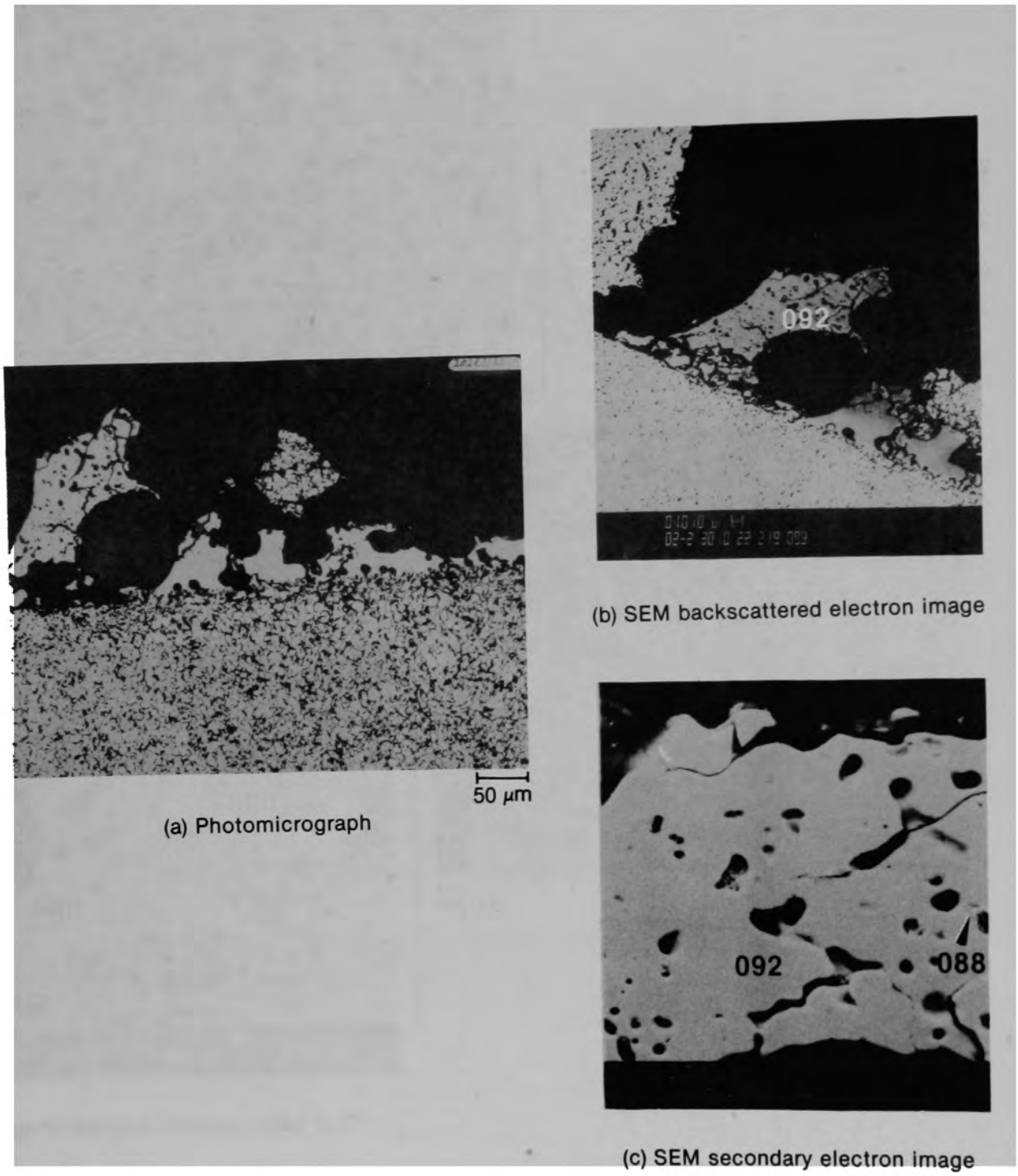

Figure C-256. Photographs of material from location F of Particle 10E (E9, 74 cm).

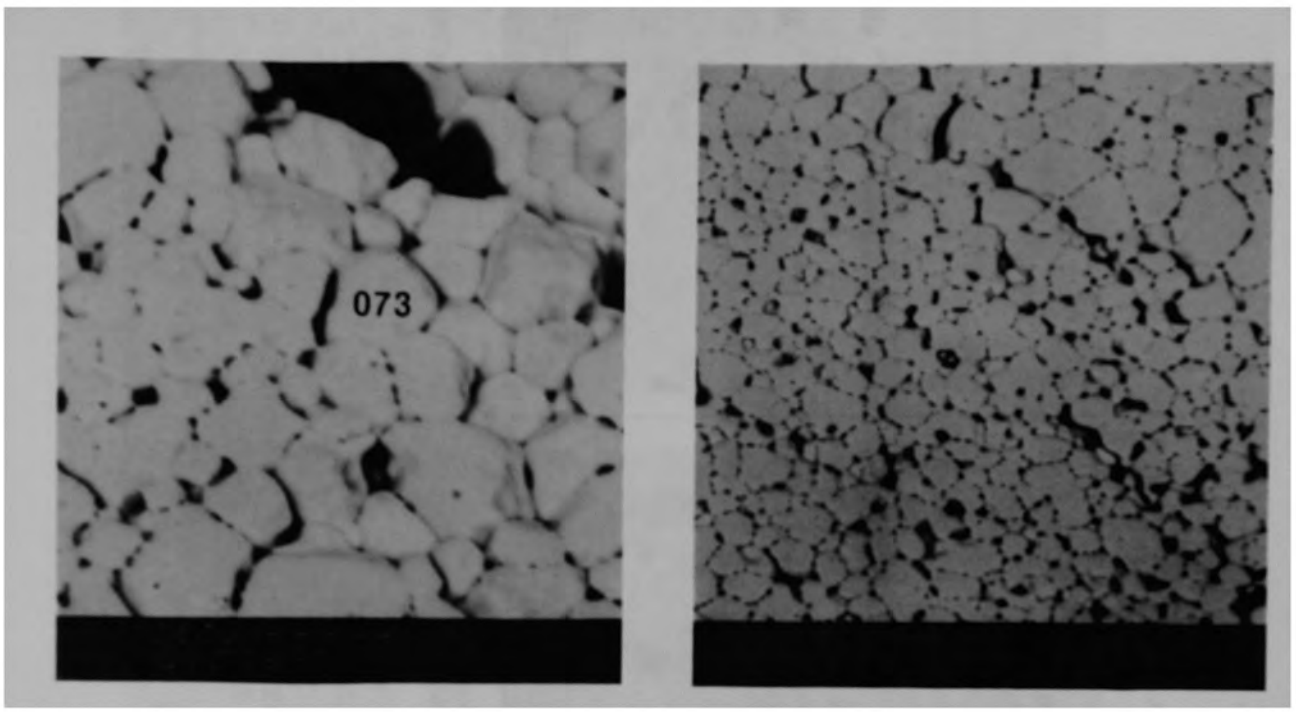

Figure C-257. SEM backscattered electron images of material from location G of Particle 10E (E9, 74 cm).

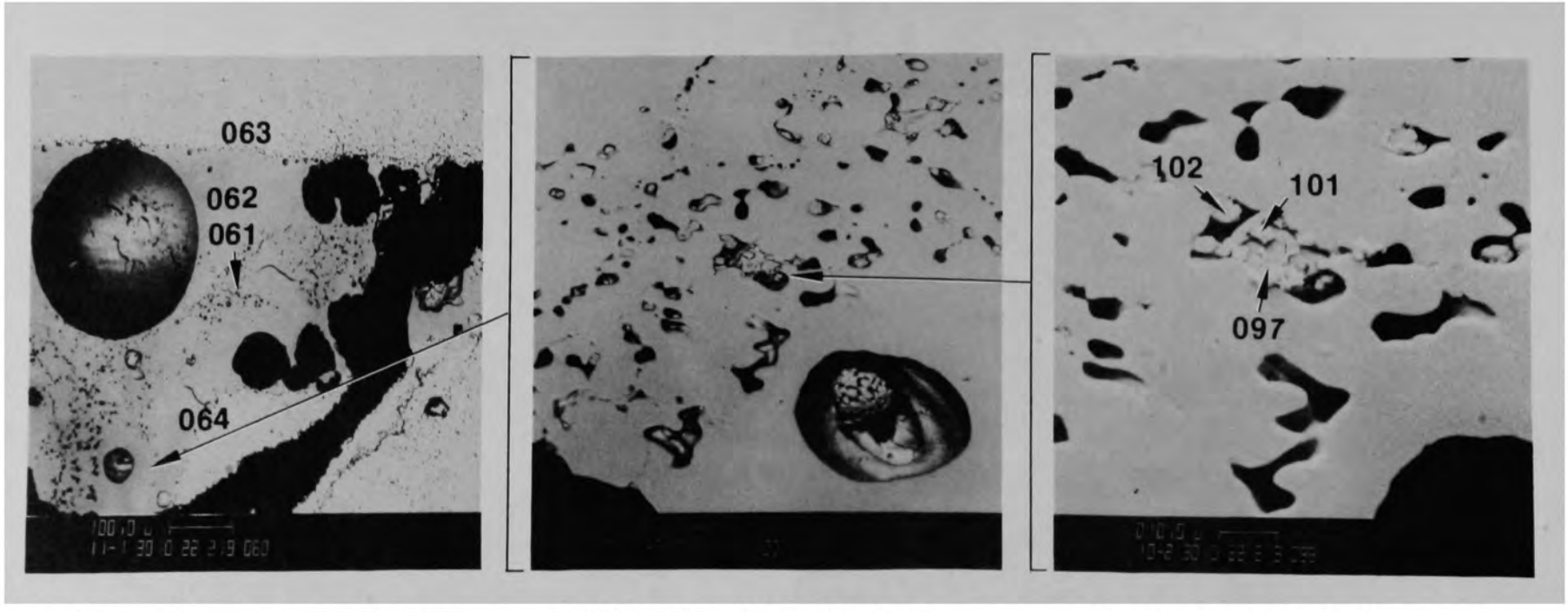

(a) SEM backscattered electron image (b) SEM backscattered electron image (c) SEM secondary electron image

Figure C-258. SEM electron images of material from location H of Particle 10E (E9, 74 cm).

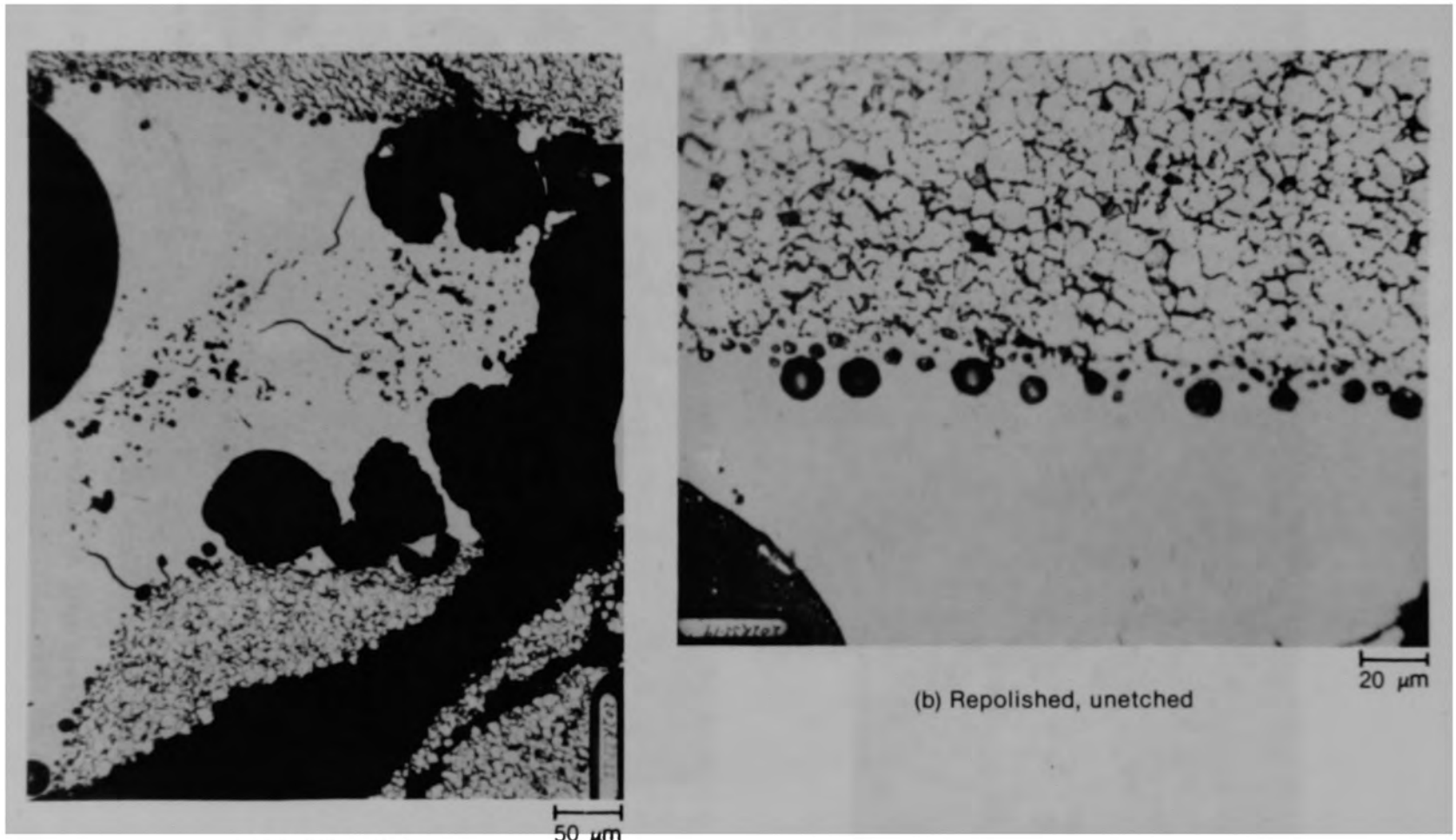

(a) Cladding etch

(b) Repolished, unetched

Figure C-259. Photomicrographs of material from location H of Particle 10E (E9, 74 cm).

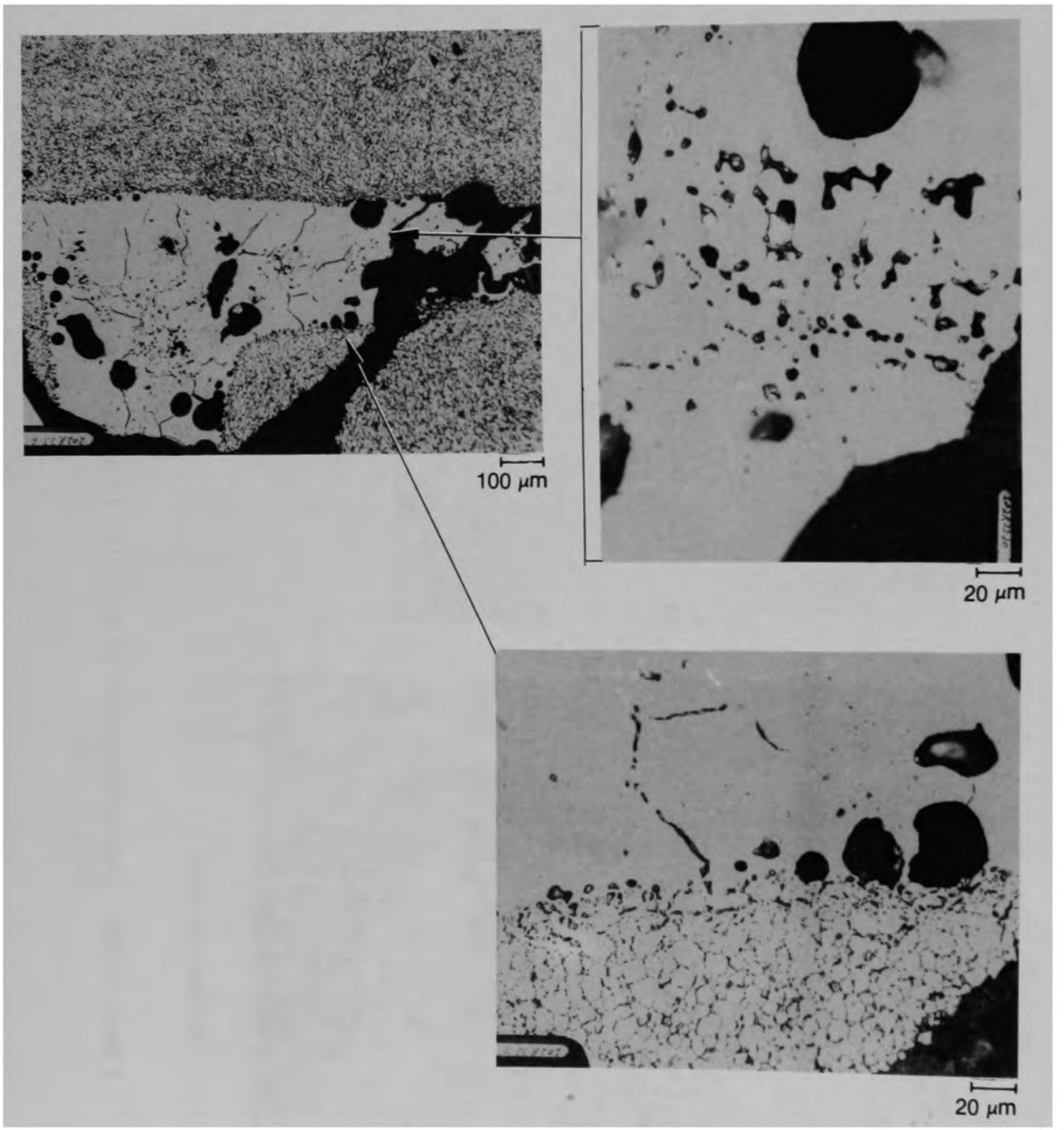

Figure C-260. Photomicrographs of material from location H of Particle 10E (E9, 74 cm).

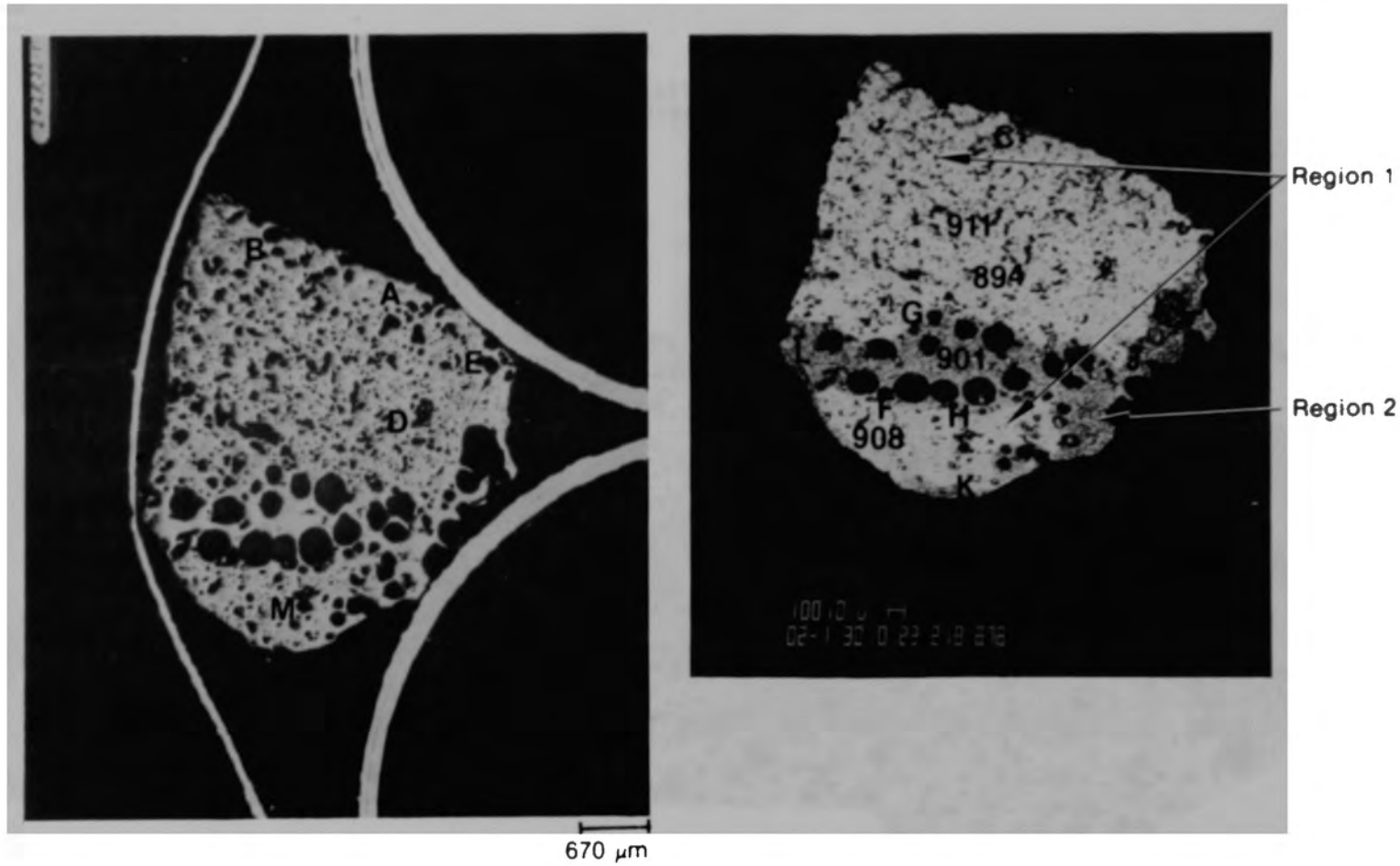

Figure C-261. Photomacrographs of Particle 10F (E9, 74 cm) showing two regions.

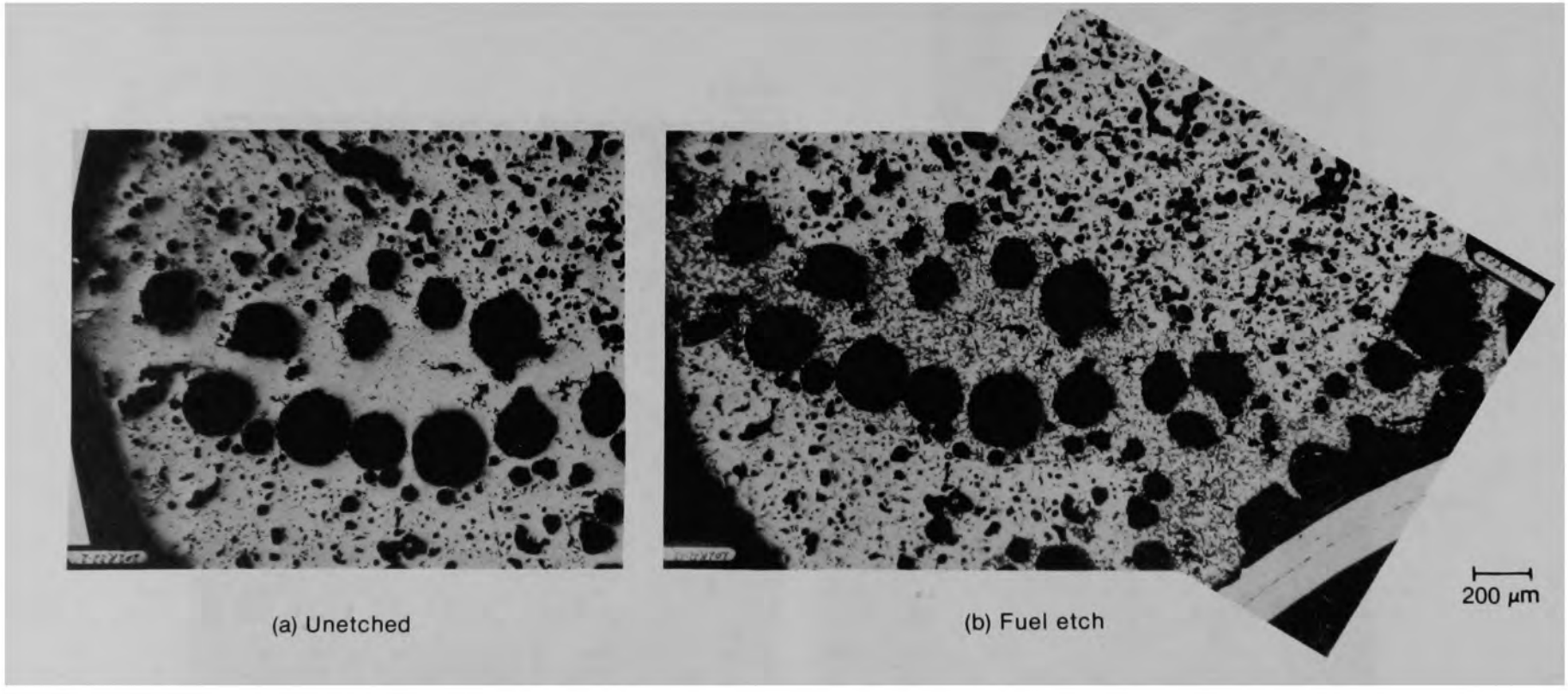

Figure C-262. Photomicrographs of material from Region 2 of Particle 10F (E9, 74 cm) showing effects of etch.

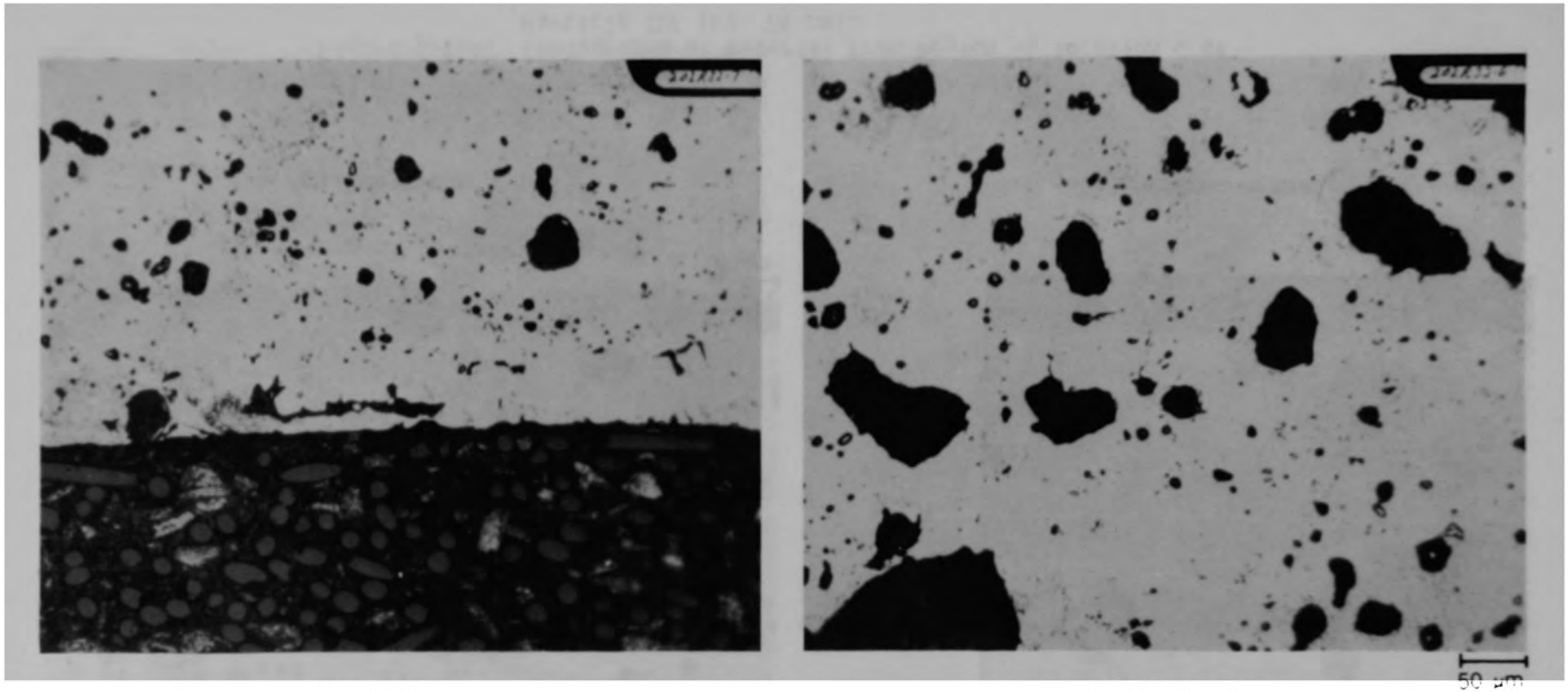

(a) Location A

(b) Location B

Figure C-263. Photomicrographs of material from Region 1 of Particle 10F (E9, 74 cm).

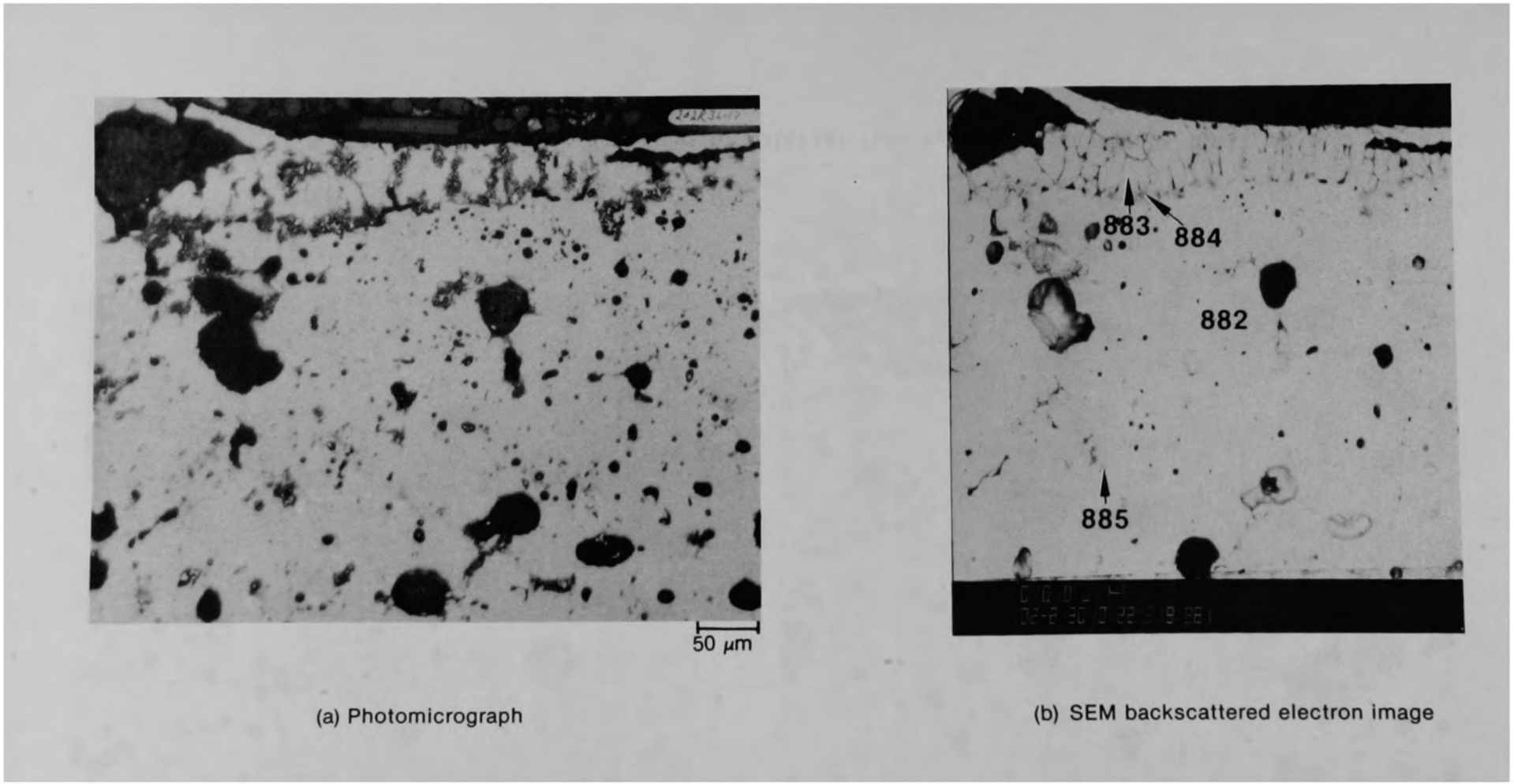

Figure C-264. Photographs of material from Region 1, location C of Particle 10F (E9, 74 cm).

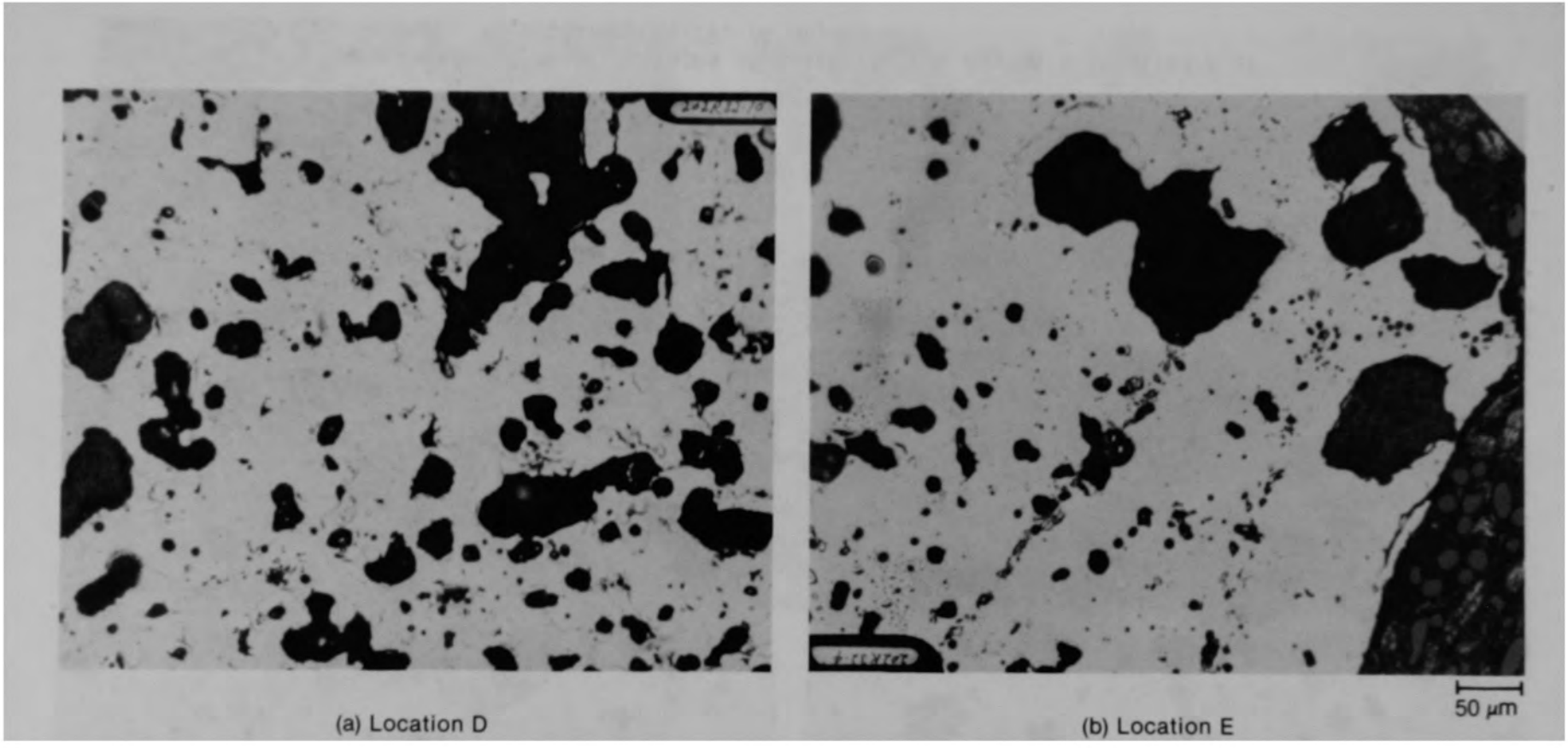

Figure C-265. Photomicrographs of material from Region 1 of Particle 10F (E9, 74 cm).

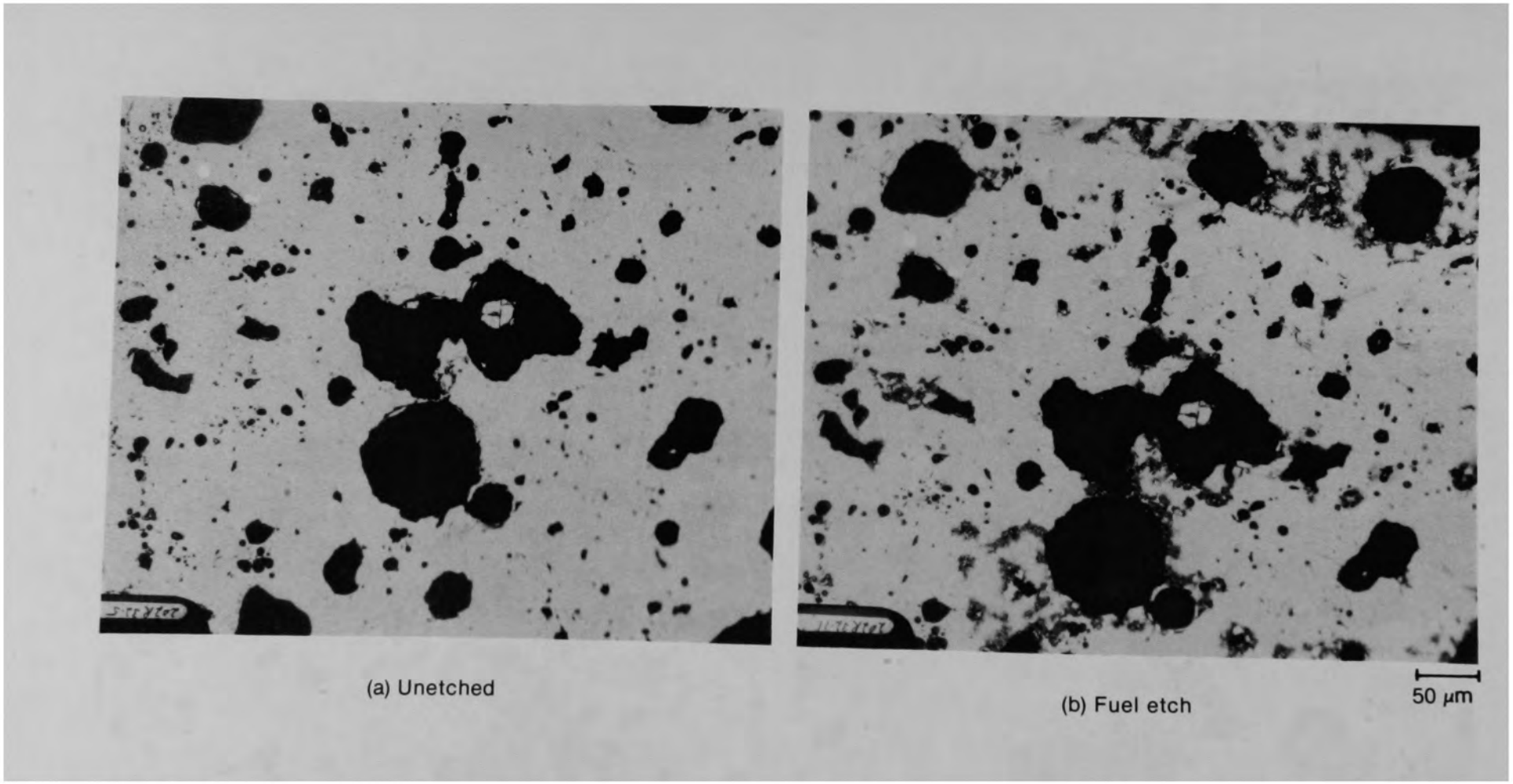

Figure C-266. Photomicrographs of material from Region 1 location M of Particle 10F (E9, 74 cm).

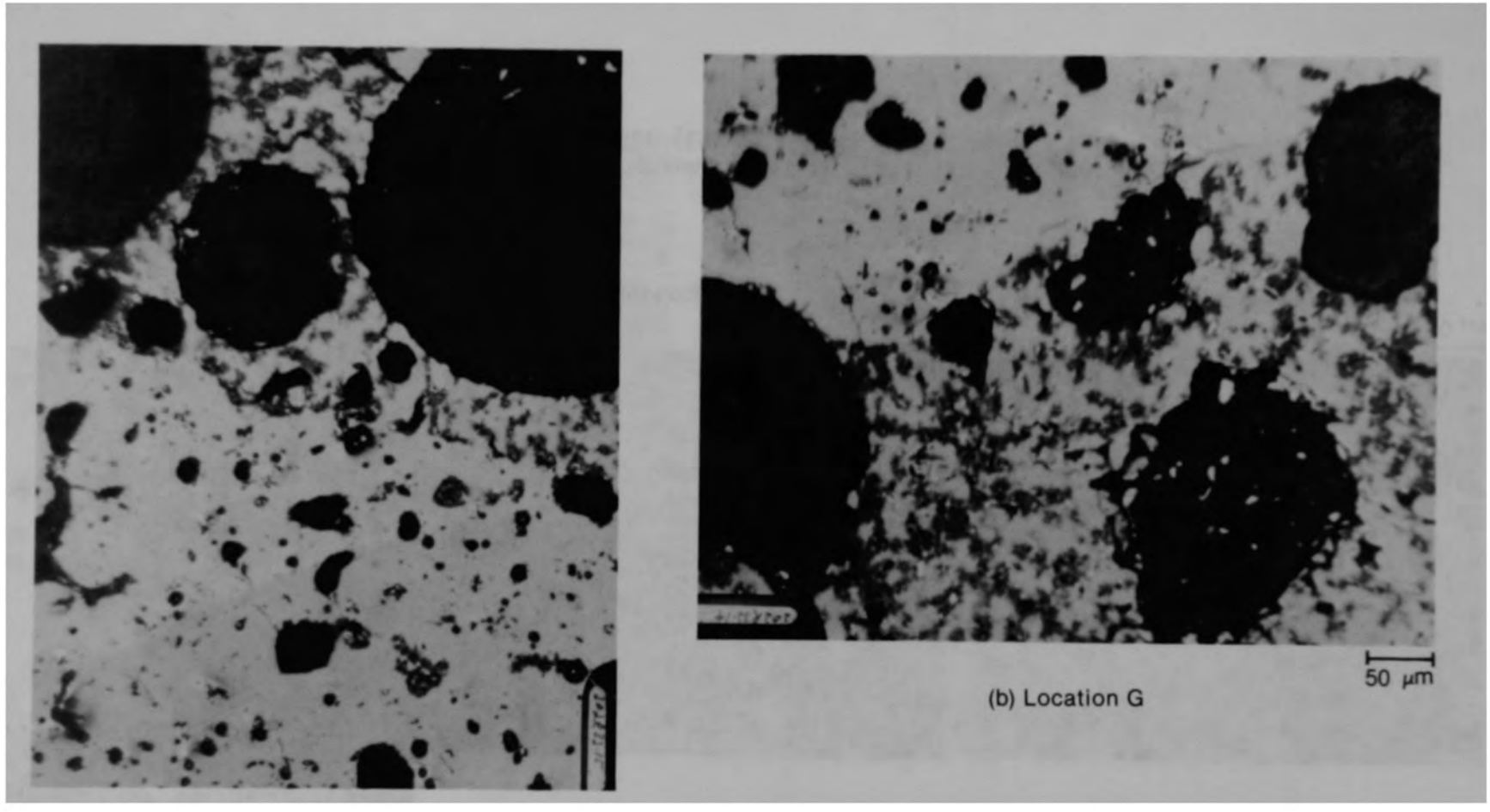

(a) Location F

(b) Location G

Figure C-267. Photomicrographs of etched material from Region 2 of Particle 10F (E9, 74 cm).

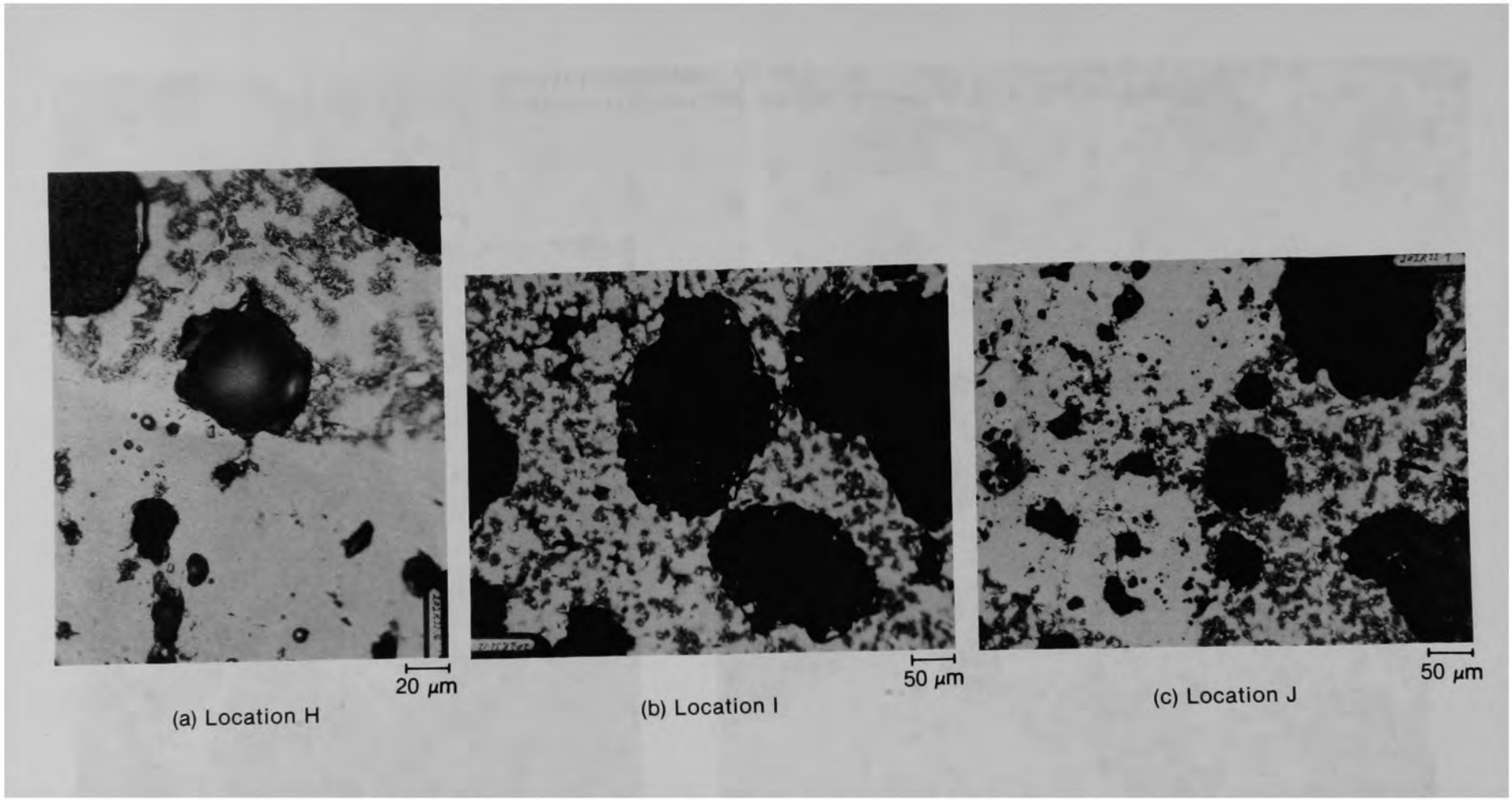

Figure C-268. Photomicrographs of etched material from Region 2 of Particle 10F (E9, 74 cm).

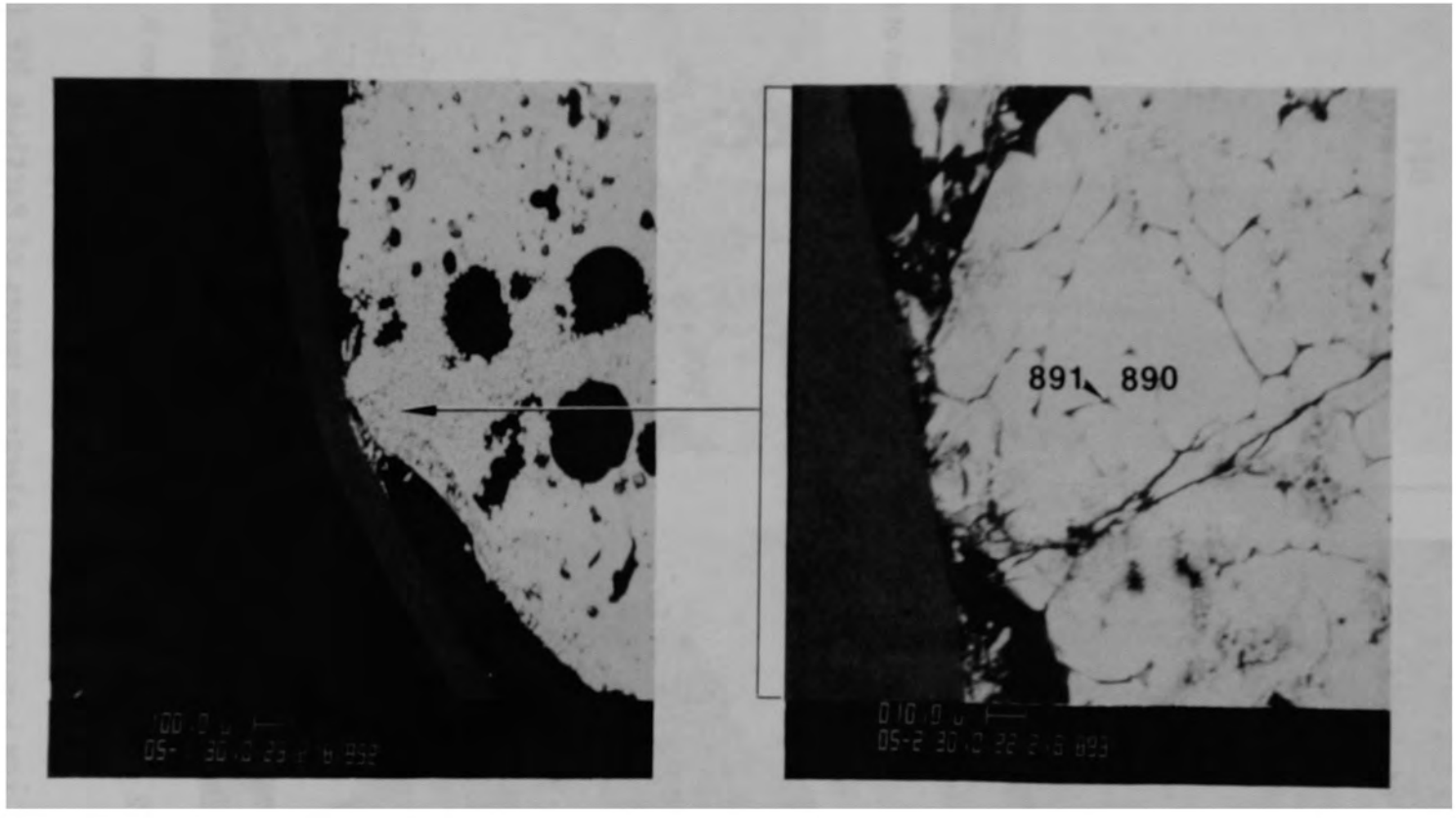

Figure C-269. SEM backscattered electron images of Region 2, location L of Particle 10F (E9, 74 cm).

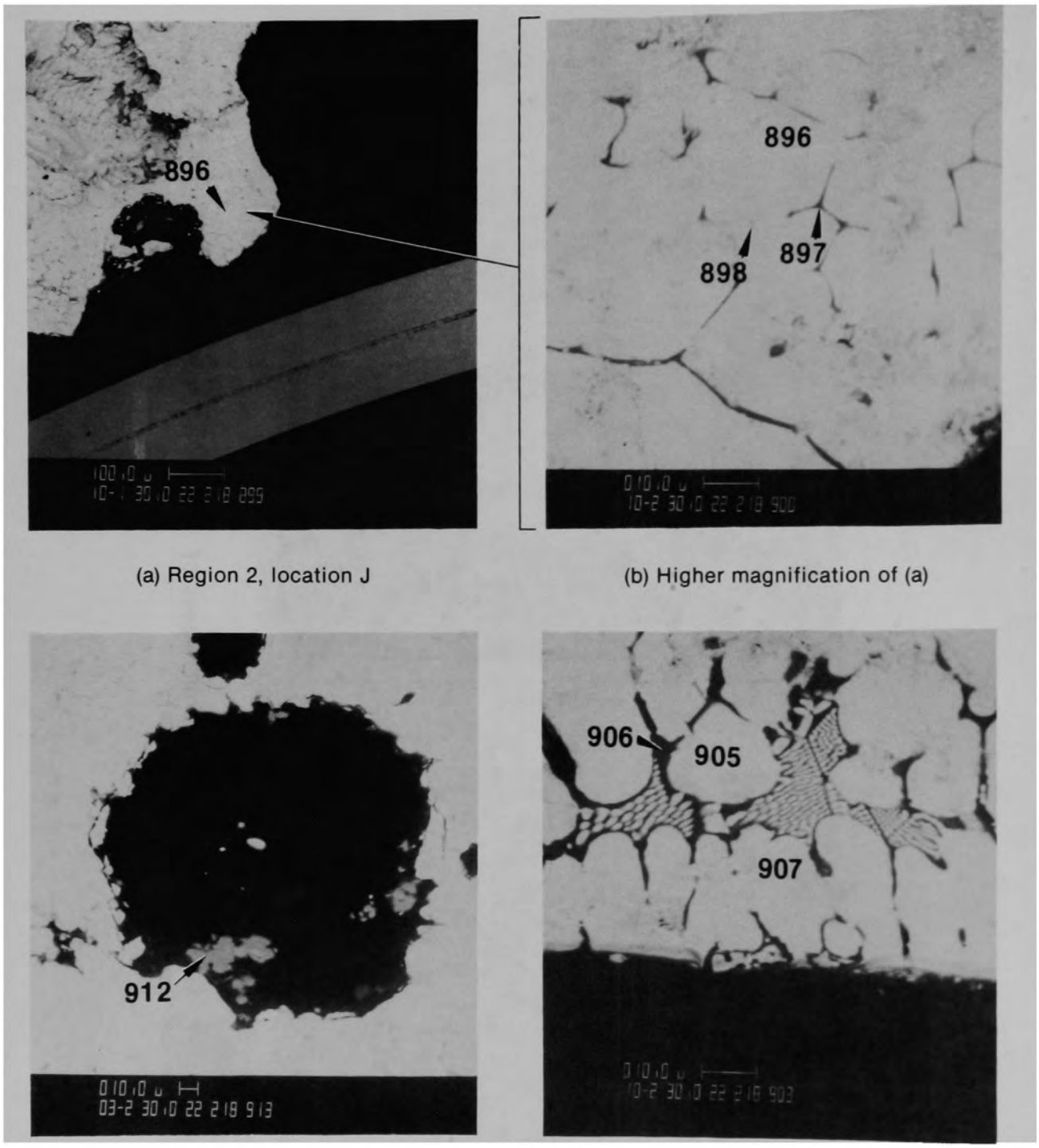

(a) Region 2, location J

(b) Higher magnification of (a)

(c) Region 2, location I

(d) Region I, location K

Figure C-270. SEM backscattered electron images of Particle 10F (E9, 74 cm).

Figure C-271. Photomacrograph of Particle 11B (E9, 94 cm).

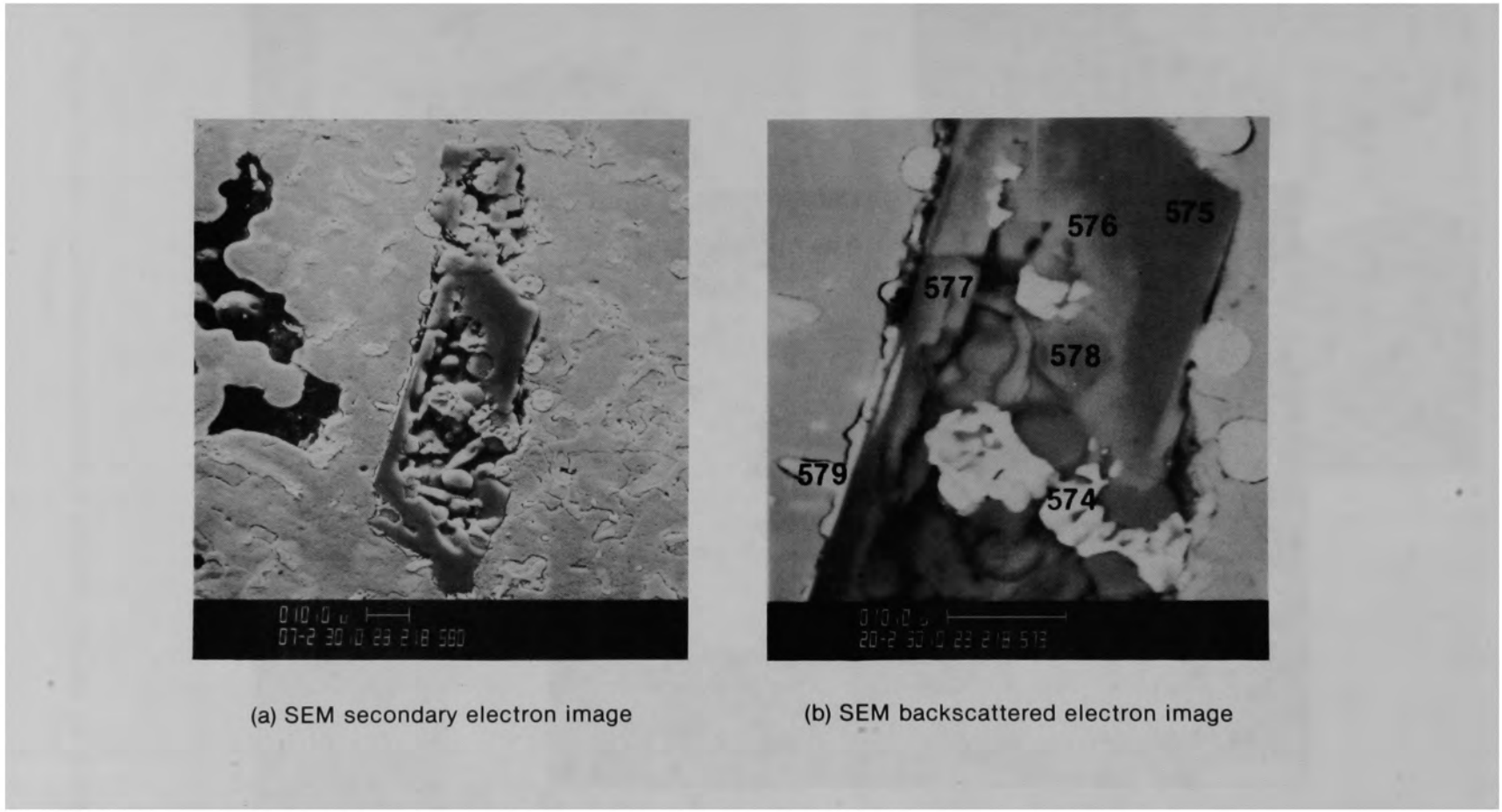

(a) SEM secondary electron image

(b) SEM backscattered electron image

Figure C-272. SEM electron images of material from location A of Particle 11B (E9, 94 cm).

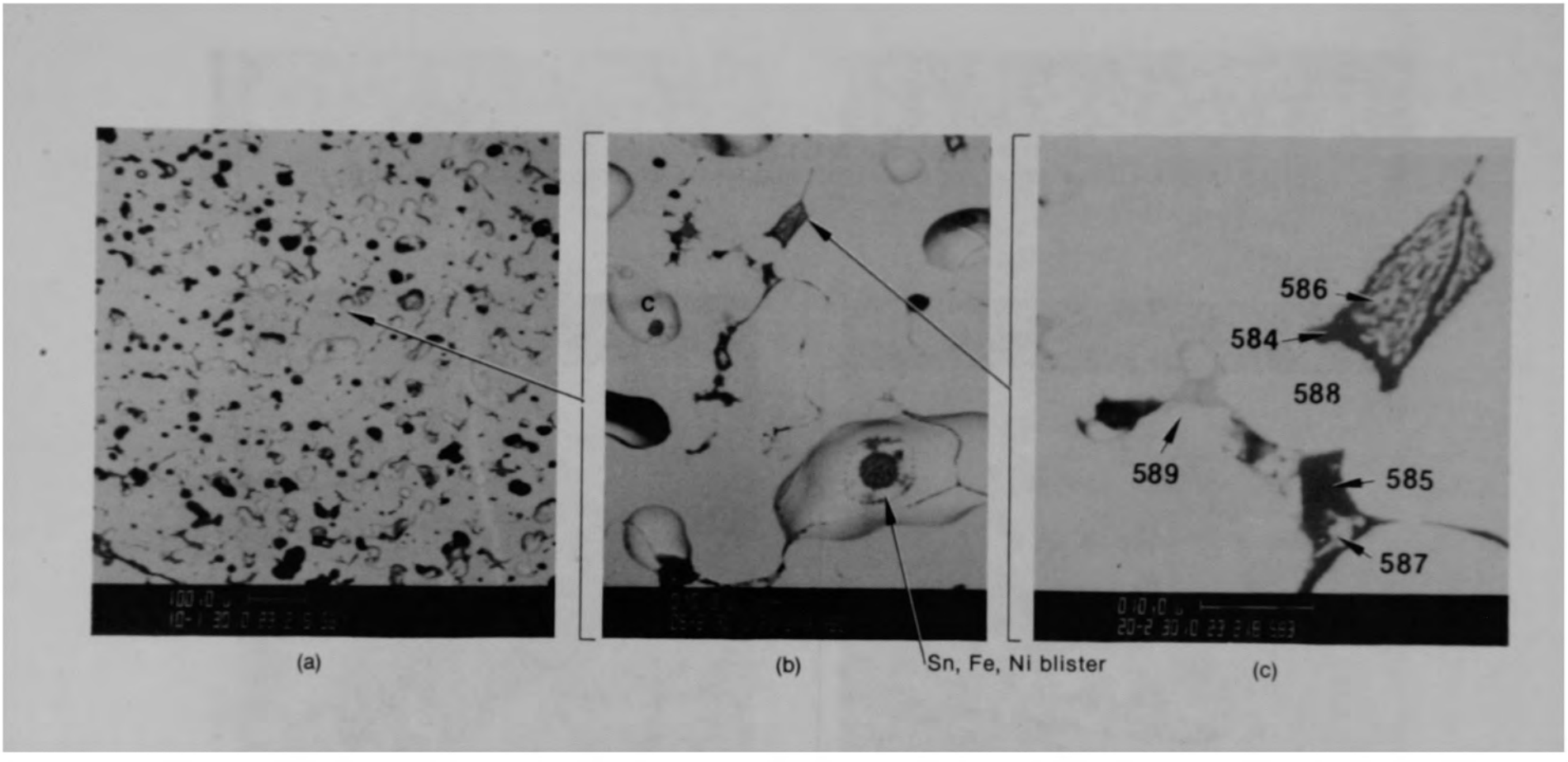

Figure C-273. SEM backscattered electron images of material from location B of Particle 11B (E9, 94 cm) showing inclusions in the ceramic material.

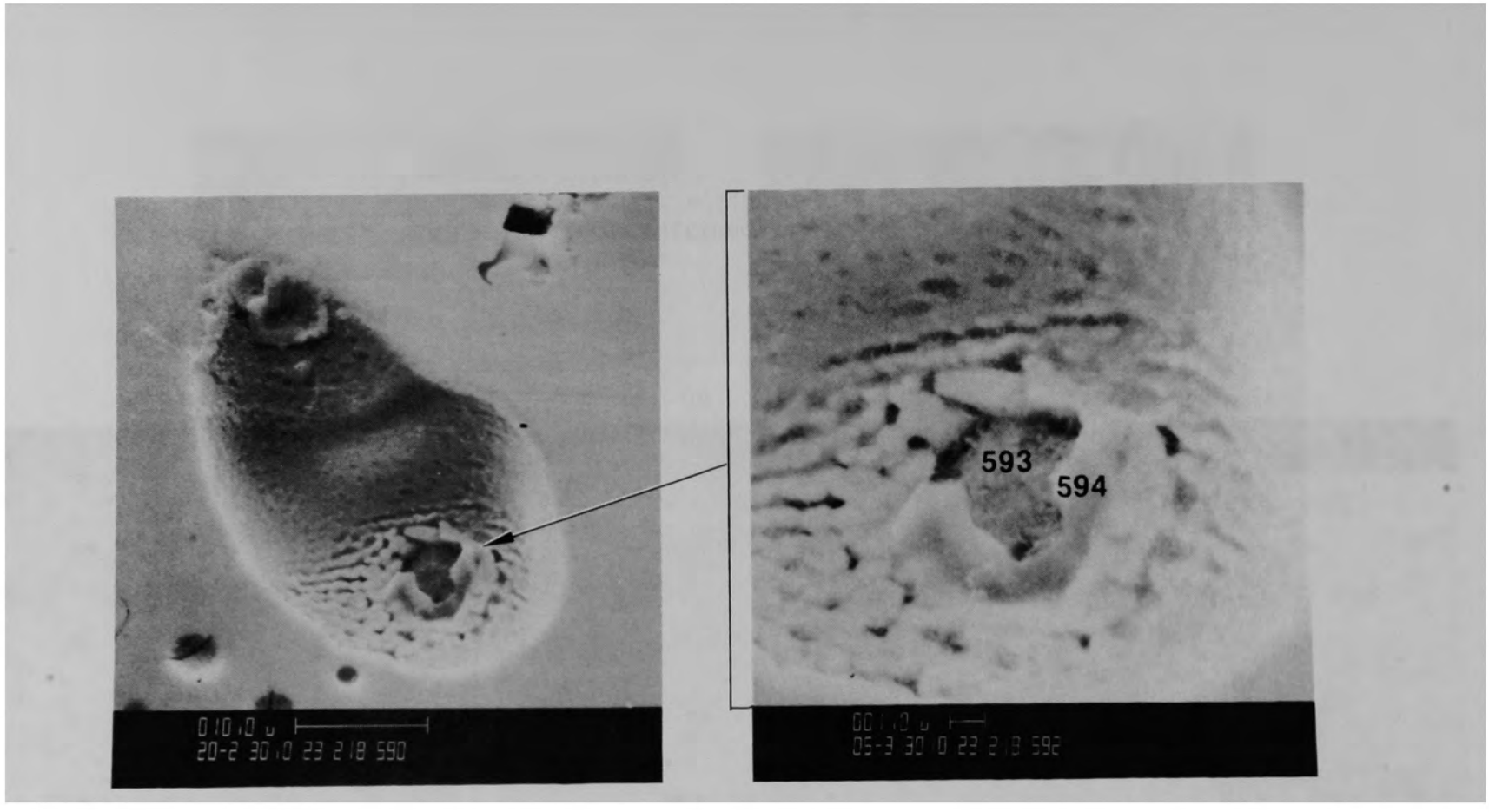

Figure C-274. SEM secondary electron images of material from location C, Figure C-273b, of Particle 11B (E9, 94 cm).

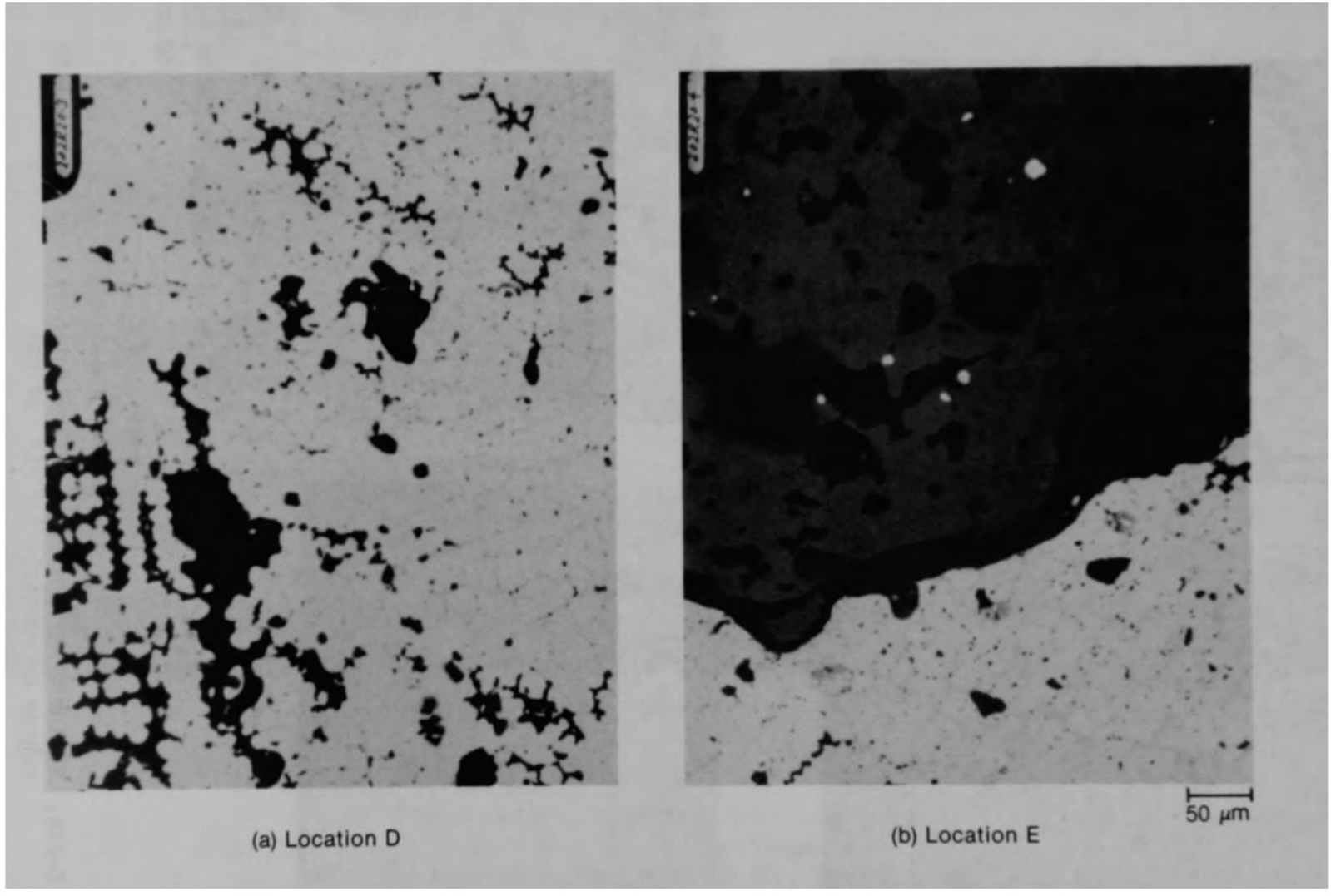

Figure C-2/5. Photomicrographs of material from metallic and interface regions of Particle 11B (E9, 94 cm).

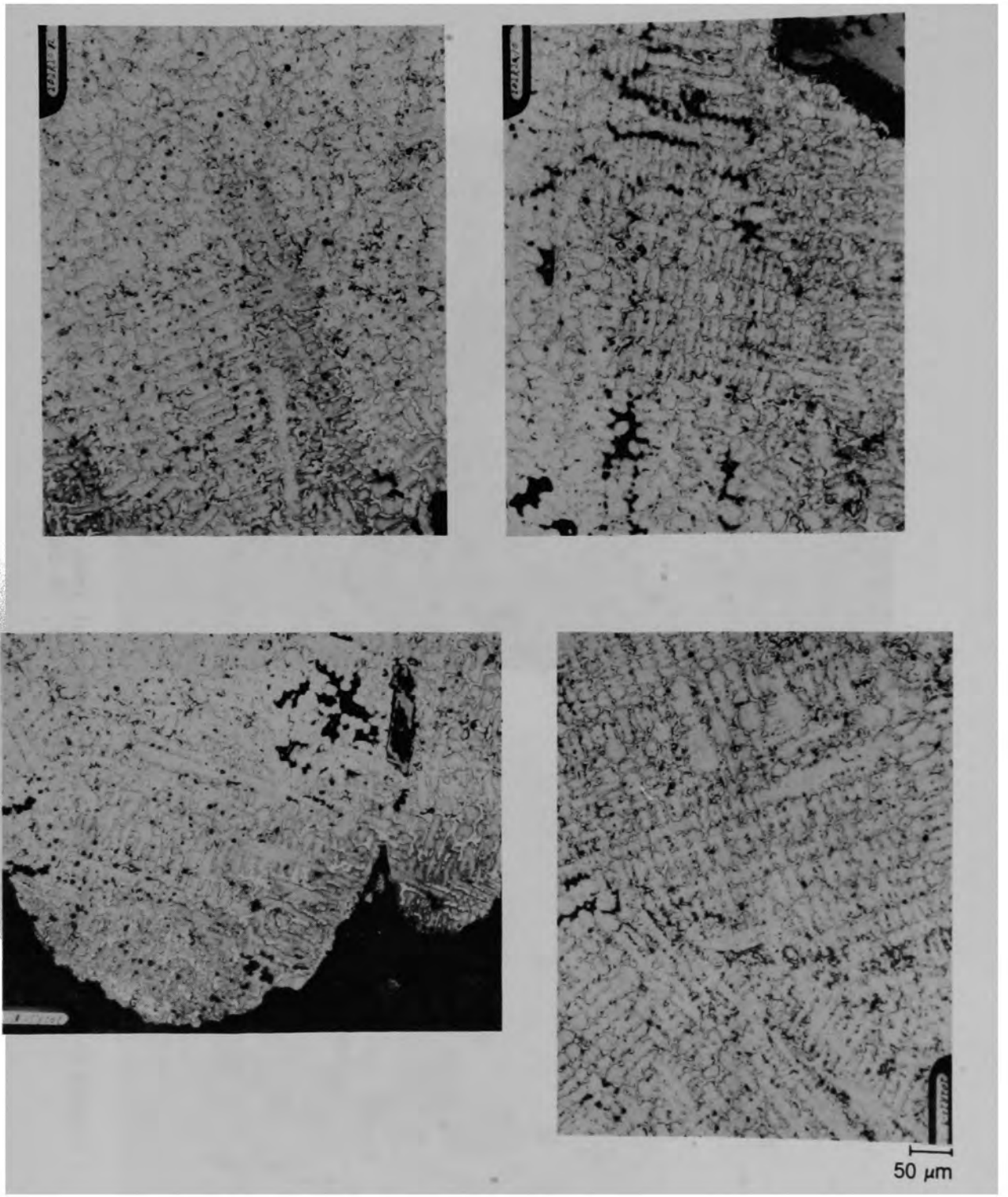

Figure C-276. Photomicrographs of Ag etched material from the metallic region of Particle 11B (E9, 94 cm).

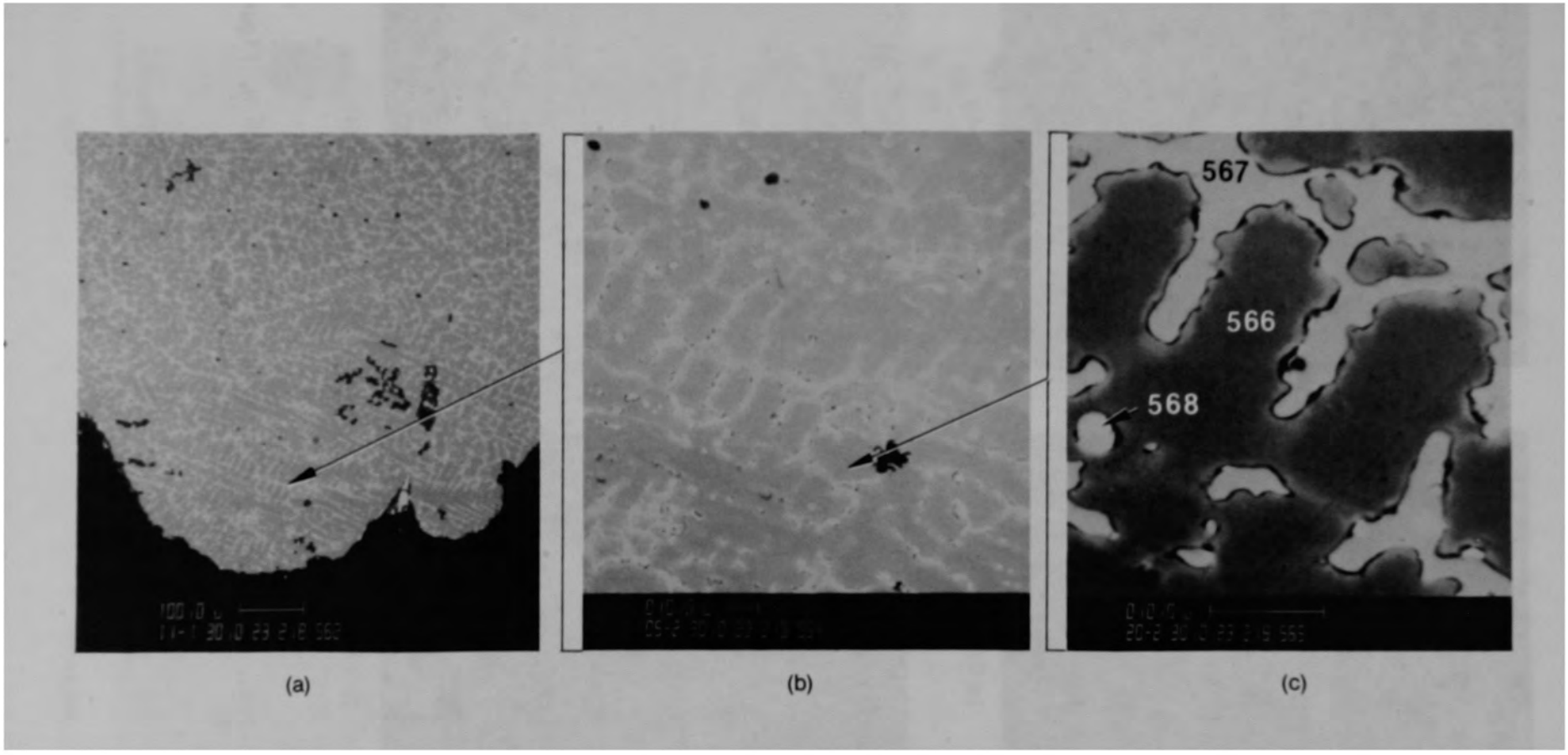

Figure C-277. SEM backscattered electron images of material from location H of Particle 11B (E9, 94 cm).

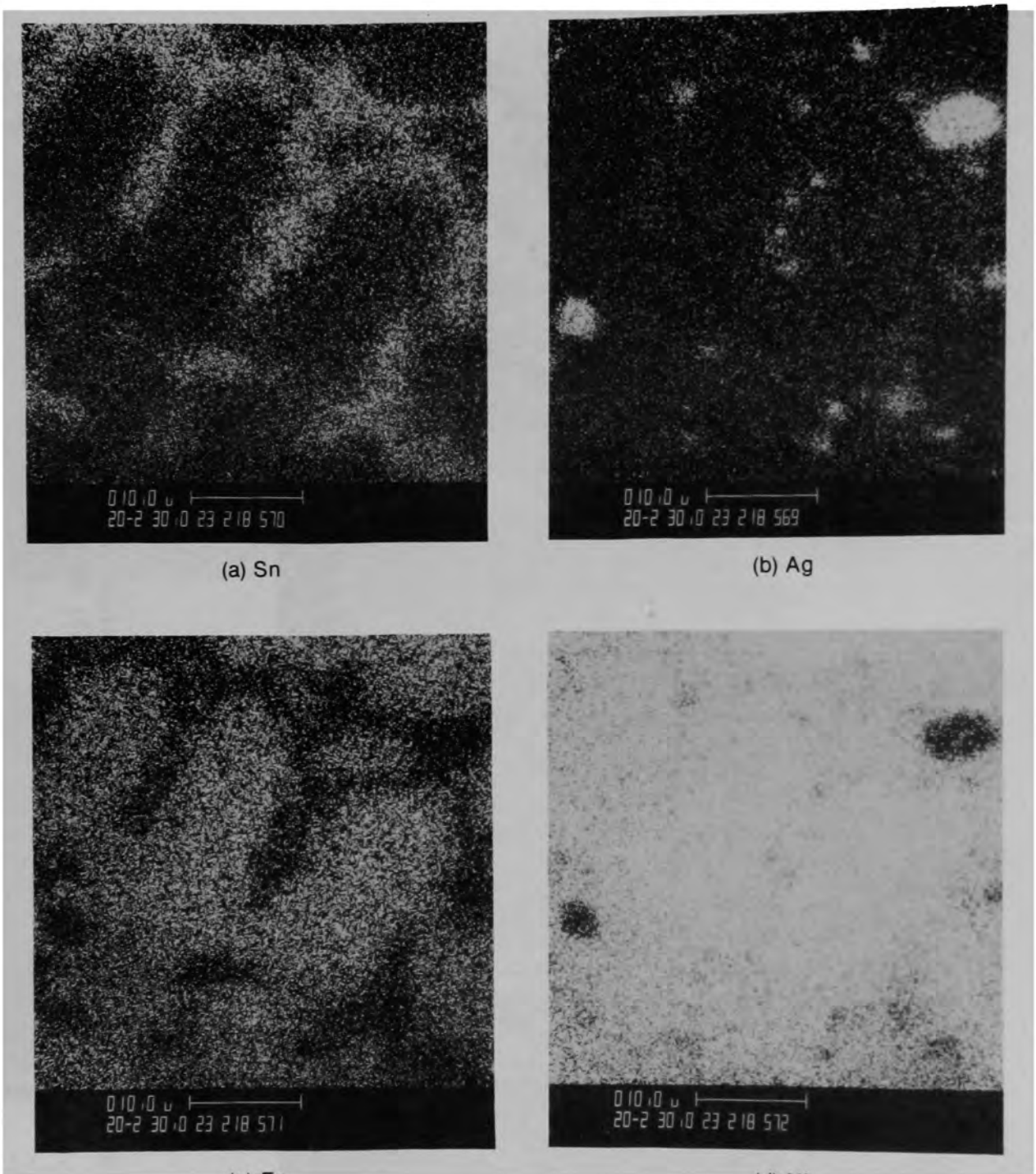

Figure C-278. X-ray dot maps of material from location H, Figure C-277c, of Particle 11B (E9, 94 cm).

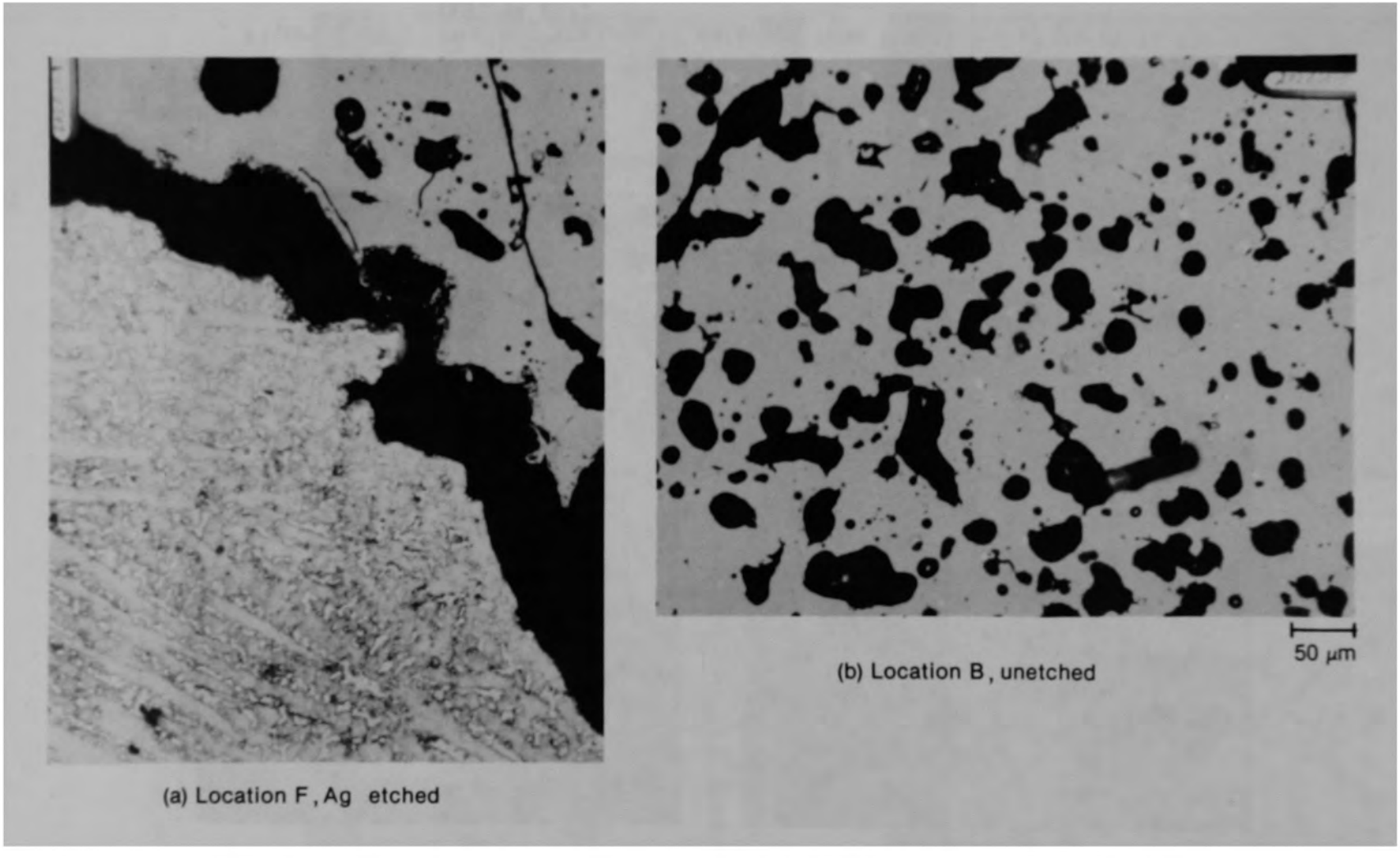

Figure C-279. Photomicrographs of material from the ceramic and interface regions of Particle 118 (E9, 94 cm).

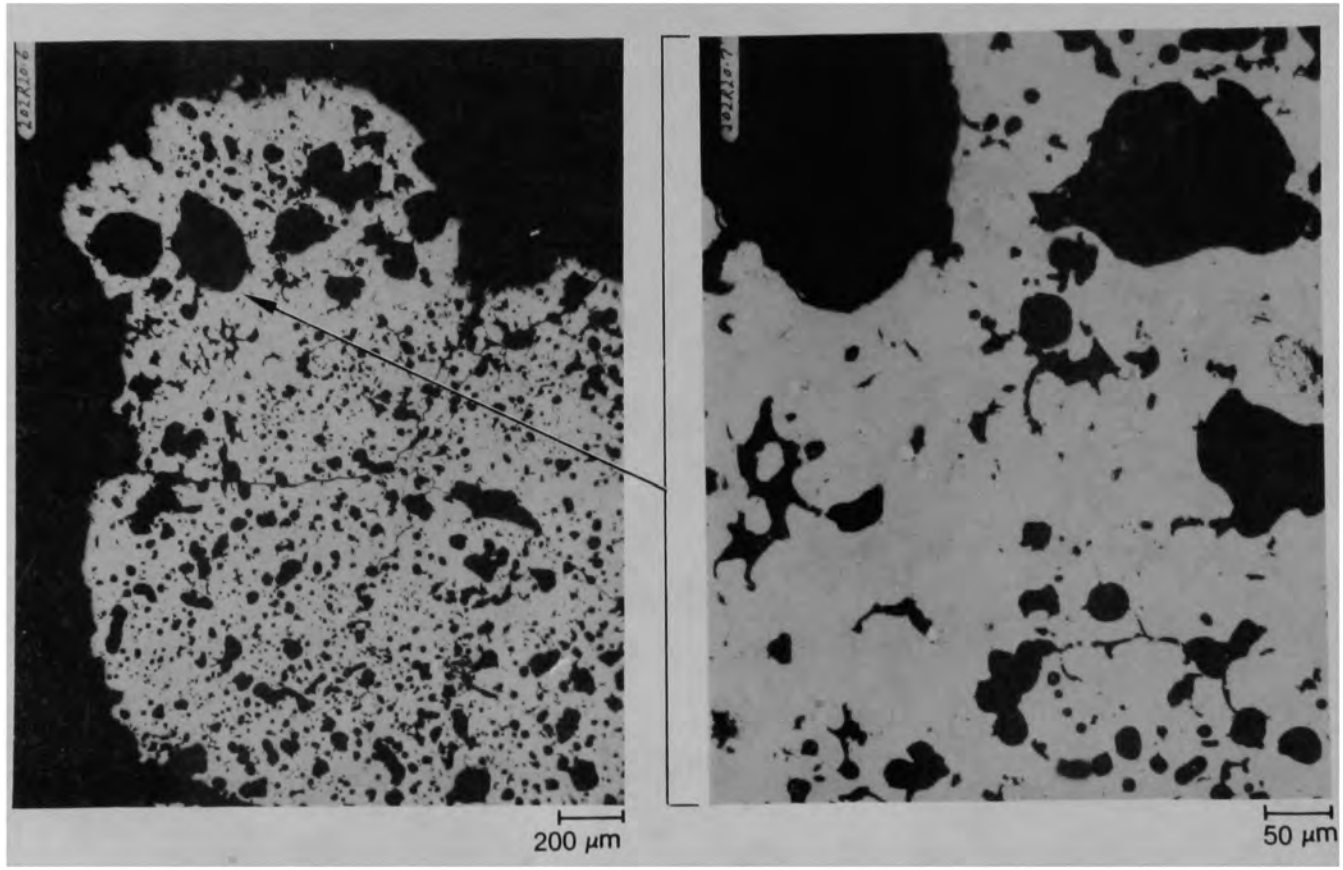

Figure C-280. Photomicrographs of material from location G of Particle 11B (E9, 94 cm).

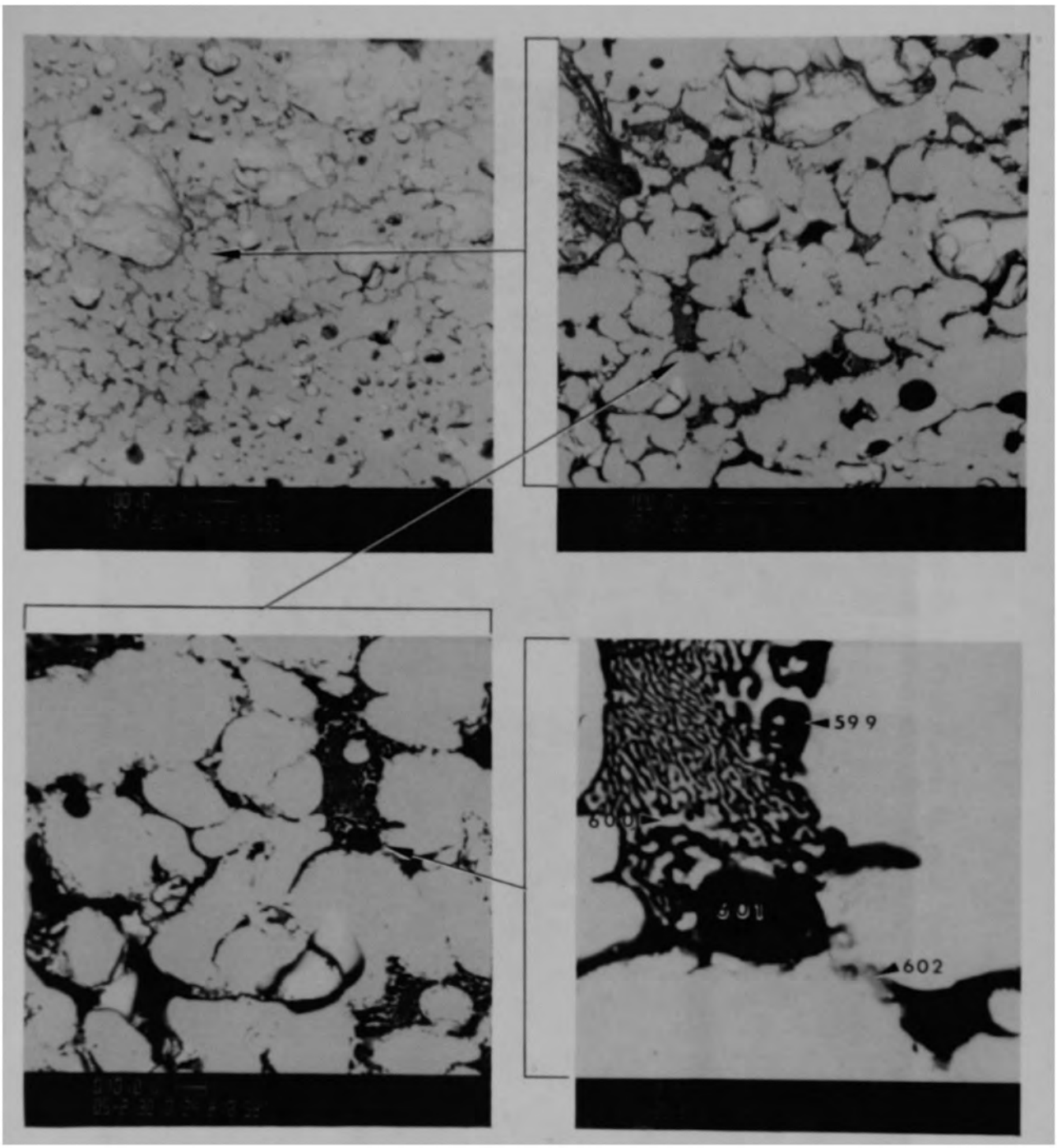

Figure C-281. SEM backscattered electron images of material from location G of Particle 11b (E9, 94 cm).

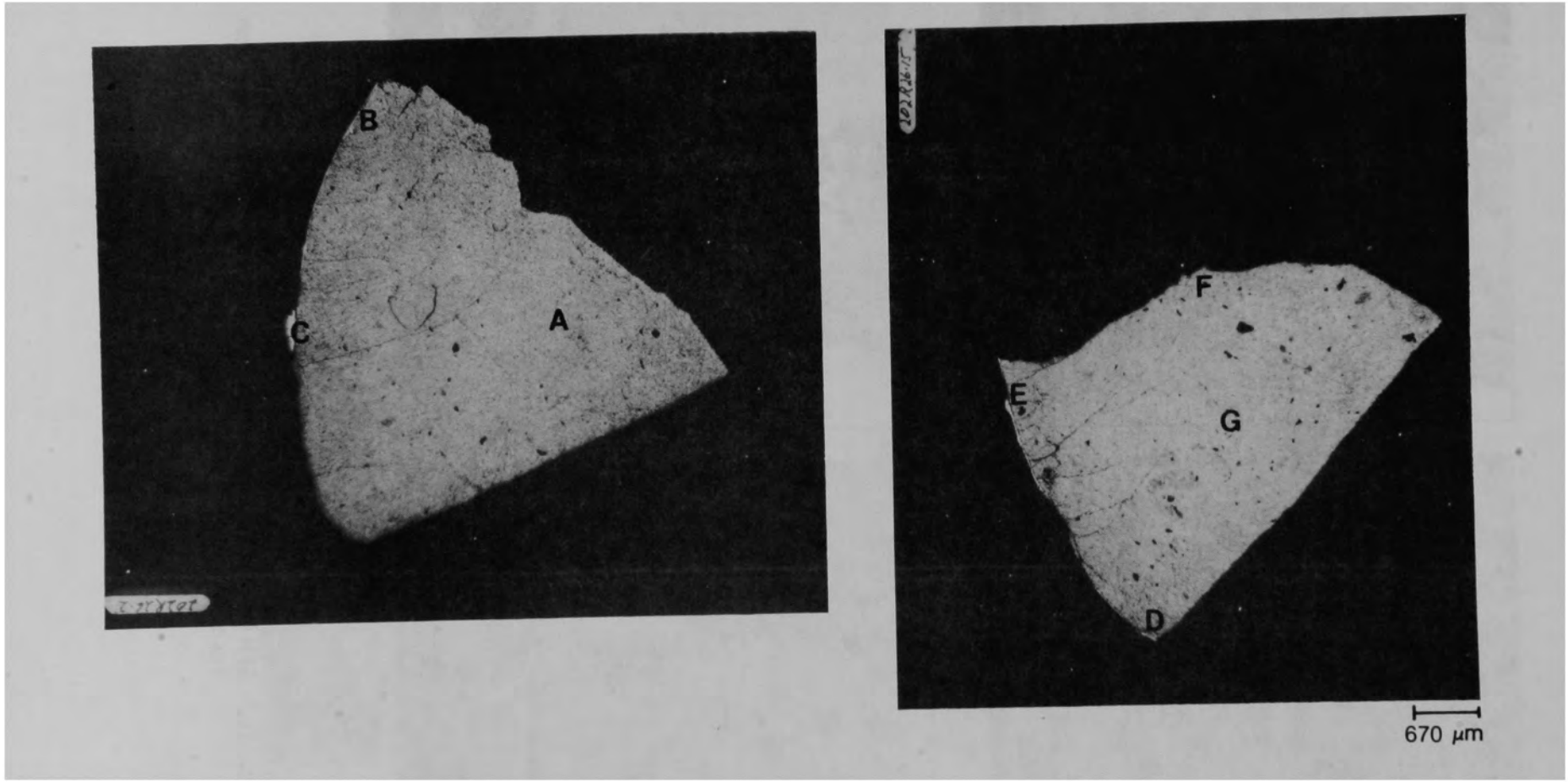

Figure C-282. Photomacrographs of Particle 11C (E9, 94 cm).

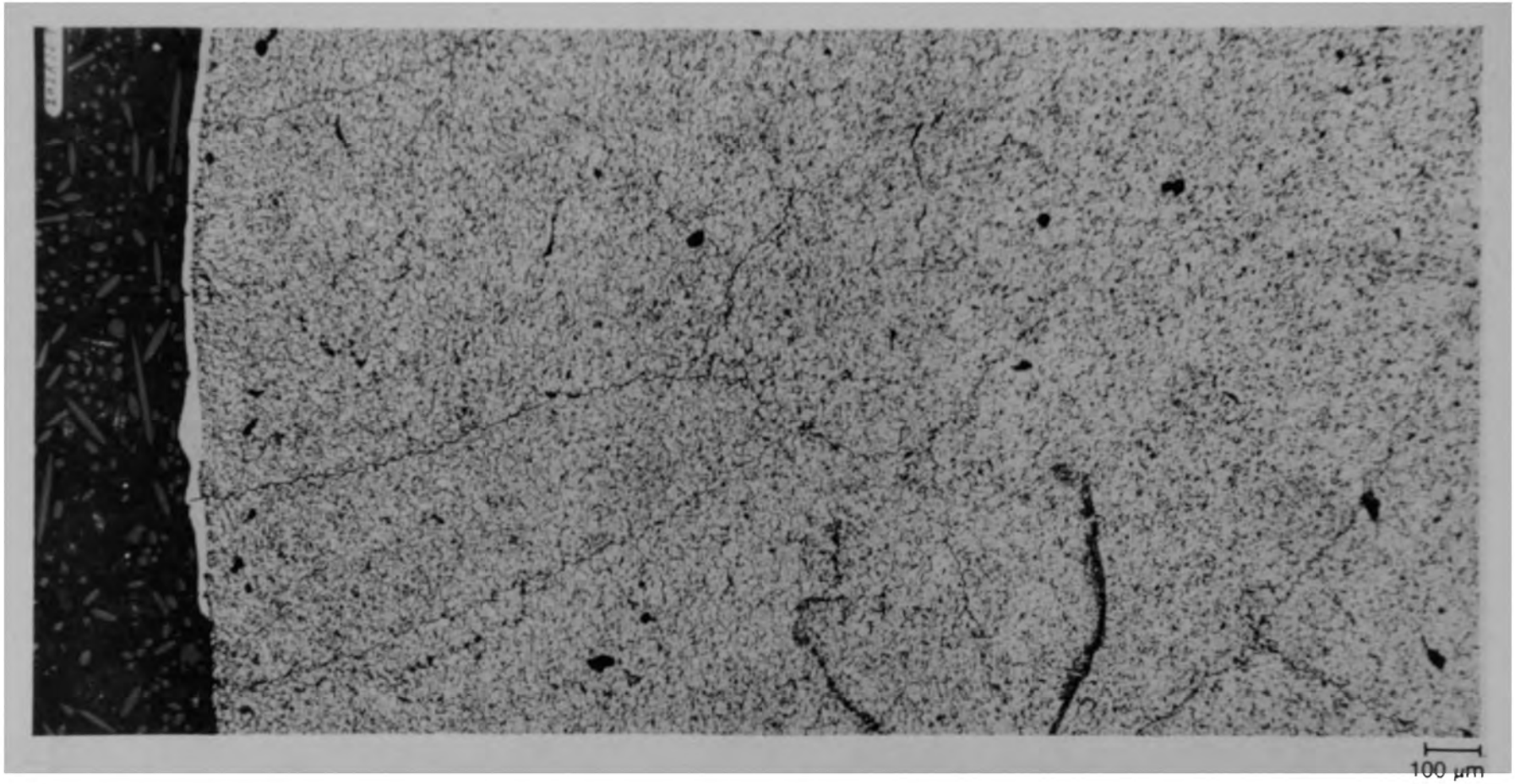

Figure C-283. Photomicrographs of a cross section of Particle 11C (E9, 94 cm) showing uniformity of grain size.

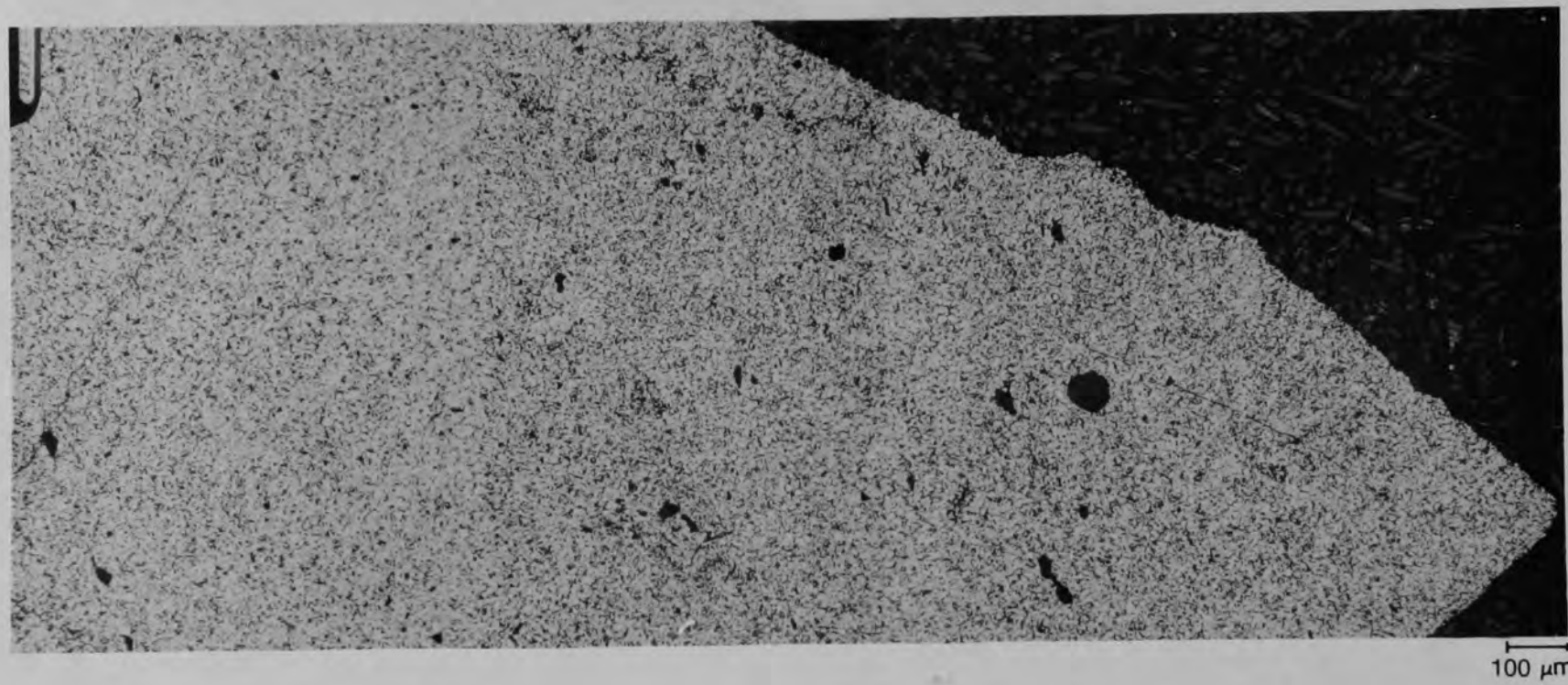

Figure C-284. Photomicrographs of a cross section of Particle 11C (E9, 94 cm) showing uniformity of grain size.

Figure C-285. Photomicrograph of material from location A of Particle 11C (E9, 94 cm) showing high porosity at grain boundaries.

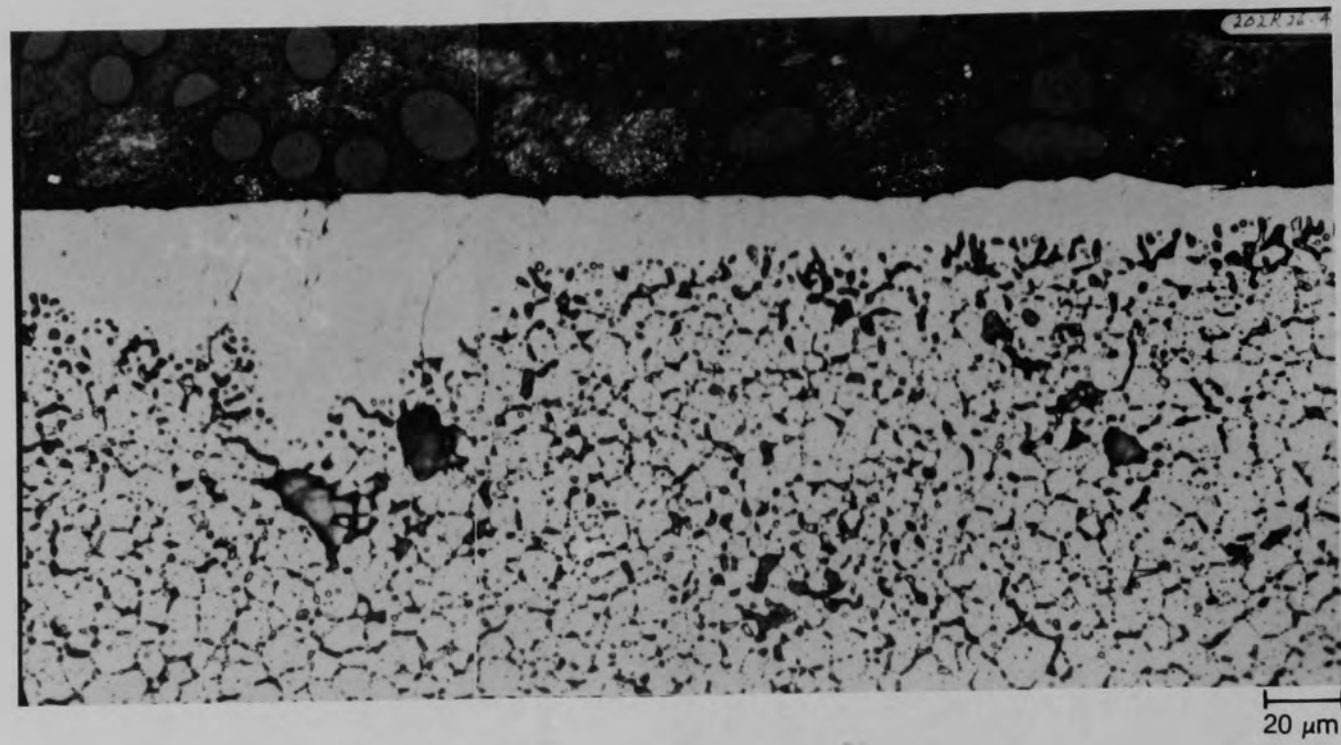

Figure C-286. Photomicrographs of material from location B of Particle 11C (E9, 94 cm).

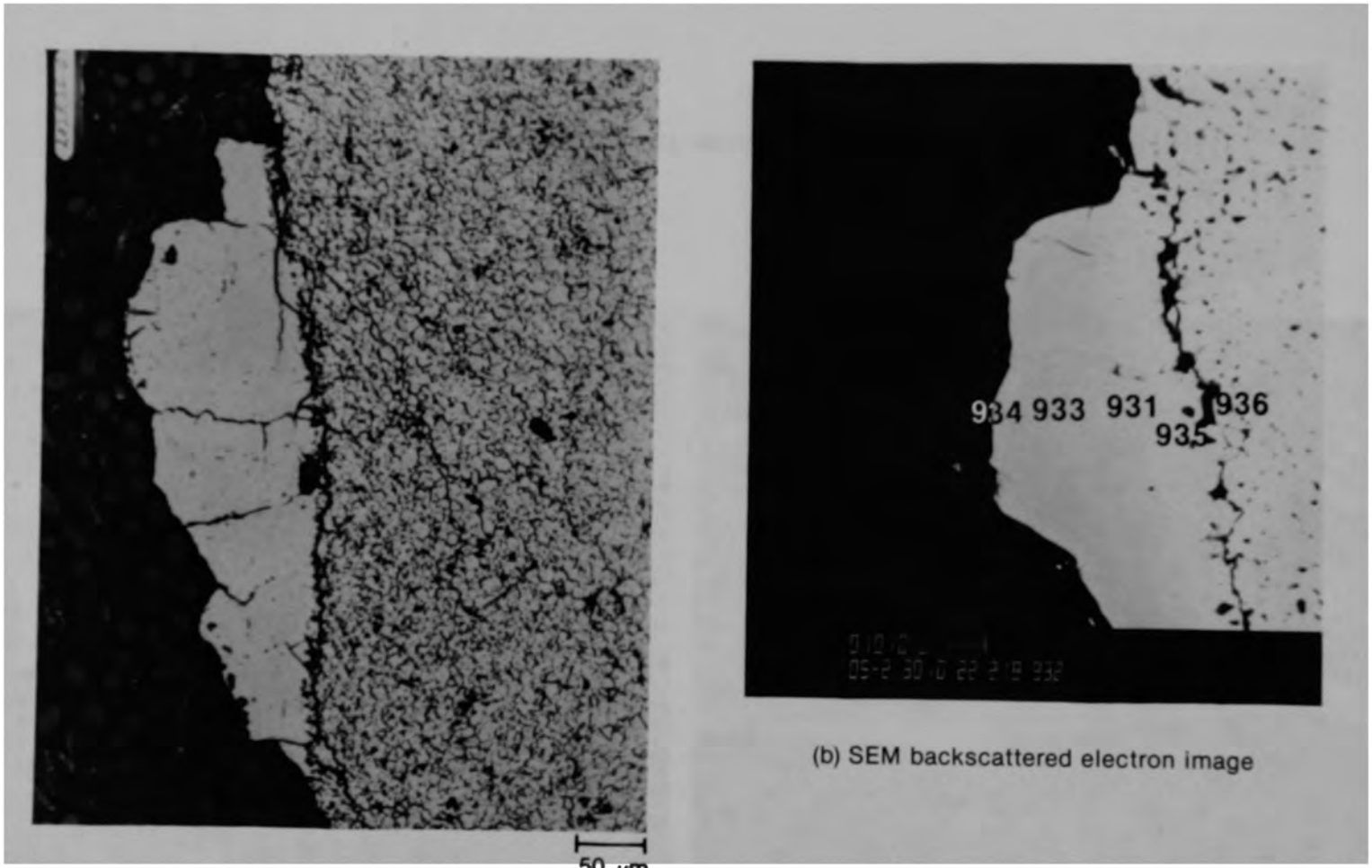

Figure C-287. Photographs of material from location C of Particle 11C (E9, 94 cm).

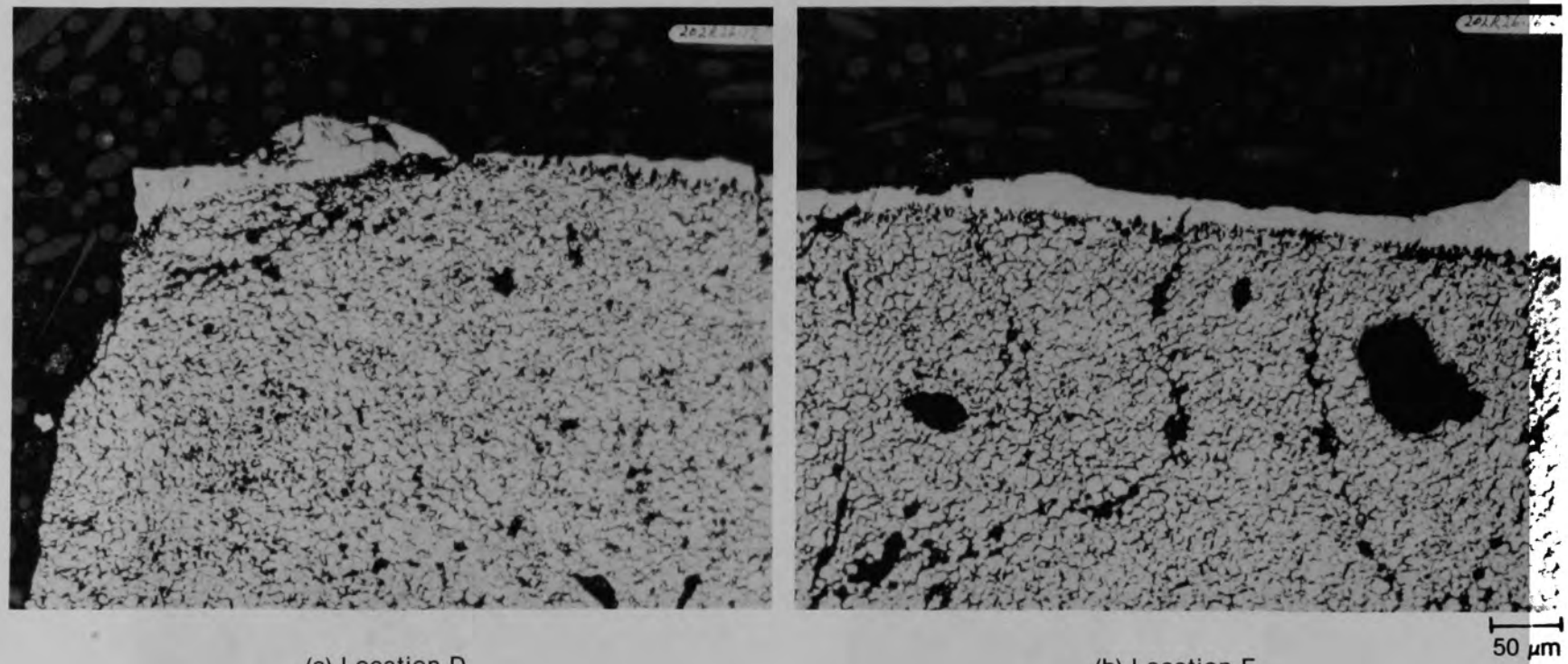

(a) Location D

(b) Location E

Figure C-288. Photomicrographs of material from edge of Particle 11C(E9, 94 cm).

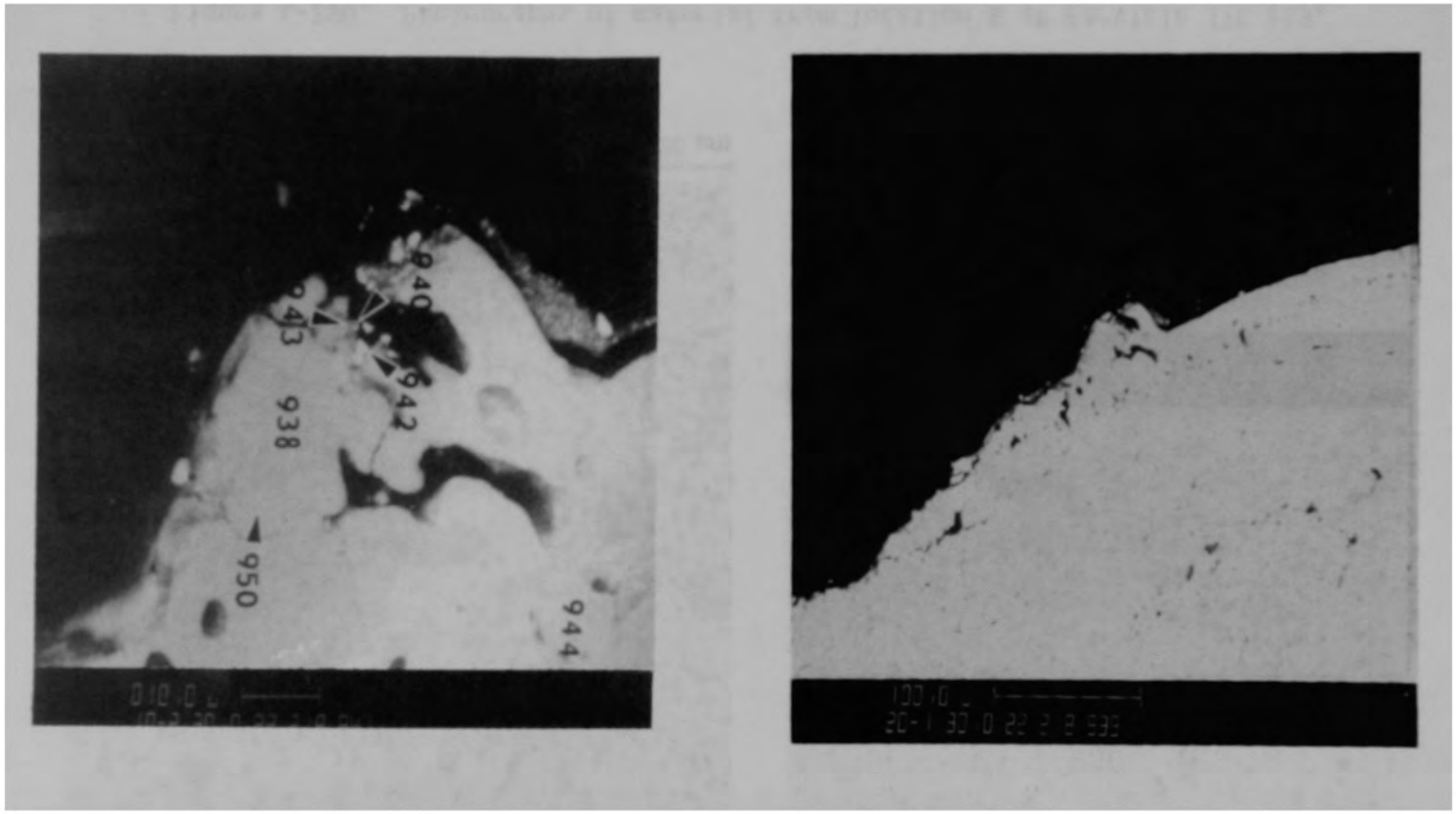

Figure C-289. SEM backscattered electron image of material from location F of Particle 11C (E9, 94 cm).

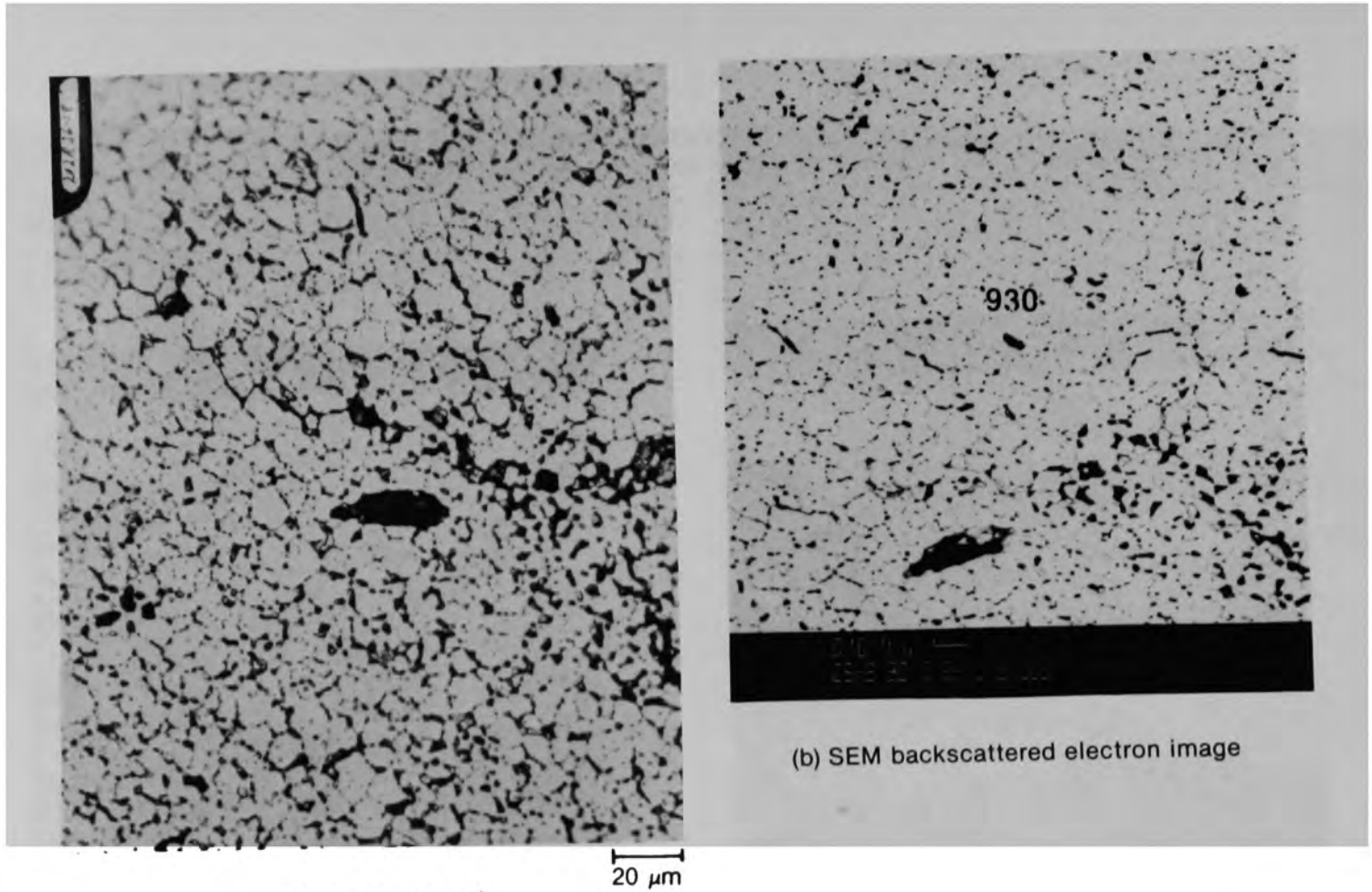

Figure C-290. Photographs of material from location G of Particle 11C (E9, 94 cm).

APPENDIX D

ELEMENTAL ANALYSIS

APPENDIX D
ELEMENTAL ANALYSIS

This Appendix contains results of the elemental analysis performed on the TMI-2 core debris grab samples, using inductively coupled plasma spectroscopy. The analysis was performed on the nonvolatile dissolved portions of the particles and aliquots. The results are given in mg element/g sample (Tables D-1 through D-10).

The uncertainties are large (~50%) for some analyses. The uncertainties were determined by comparing the results of the elemental analysis with those of the fissile/fertile material content analysis (Appendix E). The large uncertainties are caused by the small (<10 mg) sample portions and possible losses during the dissolution and analysis. Analysis of small portions was required because of high radiation levels associated with some samples.

TABLE D-1. RESULTS OF ELEMENTAL ANALYSIS OF SAMPLE 1
(mg element/g sample)

Element	Particle Size Fraction (μm) >4000 Particle 1A	>4000 Particle 1B	>4000[a] Particle 1C	>4000[a] Particle 1D	>4000 Particle 1E	1680-4000 Particle 1F	1680-4000 Particle 1G	1680-4000 Particle 1H
Ag	--[b]	<5.0 E-1	5.0 E-1	<8 E-1	2.3	1.1	1.1	3.3
Al	--[b]	4.0	4.0	1.2 E+1	4.0	3.0	7.5	<1.0
B	--[b]	<7.0 E-1	<6 E-1	<1.0	<4.0 E-1	<5.0 E-1	<8.0 E-1	<4.0 E-1
Ca	--[b]	3.0 E-1	<1.0 E-1	2.0 E-1	1.0 E-1	<1.0 E-1	<1.0 E-1	<8.0 E-2
Cr	--[b]	8.0 E-1	<4.0 E-1	3.0	4.7	5.0	4.4	2.6
Cu	--[b]	3.3 E-1	<3.0 E-1	1.0	4.0 E-1	5.0 E-1	8. E-1	<1.9 E-1
Fe	--[b]	4.0	1.0 E-1	4.4	7.5	5.0	1.95 E+1	3.3
Gd	--[b]	9.0 E-1	8.0 E-1	<1.0	<5.0 E-1	7.0 E-1	<1.0	5.0 E-1
In	--[b]	<4.0	<7.0	<6.0	<2.0	3.0	<5.0	7.2
Mn	--[b]	2.0 E-1	<1.0 E-1	2.0 E-1	2.0 E-1	3.3 E-1	5.2 E-1	1.1 E-1
Mo	--[b]	<1.0	<1.0	<2.0	<8.0 E-1	<1.0	<1.0	<8.0 E-1
Ni	--[b]	1.0	<6.0 E-1	<1.0	8.0 E-1	1.0	<8.0 E-1	4.1
Nb	--[b]	4.0	<4.0	<6.0	<2.0	<3.	5.0	<2.0
Si	--[b]	7.0	<9.0 E-1	7.8	5.5	4.1	2.3	3.9
Sn	--[b]	<7.0	<6.0	2.0 E+1	7.6	<5.0	<8.0	<4.0
Te	--[b]	5.0	<2.0	<4.0	3.0	4.0	<3.0	3.0
U	--[b]	8.31 E+2	9.78 E+1	2.64 E+2	1.78 E+2	5.70 E+2	5.73 E+2	4.72 E+2
Zr	--[b]	1.3 E+1	1.42 E+1	1.6 E+1	6.56 E+2	1.37 E+2	1.38 E+2	3.67 E+2

Element	1000-1680[a] Particle 1I	1000-1680 Particle 1J	1000-1680 Particle 1K	707-1000 Aliquot	297-707 Aliquot	149-297 Aliquot	74-149 Aliquot	30-74 Aliquot
Ag	1.5 E+1	8.0 E-1	9.0 E-1	6.0 E-1	9.0 E-1	1.5	1.3	1.8
Al	1.1	5.5	6.7	3.0	3.3	4.0	6.0	8.0
B	<2.0	<5.0 E-1	<6.0 E-1	<4.0 E-1	<4.0 E-1	<6.0 E-1	<1.0	<1.3
Ca	0.7	<1.0 E-1	<1.0 E-1	<1.0 E-1	4.6 E-1	4.7	3.7	4.8
Cr	6.4	7.3	3.4	6.8	5.3	8.3	6.9	1.10 E+1
Cu	1.8	<2.7 E-1	<3.3 E-1	4.0 E-1	4.0 E-1	<3.1 E-1	<4.8 E-1	<6.3 E-1
Fe	1.6 E+1	1.46 E+1	2.0	1.02 E+1	1.12 E+1	1.91 E+1	2.19 E+1	4.13 E+1
Gd	<2.0	<8.0 E-1	<9.0 E-1	<6.0 E-1	<5.0 E-1	<9.0 E-1	<1.3	<1.8
In	3.9 E+1	<3.0	<4.0	5.0	4.0	<4.0	<6.0	<7.0
Mn	1.6	4.9 E-1	3.5 E-1	3.6 E-1	3.9 E-1	5.5 E-1	5.2 E-1	1.00
Mo	<4.0	<1.0	<1.0	<1.0	<1.0	<1.0	<2.0	<3.0
Ni	5.4	1.8	1.0	4.01 E+1	3.3	7.1	8.8	9.8
Nb	<1.1 E+1	<3.0	<4.0	1.4	<2.0	<4.0	<6.0	<8.0
Si	1.0 E+1	5.4	7.2	3.5	4.6	7.6	9.0	3.33 E+1
Sn	6.4 E+1	<5.0	<7.0	8.6	7.0	<6.0	1.9 E+1	2.5 E+1
Te	<7.0	<2.0	<3.0	<2.0	<1.0	<2.0	8.0	<5.0
U	<6.1 E+1	6.40 E+2	5.66 E+2	5.19 E+2	5.32 E+2	4.54 E+2	4.11 E+2	3.65 E+2
Zr	3.85 E+2	1.46 E+2	1.31 E+2	1.01 E+2	1.68 E+2	3.30 E+2	3.23 E+2	3.40 E+2

a. Uncertainty is 30-50% because of problems associated with the analysis.

b. Not reported because of analysis problems.

TABLE D-2. RESULTS OF ELEMENTAL ANALYSIS OF SAMPLE 3
(mg element/g sample)

Element	Particle Size Fraction (μm) >4000[a] Particle 3A	>4000[a] Particle 3B	>4000 Particle 3C	>4000[a] Particle 3D	>4000 Particle 3E	1680-4000[a] Particle 3F	1680-4000 Particle 3G	1680-4000 Particle 3H
Ag	4.1 E-1	2.7	--[b]	2.0 E-1	8.1 E-1	<7.0 E-1	<8.0 E-1	<6.0 E-1
Al	<4.0 E-1	6.0	--[b]	<5.0 E-1	<5.0 E-1	<4.0	6.0	5.0
B	<9.0 E-2	<1.0	--[b]	<1.0 E-1	<1.0 E-1	<9.0 E-1	<1.0	<8.0 E-1
Co	<2.0 E-2	<2.0 E-1	--[b]	<5.0 E-2	<2.0 E-2	<2.0 E-1	<2.0 E-1	3.0 E-1
Cr	4.0 E-1	4.4	--[b]	<7.0 E-2	2.0 E-1	<6.0 E-1	4.0	4.5
Cu	9.0 E-2	<5.2 E-1	--[b]	<6.1 E-2	<6.1 E-2	<5.0 E-1	2.3	<3.9 E-1
Fe	2.7 E-1	5.5	--[b]	<5.0 E-2	<5.0 E-2	7.0 E-1	8.0	9.3
Ga	2.7 E-1	<2.0	--[b]	5.4 E-1	6.8 E-1	<1.0	<1.0	<1.0
In	1.0	<6.0	--[b]	1.0	<7.0 E-1	<6.0	<6.0	<5.0
Mn	3.7 E-2	<1.0 E-1	--[b]	5.9 E-2	1.1 E-1	2.0 E-1	2.0 E-1	<2.0 E-1
Mo	5.3 E-1	<2.0	--[b]	6.6 E-1	1.0	<2.0	<2.0	<2.0
Ni	<9.0 E-2	<1.0	--[b]	<1.0 E-1	2.0 E-1	<9.3 E-2	2.0	<8.0 E-1
Nb	<6.0 E-1	<6.0	--[b]	8.8 E-1	1.3	<6.0	<6.0	<5.0
Si	1.1	3.17 E+1	--[b]	3.8 E-1	8.1 E-1	1.0 E+1	6.0	2.4
Sn	2.0	<1.0 E+1	--[b]	<1.0 E-1	2.4	<9.0	<1.0 E+1	1.6 E+1
Te	<4.0 E-1	8.0	--[b]	5.0 E-1	<5.0 E-1	<4.0	<4.0	<3.0
U	3.82 E+1	<3.6 E+1	--[b]	4.82 E+2	7.24 E+2	1.00 E+3	2.76 E+2	4.46 E+2
Zr	2.31 E+1	7.10 E+2	--[b]	9.52	2.28 E+1	5.06 E+1	3.80 E+1	1.0 E+2

Element	1000-1680 Particle 3I	1000-1680[a] Particle 3J	1000-1680[a] Particle 3K	707-1000 Aliquot	297-707 Aliquot	149-297 Aliquot	74-149[a] Aliquot	30-74[a] Aliquot	<30 Aliquot
Ag	<6.0 E-1	1.0	8.2 E-1	1.4	1.7	1.8	6.0	2.2	--[b]
Al	2.0	2.0	1.8	2.0	<2.0	2.3	4.2	1.4 E+1	--[b]
B	<4.0 E-1	<3.0 E-1	<2.0 E-1	4.0 E-1	<6.0 E-1	<1.0 E-1	<0.7	<8.0 E-1	--[b]
Co	<2.0 E-1	<1.0 E-2	<7.0 E-2	1.0 E-1	2.0 E-1	1.0	1.9	3.0	--[b]
Cr	4.6	<2.0 E-1	3.83	9.98	5.7	7.4	7.4	8.0	--[b]
Cu	<2.0 E-1	<1.5 E-1	2.0 E-1	<1.9 E-1	2.8 E-1	2.0 E-1	<3.5 E-1	8.0 E-1	--[b]
Fe	6.7	1.5	4.76	1.26 E+1	1.26 E+1	1.89 E+1	1.7 E+1	2.3 E+1	--[b]
Ga	<6.0 E-1	<4.0 E-1	5.2 E-1	<5.0 E-1	<8.0 E-1	3.9 E-1	<1.0	<1.0	--[b]
In	<2.0	<2.0	<1.0	5.0	7.0	3.42	<4.2	1.0 E+1	--[b]
Mn	2.8 E-1	<3.0 E-2	2.0 E-1	4.8 E-1	3.7 E-1	4.06 E-1	4.7 E-1	4.3 E-1	--[b]
Mo	<8.0 E-1	<6.0 E-1	1.0	<8.0 E-1	<1.0	<3.0 E-1	<1.4	1.7	--[b]
Ni	8.0 E-1	6.0 E-1	4.0 E-1	1.80 E+1	2.0	7.76	7.8	8.0	--[b]
Nb	<2.0	<2.0	<1.0	<2.0	<3.0	<8.0 E-1	<4.2	<5.0	--[b]
Si	3.0	5.8	3.0	2.7	5.4	3.9 E-1	2.1	1.6 E+1	--[b]
Sn	<4.0	5.9	3.7	<4.0	<6.0	4.03	<6.9	<8.0	--[b]
Te	<2.0	<1.0	<7.0 E-1	<1.0	<2.0	<6.0 E-1	<2.8	7.0	--[b]
U	5.59 E+1	1.12 E+2	4.80 E+1	5.79 E+2	4.17 E+2	3.72 E+2	3.54 E+2	3.17 E+2	--[b]
Zr	8.56 E+1	2.69 E+2	9.23 E+1	1.95 E+2	8.14 E+1	1.75 E+1	3.2 E+2	3.55 E+2	--[b]

a. Uncertainty is 30-50% because of problems associated with the analysis.

b. Not reported because of analysis problems.

TABLE D-3. RESULTS OF ELEMENTAL ANALYSIS OF SAMPLE 4
(mg element/g sample)

Element	Particle Size Fraction (μm) >4000 Particle 4A	>4000[a] Particle 4B	>4000 Particle 4C	>4000[a] Particle 4D	>4000 Particle 4E
Ag	1.4	<0.7	4.6 E-1	--[b]	1.2
Al	5.1	5.6	2.0	--[b]	5.0
B	<0.6	<0.9	<3.0 E-1	--[b]	<8.3 E-1
Cd	<0.1	3.7 E-1	<7.0 E-2	--[b]	3.3 E-1
Cr	5.1	2.4	3.8	--[b]	2.2
Cu	1.6	<4.6 E-1	<1.6 E-1	--[b]	<4.2 E-1
Fe	1.3 E+1	1.5	3.0	--[b]	3.0
Gd	<0.8	<1.3	9.2 E-1	--[b]	<1.0
In	<3.0	1.1 E+1	<2.0	--[b]	<5.0
Mn	1.8 E-1	9.0 E-2	7.0 E-2	--[b]	<8.0 E-2
Mo	<1.0	<1.9	<7.0 E-1	--[b]	<1.7
Ni	5.9	1.9	2.1	--[b]	<8.3 E-1
Nb	<3.0	<6.0	<2.0	--[b]	<5.0
Si	4.0	26.0 E+1	7.70	--[b]	1.0 E+1
Sn	1.1 E+1	<9.3	<3.3	--[b]	<8.0
Te	4.6	<3.7	2.6	--[b]	6.7
U	9.38 E+2	5.83 E+2	5.14 E+2	--[b]	8.83 E+2
Zr	1.34 E+2	1.8 E+1	1.23 E+1	--[b]	2.62 E+1

a. Uncertainty is 30-50% because of problems associated with the analysis.

b. Not reported because of analysis problems.

TABLE D-4. RESULTS OF ELEMENTAL ANALYSIS OF SAMPLE 5
(mg element/g sample)

Element	Particle Size Fraction (μm)					
	>4000[a] Particle 5A	>4000 Particle 5B	>4000 Particle 5C	>4000[a] Particle 5D	>4000 Particle 5E	1680-4000 Particle 5F
Ag	1.0	6.7 E-1	5.0 E-1	9.2 E-1	--[b]	--[b]
Al	5.0	2.9	2.0	4.0	--[b]	--[b]
B	<8.0 E-1	<0.5	1.1	[illegible]	--[b]	--[b]
Cd	<2.0 E-1	1.9 E-1	<7.0 E-2	<1.0 E-1	--[b]	--[b]
Cr	2.4	1.1	1.3	2.1	--[b]	--[b]
Cu	<4.1 E-1	<0.2	4.0 E-1	<3.3 E-1	--[b]	--[b]
Fe	1.0	1.3	1.1	5.3 E-1	--[b]	--[b]
Gd	<1.0	<7.0 E-1	<5.0 E-1	<9.2 E-1	--[b]	--[b]
In	1.0 E+1	<3.0	4.0	7.9	--[b]	--[b]
Mn	<8.2 E-1	<1.0 E-1	7.0 E-2	<7.0 E-2	--[b]	--[b]
Mo	<2.0	2.7	<7.0 E-1	<1.3	--[b]	--[b]
Ni	2.0	2.8	7.0 E-1	<6.6 E-1	--[b]	--[b]
Nb	<5.0	<3.0	<2.0	<4.0	--[b]	--[b]
Si	2.05 E+1	1.55 E+1	3.0	2.0	--[b]	--[b]
Sn	<8.0	<5.0	7.1	1.3 E+1	--[b]	--[b]
Te	<3.0	<2.0	3.0	<2.6	--[b]	--[b]
U	6.2 E+2	8.52 E+2	5.74 E+2	8.96 E+2	--[b]	--[b]
Zr	8.56 E+1	4.14 E+1	3.9 E+1	4.1	--[b]	--[b]

Element	1680-4000 Particle 5G	1680-4000 Particle 5H	1000-1680[a] Particle 5I	1000-1680 Particle 5J	1000-1680 Particle 5K	<1000[a] Aliquot
Ag	--[b]	--[b]	2.4 E-1	--[b]	--[b]	2.0
Al	--[b]	--[b]	7.1 E-1	--[b]	--[b]	2.0
B	--[b]	--[b]	<1.0 E-1	--[b]	--[b]	<4.0 E-1
Cd	--[b]	--[b]	<2.0 E-2	--[b]	--[b]	1.0 E-1
Cr	--[b]	--[b]	5.2 E-1	--[b]	--[b]	8.0 E-1
Cu	--[b]	--[b]	1.0 E-1	--[b]	--[b]	<1.9 E-1
Fe	--[b]	--[b]	1.1	--[b]	--[b]	3.74
Gd	--[b]	--[b]	<2.0 E-1	--[b]	--[b]	<5.0 E-1
In	--[b]	--[b]	<7.0 E-1	--[b]	--[b]	<2.0
Mn	--[b]	--[b]	2.0 E-2	--[b]	--[b]	<3.9 E-2
Mo	--[b]	--[b]	<2.0 E-1	--[b]	--[b]	<8.0 E-1
Ni	--[b]	--[b]	3.6 E-1	--[b]	--[b]	1.03 E+1
Nb	--[b]	--[b]	7.0 E-1	--[b]	--[b]	<2.0
Si	--[b]	--[b]	2.0	--[b]	--[b]	9.75
Sn	--[b]	--[b]	2.4	--[b]	--[b]	7.7 E-1
Te	--[b]	--[b]	9.0 E-1	--[b]	--[b]	<1.0
U	--[b]	--[b]	1.72 E+2	--[b]	--[b]	3.13 E+2
Zr	--[b]	--[b]	8.40 E+1	--[b]	--[b]	2.87 E+1

a. Uncertainty is 30-50% because of problems associated with the analysis.

b. Not reported because of analysis problems.

TABLE D-5. RESULTS OF ELEMENTAL ANALYSIS OF SAMPLE 6
(mg element/g sample)

Element	>4000[a] Particle 6A	>4000 Particle 6B	>4000 Particle 6C	>4000 Particle 6D	>4000[a] Particle 6E	1680-4000 Particle 6F	1680-4000 Particle 6G	1680-4000[a] Particle 6H
	Particle Size Fraction (μm)							
Ag	1.0	1.2	2.6	8.0 E-1	5.1	2.1	8.1 E-1	6.4 E-1
Al	<4.0	1.0	2.83 E+1	3.0	3.0	3.0	<7.0 E-1	<6.0 E-1
B	<9.0 E-1	<2.0 E-1	<2.0 E-1	<6.0 E-1	<6.0 E-1	<4.0 E-1	<2.0 E-1	<1.0 E-1
Cd	<4.0 E-1	1.0 E-1	<5.0 E-2	2.0 E-1	4.0 E-1	3.3 E-1	7.0 E-2	<3.0 E-2
Cr	<5.0 E-1	<1.0 E-1	<1.0 E-1	<3.0 E-1	<4.0 E-1	8.07 E+1	6.3 E-1	<9.0 E-2
Cu	<4.6 E-1	<9.1 E-2	<1.2 E-1	<2.8 E-1	<3.0 E-1	2.2 E-1	<8.72 E-2	<7.3 E-2
Fe	2.7	1.4	1.0	<2.0 E-1	1.4	3.14 E+2	<7.0 E-2	<6.0 E-2
Ga	2.6	<3.0 E-1	<3.0 E-1	<8.0 E-1	8.0 E-1	<6.0 E-1	8.7 E-1	6.1 E-1
In	<5.0	<1.0	<1.0	7.0	<3.0	<3.0	2.0	<9.0 E-1
Mn	2.0 E-1	<1.8 E-1	<2.5 E-1	<6.0 E-2	<5.8 E-2	6.3	1.2 E-1	6.7 E-2
Mo	<2.0	<4.0 E-1	<5.0 E-1	<1.0	<1.0	<8.7 E-1	9.4 E-1	<3.0 E-1
Ni	3.3	<2.0 E-1	<2.0 E-1	<6.0 E-1	<6.0 E-1	4.31 E+1	<2.0 E-1	<1.0 E-1
Nb	<5.0	<1.0	<1.0	<3.0	<3.0	<3.0	1.9	<1.5
Si	2.7	<4.0	7.20	1.12 E+1	5.6 E-1	3.0	5.2 E-1	1.0
Sn	<9.0	1.72 E+1	5.0	<6.0	2.59 E+1	8.7	<2.0	<1.0
Te	<4.0	<7.4 E+1	<1.0	<2.0	<2.0	<2.0	<7.0 E-1	<6.0 E-1
U	1.02 E+3	<6.2	<5.9 E+1	8.14 E+1	<2.0 E+1	<1.5 E+1	8.96 E+2	7.06 E+2
Zr	2.49 E+1	3.40 E+2	7.63 E+2	8.1	1.45 E+3	6.00 E+2	4.92	3.70

Element	1000-1680[a] Particle 6I	1000-1680 Particle 6J	1000-1680 Particle 6K	707-1000 Aliquot	297-707[a] Aliquot	149-297[a] Aliquot	74-149[a] Aliquot	30-74[a] Aliquot
Ag	1.4	1.8	2.0	2.82	1.02 E+1	3.7 E-1	2.36 E+1	2.68 E+1
Al	5.0	1.0	3.0	1.3	3.55	3.54 E-1	1.9	1.54 E+1
B	<3.0 E-1	1.0	5.0 E-1	<1.0 E-1	<1.0 E-1	1.0 E-1	3.0 E-1	6.0 E-1
Cd	2.9	<3.0 E-2	1.0 E-1	1.0 E-1	3.3 E-1	1.2	1.5	2.2
Cr	6.2	3.0 E-1	2.0	5.56	8.51	7.71	6.90	5.0
Cu	5.2 E-1	<8.8 E-2	<1.0 E-1	1.0 E-1	<5.1 E-2	7.0 E-2	1.0 E-1	6.0 E-1
Fe	2.26 E+1	3.0 E-1	2.7	8.46	1.37 E+1	1.56 E-1	1.45 E+1	1.79 E+1
Gd	<4.0 E-1	<3.0 E-1	7.6	4.4 E-1	4.5 E-1	2.1 E-1	3.8 E-1	<9.0 E-1
In	8.52	<1.0	<7.0	<6.0 E-1	2.74	3.18	5.11	<4.0
Mn	2.6 E-1	3.0 E-2	2.1 E-1	2.4 E-1	4.0 E-1	4.1 E-1	3.3 E-1	4.0 E-1
Mo	<6.0 E-1	<3.0 E-1	<5.0 E-1	4.8 E-1	<2.0 E-1	3.4 E-1	6.6 E-1	<1
Ni	3.2 E+1	<2.0 E-1	5.0 E-1	1.51 E+1	4.08	7.34	7.20	7.4
Nb	<2.0	<1.0	<2.0	1.0	1.3	8.8 E-1	1.3	<4.0
Si	1.6	4.87	4.4	1.2	2.23	2.75	3.87	1.26 E+1
Sn	1.24 E+1	<2.0	<3.0	4.66	2.1	2.18	2.7	<6.25
Te	<1.0	1.0	<1.0	<4.0 E-1	<4.0 E-1	<3.0 E-1	<5.5 E-1	<2.0
U	1.13 E+2	1.29 E+2	7.02 E+2	5.46 E+2	4.44 E+2	3.11 E+2	3.19 E+2	2.85 E+2
Zr	2.20 E+2	5.38 E+2	7.45 E+1	1.52 E+2	1.73 E+2	6.54 E+1	3.31 E+2	2.89 E+2

a. Uncertainty is 30-50% because of problems associated with the analysis.

TABLE D-6. RESULTS OF ELEMENTAL ANALYSIS OF SAMPLE 7
(mg element/g sample)

Element	Particle Size Fraction (μm) >4000[a] Particle 7A	>4000 Particle 7B	>4000 Particle 7C	>4000 Particle 7D	>4000 Particle 7E	1680-4000[a] Particle 7F	1680-4000 Particle 7G	1680-4000[a] Particle 7H	1000-1680 Particle 7I
Ag	3.0	--[b]	--[b]	--[b]	--[b]	<1.0 E+1	<1.0	<6.0 E-1	--[b]
Al	1.0 E+1	--[b]	--[b]	--[b]	--[b]	<5.0 E+1	5.0	<3.0	--[b]
B	4.0	--[b]	--[b]	--[b]	--[b]	<1.0 E+1	2.0	<8.0 E-1	--[b]
Ca	7.0 E-1	--[b]	--[b]	--[b]	--[b]	<2.0	3.0 E-1	<2.0 E-1	--[b]
Cr	1.0 E+[illegible]	--[b]	--[b]	--[b]	--[b]	5.8 E+1	9.7	2.7	--[b]
Cu	2.0	--[b]	--[b]	--[b]	--[b]	2.0 E+1	8.0 E-1	8.0 E-1	--[b]
Fe	2.0 E+1	--[b]	--[b]	--[b]	--[b]	1.0 E+1	9.5	6.0 E-1	--[b]
Gd	<3.0	--[b]	--[b]	--[b]	--[b]	<2.0 E+1	<1.0	<1.0	--[b]
In	2.0 E+[illegible]	--[b]	--[b]	--[b]	--[b]	<7.0 E+1	<5.0	<5.0	--[b]
Mn	4.0 E-1	--[b]	--[b]	--[b]	--[b]	2.0	4.3 E-1	2.0 E-1	--[b]
Mo	<4.0	--[b]	--[b]	--[b]	--[b]	<2.0	<2.0	<2.0	--[b]
Ni	7.8	--[b]	--[b]	--[b]	--[b]	<1.0 E+1	2.0	2.0	--[b]
Nb	<1.0 E+1	--[b]	--[b]	--[b]	--[b]	<7.0 E+1	<5.0	<5.0	--[b]
Si	4.64 E+1	--[b]	--[b]	--[b]	--[b]	3.07 E+[illegible]	2.18 E+1	1.75 E+1	--[b]
Sn	<2.0 E+1	--[b]	--[b]	--[b]	--[b]	<1.0 E+2	1.6 E+1	<8.0	--[b]
Te	<7.0	--[b]	--[b]	--[b]	--[b]	<5.0 E+1	<3.0	<3.0	--[b]
U	5.91 E+[illegible]	--[b]	--[b]	--[b]	--[b]	7.2 E+[illegible]	5.19 E+[illegible]	5.25 E+[illegible]	--[b]
Zr	1.29 E+[illegible]	--[b]	--[b]	--[b]	--[b]	3.1 E+[illegible]	1.34 E+[illegible]	3.9	--[b]

Element	1000-1680[a] Particle 7J	1000-1680 Particle 7K	707-1000[a] Aliquot	297-707[a] Aliquot	149-297 Aliquot	74-149[a] Aliquot	30-74 Aliquot	20-30[a] Aliquot	<20[a] Aliquot
Ag	<2.0	2.0	6.0 E-1	<1.0	--[b]	2.1 E+1	--[b]	1.3 E+1	<8.0
Al	1.0 E+1	7.0	3.0	1.0 E+1	--[b]	2.0 E+1	--[b]	2.0 E+1	7.0 E+1
B	1.0 E+1	4.0	<4.0 E-1	<2.0	--[b]	<4.0	--[b]	<3.0	<1.0 E+1
Ca	2.0	<2.0 E-1	2.0 E-1	<4.0 E-1	--[b]	<8.0 E-1	--[b]	<6.0 E-1	<2.0
Cr	1.2 E+2	9.9	4.9	1.9 E+1	--[b]	<6.6 E+1	--[b]	4.0	4.8 E+2
Cu	2.0	1.0	4.0 E-1	2.0	--[b]	4.0	--[b]	3.0	1.0 E+1
Fe	<4.9 E+[illegible]	1.1 E+1	6.4	3.0 E+1	--[b]	4.5 E+1	--[b]	2.0 E+1	2.0 E+[illegible]
Gd	<3.0	<2.0	<6.0 E-1	<2.0	--[b]	<6.0	--[b]	<4.0	<2.0 E+1
In	2.0 E+[illegible]	1.0 E+[illegible]	5.0	<1.0 E+[illegible]	--[b]	<2.0 E+1	--[b]	<2.0 E+1	<7.0 E+1
Mn	2.0	4.4 E-1	2.2 E+1	6.4 E+1	--[b]	1.2	--[b]	6.0 E-1	7.0
Mo	<4.0	<2.0	<9.0 E-1	<4.0	--[b]	<8.0	--[b]	<6.0	<2.0 E+1
Ni	5.8 E+1	<1.0	<9.0 E-1	4.0	--[b]	8.0	--[b]	6.0	2.0 E+[illegible]
Nb	<1.0 E+1	<7.0	<3.0	<1.0 E+1	--[b]	<2.0 E+1	--[b]	<2.0 E+1	<7.0 E+1
Si	5.75 E+[illegible]	2.30 E+1	9.22	4.82 E+1	--[b]	1.19 E+[illegible]	--[b]	8.50 E+1	3.1[illegible] E+[illegible]
Sn	<2.0 E+1	2.3 E+[illegible]	8.6	<2.0 E+1	--[b]	<4.0 E+1	--[b]	<3.0 E+1	<1.0 E+[illegible]
Te	<8.0	<5.0	<2.0	<7.0	--[b]	<2.0 E+1	--[b]	<1.0 E+1	<4.0 E+1
U	4.05 E+2	6.85 E+2	3.72 E+2	1.54 E+2	--[b]	5.20 E+2	--[b]	1.9 E+2	<4.0 E+[illegible]
Zr	2.5 E+1	1.44 E+2	5.62 E+1	2.53 E+2	--[b]	4.35 E+[illegible]	--[b]	1.75 E+[illegible]	1.6 E+[illegible]

a. Uncertainty is 30-50% because of problems associated with the analysis.

b. Not reported because of analysis problems.

TABLE D-7. RESULTS OF ELEMENTAL ANALYSIS OF SAMPLE 8
(mg element/g sample)

Element	>4000[a] Particle 8A	>4000 Particle 8B	>4000 Particle 8C	>4000 Particle 8D	>4000[a] Particle 8E	1680-4000[a] Particle 8F	1680-4000 Particle 8G	1680-4000[a] Particle 8H	1000-1680[a] Particle 8I
	Particle Size Fraction (μm)								
Ag	<2.0	<8.0 E-1	--[b]	--[b]	4.0	2.0	<3.0	<2.0	<8.0 E-1
Al	2.0 E+1	<4.0	--[b]	--[b]	2.0 E+1	9.0	3.7 E+1	1.0 E+1	6.0
B	<3.0	<1.0	--[b]	--[b]	<3.0	<2.0	<4.2	<2.0	<1.0
Cd	<5.0 E-1	<2.0 E-1	--[b]	--[b]	<6.0 E-1	<3.0 E-1	<8.3 E-1	<4.0 E-1	<2.0 E-1
Cr	6.5	1.0	--[b]	--[b]	7.5	3.0	1.1 E+1	3.0	<6.0 E-1
Cu	3.0	1.0	--[b]	--[b]	5.0	2.0	2.1	2.0	1.0
Fe	2.0	<4.0 E-1	--[b]	--[b]	5.0	2.4 E+1	1.7 E+1	1.1 E+1	6.3
Gd	<4.0	<1.0	--[b]	--[b]	<4.0	<2.0	<5.8	<3.0	<1.0
In	<2.0 E+1	<6.0	--[b]	--[b]	<2.0 E+1	<9.0	<2.5 E+1	<1.0 E+1	<6.0
Mn	<3.0 E+1	<1.0 E-1	--[b]	--[b]	6.0 E-1	3.0 E-1	8.3 E-1	4.0 E-1	3.1 E-1
Mo	<5.0	<2.0	--[b]	--[b]	<6.0	<3.0	<8.3	<4.0	<2.0
Ni	5.0	<1.0	--[b]	--[b]	<3.0	6.3	<4.2	<2.0	<1.0
Nb	<2.0 E+1	<6.0	--[b]	--[b]	<2.0 E+1	<9.0	<2.5 E-1	<1.0 E+1	<6.0
Si	5.15 E+1	2.28 E+1	--[b]	--[b]	5.5 E+1	3.15 E+1	7.0 E+1	4.97 E+1	3.47 E+1
Sn	<3.0 E+1	<1.0 E+1	--[b]	--[b]	<3.0 E+1	<2.0 E+1	<4.1 E+1	<2.0 E+1	<1.0 E+1
Te	<1.0 E+1	<4.0	--[b]	--[b]	<1.0 E+1	<6.0	<1.6 E+1	<9.0	<4.0
U	7.15 E+2	8.12 E+2	--[b]	--[b]	9.66 E+2	5.52 E+2	7.84 E+2	6.91 E+2	2.22 E+2
Zr	8.0 E+1	8.0	--[b]	--[b]	5.0 E+2	3.0 E+2	1.62 E+2	8.0 E+1	5.0 E+1

Element	1000-1680[a] Particle 8J	1000-1680 Particle 8K	707-1000[a] Aliquot	297-707[a] Aliquot	149-297[a] Aliquot	74-149[a] Aliquot	30-74[a] Aliquot	20-30 Aliquot	<20[a] Aliquot	Sweepings[a]
Ag	<8.0	<1.0	<2.0	<3.0	8.1	5.4	<3.0	--[b]	1.1 E+1	4.0
Al	6.0 E+1	1.0 E+1	<1.0 E+1	2.0 E+1	<5.0	1.1 E+1	2.0 E+1	--[b]	2.93 E+1	<1.0 E+1
B	<1.0 E+1	4.0	5.0	6.0	<1.0	<7.0 E-1	<0.0	--[b]	2.0	1.3 E+1
Cd	<2.0	<4.0 E-1	<5.0 E-1	<6.0 E-1	5.0 E-1	1.5	1.0	--[b]	2.0	2.1
Cr	2.9 E+1	8.8	9.6	1.3 E+1	4.9	3.3	7.0 E+1	--[b]	2.2	1.4 E+1
Cu	1.0 E+1	<9.0 E-1	4.0	5.0 E	1.0	1.8	4.0	--[b]	1.0	3.0
Fe	3.4 E+1	1.5 E+1	7.2	6.3	1.7 E+1	2.65 E+1	6.0	--[b]	1.9 E+1	2.9 E+1
Gd	<1.0 E+1	<3.0	<3.0	<4.0	<2.0	<1.0	<5.0	--[b]	<2.0	<4.0
In	<6.0 E+1	<1.0 E+1	<1.0 E+1	<2.0 E+1	<7.0	<4.0	<2.0 E+1	--[b]	1.0 E+1	4.0 E+1
Mn	2.0	4.0 E-1	5.0 E-1	6.0 E-1	3.9 E-1	7.2 E-1	1.2	--[b]	3.8 E-1	1.6
Mo	<2.0 E+1	<4.0	<5.0	<6.0	<2.0	<1.0	<7.0	--[b]	<2.0	<6.0
Ni	<1.0 E+1	<2.0	5.0	6.0	8.6	8.9	1.5 E+1	--[b]	6.5	6.0
Nb	<6.0 E+1	<1.0 E+1	<1.0 E+1	<2.0 E+1	<7.0	<4.0	<2.0 E+1	--[b]	<7.0	<2.0 E+1
Si	3.76 E+2	5.76 E+1	6.58 E+1	9.50 E+1	3.45 E+1	1.61 E+1	9.31 E+1	--[b]	2.98 E+1	8.52 E+1
Sn	<1.0 E+2	<2.0 E+1	4.8 E+1	<3.0 E+1	<1.0 E+1	<7.0	<4.0 E+1	--[b]	<1.0 E+1	6.0 E+1
Te	<4.0 E+1	<7.0	<1.0 E+1	<1.0 E+1	<5.0	<3.0	<1.0 E+1	--[b]	1.0 E+1	<1.0 E+1
U	6.3 E+2	8.10 E+2	2.80 E+2	4.21 E+2	3.18 E+2	4.77 E+2	4.28 E+2	--[b]	4.87 E+2	9.90 E+2
Zr	5.0 E+2	2.0 E+2	3.08 E+2	3.9 E+1	1.84 E+2	2.60 E+2	2.74 E+2	--[b]	1.30 E+2	3.97 E+2

a. Uncertainty is 30-50% because of problems associated with the analysis.

b. Not reported because of analysis problems.

TABLE D-8. RESULTS OF ELEMENTAL ANALYSIS OF SAMPLE 9
(mg element/g sample)

Element	Particle Size Fraction (μm)									
	<4000 Particle 9A	>4000 Particle 9B	<4000 Particle 9C	<4000[a] Particle 9D	>4000 Particle 9E	1680-4000[a] Particle 9F	1680-4000[a] Particle 9G	1680-4000[a] Particle 9H	1000-1680 Particle 9I	1000-1680[a] Particle 9J
Ag	8.0 E-1	1.7	7.5 E-1	1.6 E+1	--[b]	1.2 E+1	1.8 E+1	2.0	<3.0 E-1	<2.0
Al	2.66 E+1	<1.0	<7.0 E-1	1.0 E+2	--[b]	8.0	1.0 E+1	<5.0	<2.0	5.3
B	<6.0 E-1	<3.0 E-1	<2.0 E-1	<2.0	--[b]	<1.0	<2.0	1.0	1.5	<1.0
Cd	<1.0 E-1	<7.0 E-2	<4.0 E-2	<4.0 E-1	--[b]	<3.0 E-1	<4.0 E-1	<2.0 E-1	<9.0 E-2	3.0 E-1
Cr	7.0 E-1	9.3	1.4	<1.0	--[b]	6.1	3.0	4.6	<3.0 E-1	5.0
Cu	<3.0 E-1	<2.0 E-1	2.0 E-1	3.0	--[b]	1.0	2.0	<6.0 E-1	<2.0 E-1	7.0 E-1
Fe	1.1 E+1	2.93 E+1	4.25	1.1 E+1	--[b]	1.7 E+1	4.0	3.9	4.1	4.2
Gd	<8.0 E-1	<5.0 E-1	5.2 E-1	<3.0	--[b]	<2.0	<3.0	<2.0	<6.0 E-1	<2.0
In	<3.0 E-1	<2.0	<1.0	<1.0 E+1	--[b]	<8.0	<1.0 E+1	<7.0	<3.0	<8.0
Mn	2.6 E-2	6.4 E-1	1.4 E-1	4.0 E-1	--[b]	4.4 E-1	<2.0 E-1	2.0 E-1	1.3 E-1	<3.0 E-1
Mo	<1.0	<7.0 E-1	<4.0 E-1	<4.0	--[b]	<3.0	<4.0	<2.0	<9.0 E-1	<3.0
Ni	2.8	7.20	2.5	2.86 E+1	--[b]	7.2	9.46 E+1	2.0	9.0 E-1	<3.0
Nb	<3.0	<2.0	<1.0	<1.0 E+1	--[b]	<8.0	<1.0 E+1	<7.0	<3.0	<8.0
Si	1.29 E+1	9.47	5.30	4.91 E+1	--[b]	4.22 E+1	6.95 E+1	3.18 E+1	1.29 E+1	3.14 E+1
Sn	<6.0	6.7	<2.0	1.00 E+2	--[b]	<1.0 E+1	<2.0 E+1	<1.0 E+1	<4.0	<1.0 E+1
Te	<2.0	3.0	<7.0 E-1	<7.0	--[b]	<6.0	<9.0	<5.0	<2.0	<6.0
U	4.64 E+2	5.55 E+2	7.84 E+2	1.1 E+2	--[b]	6.69 E+2	1.32 E+2	4.23 E+2	1.43 E+2	4.54 E+2
Zr	6.21 E+1	2.42 E+2	5.22 E+1	7.41 E+1	--[b]	1.94 E+2	5.7	5.21 E+1	7.27 E+1	5.59 E+1

Element	1000-1680 Particle 9K	707-1000[a] Aliquot	297-707 Aliquot	149-297[a] Aliquot	74-149 Aliquot	30-74 Aliquot	20-30[a] Aliquot	<20[a] Aliquot	Composite[a]
Ag	--[b]	2.0	--[b]	2.0 E+1	1.2 E+1	6.1	1.3 E+1	1.2 E+1	1.9 E+1
Al	--[b]	9.0	--[b]	3.0 E+1	9.0	1.0 E+1	2.0 E+1	9.0	2.0 E+1
B	--[b]	<2.0	--[b]	<6.0	<2.0	<9.0 E-1	<3.0	<1.0	5.0
Cd	--[b]	<3.0 E-1	--[b]	2.0	6.0 E-1	1.0	1.0	1.0	2.0
Cr	--[b]	7.2	--[b]	1.0 E+1	7.8	8.6	5.0	3.5	6.5
Cu	--[b]	2.0	--[b]	6.0	2.0	9.0 E-1	3.0	1.0	4.0
Fe	--[b]	9.9	--[b]	8.7 E+1	1.4 E+1	1.89 E+1	2.6 E+1	2.2 E+1	3.1 E+1
Gd	--[b]	2.0	--[b]	<8.0	<2.0	<1.0	<4.0	<2.0	<4.0
In	--[b]	<9.0	--[b]	<3.0 E+1	<9.0	<5.0	3.0 E+1	<9.0	2.3 E+1
Mn	--[b]	3.0 E-1	--[b]	1.0	5.7 E-1	4.3 E-1	6.0 E-1	5.8 E-1	8.0 E-1
Mo	--[b]	<3.0	--[b]	<1.0 E+1	<3.0	<2.0	<6.0	<3.0	<5.0
Ni	--[b]	2.0	--[b]	1.0 E+1	4.8	6.4	6.0	5.5	5.0
Nb	--[b]	<9.0	--[b]	<3.0 E+1	<9.0	<5.0	<9.0	<2.0 E+1	<1.5
Si	--[b]	3.51 E+1	--[b]	1.69 E+2	4.50 E+1	2.14 E+1	6.56 E+1	3.96 E+1	8.00 E+1
Sn	--[b]	3.0 E+1	--[b]	<6.0 E+1	<2.0 E+1	<9.0	<3.0 E+1	<1.0 E+1	5.0 E+1
Te	--[b]	<6.0	--[b]	<2.0 E+1	<6.0	<4.0	<1.0 E+1	<6.0	<1.0 E+1
U	--[b]	5.07 E+2	--[b]	6.71 E+2	3.45 E+2	3.39 E+2	1.7 E+2	5.00 E+2	4.56 E+2
Zr	--[b]	4.29 E+2	--[b]	3.61 E+2	1.51 E+2	1.98 E+2	9.14 E+1	1.38 E+2	2.74 E+2

a. Uncertainty is 30-50% because of problems associated with the analysis.

b. Not reported because of analysis problems.

TABLE D-9. RESULTS OF ELEMENTAL ANALYSIS OF SAMPLE 10
(mg element/g sample)

Element	Particle Size Fraction (μm) >4000 Particle 10A	>4000 Particle 10B	>4000 Particle 10C	>4000[a] Particle 10D	>4000[a] Particle 10E	1680-4000 Particle 10F	1680-4000 Particle 10G	1680-4000 Particle 10H	1000-1680[a] Particle 10I
Ag	--[b]	9.1 E-1	6.3 E-1	5.6 E-1	1.1	1.0	1.0	8.0 E-1	<1.0
Al	--[b]	<8.0 E-1	<4.0 E-1	<1.0	<9.0 E-1	<4.0	<3.0	3.0	<5.0
B	--[b]	<2.0 E-1	<9.0 E-2	<3.0 E-1	<2.0 E-1	<1.0	<8.0 E-1	<6.0 E-1	<1.0
Cd	--[b]	<4.0 E-2	<2.0 E-2	<5.0 E-2	9.0 E-2	2.0 E-1	3.0 E-1	<1.0 E-1	<3.0 E-1
Cr	--[b]	1.9	<6.0 E-2	3.0 E-1	3.0 E-1	<6.0 E-1	<5.0 E-1	3.2	2.0
Cu	--[b]	2.0 E-1	9.0 E-2	3.0 E-1	2.0 E-1	<5.0 E-1	<4.0 E-1	<3.0 E-1	<1.0
Fe	--[b]	3.4	<4.0 E-2	<1.0 E-1	1.4	6.0	2.4	4.1	1.3 E+1
Gd	--[b]	1.2	9.0 E-1	7.2 E-1	6.1 E-1	<1.0	<1.0	<8.0 E-1	<2.0
In	--[b]	2.0	<6.0 E-1	3.0	3.0	<6.0	<5.0	<3.0	<8.0
Mn	--[b]	2.3 E-1	1.2 E-1	1.6 E-1	1.1 E-1	2.0 E-1	2.0 E-1	1.8 E-1	3.0 E-1
Mo	--[b]	<4.0 E-1	<2.0 E-1	<5.0 E-1	<4.0 E-1	<2.0	<2.0	<1.0	<3.0
Ni	--[b]	3.5	2.0 E-1	<3.0 E-1	1.3	2.0	<8.0 E-1	2.4	5.8
Nb	--[b]	<1.0	<6.0 E-1	<2.0	<1.0	<6.0	<5.0	<3.0	<8.0
Si	--[b]	4.81	9.5 E-1	2.5	1.2	3.1	2.3	4.1	1.2 E+1
Sn	--[b]	<2.0	1.9	<3.0	4.4	<1.0 E+1	<8.0	<6.0	<1.0 E+1
Te	--[b]	<8.0 E-1	<4.0 E-1	<1.0	<9.0 E-1	<4.0	<3.0	<2.0	<5.0
U	--[b]	8.83 E+2	7.09 E+2	6.09 E+2	6.49 E+2	6.31 E+2	8.06 E+2	6.84 E+2	3.53 E+2
Zr	--[b]	6.93 E+1	3.28	2.7	7.54 E+1	3.96 E+1	3.7	3.89 E+1	2.4 E+1

Element	1000-1680 Particle 10J	1000-1680[a] Particle 10K	707-1000 Aliquot	297-707[a] Aliquot	149-297[a] Aliquot	74-149[a] Aliquot	30-74[a] Aliquot	20-30 Aliquot	Sweepings
Ag	<1.0	<1.0	1.2	<1.0	<4.0	4.0	6.6	5.5	2.5 E+1
Al	8.0	<6.0	3.4	1.0 E+1	3.0 E+1	1.0 E+1	8.4	8.0	5.0 E+1
B	<1.0	<1.0	3.0 E-1	<2.0	<6.0	<2.0	<8.0 E-1	<8.0 E-1	<4.0
Cd	<3.0 E-1	6.0 E-1	7.0 E-2	<3.0 E-1	<1.0	<3.0 E-1	1.0	8.0 E-1	<8.0 E-1
Cr	2.0	<8.0 E-1	4.6	<1.0	<3.0	<1.0	3.4	3.3	<2.0
Cu	1.0	<7.0 E-1	6.9 E-1	<8.0 E-1	6.0	<8.0 E-1	<4.0 E-1	<4.0 E-1	<2.0
Fe	3.0	2.0	7.27	9.8	3.0 E+1	9.9	1.80 E+1	1.4 E+1	2.6 E+1
Gd	<2.0	<2.0	<5.0 E-1	<2.0	<8.0	<2.0	<1.0	<1.0	<5.0
In	<8.0	<8.0	<2.0	<1.0 E+1	<3.0 E+1	<1.0 E+1	<5.0	<5.0	<2.0 E+1
Mn	<1.0 E-1	3.0 E-1	1.9 E-1	3.0 E-1	2.6	3.0 E-1	4.2 E-1	3.3 E-1	8.0 E-1
Mo	<3.0	<3.0	<7.0 E-1	<3.0	<1.0 E+1	<3.0	<2.0	<2.0	<8.0
Ni	<1.0	7.2	1.4	<2.0	<6.0	<2.0	5.3	4.9	8.0
Nb	<8.0	<8.0	<2.0	<1.0 E+1	<3.0 E+1	<1.0 E+1	<5.0	<5.0	<2.0 E+1
Si	1.4 E+1	1.0 E+1	9.60	3.97 E+1	1.51 E+2	4.67 E+1	6.72	2.34 E+1	1.19 E+2
Sn	<1.0 E+1	<1.0 E+1	6.9	<2.0 E+1	<6.0 E+1	<2.0 E+1	<8.0	<8.0	<4.0 E+1
Te	<5.0	<6.0	<1.0	<7.0	<2.0 E+1	<7.0	<3.0	<3.0	<2.0
U	5.37 E+2	9.67 E+2	6.43 E+2	3.77 E+2	3.30 E+2	1.71 E+2	3.67 E+2	4.68 E+2	6.21 E+2
Zr	8.59 E+1	5.6	2.10 E+2	6.50 E+1	2.24 E+2	1.26 E+2	1.63 E+2	1.56 E+2	4.24 E+2

a. Uncertainty is 30-50% because of problems associated with the analysis.

b. Not reported because of analysis problems.

TABLE D-10. RESULTS OF ELEMENTAL ANALYSIS OF SAMPLE 11
(mg element/g sample)

Element	Particle Size Fraction (μm)								
	>4000[a] Particle 11A	>4000 Particle 11B	>4000[a] Particle 11C	>4000[a] Particle 11D	>4000[a] Particle 11E	1680-4000 Particle 11F	1680-4000[a] Particle 11G	1680-4000 Particle 11H	1000-1680[a] Particle 11I
Ag	2.0	--[b]	8.4	<7.0	<1.0	9.0 E-1	2.0	--[b]	<2.0
Al	1.0 [illegible]	--[b]	2.0 E+1	[illegible]	1.0 E+1	4.0	4.19 E+1	--[b]	2.7 E+1
B	2.0	--[b]	<3.0	<9.0	<2.0	<6.0 E-1	<1.0	--[b]	2.0
Ca	4.0 E-1	--[b]	<6.0 E-1	<2.0	<4.0 E-1	<1.0 E-1	<3.0 E-1	--[b]	<4.0 E-1
Cr	5.4	--[b]	<2.0	2.0 E+1	<1.0	8.3	<8.0 E-1	--[b]	<1.0
Cu	2.0	--[b]	3.0	9.0	<9.0 E-1	<3.0 E-1	<7.0 E-1	--[b]	2.0
Fe	1.1 E+1	--[b]	6.8	7.0	3.0	1.30 E+1	2.0	--[b]	5.2
Ga	3.0	--[b]	<4.0	<1.0 E+1	<3.0	<9.0 E-1	<2.0	--[b]	<3.0
In	1.0 E+1	--[b]	<2.0 E+1	<5.0 E+1	<1.0 E+1	<4.0	<8.0	--[b]	<1.0 E+1
Mg	4.0 E-1	--[b]	5.0 E-1	2.0	<2.0 E-1	4.0 E-1	<1.0 E-1	--[b]	<2.0 E-1
Mn	4.0	--[b]	<6.0	<2.0 E+1	<4.0	<1.0	<3.0	--[b]	<4.0
Mo	2.0	--[b]	<3.0	<9.0	<2.0	<6.0 E-1	<1.0	--[b]	<2.0
Ni	1.0 E+1	--[b]	<2.0 E+1	<6.0 E+1	<1.0 E+1	<4.0	<8.0	--[b]	<1.0 E+1
Si	4.8[illegible] E+1	--[b]	9.03 E+1	3.98 E+2	5.00 E+1	1.76 E+1	3.38 E+1	--[b]	5.64 E+1
Sn	2.0 E+1	--[b]	<3.0 E+1	<9.0 E+1	<2.0 E+1	<6.0	<1.0 E+1	--[b]	4.0 E+1
Te	8.0	--[b]	<1.0 E+1	<4.0 E+1	<7.0	<3.0	<5.0	--[b]	<8.0
U	1.00 E+3	--[b]	1.12 E+3	1.14 E+3	5.61 E+2	8.23 E+2	1.03 E+3	--[b]	7.12 E+2
Zr	5.46 E+1	--[b]	5.0	2.0 E+1	<3.0	8.70 E+1	3.0	--[b]	2.14 E+1

Element	1000-1680[a] Particle 11J	1000-1680[a] Particle 11K	707-1000[a] Aliquot	149-707[a] Aliquot	74-149[a] Aliquot	30-74[a] Aliquot	20-30[a] Aliquot	[illegible]
Ag	1.0	1.0	3.0	2.0 E+1	1.8 E+1	2.0 E+1	2.3 E+1	--[b]
Al	6.0	6.0	2.0 E+1	2.0 E+1	1.0 E+1	1.0 E+1	1.0 E+1	--[b]
B	1.0	2.0	4.0	3.0	2.0	<2.0	4.0	--[b]
Ca	<2.0 E-1	<3.0 E-1	<8.0 E-1	2.0	2.0	2.0	5.0	--[b]
Cr	<6.0 E-1	<9.0 E-1	<2.0	1.3 E+1	<1.0	1.2 E+1	1.2 E+1	--[b]
Cu	1.0	<8.0 E-1	<2.0	3.0	2.0	4.0	8.8	--[b]
Fe	2.0	3.1	3.0	3.0 E+1	1.6 E+1	2.2 E+1	3.6 E+1	--[b]
Ga	<1.0	<2.0	<6.0	<4.0	<3.0	<3.0	<5.0	--[b]
In	<6.0	<9.0	<2.0 E+1	<2.0 E+1	<1.0 E+1	<1.0 E+1	<2.0 E+1	--[b]
Mg	<1.0 E-1	3.0 E-1	<4.0 E-1	1.0	4.0 E-1	5.0 E-1	7.0 E-1	--[b]
Mn	<2.0	<3.0	<8.0	<6.0	<4.0	<5.0	<7.0	--[b]
Mo	<1.0	<2.0	<4.0	6.0	<2.0	5.0	7.0	--[b]
Ni	<6.0	<9.0	<2.0 E+1	<2.0 E+1	<1.0 E+1	<1.0 E+1	<2.0 E+1	--[b]
Si	2.59 E+1	4.40 E+1	1.20 E+2	5.3 E+1	4.42 E+1	3.5 E+1	6.5 E+1	--[b]
Sn	<1.0 E+1	<2.0 E+1	<4.0 E+1	<3.0 E+1	<2.0 E+1	<2.0 E+1	<4.0 E+1	--[b]
Te	<4.0	<6.0	<2.0 E+1	<1.0 E+1	<7.0	<9.0	<1.0 E+1	--[b]
U	6.34 E+2	9.67 E+2	1.38 E+3	7.08 E+2	4.05 E+2	3.37 E+2	4.2 E+2	--[b]
Zr	2.0	3.0	5.83 E+2	1.31 E+3	3.94 E+2	4.88 E+2	4.3 E+2	--[b]

a. Uncertainty is 30-[illegible]1 because of problem associated with the analysis.

b. Not reported because of analysis problems.

APPENDIX E
RADIOCHEMICAL ANALYSES

APPENDIX E
RADIOCHEMICAL ANALYSES

This appendix contains results of the radiochemical analyses of the TMI-2 core debris grab samples (Tables E-1 through E-12). All analyses were performed on the same portions of each sample. Gamma emitting radionuclides measured by gamma spectroscopy were ^{60}Co, ^{106}Ru, ^{110m}Ag, ^{125}Sb, ^{134}Sc, ^{137}Cs, ^{144}Ce, ^{154}Eu, and ^{155}Eu. Results of the ^{90}Sr analysis were obtained by radiochemical separation and subsequent beta emitter analysis. The ^{129}I and fissile/fertile material results were obtained by neutron activation analysis, with subsequent gamma spectroscopy and delayed neutron analysis, respectively. Results of all analyses are reported in μCi/g sample, except for the fissile/fertile material contents which are reported in mg.

TABLE E-1. RESULTS OF RADIONUCLIDE ANALYSIS OF SAMPLE 1
(μCi/g sample)

Radionuclide	Particle Size Fraction (μm) >4000 Particle 1A	>4000[a] Particle 1B	>4000[a] Particle 1C	>4000 Particle 1D	>4000 Particle 1E	1680-4000[a] Particle 1F	1680-4000 Particle 1G	1680-4000 Particle 1H
^{60}Co	2.55 ± 0.14 E+1	1.45 ± 0.15 E+1	5.80 ± 0.73	1.99 ± 0.31 E+1	1.37 ± 0.09 E+1	6.48 ± 0.64	9.34 ± 0.88	7.85 ± 0.49 E+1
^{90}Sr	2.5 ± 0.1 E+2	9.4 ± 0.1 E+1	1.47 ± 0.06 E+2	2.1 ± 0.1 E+3	7.9 ± 0.3 E-1	7.3 ± 0.3 E+1	9.0 ± 0.4 E+1	4.4 ± 0.2 E+3
^{106}Ru	7.10 ± 0.40 E+1	1.24 ± 0.12 E+3	4.47 ± 0.57 E+1	8.99 ± 1.37 E+2	2.72 ± 0.18 E+2	3.51 ± 0.39 E+1	7.33 ± 0.74 E+1	1.07 ± 0.07 E+2
^{110m}Ag	--[b]	--[b]	--[b]	--[b]	--[b]	--[b]	--[b]	--[b]
^{125}Sb	1.20 ± 0.07 E+2	6.26 ± 0.65 E+1	8.2 ± 1.5 E+1	1.36 ± 0.22 E+1	9.24 ± 0.61 E+1	1.65 ± 0.18 E+1	1.84 ± 0.24 E+1	1.48 ± 0.13 E+1
^{129}I	5.5 ± 0.4 E-5	--[b]	--[b]	5.8 ± 2.8 E-5	6.82 ± 0.04 E-4	1.4 ± 0.2 E-4	2.1 ± 0.3 E-4	--[b]
^{134}Cs	5.36 ± 0.31	2.95 ± 0.44	5.05 ± 0.57 E+1	1.08 ± 0.17 E+1	3.54 ± 0.23 E+1	8.96 ± 0.7 E+1	9.98 ± 0.86 E+1	6.29 ± 0.44
^{137}Cs	2.98 ± 0.16 E+2	5.34 ± 0.54 E+1	8.70 ± 0.10 E+2	2.02 ± 0.31 E+2	8.38 ± 0.54 E+2	1.58 ± 0.13 E+3	1.71 ± 0.15 E+3	1.15 ± 0.07 E+2
^{144}Ce	1.74 ± 0.14 E+2	3.07 ± 0.33 E+3	1.87 ± 0.23 E+3	3.14 ± 0.49 E+3	7.32 ± 0.59 E+2	2.45 ± 0.22 E+3	2.31 ± 0.22 E+3	2.18 ± 0.15 E+3
^{154}Eu	7.98 ± 0.96 E-1	4.69 ± 0.49 E+1	3.19 ± 0.38 E+1	4.63 ± 0.71 E+1	1.05 ± 0.08 E+1	4.58 ± 0.40 E+1	3.54 ± 0.33 E+1	3.02 ± 0.20 E+1
^{155}Eu	9.5 ± 1.9	1.3 ± 0.2 E+2	8.0 ± 1.3 E+1	1.25 ± 0.25 E+2	3.5 ± 0.7 E+1	9.9 ± 2.0 E+1	9.5 ± 1.9 E+1	8.3 ± 1.8 E+1

Radionuclide	1000-1680 Particle 1I	1000-1680 Particle 1J	1000-1680 Particle 1K	707-1000 Aliquot	297-707[a] Aliquot	149-297 Aliquot	74-149 Aliquot	30-74[a] Aliquot
^{60}Co	1.67 ± 0.20 E+1	1.71 ± 0.10	8.2 ± 0.7	2.3 ± 0.2 E+2	4.06 ± 0.02 E+1	8.1 ± 0.6 E+1	1.1 ± 0.1 E+2	1.4 ± 0.1 E+2
^{90}Sr	1.65 ± 0.08 E+2	5.2 ± 0.3 E+3	4.3 ± 0.2 E+3	3.9 ± 0.2 E+3	3.4 ± 0.1 E+3	3.6 ± 0.2 E+3	3.1 ± 0.1 E+3	3.2 ± 0.2 E+3
^{106}Ru	7.00 ± 0.85 E+1	7.5 ± 0.5	4.6 ± 0.4 E+1	5.6 ± 0.4 E+3	1.24 ± 0.08	1.5 ± 0.1 E+2	2.7 ± 0.3 E+2	2.40 ± 0.2 E+2
^{110m}Ag	7.43 ± 0.92	--[b]	--[b]	3.7 ± 0.9	9.1 ± 1.7 E-1	1.3 ± 0.3	1.8 ± 0.4	2.2 ± 0.4
^{125}Sb	2.17 ± 0.25 E+2	9.6 ± 0.9 E-1	4.9 ± 0.8	1.91 ± 0.13 E+2	1.8 ± 0.1 E+2	3.4 ± 0.2 E+2	4.8 ± 0.5 E+2	4.5 ± 0.3 E+2
^{129}I	1.63 ± 0.01 E-3	5.6 ± 1.7 E-5	--[b]	1.04 ± 0.01 E-3	1.29 ± 0.04 E-3	3.13 ± 0.05 E-3	1.94 ± 0.03 E-3	6.79 ± 0.07 E-3
^{134}Cs	6.29 ± 0.72 E+1	2.71 ± 0.18	5.1 ± 0.4	5.6 ± 0.4 E+1	2.2 ± 0.2 E+1	4.4 ± 0.3 E+1	5.1 ± 0.5 E+1	7.13 ± 0.51 E+1
^{137}Cs	1.14 ± 0.13 E+3	4.81 ± 0.26 E+1	8.7 ± 0.7 E+1	1.06 ± 0.4 E+3	5.4 ± 0.3 E+2	9.1 ± 0.6 E+2	1.0 ± 0.1 E+3	1.35 ± 0.09 E+3
^{144}Ce	--[b]	2.80 ± 0.17 E+2	2.5 ± 0.2 E+3	2.3 ± 0.2 E+3	2.0 ± 0.2 E+3	1.55 ± 0.12 E+3	1.7 ± 0.2 E+3	1.57 ± 0.14 E+3
^{154}Eu	9.8 ± 2.5 E-1	4.73 ± 0.26	4.8 ± 0.4 E+1	4.5 ± 0.4 E+1	3.6 ± 0.2 E+1	2.4 ± 0.2 E+1	3.4 ± 0.4 E+1	2.49 ± 0.22 E+1
^{155}Eu	--[b]	1.05 ± 0.18 E+1	1.0 ± 0.2 E+2	1.1 ± 0.2 E+2	8.0 ± 1.6 E+1	6.7 ± 1.3 E+1	6.9 ± 1.4 E+1	5.6 ± 1.1 E+1

a. Uncertainty is ~30% because of problems associated with the analysis.

b. Not detected.

TABLE E-. . RESULTS OF RADIONUCLIDE ANALYSIS OF SAMPLE 3
(μCi/g sample)

Radionuclide	Particle Size Fraction					
	>4000 Particle 3A	-4000[a] Particle 3B	-4000[a] Particle 3C	>4000 Particle 3D	>4000 Particle 3E	1680-4000[a] Particle 3F
^{60}Co	4.67 ± 0.27 E+1	5.94 ± 0.41 E+1	1.30 ± 0.08 E+1	2.03 ± 0.29	1.33 ± 0.24	2.70 ± 0.33
^{90}Sr	7.5 ± 0.4 E+3	2.6 ± 0.1 E+3	5.3 ± 0.1 E+3	4.1 ± 0.2 E+3	8.4 ± 0.4 E+3	9.2 ± 0.4 E+3
^{106}Ru	6.75 ± 0.36 E+1	3.76 ± 0.35	4.03 ± 0.24 E+1	1.46 ± 0.08 E+3	1.43 ± 0.08 E+3	1.73 ± 0.20 E+3
^{110m}Ag	±b	±b	±b	±b	±b	±b
^{125}Sb	4.63 ± 0.29 E+1	6.95 ± 0.50	1.86 ± 0.13 E+1	1.34 ± 0.08 E+2	1.25 ± 0.08 E+2	6.40 ± 0.73 E+1
^{129}I	1.1 ± 0.5 E-5	5.8 ± 1.9 E-4		8.4 ± 0.3 E-5	1.43 ± 0.04 E-3	2.4 ± 0.3 E-4
^{134}Cs	3.25 ± 0.16	5.00 ± 0.42 E+1	2.23 ± 0.18	5.66 ± 0.32 E+1	5.19 ± 0.30 E+1	2.93 ± 0.33 E+1
^{137}Cs	5.87 ± 0.34 E+1	1.17 ± 0.08 E+2	4.65 ± 0.28 E+1	9.49 ± 0.52 E+2	8.36 ± 0.47 E+2	5.00 ± 0.60 E+2
^{144}Ce	1.77 ± 0.12 E+1	5.79 ± 0.52 E+1	1.76 ± 0.11 E+1	3.73 ± 0.24 E+2	3.92 ± 0.25 E+2	4.6 ± 0.53 E+1
^{154}Eu	3.00 ± 0.19 E+1	7.15 ± 0.75 E+1	2.24 ± 0.14 E+1	6.67 ± 0.41 E+1	6.83 ± 0.42 E+1	7.87 ± 0.91 E+1
^{155}Eu	1.4 ± 1.5 E+1	2.92 ± 0.59	6.99 ± 0.41 E+1	1.59 ± 0.32 E+2	1.36 ± 0.27 E+2	2.07 ± 0.40 E+2

Radionuclide	1680-4000 Particle 3G	1680-4000[a] Particle 3H	1000-1680 Particle 3I	1000-1680[a] Particle 3J	1000-1680 Particle 3K	707-1000 Aliquot
^{60}Co	6.41 ± 0.75	6.14 ± 0.71	7.13 ± 0.49 E+1	2.09 ± 0.27 E+1	6.43 ± 0.41	9.21 ± 0.59 E+1
^{90}Sr	1.10 ± 0.05 E+3	7.8 ± 0.1 E+3	3.8 ± 0.2 E+3	1.89 ± 0.09 E+3	3.5 ± 0.1 E+3	4.4 ± 0.2 E+3
^{106}Ru	1.81 ± 0.21 E+2	3.6 ± 0.47 E+1	2.39 ± 0.17 E+2	2.05 ± 0.74 E+1	4.17 ± 0.28 E+1	2.07 ± 0.24 E+2
^{110m}Ag	±b	±b	±b	±b	±b	±b
^{125}Sb	1.88 ± 0.22 E+2	4.4 ± 1.3	4.45 ± 0.38 E+1	2.39 ± 0.30 E+1	9.1 ± 0.81	3.37 ± 0.25 E+1
^{129}I	1.5 ± 0.3 E-4	3.1 ± 0.7 E-4			2.0 ± 0.3 E-4	
^{134}Cs	1.06 ± 0.12 E+1	6.57 ± 0.71 E+1	4.80 ± 0.33 E+1	6.48 ± 0.78	1.16 ± 0.07 E+1	3.10 ± 0.20 E+1
^{137}Cs	3.95 ± 0.45 E+2	1.13 ± 0.13 E+3	9.32 ± 0.63 E+2	1.03 ± 0.12 E+2	2.05 ± 0.12 E+2	5.40 ± 0.34 E+2
^{144}Ce	5.70 ± 0.69 E+1	1.55 ± 0.19 E+3	2.55 ± 0.19 E+3	1.31 ± 0.18 E+3	2.53 ± 0.16 E+3	2.38 ± 0.16 E+3
^{154}Eu	4.34 ± 0.55	2.54 ± 0.30 E+1	4.29 ± 0.31 E+1	2.33 ± 0.28 E+1	4.69 ± 0.28 E+1	4.46 ± 0.30 E+1
^{155}Eu	2.82 ± 0.33 E+1	5.6 ± 1.1 E+1	1.13 ± 0.23 E+2	5.72 ± 0.66 E+1	1.10 ± 0.22 E+2	1.00 ± 0.20 E+2

Radionuclide	297-707 Aliquot	149-297 Aliquot	74-149 Aliquot	30-74[a] Aliquot	<30 Aliquot
^{60}Co	2.21 ± 0.18 E+1	6.61 ± 0.37 E+1	8.59 ± 0.61 E+1	1.40 ± 0.09 E+2	1.02 ± 0.26 E+2
^{90}Sr	3.1 ± 0.2 E+3	2.62 ± 0.09 E+3	2.9 ± 0.2 E+3	3.6 ± 0.2 E+3	9.0 ± 0.2 E+2
^{106}Ru	1.19 ± 0.09 E+2	3.09 ± 0.17 E+2	2.33 ± 0.17 E+2	6.50 ± 0.44 E+2	2.46 ± 0.63 E+2
^{110m}Ag	±b	±b	1.22 ± 0.33	±b	±b
^{125}Sb	1.93 ± 0.19 E+2	1.09 ± 0.06 E+2	1.93 ± 0.14 E+2	2.21 ± 0.15 E+2	1.78 ± 0.46 E+2
^{129}I	1.6 ± 0.2 E-4		7.6 ± 0.3 E-4	5.6 ± 0.4 E-4	1.17 ± 0.01 E-3
^{134}Cs	3.50 ± 0.27 E+1	4.31 ± 0.24 E+1	5.15 ± 0.37 E+1	5.16 ± 0.35 E+1	2.87 ± 0.74 E+1
^{137}Cs	8.90 ± 0.60 E+2	6.6 ± 1.7 E+2	8.35 ± 0.65 E+2	9.00 ± 0.49 E+2	9.05 ± 0.64 E+2
^{144}Ce	1.80 ± 0.15 E+3	1.64 ± 0.10 E+3	1.48 ± 0.12 E+3	1.19 ± 0.09 E+3	7.5 ± 2.0 E+2
^{154}Eu	1.73 ± 0.14 E+2	1.05 ± 0.28 E+1	3.16 ± 0.26 E+1	2.59 ± 0.16 E+1	2.30 ± 0.19 E+1
^{155}Eu	4.9 ± 1.0 E+1	3.07 ± 0.79 E+1	3.83 ± 0.31 E+1	8.2 ± 1.6 E+1	6.3 ± 1.3 E+1

a. Uncertainty is ~1 because of problems associated with the analysis.

b. Not detected.

TABLE E-3. RESULTS OF RADIONUCLIDE ANALYSIS OF SAMPLE 4
(μCi/g sample)

Radionuclide	Particle 4A	Particle 4B[a]	Particle 4C	Particle 4D[a]	Particle 4E[a]
^{60}Co	6.45 ± 0.73 E+1	5.33 ± 0.33 E+1	2.51 ± 0.17 E+2	1.77 ± 0.33	1.99 ± 0.20 E+1
^{90}Sr	5.9 ± 0.3 E+3	9.4 ± 0.4 E+1	1.9 ± 0.1 E+3	5.4 ± 0.3 E+3	9.2 ± 0.5 E+3
^{106}Ru	1.52 ± 0.17 E+3	1.12 ± 0.71 E+3	6.00 ± 0.41 E+2	9.4 ± 1.2 E+2	1.37 ± 0.15 E+3
^{110m}Ag	--[b]	--[b]	--[b]	--[b]	--[b]
^{125}Sb	9.9 ± 1.1 E+1	3.21 ± 0.25 E+1	4.94 ± 0.38 E+1	9.7 ± 1.2 E+1	6.43 ± 0.72 E+2
^{129}I	1.0 ± 0.2 E-4	2.7 ± 0.6 E-5	4.9 ± 1.3 E-5	7.8 ± 3.0 E-4	--[b]
^{134}Cs	4.64 ± 0.54 E+1	8.16 ± 0.61	1.34 ± 0.10 E+1	1.13 ± 0.14 E+2	2.44 ± 0.26 E+1
^{137}Cs	7.77 ± 0.86 E+2	1.68 ± 0.10 E+2	3.65 ± 0.24 E+2	2.52 ± 0.31 E+3	4.00 ± 0.42 E+2
^{144}Ce	3.91 ± 0.46 E+3	3.65 ± 0.25 E+3	2.51 ± 0.19 E+3	2.96 ± 0.38 E+3	3.80 ± 0.41 E+3
^{154}Eu	6.82 ± 0.77 E+1	4.39 ± 0.28 E+1	2.03 ± 0.16 E+1	3.89 ± 0.50 E+1	6.34 ± 0.68 E+1
^{155}Eu	1.43 ± 0.29 E+2	1.40 ± 0.28 E+2	1.07 ± 0.21 E+2	3.99 ± 0.77 E+1	1.29 ± 0.14 E+2

a. Uncertainty is ~30% because of problems associated with the analysis.

b. Not detected.

TABLE E-4. RESULTS OF RADIONUCLIDE ANALYSIS OF SAMPLE 5 (μCi/g sample)

Radionuclide	Particle Size Fraction (μm) >4000[a] Particle 5A	>4000 Particle 5B	>4000 Particle 5C	>4000[a] Particle 5D	>4000 Particle 5E	1680-4000[a] Particle 5F
^{60}Co	2.06 ± 0.36 E+1	4.51 ± 0.31 E+1	3.94 ± 0.28 E+1	2.81 ± 0.25	1.20 ± 0.09 E+2	2.07 ± 0.19
^{90}Sr	6.[illegible] ± 0.3 E+3	4.0 ± 0.2 E+1	4.5 ± 0.2 E+3	6.2 ± 0.3 E+3	3.2 ± 0.2 E+2	8.2 ± 0.4 E+1
^{106}Ru	1.20 ± 0.21 E+3	1.25 ± 0.08 E+3	1.04 ± 0.07 E+3	5.40 ± 0.36 E+2	1.19 ± 0.08 E+3	5.58 ± 0.34 E+2
^{110m}Ag	--[b]	--[b]	--[b]	--[b]	--[b]	--[b]
^{125}Sb	9.11 ± 0.16 E+1	1.47 ± 0.10 E+2	2.47 ± 0.24 E+1	3.56 ± 0.28 E+1	3.00 ± 0.22 E+2	6.35 ± 0.40 E+1
^{129}I	1.1 ± 0.2 E-4	--[b]	3.0 ± 0.9 E-5	1.9 ± 0.3 E-4	--[c]	1.3 ± 0.3 E-3
^{134}Cs	1.[illegible] ± 0.23 E+2	1.53 ± 0.11 E+1	9.55 ± 0.75	2.25 ± 0.15 E+1	6.78 ± 0.55	2.92 ± 0.18 E+1
^{137}Cs	2.14 ± 0.38 E+2	2.95 ± 0.20 E+2	1.64 ± 0.11 E+2	6.89 ± 0.45 E+2	1.48 ± 0.11 E+2	7.90 ± 0.47 E+2
^{144}Ce	3.60 ± 0.65 E+3	3.[illegible] ± 0.27 E+3	3.15 ± 0.24 E+3	1.81 ± 0.13 E+3	2.13 ± 0.17 E+3	1.86 ± 0.12 E+3
^{154}Eu	6.54 ± 0.11 E+1	5.[illegible] ± 0.42 E+1	4.27 ± 0.32 E+1	1.58 ± 0.12 E+1	3.82 ± 0.29 E+1	1.73 ± 0.12 E+1
^{155}Eu	1.48 ± 0.29 E+[illegible]	1.33 ± 0.27 E+2	1.35 ± 0.27 E+2	8.1 ± 1.6 E+1	9.9 ± 2.0 E+1	7.4 ± 1.5 E+1

Radionuclide	1680-4000 Particle 5G	1680-4000 Particle 5H	1000-1680 Particle 5I	1000-1680[a] Particle 5J	<1000[a] Aliquot
^{60}Co	3.10 ± 0.18 E+1	--[c]	6.57 ± 0.40 E-1	1.09 ± 0.18	5.53 ± 0.34 E+1
^{90}Sr	5.0 ± 0.2 E+1	--[c]	3.9 ± 0.1 E+3	2.9 ± 0.1 E+3	--[c]
^{106}Ru	6.93 ± 0.38 E+2	--[c]	1.44 ± 0.09 E+3	1.29 ± 0.09 E+3	6.53 ± 0.40 E+2
^{110m}Ag	--[b]	--[c]	--[b]	--[b]	--[b]
^{125}Sb	1.32 ± 0.11 E+1	--[c]	1.02 ± 0.07 E+2	1.1[illegible] ± 0.08 E+2	8.01 ± 0.55 E+1
^{129}I	5.5 ± 0.8 E-4	--[c]	--[b]	5.4 ± 0.9 E-5	--[c]
^{134}Cs	2.[illegible] ± 0.26	--[c]	3.17 ± 0.[illegible]0 E+1	3.29 ± 0.23 E+1	9.85 ± 0.59 E+1
^{137}Cs	3.78 ± 0.21 E+1	--[c]	5.08 ± 0.31 E+2	5.36 ± 0.37 E+2	1.71 ± 0.10 E+3
^{144}Ce	2.36 ± 0.14 E+3	--[c]	3.56 ± 0.25 E+3	3.40 ± 0.26 E+3	2.24 ± 0.17 E+3
^{154}Eu	2.94 ± 0.18 E+1	--[c]	6.26 ± 0.42 E+1	6.23 ± 0.45 E+1	3.54 ± 0.25 E+1
^{155}Eu	1.02 ± 0.20 E+[illegible]	--[c]	1.62 ± 0.32 E+2	1.39 ± 0.28 E+2	1.06 ± 0.20 E+2

a. Uncertainty is >30% because of problems associated with the analysis.

b. Not detected.

c. Not reported because a portion of the sample was lost in analysis.

TABLE E-5. RESULTS OF RADIONUCLIDE ANALYSIS OF SAMPLE 6
(μCi/g sample)

Radionuclide	Particle Size Fraction (μm) >4000 Particle 6A	>4000 Particle 6B	>4000 Particle 6C	>4000 Particle 6D	>4000 Particle 6E	1680-4000 Particle 6F	1680-4000 Particle 6G	1680-4000 Particle 6H
^{60}Co	6.07 ± 0.67	1.66 ± 0.09	3.34 ± 0.23	--[b]	1.24 ± 0.09	4.89 ± 0.35	9.3 ± 2.1 E-1	--[b]
^{90}Sr	3.5 ± 0.2 E+3	7.9 ± 0.7 E+1	2.7 ± 0.2 E+2	2.3 ± 0.1 E+1	3.8 ± 0.4 E+1	1.5 ± 0.2 E+2	1.4 ± 0.1 E+1	1.19 ± 0.06 E+2
^{106}Ru	1.07 ± 0.11 E+3	2.39 ± 0.23	1.16 ± 0.07 E+2	9.15 ± 0.62 E+2	1.32 ± 0.14	7.0 ± 1.0	1.03 ± 0.06 E+3	8.05 ± 0.45 E+2
^{110m}Ag	--[b]	--[b]	--[b]	--[b]	--[b]	--[b]	--[b]	--[b]
^{125}Sb	9.74 ± 0.99 E+1	3.05 ± 0.17 E+2	4.22 ± 0.26 E+1	6.95 ± 0.53 E+1	2.40 ± 0.16 E+1	1.46 ± 0.11 E+1	9.97 ± 0.66 E+1	8.16 ± 0.50 E+1
^{129}I	1.6 ± 0.6 E-3	4.8 ± 0.7 E-3	2.2 ± 0.8 E-5	6.64 ± 0.07 E-3	2.9 ± 0.9 E-5	1.6 ± 0.4 E-4	3.5 ± 0.6 E-5	4.47 ± 0.06 E-4
^{134}Cs	3.90 ± 0.39 E+1	7.11 ± 0.40	9.73 ± 0.59	5.47 ± 0.38 E+1	2.22 ± 0.15	3.25 ± 0.20 E+1	1.69 ± 0.09 E+2	4.67 ± 0.26 E+1
^{137}Cs	1.19 ± 0.12 E+3	1.24 ± 0.07 E+3	1.82 ± 0.11 E+2	1.30 ± 0.09 E+3	4.41 ± 0.29 E+1	6.22 ± 0.38 E+2	3.79 ± 0.21 E+3	1.07 ± 0.06 E+3
^{144}Ce	3.65 ± 0.38 E+3	2.84 ± 0.98 E+3	1.96 ± 0.17 E+2	2.66 ± 0.21 E+3	1.91 ± 0.38	1.84 ± 0.35 E+1	3.06 ± 0.20 E+3	2.50 ± 0.16 E+3
^{154}Eu	2.88 ± 0.30 E+1	--[b]	2.93 ± 0.25	3.25 ± 0.25 E+1	--[b]	--[b]	4.34 ± 0.28 E+1	2.46 ± 0.16 E+1
^{155}Eu	1.51 ± 0.30 E+2	2.21 ± 0.88 E+1	1.03 ± 0.07 E+1	1.16 ± 0.23 E+2	--[b]	--[b]	1.37 ± 0.27 E+2	--[b]

Radionuclide	1000-1680 Particle 6I	1000-1680 Particle 6J	1000-1680 Particle 6K	707-1000 Aliquot	297-707[a] Aliquot	149-297[a] Aliquot	74-149[a] Aliquot	30-74 Aliquot
^{60}Co	2.74 ± 0.16 E+2	7.33 ± 0.43	6.87 ± 0.55	1.43 ± 0.08 E+2	5.15 ± 0.29 E+1	9.21 ± 0.59 E+1	1.11 ± 0.06 E+2	1.25 ± 0.09 E+2
^{90}Sr	3.8 ± 0.2 E+2	1.4 ± 0.6 E+3	4.2 ± 0.2 E+3	8.9 ± 0.4 E+1	1.14 ± 0.05 E+2	2.5 ± 0.1 E+3	2.3 ± 0.1 E+3	2.6 ± 0.1 E+3
^{106}Ru	2.64 ± 0.16 E+3	2.92 ± 0.16 E+2	5.81 ± 0.35 E+2	4.20 ± 0.23 E+2	2.19 ± 0.13 E+2	2.94 ± 0.17 E+2	3.74 ± 0.21 E+2	5.23 ± 0.37 E+2
^{110m}Ag	--[b]	--[b]	--[b]	--[b]	--[b]	--[b]	--[b]	--[b]
^{125}Sb	8.28 ± 0.49 E+1	1.78 ± 0.11 E+1	8.15 ± 0.59 E+1	8.77 ± 0.52 E+1	9.77 ± 0.57 E+1	1.46 ± 0.08 E+2	1.89 ± 0.11 E+2	1.67 ± 0.12 E+2
^{129}I	9.49 ± 0.03 E-4	2.1 ± 0.1 E-5	1.21 ± 0.03 E-3	5.0 ± 0.1 E-4	4.77 ± 0.05 E-4	6.7 ± 0.3 E-4	1.92 ± 0.02 E-3	2.4 ± 0.1 E-3
^{134}Cs	2.08 ± 0.34	4.97 ± 0.57 E-1	1.76 ± 0.10 E+2	5.66 ± 0.31 E+1	5.82 ± 0.32 E+1	5.36 ± 0.30 E+1	4.81 ± 0.27 E+1	5.00 ± 0.35 E+1
^{137}Cs	2.98 ± 0.18 E+1	1.10 ± 0.06 E+1	4.06 ± 0.24 E+3	1.23 ± 0.07 E+3	1.13 ± 0.06 E+3	1.07 ± 0.06 E+3	9.58 ± 0.53 E+2	9.54 ± 0.67 E+2
^{144}Ce	3.20 ± 0.34 E+2	6.90 ± 0.44 E+2	3.48 ± 0.24 E+3	2.29 ± 0.15 E+3	2.11 ± 0.15 E+3	1.40 ± 0.09 E+3	1.27 ± 0.09 E+3	1.11 ± 0.09 E+3
^{154}Eu	5.04 ± 0.64	1.34 ± 0.08 E+1	5.07 ± 0.34 E+1	3.63 ± 0.22 E+1	3.55 ± 0.22 E+1	2.16 ± 0.14 E+1	2.14 ± 0.14 E+1	1.83 ± 0.14 E+1
^{155}Eu	--[c]	--[c]	--[c]	1.07 ± 0.21 E+2	9.19 ± 1.80 E+1	6.7 ± 1.3 E+1	7.8 ± 1.6 E+1	4.5 ± 0.9 E+1

a. Uncertainty is ~30% because of problems associated with the analysis.

b. Not detected.

c. Not reported because of problems associated with the analysis.

TABLE E-6. RESULTS OF RADIONUCLIDE ANALYSIS OF SAMPLE 7 (μCi/g sample)

Radionuclide	Particle Size Fraction (μm)					
	>4000[a] Particle 7A	>4000 Particle 7B	>4000[a] Particle 7C	>4000 Particle 7D	>4000[a] Particle 7E	1680-4000[a] Particle 7F
^{60}Co	2.06 ± 0.03 E+1	1.49 ± 0.53 E+1	5.86 ± 0.75	2.06 ± 0.03 E+1	4.91 ± 0.11 E+1	4.06 ± 0.32
^{90}Sr	5.35 ± 0.58 E+3	2.33 ± 0.23 E+4	1.72 ± 0.17 E+3	1.58 ± 0.11 E+3	2.73 ± 0.30 E+4	1.32 ± 0.10 E+4
^{106}Ru	1.05 ± 0.14 E+2	7.58 ± 0.28 E+2	6.18 ± 0.98 E+1	1.04 ± 0.01 E+2	1.04 ± 0.01 E+3	2.25 ± 0.28 E+1
^{125}Sb	5.11 ± 0.66 E+1	1.35 ± 0.11 E+2	3.42 ± 0.49 E+1	6.53 ± 0.11 E+1	9.97 ± 0.45 E+1	1.08 ± 0.15 E+1
^{129}I	--[b]	6.16 ± 0.20 E-3	1.46 ± 0.28 E-4	9.06 ± 2.15 E-5	8.27 ± 2.39 E-4	--[b]
^{134}Cs	8.03 ± 0.24 E+1	2.02 ± 0.05 E+2	9.80 ± 0.24 E+1	1.42 ± 0.11	3.11 ± 0.11 E+1	2.27 ± 0.06 E+1
^{137}Cs	1.47 ± 0.01 E+3	5.43 ± 0.02 E+3	1.77 ± 0.07 E+1	3.17 ± 0.03 E+1	7.46 ± 0.04 E+2	4.22 ± 0.02 E+2
^{144}Ce	5.28 ± 0.31 E+3	2.02 ± 0.31 E+1	2.67 ± 0.09 E+3	5.90 ± 0.31 E+2	3.26 ± 0.15 E+3	1.37 ± 0.11 E+3
^{154}Eu	9.8 ± 1.1 E+1	2.04 ± 0.61 E+1	5.01 ± 0.51 E+1	7.35 ± 0.92	4.39 ± 0.51 E+1	2.66 ± 0.20 E+1
^{155}Eu	2.15 ± 0.71 E+2	1.06 ± 0.35 E+2	1.13 ± 0.37 E+2	2.04 ± 0.67 E+1	1.34 ± 0.44 E+2	5.2 ± 1.7 E+1

Radionuclide	1680-4000[a] Particle 7G	1680-4000 Particle 7H	1000-1680[a] Particle 7I	1000-1680[a] Particle 7J	1000-1680 Particle 7K	707-1000[a] Aliquot
^{60}Co	1.26 ± 0.07 E+1	5.23 ± 0.53	5.98 ± 0.42	1.17 ± 0.75 E+1	9.61 ± 0.43	5.43 ± 0.27
^{90}Sr	8.67 ± 1.45 E+3	6.96 ± 0.63 E+3	9.51 ± 0.91 E+3	3.37 ± 0.34 E+3	6.78 ± 0.71 E+3	3.49 ± 0.35 E+3
^{106}Ru	4.49 ± 0.70 E+1	9.13 ± 0.14 E+2	3.93 ± 0.42 E+1	5.76 ± 0.70 E+1	5.06 ± 0.42 E+1	9.74 ± 0.35 E+1
^{125}Sb	1.28 ± 0.33 E+1	7.75 ± 0.51 E+1	1.06 ± 0.15 E+1	2.39 ± 0.39 E+1	1.14 ± 0.16 E+1	8.63 ± 0.11
^{129}I	5.28 ± 1.42 E-5	--[b]	4.77 ± 0.30 E-3	--[b]	8.56 ± 4.34 E-5	--[b]
^{134}Cs	6.66 ± 0.12 E+1	6.61 ± 0.12 E+1	1.33 ± 0.06 E+1	6.49 ± 0.12 E+1	1.18 ± 0.05 E+1	7.63 ± 0.03
^{137}Cs	1.110 ± 0.005 E+3	1.410 ± 0.006 E+3	2.46 ± 0.02 E+2	1.140 ± 0.005 E+3	2.13 ± 0.02 E+2	1.33 ± 0.01 E+3
^{144}Ce	2.64 ± 0.15 E+3	2.64 ± 0.15 E+3	1.58 ± 0.10 E+3	--[b]	--[b]	1.45 ± 0.07 E+3
^{154}Eu	4.60 ± 0.51 E+1	3.78 ± 0.51 E+1	2.76 ± 0.31 E+1	5.52 ± 0.51 E+1	5.31 ± 0.31 E+1	2.72 ± 0.19 E+2
^{155}Eu	1.04 ± 40 E+2	8.8 ± 2.9 E+1	5.8 ± 1.9 E+2	1.22 ± 40 E+2	1.09 ± 0.36 E+2	6.21 ± 0.20 E+1

Radionuclide	297-707 Aliquot	149-297[a] Aliquot	74-149[a] Aliquot	30-74[a] Aliquot	20-30 Aliquot	<20[a] Aliquot
^{60}Co	1.31 ± 0.04 E+1	1.14 ± 0.31 E+2	6.30 ± 0.11 E+1	5.76 ± 0.11 E+1	1.14 ± 0.02 E+2	3.63 ± 0.10 E+2
^{90}Sr	2.74 ± 0.29 E+3	3.71 ± 0.34 E+3	5.39 ± 0.67 E+3	--[b]	3.29 ± 0.25 E+3	3.04 ± 0.30 E+3
^{106}Ru	3.65 ± 0.14 E+1	2.95 ± 1.47 E+2	1.49 ± 0.05 E+2	1.21 ± 0.07 E+2	8.29 ± 0.14 E+2	1.74 ± 0.05 E+2
^{125}Sb	1.59 ± 0.10 E+1	1.23 ± 0.06 E+2	1.21 ± 0.03 E+2	7.70 ± 0.35 E+1	--[b]	3.23 ± 0.23 E+2
^{129}I	--[b]	2.25 ± 0.30 E-4	4.56 ± 1.33 E-4	--[b]	4.57 ± 0.48 E-4	--[b]
^{134}Cs	4.84 ± 0.24	7.44 ± 0.18 E+1	4.75 ± 0.09 E+1	2.49 ± 0.09 E+1	3.90 ± 0.12 E+1	1.63 ± 0.71 E+1
^{137}Cs	1.09 ± 0.08 E+2	1.46 ± 0.01 E+3	9.07 ± 0.03 E+2	4.76 ± 0.03 E+2	7.75 ± 0.04 E+2	3.32 ± 0.02 E+2
^{144}Ce	1.07 ± 0.06 E+3	2.79 ± 0.22 E+3	1.63 ± 0.11 E+3	1.01 ± 0.12 E+3	2.17 ± 0.15 E+3	9.63 ± 1.09 E+2
^{154}Eu	1.84 ± 0.10 E+1	5.20 ± 0.76 E+1	2.86 ± 0.31 E+1	2.04 ± 0.41 E+1	3.58 ± 0.51 E+1	1.63 ± 0.31 E+1
^{155}Eu	4.2 ± 1.4 E+1	1.05 ± 0.34 E+2	5.3 ± 1.7 E-1	3.3 ± 1.1 E+1	7.5 ± 2.5 E+1	3.3 ± 1.1 E+1

a. Uncertainty is ±30% because of problems associated with the analysis.

b. Not detected.

TABLE E-7. RESULTS OF GAMMA SPECTROSCOPY ANALYSIS OF SAMPLE 8
(μCi/g sample)

Radionuclide	Particle Size Fraction (μm) >4000[a] Particle 9A	>4000 Particle 9B	>4000[a] Particle 9C	>4000 Particle 9D	>4000 Particle 9E	1680-4000 Particle 9F
^{60}Co	5.55 ± 0.11 E+1	--[b]	6.72 ± 0.43	9.18 ± 0.43	5.15 ± 0.08 E+1	2.54 ± 0.05 E+1
^{90}Sr	5.67 ± 0.61 E+3	--[b]	1.37 ± 0.15 E+4	--[c]	5.31 ± 0.51 E+3	1.59 ± 0.14 E+3
^{106}Ru	8.29 ± 0.14 E+2	--[b]	4.35 ± 0.56 E+1	3.370 ± 0.004 E+3	6.60 ± 0.28 E+1	1.97 ± 0.14 E+1
^{125}Sb	--[c]	--[b]	2.09 ± 0.26 E+1	2.11 ± 0.24 E+1	3.23 ± 0.15 E+1	5.37 ± 0.67
^{129}I	--[c]	--[b]	--[c]	--[c]	--[c]	--[c]
^{134}Cs	5.19 ± 0.12 E+1	--[b]	4.98 ± 0.11 E+1	5.60 ± 0.09 E+1	1.06 ± 0.03 E+1	1.64 ± 0.12
^{137}Cs	9.85 ± 0.04 E+2	--[b]	8.93 ± 0.04 E+2	9.85 ± 0.03 E+2	2.84 ± 0.01 E+2	3.67 ± 0.04 E+1
^{144}Ce	3.26 ± 0.15 E+3	--[b]	2.02 ± 0.15 E+3	2.95 ± 0.15 E+3	1.65 ± 0.09 E+3	9.94 ± 0.62 E+2
^{154}Eu	5.41 ± 0.51 E+1	--[b]	3.98 ± 0.31 E+1	5.41 ± 0.31 E+1	1.33 ± 0.20 E+1	1.43 ± 0.10 E+1
^{155}Eu	--[c]	--[b]	7.7 ± 2.5 E+1	1.13 ± 0.37 E+2	6.7 ± 2.2 E+1	5.7 ± 1.9 E+1

Radionuclide	1680-4000[a] Particle 8G	1680-4000 Particle 8H	1000-1680[a] Particle 8I	1000-1680[a] Particle 8J	1000-1680 Particle 8K	707-1000 Aliquot
^{60}Co	6.40 ± 0.75	3.95 ± 0.11 E+1	1.53 ± 0.14 E+1	12.3 ± 0.4 E+1	1.07 ± 0.05 E+1	5.14 ± 0.08 E+1
^{90}Sr	9.62 ± 1.01 E+3	5.47 ± 0.61 E+3	1.29 ± 0.09 E+3	8.10 ± 0.81 E+3	1.03 ± 0.10 E+4	2.43 ± 0.20 E+3
^{106}Ru	7.44 ± 1.26 E+1	9.41 ± 0.14 E+2	8.88 ± 1.92 E+1	7.3 ± 1.7	3.51 ± 0.42 E+1	5.76 ± 0.28 E+1
^{125}Sb	5.36 ± 0.66 E+1	5.72 ± 0.32 E+1	3.82 ± 0.91 E+1	6.15 ± 0.91	1.87 ± 0.26 E+1	2.49 ± 0.15 E+1
^{129}I	3.83 ± 1.34 E-4	--[c]	5.08 ± 1.86 E-5	--[c]	--[c]	--[c]
^{134}Cs	1.31 ± 0.02 E+2	1.25 ± 0.71 E+1	1.36 ± 0.03 E+2	1.37 ± 0.03 E+1	3.00 ± 0.82 E+1	7.32 ± 0.35
^{137}Cs	2.350 ± 0.009 E+3	2.07 ± 0.02 E+2	2.51 ± 0.13 E+3	2.54 ± 0.01 E+2	5.28 ± 0.03 E+2	1.80 ± 0.01 E+2
^{144}Ce	3.11 ± 0.31 E+3	3.73 ± 0.15 E+3	2.54 ± 0.5 E+3	5.28 ± 0.62 E+2	2.48 ± 0.15 E+3	1.54 ± 0.09 E+3
^{154}Eu	5.41 ± 0.61 E+1	6.84 ± 0.51 E+1	1.18 ± 0.11 E+2	8.27 ± 0.12	4.70 ± 0.41 E+1	2.55 ± 0.20 E+1
^{155}Eu	1.15 ± 0.38 E+2	1.47 ± 0.48 E+2	3.11 ± 1.02 E+2	1.56 ± 0.52 E+1	1.00 ± 0.33 E+2	6.6 ± 2.2 E+1

Radionuclide	297-707[a] Aliquot	149-297 Aliquot	74-149 Aliquot	30-74 Aliquot	20-30[a] Aliquot	<20 Aliquot	Sweepings[a]
^{60}Co	2.63 ± 0.53 E+1	4.48 ± 0.11 E+1	9.39 ± 0.21 E+1	8.86 ± 0.10 E+1	8.85 ± 0.15	7.68 ± 0.21 E+1	8.22 ± 0.21
^{90}Sr	4.81 ± 0.51 E+3	3.26 ± 0.34 E+3	5.45 ± 0.57 E+3	5.74 ± 0.67 E+3	1.52 ± 0.10 E+4	3.85 ± 0.40 E+3	7.84 ± 0.76 E+3
^{106}Ru	4.78 ± 0.28 E+1	1.62 ± 0.07 E+2	1.29 ± 0.01 E+3	1.77 ± 0.06 E+2	2.92 ± 0.01 E+1	4.49 ± 0.11 E+2	6.46 ± 0.14 E+1
^{125}Sb	6.05 ± 0.73	9.43 ± 0.36 E+1	3.18 ± 0.06 E+2	1.59 ± 0.03 E+2	--[c]	1.75 ± 0.05 E+2	1.04 ± 0.07 E+1
^{129}I	--[c]	--[c]	1.89 ± 0.07 E-3	1.26 ± 0.12 E-3	1.80 ± 0.29 E-3	6.81 ± 0.38 E-4	--[c]
^{134}Cs	3.66 ± 0.24	2.92 ± 0.09 E+1	4.60 ± 0.12 E+1	3.79 ± 0.08 E+1	4.30 ± 0.01	7.32 ± 0.12 E+1	8.38 ± 0.24
^{137}Cs	6.60 ± 0.06 E+1	5.69 ± 0.03 E+2	9.65 ± 0.04 E+2	7.70 ± 0.03 E+2	8.950 ± 0.004 E+1	1.780 ± 0.006 E+3	1.700 ± 0.009 E+2
^{144}Ce	1.30 ± 0.08 E+3	1.37 ± 0.12 E+3	1.85 ± 0.14 E+3	1.37 ± 0.11 E+3	1.57 ± 1.33 E+2	2.02 ± 0.15 E+3	5.12 ± 0.31 E+2
^{154}Eu	2.55 ± 0.20 E+1	2.15 ± 0.41 E+1	3.47 ± 0.41 E+1	2.15 ± 0.31 E+1	2.92 ± 0.43	3.06 ± 0.51 E+1	9.30 ± 1.02
^{155}Eu	5.3 ± 1.7 E+1	4.8 ± 1.6 E+1	7.5 ± 2.5 E+1	4.6 ± 1.5 E+1	--[c]	6.8 ± 2.2 E+1	2.02 ± 0.66 E+1

a. Uncertainty is ~30% because of problems associated with the analysis.

b. Not reported because of problems associated with the analysis.

c. Not detected.

TABLE E-8. RESULTS OF RADIONUCLIDE ANALYSIS OF SAMPLE 9
(μCi/g sample)

Radionuclide	Particle Size Fraction (μm)					
	<4000 Particle 9A	>4000 Particle 9B	>4000 Particle 9C	>4000 Particle 9D	>4000 Particle 9E	1680-4000 Particle 9F
^{60}Co	4.41 ± 0.07 E+1	9.60 ± 0.93 E+1	3.42 ± 0.11 E+1	8.86 ± 0.43 E+1	5.72 ± 0.16 E+1	4.48 ± 0.07 E+1
^{90}Sr	5.57 ± 0.51 E+3	6.13 ± 0.61 E+3	4.69 ± 0.45 E+2	1.85 ± 0.17 E+3	1.14 ± 0.10 E+4	6.36 ± 0.67 E+3
^{106}Ru	5.21 ± 0.03 E+3	2.54 ± 0.06 E+2	1.04 ± 0.01 E+3	4.65 ± 0.03 E+4	7.91 ± 0.02 E+3	4.96 ± 0.08 E+2
^{125}Sb	1.08 ± 0.11 E+1	7.81 ± 1.48	7.42 ± 0.40 E+1	5.64 ± 0.06 E+3	6.68 ± 0.44 E+1	1.30 ± 0.30 E+1
^{129}I	9.23 ± 1.35 E-4	--[a]	--[a]	3.70 ± 0.06 E-3	--[a]	--[a]
^{134}Cs	3.30 ± 0.28	5.42 ± 0.40	1.58 ± 0.08 E+1	--[a]	2.08 ± 0.10 E+1	1.37 ± 0.06 E+1
^{137}Cs	5.70 ± 0.59 E+1	9.77 ± 0.08 E+1	2.65 ± 0.02 E+2	1.52 ± 0.30 E+1	3.50 ± 0.02 E+2	2.61 ± 0.02 E+2
^{144}Ce	2.17 ± 0.11 E+3	1.94 ± 0.10 E+3	3.57 ± 0.15 E+3	--[a]	3.73 ± 0.25 E+3	2.79 ± 0.02 E+3
^{154}Eu	3.71 ± 0.24 E+1	2.60 ± 0.02 E+1	5.72 ± 0.51 E+1	--[a]	6.86 ± 0.73 E+1	4.29 ± 0.41 E+1
^{155}Eu	7.84 ± 2.59 E+1	7.48 ± 2.46 E+1	1.51 ± 0.50 E+2	--[a]	1.48 ± 0.48 E+2	1.17 ± 0.39 E+2
	1680-4000 Particle 9G	1680-4000 Particle 9H	1000-1680 Particle 9I	1000-1680 Particle 9J	1000-1680 Particle 9K	707-1000 Aliquot
^{60}Co	5.76 ± 0.24 E+1	1.94 ± 0.07 E+1	8.00 ± 0.01 E+1	2.77 ± 0.11 E+1	--[c]	6.62 ± 0.21
^{90}Sr	1.60 ± 0.16 E+3	2.93 ± 0.34 E+3	1.08 ± 0.11 E+3	5.45 ± 0.57 E+3	--[c]	4.18 ± 0.38 E+3
^{106}Ru	1.77 ± 0.01 E+4	3.55 ± 0.93 E+2	9.69 ± 0.14 E+2	1.67 ± 0.03 E+3	--[c]	3.93 ± 0.14 E+3
^{125}Sb	1.61 ± 0.02 E+3	1.29 ± 0.18 E+1	--[a]	--[a]	--[c]	2.71 ± 0.11 E+1
^{129}I	1.12 ± 0.44 E-3	--[a]	--[a]	--[a]	--[c]	--[a]
^{134}Cs	--[a]	4.46 ± 0.53	4.01 ± 0.83	3.42 ± 0.12 E+1	--[c]	9.68 ± 0.24
^{137}Cs	2.71 ± 1.17 E+1	7.97 ± 0.11 E+1	6.07 ± 0.10 E+1	6.40 ± 0.04 E+2	--[c]	1.780 ± 0.009 E+3
^{144}Ce	--[a]	1.65 ± 0.14 E+3	--[a]	4.97 ± 0.31 E+3	--[c]	1.61 ± 0.08 E+3
^{154}Eu	--[a]	2.95 ± 2.04 E+1	7.76 ± 0.71 E+1	8.48 ± 0.61 E+1	--[c]	2.76 ± 0.20 E+2
^{155}Eu	--[a]	6.48 ± 2.73 E+1	--[a]	--[a]	--[c]	6.1 ± 2.0 E+1
	297-707[b] Aliquot	149-297[b] Aliquot	74-149[b] Aliquot	30-74 Aliquot	20-30 Aliquot	<20 Aliquot
^{60}Co	4.70 ± 0.21 E+1	4.03 ± 0.06 E+1	1.71 ± 0.03 E+1	1.07 ± 0.07 E+3	6.03 ± 0.08 E+1	7.04 ± 0.21 E+1
^{90}Sr	3.74 ± 0.40 E+3	6.07 ± 0.51 E+3	2.89 ± 0.29 E+3	2.89 ± 0.29 E+3	2.28 ± 0.23 E+3	4.55 ± 0.51 E+3
^{106}Ru	7.72 ± 1.69 E+1	7.44 ± 0.28 E+1	5.71 ± 2.00 E+1	4.45 ± 0.07 E+2	2.05 ± 0.04 E+2	4.49 ± 0.24 E+2
^{125}Sb	--[a]	--[a]	4.29 ± 0.11 E+1	1.49 ± 0.03 E+2	1.03 ± 0.01 E+2	--[a]
^{129}I	--[a]	--[a]	--[a]	--[a]	--[a]	1.06 ± 0.50 E-3
^{134}Cs	3.16 ± 0.05 E+1	2.01 ± 0.03 E+1	1.14 ± 0.30 E+1	3.46 ± 0.07 E+1	3.52 ± 0.06 E+1	8.85 ± 0.23 E+1
^{137}Cs	5.98 ± 0.02 E+2	3.87 ± 0.01 E+2	2.35 ± 0.04 E+2	7.06 ± 0.03 E+2	7.87 ± 0.02 E+2	2.140 ± 0.008 E+3
^{144}Ce	7.30 ± 1.55 E+2	7.30 ± 0.47 E+2	4.71 ± 0.40 E+2	1.10 ± 0.01 E+3	9.78 ± 0.62 E+2	2.17 ± 0.15 E+3
^{154}Eu	1.33 ± 0.31 E+1	1.32 ± 0.10 E+1	8.17 ± 1.17	2.25 ± 0.31 E+1	1.33 ± 0.20 E+1	2.86 ± 0.51 E+1
^{155}Eu	2.68 ± 0.88 E+1	2.40 ± 0.79 E+1	1.54 ± 0.51 E+1	5.40 ± 1.80 E+1	3.2 ± 1.1 E+1	7.7 ± 2.5 E+1

a. Not detected.

b. Associated uncertainty is 30-50%.

c. Not reported because of problems associated with the analysis.

TABLE E-9. RESULTS OF RADIONUCLIDE ANALYSIS OF SAMPLE 10
(μCi/g sample)

Radionuclide	Particle Size Fraction (μm) >4000 Particle 10A	>4000 Particle 10B	>4000 Particle 10C	>4000 Particle 10D	>4000 Particle 10E	1680-4000[a] Particle 10F
^{60}Co	9.07 ± 0.53	1.95 ± 0.08 E+1	--[b]	--[c]	1.28 ± 0.11 E+1	9.60 ± 0.45
^{90}Sr	2.22 ± 0.23 E+4	9.67 ± 0.92 E+3	6.19 ± 0.60 E+3	--[c]	4.62 ± 0.53 E+3	1.59 ± 0.76 E+3
^{106}Ru	6.76 ± 0.11 E+2	8.57 ± 0.14 E+2	5.62 ± 0.28 E+2	--[c]	1.36 ± 0.03 E+3	7.37 ± 0.10 E+2
^{125}Sb	2.91 ± 0.24 E+1	5.40 ± 0.37 E+1	9.94 ± 0.93 E+1	--[c]	2.24 ± 0.13 E+2	4.85 ± 0.24 E+1
^{129}I	--[b]	7.53 ± 0.48 E-5	1.32 ± 0.11 E-3	--[c]	9.25 ± 0.12 E-4	--[b]
^{134}Cs	1.12 ± 0.05 E+1	1.39 ± 0.08 E+1	1.57 ± 0.02 E+2	--[c]	2.55 ± 0.05 E+2	1.08 ± 0.07 E+1
^{137}Cs	2.50 ± 0.02 E+2	2.63 ± 0.02 E+2	4.38 ± 0.01 E+3	--[c]	4.00 ± 0.01 E+3	1.84 ± 0.01 E+2
^{144}Ce	2.03 ± 0.14 E+3	2.95 ± 0.15 E+3	1.86 ± 0.15 E+3	--[c]	3.88 ± 0.31 E+3	2.21 ± 0.11 E+3
^{154}Eu	2.86 ± 0.81 E+1	4.39 ± 0.51 E+1	1.74 ± 0.31 E+1	--[c]	7.46 ± 1.02 E+1	3.91 ± 0.31 E+1
^{155}Eu	1.31 ± 0.43 E+2	1.52 ± 0.50 E+2	5.7 ± 1.9 E+1	--[c]	1.66 ± 0.55 E+2	1.01 ± 0.16 E+2

Radionuclide	1680-4000 Particle 10G	1680-4000 Particle 10H	1000-1680[a] Particle 10I	1000-1680[a] Particle 10J	1000-1680[a] Particle 10K	707-1000 Aliquot
^{60}Co	--[c]	3.63 ± 0.11 E+1	6.65 ± 0.35 E+1	1.28 ± 0.04 E+1	7.04 ± 0.21 E+1	3.35 ± 0.96 E+1
^{90}Sr	--[c]	9.11 ± 1.01 E+3	2.33 ± 0.20 E+3	2.63 ± 0.30 E+3	1.23 ± 0.11 E+4	5.78 ± 0.58 E+3
^{106}Ru	--[c]	6.94 ± 0.13 E+2	3.15 ± 0.07 E+1	5.75 ± 0.05 E+2	1.19 ± 0.01 E+3	4.19 ± 1.12 E+2
^{125}Sb	--[c]	2.75 ± 0.27 E+1	5.90 ± 1.80 E+1	2.68 ± 0.13 E+1	1.49 ± 0.05 E+2	3.29 ± 0.31 E+1
^{129}I	--[c]	8.59 ± 1.63 E-5	--[b]	1.16 ± 0.54 E-4	--[b]	--[b]
^{134}Cs	--[c]	8.38 ± 0.59	1.36 ± 0.17	7.60 ± 0.03	1.79 ± 0.09 E+1	3.49 ± 0.11 E+1
^{137}Cs	--[c]	1.63 ± 0.02 E+2	2.37 ± 0.01 E+1	1.45 ± 0.01 E+2	3.15 ± 0.03 E+2	8.07 ± 0.03 E+2
^{144}Ce	--[c]	3.26 ± 0.15 E+3	1.16 ± 0.07 E+3	1.47 ± 0.07 E+3	3.11 ± 0.15 E+3	1.88 ± 0.14 E+3
^{154}Eu	--[c]	4.70 ± 0.41 E+1	1.79 ± 0.41 E+1	2.40 ± 2.05 E+1	4.80 ± 0.41 E+1	2.45 ± 0.41 E+1
^{155}Eu	--[c]	1.43 ± 0.47 E+2	5.60 ± 1.85 E+1	7.10 ± 2.35 E+2	1.48 ± 0.49 E+2	7.4 ± 2.4 E+1

Radionuclide	297-707 Aliquot	149-297 Aliquot	74-149 Aliquot	30-74 Aliquot	<30 Aliquot	Sweepings[a]
^{60}Co	3.54 ± 0.06 E+1	4.27 ± 0.11 E+1	4.83 ± 0.08 E+1	9.07 ± 0.21 E+1	9.18 ± 0.21 E+1	1.55 ± 0.02 E+1
^{90}Sr	3.29 ± 0.38 E+3	2.23 ± 0.20 E+3	2.17 ± 0.29 E+3	3.42 ± 0.32 E+3	5.86 ± 0.58 E+3	6.07 ± 0.68 E+3
^{106}Ru	3.03 ± 0.04 E+2	1.57 ± 0.07 E+2	2.40 ± 0.06 E+2	5.27 ± 0.11 E+2	8.57 ± 0.14 E+2	6.46 ± 0.14 E+1
^{125}Sb	2.42 ± 0.01 E+2	8.87 ± 0.34 E+1	--[b]	1.06 ± 0.04 E+2	--[b]	2.75 ± 0.07 E+1
^{129}I	1.69 ± 0.54 E-4	3.69 ± 1.07 E-4	--[b]	2.98 ± 2.23 E-4	5.05 ± 1.70 E-4	9.23 ± 1.35 E-4
^{134}Cs	1.59 ± 0.06 E+1	3.20 ± 0.09 E+1	2.11 ± 0.59 E+1	3.52 ± 0.11 E+1	3.55 ± 0.11 E+1	7.56 ± 0.12
^{137}Cs	3.04 ± 0.01 E+2	6.71 ± 0.03 E+2	4.30 ± 0.02 E+2	7.20 ± 0.40 E+2	7.77 ± 0.40 E+2	1.71 ± 0.61 E+2
^{144}Ce	1.53 ± 0.07 E+3	8.85 ± 0.93 E+2	--[b]	1.86 ± 0.15 E+3	2.17 ± 0.15 E+3	3.57 ± 0.15 E+2
^{154}Eu	2.11 ± 0.50 E+1	1.23 ± 0.31 E+1	2.15 ± 0.20 E+1	2.76 ± 0.41 E+1	3.68 ± 0.51 E+1	5.21 ± 0.71
^{155}Eu	5.25 ± 1.75 E+1	2.96 ± 0.97 E+1	--[b]	6.9 ± 2.3 E+1	7.5 ± 2.5 E+1	1.17 ± 0.39 E+1

a. Uncertainty is 30 to 50% because of problems associated with the analysis.

b. Not detected.

c. Not reported because of problems associated with the analysis.

TABLE E-10. RESULTS OF RADIONUCLIDE ANALYSIS OF SAMPLE 11
(μCi/g sample)

Radionuclide	Particle Size Fraction (μm)					
	>4000 Particle 11A	>4000 Particle 11B	>4000 Particle 11C	>4000 Particle 11D	>4000[a] Particle 11E	1680-4000[a] Particle 11F
^{60}Co	2.73 ± 0.05 E+1	1.98 ± 0.05 E+1	--[b]	--[b]	--[c]	1.94 ± 0.06 E+1
^{90}Sr	3.37 ± 0.34 E+2	3.74 ± 0.40 E+4	--[b]	--[b]	2.46 ± 0.29 E+3	2.94 ± 0.03 E+4
^{106}Ru	4.37 ± 0.06	2.49 ± 0.04 E+2	--[b]	--[b]	2.16 ± 0.08 E+2	2.66 ± 0.06 E+2
^{125}Sb	9.18 ± 0.17	2.10 ± 0.10 E+1	--[b]	--[b]	4.02 ± 0.28 E+1	3.19 ± 0.16 E+1
^{129}I	--[c]	--[c]	--[b]	--[b]	5.05 ± 0.40 E-4	2.57 ± 1.12 E-5
^{134}Cs	2.95 ± 0.24 E+1	9.21 ± 0.35	--[b]	--[b]	3.23 ± 0.08 E+1	1.10 ± 0.05 E+1
^{137}Cs	1.040 ± 0.007 E+1	1.73 ± 0.01 E+2	--[b]	--[b]	1.850 ± 0.005 E+3	2.14 ± 0.01 E+2
^{144}Ce	1.46 ± 0.07 E+1	1.06 ± 0.06 E+3	--[b]	--[b]	--[c]	1.32 ± 0.08 E+3
^{154}Eu	1.02 ± 0.10	8.0 ± 1.4	--[b]	--[b]	--[c]	7.35 ± 1.55
^{155}Eu	--[b]	--[b]	--[b]	--[b]	3.66 ± 1.20 E+1	--[b]
	1680-4000 Particle 11G	1680-4000 Particle 11H	1000-1680 Particle 11I	1000-1680 Particle 11J	1000-1680 Particle 11K	707-1000[a] Aliquot
^{60}Co	--[c]	1.60 ± 0.32 E-1	7.26 ± 0.32	--[c]	9.61 ± 0.53	1.14 ± 0.14
^{90}Sr	9.31 ± 0.91 E+3	1.40 ± 0.13 E+4	4.89 ± 0.51 E+3	7.64 ± 0.74 E+3	5.06 ± 0.58 E+3	6.41 ± 0.67 E+2
^{106}Ru	9.13 ± 0.14 E+2	6.74 ± 0.14 E+2	3.79 ± 0.05 E+2	1.56 ± 0.05 E+3	4.65 ± 0.08 E+2	2.43 ± 0.84
^{125}Sb	--[c]	4.11 ± 0.42 E+1	--[c]	2.48 ± 0.20 [illegible]	6.61 ± 0.25 E+1	3.00 ± 0.53
^{129}I	3.72 ± 0.28 E-4	4.44 ± 0.32 E-4	--[c]	--[c]	1.73 ± 0.51 E-4	--[c]
^{134}Cs	6.14 ± 0.12 E+1	2.95 ± 0.12 E+1	1.89 ± 0.23	5.08 ± 0.83 E+2	9.92 ± 0.42	1.02 ± 0.16
^{137}Cs	1.640 ± 0.007 E+3	6.96 ± 0.05 E+2	3.48 ± 0.51 E+1	9.28 ± 0.03 E+3	3.03 ± 0.02 E+2	2.17 ± 0.05 E+1
^{144}Ce	2.64 ± 0.15 E+3	2.02 ± 0.15 E+3	2.30 ± 0.11	3.26 ± 0.47 E+3	--[c]	--[c]
^{154}Eu	3.47 ± 0.51 E+1	2.04 ± 0.41 E+1	4.80 ± 0.20 E+1	6.01 ± 0.01 E+1	1.33 ± 0.10 E+1	--[c]
^{155}Eu	--[c]	8.7 ± 2.8 E+1	--[c]	--[c]	--[b]	--[c]
	297-707[a] Aliquot	149-297 Aliquot	74-149 Aliquot	30-74 Aliquot	<30 Aliquot	Sweepings[a]
^{60}Co	6.40 ± 0.21	1.01 ± 0.02 E+2	8.86 ± 0.21 E+1	1.59 ± 0.03 E+2	2.61 ± 0.04 E+2	3.12 ± 0.53 E+1
^{90}Sr	--[b]	6.33 ± 0.76 E+3	3.04 ± 0.29 E+3	3.64 ± 0.40 E+3	4.05 ± 0.34 E+3	7.09 ± 0.67 E+3
^{106}Ru	8.15 ± 0.28 E+1	4.42 ± 0.09 E+2	3.05 ± 0.10 E+2	8.57 ± 0.13 E+2	5.90 ± 0.14 E+2	1.54 ± 0.04 E+2
^{125}Sb	1.23 ± 0.08 E+1	1.10 ± 0.04 E+2	1.81 ± 0.05 E+2	2.01 ± 0.07 E+2	3.83 ± 0.11 E+2	8.26 ± 0.18 E+1
^{129}I	--[c]	--[c]	5.43 ± 0.53 E-4	2.6 ± 1.1 E-5	1.17 ± 0.11 E-3	6.05 ± 1.90 E-3
^{134}Cs	5.31 ± 0.36	4.60 ± 0.11 E+1	5.90 ± 0.12 E+1	3.90 ± 0.12 E+1	5.08 ± 0.24 E+1	2.67 ± 0.05 E+1
^{137}Cs	1.010 ± 0.007 E+2	1.020 ± 0.004 E+3	1.240 ± 0.005 E+3	8.42 ± 0.06 E+2	1.100 ± 0.007 E+3	4.98 ± 0.02 E+2
^{144}Ce	9.47 ± 0.47 E+2	--[c]	1.54 ± 0.14 E+3	1.38 ± 0.15 E+3	1.29 ± 0.20 E+3	1.15 ± 0.06 E+3
^{154}Eu	1.74 ± 0.10 E+1	2.25 ± 0.41 E+1	2.35 ± 0.41 E+1	1.43 ± 0.61 E+1	1.43 ± 0.61 E+1	1.43 ± 0.20 E+1
^{155}Eu	3.9 ± 1.3 E-1	5.3 ± 1.7 E+1	5.8 ± 1.9 E+1	4.8 ± 1.65 E+1	4.9 ± 1.6 E+1	5.9 ± 1.7 E+1

a. Uncertainty is 30 to 50% because of problems associated with the analysis.

b. Not reported because of problems associated with the analysis.

c. Not detected.

TABLE E-11. FISSILE/FERTILE MATERIAL CONTENT OF TMI-2 CORE DEBRIS GRAB SAMPLES

Particle Size Fraction (μm)	Particle/Aliquot	Fissile (mg)	Fertile (mg)	Enrichment (wt%)	Particle/Aliquot Weight (mg)
Sample 1					
>4000	Particle 1A	2.4 ± 0.1 E-1	7.5 ± 0.1	3.0 ± 0.4	84
>4000	Particle 1B	2.2 ± 0.1 E-1	1.10 ± 0.07 E+1	2.0 ± 0.2	15
>4000	Particle 1C	1.4 ± 0.1 E-1	5.2 ± 0.9	2.6 ± 0.5	15
>4000	Particle 1D	1.4 ± 0.1 E-1	5.4 ± 1.0	2.4 ± 0.5	7
>4000	Particle 1E	1.4 ± 0.1 E-1	5.0 ± 0.9	2.6 ± 0.5	29
1680-4000	Particle 1F	2.6 ± 0.1 E-1	1.08 ± 0.09 E+1	2.3 ± 0.2	20
1680-4000	Particle 1G	1.6 ± 0.1 E-1	7.9 ± 1.0	2.0 ± 0.3	15
1680-4000	Particle 1H	4.2 ± 0.2 E-1	1.5 ± 0.1 E+1	2.7 ± 0.2	33
1000-1680	Particle 1I	--[a]	--[a]	--[a]	--[a]
1000-1680	Particle 1J	3.2 ± 0.1 E-1	1.48 ± 0.9 E+1	2.2 ± 0.2	24
1000-1680	Particle 1K	2.5 ± 0.1 E-1	9.8 ± 0.09	2.4 ± 0.3	19
707-1000	Aliquot	3.7 ± 0.1 E-1	1.68 ± 0.09 E+1	2.2 ± 0.2	26
297-707	Aliquot	4.0 ± 0.2 E-1	1.65 ± 0.09 E+1	2.4 ± 0.2	35
149-297	Aliquot	2.1 ± 0.2 E-1	8.8 ± 0.9	2.3 ± 0.3	23
74-149	Aliquot	1.2 ± 0.1 E-1	4.8 ± 0.8	2.2 ± 0.4	12
30-74	Aliquot	7.5 ± 0.1 E-2	3.2 ± 0.8	2.3 ± 0.7	10
Sample 3					
>4000	Particle 3A	6.2 ± 0.4 E-1	2.2 ± 0.1 E+1	2.7 ± 0.2	56
>4000	Particle 3B	<1.6 E-2	<0.7	--	23
>4000	Particle 3C	--[a]	--[a]	--[a]	39
>4000	Particle 3D	1.9 ± 0.03	8.3 ± 0.3 E+1	2.23 ± 0.06	97
>4000	Particle 3E	1.3 ± 0.02	5.8 ± 0.2 E+1	2.2 ± 0.1	69
1680-4000	Particle 3F	3.8 ± 0.1 E-1	--[b]	--[b]	15
1680-4000	Particle 3G	8.2 ± 0.1 E-2	2.8[c]	2.8	10
1680-4000	Particle 3H	9.8 ± 0.1 E-2	4.8 ± 1.0	2.0 ± 0.5	14
1000-1680	Particle 3I	4.6 ± 0.1 E-1	--[b]	--[b]	25
1000-1680	Particle 3J	1.1 ± 0.1 E-1	3.9 ± 0.8	2.7 ± 0.6	17
1000-1680	Particle 3K	6.4 ± 0.2 E-1	2.9 ± 0.1 E+1	2.2 ± 0.1	45
707-1000	Aliquot	4.3 ± 0.1 E-1	1.9 E+1[c]	2.3[c]	30
297-707	Aliquot	2.2 ± 0.1 E-1	8.7[c]	2.4[c]	18
149-297	Aliquot	1.15 ± 0.02	--[b]	--[b]	114
74-149	Aliquot	1.7 ± 0.1 E-1	7.0[c]	2.3	22
30-74	Aliquot	1.8 ± 0.1 E-1	6.4 ± 1.0	2.6 ± 0.4	25
20-30	Aliquot	1.5 ± 1.2 E-2	<1	--[b]	4

TABLE E-11. (continued)

Particle Size Fraction (μm)	Particle/Aliquot	Fissile (mg)	Fertile (mg)	Enrichment (wt%)	Particle/Aliquot Weight (mg)
Sample 4					
>4000	Particle 4A	4.6 ± 0.2 E-1	1.86 E+1[c]	2.4[c]	22
>4000	Particle 4B	2.1 ± 0.2 E-1	5.6 ± 0.9	3.6 ± 0.6	7
>4000	Particle 4C	5.9 ± 0.1 E-1	1.93 E+1[c]	3.0[c]	38
>4000	Particle 4D	2.8 ± 0.1 E-1	1.05 E+1[c]	2.6[c]	14
>4000	Particle 4E	3.2 ± 0.1 E-1	1.4 E+1[c]	2.2[c]	15
Sample 5					
>4000	Particle 5A	2.3 ± 0.1 E-1	8.7 ± 1.0	2.6 ± 0.3	11
>4000	Particle 5B	5.5 ± 0.2 E-1	2.4 ± 0.1 E+1	2.3 ± 0.1	26
>4000	Particle 5C	5.3 ± 0.1 E-1	1.9 E+1[c]	2.66[c]	24
>4000	Particle 5D	5.4 ± 0.1 E-1	1.9 E+1[c]	2.75[c]	27
>4000	Particle 5E	2.3 ± 0.1 E-1	7.4 ± 0.9	3.1 ± 0.4	21
1680-4000	Particle 5F	6.5 ± 0.3 E-1	2.2 ± 0.1 E+1	2.9 ± 0.2	39
1680-4000	Particle 5G	--[a]	--[a]	--[a]	89
1000-1680	Particle 5H	<0.1	--[a]	--[a]	6
1000-1680	Particle 5I	4.1 ± 0.1 E-1	1.7 E+1[b]	2.4[b]	37
1000-1680	Particle 5J	--[a]	--[a]	--[a]	24
<1000	Aliquot	8.1 ± 0.2 E-1	2.8 ± 0.1 E+1	2.8 ± 0.1	43
Sample 6					
<4000	Particle 6A	4.5 ± 0.2 E-1	1.2 ± 0.1 E+1	2.9 ± 0.2	12
<4000	Particle 6B	<0.01	<1	--[a]	65
<4000	Particle 6C	5.7 ± 0.1 E-1	<1	--[a]	40
<4000	Particle 6D	5.6 ± 0.1 E-1	1.9 ± 0.1 E+1	2.8 ± 0.2	25
<4000	Particle 6E	<0.01	<1	--[a]	26
1680-4000	Particle 6F	<0.01	<1	--[a]	33
1680-4000	Particle 6G	2.16 ± 0.03	7.7 ± 0.2 E+1	2.7 ± 0.1	94
1680-4000	Particle 6H	2.43 ± 0.03	9.1 ± 0.2 E+1	2.6 ± 0.1	101
1000-1680	Particle 6I	1.2 ± 0.1 E-1	3.3 ± 0.8	3.4 ± 0.9	41
1000-1680	Particle 6J	2.8 ± 0.1 E-1	8.7 ± 0.9	3.1 ± 0.4	71
1000-1680	Particle 6K	9.2 ± 0.2 E-1	3.3 ± 0.1 E+1	2.7 ± 0.1	43
707-1000	Aliquot	2.08 ± 0.02	8.1 ± 0.2 E+1	2.5 ± 0.1	139
297-707	Aliquot	1.72 ± 0.03	7.3 ± 0.2 E+1	2.3 ± 0.1	130
149-297	Aliquot	1.36 ± 0.05	5.1 ± 0.2 E+1	2.6 ± 0.1	135
74-149	Aliquot	7.9 ± 0.02 E-1	3.3 ± 0.1 E+1	2.3 ± 0.1	87
30-74	Aliquot	1.5 ± 0.1 E-1	5.1 ± 0.9	2.9 ± 0.5	22

TABLE E-11. (continued)

Particle Size Fraction (μm)	Particle/Aliquot	Fissile (mg)	Fertile (mg)	Enrichment (wt%)	Particle/Aliquot Weight (mg)
Sample 7					
>4000	Particle 7A	1.1 ± 0.1 E-1	4.8 ± 0.8	2.2 ± 0.4	7
>4000	Particle 7B	2.4 ± 0.1 E-1	9.2 ± 0.8	2.5 ± 0.2	11
>4000	Particle 7C	1.1 ± 0.1 E-1	4.6 ± 0.7	2.2 ± 0.4	6
>4000	Particle 7D	--[c]	--[c]	--[c]	11
>4000	Particle 7E	9.1 ± 0.1 E-2	1.7 ± 0.7	4.9 ± 1.9	4
1680-4000	Particle 7F	1.9 ± 0.1 E-2	9.2 ± 6.6 E-1	2.0 ± 0.2	3
1680-4000	Particle 7G	1.8 ± 0.1 E-1	8.5 ± 0.7	2.0 ± 0.2	13
1680-4000	Particle 7H	3.2 ± 0.1 E-1	1.00 ± 0.08 E+1	3.1 ± 0.3	14
1000-1680	Particle 7I	2.6 ± 0.1 E-2	1.5 ± 0.7	1.7 ± 1.1	3
1000-1680	Particle 7J	7.8 ± 0.1 E-2	3.5 ± 0.7	2.2 ± 0.5	5
1000-1680	Particle 7K	1.6 ± 0.1 E-1	6.6 ± 0.7	2.3 ± 0.3	10
707-1000	Aliquot	2.6 ± 0.1 E-1	1.21 ± 0.08 E+1	2.2 ± 0.2	29
297-707	Aliquot	5.2 ± 0.1 E-2	3.6 ± 0.7	1.4 ± 0.4	7
149-297	Aliquot	--[a]	--[a]	--[a]	6
74-149	Aliquot	5.2 ± 0.1 E-2	3.4 ± 0.7	1.5 ± 0.4	4
30-74	Aliquot	1.3 ± 0.1 E-2	1.1 ± 0.7	1.2 ± 1.2	2
20-30	Aliquot	5.4 ± 0.1 E-2	2.4 ± 0.7	2.2 ± 0.8	4
<20	Aliquot	1.6 ± 0.1 E-2	<1	--[a]	2
Sample 8					
>4000	Particle 8A	9.9 ± 0.1 E-2	5.3 ± 0.8	1.8 ± 0.3	13
>4000	Particle 8B	3.0 ± 0.1 E-1	1.05 ± 0.08 E+1	2.8 ± 0.2	13
>4000	Particle 8C	5.9 ± 0.1 E-2	2.3 ± 0.7	2.5 ± 0.9	6
>4000	Particle 8D	7.7 ± 0.1 E-2	4.1 ± 0.7	1.8 ± 0.4	4[d]
>4000	Particle 8E	1.3 ± 0.1 E-1	5.9 ± 0.8	2.1 ± 0.3	5[d]
1680-4000	Particle 8F	1.1 ± 0.1 E-1	5.0 ± 0.8	2.0 ± 0.4	7
1680-4000	Particle 8G	5.2 ± 0.1 E-2	3.3 ± 0.7	1.5 ± 0.5	3[d]
1680-4000	Particle 8H	1.1 ± 0.1 E-1	5.4 ± 0.8	2.0 ± 0.4	5[d]
1000-1680	Particle 8I	5.1 ± 0.1 E-2	3.8 ± 0.8	1.3 ± 0.4	11
1000-1680	Particle 8J	1.0 ± 1.2 E-2	1.8 ± 0.7	--[c]	5
1000-1680	Particle 8K	1.2 ± 0.1 E-1	4.9 ± 0.7	2.4 ± 0.4	8
707-1000	Aliquot	4.2 ± 1.2 E-2	2.3 ± 0.7	1.8 ± 0.8	5
297-707	Aliquot	4.9 ± 1.2 E-2	3.0 ± 0.7	1.6 ± 0.6	6
149-297	Aliquot	7.7 ± 1.2 E-2	3.4 ± 0.8	2.2 ± 0.6	8
74-149	Aliquot	2.3 ± 0.1 E-1	9.1 ± 0.8	2.5 ± 0.3	19
30-74	Aliquot	3.4 ± 1.2 E-2	1.9 ± 0.7	1.7 ± 0.9	4
20-30	Aliquot	6.4 ± 1.2 E-2	1.9 ± 0.8	3.3 ± 1.4	7
<20	Aliquot	1.6 ± 0.1 E-1	6.2 ± 0.8	2.5 ± 0.4	9
Sweepings	Aliquot	1.2 ± 0.1 E-1	5.6 ± 0.8	2.0 ± 0.3	9

TABLE E-11. (continued)

Particle Size Fraction (μm)	Particle/Aliquot	Fissile (mg)	Fertile (mg)	Enrichment (wt%)	Particle/Aliquot Weight (mg)
Sample 9					
>4000	Particle 9A	2.6 ± 0.1 E-1	9.7 ± 0.8	2.6 ± 0.2	20
>4000	Particle 9B	5.3 ± 0.1 E-1	2.02 ± 0.09 E+1	2.6 ± 0.1	33
>4000	Particle 9C	1.46 ± 0.03	5.8 ± 0.1 E+1	2.46 ± 0.07	64
>4000	Particle 9D	<0.01	<1	--[a]	7
>4000	Particle 9E	6.6 ± 0.1 E-2	2.4 ± 0.1 E+1	2.7 ± 0.1	30
1680-4000	Particle 9F	1.7 ± 0.1 E-1	7.5 ± 0.8	2.2 ± 0.3	9
1680-4000	Particle 9G	<0.01	1.2 ± 0.7	--[a]	5
1680-4000	Particle 9H	9.7 ± 0.1 E-2	4.7 ± 0.8	2.0 ± 0.4	9
1000-1680	Particle 9I	1.2 ± 0.1 E-1	3.8 ± 0.8	3.0 ± 0.6	28
1000-1680	Particle 9J	1.3 ± 0.1 E-1	6.7 ± 0.8	2.0 ± 0.3	8
1000-1680	Particle 9K	--[a]	<1[a]	--[a]	--[a]
707-1000	Aliquot	1.0 ± 0.1 E-1	3.2 ± 0.8	3.1 ± 0.8	9
297-707	Aliquot	<0.1	1.3 ± 0.7	--[a]	2
149-297	Aliquot	4.0 ± 0.1 E-2	2.0 ± 0.7	1.9 ± 0.9	8
74-149	Aliquot	6.4 ± 0.1 E-2	2.5 ± 0.7	2.5 ± 0.8	7
30-74	Aliquot	1.7 ± 0.1 E-1	4.7 ± 0.7	2.4 ± 0.4	12
20-30	Aliquot	4.8 ± 0.1 E-2	1.8 ± 0.7	2.6 ± 1.2	7
<20	Aliquot	1.6 ± 0.1 E-1	7.5 ± 0.8	2.0 ± 0.3	10
Sweepings	--	5.5 ± 1.2 E-2	3.2 ± 0.7	1.7 ± 0.5	7
Sample 10					
>4000	Particle 10A	2.06 ± 0.03	1.10 ± 0.02 E+2	1.83 ± 0.05	131
>4000	Particle 10B	1.53 ± 0.03	5.2 ± 0.1 E+1	2.86 ± 0.09	66
>4000	Particle 10C	3.21 ± 0.05	1.21 ± 0.03 E+2	2.58 ± 0.06	153
>4000	Particle 10D	1.14 ± 0.02	3.8 ± 0.1 E+1	2.9 ± 0.1	44
>4000	Particle 10E	1.11 ± 0.02	4.5 ± 0.1 E+1	2.41 ± 0.08	58
1680-4000	Particle 10F	1.42 ± 0.01 E-1	7.7 ± 0.8	1.8 ± 0.2	12
1680-4000	Particle 10G	4.7 ± 0.1 E-1	1.62 ± 0.09 E+1	2.8 ± 0.2	18
1680-4000	Particle 10H	4.0 ± 0.1 E-1	1.74 ± 0.08 E+1	2.2 ± 0.1	22
1000-1680	Particle 10I	8.0 ± 1.0 E-2	5.8 ± 0.8	1.4 ± 0.3	10
1000-1680	Particle 10J	1.5 ± 0.1 E-1	5.4 ± 0.7	2.8 ± 0.4	10
1000-1680	Particle 10K	2.7 ± 0.1 E-1	1.13 ± 0.08 E+1	2.3 ± 0.2	12
707-1000	Aliquot	6.3 ± 0.2 E-1	2.67 ± 0.9 E+1	2.3 ± 0.1	41
297-707	Aliquot	9.7 ± 1.2 E-2	3.6 ± 0.7	2.6 ± 0.6	8
149-297	Aliquot	1.2 ± 1.2 E-2	1.7 ± 0.7	--[a]	2
74-149	Aliquot	4.0 ± 1.2 E-2	9.1 ± 7.2 E-1	4.2 ± 3.2	7
30-74	Aliquot	2.4 ± 0.1	9.5 ± 0.8	2.4 ± 0.2	17
20-30	Aliquot	2.4 ± 0.1 E-1	1.01 ± 0.08 E+1	2.3 ± 0.2	15
Sweepings	Aliquot	3.0 ± 1.2 E-2	1.8 ± 0.7	1.7 ± 0.9	14

TABLE E-11. (continued)

Particle Size Fraction (μm)	Particle/Aliquot	Fissile (mg)	Fertile (mg)	Enrichment (wt%)	Particle/Aliquot Weight (mg)
Sample 11					
>4000	Particle 11A	1.8 ± 0.1 E-1	6.4 ± 0.7	2.8 ± 0.4	6[d]
>4000	Particle 11B	2.4 ± 0.1 E-1	1.08 ± 0.08 E+1	2.2 ± 0.2	15
>4000	Particle 11C	1.1 ± 0.1 E-1	6.4 ± 0.7	1.6 ± 0.3	5[d]
>4000	Particle 11D	3.1 ± 1.2 E-2	2.4 ± 0.7	1.2 ± 0.6	1[d]
>4000	Particle 11E	1.3 ± 0.1 E-1	5.7 ± 0.7	2.2 ± 0.3	7
1680-4000	Particle 11F	3.7 ± 0.1 E-1	1.46 ± 0.08 E+1	2.5 ± 0.2	20
1680-4000	Particle 11G	2.6 ± 0.1 E-1	9.4 ± 0.8	2.7 ± 0.3	10
1680-4000	Particle 11H	3.4 ± 0.1 E-1	1.21 ± 0.08 E+1	2.8 ± 0.2	15
1000-1680	Particle 11I	1.0 ± 0.1 E-1	5.3 ± 0.7	1.8 ± 0.3	6
1000-1680	Particle 11J	2.6 ± 0.1 E-1	1.04 ± 0.08 E+1	2.5 ± 0.2	10
1000-1680	Particle 11K	1.9 ± 0.1 E-1	8.1 ± 0.8	2.3 ± 0.3	9
707-1000	Aliquot	<0.01	1.9 ± 0.7	--[a]	3
297-707	Aliquot	6.7 ± 1.2 E-2	3.5 ± 0.7	1.9 ± 0.5	8
149-297	Aliquot	7.5 ± 1.2 E-2	2.8 ± 0.7	2.6 ± 0.8	7
74-149	Aliquot	5.3 ± 1.2 E-2	3.3 ± 0.7	1.6 ± 0.5	5
30-74	Aliquot	5.5 ± 1.2 E-2	2.7 ± 0.8	2.0 ± 0.7	6
20-30	Aliquot	3.4 ± 1.2 E-2	2.2 ± 0.7	1.5 ± 0.7	3
Sweepings	Aliquot	1.0 ± 0.1 E-1	4.2 ± 0.7	2.4 ± 0.5	8

a. Not measured.

b. Not reported because of problems associated with the analysis.

c. Calculated based on mass spectrometry enrichment analysis.

d. Uncertainty is ~50% because of small sample weights.

TABLE E-12. RADIONUCLIDE CONCENTRATIONS OF THE INSOLUBLE PORTIONS OF THE RECOMBINED BULK SAMPLES FROM THE H8 AND E9 CORE LOCATIONS (μCi/g insoluble material)

Radionuclide	H8 Location				
	Sample 1 (0.41 g)[a]	Sample 7	Sample 3 (1.20 g)[a]	Sample 8 (0.60 g)[a]	Sample 9 (0.200 g)[a]
^{60}Co	3.91 ± 0.05 E+1	--[b]	1.98 ± 0.04	1.97 ± 0.04	1.36 ± 0.03
^{106}Ru	9.36 ± 0.14 E+1	--[b]	1.88 ± 0.04 E+1	7.06 ± 0.21	1.93 ± 0.04 E+1
^{125}Sb	6.34 ± 0.27	--[b]	1.10 ± 0.04	1.81 ± 0.20 E-1	3.09 ± 0.39 E-1
^{134}Cs	4.2 ± 1.0 E-1	--[b]	9.0 ± 1.4 E-2	5.82 ± 0.97 E-2	2.81 ± 0.16 E-1
^{137}Cs	9.52 ± 0.19	--[b]	2.54 ± 0.03	1.27 ± 0.02	5.74 ± 0.05
^{144}Ce	1.74 ± 0.24 E+2	--[b]	1.31 ± 0.08 E+2	4.06 ± 0.38 E+1	1.78 ± 0.28 E+1
^{154}Eu	2.12 ± 0.22	--[b]	2.21 ± 0.07	4.81 ± 0.31 E-1	2.51 ± 0.25 E-1
^{155}Eu	5.3 ± 1.8	--[b]	3.4 ± 1.1	1.12 ± 0.37	5.2 ± 1.7 E-1

Radionuclide	E9 Location				
	Sample 4 (.090 g)[a]	Sample 5	Sample 6 (1.54 g)[a]	Sample 10 (0.34 g)[a]	Sample 11 (1.5 g)[a]
^{60}Co	1.40 ± 0.06 E+1	--[b]	3.06 ± 0.13	5.27 ± 0.06	2.15 ± 0.04
^{106}Ru	2.67 ± 0.01 E+3	--[b]	7.13 ± 0.05 E+2	1.34 ± 0.01 E+2	2.14 ± 0.04 E+1
^{125}Sb	1.37 ± 0.15 E+1	--[b]	7.41 ± 0.32	3.28 ± 0.08	2.40 ± 0.06
^{134}Cs	--[c]	--[b]	--[c]	1.19 ± 0.03	2.76 ± 0.18 E-1
^{137}Cs	3.17 ± 0.35	--[b]	4.72 ± 0.12	2.59 ± 0.01 E+1	5.67 ± 0.05
^{144}Ce	6.42 ± 0.31 E+3	--[b]	2.00 ± 0.22 E+2	2.59 ± 0.34 E+1	6.29 ± 0.53 E+1
^{154}Eu	1.02 ± 0.03 E+2	--[b]	2.61 ± 0.26	2.68 ± 0.35 E-1	7.46 ± 0.47 E-1
^{155}Eu	1.91 ± 0.63 E+2	--[b]	6.9 ± 2.3	6.6 ± 2.2 E-1	1.76 ± 0.58

a. Grams of insoluble material.

b. No insoluble material.

c. Not detected.

APPENDIX F
TMI-2 CORE NODULAR ORIGEN-2 CALCULATIONS

APPENDIX F

TMI-2 CORE NODULAR ORIGEN-2 CALCULATIONS[a]

Core inventory calculations using the ORIGEN-2 code have been made based on the average burnup estimates for the TMI-2 core.[b] Therefore, to provide a more accurate estimate of radionuclide inventories and concentrations in the core, the 177 individual assembly power histories were obtained from GPU Nuclear Inc. Figure F-1 shows the grid location, identification, and initial enrichment at each location.

It was determined from the initial data that a burnup summary map could be developed for the TMI-2 core. For this analysis, the axial core height (~3.9 m) was divided into seven arbitrary axial zones, each 55.6 cm in height. The average burnup then was calculated for each of the seven axial zones of each assembly, a total of 1239 nodes.

The burnup nodes were then divided into four subgroups for each initial enrichment group (1.98%, 2.64%, and 2.98% ^{235}U enrichment). Table F-1 shows the number of burnup nodes in each subgroup, the initial enrichment, number of metric tons of uranium (^{235}U + ^{238}U) in each group, the average burnup (MWd/MTU) for each group, and the maximum and minimum burnup zones for each group. Figures F-2 through F-8 show the burnup for all fuel assemblies in the seven axial burnup zones.

Table F-2 lists the full core and initial enrichment zone radionuclide inventories for April 1, 1984, the date used for decay correction purposes for the measured radionuclide concentration. Table F-3 contains the average radionuclide concentrations for the entire core and each enrichment group. Tables F-4 through F-6 give the radionuclide concentrations for each of the individual burnup subgroups.

---

a. B. G. Schnitzler and J. B. Briggs, TMI-2 Isotopic Inventory Calculations, EGG-PBS-6798, July 1985 (draft).

b. R. J. Davis et al., Radionuclide Mass Balance for the TMI-2 Accident: Data through 1979 and Preliminary Assessment of Uncertainties, GEND-INF-047, November 1984.

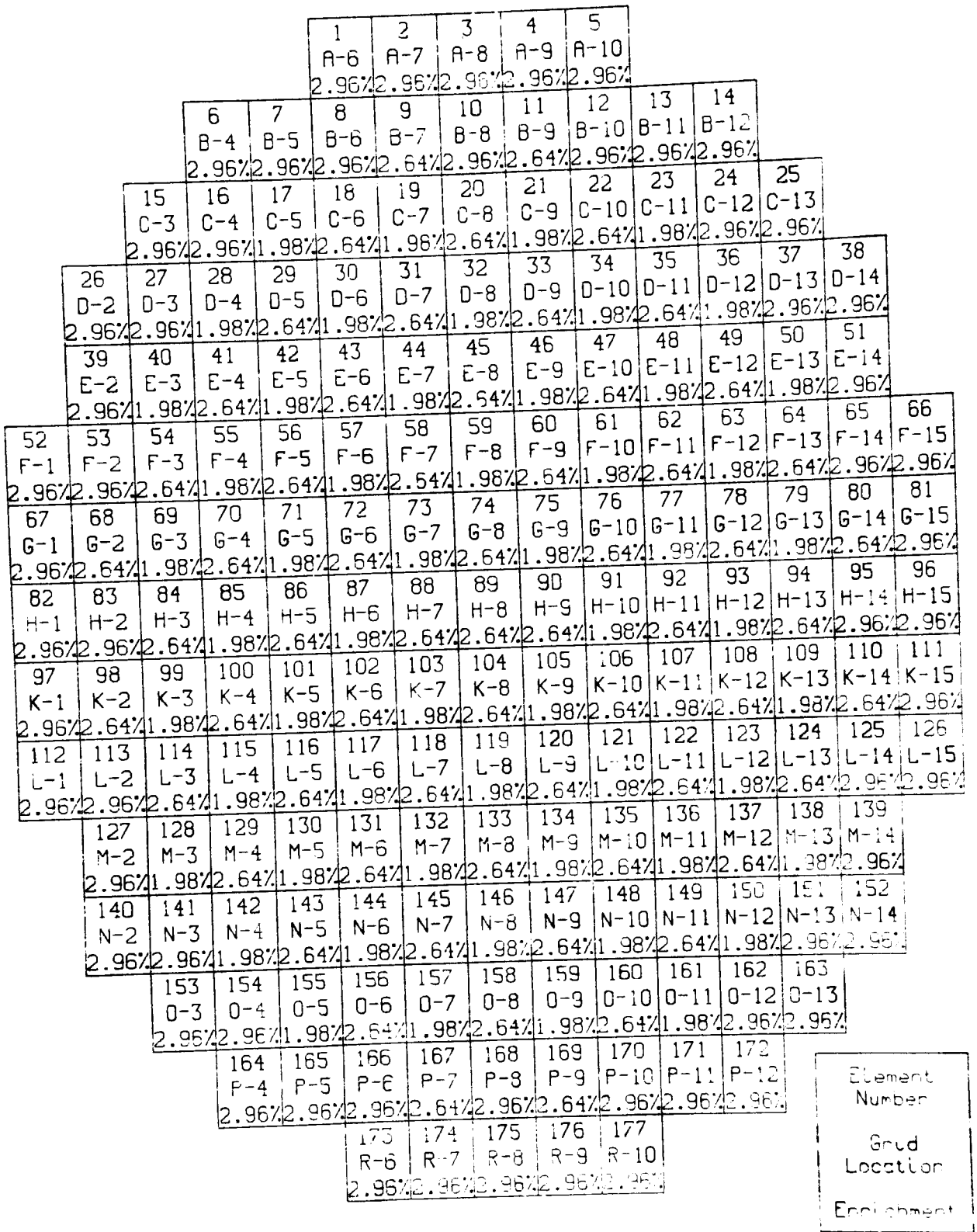

Figure F-1. TMI-2 element location and enrichment map.

TABLE F-1. TMI-2 REACTOR CORE FUEL NODE SUMMARY

Fuel Group	Number of Fuel Nodes	Initial Enrichment (wt%)	Initial Uranium (metric ton)	Average Burnup (MWd/MTU)	Minimum Burnup (MWd/MTU)	Maximum Burnup (MWd/MTU)
1	72	1.98	4.7684	1863	1436	2240
2	68	1.98	4.5035	2746	2488	3158
3	152	1.98	10.067	3637	3190	4021
4	100	1.98	6.6228	4391	4087	4905
5	105	2.64	6.9540	2239	1647	2741
6	76	2.64	5.0334	3552	2810	3890
7	230	2.64	15.233	4315	3907	4952
8	16	2.64	1.0597	5465	5227	6213
9	136	2.96	9.0071	1548	910	2020
10	164	2.96	10.861	2644	2100	3143
11	76	2.96	5.0334	3554	3261	4192
12	44	2.96	2.9140	4878	4453	5572

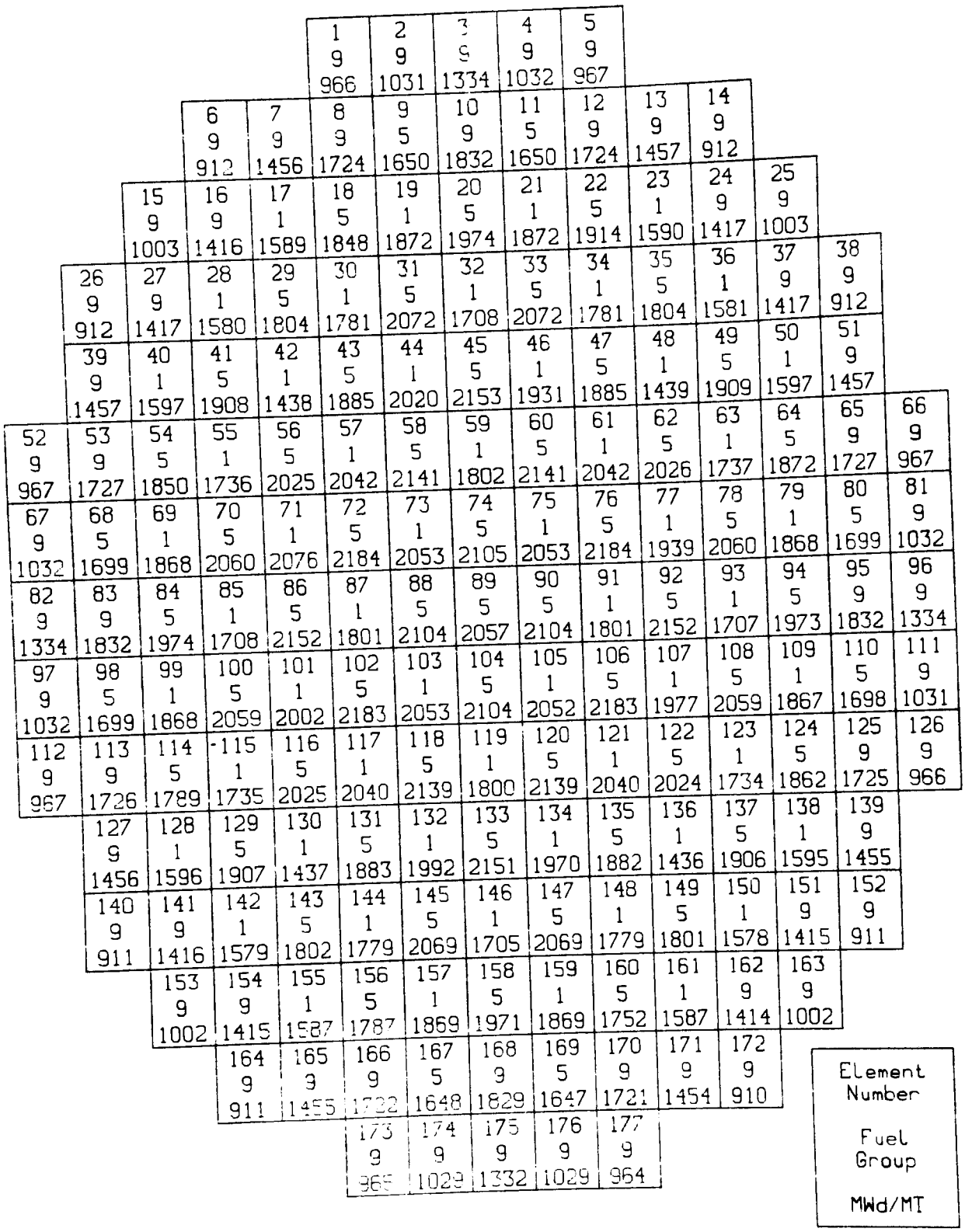

Figure F-2. TMI-2 burnup for Axial Level 1 of 7 (levels numbered from top of core).

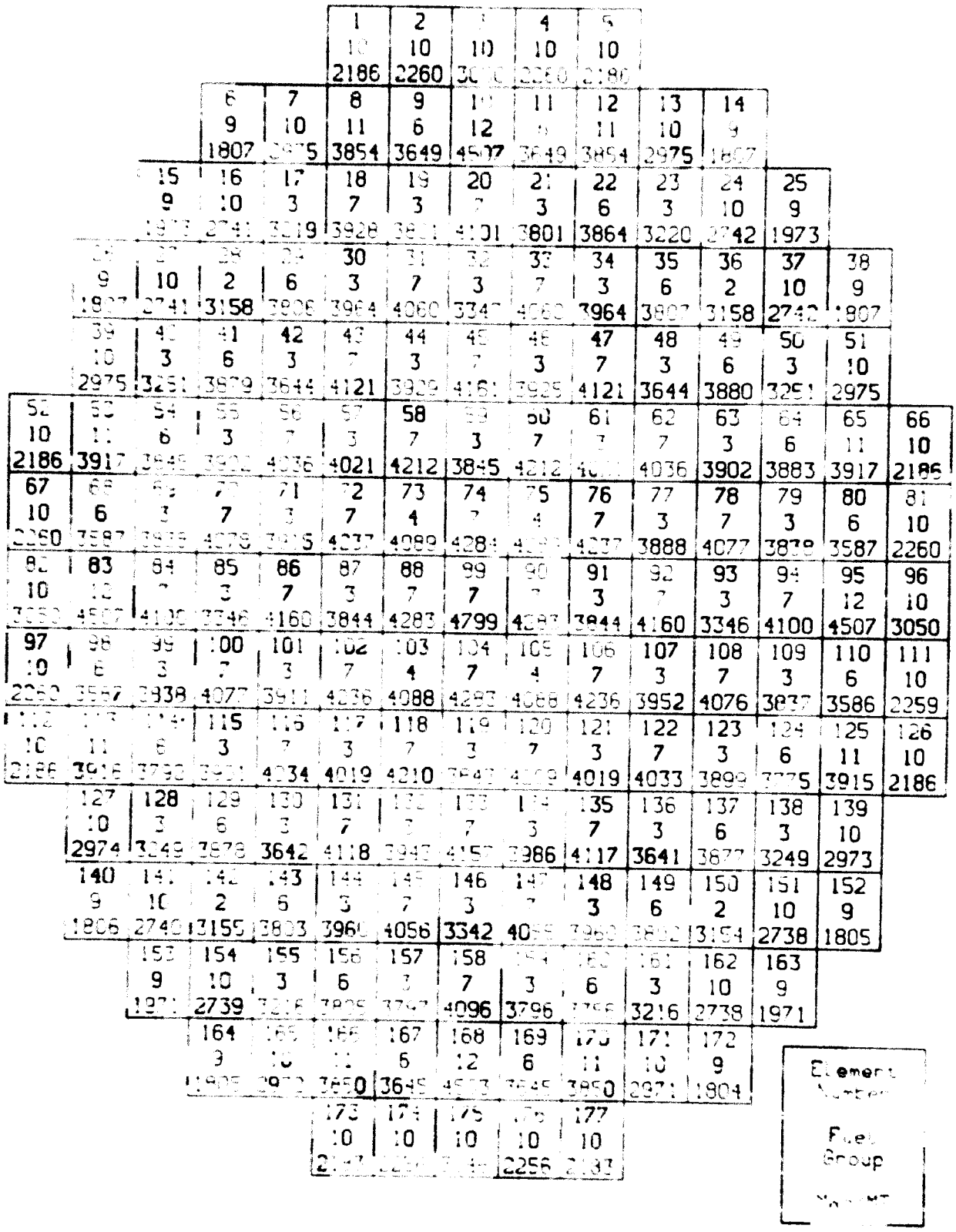

Figure F-3. TMI-2 burnup for Axial Level 2 of 7 (levels numbered from top of core).

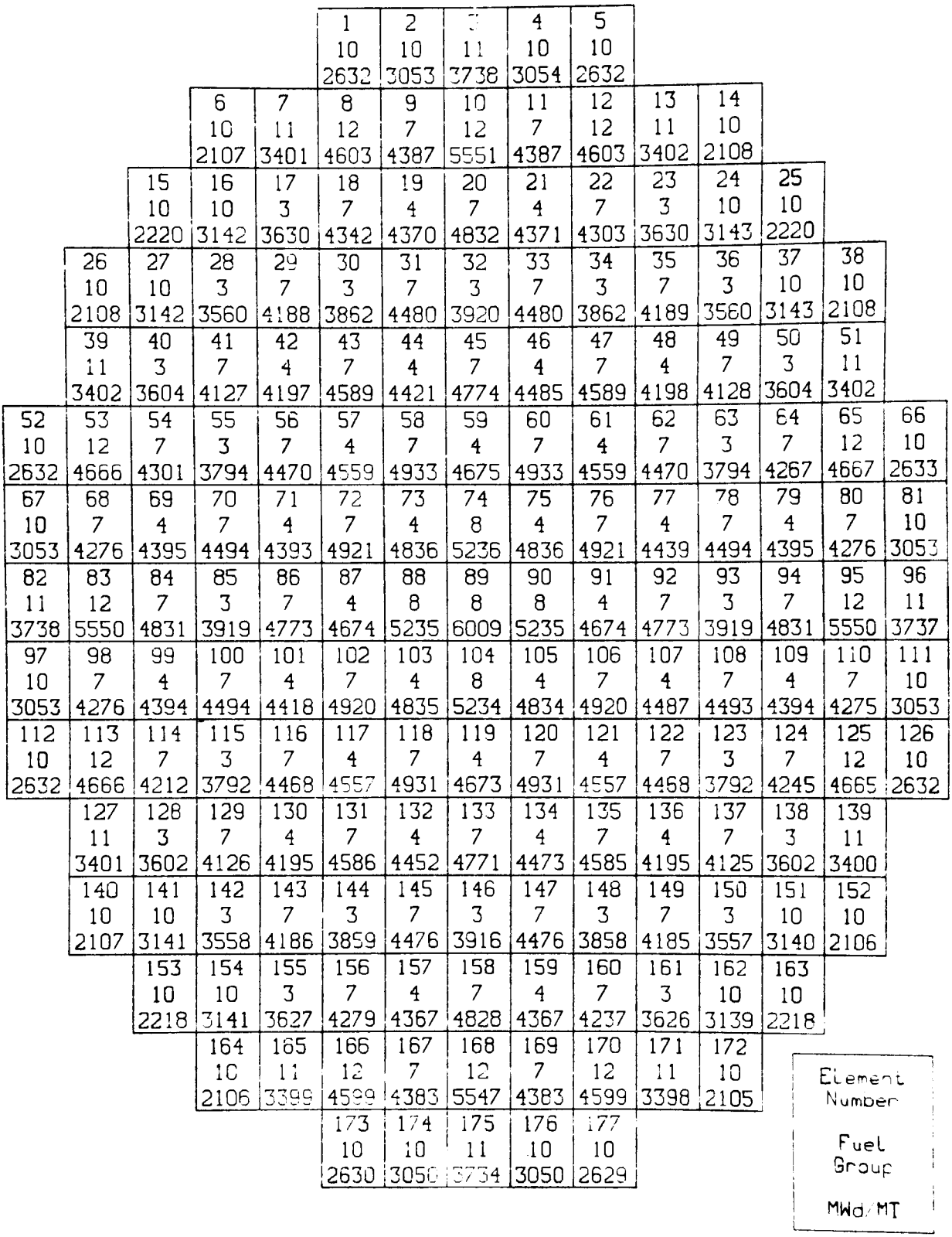

Figure F-4. TMI-2 burnup for Axial Level 3 of 7 (levels numbered from top of core).

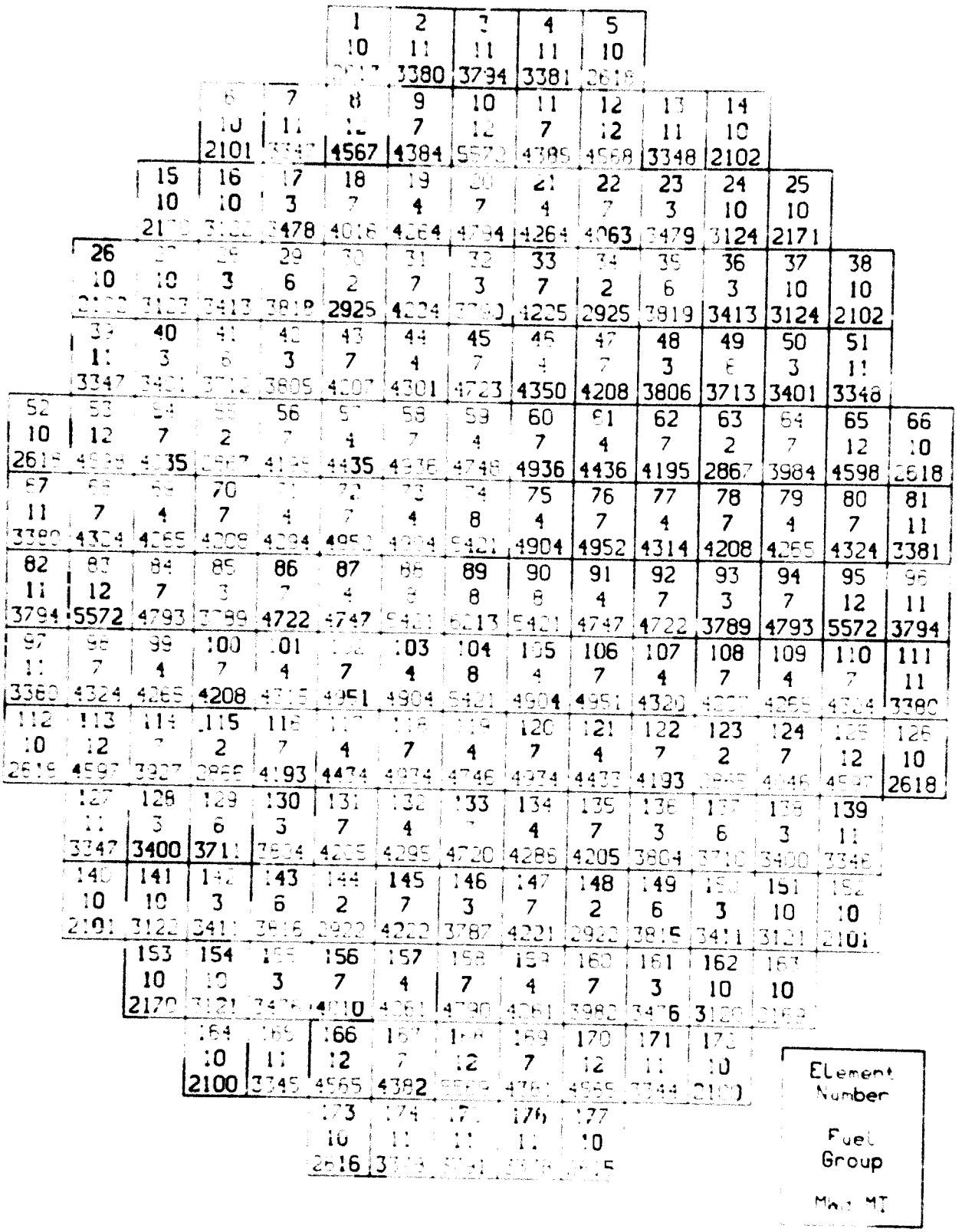

Figure F-5. TMI-2 burnup for Axial Level 4 of 7 (levels numbered from top of core).

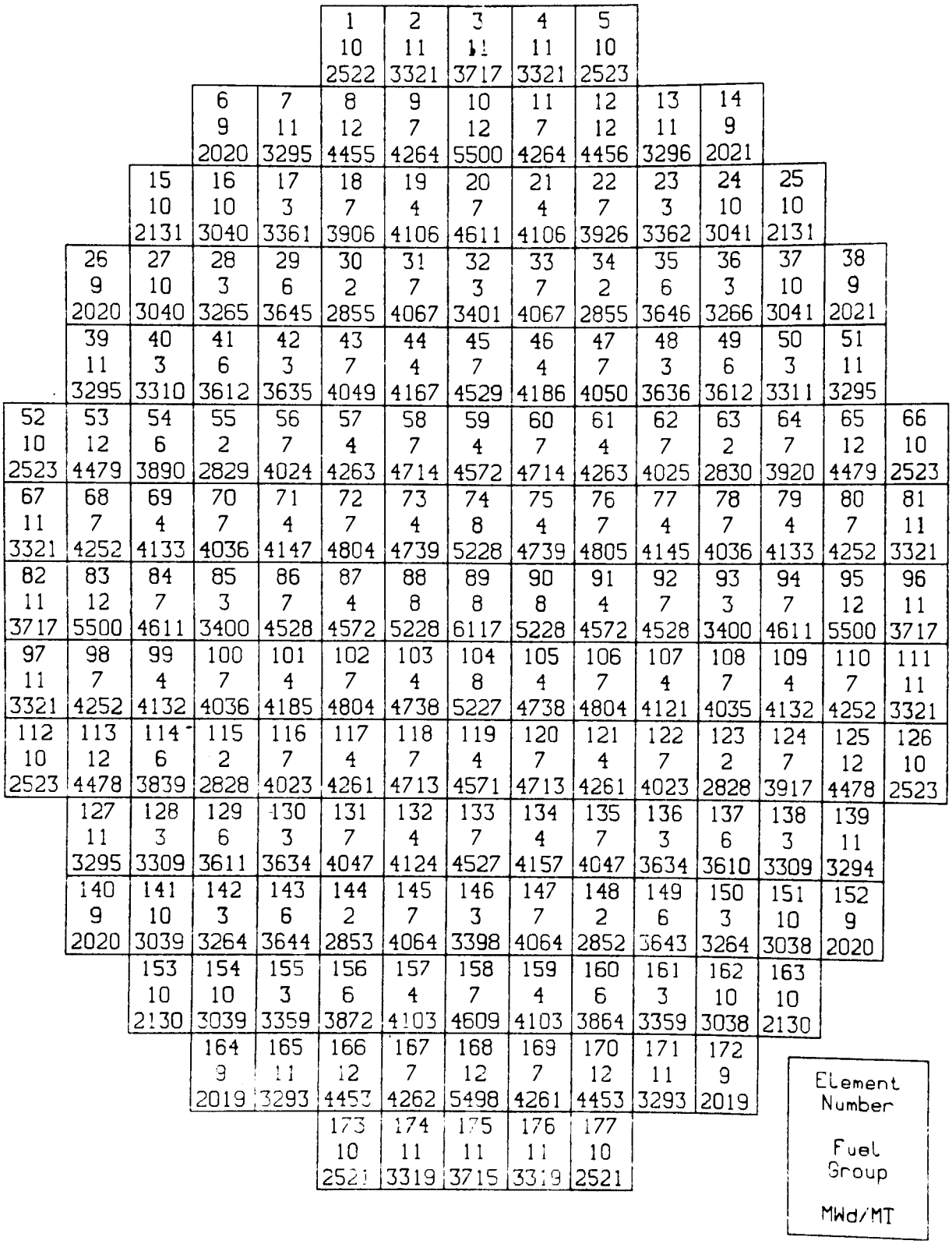

Figure F-6. TMI-2 burnup for Axial Level 5 of 7 (levels numbered from top of core).

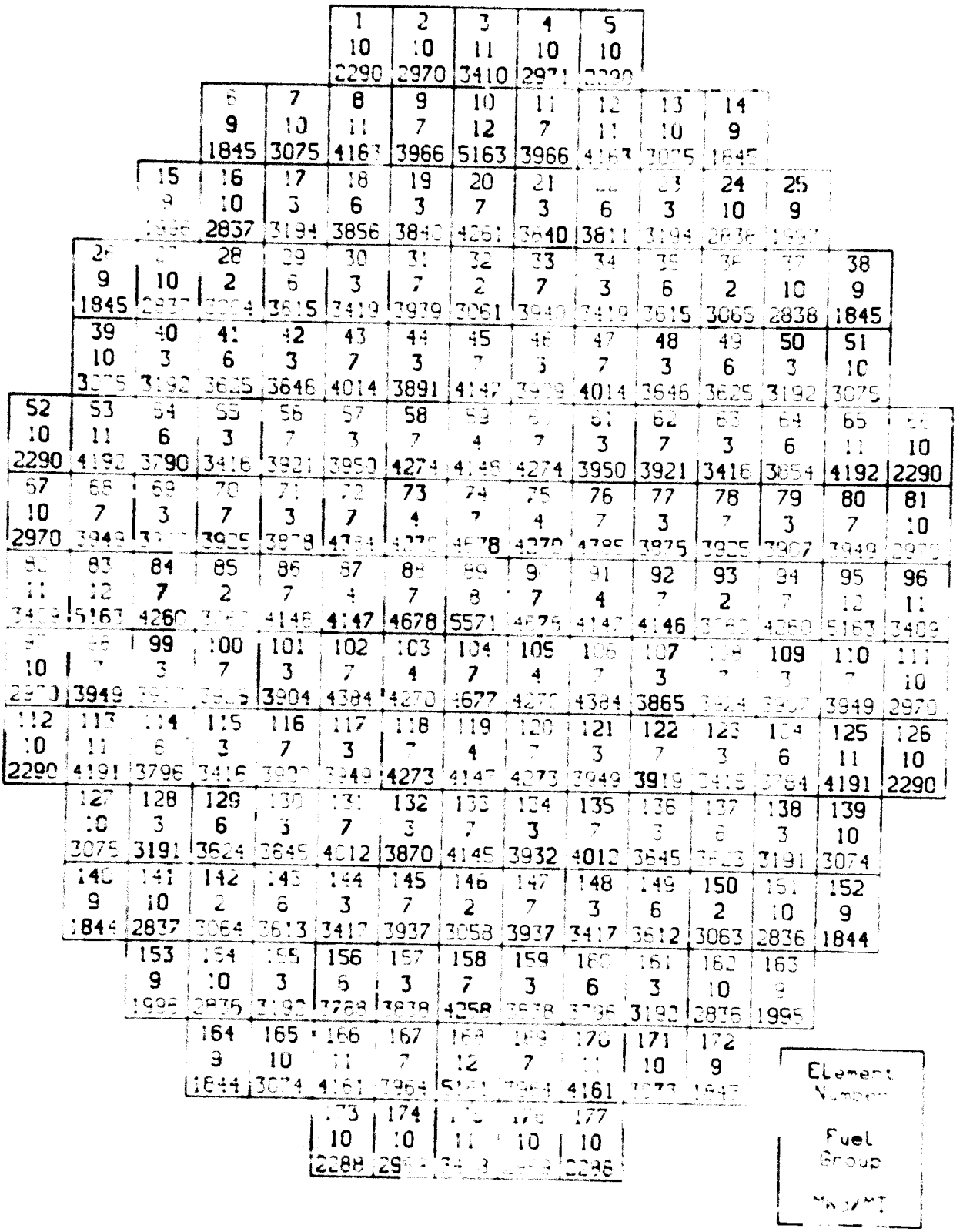

Figure F-7. TMI-2 burnup for Axial Level 6 of 7 (levels numbered from top of core).

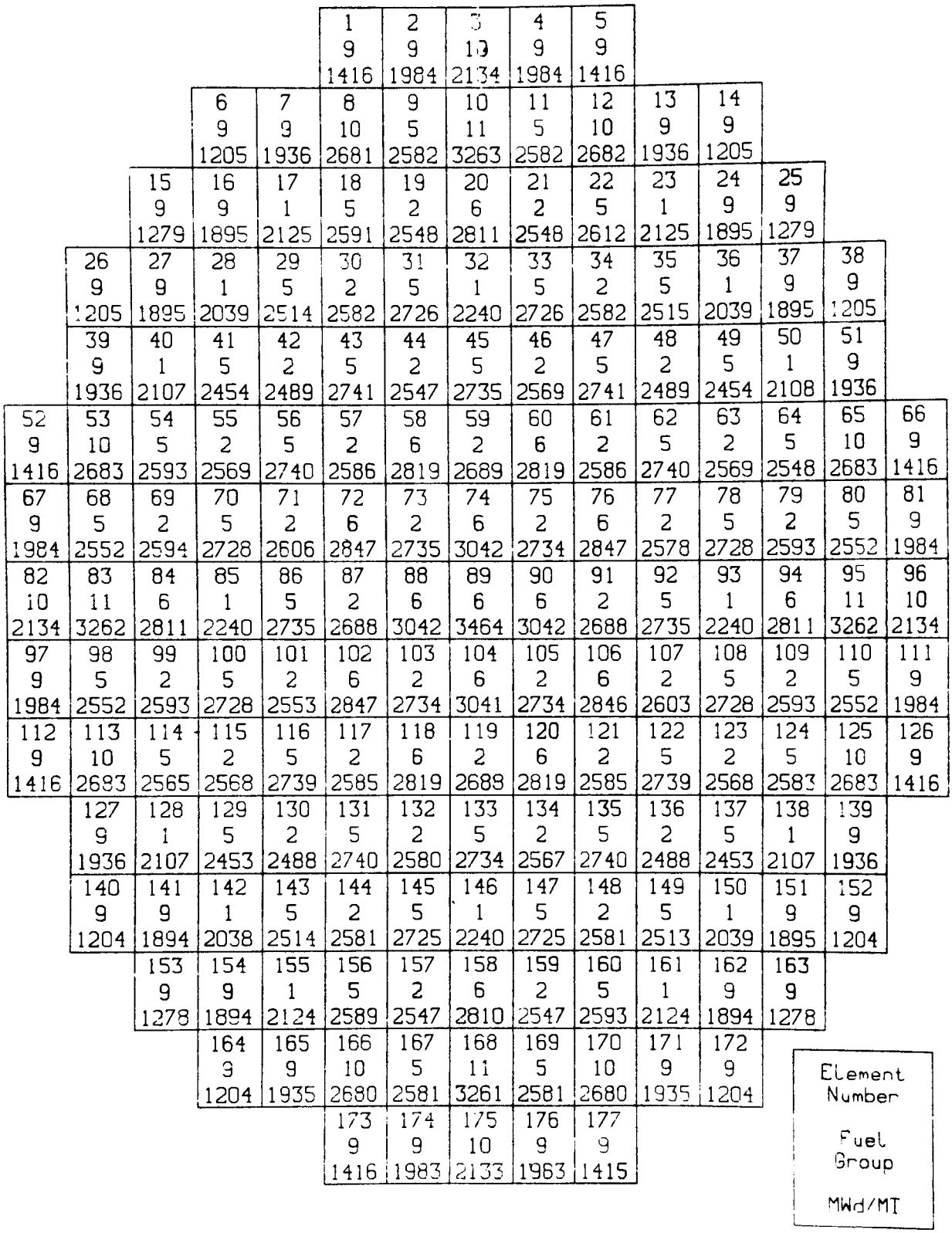

Figure F-8. TMI-2 burnup for Axial Level 7 of 7 (levels numbered from top of core).

TABLE F-2 TMI-2 ISOTOPIC ACTIVITY SUMMARY (CURIES) FOR FULL CORE (MARCH 1984).

	FULL CORE	ALL 1.98%	ALL 2.64%	ALL 2.96%
TH231	3.899E+00	9.256E-01	1.373E+00	1.601E+00
TH234	2.662E+01	8.529E+00	9.231E+00	9.059E+00
PA233	1.20CE+00	4.536E-01	4.638E-01	2.827E-01
PA234M	2.682E+01	8.529E+00	9.231E+00	9.059E+00
U234	9.758E-02	3.179E-02	3.657E-02	2.721E-02
U235	3.899E+00	9.256E-01	1.373E+00	1.601E+00
U236	3.303E+00	1.010E+00	1.313E+00	9.612E-01
U237	4.704E-02	2.261E-02	1.768E-02	6.754E-03
U238	2.662E+01	8.529E+00	9.231E+00	9.059E+00
NP237	1.200E+00	4.536E-01	4.638E-01	2.827E-01
NP239	4.085E-01	2.342E-01	1.387E-01	3.563E-02
PU236	6.217E-02	2.719E-02	2.411E-02	1.087E-02
PU238	1.053E+03	4.612E+02	4.078E+02	1.839E+02
PU239	9.336E+03	3.494E+03	3.450E+03	2.392E+03
PU240	2.860E+03	1.228E+03	1.086E+03	5.456E+02
PU241	1.918E+05	9.217E+04	7.206E+04	2.753E+04
PU242	3.302E-01	1.751E-01	1.189E-01	3.617E-02
AM241	1.761E+03	8.468E+02	6.617E+02	2.528E+02
AM242M	7.286E-01	3.801E-01	2.645E-01	8.395E-02
AM242	7.249E-01	3.782E-01	2.632E-01	8.353E-02
AM243	4.085E-01	2.342E-01	1.387E-01	3.563E-02
CM242	1.547E+00	8.192E-01	5.561E-01	1.715E-01
CM243	1.110E-01	6.395E-02	3.745E-02	9.601E-03
CM244	4.342E+00	2.662E+00	1.370E+00	3.092E-01
H 3	3.196E+03	1.073E+03	1.251E+03	8.723E+02
SR 79	3.542E+00	1.157E+00	1.392E+00	9.933E-01
KR 85	7.031E+04	2.231E+04	2.779E+04	2.021E+04
SR 89	8.011E-04	2.509E-04	3.170E-04	2.332E-04
SR 90	6.625E+05	2.089E+05	2.621E+05	1.915E+05
Y 90	6.627E+05	2.090E+05	2.621E+05	1.916E+05
Y 91	2.886E-02	9.086E-03	1.141E-02	8.360E-03
ZR 93	1.675E+01	5.350E+00	6.612E+00	4.787E+00
NB 93M	3.710E+00	1.186E+00	1.464E+00	1.060E+00
ZR 95	2.034E-01	6.530E-02	8.022E-02	5.785E-02
NB 95	4.515E-01	1.450E-01	1.781E-01	1.284E-01
NB 95M	1.509E-03	4.844E-04	5.951E-04	4.292E-04
TC 99	1.200E+02	3.895E+01	4.721E+01	3.380E+01
RU103	6.165E-07	2.110E-07	2.411E-07	1.645E-07
RU106	1.149E+05	4.391E+04	4.410E+04	2.687E+04
RH106	1.149E+05	4.391E+04	4.410E+04	2.687E+04
PD107	3.771E-01	1.484E-01	1.441E-01	8.458E-02
AG110	2.783E-01	1.266E-01	1.063E-01	4.533E-02
AG110M	2.092E+01	9.522E+00	7.992E+00	3.408E+00
CD113M	2.422E+02	9.041E+01	9.204E+01	5.971E+01
SN119M	1.988E+01	7.310E+00	7.567E+00	5.004E+00
SN121M	9.562E-01	3.428E-01	3.726E-01	2.408E-01
SN123	5.303E+00	1.903E+00	2.033E+00	1.367E+00
SB125	3.598E+04	1.351E+04	1.413E+04	9.336E+03
TE125M	9.024E+03	3.297E+03	3.449E+03	2.278E+03
SN126	5.338E+00	1.908E+00	2.054E+00	1.375E+00
SB126	7.474E-01	2.672E-01	2.876E-01	1.926E-01
SB126M	5.338E+00	1.908E+00	2.054E+00	1.375E+00
TE127	3.072E+00	1.092E+00	1.188E+00	7.918E-01
TE127M	3.136E+00	1.115E+00	1.213E+00	8.083E-01
I129	2.294E-01	7.801E-02	8.958E-02	6.182E-02
CS134	3.699E+04	1.403E+04	1.517E+04	7.793E+03
CS135	3.305E+00	9.396E-01	1.236E+00	1.132E+00
CS137	7.605E+05	2.476E+05	2.995E+05	2.134E+05
BA137M	7.194E+05	2.343E+05	2.833E+05	2.018E+05
CE144	2.752E+05	8.821E+04	1.066E+05	7.640E+04
PR144	2.752E+05	8.822E+04	1.066E+05	7.640E+04
PR144M	3.303E+03	1.059E+03	1.303E+03	9.408E+02
PM147	5.366E+05	2.665E+05	3.278E+05	2.423E+05
SM151	1.039E+04	3.173E+03	3.918E+03	3.294E+03
EU152	4.319E+01	1.411E+01	1.720E+01	1.188E+01
EU153	3.351E-01	1.316E-01	1.305E-01	6.499E-02
EU154	6.385E+03	2.526E+03	2.480E+03	1.279E+03
EU155	1.612E+04	5.566E+03	6.159E+03	4.395E+03

TABLE F-3 TMI-2 SPECIFIC ACTIVITY SUMMARY (CURIES/GRAM U) FOR FULL CORE (MARCH 1984).

	FULL CORE	ALL 1.98%	ALL 2.64%	ALL 2.96%
TH231	4.778E-08	3.586E-08	4.885E-08	5.779E-08
TH234	3.286E-07	3.305E-07	3.284E-07	3.271E-07
PA233	1.470E-08	1.757E-08	1.650E-08	1.021E-08
PA234M	3.286E-07	3.305E-07	3.284E-07	3.271E-07
U234	1.196E-09	1.232E-09	1.372E-09	9.826E-10
U235	4.778E-08	3.586E-08	4.885E-08	5.779E-08
U236	4.048E-08	3.912E-08	4.670E-08	3.543E-08
U237	5.764E-10	8.761E-10	6.289E-10	2.439E-10
U238	3.286E-07	3.305E-07	3.284E-07	3.271E-07
NP237	1.470E-08	1.757E-08	1.650E-08	1.021E-08
NP239	5.005E-09	9.074E-09	4.933E-09	1.286E-09
PU236	7.618E-10	1.053E-09	8.579E-10	3.925E-10
PU238	1.290E-05	1.787E-05	1.451E-05	6.639E-06
PU239	1.144E-04	1.354E-04	1.228E-04	8.636E-05
PU240	3.504E-05	4.759E-05	3.864E-05	1.970E-05
PU241	2.350E-03	3.571E-03	2.564E-03	9.941E-04
PU242	4.046E-09	6.784E-09	4.230E-09	1.306E-09
AM241	2.158E-05	3.281E-05	2.354E-05	9.128E-06
AM242M	8.927E-09	1.473E-08	9.409E-09	3.031E-09
AM242	8.883E-09	1.466E-08	9.362E-09	3.016E-09
AM243	5.005E-09	9.074E-09	4.933E-09	1.286E-09
CM242	1.695E-08	3.174E-08	1.979E-08	6.193E-09
CM243	1.360E-09	2.478E-09	1.332E-09	3.466E-10
CM244	5.320E-08	1.032E-07	4.876E-08	1.116E-08
H 3	3.916E-05	4.157E-05	4.450E-05	3.150E-05
SE 79	4.340E-08	4.483E-08	4.952E-08	3.586E-08
KR 85	8.616E-04	8.646E-04	9.886E-04	7.299E-04
SR 89	9.815E-12	9.721E-12	1.128E-11	8.420E-12
SR 90	8.118E-03	8.094E-03	9.324E-03	6.916E-03
Y 90	8.120E-03	8.096E-03	9.327E-03	6.918E-03
Y 91	3.536E-10	3.520E-10	4.060E-10	3.018E-10
ZR 93	2.052E-07	2.073E-07	2.352E-07	1.729E-07
NB 93M	4.545E-08	4.594E-08	5.210E-08	3.826E-08
ZR 95	2.492E-09	2.530E-09	2.854E-09	2.089E-09
NB 95	5.533E-09	5.618E-09	6.336E-09	4.638E-09
NB 95M	1.849E-11	1.877E-11	2.117E-11	1.550E-11
TC 99	1.470E-06	1.509E-06	1.680E-06	1.221E-06
RU103	7.554E-15	8.174E-15	8.577E-15	5.939E-15
RU106	1.408E-03	1.701E-03	1.569E-03	9.703E-04
RH106	1.408E-03	1.701E-03	1.569E-03	9.703E-04
PD107	4.621E-09	5.750E-09	5.128E-09	3.054E-09
AG110	3.410E-09	4.907E-09	3.782E-09	1.637E-09
AG110M	2.564E-07	3.689E-07	2.843E-07	1.231E-07
CD113M	2.967E-06	3.503E-06	3.275E-06	2.156E-06
SN119M	2.436E-07	2.832E-07	2.692E-07	1.807E-07
SN121M	1.172E-08	1.328E-08	1.326E-08	8.694E-09
SN123	6.498E-08	7.374E-08	7.233E-08	4.937E-08
SB125	4.531E-04	5.234E-04	5.028E-04	3.371E-04
TE125M	1.106E-04	1.277E-04	1.227E-04	8.226E-05
SN126	6.541E-08	7.394E-08	7.309E-08	4.966E-08
SB126	9.157E-09	1.035E-08	1.023E-08	6.952E-09
SB126M	6.541E-08	7.394E-08	7.309E-08	4.966E-08
TE127	3.764E-08	4.230E-08	4.227E-08	2.859E-08
TE127M	3.843E-08	4.319E-08	4.316E-08	2.918E-08
I129	2.811E-09	3.022E-09	3.187E-09	2.232E-09
CS134	4.533E-04	5.436E-04	5.398E-04	2.814E-04
CS135	4.053E-08	3.641E-08	4.397E-08	4.088E-08
CS137	9.316E-03	9.594E-03	1.065E-02	7.704E-03
BA137M	8.815E-03	9.076E-03	1.008E-02	7.288E-03
CE144	3.372E-03	3.418E-03	3.864E-03	2.831E-03
PR144	3.372E-03	3.418E-03	3.864E-03	2.831E-03
PR144M	4.047E-05	4.101E-05	4.637E-05	3.397E-05
PM147	1.025E-02	1.032E-02	1.166E-02	8.749E-03
SM151	1.272E-04	1.229E-04	1.394E-04	1.189E-04
EU152	5.292E-07	5.467E-07	6.121E-07	4.288E-07
EU153	4.106E-09	5.101E-09	4.928E-09	2.346E-09
EU154	7.824E-05	9.788E-05	9.179E-05	4.617E-05
EU155	1.975E-04	2.157E-04	2.191E-04	1.587E-04

TABLE F-4 TMI-2 SPECIFIC ACTIVITY SUMMARY (CURIES/GRAM U) FOR 1.98% INITIAL ENRICHMENT ZONES (MARCH 1984).

	ALL 1.98%	GROUP 1	GROUP 2	GROUP 3	GROUP 4
TH231	3.586E-08	3.866E-08	3.694E-08	3.529E-08	3.396E-08
TH234	3.305E-07	3.301E-07	3.303E-07	3.305E-07	3.307E-07
PA233	1.757E-08	8.721E-09	1.369E-08	1.919E-08	2.416E-08
PA234M	3.305E-07	3.301E-07	3.303E-07	3.305E-07	3.307E-07
U234	1.232E-09	6.868E-10	9.868E-10	1.338E-09	1.652E-09
U235	3.586E-08	3.868E-08	3.695E-08	3.529E-08	3.396E-08
U236	3.912E-08	2.333E-08	3.312E-08	4.235E-08	4.970E-08
U237	3.761E-10	1.719E-10	4.763E-10	9.655E-10	1.522E-09
U238	3.305E-07	3.301E-07	3.303E-07	3.305E-07	3.307E-07
NP237	1.757E-08	8.721E-09	1.369E-08	1.919E-08	2.416E-08
NP239	9.074E-09	7.073E-10	2.458E-09	8.790E-09	2.028E-08
PU236	1.053E-09	2.936E-10	6.494E-10	1.160E-09	1.715E-09
PU238	1.787E-05	4.986E-06	1.108E-05	1.968E-05	2.910E-05
PU239	1.354E-04	8.694E-05	1.189E-04	1.458E-04	1.659E-04
PU240	4.759E-05	1.764E-05	3.391E-05	5.299E-05	7.035E-05
PU241	3.571E-03	7.006E-04	1.942E-03	3.936E-03	6.203E-03
PU242	6.753E-09	6.419E-10	2.630E-09	7.098E-09	1.358E-08
AM241	3.491E-05	9.437E-06	1.784E-05	3.616E-05	5.699E-05
AM242M	1.473E-08	1.652E-09	5.282E-09	1.576E-08	2.836E-08
AM242	1.476E-08	1.644E-09	6.225E-09	1.568E-08	2.824E-08
AM243	9.074E-09	4.073E-10	2.458E-09	8.790E-09	2.028E-08
CM242	3.174E-08	3.198E-09	1.274E-08	3.348E-08	6.268E-08
CM243	2.033E-09	1.115E-10	6.727E-10	2.402E-09	5.534E-09
CM244	4.103E-05	2.155E-09	1.910E-08	9.055E-08	2.527E-07
CM 3	4.163E-05	2.257E-05	3.372E-05	4.522E-05	5.510E-05
CM 79	4.463E-03	2.515E-08	3.690E-08	4.869E-08	5.858E-08
ERSR 85	8.646E-04	4.960E-04	7.190E-04	9.379E-04	1.119E-03
SR 89	9.701E-12	5.678E-12	8.149E-12	1.053E-11	1.248E-11
SR 90	8.094E-03	4.672E-03	6.750E-03	8.778E-03	1.044E-02
Y 90	8.096E-03	4.673E-03	6.752E-03	8.780E-03	1.045E-02
Y 91	3.520E-10	2.042E-10	2.942E-10	3.817E-10	4.533E-10
ZR 93	2.073E-07	1.180E-07	1.716E-07	2.250E-07	2.691E-07
NB 93M	4.594E-08	2.612E-08	3.805E-08	4.986E-08	5.968E-08
ZR 95	2.530E-09	1.431E-09	2.091E-09	2.747E-09	3.295E-09
NB 95	5.618E-09	3.178E-09	4.642E-09	6.098E-09	7.315E-09
NB 95M	1.877E-11	1.062E-11	1.551E-11	2.039E-11	2.444E-11
TC 99	1.509E-06	8.453E-07	1.242E-06	1.639E-06	1.973E-06
RU103	9.174E-15	4.267E-15	6.522E-15	8.910E-15	1.100E-14
RU106	1.701E-03	7.724E-04	1.280E-03	1.865E-03	2.410E-03
RH106	1.701E-03	7.724E-04	1.280E-03	1.865E-03	2.410E-03
PD107	5.750E-09	2.490E-09	4.245E-09	6.315E-09	8.272E-09
AG110	4.907E-09	1.137E-09	2.782E-09	5.373E-09	8.370E-09
AG110M	3.699E-07	8.546E-08	2.092E-07	4.040E-07	6.293E-07
CD113M	3.503E-06	1.850E-06	2.803E-06	3.813E-06	4.703E-06
SN119M	2.832E-07	1.543E-07	2.299E-07	3.080E-07	3.751E-07
SN121M	1.328E-08	6.293E-09	1.013E-08	1.459E-08	1.853E-08
SN123	7.374E-08	4.038E-08	6.003E-08	8.018E-08	9.739E-08
SB125	5.234E-04	2.798E-04	4.217E-04	5.698E-04	6.982E-04
TE125M	1.277E-04	6.829E-05	1.029E-04	1.391E-04	1.704E-04
SN126	7.394E-08	3.945E-08	5.953E-08	8.051E-08	9.871E-08
SB126	1.035E-08	5.523E-09	8.334E-09	1.127E-08	1.382E-08
SB126M	7.394E-08	3.945E-08	5.952E-08	8.051E-08	9.871E-08
TE127	4.230E-08	2.200E-08	3.369E-08	4.612E-08	5.704E-08
TE127M	4.319E-08	2.246E-08	3.440E-08	4.709E-08	5.823E-08
I129	3.022E-09	1.617E-09	2.437E-09	3.291E-09	4.029E-09
CS134	5.436E-04	2.649E-04	3.497E-04	6.011E-04	8.619E-04
CS135	3.041E-08	2.960E-08	3.439E-08	3.793E-08	4.038E-08
CS137	9.594E-03	5.321E-03	7.859E-03	1.043E-02	1.260E-02
BA137M	9.076E-03	5.033E-03	7.433E-03	9.863E-03	1.192E-02
CE144	3.418E-03	1.935E-03	2.625E-03	3.710E-03	4.449E-03
PR144	3.418E-03	1.935E-03	2.625E-03	3.710E-03	4.449E-03
PR144M	4.101E-05	2.322E-05	3.390E-05	4.452E-05	5.339E-05
PM147	1.032E-03	9.127E-04	8.728E-04	1.118E-03	1.314E-03
SM151	1.229E-04	9.049E-05	1.130E-04	1.301E-04	1.422E-04
EU152	5.467E-07	3.104E-07	4.742E-07	6.023E-07	6.824E-07
EU153	5.101E-09	1.318E-09	3.178E-09	5.710E-09	8.219E-09
EU154	9.786E-05	2.906E-05	6.112E-05	1.079E-04	1.582E-04
EU155	2.157E-04	1.251E-04	1.797E-04	2.334E-04	2.786E-04

TABLE F-5 TAI-2 SPECIFIC ACTIVITY SUMMARY (CURIES/GRAM U) FOR 2.64% INITIAL ENRICHMENT ZONES (MARCH 1984).

	ALL 2.64%	GROUP 5	GROUP 6	GROUP 7	GROUP 8
TH231	4.385E-08	5.191E-08	4.913E-08	4.760E-08	4.537E-08
TH234	3.284E-07	3.281E-07	3.284E-07	3.286E-07	3.289E-07
PA233	1.650E-08	8.654E-09	1.536E-08	1.974E-08	2.699E-08
PA234M	3.284E-07	3.281E-07	3.284E-07	3.286E-07	3.289E-07
U234	1.372E-09	8.056E-10	1.302E-09	1.606E-09	2.090E-09
U235	4.885E-08	5.191E-08	4.913E-08	4.759E-08	4.537E-08
U236	4.670E-08	2.946E-08	4.512E-08	5.376E-08	6.620E-08
U237	6.289E-10	1.455E-10	5.025E-10	8.316E-10	1.501E-09
U238	3.284E-07	3.281E-07	3.284E-07	3.286E-07	3.289E-07
NP237	1.650E-08	8.654E-09	1.536E-08	1.974E-08	2.699E-08
NP239	4.933E-09	3.060E-10	2.725E-09	6.739E-09	1.997E-08
PU236	8.579E-10	2.701E-10	7.231E-10	1.103E-09	1.852E-09
PU238	1.451E-05	4.582E-06	1.223E-05	1.864E-05	3.128E-05
PU239	1.228E-04	8.223E-05	1.201E-04	1.393E-04	1.650E-04
PU240	3.864E-05	1.580E-05	3.500E-05	4.815E-05	6.968E-05
PU241	2.564E-03	5.930E-04	2.048E-03	3.390E-03	6.120E-03
PU242	4.230E-09	5.115E-10	2.840E-09	5.759E-09	1.336E-08
AM241	2.354E-05	5.445E-06	1.881E-05	3.113E-05	5.620E-05
AM242M	9.409E-09	1.315E-09	6.649E-09	1.278E-08	2.738E-08
AM242	9.362E-09	1.309E-09	6.616E-09	1.272E-08	2.724E-08
AM243	4.933E-09	3.060E-10	2.725E-09	6.739E-09	1.997E-08
CM242	1.979E-08	2.534E-09	1.355E-08	2.691E-08	6.059E-08
CM243	1.332E-09	8.317E-11	7.379E-10	1.821E-09	5.371E-09
CM244	4.076E-08	1.526E-09	2.170E-08	6.555E-08	2.474E-07
H 3	4.450E-05	2.635E-05	4.242E-05	5.196E-05	6.655E-05
SE 79	4.952E-08	3.000E-08	4.744E-08	5.754E-08	7.270E-08
KR 85	9.886E-04	6.080E-04	9.499E-04	1.145E-03	1.433E-03
SR 89	1.128E-11	7.021E-12	1.086E-11	1.302E-11	1.618E-11
SR 90	9.324E-03	5.759E-03	8.967E-03	1.079E-02	1.347E-02
Y 90	9.327E-03	5.760E-03	8.970E-03	1.079E-02	1.347E-02
Y 91	4.060E-10	2.516E-10	3.907E-10	4.693E-10	5.847E-10
ZR 93	2.352E-07	1.440E-07	2.258E-07	2.727E-07	3.424E-07
NB 93M	5.210E-08	3.186E-08	5.000E-08	6.041E-08	7.587E-08
ZR 95	2.854E-09	1.740E-09	2.737E-09	3.311E-09	4.168E-09
NB 95	6.336E-09	3.863E-09	6.078E-09	7.352E-09	9.254E-09
NB 95M	2.117E-11	1.291E-11	2.031E-11	2.457E-11	3.092E-11
TC 99	1.680E-06	1.018E-06	1.609E-06	1.952E-06	2.464E-06
RU103	8.577E-15	4.937E-15	8.133E-15	1.008E-14	1.310E-14
RU106	1.569E-03	8.040E-04	1.455E-03	1.886E-03	2.599E-03
RH106	1.569E-03	8.040E-04	1.455E-03	1.886E-03	2.599E-03
PD107	5.128E-09	2.517E-09	4.719E-09	6.209E-09	8.719E-09
AG110	3.782E-09	1.056E-09	3.098E-09	4.917E-09	8.672E-09
AG110M	2.843E-07	7.943E-08	2.329E-07	3.697E-07	6.520E-07
CD113M	3.275E-06	1.882E-06	3.101E-06	3.648E-06	5.026E-06
SN119M	2.692E-07	1.584E-07	2.563E-07	3.148E-07	4.051E-07
SN121M	1.326E-08	7.107E-09	1.240E-08	1.580E-08	2.128E-08
SN123	7.233E-08	4.282E-08	6.896E-08	8.447E-08	1.082E-07
SB125	5.026E-04	2.923E-04	4.776E-04	5.895E-04	7.629E-04
TE125M	1.227E-04	7.133E-05	1.166E-04	1.439E-04	1.862E-04
SN126	7.309E-08	4.253E-08	6.945E-08	8.568E-08	1.108E-07
SB126	1.023E-08	5.954E-09	9.723E-09	1.199E-08	1.551E-08
SB126M	7.309E-08	4.253E-08	6.945E-08	8.568E-08	1.108E-07
TE127	4.227E-03	2.416E-08	4.003E-08	4.974E-08	6.493E-08
TE127M	4.316E-08	2.466E-08	4.087E-08	5.078E-08	6.628E-08
I129	3.187E-09	1.868E-09	3.033E-09	3.730E-09	4.802E-09
CS134	5.398E-04	1.889E-04	4.685E-04	6.860E-04	1.089E-03
CS135	4.397E-08	3.687E-08	4.385E-08	4.681E-08	5.044E-08
CS137	1.065E-02	6.409E-03	1.019E-02	1.240E-02	1.573E-02
BA137M	1.008E-02	6.063E-03	9.641E-03	1.173E-02	1.488E-02
CE144	3.864E-03	2.357E-03	3.707E-03	4.483E-03	5.642E-03
PR144	3.864E-03	2.357E-03	3.707E-03	4.483E-03	5.642E-03
PR144M	4.637E-05	2.828E-05	4.448E-05	5.380E-05	6.770E-05
PM147	1.166E-02	7.407E-03	1.129E-02	1.341E-02	1.642E-02
SM151	1.394E-04	1.076E-04	1.387E-04	1.522E-04	1.687E-04
EU152	6.121E-07	3.626E-07	6.039E-07	7.134E-07	8.364E-07
GD153	4.926E-09	1.449E-09	4.219E-09	6.387E-09	1.023E-08
EU154	9.179E-05	3.083E-05	7.866E-05	1.172E-04	1.908E-04
EU155	2.191E-04	1.387E-04	2.111E-04	2.521E-04	3.134E-04

TABLE F-6 TNI-2 SPECIFIC ACTIVITY SUMMARY (CURIES/GRAM U) FOR 2.96% INITIAL ENRICHMENT ZONES (MARCH 1964).

	ALL 2.96%	GROUP 9	GROUP 10	GROUP 11	GROUP 12
TH231	5.779E-06	6.030E-08	5.784E-08	5.587E-08	5.312E-08
TH234	3.271E-07	3.267E-07	3.271E-07	3.274E-07	3.277E-07
PA233	1.021E-08	5.071E-09	9.671E-09	1.410E-08	2.144E-08
PA234M	3.271E-07	3.267E-07	3.271E-07	3.274E-07	3.277E-07
U234	9.826E-10	5.586E-10	9.591E-10	1.304E-09	1.831E-09
U235	5.779E-06	6.030E-08	5.784E-08	5.587E-06	5.312E-08
U236	3.543E-08	2.113E-08	3.518E-08	4.635E-06	6.165E-08
U237	2.439E-10	3.893E-11	1.742E-10	3.895E-10	8.910E-10
U238	3.271E-07	3.267E-07	3.271E-07	3.274E-07	3.277E-07
NP237	1.021E-08	5.071E-09	9.671E-09	1.410E-08	2.144E-08
NP239	1.286E-09	3.165E-11	4.212E-10	1.729E-09	7.656E-09
PU236	3.925E-10	1.022E-10	3.174E-10	6.028E-10	1.211E-09
PU238	6.639E-06	1.735E-06	5.377E-06	1.019E-05	2.046E-05
PU239	8.636E-05	5.422E-05	8.681E-05	1.110E-04	1.419E-04
PU240	1.970E-05	6.690E-06	1.773E-05	2.968E-05	5.024E-05
PU241	9.941E-04	1.587E-04	7.102E-04	1.584E-03	3.632E-03
PU242	1.306E-09	8.482E-11	6.559E-10	1.587E-09	6.356E-09
AM241	9.128E-06	1.457E-06	6.521E-06	1.454E-05	3.335E-05
AM242M	3.031E-09	2.314E-10	1.662E-09	4.737E-09	1.390E-08
AM242	3.016E-09	2.302E-10	1.653E-09	4.714E-09	1.383E-08
AM243	1.286E-09	3.165E-11	4.212E-10	1.729E-09	7.656E-09
CM242	6.193E-09	4.301E-10	3.224E-09	9.526E-09	2.944E-08
CM243	3.466E-10	8.597E-12	1.141E-10	4.670E-10	2.059E-09
CM244	1.116E-08	9.823E-11	2.244E-09	1.248E-08	7.666E-08
H 3	3.150E-05	1.786E-05	3.087E-05	4.189E-05	5.820E-05
SE 79	3.586E-08	2.072E-08	3.532E-08	4.741E-08	6.494E-08
KR 85	7.299E-04	4.269E-04	7.211E-04	9.612E-04	1.304E-03
SR 89	8.420E-12	4.973E-12	8.339E-12	1.105E-11	1.488E-11
SR 90	6.916E-03	4.058E-03	6.838E-03	9.098E-03	1.231E-02
Y 90	6.916E-03	4.059E-03	6.840E-03	9.100E-03	1.231E-02
Y 91	3.014E-10	1.776E-10	2.987E-10	3.967E-10	5.355E-10
ZR 93	1.729E-07	1.007E-07	1.706E-07	2.279E-07	3.101E-07
NB 93M	3.826E-08	2.228E-08	3.775E-08	5.045E-08	6.868E-08
ZR 95	2.089E-09	1.213E-09	2.060E-09	2.757E-09	3.760E-09
NB 95	4.639E-09	2.694E-09	4.574E-09	6.121E-09	8.349E-09
NB 95M	1.550E-11	9.002E-12	1.528E-11	2.045E-11	2.790E-11
TC 99	1.221E-06	7.058E-07	1.202E-06	1.613E-06	2.208E-06
RU103	5.939E-15	3.287E-15	5.788E-15	7.960E-15	1.125E-14
RU106	9.703E-04	4.797E-04	9.202E-04	1.342E-03	2.039E-03
RH106	9.703E-04	4.797E-04	9.202E-04	1.342E-03	2.039E-03
PD107	3.054E-09	1.439E-09	2.905E-09	4.276E-09	6.661E-09
AG110	1.637E-09	3.777E-10	1.269E-09	2.532E-09	5.374E-09
AG110M	1.231E-07	2.840E-08	9.542E-08	1.904E-07	4.041E-07
CD113M	2.156E-06	1.190E-06	2.097E-06	2.891E-06	4.107E-06
SN119M	1.807E-07	1.018E-07	1.767E-07	2.408E-07	3.367E-07
SN121	8.594E-09	4.509E-09	8.343E-09	1.188E-08	1.751E-08
SN123	4.937E-08	2.796E-08	4.836E-08	6.570E-08	9.143E-08
SB125	3.371E-04	1.878E-04	3.289E-04	4.508E-04	6.347E-04
TE125M	8.226E-05	4.584E-05	6.027E-05	1.100E-04	1.549E-04
SN126	4.966E-08	2.771E-08	4.847E-08	6.638E-08	9.335E-08
SB126	6.952E-09	3.860E-09	6.786E-09	9.293E-09	1.307E-08
SB126M	4.966E-08	2.771E-08	4.847E-08	6.638E-08	9.335E-08
TE127	2.859E-08	1.570E-08	2.760E-08	3.840E-08	5.457E-08
TE127M	2.918E-06	1.603E-08	2.838E-08	3.920E-08	5.572E-08
I129	2.232E-09	1.255E-09	2.154E-09	2.977E-09	4.161E-09
CS134	2.314E-04	8.286E-05	2.390E-04	4.292E-04	8.008E-04
CS135	4.088E-08	3.290E-08	4.184E-08	4.673E-08	5.195E-08
CS137	7.704E-03	4.427E-03	7.577E-03	1.020E-02	1.404E-02
BA137M	7.298E-03	4.188E-03	7.168E-03	9.652E-03	1.328E-02
CE144	2.931E-03	1.645E-03	2.792E-03	3.736E-03	5.094E-03
PR144	2.931E-03	1.645E-03	2.792E-03	3.736E-03	5.094E-03
PR144M	3.397E-05	1.974E-05	3.351E-05	4.443E-05	6.113E-05
PM147	8.749E-03	5.259E-03	9.710E-03	1.142E-02	1.512E-02
SM151	1.189E-04	8.604E-05	1.221E-04	1.435E-04	1.667E-04
EU154	4.298E-07	2.079E-07	4.312E-07	6.030E-07	7.970E-07
GD153	2.346E-09	4.076E-10	1.876E-09	3.752E-09	7.440E-09
EU154	4.617E-05	1.314E-05	3.860E-05	7.050E-05	1.351E-04
EU155	1.587E-04	9.638E-05	1.578E-04	2.060E-04	2.740E-04

APPENDIX G

SURFACE AREA CALCULATION FOR PARTICLE SIZE FRACTIONS

APPENDIX G
SURFACE AREA CALCULATION FOR PARTICLE SIZE FRACTIONS

Surface area ratios were calculated for particle size fractions sieved from the TMI-2 core debris grab samples. The results of the calculation were used for evaluating the correlation between the surface area of particle size fractions and element fission product concentrations measured for the samples. For the calculational model, particles were assumed to have similar shapes and a constant particle density. The specific surface area ratio difference between the minimum particle size fraction (30 to 74 μm) and the maximum (1680 to 4000 μm) fraction is approximately a factor of 50.

Assumptions for Surface Area Calculation

Assumptions

1. Particle shapes are approximated to be similar.
2. Particle density is constant for individual particles.
3. Particle size distribution is described to be logarithmically linear for cumulative weight fraction and particle size.
4. Effective diameter represents particle size.

Nomenclature

F = Cumulative weight fraction for a certain particle size

R = Particle size (effective diameter) in μm

S = Surface area of distinct particle (cm^2)

W = Weight of distinct particle (mg)

D = Effective particle density used in the relationship between W and R

k = Effective surface area coefficient used in the relationship between S and R

a,b = Particle size distribution coefficients used in the relationship between F and R

T = Total weight of all particle size fractions (mg)

N_x^y = Number of particles in the diameter range from x to y

A_x^y = Surface area of particles in the diameter range from x to y (cm^2)

i = Identification for a certain particle size fraction

A_i = Average specific surface area for a certain particle size fraction i (cm^2)

C = Average specific surface area for all particle size fractions (cm^2).

Formulation

From Assumption 3, the relationship between F (cumulative weight fraction) and R (effective diameter) can be described as

$$F = aR^b \qquad (1)$$

where a and b are determined from the relationship between F and R.

The weight (W) and surface area (S) of a particle with diameter R can be approximated as follows:

$$W = DR^3 \tag{2}$$

$$S = kR^2 \tag{3}$$

where D and k are assumed to be constant.

The number of particles included in the diameter range from R to R + dR is derived from Equations 1 and 2, and the total sample weight (T).

$$dF = abR^{b-1}dR$$

$$N_R^{R+dR} = \frac{TdF}{dR^3}$$

$$= \frac{Tab}{D} R^{b-4}dR \tag{4}$$

The surface area of particles included in the above diameter range is described as

$$A_R^{R+dR} = kR^2 \cdot N_R^{R+dR}$$

$$= \frac{kTab}{D} R^{b-2}dR \ .$$

The average specific surface area for particle size fraction i can be derived as follows:

$$A_i = A_{r_{i1}}^{r_{12}} / T[F(r_{12}) - F(r_{i1})]$$

$$= \int_{r_{i1}}^{r_{i2}} \frac{kTab}{b} R^{b-2} dR / Ta(r_{i2}^b - r_{i1}^b)$$

$$= \frac{k}{D} \cdot \frac{b}{r_{i2}^b - r_{i1}^b} \int_{r_{i1}}^{r_{i2}} R^{b-2} dR \ .$$

When $b \neq 1$,

$$A_i = \frac{k}{D} \cdot \frac{\log(r_{i2}/r_{i1})}{r_{i2} - r_{i1}} \tag{6}$$

and when $b \neq 1$,

$$A_i = \frac{k}{D} \cdot \frac{b}{b-1} \cdot \frac{r_{i2}^{b-1} - r_{i1}^{b-1}}{r_{i2}^b - r_{i1}^b} \tag{7}$$

where r_{i1} and r_{i2} indicate the diameter range of the particle size fraction i.

The specific surface area averaged for all particle size fractions may be used as a normalization standard.

When $b = 1$,

$$C = \frac{k}{D} \cdot \frac{\log(r_{max}/r_{min})}{r_{max} - r_{min}}$$

$$A_i/C = \frac{\log(r_{i2}/r_{i1})}{\log(r_{max}/r_{min})} \cdot \frac{r_{max} - r_{min}}{r_{i2} - r_{i1}} \ . \tag{8}$$

When $b \neq 1$,

$$C = \frac{k}{D} \cdot \frac{b}{b-1} \cdot \frac{r_{max}^{b-1} - r_{min}^{b-1}}{r_{max}^{b} - r_{min}^{b}}$$

$$A_i/C = \frac{r_{i2}^{b-1} - r_{i1}^{b-1}}{r_{max}^{b-1} - r_{min}^{b-1}} \cdot \frac{r_{max}^{b} - r_{min}^{b}}{r_{i2}^{b} - r_{i1}^{b}} \cdot \qquad (9)$$

Application to Grab Sample Particle Size Distribution

The particle size distribution coefficient b in Equation (1) can be determined for the core debris grab samples (See Figure 15 of Reference G-1) by

$$A_i/C = \frac{r_{i2}^{0.59} - r_{i1}^{0.59}}{r_{max}^{0.59} - r_{min}^{0.59}} \quad \frac{r_{max}^{1.59} - r_{min}^{1.59}}{r_{i2}^{1.59} - r_{i1}^{1.59}} \cdot$$

Results of the application to the core debris grab sample particle size distribution are shown in the Table G-1.

TABLE G-1. NORMALIZED SURFACE AREA FOR TMI-2 CORE DEBRIS GRAB SAMPLES

Particle Size Range (μm)		Normalized Surface Area per Unit Mass	
r_{i1}	r_{i2}	(30 μm)[a]	(20 μm)[b]
1680	4000	0.57	0.56
1000	1680	1.18	1.17
707	1000	1.85	1.83
297	707	3.21	3.17
149	297	7.16	7.07
74	149	14.3	14.1
30	74	31.0	30.6
20	30	--	62.4

a. For samples sieved to 30 μm.

b. For samples sieved to 20 μm.

Reference

G-1. D. W. Akers and B. A. Cook, Draft Preliminary Report: TMI-2 Core Debris Grab Samples--Analysis of First Group of Samples, EGG-TMI-6630, June 1984, draft.

APPENDIX H

THERMAL ANALYSIS OF TMI-2 CORE DEBRIS SAMPLES

J. R. Jewett
Rockwell Hanford Operations

Rockwell Hanford Operations

SUPPORTING DOCUMENT

Number	Rev. No.	Page 1 of Total Pages
SD-WM-TRP-009	Rev. 0	13

PROGRAM: WASTE MANAGEMENT

Document Title:
Thermal Analysis of TMI-2 Core Debris Samples

Baseline Document: ☐ Yes ☒ No

Key Words:
Zirconium, Core Debris, TMI, DTA, Pyrophoricity

WBS No or Work Package No: X762B

Prepared by (Name and Dept. No.): J. R. Jewett/65450 — Date: 10/10/84

See reverse side for additional approvers

Abstract

Differential thermal analyses (DTA) were conducted on samples of Three Mile Island core debris. The samples generally showed little thermal activity; however, one sample gave a large broad exotherm starting at 550°C.

Distribution

Department of Energy
Richland Operations Office

* M. Dayani — Fed/700
* J. D. White — Fed/700

EG&G Idaho (TMI)
Middletown, Pennsylvania

* G. J. Quinn
* H. M. Burton (10)
† Joe Carlson

Department of Energy
TMI Site

* W. W. Bixby

Rockwell Hanford Operations

* J. N. Appel	2750E/200E
* J. S. Buckingham	MO-037/200W
* B. D. Bullough	MO-922/200E
* T. D. Cooper	284-5[illegible]/200W
* J. O. Henrie (3)	2750E/200E
* J. R. Jewett (3)	MO-037/200W
* J. P. Sloughter	2704S/200W

(Continued on reverse side)

*COMPLETE DOCUMENT
(No asterisk: title page summary or revision page only)

Release Stamp

OFFICIAL RELEASE
OCT 19 1984

Prepared By _____

Used By _____

19

A-6400-073 (R-2-83)

Rockwell Hanford Operations

Page	Number
2	SD-WM-TRP-009

SUPPORTING DOCUMENT

Approvals

☒	H. E. McGuire	Program Office
☒	J. O. Henrie	Research and Engineering
☐		Plant Operations
☐		Health, Safety and Environment
☐		Quality Assurance
☐		Training
☐		End Function
☐		End Function
☐		
☐		
☐		
☐		
☒	J. S. Buckingham	Approval Authority

* Distribution	Name	Mail Address

A-6400-073R (2-83)

THERMAL ANALYSIS OF TMI-2 CORE DEBRIS SAMPLES

Differential thermal analyses (DTA) have been conducted on seven samples of core debris from Three Mile Island Unit 2 (TMI-2). The samples were received from D. W. Akers of EG&G Idaho on August 23, 1984. The attached table summarizes the appearances of the samples.

Each sample was heated from 30°C to 1000°C at 10 deg/min while monitoring the heat energy being absorbed or produced by the sample, using a Perkin-Elmer DTA 1700 DTA System. Each sample was packaged separately in a small glass vial and weighed in the range 10-20 mg. Each sample was consumed completely in the test, leaving a dark powder residue.

The attached figures give the DTA results. The samples generally showed little or no thermal activity. In exception, sample #262 gave a large broad exotherm of 761 cal/g, spanning nearly 500 degrees, starting at about 550°C. This exotherm is at much greater temperatures than those observed for samples of zirconium powder and partially oxidized zirconium powder (Reference). If the exotherm is due to the oxidation of zirconium, the zirconium must be coated with a thick non-combustible (oxide?) layer which protects it at lower temperatures.

Samples #245 and Spl #5 both showed about 100 cal/g of exothermic activity in the 200-600°C region, with most of it occurring in a peak from about 550°C to 600°C. Similar activity, but greatly reduced in magnitude, was also observed in sample #247.

"Blank" runs, conducted in the same way (except without samples) have been included in the figures to demonstrate the baseline and run-to-run variation inherent in the measurement method.

TABLE

Appearance of Sample Materials As Received

Sample	Appearance
#245	single, black, obsidian-like particle
#246	one large black particle plus black fines
#247	single, black, obsidian-like particle
#258	single brownish shard
#262	single black particle
#265	single black obsidian-like particle
Spl #5	single black particle plus black fines

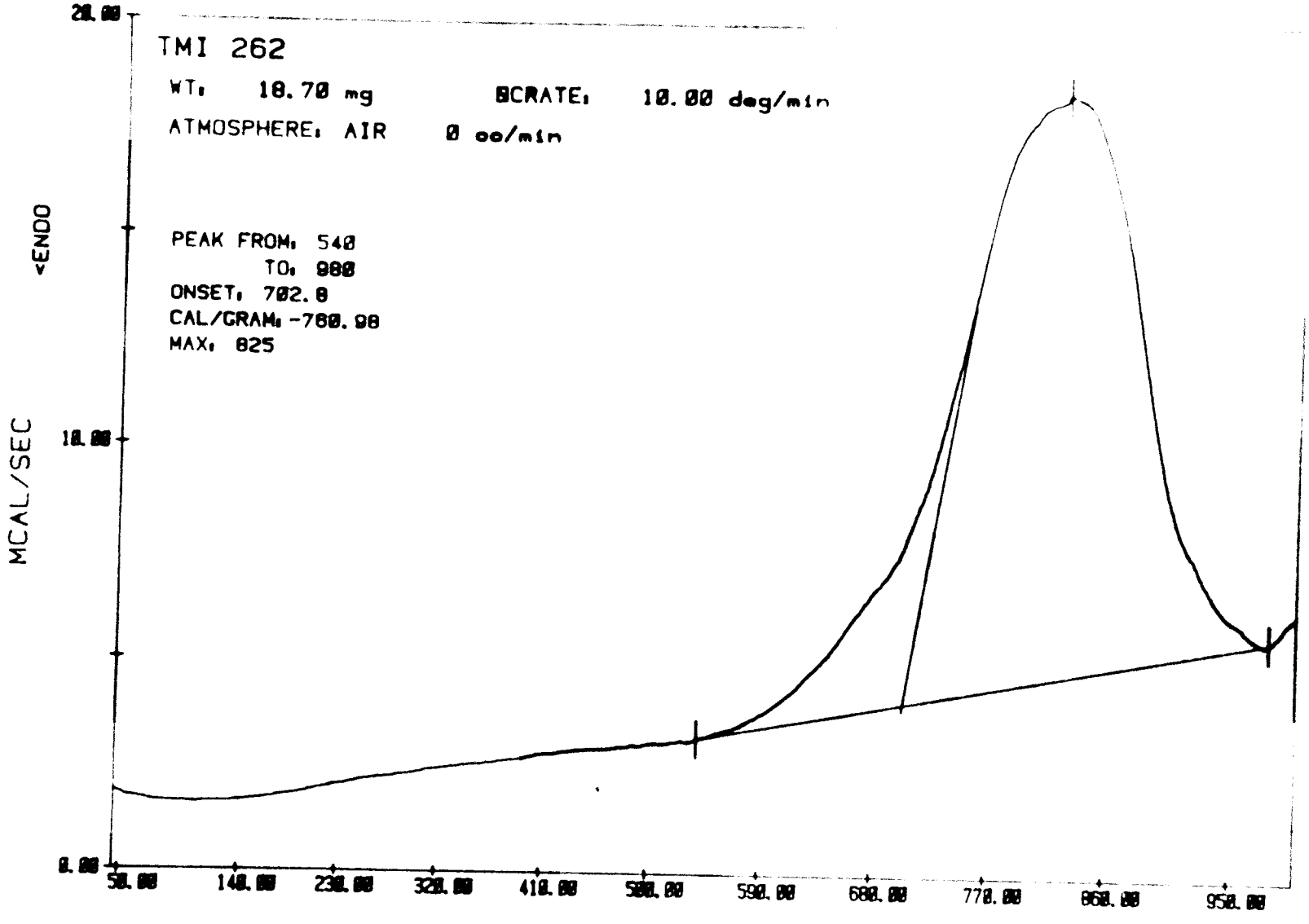
TMI 262
WT: 18.70 mg
BCRATE: 10.00 deg/min
ATMOSPHERE: AIR 0 cc/min
PEAK FROM: 540
TO: 980
ONSET: 702.8
CAL/GRAM: -760.98
MAX: 825
<ENDO
MCAL/SEC
20.00
10.00
0.00
50.00
140.00
230.00
320.00
410.00
500.00
590.00
680.00
770.00
860.00
950.00
JKW
FILE: 262PK.DT
DATE: 84/09/20
TIME: 12:04
TEMPERATURE (C)
DTA

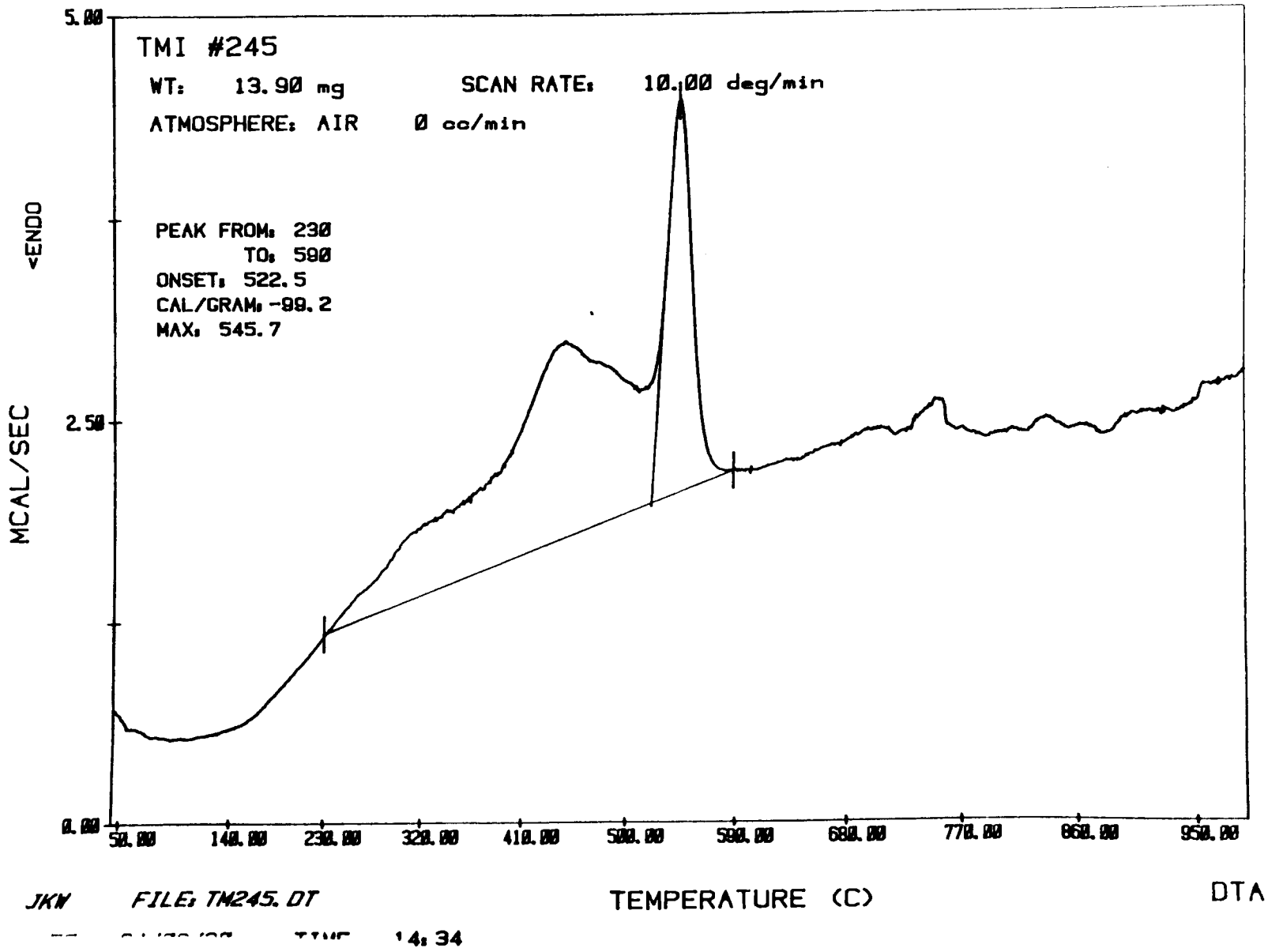
TMI #245
WT: 13.90 mg
SCAN RATE: 10.00 deg/min
ATMOSPHERE: AIR 0 cc/min
PEAK FROM: 230
TO: 590
ONSET: 522.5
CAL/GRAM: -99.2
MAX: 545.7
<ENDO
MCAL/SEC
5.00
2.50
0.00
50.00
140.00
230.00
320.00
410.00
500.00
590.00
680.00
770.00
860.00
950.00
JKW
FILE: TM245.DT
TEMPERATURE (C)
DTA
TIME 14:34

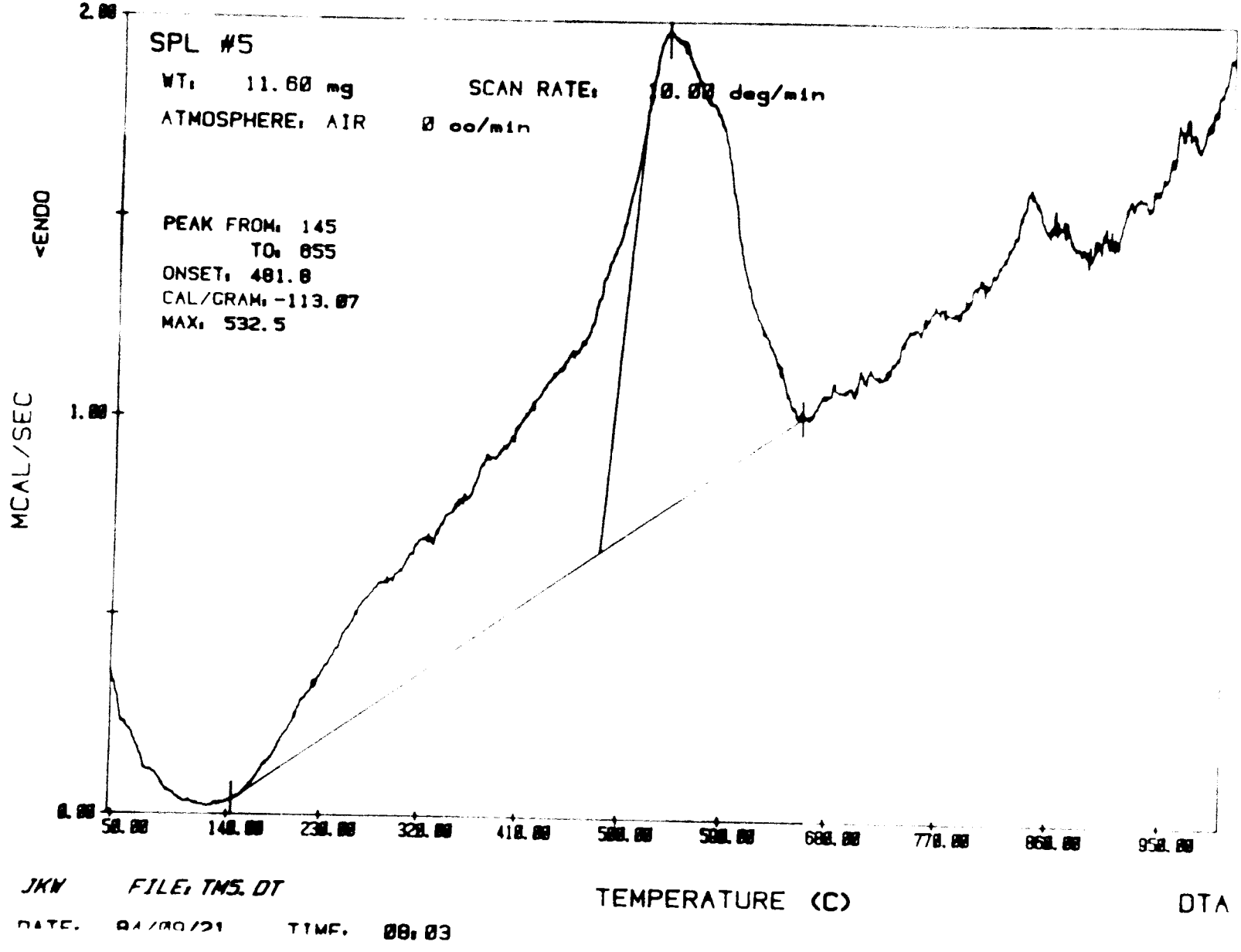
SPL #5
WT: 11.60 mg
SCAN RATE: 10.00 deg/min
ATMOSPHERE: AIR 0 cc/min
PEAK FROM: 145
TO: 855
ONSET: 481.8
CAL/GRAM: -113.07
MAX: 532.5
<ENDO
MCAL/SEC
2.00
1.00
0.00
50.00
140.00
230.00
320.00
410.00
500.00
590.00
680.00
770.00
860.00
950.00
JKW
FILE: TMS.DT
DATE: 94/09/21
TIME: 08:03
TEMPERATURE (C)
DTA

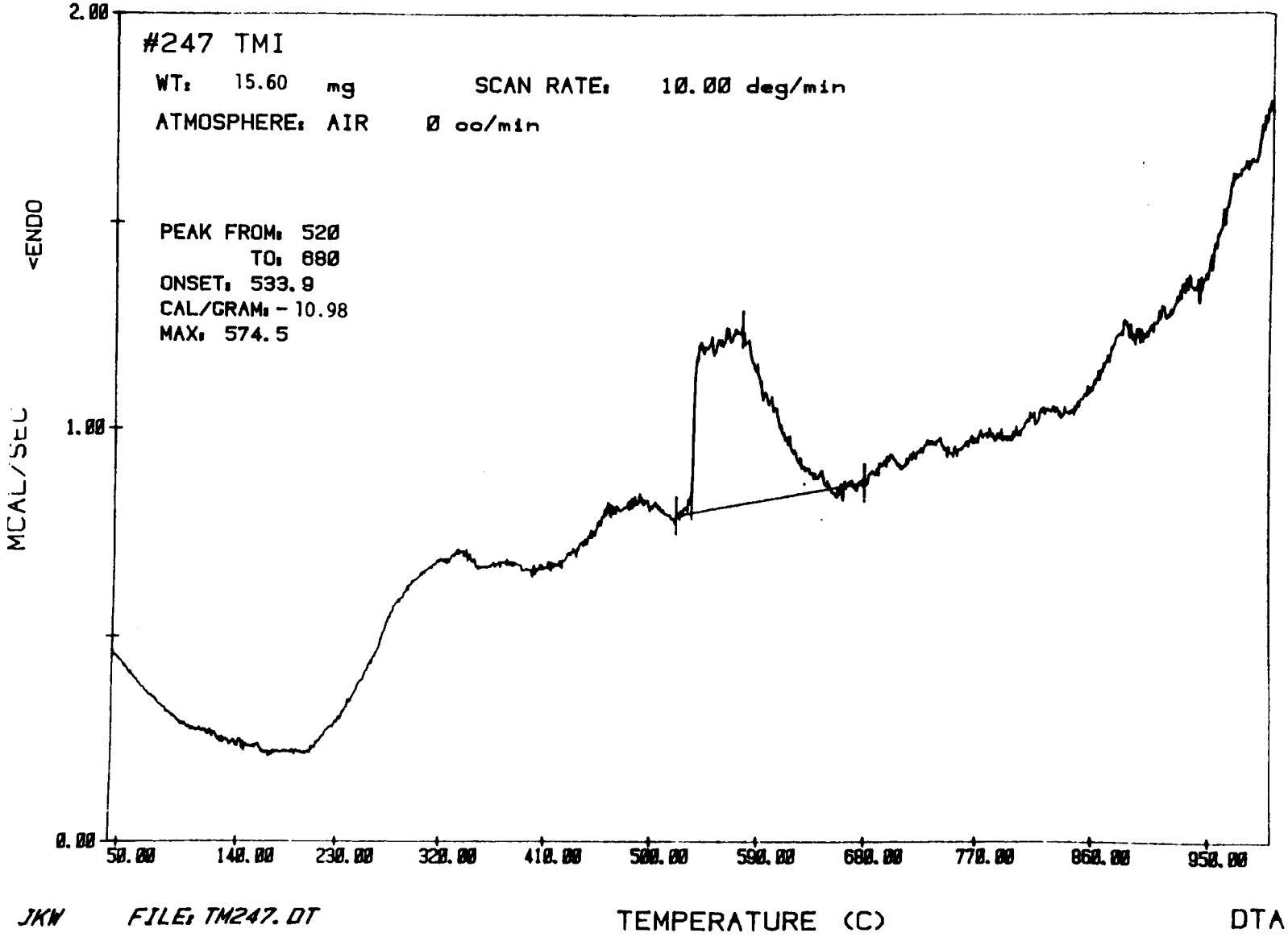
#247 TMI
WT: 15.60 mg
SCAN RATE: 10.00 deg/min
ATMOSPHERE: AIR 0 cc/min
PEAK FROM: 520
TO: 680
ONSET: 533.9
CAL/GRAM: -10.98
MAX: 574.5
<ENDO
MCAL/SEC
2.00
1.00
0.00
50.00
140.00
230.00
320.00
410.00
500.00
590.00
680.00
770.00
860.00
950.00
JKW
FILE: TM247.DT
TEMPERATURE (C)
DTA

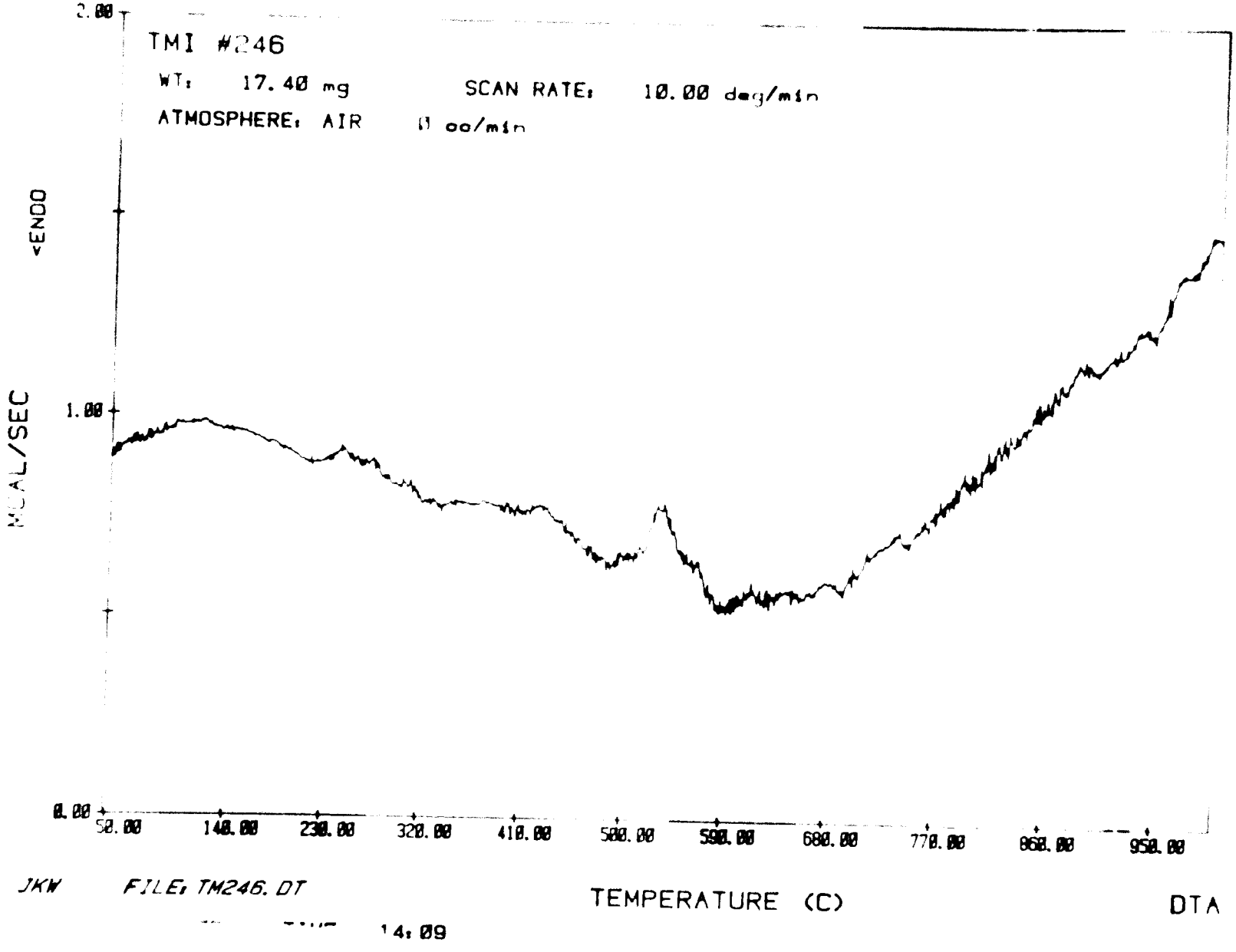
TMI #246
WT: 17.40 mg
SCAN RATE: 10.00 deg/min
ATMOSPHERE: AIR
<ENDO
MCAL/SEC
2.00
1.00
0.00
50.00
140.00
230.00
320.00
410.00
500.00
590.00
680.00
770.00
860.00
950.00
JKW
FILE: TM246.DT
14:09
TEMPERATURE (C)
DTA

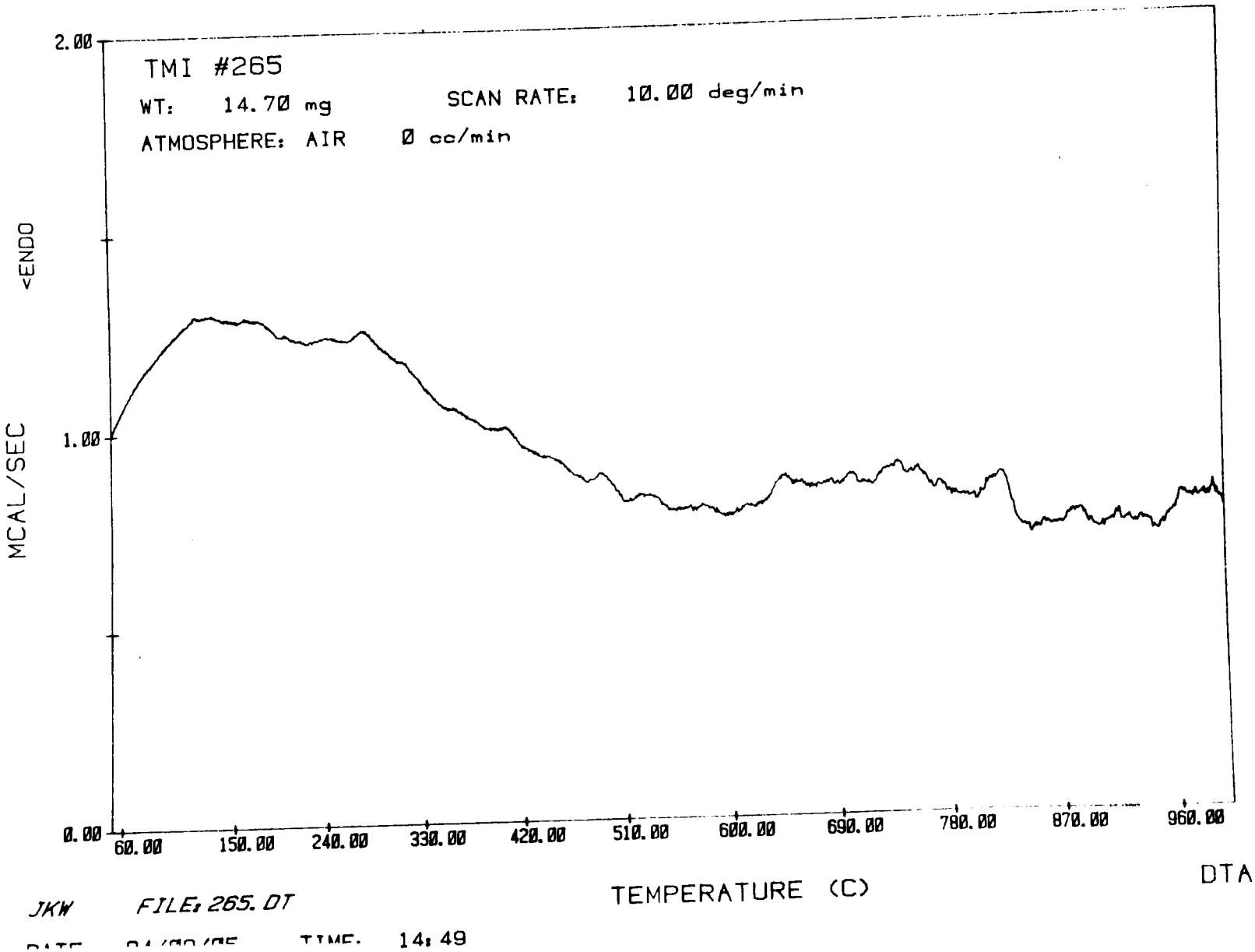
TMI #265
WT: 14.70 mg
SCAN RATE: 10.00 deg/min
ATMOSPHERE: AIR 0 cc/min
<ENDO
MCAL/SEC
2.00
1.00
0.00
60.00
150.00
240.00
330.00
420.00
510.00
600.00
690.00
780.00
870.00
960.00
TEMPERATURE (C)
DTA
JKW
FILE: 265.DT
TIME: 14:49

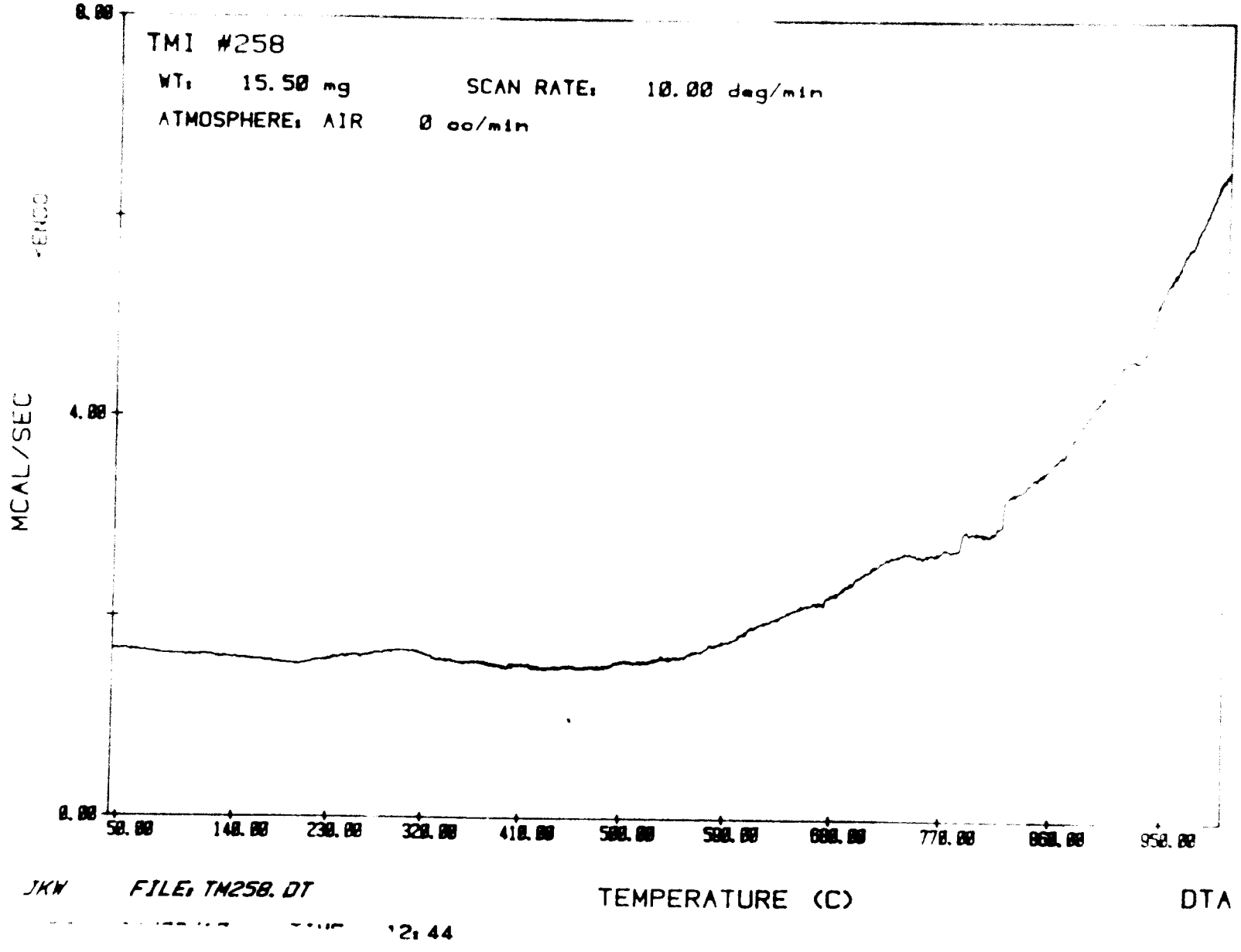
TMI #258
WT: 15.50 mg
SCAN RATE: 10.00 deg/min
ATMOSPHERE: AIR 0 cc/min
MCAL/SEC
8.00
4.00
0.00
50.00
140.00
230.00
320.00
410.00
500.00
590.00
680.00
770.00
860.00
950.00
JKW
FILE: TM258.DT
TEMPERATURE (C)
DTA

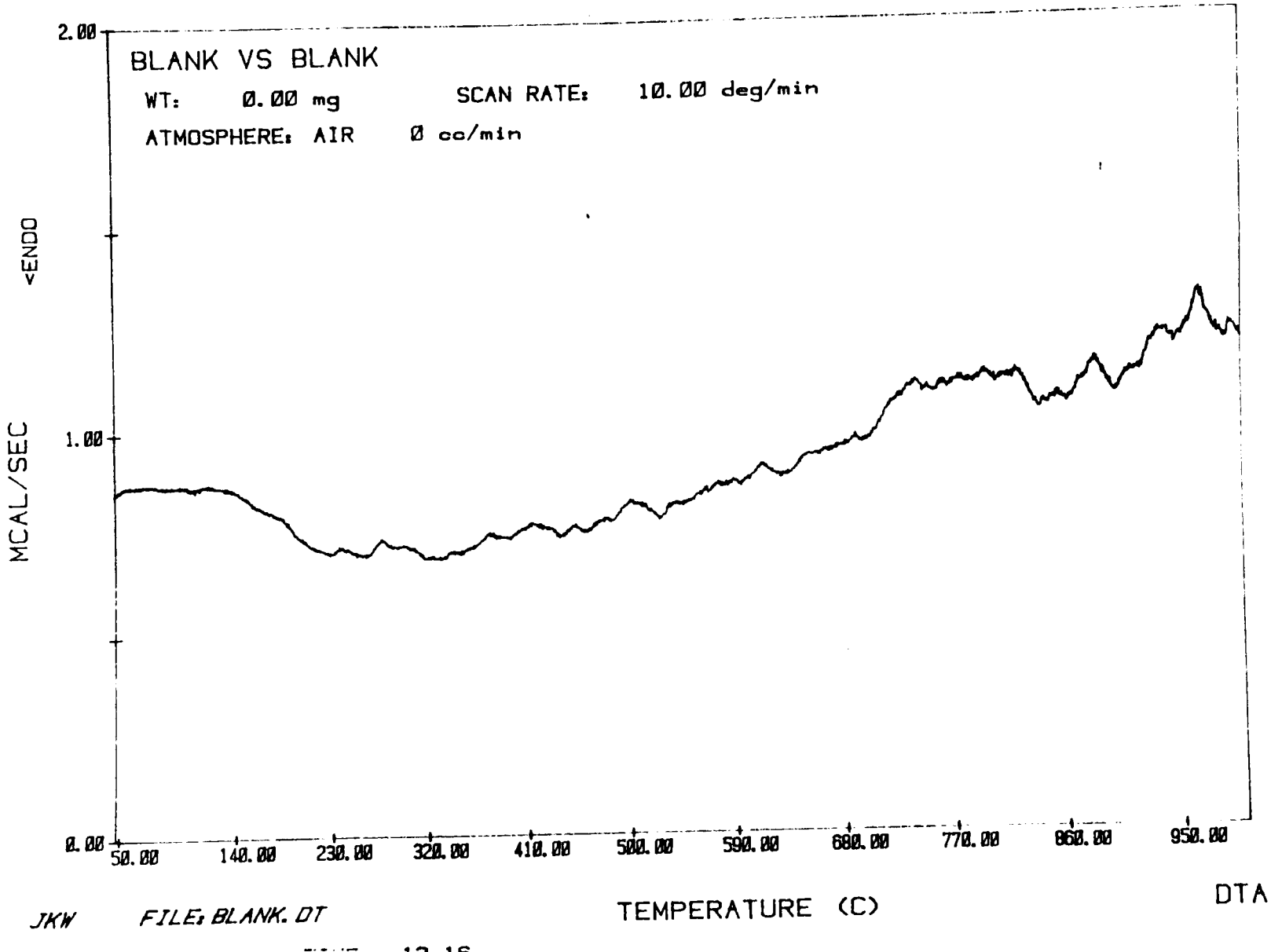
BLANK VS BLANK
WT: 0.00 mg
SCAN RATE: 10.00 deg/min
ATMOSPHERE: AIR 0 cc/min
<ENDO
MCAL/SEC
2.00
1.00
0.00
50.00
140.00
230.00
320.00
410.00
500.00
590.00
680.00
770.00
860.00
950.00
TEMPERATURE (C)
DTA
JKW
FILE: BLANK.DT
12:16

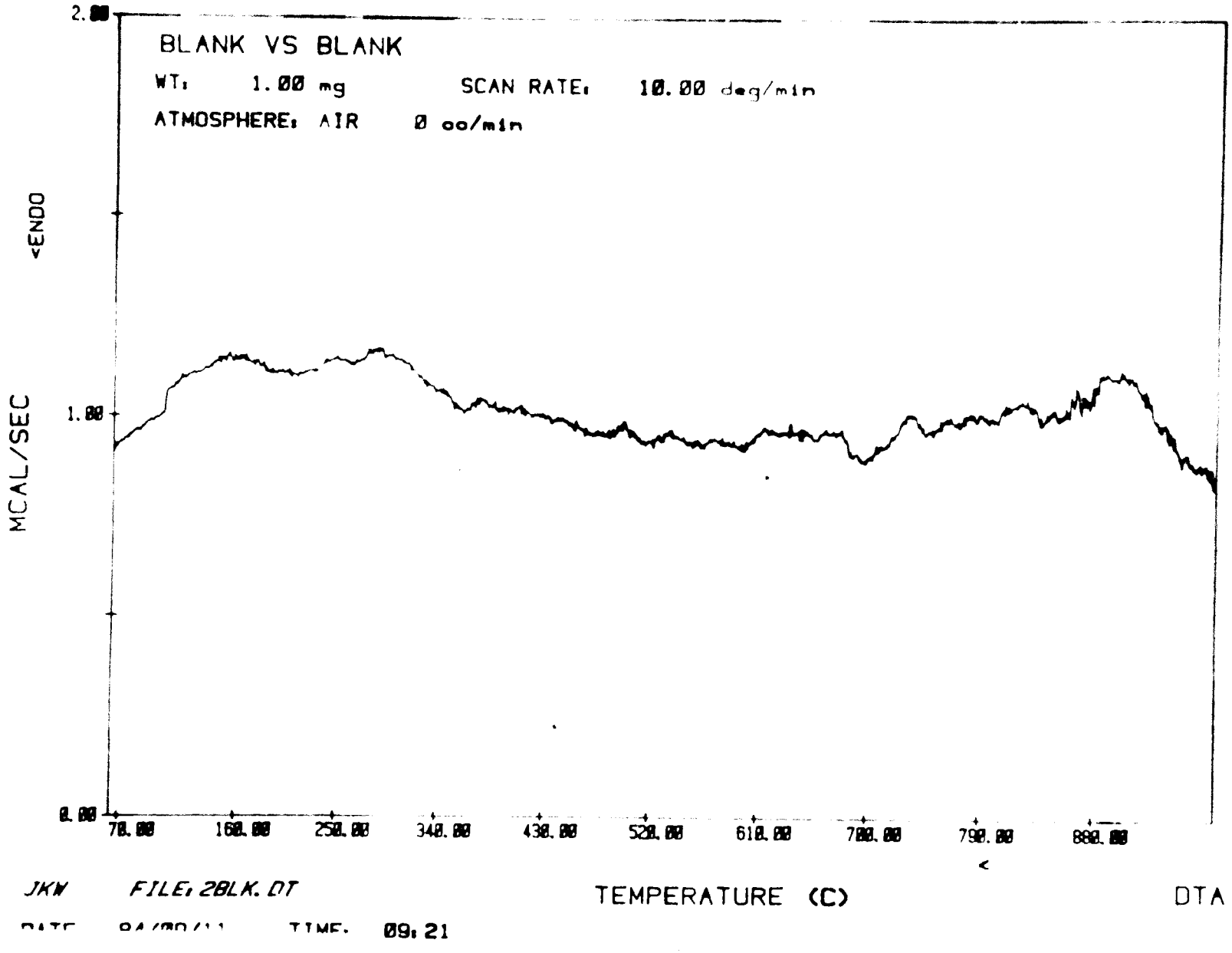
BLANK VS BLANK
WT: 1.00 mg
SCAN RATE: 10.00 deg/min
ATMOSPHERE: AIR 0 cc/min
<ENDO
MCAL/SEC
2.00
1.00
0.00
70.00
160.00
250.00
340.00
430.00
520.00
610.00
700.00
790.00
880.00
JKW
FILE: 2BLK.DT
TEMPERATURE (C)
DTA
TIME: 09:21

SI-H.